DOE/ER/13000--711

STANFORD SYNCHROTRON RADIATION LABORATORY

DISCLAIMER

This report was prepared as an account of work sponsored by an agency of the United States Government. Neither the United States Government nor any agency thereof, nor any of their employees, makes any warranty, express or implied, or assumes any legal liability or responsibility for the accuracy, completeness, or usefulness of any information, apparatus, product, or process disclosed, or represents that its use would not infringe privately owned rights. Reference herein to any specific commercial product, process, or service by trade name, trademark, manufacturer, or otherwise does not necessarily constitute or imply its endorsement, recommendation, or favoring by the United States Government or any agency thereof. The views and opinions of authors expressed herein do not necessarily state or reflect those of the United States Government or any agency thereof.

ACTIVITY REPORT FOR 1987

DISTRIBUTION OF THIS DOCUMENT IS UNLIMITED

MASTER

ABOUT THE STANFORD SYNCHROTRON RADIATION LABORATORY

SSRL is a national facility supported primarily by the Department of Energy for the utilization of synchrotron radiation for basic and applied research in the natural sciences and engineering. It is a user-oriented facility which welcomes proposals for experiments from all researchers.

The synchrotron radiation is produced by the 4 GeV storage ring, SPEAR, and the 15 GeV storage ring, PEP, operated by the Stanford Linear Accelerator Center (SLAC). SPEAR is dedicated to the production of synchrotron radiation during 50% of its operations time or about 4 months per year. The remainder of the time synchrotron radiation may be used parasitically during colliding beam runs for high energy physics experiments. Operation on PEP is generally parasitic.

SSRL currently has 24 experimental stations on the SPEAR and PEP storage rings. There are 158 active proposals for experimental work from 114 institutions involving approximately 650 scientists. There is normally no charge for use of beam time by experimenters.

Additional information for prospective users is contained in the booklet "SSRL User Guide". Further information about the facility may be obtained by writing or telephoning Katherine Cantwell at SSRL, SLAC Bin 69, P.O. Box 4349, Stanford, CA 94309 -0210 - telephone (415) 926-3191.

This report summarizes the activity at SSRL for the period January 1, 1987 to December 31, 1987.

SSRL is supported by the Department of Energy, Office of Basic Energy Sciences: and the National Institutes of Health, Biotechnology Resource Program, Division of Research Resources.

DISCLAIMER

Portions of this document may be illegible in electronic image products. Images are produced from the best available original document.

Stanford Synchrotron Radiation Laboratory
1987 ACTIVITY REPORT
TABLE OF CONTENTS

		Page
I	**Laboratory Operations**	1
	Operations Division Activities	2
	Beam and SPEAR Usage Tables	2
II	**Accelerator Physics Program**	9
	SPEAR Accelerator Physics Activities	9
	3 GeV Injector Plans	10
	Accelerator Physics Studies on PEP	10
III	**Experimental Facilities**	17
	X-ray Facilities	17
	VUV Facilities	18
	Biotechnology Facilities	20
	PRT Experimental Facilities	20
	Support Facilities	26
IV	**Engineering Division**	27
	Mechanical Engineering	27
	Electrical Engineering	28
V	**Conferences and Workshops**	31
	Workshop on PEP as a Synchrotron Radiation Source	31
	Fourteenth Annual SSRL Users Group Meeting	32
	First SSRL Rotation Camera Users Meeting	32
VI	**SSRL Organization**	33
	SSRL Functional Organization	33
	SSRL Advisory Panels	36
VII	**Experimental Progress Reports**	37
	Index to Experimental Progress Reports	37
	Materials Proposals	44
	Biology Proposals	131
	VUV Proposals	171
VIII	**Active Proposals**	219
IX	**SSRL Experimenters and Proposals by Institution**	242
X	**SSRL Publications**	252
	Publications	252
	Theses	265

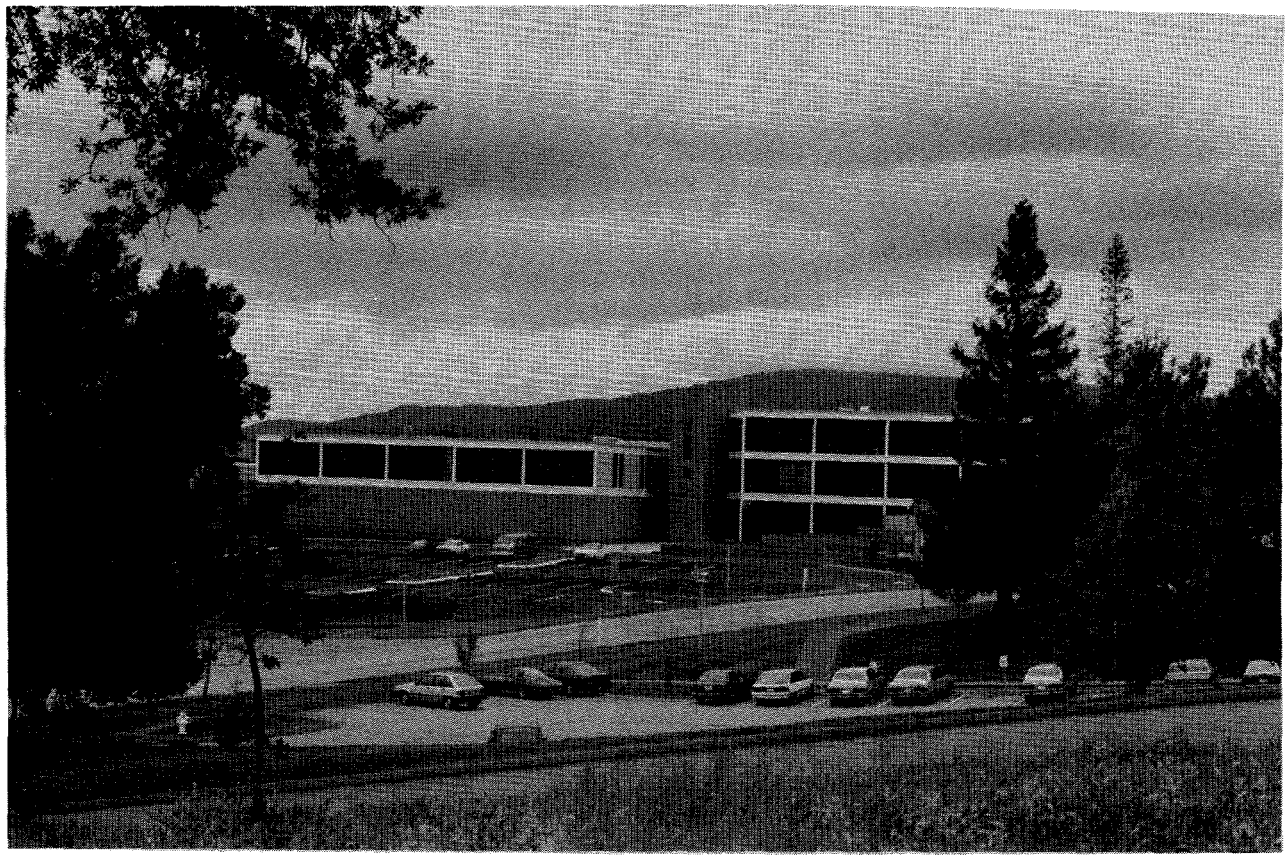

Photo- G. Brown

The new SSRL Laboratory-Office-Shop-Building (LOS) completed under the SEP project funded by the DOE. The LOS houses the SSRL administrative, engineering and scientific staff and is located just outside the SLAC research yard.

SSRL Activity Report 1987

INTRODUCTION

During 1987, SSRL achieved many significant advances and reached several major milestones utilizing both SPEAR and PEP as synchrotron radiation sources as described in this report. Perhaps the following two are worthy of particular mention:

1. SPEAR reached an all time high of 4,190 delivered user-shifts during calendar year 1987. Highlights of the many scientific results are given below.

2. During a 12 day run in December of 1987, PEP was operated in a low emittance mode (calculated emittance 6.4 nanometer-radians) at 7.1 GeV with currents up to 33 mA. A second undulator beam line on PEP was commissioned during this run and used to record many spectra showing the extremely high brightness of the radiation. PEP is now by far the highest brightness synchrotron radiation source in the world.

It is gratifying to note that work done at SSRL has been recognized by an impressive array of awards during 1987 as listed at the end of this introduction.

FACILITY DEVELOPMENT

Laboratory operations are reviewed in Section I of this report. During 1987, the SLAC Linear Collider (SLC) was being commissioned, resulting in limited injection opportunities during dedicated runs on SPEAR. Typically, injection was available once every 12 hours. Due to the usually long lifetimes on SPEAR this was not a major problem during runs for experiments. However, the limited injection opportunities made it difficult or impossible to pursue accelerator physics studies to improve the performance of the SPEAR ring and train graduate students in accelerator physics.

These limitations on injection from the SLAC linac will be a thing of the past once the new 3 GeV dedicated synchrotron injector to SPEAR is completed in 1990. This major construction project was started in October, 1987. (Actually, its official start was delayed until February, 1988 due to delays in the federal budget process for fiscal year 1988.) This injector will end dependence on the SLAC linac schedule and eliminate interference with SLC operation. As a full energy injector, it will improve the stability and reproducibility of the photon beams from SPEAR, as well as providing more running time at a lower cost per shift. It will also facilitate the reduction of the SPEAR emittance and will increase opportunities for accelerator physics studies to improve the performance of the SPEAR storage ring and train graduate students. The injector project is described in Section II of this report.

In October, 1987 SSRL conducted a Workshop on PEP as a Synchrotron Radiation Source attended by 125 scientists from many laboratories in the US, Europe and Japan. An accelerator physics working group provided a critical assessment of PEP's potential as a low emittance storage ring. Nine working groups dealing with different applications discussed many experiments that could be done on PEP, particularly experiments that would make use of its unique features. *[See Section V.]*

With the major interest in PEP as a synchrotron radiation source that was evident at the PEP Workshop, and the dramatic demonstration of PEP's capabilities in the December, 1987 run, it became clear that PEP will be extremely important to national needs in synchrotron radiation research. Even in parasitic operation during colliding beam runs (which are scheduled to resume in August, 1988 after a two year period with no colliding beam operation) PEP offers x-ray beams above 10 keV with an order of magnitude higher brightness than any other source. During the 2-3 months per year available for dedicated low emittance operation, even much higher brightness can be reached.

Experiments using these higher levels of brightness and coherent power will start now, rather than waiting until the mid 1990's when new, third generation rings designed for these performance levels are expected to start operation. Furthermore, PEP could serve as a test bed for these new rings and for the development of their insertion devices and beam line instrumentation.

In addition, PEP has characteristics (particularly its 2200 meter circumference, its 117 meter long straight sections and its 16 GeV energy) that offer the potential to achieve performance levels exceeding those of the third generation rings now in design and construction at other labs. For example, calculations indicate that, with the use of 100-200 meters of damping wigglers in the long straight sections, the emittance of PEP could be reduced to less than one nanometer-radian at 6 GeV. PEP could therefore be the prototype of a diffraction-limited x-ray source for the future. *[See Section II.]*

The utilization of PEP however, will be limited by its dependence on the SLAC linac for injection, in the same way that this presently limits SPEAR. Therefore our thoughts turned to possibilities for injection to PEP independent of the SLAC linac. A plan was developed to enlarge the SPEAR 3 GeV synchrotron injector from a circumference of 100 meters to 133 meters, so that it could be later upgraded to function at 5 GeV, a level considered to be a reasonable minimum injection energy for PEP. The 5 GeV beam from this ring would be transported through a 120 meter tunnel, at the end of which it would connect to the present electron injection line of the PEP ring. After injection at 5 GeV, the energy of PEP would be ramped to the higher energy that would be needed for most synchrotron radiation experiments. Although this scheme would not provide full energy injection into PEP, it is the quickest and most cost-effective path to achieving dedicated injection. *[See Section II.]*

The addition of 5 new experimental stations on SPEAR during 1987, plus the simultaneous operation of SPEAR and PEP, placed severe demands on the SSRL technical and scientific staff. Budget constraints have prevented the staff from growing at a rate commensurate with the increased number of stations and user community. In addition to the new beam line that was commissioned on PEP, two new participating research team (PRT) beam lines were commissioned on the SPEAR storage ring. These were Beam Lines VIII and X, a joint effort of several US national laboratories in collaboration with the University of California system and SSRL. The national laboratories are Lawrence Livermore, Los Alamos and Sandia. The Lawrence Livermore Laboratory is the lead laboratory for the entire effort. This collaboration added significantly to SSRL's experimental capabilities with two magnificent new monochromators in the VUV and soft x-ray spectral region plus a hard x-ray station operating off a very powerful 15 period, 1.4 Tesla hybrid wiggler magnet. *[See Section III.]*

Although accelerator physics studies were severely limited because of the lack of the adequate opportunities for frequent injection into SPEAR, some studies were carried out as described in Section II. These include studies of ramping, ion clearing, stability, wiggler characterization, filling patterns, timing mode, beam steering and operation at energies above 3 GeV.

During the 12-day low emittance run on PEP, a group of more than 20 scientists from SSRL, SLAC, Argonne National Laboratory, Brookhaven National Laboratory and the Lawrence Berkeley Laboratory collaborated in a wide range of studies to characterize the low emittance lattice, evaluate single and multi-bunch instability limits, study the beam steering and stabilizing system and determine aperture requirements for injection. In addition, many detailed studies of the characteristics of the undulator beam in low emittance operation were carried out. *[See Section II.]*

Improvements to the large and increasing range of SSRL experimental facilities are described in Section III of this report. This includes the commissioning of new facility beam lines and the improvements to existing facility beam lines that serve both the VUV and x-ray parts of the spectrum. Significant improvements have been made in the output flux, reliability and user-friendliness of the systems. The very significant capabilities that SSRL offers for protein crystallography, x-ray absorption spectroscopy and small angle scattering are also described in Section III.

During 1987, the SSRL enhancement project (SEP) was essentially completed. This very successful construction project provided a number of major new capabilities to the laboratory including two beam lines on the PEP storage ring, a major upgrade in the steering and stabilizing systems for SPEAR and PEP, additions to the nuclear physics injector (NPI) system to enable it to provide injection into the SPEAR and PEP storage rings and a new laboratory/office/shop (LOS) building. The LOS building provides new support facilities including a machine shop, a vacuum assembly area, a metrology/mirror coating facility, a vacuum clean room, a VUV research laboratory, an x-ray laboratory, an electronics shop, a biotechnology laboratory, a design/drafting area and a central computer facility as well as numerous staff offices, conference rooms and a library. Providing all these facilities in one centralized location is expected to increase efficiency as well as free up much needed space close to the beam lines for users.

A major improvement in computational facilities is underway at SSRL with the introduction of the new VAX 8700 computer system which will replace the VAX 11/780 and VAX 11/750 systems. The beam line computers are also being upgraded.

The broad range of engineering efforts at SSRL in 1987 are described in Section IV of this report. The major activities include the design of a pinhole camera system for PEP Beam Line 1B, studies of beryllium window heating, thermal-structural analysis of several SSRL beam line components, the introduction of computer aided design systems, improvements to beam line control, wiggler control and beam line steering and stabilization systems and the development of beam line and storage ring status monitoring systems.

HIGHLIGHTS OF RESEARCH ACTIVITIES

X-ray and Materials Research

Synchrotron radiation research at x-ray wavelengths now impacts an astonishing diversity of disciplines. At SSRL, vigorous programs are being pursued in materials sciences, chemical sciences, biology, medicine, and fundamental physics. These studies are carried out in many variants on the three basic interactions of photons with matter: absorption, elastic scattering, and inelastic scattering. Through absorption spectroscopies, once can decipher the local atomic and electronic structure of materials; through elastic scattering one can probe correlations from a few Å to a few microns; and with inelastic scattering one can probe excitations in matter from a few meV to several hundred electron volts.

Because of this diversity of research, no overview can possibly substitute for the individual research reports presented in the Activity Report. However, we would like to call to the reader's attention the intense work proceeding on the high transition temperature superconductors *(868M, 984M, 1073M, 1079M, 1097Mp, 2023Mp)*. In these experiments, near-edge and extended x-ray absorption fine structures have been measured and applied to understanding the dependence of electronic and atomic structure upon preparation techniques, stoichiometry, transition temperature, and so forth.

High-resolution scattering continued to play an important role in x-ray research at SSRL. Of particular note is the work of Brock et al. *(1011M)* on orientational ordering in tilted hexatic liquid crystal films. This program is exploring the fascinating interplay between position order parameters and bond orientation order parameters, in very thin freely suspended liquid crystal films. The detailed phase diagrams of these systems are now being studied, and have already contributed greatly to the understanding of critical phenomena in 2 and 3 dimensions.

The resonant nuclear scattering program at SSRL *(8003M)* has achieved a major milestone, with the observation of the resonant diffraction signal from Fe-57 enriched crystals of Yttrium-Iron-Garnet. The rich time structure arising from the interference of the hyperfine sublevels has confirmed previous observations by other groups, and the time structure has been effectively modified by the interposition of resonant absorber,

which effectively "blanks out" selected lines.

Finally, the medical imaging group *(1046B)* has made significant progress in its quest for clinically useful images of the coronary vascular system of humans. In a series of trials on three human patients, profiles of the coronary arterial tree were obtained for various orientations of the patient, to test the ability to resolve the arteries from the ventricular background. Although analysis is not yet complete on this data, preliminary results appear to be very promising.

Biotechnology

This has been a particularly significant year for achievements in the biotechnology area at SSRL. Perhaps most important has been the dramatic success realized through the use of multiple-wavelength phasing to solve the classic phase problem for crystallographic studies of proteins. Using data collected with the multi-wire SSRL area detector, several structures have now been fully solved. The structure of a copper-containing "blue" protein from cucumbers, which defied solution over a 10-year period by conventional approaches, has been phased and the structure refinement is well along *(1004B)*. Structures of a iron-containing ferredoxin and a selenium containing biotin-streptavidin complex (for which data on the later was partly collected at SSRL and partly at the Photon Factory) have also been obtained *(1087Bp)*. Promising data is reported on a fourth structure, amicyanin, and solution appears likely to soon be achieved *(8105B)*. This work clearly demonstrates the potential of this new approach based on multiple wavelength phasing to solution of protein structures.

The more classical approach of using several protein crystals containing heavy atom derivatives has also met with success for data collected on the rotation camera at SSRL. Six reports deal with structural work being done on this instrument. One particular highlight is the complete structure determination of an important oncogene protein isolated from human tumors *(1A56)*. Another result with wide-ranging implications for protein crystallography using synchrotron sources is the observation of a dramatic improvement in crystal lifetimes upon cooling to temperatures of around 100 K using a new "flash freezing" technique *(1A32B)*.

X-ray absorption spectroscopy continues to find wide use in the study of the electronic and structural properties of metal ions in biological systems. Several studies have resulted in a dramatic advancement of our understanding of the structure and function of manganese in the oxygen-evolving photosynthetic system *(2010Bp,1001B, 1085Bp)*. Nickel-containing enzymes have also been isolated relatively recently from organisms like methanogenic bacterial and XAS studies have helped in defining the nature of the active site *(969 Bp)*. The spectral range of 2-4 keV, which contains the K absorption edges of elements like S, Cl, and P and the L edges of the second row transition elements, has been opened up through the use of the Beam Line VI wiggler run at low magnetic field in undulator mode. Studies have revealed new information about the nature of sulfur in the iron-molybdenum cofactor from nitrogenase *(8116B)* and appear promising for phosphorous-containing materials *(1001B)*.

VUV and Soft X-ray

During 1987 great progress was made in using EXAFS, SEXAFS, NEXAFS *(Near-Edge X-Ray Absorption Fine Structure)*, PED *(Photoelectron Diffraction)* and ARPEFS *(Angle-Resolved Photoemission Extended Fine Structure)* to determine electronic and structural properties. These techniques are now being applied to problems with ever-increasing sophistication. The structure of P impurities in GaAs has been determined by EXAFS, as has the microsccpic structure of sulfur doped $Al_xGa_{1-x}As$ *(1013Vp)*, thus extending this technique to highly dilute systems. Anisotropy in the surface vibrational amplitudes for Cl chemisorbed on Cu(100) has been examined for the first time with SEXAFS *(947V)*. The surface structure of ordered S overlayers on Fe(001) and Cr(001) were determined by ARPEFS in a continued successful application of this technique *(943Vp)*, and Beam Line VI was used for the first time in PED experiments, based on the Co 1s core line, to determine the surface geometry for (1x1) Co/Cu(001) *(9900V)*. The electronic properties of clean and hydro-

gen terminated Si surfaces, as well as SiGe alloys, have been studied in Si K-edge absorption experiments *(8104V)*. The same approach has been used for valency studies of Yb-compounds in this case based on the Yb $L_{II, III}$ absorption spectra *(941Vp)*. Major advances have been made using NEXAFS, in combination with the highly polarized synchrotron radiation, to determine the orientations and bonding distances for chemisorbed organic molecules on metal surfaces, e.g. methyl acetylide on Ag(110) *(963V)* and benzen-ethiol on Mo(110) *(1080Vp)*, further opening up the field of surface reactions for this kind of studies.

The electronic and structural properties of metal/semiconductor interfaces and heterostructures have continued to be the subject of both intense and successful studies. A detailed study of the bonding of arsenic and hydrogen to the Si(111) surface has been completed *(908Vp)*, as part of a broader reseach program on the GaAs-on-Si system. The effects of temperature and doping on the Fermi level pinning position in the bandgap of III-V semiconductors have been examined in the pursuit of understanding the basic mechanism behind Schottky barrier formation *(935Vp)*. The effect of strain on the band structure of $In_xGa_{1-x}As$, as manifested in the deformation potential of the upper valence bands, has been elucidated in detail *(8104V)* with important implications for understanding pseudo-morphic heterostructures in general. Excellent progress is also reported on photoelectron spectroscopic studies of metal ion sites for systems which are of interest in catalysis *(1022Vp)*.

Electron correlation effects in narrow band materials, predominantly 4f and 5f containing lanthanides and actinides, have been studied with photoemission and resonance photoemission successfully for many years at SSRL. With the advent of the new high Tc materials these studies have intensified *(1028V, 8000V)*.

The basic photoionization processes, in particular phenomena for excitation energies close to ionization thresholds, have received continued interest. These studies include valence and core level satellites for argon and lithium, respectively, photoelectron asymmetry parameter for the sulfur 2p level in SO_2 and autoionization resonances in He and Kr *(943 Vp)*. Resonances in the K-edge absorption spectrum of solid Be have been reported *(9901V)* and work on solid state effects in photoionization cross sections has continued *(8000V)*.

The research efforts in x-ray lithography focussed on radiation damage in masks *(1L09V)* and on resist properties *(8104V)*. Finally, during 1987 the first results were obtained using an imaging photoelectron microscope *(8104V)*.

Herman Winick
Acting Director
(Arthur Bienenstock is on sabbatical)

1987 AWARDS BASED ON SSRL WORK

Oliver E. Buckley Condensed Matter Physics Prize of the American Physical Society to **Robert J. Birgeneau** (MIT) for "his use of neutron and x-ray scattering experiments to determine the phases and phase transitions of low dimensional systems."

Third Patterson Award of the American Crystallographic Association to **David and Lieselotte Templeton** (LBL) for "recognition of significant achievements in the accurate measurement of anomalous scattering terms at wavelengths near absorption edges using synchrotron radiation and pioneering contributions to our understanding of anomalous scattering of x-rays."

Ernest Orlando Lawrence Memorial Award of the Department of Energy to **David Moncton** (EXXON/Argonne National Lab) "for the development of high resolution synchrotron x-ray scattering techniques and their applications to diverse materials systems."

Prize for Achievement in Accelerator Physics and Technology of the U.S. Particle Accelerator School to **Klaus Halbach** (LBL) for "making high field permanent magnets practical tools for accelerator technology."

J.D. Hanawalt Award of the International Centre for Diffraction Data to **William Parrish** (IBM San Jose) for "excellence in the field of powder diffraction."

Department of Energy's 1987 Materials Sciences Research Competition winner, **Herman Winick** (SSRL) in the category of Significant Implication for Energy Related Technology in Solid State Physics for "development of high brilliance, high flux synchrotron radiation beams with wiggler and undulator magnet insertion devices".

The first **Barrett Award** of the Annual Denver Conferences on Application of X-ray Analysis to **William Parrish** (IBM San Jose) for outstanding contributions to powder diffraction.

MRS 1987 Graduate Student Award to **Lane C. Wilson** (Stanford University) for outstanding thesis research.

I. LABORATORY OPERATIONS

SSRL operations were at an all time high in 1987. Five new branch lines were opened to users. The highest number ever of 8-hour user shifts, 4190, were delivered. A record number of SPEAR shifts, 396, were scheduled in three separate dedicated runs. The first run (January 2 to February 7) was a continuation of the winter 1986 run. A second dedicated run, March 18 through May 2, followed shortly. An unexpected opportunity for dedicated time arose in fall 1987, and, on short notice, the third run occurred from October 26 to December 24.

SPEAR is usually injected for SSRL running from the Nuclear Physics Injector (NPI) Gun at Sector 25 of the LINAC. If the SLAC Linear Collider (SLC) is running simultaneously with SPEAR, injection has been limited to once every 12 hours. The November 1986 to February 1987 run was the first operation in the 12 hour injection mode (see 1986 Activity Report). In spite of this, the run was fairly successful, resulting in average currents and lifetimes at injection of 65 mA and 15 hours respectively. The March/April 1987 run, also in this mode, resulted in average beam currents of 72 mA and average lifetimes of 25 hrs. At lower currents, lifetimes approached 45 hours. This improved performance was due primarily to the fact that SPEAR remained under vacuum for the two months prior to the spring 1987 run. In fact, the spring run provided some of the stablest running SSRL has experienced in the past several years.

The fall 1987 run was anticipated to be very good because of the experience in the spring and because more frequent injection would be available. A number of problems, however, caused the performance of SPEAR to be poor. The two major problems were primarily vacuum related. A SPEAR valve bellows, and subsequently a bellows in SPEAR itself, developed leaks. The second leak required venting part of the ring and repairing the drift tube. Because of these failures the pressure in SPEAR during the fall run was not as low as usual, resulting in shorter lifetimes and lower initial current. During this run the average lifetimes and currents at injection were 10 hours and 55 mA.

Since 1985 SLAC has been heavily involved in the construction and commissioning of the Linear Collider. This program has made planning for, and execution of, synchrotron radiation running more difficult. In particular, every attempt has been made to place the synchrotron radiation runs where they have the least impact on the SLC program. Since SLC is still in the construction/commissioning stage there have been difficulties in developing long-term schedules. SPEAR performance has also suffered since SLAC manpower is heavily committed to the SLC program. This year, for instance, only 65% of the scheduled beam was delivered and the fall run hit a low of 59%.

Neither SPEAR nor PEP has run for high energy physics since early 1986 which has meant no parasitic operation for synchrotron radiation research. [A dedicated machine physics run was held on PEP in December which is described in the Accelerator Physics chapter.] Parasitic operation on SPEAR is used by synchrotron radiation researchers for training new users and students, testing equipment and performing research, particularly in the VUV, which can utilize the lower energy, lower currents and shorter lifetimes. SLAC's present plans are to recommence high energy physics programs on both SPEAR and PEP in August of 1988.

One of the characteristics of the SPEAR ring is its excellent timing properties. Timing mode has four individual bunches of electrons equally spaced in the SPEAR ring and therefore separated by 190 ns. The higher current per bunch in timing mode results in a shorter lifetime and the need for more frequent injection. For this reason timing mode is not scheduled when SSRL does not have on-demand access to the LINAC. Since the fall period was under conditions of on-demand injection, timing mode was run for the last three weeks, December 5 to 24th. Although the currents and lifetimes were still lower than in multi-bunch operation, timing mode this fall was less troubled than previously experienced.

OPERATIONS DIVISION ACTIVITIES

The Operations Division had a challenging year in 1987 with the spring and fall runs each presenting their own and different sets of demands. The spring run had limited injection and required very close coordination with SLAC operations to insure that SLC requirements did not compromise the SSRL program. Although unlimited injection was available during the fall run, a number of SPEAR related problems required close SSRL operations coordination to insure that the problems affecting SPEAR performance were identified and repaired. In spite of these problems, both runs ended well.

The addition of 5 new stations plus running on PEP necessitated double staffing of duty operators. Since the Operations group has insufficient staff to provide two duty operators simultaneously, members of other SSRL groups were trained as "temporary" duty operators over the past year. This has added depth to the Operations staff and allowed it to deal with user demand during dedicated runs.

During the long May through October shutdown, the groups' activities shifted to construction and maintenance. During the past year, the Operations Division has participated in the construction of a number of beam and branch lines, including PEP 1B, Beam Line V, and Beam Line X. In addition, the Operations group provides much of labor for beam line upgrades and routine maintenance.

During the coming year, the vacuum group and mirror coating facility will move to the new Laboratory-Office-Shop Building (LOS). A precision machine shop in the LOS will be established. The machine shop in Building 120 will remain as a staff and user shop and will be upgraded. The Operations group will be working with users to insure that these changes do not affect the user support normally provided by the vacuum and operations groups.

Beam and SPEAR Usage Tables

The following tables and graphs contain statistics on SPEAR running, experimental use and characteristics of SSRL stations. For earlier information, consult previous Activity Reports.

Table 1 (and the accompanying graph) show the number of SPEAR shifts scheduled and delivered since dedicated running commenced in 1979.

Tables 2 and 3 and the accompanying graph illustrate the use of beam at SSRL for experimental purposes.

Table 4 shows the number of shifts requested versus the number of shifts actually assigned for dedicated time and Table 5 lists the characteristics of the 24 SSRL SPEAR and PEP experimental stations.

TABLE 1

BEAM TIME STATISTICS/DEDICATED TIME

DEDICATED RUN	Scheduled Hours	Delivered Hours	%Del
10/20 to 11/05/79	152	95.3	62%
12/03 to 12/21/79	352	299.4	85%
02/08 to 03/05/80	472	366.3	77%
04/16 to 05/19/80	764	588.2	76%
06/30 to 07/30/80	726	320.4	44%
09/29 to 10/14/80	336	194.9	58%
12/02 to 12/22/80	440	309	70%
01/26 to 03/03/81	792	600.9	76%
05/16 to 06/30/81	988	727	73%
11/18 to 12/21/81	546	363.6	66%
01/08 to 02/22/82	748	612.5	81%
03/09 to 04/26/82	995	830.9	83%
10/15 to 11/05/82	473	316	66%
12/27 to 02/22/83	1050	825.6	78%
05/09 to 06/30/83	1195	960.3	80%
11/07 to 12/23/83	857	662.8	77%
03/21 to 04/30/84	835	674.3	80%
01/10 to 02/21/85	905	606.6	67%
03/15 to 07/22/85	1502	1056.5	70%
10/14 to 11/11/85	416	203.7	48%
04/11 to 06/30/86	1550	1106.5	71%
11/17 to 12/24/86	832	544.7	65%
01/02 to 02/07/87	696	522	75%
03/18 to 05/02/87	1112	769	69%
10/26 to 12/24/87	1360	801	59%

The history of dedicated time at SSRL/SPEAR since its inception in1979 is shown. Until 1986 SSRL received one-half of the SPEAR operating time in a mode dedicated to synchrotron radiation while the other half was used for colliding beam physics. For the last two years there has been no colliding beam program on SPEAR. Dedicated shifts have been limited by SSRL budgetary considerations, construction and the SLC schedule. It is anticipated that high energy physics will resume in the summer of 1988. Delivered SPEAR beam time has ranged from 44% to 85% over the 25 SSRL dedicated runs with an average delivery of 71%. The delivery rate for 1987, 65%, was below average.

Scheduled and Delivered Shifts

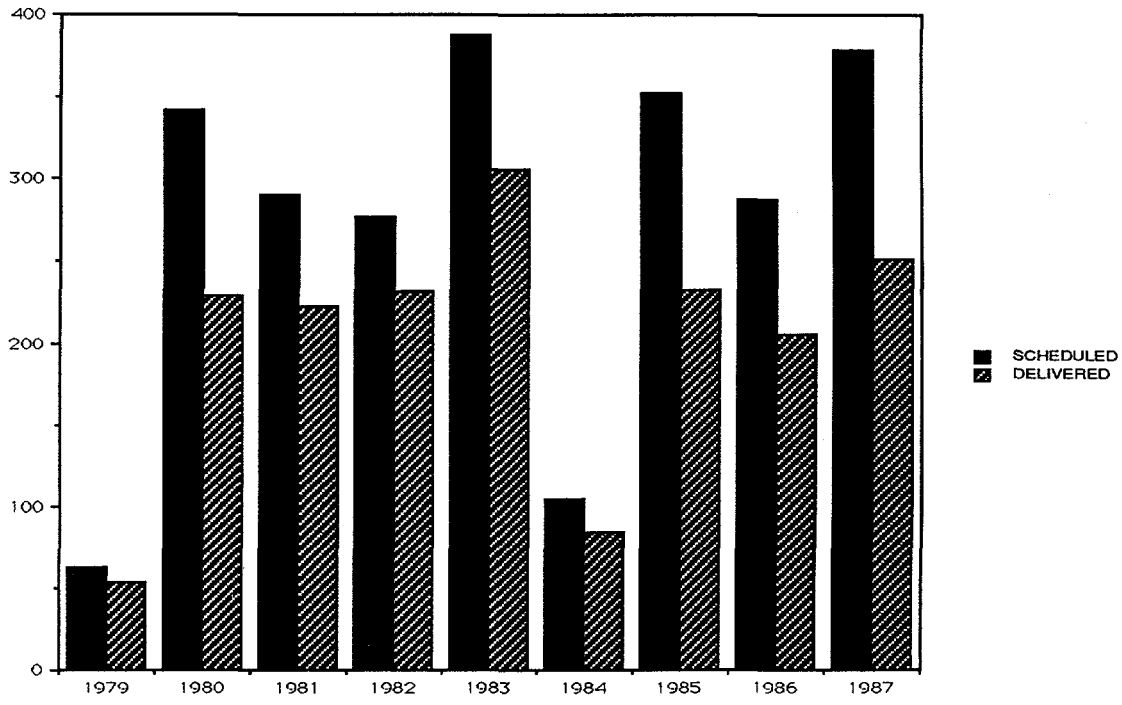

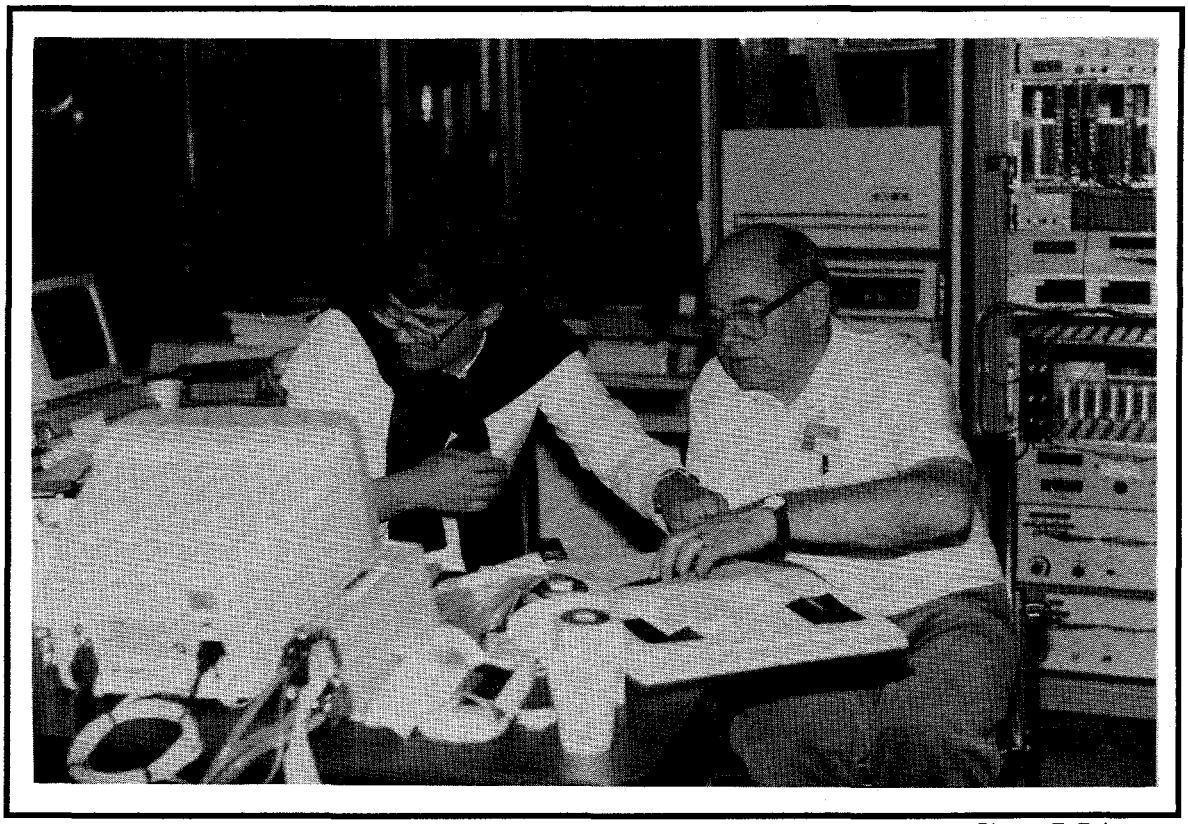

Photo - Z. Rek

John Kinney (LLNL) and Ulrich Bonse (Universiy of Dortmund) doing chemically specific 3-dimensional x-ray microtomography on SSRL Station II-3

TABLE 2

USER SHIFTS BY EXPERIMENTAL STATION
CALENDAR 1987

Experimental Station	01/02/87 02/07/87 Dedicated	03/18/87 05/02/87 Dedicated	10/26/87 12/24/87 Dedicated	Total Shifts per Station
Beam Line I				
I-1	71	83	86	240
I-2	Under Construction	0 (80)	18 (40)	18 (120)
I-4	0 (60)*	40 (14)	58 (14)	98 (88)
I-5	54 (13)	68 (15)	75	197 (28)
Beam Line II				
II-2	69	76	85	230
II-3	20 (54)	0 (81)	0 (87)	20 (222)
II-4	36 (19)	85	86	207 (19)
Beam Line III				
III-1	69	83	97	249
III-2	Under Construction	80	66 (19)	146 (19)
III-3	73	82 (2)	87	242 (2)
III-4	0 (65)	81	63	144 (65)
Beam Line IV				
IV-1	68	80	85	233
IV-2	68	85	86	239
IV-3	63	73	86	222
Beam Line VI				
VI-2	72	71 (6)	74 (8)	217 (14)
Beam Line VII				
VII-1	54	85	74	213
VII-2	67	82	81	230
VII-3	67	86	83	236
Beam Line VIII				
VIII-1	Under Construction	48 (33)	0 (50)	48 (83)
VIII-2	Under Construction	0 (50)	0 (50)	
Beam Line X				
X-2	Under Construction		43 (8)	43 (8)
	TOTALS - Dedicated Running			
	851 (211)	1288 (231)	1333 (276)	3472 (718)

* ( ) = facility characterization time

In 1987, 3472 8-hour shifts were actually used by experimenters for data taking on SSRL's 21 operating SPEAR stations. Additional shifts were used for Machine Physics studies (fall run only) and beam line check out between experimenters. A total of 718 (17% of the total user shifts) were used by SSRL staff and collaborators for characterization, up-grading and commissioning time. In 1987 time was used to commission stations I-2, I-4, VIII-1 and VIII-2. In addition, characterization time is used for continuing developmental studies such as section topography on I-4, multilayer monochromators on III-4, beam characterization, orbit and glitch studies on II-3. In general, II-3 is reserved exclusively for photon beam studies and instrumentation development.

TABLE 3

SUMMARY OF SHIFTS USED FOR SSRL EXPERIMENTS
CALENDAR 1987

RUN PERIODS	01/02/87 to 02/07/87	03/18/87 to 05/02/87	10/26/87 to 12/24/87	TOTALS for PERIODS
User Shifts (Dedicated)	1062	1519	1609	4190
Proposals Run (Dedicated)	54	88	86	228
Users/Shifts (Dedicated)	16.3	15.8	16.1	16.0

In 1987 SSRL averaged 16 data-taking users per shift on its 21 SPEAR stations. The largest number ever, 4190, 8-hour user shifts were delivered to 228 experiments.

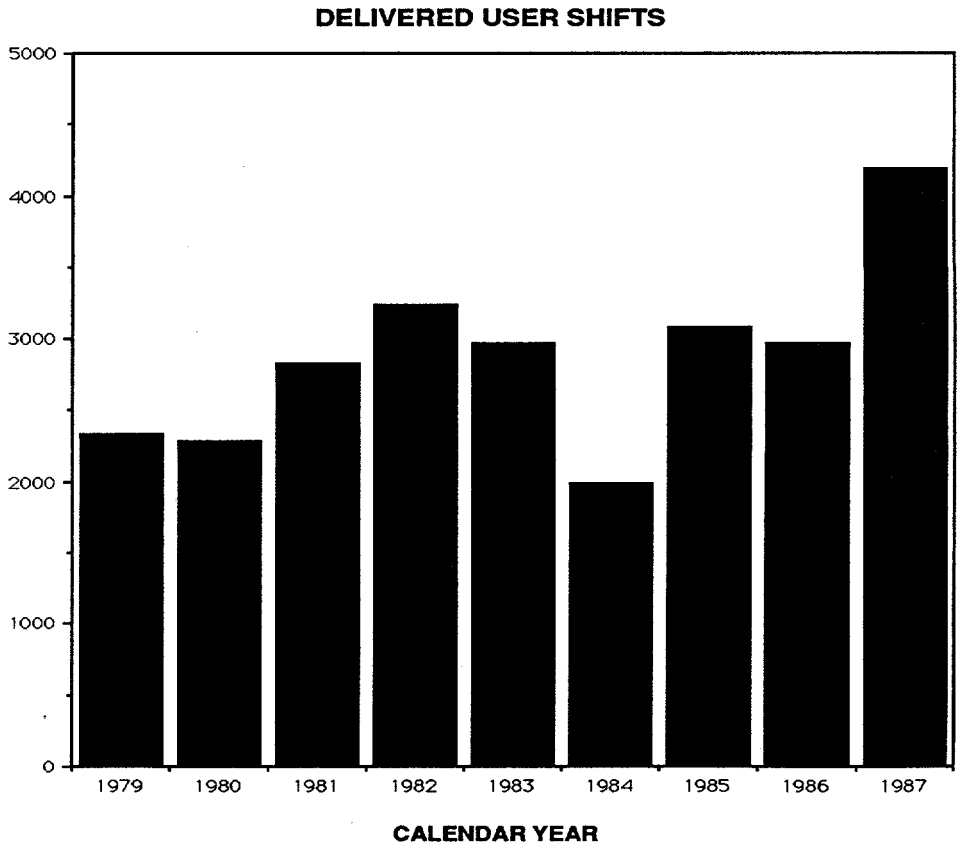

TABLE 4

DEDICATED DEMAND vs ACCOMMODATION ON SSRL EXPERIMENTAL STATIONS

March 1987-December 1987*

Numbers in Italics are Spring Run

Station	Shifts Requested	Shifts Assigned	%Assign	Proposals Requested	Proposals Assigned	%Assign
Bending Magnets						
I-5	133	91	68%	12	8	67%
	244	*121*	*50%*	*15*	*9*	*60%*
II-2	81	82	101%	6	6	100%
	133	*120*	*90%*	*10*	*7*	*70%*
II-3	used for facility characterization projects					
	used for facility characterization projects					
II-4	169	100	59%	8	6	75%
	287	*128*	*45%*	*11*	*11*	*100%*
Wigglers						
End Stations						
IV-2	153	90	59%	7	4	57%
	272	*124*	*46%*	*15*	*10*	*67%*
VI-2**	117	33	28%	5	3	60%
	257	*23*	*9%*	*13*	*2*	*15%*
VII-2	147	93	63%	6	5	83%
	223	*152*	*68%*	*10*	*5*	*50%*
Side Stations						
IV-3	156	91	58%	10	7	70%
	195	*124*	*64%*	*12*	*9*	*75%*
VII-3, IV-1	431	179	42%	31	15	48%
	528	*212*	*40%*	*39*	*20*	*51%*
VUV/Soft X-ray Lines						
Grasshoppers (2)						
	384	186	48%	11	7	64%
	306	*268*	*88%*	*9*	*8*	*89%*
Jumbo	201	93	46%	7	4	57%
	162	*131*	*81%*	*3*	*3*	*100%*

* statitics for winter run included in 1986 report
**general user time only

Demand for experimental time on the SSRL branch lines varies considerably. In 1987 approximately 50% of requested shifts were assigned. This is considerably less than in recent years. In particular, 65% was assigned in 1986. The demand is generally highest on the wiggler end and side stations as well as the grasshopper lines. Station II-4, the white radiation line, experienced a large increase in demand over 1986.

The percentage of proposals receiving beam time is often higher than the percentage of shifts accommodated since most experimenters do not receive the full allotment of shifts requested. Demand is also limited by perceived availability of beam time. Experimenters have indicated that they could use much more time if it were available. In addition, many new groups are discouraged from starting programs based on synchrotron radiation at SSRL since the time available is so limited and the time from application (6 months to two years) often long.

TABLE 5

CHARACTERISTICS OF SSRL EXPERIMENTAL STATIONS

SSRL presently has 24 experimental stations 22 of which are located on SPEAR and two on PEP. 11 of these stations are based on insertion devices while the remainder use bending magnet radiation.

	Horizontal Angular Acceptance (Mrad)	Mirror Cut Off (keV)	Monochromator	Energy Range (eV)	Resolution Δ/E	Approximate Spot Size HgtxWdth (mm)	Dedicated Instrumentation
INSERTION DEVICES STATIONS							
WIGGLER LINES - X-RAY							
End Stations							
IV-2 (8-Pole)							
Focused	4.6	10.2	Double Crystal	2800-10200	$\sim 5 \times 10^{-4}$	2.0 x 6.0	
Unfocused	1.0		Double Crystal	2800-45000	$\sim 10^{-4}$	2.0 x 20.0	
VI-2 (54-Pole)							
Focused	2.3	22	Double Crystal	2800-21000	$\sim 5 \times 10^{-4}$	2.0 x 6.0	
Unfocused	1.0		Double Crystal	2800-45000	$\sim 10^{-4}$	2.0 x 20.0	
VII-2 (8-Pole)							Six-circle Diffractometer
Focused	4.6	10.2	Double Crystal	2800-10200	$\sim 5 \times 10^{-4}$	2.0 x 6.0	
Unfocused	1.0		Double Crystal	2800-45000	$\sim 10^{-4}$	2.0 x 20.0	
X-2 (31-Pole)							
Focused	2.3	22	Double Crystal	2800-21000	$\sim 5 \times 10^{-4}$	2.0 x 6.0	
Unfocused	1.0		Double Crystal	2800-45000	$\sim 10^{-4}$	2.0 x 20.0	
Side Stations							
IV-1	1.0		Double Crystal	2800-45000	$\sim 5 \times 10^{-4}$	2.0 x 20.0	
IV-3	1.0		Double Crystal	2800-45000	$\sim 10^{-4}$	2.0 x 20.0	Two-circleDiffractometer
VII-1	1.0		Curved Crystal	6000-13000	$\sim 8 \times 10^{-4}$	0.6 x 3.0	Rotation Camera
VIII-3	1.0		Double Crystal	2800-45000	$\sim 10^{-4}$	2.0 x 20.0	
Undulator Lines - VUV/Soft X-Ray							
V-2	1.5		Rowland Circle-Multiple Grating	10-1200	≥ 7%	6.0 x 8.0	Angle Integrated e-Spectrometer
Undulator Lines - X-Ray							
PEP 1B	FULL		Double Crystal	12000-42000	$\sim 10^{-5}$	0.6 x 6.0	
PEP 5B	FULL	15.0	Double Crystal	12000-20000	$\sim 10^{-5}$	0.6 x 3.0	Six-circle Diffractometer
BENDING MAGNET STATIONS							
X-Ray							
I-4	2.0		Curved Crystal	6700-10800	0.3×10^{-3}	0.25 x 0.5	Small Angle Scattering Detector
I-5	1.0		Double Crystal	2800-30000	$\sim 10^{-4}$	3 x 20	Area Detector/CAD-4
II-2 (Focused)	4.8	8.9	Double Crystal	2800-8900	$\sim 5 \times 10^{-4}$	1 x 4	
II-3	1.0		Double Crystal	2800-30000	$\sim 5 \times 10^{-4}$	3 x 20	
II-4	1.0		None	3200-30000		3.5 x 18	
VUV/Soft X-Ray							
I-1	2.0		Grasshopper	32-1000	Δλ = .1–.2 Å	1.0 x 1.0	
I-2	4.0		6m TGM	8-180	Δλ = .06–3 Å	TBD	
III-1	2.0		Grasshopper	25-1200	Δλ = .05-2 Å	1.0 x 1.0	
III-2	4.0		Seya-Namioka	5-50	Δλ = .2-6 Å	2 x7	
III-3	8-10	4.5	UHV Double Crystal (Jumbo)	800-4500	0.35 - 7 eV Å	2.0 x 4.0	
III-4	0.6		Multilayer	0-3000	White or Δλ/λ = .3%	2 x 8	Vaccum Diffractometer/ Lithography Exposure Station
VIII-1	12		6m TGM	8-180	Δλ = .06-3 Å	$1mm^2$	Angle Resolved e-Spectrometer
VIII-2	5		6m SGM	50-1000	$E/\Delta E \leq 22000$	$1mm^2$	Angle Resolved e-Spectrometer

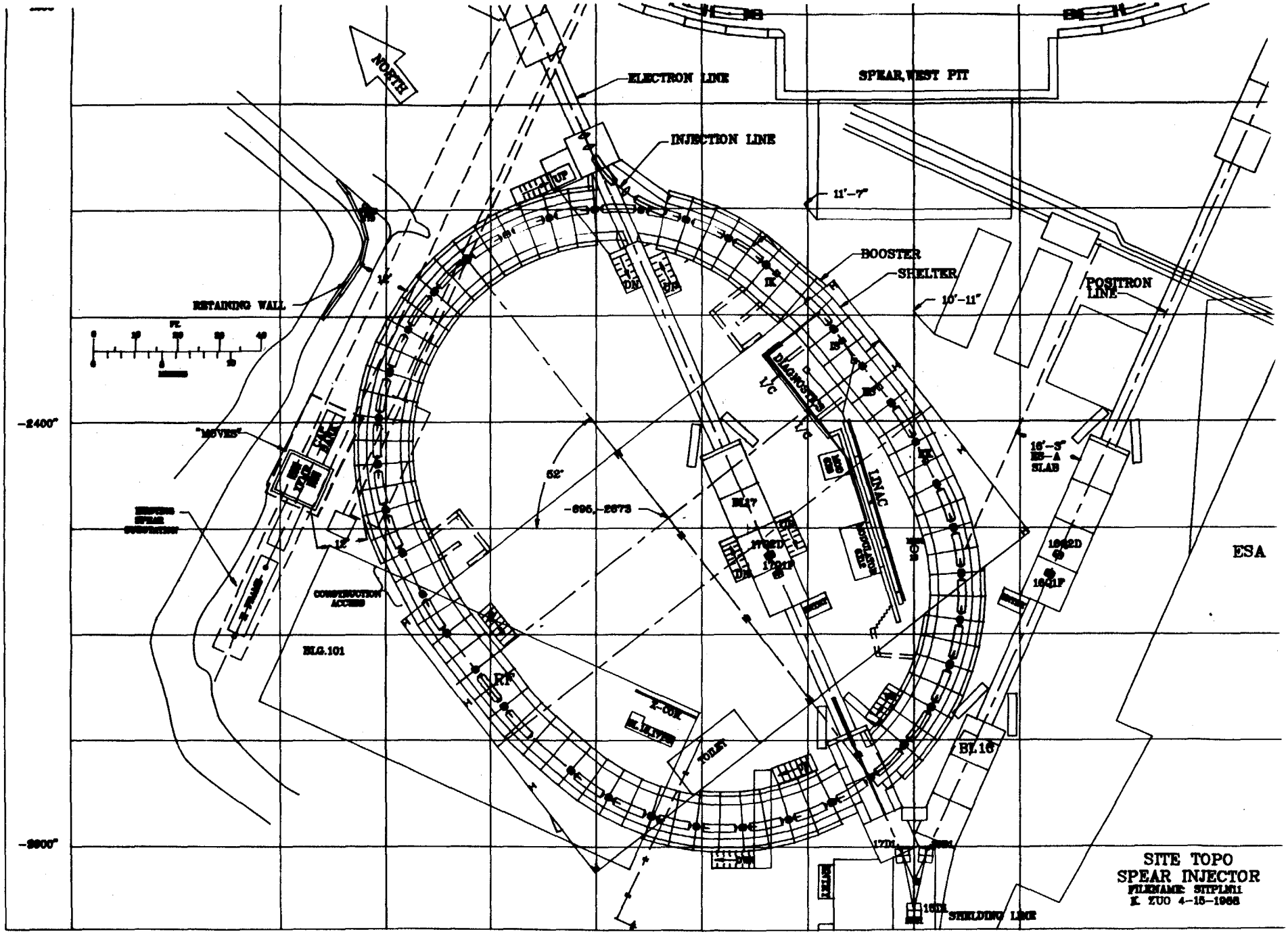
NORTH
ELECTRON LINE
SPEAR WEST PIT
INJECTION LINE
11'-7"
BOOSTER
SHELTER
POSITRON
LINE
10'-11"
RETAINING WALL
14'
-2400"
"MOVIES"
52°
-696,-2673
LINAC
16'-3"
ES-A
SLAB
ESA
12'
CONSTRUCTION
ACCESS
BLG.101
RF
EL 16
-2900"
SHIELDING LINE
SITE TOPO
SPEAR INJECTOR
FILENAME: SITPLN11
K. YUO 4-15-1988

II ACCELERATOR PHYSICS PROGRAM

The Accelerator Physics group's activities concentrated on three major goals: to improve SPEAR operation, to implement low emittance operation of PEP and to design and construct a separate, full energy SPEAR injector.

SPEAR ACCELERATOR PHYSICS ACTIVITIES

During the spring 1987 run, most of the machine physics shifts were aimed at improving the normal operating condition of SPEAR. Specifically, the closed orbit correction scheme was cleared of various software problems and wrong corrector assignments. In addition, energy ramping was studied. The orbit control during ramping was found to be faulty and improvements were made.

Virtually no machine physics shifts were available during the fall run due to hardware failure and pressure for user shifts. A few shifts were devoted to ramping studies to reach energies above 3.0 GeV, to studies of optimum filling patterns, ion problems and dynamic aperture. Other studies on beam stability were done parasitically.

The particular activities are listed below.

Ramping Studies: Studies were performed of different methods of controlling the ramping rates of the various SPEAR components from injection to final energy.

Ion Clearing: Studies of the effectiveness of biasing the position monitoring buttons in SPEAR straight section 7S8 for clearing ions from the Beam Line VI Wiggler vacuum chamber were made. No ion clearing effect was detected.

Long Term Stability: Measurements were made of the long term beam position stability of the SPEAR electron beam using a pinhole camera in Beam Line II and split ion chamber position monitors. Diurnal effects were observed, perhaps related to thermal conditions.

Beam Line X Wiggler Characterization: The corrector values for compensating the effect of the residual field integral of the Beam Line X Wiggler on the stored electron beam were measured and saved for automatic compensation by the SPEAR computer.

Alternate Filling Patterns: Studies were performed of nonstandard filling patterns suitable for doing time resolved photo-electron spectroscopy of surfaces on a sub micro-second time scale. The desired fill patterns were achievable but, due to bunch to bunch intensity variations, a fast beam monitor may be required.

Dynamic Aperture Studies: An investigation of the effects of sextupolar fields on the dynamic aperture of SPEAR was carried out. This work was done as part of one of the first Stanford University student theses in Accelerator Physics at SSRL.

Sextupoles are used to make the chromaticity positive, but the non-linearity of the field also causes the oscillatory motions to become unstable at some amplitude. This limiting amplitude, the dynamic aperture, depends on the position of the sextupoles around the ring as well as their strengths. A large dynamic aperture is necessary in the design of future low-emittance rings which have very strong sextupoles.

In the normal operation of SPEAR the three families of sextupoles are set at low enough values such that the maximum amplitude of betatron motion is determined by the vacuum chamber size and the orbit distortion around the ring (geometric acceptance), and not by the above instability. In this respect, SPEAR's normal lattice is too "good" to demonstrate non-linear effects.

The goal of the measurements was to incease the sextupole strengths, to observe any subsequent reduction of dynamic aperture, and to compare results with computer tracking simulations. Preliminary data reduction shows that the decrease in observed beam lifetime (an indirect measure of acceptance, under certain conditions) is due to the shrinkage of the chromatic acceptance rather than the geometric acceptance. When the sextupoles are turned up to about twice their usual strengths, an appreciable number of particles populating the tails of the energy distribution become unstable and are lost.

There is no conclusive evidence of instability due to geometric aberration, as the limiting amplitude is probably still greater than the geometric acceptance. Computer tracking simulations are not completed as of this writing.

Timing Mode Operation: Studies were performed to determine an optimum filling pattern in timing mode in order to avoid poor lifetimes due to ion collection. Although results were varied, it seems clear that the problem is minimized if a large portion of the ring circumference (~50%) is left empty.

High Energy Operation: Attempts were made to ramp stored beam to higher than normal energy to test feasibility of future human angiography studies on SPEAR. It is possible to ramp beams to >3 GeV, although a tune-up of the RF system is important before doing so.

Steering Tests: The new steering installation for Beam Line X was tested and made operational. A prototype steering feedback servo system was tested prior to finalizing the design. *(See Beam Line Steering in Chapter IV for details.)* A beam position noise monitoring technique was tried.

3 GEV INJECTOR PLANS

SSRL's preparations for the construction of a dedicated 3 GeV SPEAR injector synchrotron made significant progress in 1987. This project, proposed last year and included in the President's FY '88 budget proposal, was finally approved by Congress in mid-January, 1988 after passing DOE validation, construction and cost reviews and a technical review by outside committee members. The injector will be located next to the SPEAR storage ring and will be configured such that SPEAR can be operated for synchrotron radiation production without interference with other programs on the SLAC site. Since the approval, activities are being concentrated on building up the group, preparing designs for long lead time items and prototype activities.

In view of the successful operation of PEP in the low emittance mode, it was suggested that the 3 GeV SPEAR injector could be upgraded later to 5 GeV if the circumference of the booster was increased to 133 meters. Although this would not make an ideal injector for PEP, it would provide injection when none is available during SLC running. In order to make this potential viable, a 400 foot tunnel has to be constructed from the SPEAR booster to the PEP region #10. There the beam transport line would tie into the existing electron injection line into PEP. After beam accumulation in PEP, the energy would be ramped to the final operating energy. This option is not intended to replace a full energy injector for PEP at a later date.

A separate request for funds will have to be made to cover the additional costs for later upgrade to obtain the 5 GeV capability of the SPEAR injector.

ACCELERATOR PHYSICS STUDIES ON PEP

From December 9-21, 1987 PEP was operated at 7.1 GeV in a low emittance configuration optimized for the production of high brilliance synchrotron radiation from undulators. The run was extremely successful in verifying the basic capabilities of PEP as a low emittance source of synchrotron radiation. A large amount of data was taken and is now being analyzed. Technical reports are in preparation. Four abstracts have been submitted to the April 18-21, 1988 meeting of the American Physical Society in Baltimore, where there will be a special session on synchrotron radiation sources. The titles and authors of these abstracts are given below.

The main purpose of the PEP run was to study the operational characteristics of the low emittance configuration (which was tested briefly in a one day run in March, 1986), to measure the emittance achieved, to identify possible limits on stored current and stability and to measure the characteristics of the radiation using the two undulator beam lines now installed in PEP.

These studies were carried out by physicists from SSRL, SLAC, Argonne National Laboratory, Brookhaven National Laboratory and the Lawrence Berkeley Laboratory, all of which have interest in low emittance electron rings. *(See the listing of names at the end of this report.)* The following is a brief synopsis of the work carried out and some tentative results, pending further analysis.

STUDIES PERFORMED

1. The low emittance lattice (called PEP 29) was implemented and characterized at 7.1 GeV. The results are in agreement with the model.

2. Preliminary evaluation of the data taken indicate that the measured horizontal emittance is in agreement with the value of 6.4 nanometer-radians calculated for the uncoupled horizontal emittance for this lattice at 7.1 GeV. An even lower value, consistent with a calculated horizontal emittance of 3.3 nanometer-radians, was measured by changing the damping partition, as described below. Most of the data was taken at low current (about 1 mA or less). There is some indication of emittance growth at higher currents.

3. Stored currents up to 33 mA were achieved in multi-bunch mode with reasonable stability at the higher current and very good stability at lower current. However, it was difficult to reproduce currents above about 15 mA.

4. The maximum beam lifetime ranged from about 2 hours at the highest current to 3 hours at low current, limited by the relatively high average pressure in the ring which had not been operated for about 20 months.

5. The recently completed 2nd SSRL undulator beam line (PEP 1B) was commissioned and used to make spectral and angular distribution measurements of the undulator radiation from 2.5 to 16 keV. Figure 1 is a schematic of the beam line. The sharp peaks observed in the spectral distribution (see figure 2) when a pinhole is used verify that very high brilliance has been achieved. For example, a one standard deviation width of about 60 eV was measured in a third harmonic peak at 8000 eV. This peak is more than 100 times above the baseline. The different spatial patterns of undulator radiation at the different harmonics of the spectrum from a low emittance source were clearly observed on a fluorescent screen and recorded photographically (see figure 3).

The calculated horizontal and vertical beta functions at the undulator source point in the low emittance optics are 26.4 m and 5.3 m respectively. The dispersion function there is 0.54 m and the energy spread is 0.048%.

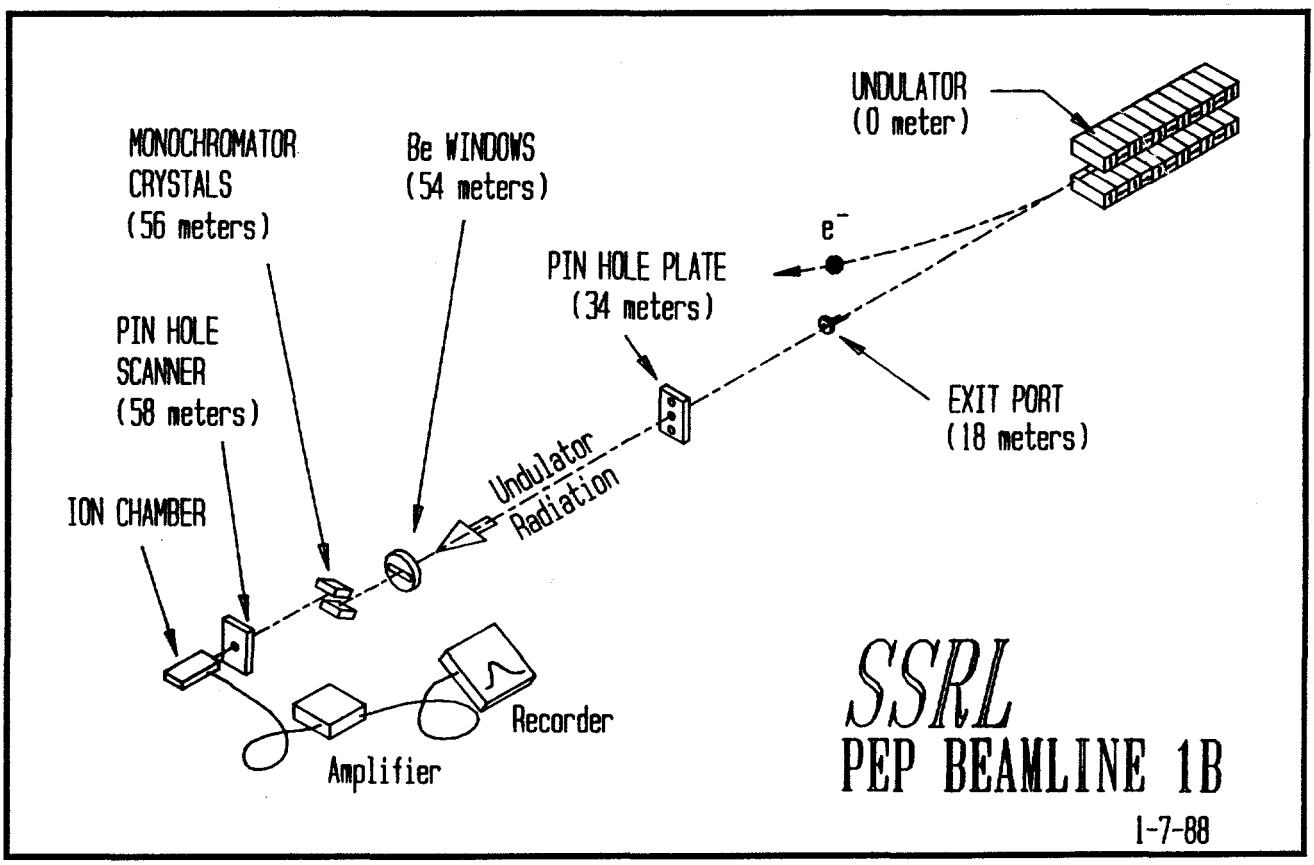

FIGURE 1

SCHEMATIC DRAWING OF THE PEP 1B UNDULATOR BEAM LINE

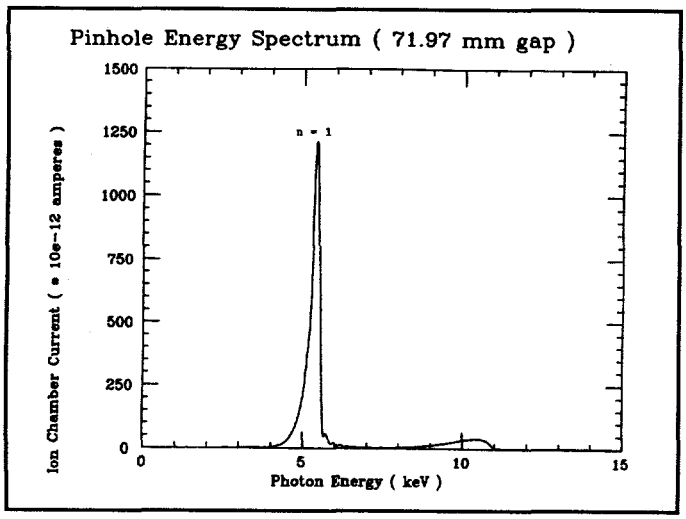

Figure 2a

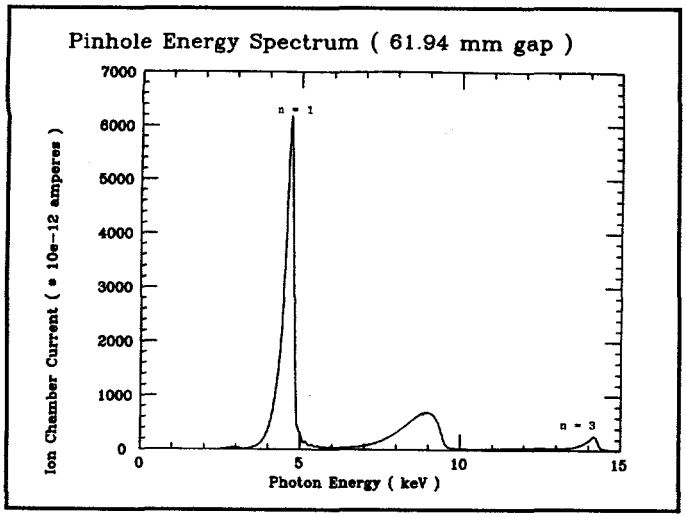

Figure 2b

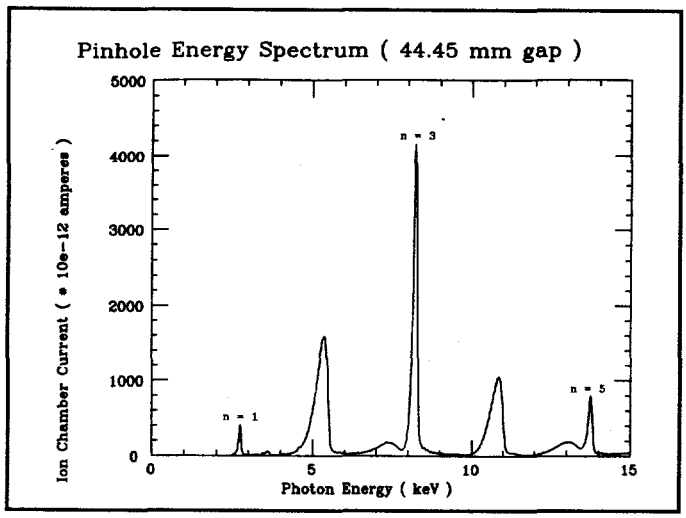

Figure 2c

FIGURE 2

Energy spectra of pinhole-collimated synchrotron radiation at three values of the strength parameter. The data was taken at low current in the low emittance mode at 7.1 GeV.

2a K=0.51, 2b K=0.76, 2c K=1.58

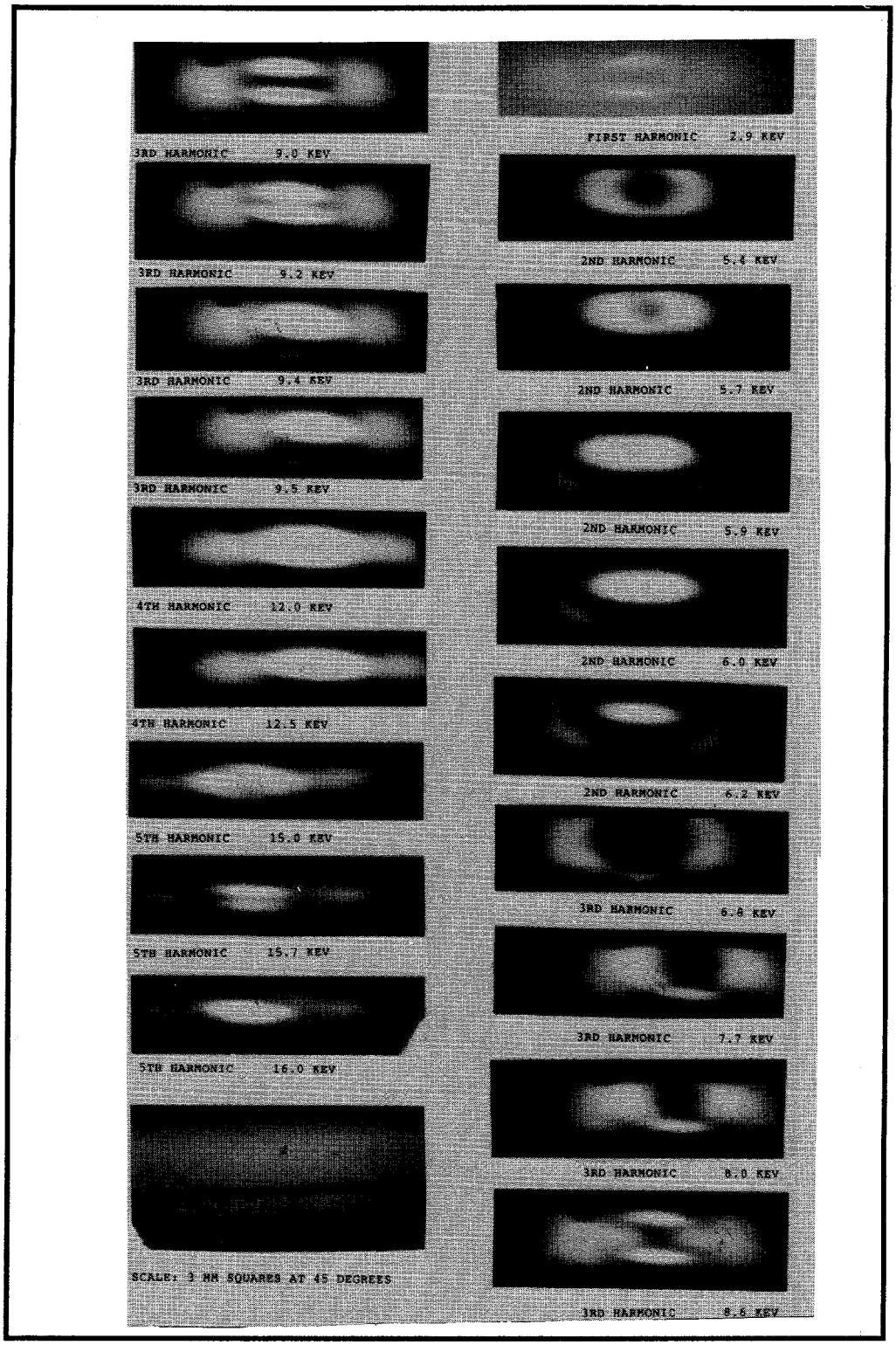

FIGURE 3

Patterns of undulator radiation observed on a fluorscent screen located at 58 meters from the undulator.

6. Measurements of the size of the electron beam in PEP were made by imaging the electron beam through a pinhole (diameter 0.13 mm) and scanning the image with a second pinhole. This pinhole camera system is installed in the new PEP beam line as shown in figure 1. The calculated horizontal beam size is 0.48 mm (one standard deviation) at the undulator source point. If the vertical to horizontal emittance ratio were 2%, the calculated vertical beam size would be so small (one standard deviation value of about 0.025 mm) that diffraction would limit the accuracy of the measurement, even using a very small pinhole and 1 Å x-ray wavelength. Furthermore, the large aspect ratio means that a small beam tilt, such as seems to be present from the patterns shown in figure 3, could cause an apparent reduction in horizontal beam size. The pinhole camera data is still being analyzed.

7. The single bunch fast head-tail instability threshold was found to be about 2 mA with an RF voltage of about 19 MV. This is lower than expected based on ring impedance measurements done in a colliding beam configuration. It was hypothesized that this could be due to a change in the "beta-weighted" ring impedance due to the very different beta functions along the interaction region in the low emittance optics compared with colliding beam optics.

This hypothesis was verified by making a modification to the low emittance optics which reduced the beta functions in these locations and observing an increase in the threshold for the fast head-tail instability. A new, yet untried, low emittance optics developed at SSRL has smaller beta functions in the interaction regions and hence should have a higher single bunch current capability. This new lattice is optimized for damping wigglers which will be used to further lower the emittance by another factor of about 10.

8. Multi bunch currents were limited by longitudinal instabilities. It was found that the threshold for multi bunch instabilities could be raised by operating one of the many unused PEP RF stations as a synchrotron tune splitting cavity, phase-locked to the main accelerating RF system and operating at a frequency 136 kHz (the revolution frequency) higher than the normal frequency (353.21 MHz). With 6 MV on the accelerating system and 1.15 MV on the tune-splitting system the measured synchrotron frequency became a function of bunch number, varying from 2.8 kHz to 2.3 kHz. This 500 Hz tune spread provided Landau damping of certain coupled-bunch instabilities with risetimes longer than about 2 milliseconds. With this system we were able to store up to about 20 mA with good stability. Higher tune splitting voltages could prove even more effective.

The effect of the longitudinal impedance of the unused accelerating cells and the tune splitter itself were identified as critical parameters. Calculations with the ZAP code showed that, in their standard configuration, the impedance of their accelerating resonance would produce an instability tenfold worse than that expected from their higher frequency modes. It was also recognized that the impedance of the tune splitter cells could cause an instability that would overpower the damping effect of the induced tune spread. By repositioning the tuners in these cavities it was possible to cancel their destabilizing effects and raise the coupled bunch longitudinal instability threshold above 33 mA. By further adjusting the tuners it should be possible to cancel the destabilitzing impedance of the tune splitter, while preserving its damping effect.

9. A study was made of PEP operation at an RF frequency 4.5 kHz above the normal frequency of 353.21 MHz, which increases the horizontal damping partition number from 1.0 to 2.0, thereby reducing the calculated horizontal emittance by about a factor of two to about 3.3 nanometer-radians. In addition, in this mode the horizontal dispersion at the symmetry straight section source point is reduced from 0.53 m to 0.25 m, reducing the dispersion contribution to the horizontal source size.

10.Studies of the operational characteristics of the photon beam position monitor, the vertical and horizontal beam steering and the vertical feedback systems were carried out. Although the photon beam from the undulator was observed to be exceptionally stable during the measurements, and, in fact, the feedback system was not necessary to make the measurements, it may be expected that the feedback system will be necessary for certain sensitive experiments. The measured vertical beam position noise spectrum was concentrated in the 5 to 100 Hz range with peaks at 12 and 28 Hz. The open-loop response of the steering servo system was measured and compensated. A factor of 5 attenuation of the 12 Hz peak was achieved in closed-loop mode. The feedback system performance was limited by the response characteristics of the high inductance vertical correctors and could be significantly im-

proved with new corrector magnets. The higher tune of the low emittance lattice results in poor sensitivity of the horizontal steering bumps. This could be improved by powering other, presently unused, corrector magnets. The effect of bending magnet fringe field pollution on the undulator beam position signal was also studied.

11. Injection efficiency as a function of vertical aperture was studied. This data is relevant to the determination of the minimum aperture that can be allowed for a fixed vacuum chamber for a small gap, short period undulator.

ABSTRACTS BASED ON THE PEP RUN SUBMITTED TO THE APRIL 18-21, 1988 MEETING OF THE AMERICAN PHYSICAL SOCIETY

Operation of PEP at Low Emittance as Synchrotron Radiation Source; H. WINICK (SSRL) for the PEP Study Group*

Experimental Study of Collective Effects for the PEP Low Emittance Optics; M. S. ZISMAN (LBL); M. ALLEN (SLAC); M. DONALD (SLAC); J. GALAYDA (BNL); A. JACKSON (LBL); S. KRAMER (ANL); L. RIVKIN (SLAC); for the PEP Study Group*

Lattice Characterization of PEP II Low Emittance Configuration; M. BORLAND (SSRL) and M. DONALD (SLAC); for the PEP Study Group*

Performance of the X-Ray Undulator on PEP; W. LAVENDER (SSRL); G BROWN (SSRL); R. COISSON (SSRL, U. PARMA); T. TROXEL (SSRL); for the PEP Study Group*

* **PEP Study Group**: (ANL) S. Kramer, M. Yoon; (BNL) B. Craft, G. Decker, J. Galayda; (LBL) A. Jackson, M. Zisman; (SLAC) M. Allen, E. Bloom, M. Donald, J. Paterson, J.-L. Pellegrin, B. Richter, L. Rivkin, H. Schwarz; (SSRL) M. Borland, G. Brown, R. Coisson, L. Emery, R. Hettel, W. Lavender, J. Safranek, T. Troxel, H. Wiedemann, H. Winick, W. Xie.

III EXPERIMENTAL FACILITIES

Experimental facilities at SSRL are of two types: general facility stations and participating research teams (PRT's). General facility stations have been funded by various government agencies, principally the DOE, NIH and NSF and are open to the general user community on a competitive basis for 100% of their operating time.

Presently, SSRL has three operating Participating Research Team's with a fourth group having recently been formed. At SSRL all present PRT's are a three-party collaboration with SSRL as one of the parties. The two outside institutions receive 2/3rds of the available beam time while 1/3 is reserved for the SSRL general users. The PRT arrangements are for a 3 year term. Renewal is based on a review which considers scientific merit and contributions to graduate education and to the SSRL user community.

The three existing PRT's are EXXON/Lawrence Berkeley Laboratory/SSRL (Beam Line VI), University of California/National Laboratories*(with LLNL as the lead lab)*/SSRL (Beam Lines VIII and X) and Xerox/Stanford/SSRL (Beam Line V). IBM/The Stanford Center for Materials Research/SSRL are presently developing a side station on Beam Line X in a PRT mode.

X-RAY FACILITIES

Improvements to Existing Facility Lines

Branch Line I-4 - A major improvement program on Branch Line I-4 has occurred with the installation of a new 8.5 degree asymmetrically cut silicon monochromator. With the new monochromator, the flux at the fundamental has increased by about 50%. Tests were performed for the first time at the third harmonic (26 KeV) and a useful spot size (1.5 x 0.5 mm) was achieved.

Branch Line IV-3 - Branch Line IV-3 is midway through a major improvement program, with significant mechanical improvements to the two-circle diffractometer, and with construction of a focussing mirror assembly in progress. The design is complete and assembly is scheduled for the summer of 1988. This focussing mirror will provide a horizontal line focus and will cut off the higher harmonics of the x-ray beam.

Branch Line VII-2 - Branch Line VII-2, which is used for high-resolution scattering studies on single crystal samples, has been modified to easily accommodate the transition from focussed to unfocussed operation. Some minor changes have been made to the absorber system, and work is in progress to convert the beam line control software to microVAXoperation.

General X-ray Facility Improvements

Monochromator Calibrators - Using the facility Beam Line II-3, experiments are underway to map the complete multiple reflection spectra of perfect crystal monochromators to aid in the choice of crystal reflections for applications within a given energy range. At the same time, a theory is being developed to utilize these reflections as calibration markers, with very high accuracy. Utilizing the dynamical theory of diffraction, it should be possible to calibrate the monochromators to an accuracy of 0.1 eV or better.

Monochromator Intensity Levelling Circuit - An intensity levelling circuit has been developed, in conjunction with Frank Bridges of the University of California at Santa Cruz. The purpose of the circuit is to provide a constant intensity to the experiment, independent of the current stored in the electron beam. This is accomplished by detuning the crystal by 50% (using the piezoelective transducer) and then continuously adjusting the transducer, via a closed-loop feedback system, to maintain a constant intensity. A prototype system has been built and tested, and a system is now available for the general user community.

X-ray Facility Experimental Stations Commissioned In 1987

PEP Beam Line 1B - The second PEP synchrotron radiation beam line, illuminated by an undulator located in symmetry straight section 1B, was commissioned during a dedicated PEP run in December, 1987. The beam line has characteristics that are identical to the beam line located at region 5B, and is optimized to produce 12 KeV radiation when PEP is operated at 14.5 GeV.

During the commissioning program, PEP was operated at 7 GeV in the normal colliding beam

configuration, as well as in a high-tune, low emittance configuration. In these modes, the angle-integrated and on-axis energy spectra were measured, as well as the electron beam spatial and angular profiles. The measurements agreed well with the theory, and the results are summarized in the Accelerator Physics Chapter.

VUV FACILITIES

The VUV facilities at SSRL are expanding. Four new experimental stations (two PRT and two facility) were commissioned in 1987 with more to come in 1988. At the same time, many improvements have been made to existing facilities. Several activities are being moved to the new LOS building or off the ground floor to make room for beam lines and setup space. In conjunction with the increase in the number of VUV and soft X-ray beam lines, three new staff members, two technicians and a scientist joined this group in 1987. The Perkin Elmer chamber was overhauled and cleaned. The VG chamber was brought back on line and was used to commission Branch Line III-2 (the 18 degree line) and for user experiments. Most of the beam line computer systems are being maintained in their current configuration awaiting the upgrade to microVAXes.

VUV Facility Experimental Stations Commissioned In 1987

Branch Line III-2 (18 degree line) - Final alignment and commissioning of Branch Line III-2 (18 degree line) took place in January 1987. Users were scheduled and successful experiments were performed during the April, 1987 run. At that time, it was determined that the M1 focussing mirror was not bending enough to produce a good focus at the entrance slit. During the summer shutdown the mirror was replaced with a thinner trial mirror made of float glass. This improved the focus enough to double the flux through the monochromator. In addition, the motions on the M1 mirror manipulator were motorized. The mirror tank hangs from the ceiling downstairs from where the user sits, so remote control is needed to access those motions from the experimental station. A further modification to the line was to shift the refocussing mirror downstream by 20 inches to produce a smaller spot size at the sample position. These improvements resulted in enhanced performance during the fall run in 1987.

Branch Line I-2 (TGM) - The redesigned branch on Beam Line I was commissioned in 1987. First light was brought through the TGM during the spring run and initial alignment of the line took place. For this run a substitute M1 mirror was used, since the ellipsoidal mirror designed to focus on the entrance slit of the monochromator was not delivered until the summer. With the new focussing mirror, monochromatic scans were achieved with all three gratings during the fall run. As part of the commissioning process, users successfully collected data. Further alignment of the optical components of the line will take place during the first run of 1988. The flux on the line is still limited by the original flat M0 mirror which has been in use for 15 years.

Improvements to Existing VUV Experimental Stations

Branch Line I-1 and Branch Line III-1 (Grasshoppers) - A theoretical study was performed to determine the improvement possible by replacing the spherical focussing mirror on the grasshopper monochromator with an elliptical one. From ray tracing it was calculated that 1.6 times the flux, or two to three times improvement in photon energy resolution would be possible (See figures 4 and 5). An elliptical mirror, holder and bender were specified and ordered for each grasshopper monochromator. They are scheduled to arrive early in 1988.

Branch Line III-3 (Jumbo) - No major changes were made on Jumbo during 1987. In the coming year the data acquisition and control system is to be upgraded to a microVAX work station operating with the new software designed by the SSRL computer group. This new system and software will not only eliminate many of the long standing bugs that have aggravated users, but bring on-line data analysis and rapid data transfer capabilities to the branch line. In accordance with the recommendations of the Users Organization, Jumbo will be the first of the VUV lines with a microVAX system, with the other stations to follow soon after.

Branch Line III-4 (Lithography Line) - Many improvements were made to Branch Line III-4 during 1987. The monochromator chamber was modified with a larger flange to allow easier access to optics. Several other small ports were added to mount gauges, viewports and other instrumentation. The computer was upgraded (and simplified) to a Macintosh improving the interface to the motor controllers. The cabling and plumbing were streamlined. Other components were rearranged to allow easy installation of user filters and to improve access in general.

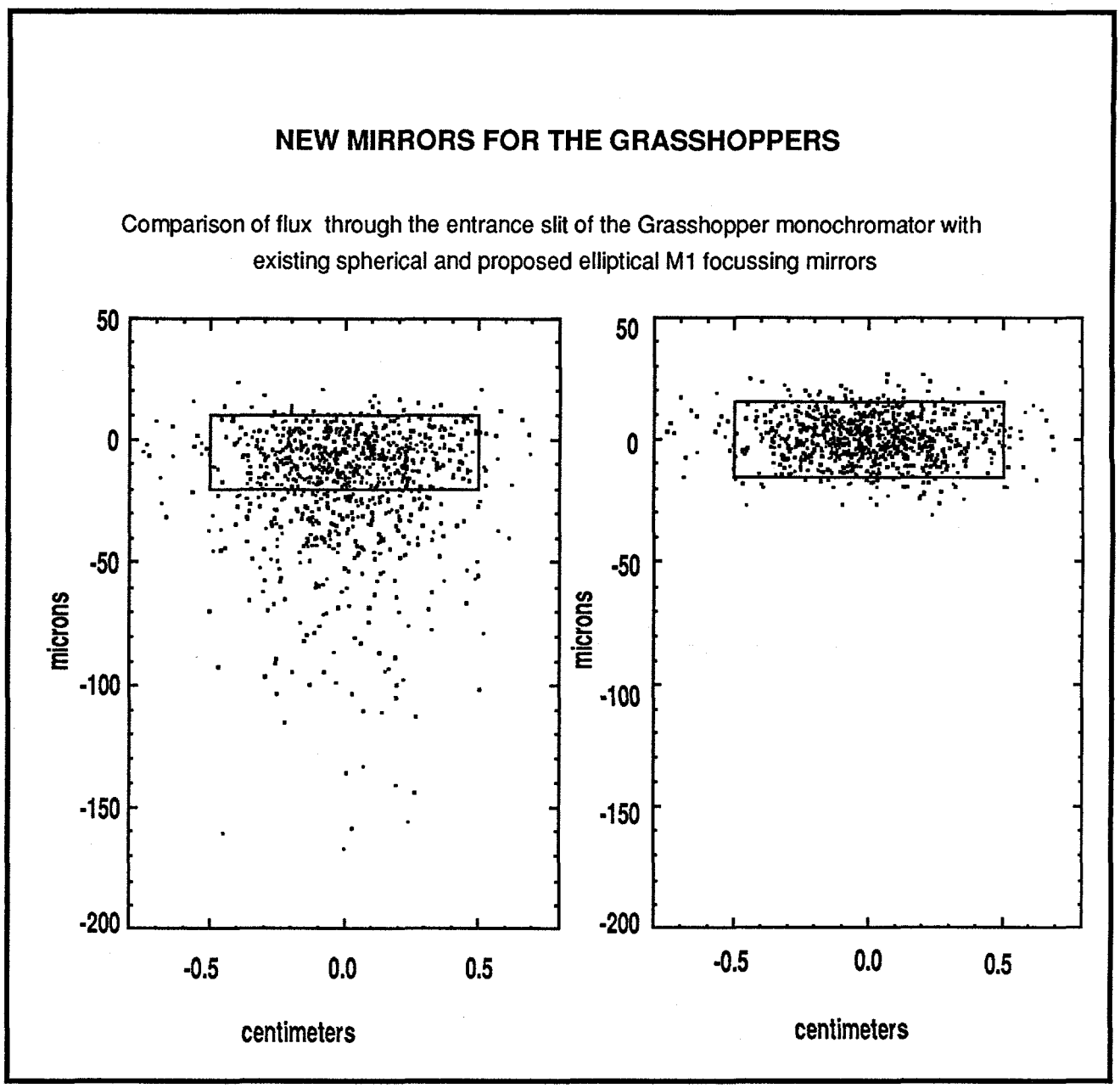

FIGURE 4

Scatter plot of rays at entrance slit with spherical M1 mirror. A slit 1 cm by 30 microns is overlaid. Only 60% of the rays make it through the slit.

FIGURE 5

Scatter plot of rays at entrance slit with elliptical M1 mirror. A slit 1 cm by 30 microns is overlaid. 90% of the rays make it through the slit.

BIOTECHNOLOGY FACILITIES

The research and user support in the Biotechnology Division at SSRL are funded jointly by the NIH Division of Research Resources and the core SSRL operations budget from the DOE. The division's responsibilities also include oversight for the computer activities at SSRL.

Facilities for Protein Crystallography - The SSRL area detector system for protein crystallography on Beam Line I-5 was very actively used during 1987 for collection of anomalous scattering data on proteins. The major facility upgrade from a PDP 11/34 to a microVAX-II GPX workstation control system was fully completed, and the system operates with significantly enhanced performance and functionality. A write-once, read many times 0.4 GByte (per side) optical disk has been added for high volume, reliable data archival.

The rotation camera beam line (Station VII-1) is a station fully dedicated to the collection of protein single crystal diffraction data and it continues to be fully scheduled. The station is essentially the same as it was during 1986. Plans are being made to provide capabilities for cooling crystals to liquid nitrogen temperatures in 1988.

The CAD-4 diffractometer system for accurate measurement of diffracted intensities continues to receive use for important experiments that investigate anomalous scattering terms. The maintenance of the PDP-8 control computer is, however, becoming an increasing headache. Plans have been made to make a conversion to microVAX control in 1988.

Facilities for X-Ray Absorption Spectroscopy - A number of new facilities are being developed for XAS measurements. The low temperature (4 K) Oxford cryostat is routinely being used for fluorescence x-ray absorption measurements of dilute biological systems. This year, the troublesome vacuum pump has been replaced by a high capacity, and very reliable, turbo-pump. This greatly simplifies the process of pumping down the cryostat and maintaining the required vacuum. Additional detectors for use in XAS measurements have been purchased and tested, and are available to users by request.

There continues to be significant progress in the development of the new HgI_2 detector systems for EXAFS and scattering studies. The project, joint with the Physics Institute of the University of Southern California, has just produced a new prototype 5 element array solid state detector system with very good capabilities for EXAFS applications. The array detector performed very well (high count-rates, good energy resolution) in tests in November, 1987 at SSRL. In 1988, development of integrated electronics for the detector array and improved packaging will continue so that multiple arrays can be stacked together.

Facilities for Small Angle Scattering - The Biotechnology SAXS camera has been upgraded to provide capability for three different types of experiments: 1) scattering from solutions, 2) diffraction from oriented membranes, and 3) diffraction from thin and mono layers. The camera can be placed on any end station (but is most frequently used on stations II-2 or IV-2). The camera now consists of two sets of slits for collimation, an ionization chamber to measure intensity of the incident beam, a sample holder, a vacuum path, a gas filled one-dimensional position-sensitive detector to measure the scattered signal, and a fluorescence screen/photo diode assembly to measure the transmission through the sample. All of the units, except the ionization chamber, can be aligned by stepping or DC motors. Different sample holders are provided for the different types of experiments, a capillary holder for the solution scattering, a disk holder for the oriented membranes and a tilt-rotation stage for the monolayers.

Signals from the detector are discriminated and fed into a time-to-digital converter, followed by a histogramming memory. Data in the histogramming memory are read by a computer, currently by PDP 11/34 computer control to be upgraded to a microVAX-II workstation in 1988.

PRT EXPERIMENTAL FACILITIES

PRT Experimental Facilities Commissioned in 1987

University Of California/National Laboratories PRT Beam Lines - During 1987, construction of three branch lines for a UC/National Laboratories PRT was completed and commissioning and several preliminary experiments were performed. These included a 8-185 eV VUV branch and a 60-1100 eV soft x-ray branch on bending-magnet Beam Line VIII and a 3-35 eV hard x-ray branch on wiggler Beam Line X. The beam lines were built under the DOE X-Ray

Calibration and Standards Facility (XCSF) project with additional funds provided by the Lawrence Livermore National Laboratory and the University of California Laboratory for Synchrotron Radiation Research. PRT members include the Livermore, Los Alamos, and Sandia National Laboratories and the University of California. LLNL is the lead laboratory for the project. These branch lines are open to the user community through SSRL's 33% share of the time.

Branch Line VIII-1 - During the spring run, the toroidal grating monochromator (TGM) was tested and calibrated by collecting absorption data from several thin foils. These tests included the use of different filters to suppress higher-order light, which was generally found to be low. Absolute photoabsorption cross sections were measured for Be, C, Si, and U foils (see figure 6 for Be data). In addition, absorption edges of many different ions in fluorescing crystals and glasses were examined using optical detection and some photoemission data for Si-on-Ge and Ge-on-Si samples were collected. The photon flux out of this monochromator has been estimated to be as much as an order of magnitude higher than that from the Grasshopper monochromator at 140 eV. The energy resolution at 100 eV photon energy has been demonstrated to be better than 0.25 eV and can undoubtedly be improved without a serious loss of intensity by careful tuning of the beam line optical elements and movable exit slit.

During the first three weeks of the fall run, a new photoelectron microscope built by Surface Science Laboratories was tested as part of the SSRL instrumentation development effort. The beam out of the TGM matched the input optics of the microscope very well. The spatial resolution of the instrument was demonstrated to be in the 2- to 5-micron range, and chemical shifts of 0.75 eV were observable in spectrometer mode. The test demonstrated the soundness of the instrument design, and was considered by all participants to be very successful.

The new angle-resolved photoelectron spectrometer system from VSW, Ltd. was also installed. It consists of a main analysis chamber with 30 ports, a 50-mm hemispherical analyzer on a goniometer, a sample-introduction system with a load lock, and the electronics required to operate the system. Unfortunately, the equipment was delivered too late to undergo complete testing and debugging before the run began and several problems developed that are currently being fixed; the system will be exercised completely before the next run. A CMA was installed in the chamber and a very nice set of resonant emission data were collected on several Ni-containing compounds, making the final run of the year at least partly successful.

All that remains to complete the beam line and station is to install the necessary CAMAC modules to accumulate the data from the photoelectron spectrometer, and make sure that the existing software can drive the analyzer electronics. These final additions should be complete before the next run begins.

Branch Line VIII-2 - The design and fabrication of the spherical grating monochromator (SGM) for the Beam Line VIII-2 soft x-ray branch was completed

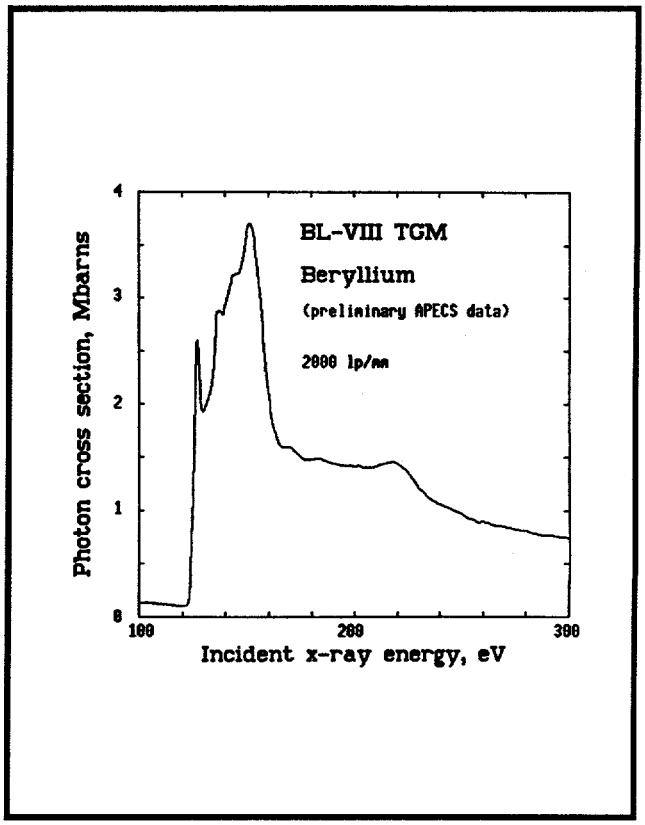

FIGURE 6
Beryillium K-Edge absorption cross-section data obtained on Branch Line VIII-1 with grating #1

early in the year. The SGM features three interchangeable ion-etched gratings from Astron, Ltd., a new scanning mechanism that utilizes flexure pivots to eliminate backlash, and a laser interferometer angle monitor for increased rotational accuracy. During the spring 1987 SPEAR run, the SGM arrived from Acton Research and was installed and aligned in record time, thereby allowing three days for preliminary measurements. Commissioning and preliminary experimental work were conducted during the fall run including testing of the new software-hardware interface, alignment of a newly installed exit mirror, resolution checks and wavelength calibration using a new prefilter set. A temporary Sandia UHV sample chamber and an SSRL Io section were installed and used to obtain near-edge carbon total electron yield data, to measure absolute photoemission cross sections of several materials in transmission, and to detect various absorption edges in the 100-1200 eV range using optical emission from fluorescing ions in numerous crystal and glasses.

Progress was made in the design, fabrication and installation of a tandem reflectometry chamber separated from the UHV chamber by means of a thin-windowed differential pumping section. In addition to the reflectivity measurements for which it was designed, this system will be used for a variety of experiments that are not compatible with UHV. A photoemission chamber was also received from VSW, Ltd., and will be installed and tested during the spring run.

Branch Line X-2 - A 15-period hybrid wiggler with neodymium-iron-boron permanent magnets (see figure 7) built at the Lawrence Berkeley Laboratory was installed and all in-alcove work for the beam line completed during the summer of 1987. Thanks to the fine efforts of the SSRL staff and the LLNL project team the carbon filter, beryllium windows, Hower-Brown monochromator and remaining beam lines components were quickly installed in time to obtain some operational experience during the fall run. First wiggler light into the Beam Line was recorded on November 14.

The wiggler has been operated at fields up to the 1.4 Tesla design maximum with no adverse effects on SPEAR operations. Initial power measurements indicate that the flux at sample is $>10^{12}$ photons/sec at 10 keV (unfocussed) with SPEAR running at 3 GeV, 50 mA and at a wiggler field of 1 Tesla. Beam profiles recorded with a CCD camera in both the focussed and unfocussed modes demonstrated satisfactory performance. Using a temporary hutch, several experiments were conducted. These include XANES/EXAFS of all metal constituents in high-temperature superconductors to study valence and site geometry, optical XANES/EXAFS for site-selective detection, Cr sites and valence in laser crystals, tomographic imaging of FeS_2 phases in coal, evanescent and standing wave measurements of thin films, and a Mossbauer nuclear scattering experiment *(see Progress Reports for Proposals 9901M and 8003M for further details).*

Design of a permanent experimental hutch is underway. It will have two sections: the front section for spectroscopy and imaging experiments; the rear section for diffraction/scattering experiments. The first section should be completed prior to the beginning of the next dedicated run. The addition of a side branch is also possible and is under consideration.

PRT Facilities Under Construction

Branch Line VI-2 - Branch Line VI-2, the first of potentially three branch lines on the EXXON/LBL/SSRL PRT beam line, has been modified to accommodate the soft x-ray branch line, VI-1. The parity of the monochromator has been reserved to permit access when VI-1 is installed in the summer of 1988. In the spring of 1988, the monochromator housing will also be so modified.

Branch Line VI-1 (LBL/EXXON/SSRL) - The Beam Line VI PRT is developing a second branch line on Beam Line VI. This will be a high flux and resolution (56-1000 eV) spherical grating monochromator accepting up to 1.1 mrad of the wiggler radiation fan. This branch line has a total horizontal deflection of 5.6 degrees from the main line and the monochromator and experimental station will be located between the existing end station, Branch Line VI-2, and Beam Line V.

During the last year problems arose because of the developmental nature of the beam line components. The decision to make the M0 mirror removable on a single flange lengthened the design process. In addition, the electroless nickel surface of the mirror was polished through to the copper substrate. This required replating, re-grinding and repolishing. The mirror is now ready, except for a last minute vacuum problem, for installation in its tank 8.8 meters downstream from the wiggler. Essentially all of the

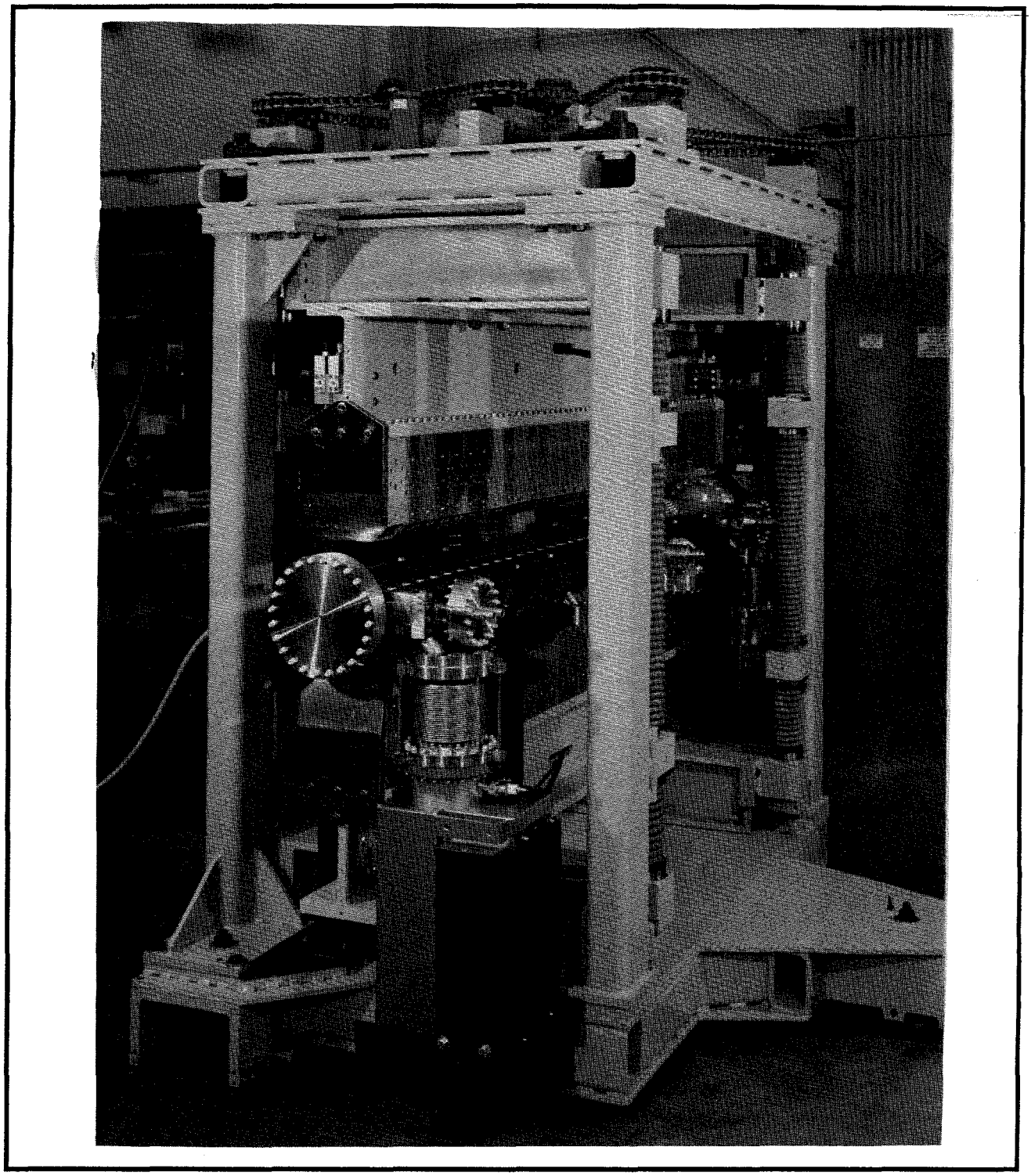

FIGURE 7

The wiggler for Beam Line X, a 15-period, variable-gap, permanent magnet-steel hybrid. At 3 GeV, the wiggler at peak field is expected to radiate approximately 3 kW in a 5-mrad horizontal fan with a 7.8-keV critical energy at 1.3 Tesla.

components up to and including M1 are finished and will be installed in 1988. The monochromator and the wavelength drive system will be assembled at LBL in the first half of the year for installation at Stanford sometime in the summer, depending on manpower availability and conflicts with the dedicated run.

The decision was made in 1987 to engage a company that had experience in precision slides and microstepper motor technology to design and fabricate the slide system for the moving slits and the grating wavelength drive. LBL is working closely with Microautomation Technology of Berkeley and expects to set a new standard in precise control of the gratings and slits. A laser interferometer system will be the position encoder for the wavelength, and Moire fringe glass scale readouts will encode the slit position. Real time closed loop software running in a system separate from the main beam line computer will read these encoders and maintain the accuracy of the system.

The system will be assembled initially with a fused silica grating from Ferranti Astron in the U.K. The advanced water-cooled grating substrates are nearing completion at Perkin Elmer, but the optimum means of applying the grating grooves requires development work which will be pursued by LBL in 1988 in collaboration with grating manufacturers. To facilitate this work, and to guarantee the success of the ruling or holographic process, whichever is chosen, twenty sample substrates having the same specifications for surface quality have been ordered from the same vendor. This will assure that the parameters chosen from the development process will produce good grating grooves on the water cooled substrates.

Photons through the exit slit of the monochromator are expected by in the next dedicated run.

Beam Line X-1 - Design has started on a soft x-ray (100-1000 eV) side station for Beam Line X. This station will have a configuration similar to Branch Line VI-1 with a high resolution spherical grating monochromator. It is being built by IBM and the Center for Materials Research at Stanford University for research in the areas of semiconductor surfaces, high resolution carbon edge studies and microscopy.

Beam Line V - This multi-undulator beam line is also known as beam line WUNDER because of its use of wiggler-undulator insertion source technology. The previous activity report focussed on the operational success of the new multi-undulator concept. This report will focus on the status of the Locust monochromator. The assembly of the monochromtor has proceeded throughout 1987 and bakeout began in February, 1988. A complete review of the design of the beam line is given in *[R.Z. Bachrach, R.D. Bringans, B.B. Pate, and R.G. Carr, in "Proceedings of the International Conference on Insertion Devices for Synchrotron Sources", edited by R. Tatchyn and I. Lindau, 1986]* which also cites the other pertinent papers. The last phase of the construction is due for completion of the spring of 1988 with testing and experimentation beginning with the June, 1988 run.

The specific focus for Beam Line V is the spectral range from 10-1000 eV and the design goal is to deliver the highest possible power density to the sample in the smallest feasible bandwidth. The design of the beam line is dominated by the increased beam power density from an undulator source which necessitated active cooling of most elements likely to be hit by the beam. In the case of optical elements, this requirement arises not only because of possible damage, but also because distortions of the optics must be minimized to maintain ultimate performance. In specifying a monochromator for this beam line, an instrument was sought which would match well to the multi-undulator and SPEAR characteristics and which would advance the state of the art. The resulting Locust monochromator implements a constant deviation Vodar geometry Rowland Circle mounting and is descended from the Grasshopper Monochromator. By using closed loop computer control and configurational changes, the design incorporates a number of features that would not be achievable with either the Grasshopper or the Extended Range Grasshopper (ERG) configuration for these optics. As with the Grasshopper, the Locust uses principally spherical or conic section optics. The Grasshopper was the first fully UHV monochromator. The Locust achieves both variable angle of incidence optics and is the first to be fully water cooled to enable it to maintain performance with the powers delivered by an undulator. The incorporation of water cooling consistent with accepted vacuum practice while maintaining the required mechanical and optical tolerances proved to be a major design problem and added immensely to the scope of design work required and the complexity of the assembly. The Locust uses an elliptically figured SiC entrance mirror fabricated by TRW, SiC entrance codling slit and both spherical and cylindrical gratings.

The refocussing system is built into the monochromator creating three work areas by providing two beams deflected horizontally at 14 degrees from mirrors 1.0 meter from the exit slit. The side stations are at 2.25 meters and the end station 3.5 meters from their respective mirrors. The two side stations have a more limited energy range than the end station, but this is offset by the participating research groups being able to maintain experimental chambers in place permanently. The end station port is for general use and has no permanently installed chamber. Provision has been developed, however, for rapidly changing and positioning chambers available for general users.

Figure 8 shows a schematic side view of the monochromator system. The refocusing and exit slit chambers are on the left, the moving chamber which houses the grating and associated optics is in the center, and the entrance chamber is on the right.

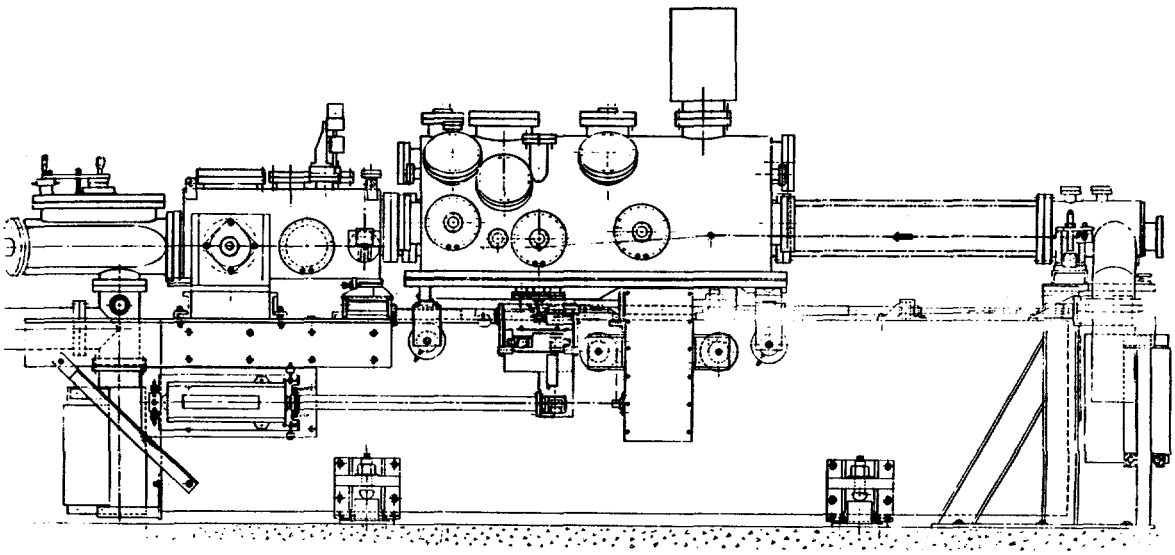

FIGURE 8

SCHEMATIC VIEW OF THE BEAM LINE V MONOCHROMATOR SYSTEM

SUPPORT FACILITIES

Laboratory/Shop/Office Building - The SSRL Laboratory-Office-Shop building was completed in February, 1988 with SSRL scientific, technical and administrative staff moving into their new quarters on February 26.

The completion of the laboratory building marks an important milestone for SSRL, as it frees up valuable user setup and experimental floor space and consolidates many activities that were formerly distributed throughout trailers and separate buildings. These include the electronic shop, the vacuum clean room, the machine shop, the mirror coating facility and the computer room. The former vacuum cleanroom and machine shop will be converted to a "staff" clean room and machine shop facilities, and will be available to the user community for their experimental programs.

The new building comprises 33,000 sq. ft. in two two-story sections. The laboratory-shop wing houses, on the first floor, a machine shop, a vacuum assembly area, a vacuum clean room, a metrology/mirror coating facility, a VUV research laboratory and an x-ray laboratory. The second floor houses the electronic shop, the biotechnology laboratory, the central computer facility and scientific staff offices, as well as a conference room and a library.

The other section of the building houses the design/drafting and engineering functions on the ground floor, and the administrative functions on the second floor. From the user perspective, the consolidation of these activities should streamline various user/facility interactions. It will also free up a significant amount of office space in the Bldg. 120 complex for PRT and user "quiet areas".

Computational Facilities - A major change in the computational support area at SSRL is being made at the current time. The central VAX 11/780, which supports the scientific applications for the laboratory, and the VAX 11/750, which supports all administrative computing at SSRL, are being replaced by a single new VAX 8700 which is being installed in the LOS building. This system will be the central node for the lab-wide ETHERNET/DECNET system which is fully implemented throughout SSRL and connects to SLAC via a LAN bridge. This new system will significantly enhance currently stretched computational capabilities. The 8700 is more than 6 times the speed of the 11/780 and will have a very large memory and disk configuration.

Another development in the computational area is the upgrade program to implement microVAX workstations as replacements for the aging PDP 11/34 branch line instrumentation control computers. Motor driver software for the interface is now almost complete and higher level applications packages (such as the EXAFS data acquisition system) are being designed. Over the next eighteen months, most of the PDP systems will be phased out and replaced by microVAXes. The new systems will also have complete data analysis software to provide for analysis in real time. All of the branch line microVAXes will interconnect over the ETHERNET with the 8700 and the outside world.

SSRL Computer LANs (Local Area Networks) - During this past year, with the assistance of the Electrical Engineering group, the SSRL Local Area Network (LAN) has also been expanded to include the new LOS building and, with the cooperation of SLAC networking, connections to the SSRL beam lines on PEP. The network is implemented via both coaxial network links and fiber optic interconnections between LOS, SPEAR and the engineering trailers. A new terminal server system based on DECserver 200/500 devices has replaced the aging, and less versatile, system which has existed at SSRL for the last four years. A new set of dial-in modems (3) are resident on the DECserver 500, providing convenient access to any of the systems on the SSRL LAN.

Biochemical Laboratory - Only a few small changes have been made in this facility which continues to receive heavy use during runs. A microfuge has been added for small volume samples. An ultracentrifuge rotor with swinging buckets is also now available for outside users.

IV ENGINEERING DIVISION

MECHANICAL ENGINEERING

An appreciable portion of the effort of the Mechanical Engineering group is devoted to design of new beam lines. In 1987, work was carried out on PEP Beam Line 1B, SPEAR Beam Lines VIII and X and the Beam Line V monochromator. All of these activities are described in the preceding chapter.

Work Completed in 1987 - Work completed includes: 1) the design of a "pin hole" device used as a diagnostic tool in PEP Beam Line 1B, 2) SSRL specific additions to the new SLAC Vacuum Specification, 3) the qualification of a new non-circular UHV sealing method developed at LBL, and 4) design of a focussing mirror following the monochromator on Branch Line IV-3.

The PEP "pin hole" allows one to image the x-ray source, and in combination with a scanning pinhole and the monochromator in the hutch, provides a method of producing a series of planar monochromatic maps of flux distribution.

The new LBL noncircular seal consists of a copper or aluminum seal with an "x" cross-section that is crushed into the corners of conventional o-ring grooves. Mating flanges need not be of similar materials, allowing a match of aluminum to stainless steel. The sealing system is currently in use at LBL, and will be used on a large rectangular flange on the mirror tank for Branch Line VI-1. Vacuum performance is similar to the conventional conflat flange.

Beryllium Window and Hybrid Wiggler Power Studies - The ME group, in collaboration with the SSRL X-Ray group, is conducting experiments to measure the temperature distribution on the first beryllium window and the power output of Beam Line VI. An infra-red camera recorded the temperature field on the window, and change in cooling water temperature near the window was used to determine approximately the power absorbed by the beryllium. Photon flux was also measured in the experimental hutch. Results so far indicate that the total power output of the wiggler appears to be lower than expected.

Lawrence Livermore National Laboratories produced temperature fields on sample beryllium windows with a calibrated laser welder. *[Holdner, F.R., et al. "Thermal Damage Study of Beryllium Windows used as Vacuum Barriers in Synchrotron Radiation Beamlines", LLNL Report UCID-21179 (September 1987)].* Temperature fields were measured with an infra-red camera and checked with thermocouples. Laser power levels were increased until the beryllium foil failed.

The ME group at SSRL, using LLNL power distributions and finite element methods, reproduced the experimental temperature distributions, thus verifying the finite element models used in window thermal predictions.

In 1988, the Mechanical Engineering and X-Ray groups will design and install an accurate calorimeter to determine the beam power following the beryllium window module. This instrument may also be installed on Beam Line X to determine its total power output.

Thermal-Structural Analysis - SSRL is now conducting almost all of its finite element analysis on PC's. The Engineering group has two Compaq 386's with 80387 floating point processors, running a thermal-structural analysis package from Algor Interactive Systems. This package includes a model drafting package, as well as accepting output from Cadkey, the SSRL standard drafting program. The Compaq has been used to run models of 5 to 6 thousand degrees of freedom in the space of 5 to 6 hours. Larger models can be run on the VAX at SSRL using similar programs from the same company. The Compaq/Algor combination has been used to examine the temperature and stress distributions on beryllium windows, crotches, masks, and mirrors.

Computer Aided Design - The Mechanical Engineering group now has two PC's dedicated to mechanical design and drafting; a Compaq 386 and an IBM AT clone. Three designers are now able to use these machines.

The designs of the PEP pin hole device and the XAFS hutch on Beam Line X-2 were done exclusively on the Mechanical Engineering CAD stations. Future efforts, such as the Beam Line II rework and Beam Line X-1 branch line design, will also be done on the CAD systems.

ELECTRICAL ENGINEERING

Beam Line Control Systems - A major activity of the Electrical Engineering group is the design, construction, maintenance and improvement of various control systems for SSRL beam lines. These control systems may be divided into the following functional catagories: vacuum controls, photon beam steering and stabilization controls, personnel protection interlock systems, communications (audio, video, data), insertion device controls and experimental station electronics.

In 1987, the EE group was involved in the design and implementation of control systems for the following new beam lines: PEP Beam Line 1B, SPEAR Beam Line VIII, and SPEAR Beam Line X. The installations of the controls sytems were completed, and the various controls were tested and commissioned. The beam lines were successfully operated with beam.

Work is continuing to standardize the beam line control systems. The goals are to simplify the operation and maintenance of these systems and to reduce the training time for technical support personnel.

Beam Line X Wiggler Control System - The Beam Line X wiggler control system, based on that of Beam Line VI, has been improved in three areas. The control panel has been simplified for easier use in routine operation. The touch panel presents all critical information, and will automatically calculate the wiggler gap for the desired field. The system will not allow fields to exceed levels that are safe as determined by the number of filters inserted. Wiggler trim currents have been optimized to minimize effects on storage ring current. Provision has been made to allow continuous scanning of the wiggler field, controlled by the experimental station computer, with a minimum effect on the storage ring current and SPEAR control computer.

Development of Beam Line and Storage Ring Status Monitoring System - Efforts are continuing to develop a central computer facility for monitoring all SSRL beam line control systems and SPEAR/PEP ring operating parameters. The purpose of the proposed computer facility is to permit centralized monitoring (and eventually, some manipulation) of the beam line control systems. The facility will also act as the interface to the SPEAR/PEP VAX computers for acquisition of storage ring data. The centralized status information will be available to SSRL operators and key personnel. Relevant information will be displayed at each beam line control station and at the main operation console in the SSRL control room. The system will be connected to the SSRL sitewide Ethernet, making the status information available to all network terminals.

The system will consist of the following major components: 1) a system supervisor computer which will also be used for software development and program maintenance, 2) a set of console computers in the main control room, 3) a set of process control computers (DEC microVAX-II's for SSRL and VAX750 for SPEAR control) with individual CAMAC serial highway drivers located central to their respective process interfaces, 4) CAMAC instrumentation crates and modules directly interfaced to the beam line control systems (or to the storage ring instrumentation, in the case of the ring control system), 5) a machine control Ethernet LAN interconnecting the system supervisor, consoles and process computers, 6) a laboratory Ethernet LAN (existing SSRL Ethernet) connecting the system supervisor computer to the terminal servers and outside world.

The supervisor computer will collect beam line statistics to investigate long term trends; for example, to identify a slow leak in the vacuum system. the Ethernet connection to the SPEAR VAX will also permit this computer to monitor SPEAR collected information, such as ring current, energy, lifetime, magnet fields and vacuum reading within the ring itself.

Beam Line Steering and Stabilization - The ninth beam line steering servo system for SPEAR and the system for PEP, servicing SPEAR Beam Line X and PEP Beam Line 1b, were commissioned during the fall of 1987. Both systems utilize in-vacuum photoemission beam position monitors similar to those used on SPEAR Beam Line VI and the PEP Beam Line 5b *(see SSRL Activity Reports for 1984 and 1985).*

While these systems can stabilize vertical beam position at the experimental station to a level of order 0.1 mm or less over the course of the delivered beam period when the beam line insertion magnets are operated in their high field configurations (>~3 kGauss for the Beam Line X 15 period hybrid wiggler, >~1 kGauss for the PEP 26 period undulator), the

stabilization level can be considerably less during low field operation because of the significant contribution to the position monitor signals from bending magnet radiation. This "pollutant" radiation can create an asymmetric illumination of the monitor electrodes, and a shift of the illumination centroid can occur as beam decays. The steering servo system incorrectly interprets such a shift as the movement of the insertion device beam and adjusts the stored beam orbit to restore the centering of the beam centroid. This mechanism can result in missteering the desired insertion device beam by as much as a millimeter over the course of a fill.

One way to reduce the inadequacies of the steering system during low field insertion magnet operation is either to situate the position monitor far back on the beam line where the bending magnet radiation can be effectively masked. This solution is frequently impractical because of the presence of a focussing mirror at a location on the beam line that is close enough to the source point that bending magnet radiation is still a problem.

Another solution is to incorporate a position monitor that can recognize the radiation pattern of the desired beam and respond only to its displacement. For undulator radiation, the task is fairly simple since the location of the desired beam coincides with the peak of the beam's transverse intensity profile. SSRL is assisting Britton Chance et al. (University of Pennsylvania) *[B. Chance, D. Schick, R. Hettel, L. Powers, Nucl. Instr. and Meth. A246 (1986) 400.]* in the development of a "vibrating reed" monitor consisting of a thin stainless steel wand that sweeps transversely through the beam at a high frequency (~200 Hz) and with a low duty cycle (~5%) to sample the beam's intensity profile. A small area on the wand is coated with a phosphor to sense the limited crossection of the beam. Vertically scattered photons are detected with a photomultiplier tube; processing electronics produces a signal proportional to the off-center position of the beam's "hot spot". A version of this monitor that operates in helium was tested on diagnostic Beam Line II-3 and on wiggler Beam Line VI over the last year. This monitor promises 10 micron accuracy independent of beam intensity. A model that functions in vacuum is being developed by Chance.

Further development and upgrading of the steering control system was carried out in 1987 under the auspices of the SEP project. A new steering servo controller printed circuit board was designed that incorporates the analog and digital circuitry required for computer control and monitoring of the high bandwidth analog servo components. Functions include an interlock that prevents the system from operating in closed-loop mode if the position monitor or other servo signals have improper magnitudes and disables the system totally if the corrector magnet actuators are not operating properly. Automatic gain control (AGC) has been implemented to normalize system gain over a dynamic range of ~30 dB in beam intensity/ current. In addition, a gain ramping circuit has been devised that effects smooth transitions between open- and closed-loop modes ("manual" and "auto") to avoid the transient "glitching" of the beam orbit that otherwise occurs during these transitions. The new steering controller was tested on SPEAR Beam Line VIII and PEP Beam Line 1B in Fall, 1987. Installation of the new units for all SSRL beam lines is scheduled for early 1988. Remote computer control and monitoring of the steering systems via the CAMAC interface is presently being implemented.

Future steering system improvement centers on the development of the 2-monitor, 4-magnet servo configuration that will stabilize both position and angle of the photon beam in the vertical plane *(described in the 1985 Activity Report).* A key component in this system is the RF beam position monitor and signal processing module that detects and decodes the position of the stored beam near the source point where it is colinear with the photon beam. A module is being developed that produces both vertical and horizontal position sensitive signals with an estimated reproducibility error of ~50 microns or better over a bandwidth of ~1 kHz. This monitor, working in conjunction with a photon monitor located many meters from the source point, should be capable of stabilizing the photon beam's position and angle to a small fraction of its transverse size and divergence parameters at the experimental station.

Members of SSRL's Biotechnology Group - "3 a.m Wating for Beam" Photo - Z. Rek
Keith Hodgson, Larry Roe *(now at W.R. Grace & Co)*, Paul Phizackerley and Britt Hedman

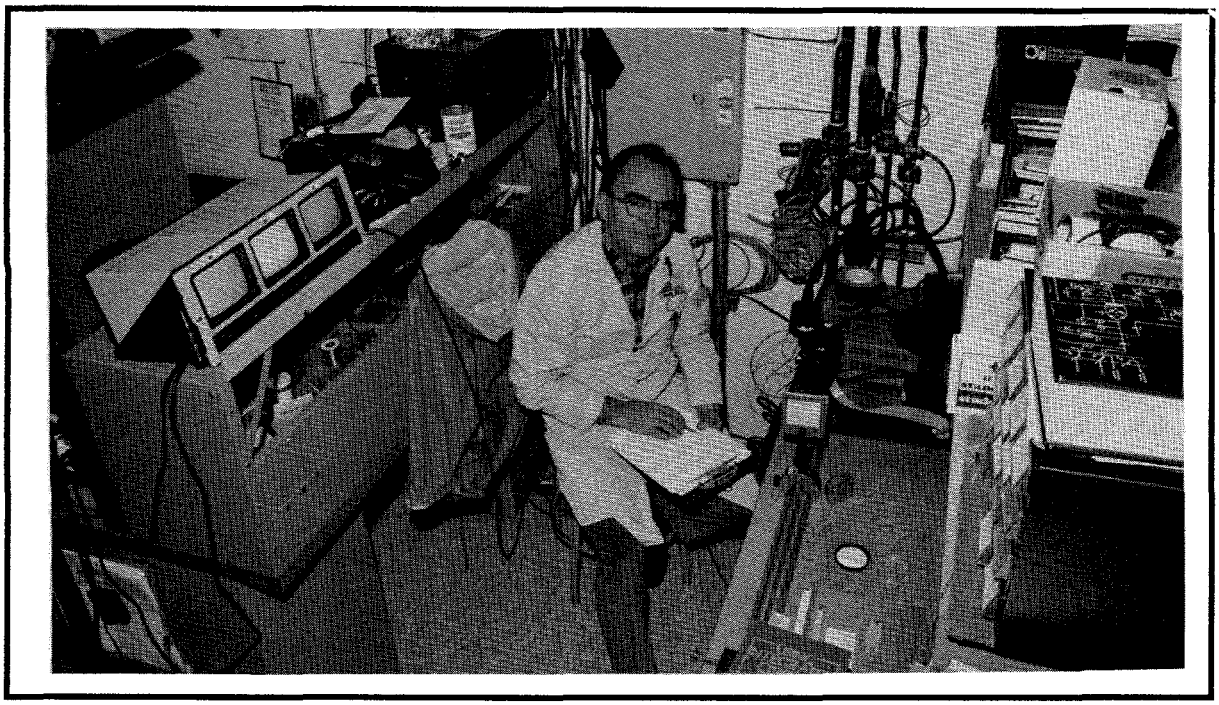

Hans Przybylski, SSRL X-ray Group, working in the electronics laboratory. Photo - C. L. Troxel, Jr.
Han's skills in precision mechanics have earned him the deserved reputation as a man who can make anthing work.

V CONFERENCES AND WORKSHOPS

WORKSHOP ON PEP AS A SYNCHROTRON RADIATION SOURCE

A Workshop on PEP as a Synchrotron Radiation Source was held by SSRL on October 20-21, 1987. PEP is a colliding-beam storage ring that has already been used for a few weeks for synchrotron radiation research parasitically during high energy physics runs.

PEP's main features as a synchrotron radiation source are high energy (up to 16 GeV with presently installed RF), long straight sections (6 are 117 meters long), large circumference (2200 meters) and low bending magnet field (0.32 Tesla at 16 GeV). It has operated in a low emittance mode with an emittance of less than 12 nanometer-radians at 8 GeV, making it the lowest emittance synchrotron radiation source. *(In December 1987, after the workshop, PEP was operated at 7.1 GeV with a calculated emittance of 6.4 nanometer-radians. See Chapter II for details.)*

At the Workshop, there were 125 registered participants (77 from government labs, 23 from universities, 16 from foreign institutions and 9 from US industry). The following charge was given to the Workshop by SSRL Director, Art Bienenstock.

A. Explore PEP's potential as a low emittance storage ring. Examine the possibilities which have been proposed for achieving that very low emittance. Provide your critical analysis of those possibilities and inform us of others which may be achievable.

B. Explore the range of insertion devices which can utilize the extreme lengths and/or high energies available on this machine.

C. Consider the potential evolution of this machine from one which will function routinely with brilliances of the order of 10^{16} as PEP functions in a parasitic mode to the projected 10^{21} with the achievement of the extremely low emittances. Define new experiments which can be performed as this evolution proceeds.

Individual contributions to the Workshop and summaries and conclusions by Working Group Leaders have been assembled into a proceedings. Copies are available on request by writing to M. Steger at SSRL, SLAC Bin #69, PO Box 4349, Stanford, CA 94309-0210.

Some highlights from the summary talks by the leaders of the 11 Working Groups are given below:

A. Detailed analysis and past experience with PEP were reviewed by 35 scientists in the Accelerator Physics Working Group. They concluded that there was good reason to expect that PEP could run at high currents (5-8 mA per bunch, 100 mA or more total current) at 8 GeV in the low emittance mode that has already been tested at low current and that no major problems were forseen that would prevent the achievement of much lower emittances with damping wigglers, as has been proposed. A list of specific accelerator physics studies that should be carried out was made.

B. The 9 Working Groups dealing with the different applications presented many experiments that could be done on PEP. Some of these could also be performed on rings such as the APS and ESRF and PEP offered an opportunity for an early start. Others could uniquely be done at PEP because of the extreme capabilities and/or potential of PEP (brightness, photon energy, coherent power, short bunches). There was considerable excitement about the prospects for carrying out these experiments, but also concern about running time, staff support and the number of beam lines and support facilities that would be available.

C. The Directors of the APS and ESRF projects, and several of their staff present at the Workshop, expressed interest to participate in machine studies and use of PEP beam lines to gain experience relevant to their projects. It is also expected that interest in using very high energy rings will grow in Japan using the Tristan 26-30 GeV storage ring that recently began operation for colliding-beam studies at KEK. A talk on Japanese planning for high energy light sources was presented to the Workshop by M. Ando from the Photon Factory.

D. There was considerable interest in very high photon energies (up to several hundred KeV) for

applications such as studies of crystal optics, Compton and magnetic scattering, and nuclear resonance spectroscopy. It was also pointed out that the high coherent power levels that PEP could produce would have application in several areas including microanalysis and the pumping of soft x-ray lasers. Interest was also shown in the possibilities to place samples very close to the source, which would allow the recording of a diffraction pattern in one shot with a time resolution of picoseconds instead of milliseconds and, conversely, to have very long beam lines to exploit the exceptional collimation of the radiation in topographic studies.

FOURTEENTH ANNUAL SSRL USERS GROUP MEETING

The Users Group Meeting was held this year on October 22 and 23, 1987. The SSRLUO Executive Committee is responsible for organizing the Users Group Meeting jointly with a representative of the SSRL scientific staff. Approximately 156 people were in attendance. The program for the meeting and the authors' abstracts are available as SSRL Report Number 87/05.

Co-Chairpersons for the meeting were Joe Wong for the Users Organization and Brad Pate for the SSRL scientific staff. Reports on individual experiments were presented in poster sessions.

FIRST SSRL ROTATION CAMERA USERS MEETING

The first SSRL Rotation Camera Users Meeting, attended by about 30 people, was held at Asilomar, California on March 23, 1987 during the Eighth West Coast Protein Crystallography Workshop. This was the first such meeting since the rotation camera facility became available to users in April, 1984. It was held at this time because many of the SSRL rotation camera users were planning to attend the Crystallography Workshop.

The meeting, chaired by Paul Phizackerley of SSRL, provided the opportunity to discuss, as a group, such topics as the functioning and capabilities of the rotation camera system, the quality of results obtained, film scanning software used, user experiences with the experimental facilities, user support, hardware and software documentation, scheduling and access to the facility, and plans for future instrumentation development.

VI SSRL ORGANIZATION

SSRL FUNCTIONAL ORGANIZATION

The SSRL administration is divided into seven functional areas each headed by a senior staff member. These are: X-ray, VUV, Biotechnology, Accelerator Physics, Operations, Engineering and Administration. In the next few months a separate organization to support the 3 GeV injector project will be developed. In addition, each experimental station and piece of specialized instrumentation is the responsibility of an SSRL staff member. The charts which follow depict these responsibilities and the functional organization of SSRL as of January 1988.

SSRL EXPERIMENTAL STATIONS
RESPONSIBLE PERSONNEL

BRANCH LINE	RESPONSIBLE SCIENTIST/ENGINEER
I-1 (Grasshopper)	I. Lindau/A. Waldhauer
I-2 (TGM)	I. Lindau/M. Rowen
I-4 (SAS)	S. Brennan/H. Tompkins
I-5 (Bend Magnet X-ray)	G. Brown/T. Troxel
II-2 (Bend Magnet X-ray)	G. Brown/T. Troxel
II-4 (White Radiation)	Z. Rek
III-1 (Grasshopper)	I. Lindau/A. Waldhauer
III-2 (SXR- 18 degree)	I. Lindau/A. Waldhauer
III-3 (SXR-Jumbo)	I. Lindau/M. Rowen
III-4 (Lithography)	P. Pianetta/A. Waldhauer
IV-1 (Wiggler)	G. Brown/T. Troxel
IV-2 (Wiggler)	G. Brown/T. Troxel
IV-3 (Wiggler)	S. Brennan/H. Tompkins
VI-2 (Wiggler)	J. Arthur/T. Troxel D. Moncton *(EXXON)*, J. Kortright*(LBL)*
VII-1 (Rotation Camera)	P. Phizackerley
VII-2 (Wiggler)	S. Brennan/H. Tompkins
VII-3 (Wiggler)	G. Brown/T. Troxel
VIII-1 (SGM)	M. Rowen, G. Tirsell *(LLNL)*
VIII-2 (TGM)	M. Rowen, S. Williams (UCLA)
X-2 (Wiggler)	S. Brennan, J. Wong (LLNL)
PEP 1B	G. Brown/T. Troxel
PEP 5B	G. Brown/T. Troxel

INSTRUMENTATION/FACILITY RESPONSIBILITIES

MATERIALS DIFFRACTOMETER: *S. Brennan/H. Tompkins*
VACUUM SAMPLE CHAMBERS: *M. Rowen*
AREA DETECTOR: *P. Phizackerley*
COMPUTER SYSTEMS: *T. Cox*
VII-2 SPECTROMETER: *S. Brennan/H. Tompkins*
BIOCHEMISTRY LABORATORY: *B. Hedman/R. Mayer*
DARKROOMS: *P. Phizckerley/Z. Rek*
BEAM LINE STEERING: *R. Hettel*
EXAFS EQUIPMENT AND SOFTWARE: *B. Hedman/R. Mayer*
SAS CAMERA (BIOLOGY): *S. Wakatsuki*
EXAFS CONSULTANT: *B. Hedman*
SCATTERING CONSULTANT: *S. Brennan*
RT-11 SOFTWARE CONSULTANT: *S. Brennan*

SSRL DEVELOPMENT PROJECTS -RESPONSIBLE PERSONNEL

BEAM LINE II - *G. BROWN (SSRL)/T. TROXEL (SSRL)/ R. BOYCE (SSRL)*

BEAM LINE V - *I. LINDAU (STANFORD)/R. BACHRACH (XEROX)/ A. WALDHAUER (SSRL)*

STATION VI-1 - *R. TATCHYN (SSRL), W. MCKINNEY (LBL) R. YOTAM (SSRL)/J. CHIN (LBL)*

3 GeV SPEAR INJECTOR - *H. WIEDEMANN*

STATION X-1 - *I. LINDAU (STANFORD), J. STOHR (IBM), M. ROWEN (SSRL)/J. MONTGOMERY (SSRL)*

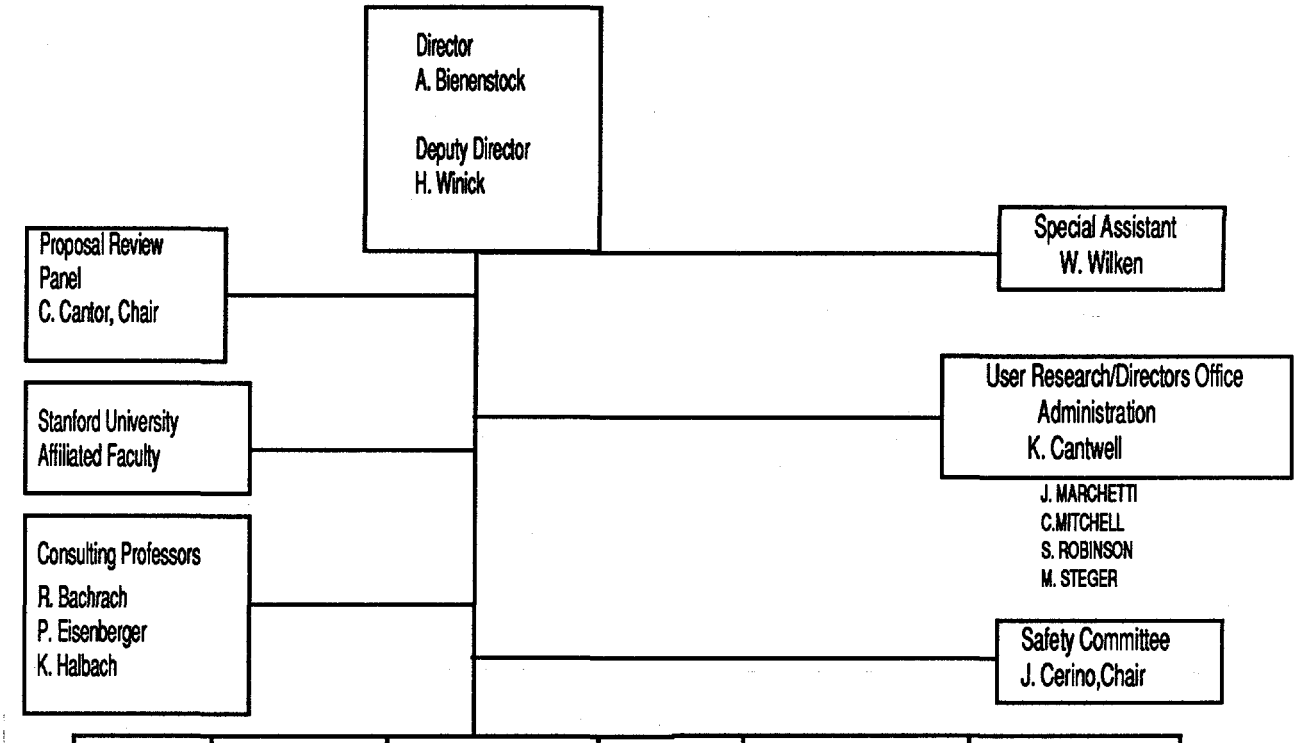

J. ARTHUR
A. BIENENSTOCK
S. BRENNAN
P. CAPEDER
G. KERR
H. PRZYBYLSKI
S. RUBY
H. TOMPKINS
C. TROXEL, JR.
T. TROXEL

R. CARR
G. HUSEK
R. MORRIS (SEL)
B. PATE
P. PIANETTA
J. PRAXEL
M. ROWEN
F. SENF
R. TATCHYN
C. TROXEL
A. WALDHAUER

B. HEDMAN
R. MAYER
E. MERRITT
P. PHIZACKERLEY
Z. REK
U. SPANN

COMPUTER RESOURCES

A. COX, Mgr
E. HUIE
A. WINSTON

J. CERINO
R. HETTEL
J. KWONG
B. LO
H. WINICK

BUSINESS ADMINISTRATION

M. BOWMAN, Mgr
M. BRUCE-HEMENWAY
L. CRUM
L. BOOKER

PERSONNEL ADMINISTRATION

S. LOVGREN, Mgr
L. BOOKER

ELECTRONICS

R. YOTAM, Mgr
C. CORK
R. GAROUTTE
R. HETTEL
M. HORTON
R. ORTIZ
J. YANG

MECHANICAL

B. YOUNGMAN, Mgr
R. BOYCE, Dep Mgr
M. DORMIANI
J. MONTGOMERY

M. STICKLER (Administration)
C. TROXEL, Mgr

ENGINEERING

D. CHARLESTON
C. TANIGUCHI (Stockroom)

OPERATORS

D. DAY, Supervisor
T. HOSTETLER, Lead
K. CULLER
J. DUNN
D. ERNST
J. HAYWARD
D. NEAR
D. ROSITCH

PLANT

A. FILIPPI
R. SILVERS

VACUUM

H. MORALES, Supervisor
T. MARTINEZ
M. NALLS
T. NEAL

SSRL Organization Chart

January 1988

SSRL ADVISORY PANELS

PROPOSAL REVIEW PANEL

A main task of the Proposal Review Panel is the review and rating of scientific proposals to SSRL based largely on reports obtained from outside (non-panel) referees. The panel met on January 9 and 10, 1987 and on July 17 and 18, 1987 at SSRL and rated the new proposals which had been received in September, 1986 and March, 1987 respectively.

As of December 31, 1987 SSRL had received a total of 2048 proposals of which 158 are presently active.

The Proposal Review Panel meets twice yearly, generally in June and January. Deadlines for receipt of proposals for consideration at the next meeting are the first of September and the first of March of each year.

The panel members in 1987 were:

Biology Sub-panel
Charles Cantor, Columbia University *(Chairperson)*
Wayne Hendrickson, Columbia University
William Orme-Johnson, MIT

Materials Sub-panel
Boris Batterman, Cornell University
Howard Birnbaum, University of Illinois
Russell Chianelli, Exxon
Denis McWhan, AT&T Bell Laboratories

VUV Sub-panel
Bernd Crasemann, University of Oregon
Charles Fadley, University of Hawaii
Warren Grobman, IBM Watson Research Center

Dr. Crasemann's term ended with the January 1988 meeting. Torgny Gustafsson, Rutgers University, is the new VUV subpanel member.

SCIENCE POLICY BOARD

The Science Policy Board reviews all aspects of SSRL operation, development and plans for the future. It reports to Stanford University President Donald Kennedy. The Board met once during this reporting peroid, on May 22 and 23, 1987. The members at the time of the meeting were:

B. McDaniel, Cornell University *(Chairperson)*
P. Chaudhari, IBM
E. Ginzton, Varian Laboratories
W. Kohn, University of California
Wm. Orme-Johnson, MIT
Y. Petroff, LURE
F. Schwettman, Hewlett-Packard

SSRL USERS ORGANIZATION

Members of the Executive Committee of the SSRLUO were appointed at the Fourteenth Annual SSRL Users Group Meeting as follows:

Joe Wong, LLNL *(Chairperson)*
Marjorie Olmstead, UC-Berkeley *(Vice-Chair)*
Frank (Bud) Bridges, University of California
Ross Bringans, Xerox
Robert Greegor, Boeing Company
Jeff Kortright, Lawrence Berkeley Laboratory
Francesco Sette, AT&T Bell Laboratories
Jo Stohr, IBM *(Past-Chairperson)*
Louis Terminello, Lawrence Berkeley Laboratory
Lane Wilson, LLNL
Katherine Cantwell, *(Secretary - SSRL Liaison)*

The Users Organization Executive Committee meets periodically throughout the year to consider and advise on matters pertinent to user interests at the Laboratory.

VII EXPERIMENTAL PROGRESS REPORTS

MATERIALS PROPOSALS **Page**

100Mp "X-Ray Absorption Studies of Disordered Systems" E.D. Crozier, N. Alberding, K.R. Bauchspiess, D. Jiang, A.J. Seary, R. Ingalls, J. Freund, B. Houser 44

822Mp "Temperature Dependence Study of Monolayers and Multilayers of the Langmuir-Blodgett Type" W.B. Yun, M. Bloch, X. Yang, J. Viccaro 46

868M "EXAFS Studies of High T_c Superconductors" J.B. Boyce, F. Bridges, T. Claeson, T.H. Geballe, C.W. Chu, J.M. Tarascon 47

918M "Investigation of the α-Fe $\rightarrow$ ε-Fe Transition Using Synchrotron Radiation" M.H. Manghnani, L.C. Ming, Y.H. Kim, N. Nakagiri 49

940M "Anomalous X-Ray Diffraction Studies of Bimetallic Catalysts: Pt-Re on SiO_2" K.S. Liang, G.H. Hughes, J.H. Sinfelt 50

956Mp "Transformation of Ca and K Catalytic Species in Lignite During Pyrolysis and Gasification: An In -Situ EXAFS Investigation" F.E. Huggins, N. Shah, G.P. Huffman, F.W. Lytle, R.B. Greegor, R.G. Jenkins 51

956Mp "EXAFS Studies of Organic Sulfur in Coal" G.P. Huffman, N. Shah, F.E. Huggins, R.B. Greegor, F.W. Lytle 53

956Mp "Investigation of the Kinetics of the Carbide Formation in HSLA Steels by EXAFS Spectroscopy" N. Shan, G.P. Huffman, F.E. Huggins, L.J. Cuddy, F.W. Lytle, R.B. Greegor 54

979M "3-D X-Ray Microtomography of Catalytic Materials" J.H. Kinney, M.C. Nichols, Q.C. Johnson, R.A. Saroyan, U. Bonse, R. Nusshardt, R. Pahl 55

983M "X-Ray Absorption Study of Amorphous Germanium at High Pressure" R. Ingalls, J. Freund, E.D. Crozier 56

984M "X-Ray Absorption Studies of High T_c Superconductors" J. Whitmore, B. Houser, Y. Ma, M. Qian, R. Ingalls, E.A. Stern, F.C. Brown, R. Kurosky, B. Thiel, J.M. Tranquada, E.D. Crozier, N. Alberding, A.J. Seary, J.P. Rice, B.G. Pazol, D.M. Ginsberg 57

988M "Actinide and Fission Product Site Speciation in Nuclear Waste Glasses" E.M. Larson, P.G. Eller, R.B. Greegor, F.W. Lytle, M.P. Eastman 58

995Mp "In-Situ X-ray Absorption Study of Pb(II) and Co(II) Sorption Complexes at the γ-Al_2O_3 Water Interface" G.E. Brown, C.J. Chisholm, K.F. Hayes, A.L. Roe, G.A. Parks, K.O. Hodgson, J.O. Leckie 59

996M "Interface Structure of $NiSi_2$/Si(111)" I.K. Robinson, R.T. Tung, R. Feidenhans'l 62

999Mp "EXAFS Study of Rare Earth Element Environments in Quenched Silicate Melts of Geochemical Interest" C.W. Ponader, G.E. Brown Jr., W.E. Jackson 64

1000Mp "Characterization of Co-Containing Oxides on Stainless Steel by e-Yield XANES Spectroscopy" F. Lytle, R. Greegor, Z. Rek, H. Ocken 65

1000Mp "Investigation of Pb Implanted TiO_2 and $SrTiO_3$ Using Total Electron Yield" R.B. Greegor, F.W. Lytle, B.C. Chakoumakos, R.C. Ewing, G.W. Arnold 66

1000Mp	"Site Selectivity in Mn Glass Using Optical XANES" R.B. Greegor, F.W. Lytle, D.R. Sandstrom, M. Weber, J. Wong	67
1001Mp	"Universal Interactions in Undulating Membranes: A Series of Synchrotron X-Ray Studies of Dilute 1-Dimensional Fluid Multilayers" C.R. Safinya, D. Roux, G.S. Smith, E.B. Sirota	68
1001Mp	"Dynamic 'Steady State' Microscopic Structure of Complex Fluids Studied in a Couette X-Ray Shear Cell" C.R. Safinya, R. Plano, E.B. Sirota, G.S. Smith	70
1001Mp	"SAXS Study of Colloidal Crystals" E.B. Sirota, S.K. Sinha, H.D. Ou-Yang, P.M. Chaiken, J.D. Axe, Y. Fujii	71
1001Mp	"Extended X-Ray Absorption Fine Structure (EXAFS) Studies of Platinum-Tin Catalysts" G. Meitzner, G.H. Via, F.W. Lytle, S.C. Fung, J.H. Sinfelt	72
1001Mp	"Sulfur K-Edge X-Ray Absorption Spectroscopy of Asphaltenes and Model Compounds" G.N. George, M.L. Gorbaty	73
1001Mp	"Scattering Studies of La_2Cu0_4 Single Crystals: Charge Density Modulations" D.E. Moncton, K.L. D'Amico, J. Bohr, J. Als-Nielsen, R.M. Fleming, J.P. Remeika, D. Vaknin	74
1001Mp	"High Resolution Powder X-Ray Diffraction" J.M. Newsam, K.S. Liang, G. Hughes	75A
1011M	"Bond Orientational Ordering in Tilted Hexatic Liquid Crystal Films" J.D. Brock, R.J. Birgeneau, J.D. Litster, B. McClain, D.Y. Noh, P.M. Horn	76
1021Mp	"Synchrotron X-Ray Polycrystalline Diffractometry - IV & V" W. Parrish, M. Hart, M. Bellotto, L. Depero, C. Erickson	77
1031M	"XAS Studies of Synthetic Models for Hydrodesulfurization Catalysts" G.S. Waldo, O. Baralt, M.D. Curtis, J.E. Penner-Hahn	78
1033M	"XAS Determination of the Chemical Forms of Sulfur in Petroleums" G.S. Waldo, R.M.K. Carlson, J.E. Penner-Hahn	79
1036Mp	"Coster-Kronig Transition Probabilities in Metals" S.L. Sorensen, R. Carr, S.J. Schaphorst, S.B. Whitfield, B. Crasemann	80
1038M	"Deep Donors in Gallium Aluminum Arsenide Semiconductor Alloys" T.M. Hayes, D.L. Williamson, P. Gibart	82
1054M	"X-Ray Induced Photo-Acoustic Emission" R.D. Day, R.W. Ryon, S. Benson	83
1056M	"Synchrotron White Beam Topography of Striations and Interface Breakdown in Alloyed GaAs" S.R. Stock, Z.U. Rek, A.G. Elliot	85
1058M	"Roughening and Deconstruction of the Au(110) Surface" G.A. Held, J.L. Jordan-Sweet, P.M. Horn, A.Mak, R.J. Birgeneau, T. Gustafsson	87
1059M	"Thermal Expansivity of γ-Mg_2Si0_4 and γ-$(Mg,Fe)_2Si0_4$ Spinels to 900°C Using Synchrotron Radiation" L.C. Ming, M.H. Manghnani, Y.H. Kim, U. Devi, D.H. Xiong, E. Ito	89
1063M	"In-Situ Surface EXAFS of Monolayers on Silver Electrodes" O.R. Melroy, M.F. Toney, M.G. Samant, J.G. Gordon, L. Blum II	91
1064M	"Static High Pressure Equation-of-State (EOS) Studies on Thorium to 100 GPa: A Preliminary Report" J. Akella, Q. Johnson, G.S. Smith, L.C. Ming	92

1066Mp	"The Use of EXAFS Spectroelectrochemistry for the In Situ Study of the Oxidation of a Copper(I) Complex in a Polymer Modified Electrode" R.C. Elder, W.R. Heineman	94
1072M	"Glancing Angle EXAFS Studies on Cu-A1 Interfaces" S.M. Heald, H. Chen	96
1073M	"X-Ray Absorption Study of Oxide Based Superconductors" S.M. Heald, C.Y. Yang, J.M. Tranquada	97
1078M	"EXAFS Studies on Powders of GaAs Treated with Co Complexes" I.L. Abrahams, C.E. Caley, S.R. Lunt, G.M. Miskelly, M.J. Sailor, P.G. Santangelo, M.H. Schmidt, B.J. Tufts, N.S. Lewis	98
1079M	"EXAFS of $YBa_2Cu_3O_{7-\delta}$ and $GdBa_2Cu_3O_{7-\delta}$ Superconductors" J.B. Boyce, F.C. Bridges, T. Claeson, T.H. Geballe, R.S. Howland	101
1081M	"Microradiography of Creep Damage in Copper" J.E. Benci, D.P. Pope	102
1097Mp	"Antisite Disorder in $YBa_2Cu_3O_7$" F.W. Lytle, E.C. Marques, R.B. Greegor, H.G. Ahlstrom, E.M. Larson, D.E. Peterson, A.J. Panson	103
1097Mp	"Rare Earth L-Edge Spectra in $Y_{1-x}M_xBa_2Cu_3O_7$" F. Lytle, R. Greegor, E. Marques, E. Larson, J. Wong, C. Violet	104
2023Mp	"Characterization of the Atomic and Electronic Structures of High T_c Superconducting Materials by XAS" S.D. Conradson, G.H. Kwei, I.D. Raistrick	105
2024Mp	"XAS Studies of Quasi-One-Dimensional Halide-Bridged Mixed Valence Platinum Compounds" S.D. Conradson, B.I. Swanson, A.P. Sattelberger	106
8001M	"Reflectivity of Thin Carbon Films" S. Brennan, M.F. Toney	107
8001M	"Fluorescence EXAFS Study of Silicon in Neodymium Iron Boron Rare-Earth Magnets" S. Brennan, A. Bienenstock, J.E. Keem	108
8001M	"Strain Distribution in Thin Aluminum Films using X-Ray Depth Profiling" M.F. Doerner, S. Brennan	109
8003M	"Time-Domain Effects in Resonant Nuclear Scattering of Synchrotron X-Rays" S.L. Ruby, J. Arthur, D. Brown, G. Shenoy, E. Alp	110
8010M	"Interferometric Study of Spherical Wave Diffraction" J. Arthur, H. Tompkins	111
8101M	"Structural Investigations of W-Ge Multilayers and Amorphous W-Ge Alloys" M. Rice, A. Bienenstock	112
8103M	"Analysis of Co Doped Iron Oxide Thin Films by X-Ray Depth Profiling" M.F. Toney, T.C. Huang, S. Brennan, Z. Rek	113
8103M	"Quantification of the Spatial Variation of Strain Fields Surrounding Laser-Drilled Holes in Silicon using White Beam Section Topography" Y.H. Chung, Z.U. Rek, S.R. Stock	115
9900M	"Two Dimensional Compressibility of Electrochemically Adsorbed Lead on Silver (111)" P.N. Ross, J.B. Kortright, O.R. Melroy, M.F. Toney, G.L. Borges, M.G. Samant, L. Blum	117
9901M	"Valence and Anti-Site Disorder in High Temperature Superconductors" J. Wong, F.W. Lytle, R.B. Greegor, C. Violet, G. Xiao, A. Panson, E. Larson, D. Peterson, T. Collings, B. Maple	118

9901M "X-Ray Tomography on Beam Line X" J.H. Kinney, Q.C. Johnson, R.A. Saroyan, M.C. Nichols, U. Bonse, R. Nusshardt 119

9901M "Beam Line X-2 Profile Measurement with a CCD Imager" J.H. Kinney, J. Wong, T. Troxel 120

9901M "EXAFS on Near Monolayer Hafnium Film" T.W. Barbee, J. Wong 121

Letters of Intent

"Bromine K-Edge Cellular Radiosensitization with Bromodeoxyuridine" D. Larson, W.J. Bodell, C. Ling, T.L. Phillips, M. Schell, D. Shrieve, T. Troxel 122

"Radius of Gyration Measurements of Soluble Chromatin Fibers" S.P. Williams, J.P. Langmore 123

"Observation of Cluster Formation in an Ionomer" A.F. Galambos, W.B. Stockton, J.T. Korberstein, A. Sen, R.A. Weiss 124

"The Microstructure of Block Copolymers Formed Via Ionic Interactions" T.P. Russell, R. Jerome, P. Charlier, M. Foucart 126

"Intercalibration of Small-Angle X-Ray and Neutron Scattering Data" T.P. Russell, J.S. Lin, S. Spooner, G.D. Wignall 128

"Solution of Phase Problem for Crystallography at a Wavelength of 3.5 Å" Q. Shen, R. Colella 130

BIOLOGY PROPOSALS

840Bp "X-Ray Absorption Spectroscopy of Mn and Fe in the Photosynthetic Apparatus" R.D. Guiles, A.E. McDermott, J.L. Cole, V.K. Yachandra, V.J. DeRose, J.-L. Zimmermann, S.L. Dexheimer, K. Sauer, M.P. Klein 131

957Bp "Anomalous Scattering of X-Rays" D.H. Templeton, L.K. Templeton 133

961B "Structure/Function Studies of Oxidases, Peroxidases and Catalases" B. Chance, L. Powers, S. Khalid, I. Ayene, R. Waterland, T.E. King, G. Bunker, K. Zhang, R. Poyton, E. Davidson 134

969B "X-Ray Absorption Spectroscopic Studies of Nickel Containing Metalloenzymes" A.K. Shiemke, M.K. Eidsness, R.A. Scott 135

981Bp "Mathematical Modeling of Multiple Wave Functions for Iron Porphyrin EXAFS Spectra" J.O. Alben, F.G. Fiamingo, A.A. Croteau, C.F. Hemann, K.A. Powell, V.M. Molleran, S. Park 137

991Bp "Technetium Diphosphonate Imaging Agents and Rhenium Therapeutic Radiopharmaceuticals" R.C. Elder, E. Deutsch 138

993B "A Copper XAS Study of Dopamine β-Hydroxylase" R.A. Scott, R.J. Sullivan, W.E. DeWolf, R.E. Dolle, L.I. Kruse 140

1001B "Biochemistry: Use Made of Beam Line VI-2 in 1986/1987" G.N. George, R.C. Prince 142

1004B "Crystal Structure Determination of Cucumber Basic Protein Using Multiple Energy Anomalous Dispersion Phasing" E.A. Merritt, R.P. Phizackerley, K.O. Hodgson, B. Hedman, H.C. Freeman, J.M. Guss 144

1007B	"Low Temperature Photolysis/Recombination of Hemoproteins Under Conditions of Nuclear Tunneling" B. Chance, G. Bunker, K. Zhang, K.S. Reddy, H. Oyanagi, S. Sligar, B. Springer	145
1030B	"L-Edge Spectroscopy of Molybdenum Compounds and Enzymes" G.N. George, W.E. Cleland J.H. Enemark, B.E. Smith, C.A. Kipke, S. Roberts, S.P. Cramer	145A
1035B	"XAS Investigations of Rieske-Like Iron Sulfur Centers" H.T. Tsang, J.E. Penner-Hahn, C.J. Batie, D.P. Ballou	146
1040B	"EXAFS Analysis of Xanthine Oxidase Complexes with Alloxanthine, Violapterin and 6–Pteridylaldehyde" R. Hille, G.N. George, M.K. Eidsness, S.P. Cramer	148
1046B	"Coronary Angiography in Human Subjects" E. Rubenstein, G.S. Brown, J.C. Giacomini, H.J. Gordon, R. Hofstadter, A.C. Thompson, H.D. Zeman	149
1085Bp	"X-Ray Absorption Spectroscopic Characterization of the Mn in Biological Systems" J.E. Penner-Hahn, V.L. Pecoraro, R.M. Fronko, H.-T. Tsang, C.F. Yocum, S. Betts	150
1087Bp	"Anomalous Diffraction Measurements from Protein Crystals" W.A. Hendrickson, J.R. Horton, C.M. Ogata, W.E. Royer, W. Yang, E.A. Merritt, R.P. Phizackerley	152
8105B	"Crystal Structure Determination of Amicyanin Using Multiple Energy Anomalous Dispersion Phasing" E.A. Merritt, R.P. Phizackerley, L. Lim, F.S. Mathews	153
8110B	"Small Angle X-Ray Scattering Studies on Cation Binding Sites and Linking Regions of Bacteriorhodopsin" S. Wakatsuki, K.O. Hodgson, R.M. Stroud, S. Doniach, U. Spann	154
8110B	"A Study of the Electronic Structure of $S_2O_6^{2-}$ by Polarized K-Edge X-Ray Absorption Spectroscopy" T.A. Tyson, A.L. Roe, B. Hedman, P. Frank, K. Hodgson	156
8110B	"A Multiple Scattering Analysis of the EXAFS Spectrum of SF_6" T.A. Tyson, B. Hedman, K.O. Hodgson	158
8116B	"XANES Spectroscopic Studies of Sulfur within Blood Cells from the Tunicate Ascidia Ceratodes" P. Frank, B. Hedman, R.M. Carlson, K.O. Hodgson	160
8116B	"Sulfur K and Molybdenum L Edge XANES of the Iron-Molybdenum Cofactor from Azotobacter Vinelandii Nitrogenase" B. Hedman, P. Frank, S.F. Gheller, A.L. Roe, W.E. Newton, K.O. Hodgson	162
1A32B	"Crystallography of Ribosomal Particles" A. Yonath, F. Frolow, K vonBoehlen, I. Makowski, H. Hope, C. Kratky, K. Bartels, H.G. Wittmann	164
1A39B	"X-Ray Crystallography of Succinyl-CoA Synthetase from Escherichia coli" W.T. Wolodko, P.M.D. Fitzgerald, M.N.G. James, W.A. Bridger	166
1A56B	"Three-Dimensional Structure of an Oncogene Protein: Catalytic Domain of Human c-H-ras p21" A.M. DeVos, L. Tong, M.V. Milburn, P.M. Matias, J. Jancarik, K. Miura, E. Ohtsuka, S. Noguchi, S. Nishimura, S.-H. Kim	167
1A66B	"Structural Studies of Antibodies, Antigens and Antibody-Antigen Complexes" I.A. Wilson, E.A. Stura, J.A. Arevalo, G. Lambert, J.M. Rini	168
1A69B	"The Crystal Structure of the Enzyme Phosphoribosyl Transferase" S.L. Edwards, J, Kraut, T. Halloran, S.E. Mills	169
1A70B	"Crystallographic Studies of Transmembrane Ion Channels" T. Earnest, M. McCarthy, M. Shuster, J. Earnest, K. Perry, W. Montfort, S. Choe, R. Stroud	170

VUV PROPOSALS

908Vp	"The Bonding of Arsenic and Hydrogen to the Si(111) Surface" R.D. Bringans, M.A. Olmstead	171
935Vp	"Fermi Level Pinning at Sb/GaAs(110) Interface: The Temperature Effects" R. Cao, K. Miyano, T. Kendelewicz, I. Lindau, W.E. Spicer	173
935Vp	"Low Temperature Deposition of Ag and Pd on HgCdTe" G.P. Carey, A.K. Wahi, T.T. Chiang, I. Lindau, W.E. Spicer	175
935Vp	"Ag/GaAs Interface: Reversibility of Fermi Level Pinning" T.T. Chiang, C.J. Spindt, G.P. Carey, A.K. Wahi, I. Lindau, W.E. Spicer	176
935Vp	"Critical Review of Valence Band Offset Measurements" R.S. List, I. Lindau, W.E. Spicer	178
935Vp	"Data Acquisition Software for the New μ-VAX Beam Line Computers" P.H. Mahowald	179
935Vp	"A Substrate Doping Variation Study of the Pinning States at Metal/GaAs(110) Interfaces" K.E. Miyano, R. Cao, T. Kendelewicz, C.J. Spindt, P.H. Mahowald, I. Lindau, W.E. Spicer	180
935Vp	"A Study of the Ag/ZnTe, Al/ZnTe, and Al/CdTe Metal/II-VI(110) Interfaces" A.K. Wahi, G.P. Carey, T. Chiang, I. Lindau, W.E. Spicer	181
941Vp	"Core Level Spectroscopy of Yb-Compounds" I. Abbati, L. Braicovich, M. Sancrotti, E. Puppin, I. Lindau, R. Eggenhoffnerr, A. Landelli, G.L. Olcese, A. Palenzona	182
943Vp	"Observation of Many New Argon Valence Satellites Near Threshold" U. Becker, B. Langer, H.G. Kerkhoff, M. Kupsch, D. Szostak, R. Wehlitz, P.A. Heimann, S.H. Liu, D.W. Lindle, T.A. Ferrett, D.A. Shirley	183
943Vp	"Photoelectron Asymmetry Parameter for the S 2p Level of SO_2" T.A. Ferrett, P.A. Heimann, H.G. Kerkhoff, U. Becker, D.W. Lindle, D.A. Shirley	184
943Vp	"Complete Photoemission Study of the He $1s^2 \rightarrow 3s3p$ Autoionizing Resonance" D.W. Lindle, T.A. Ferrett, P.A. Heimann, D.A. Shirley	185
943Vp	"A Photoemission Study of Kr 3d → Np Autoionization Resonances" D.W. Lindle, P.A. Heimann, T.A. Ferrett, M.N. Piancastelli, D.A. Shirley	186
943Vp	"Lithium 1s Main-Line and Satellite Photoemission: Resonant and Nonresonant Behavior" T.A. Ferrett, D.W. Lindle, P.A. Heimann, W.D. Brewer, U. Becker, H.G. Kerkhoff, D.A. Shirley	187
943Vp	"C(2x2)S/Cr(001) Surface and Near-Surface Structure Determined Using Angle-Resolved Photoemission Extended Fine Structure" L.J. Terminello, X.S. Zhang, Z.Q. Huang, S. Kim, A.E. Schach von Wittenau, D.A. Shirley	188
943Vp	"Chemisorption Structure of c(2x2)S/Fe(001) Determined by ARPEFS" X.S. Zhang, L.J. Terminello, S. Kim, Z.Q. Huang, A.E. Schach von Wittenau, D.A. Shirley	189
947V	"Anisotropic Vibrational Amplitudes of Surface Atoms Studied with SEXAFS" P.H. Citrin, F. Sette, T. Hashizume, F. Comin, A.A. MacDowell	190
963V	"NEXAFS Studies of π-Complex Orientation on Ag(110)" A. Muscat, R.J. Madix, J. Stohr	191

1013Vp	"Sulfur Doped $Al_xGa_{1-x}As$: Microscopic Structure of DX Centers and Compositional Ordering" F. Sette, J.E. Rowe, J.M. Poate, S.J. Pearton	193
1013Vp	"Structure of P Impurities in GaAs" F. Sette, J.E. Rowe, J.M. Poate, S.J. Pearton	194
1022Vp	"Photoelectron Spectroscopic Studies of Metal Ion Sites" K.D. Butcher, S.V. Didziulis, J. Lin, E.I. Solomon	195
1028V	"High-Photon Flux Photoemission Studies in Narrow Band Materials" J.W. Allen, J.-S. Kang, Z.-X. Shen, J.J. Yeh, W. Ellis, M.B. Maple, Y.D. Dalichaouch, B.-W. Lee, M.S. Torikachvili, J.-Z. Sun, I. Lindau	197
1080Vp	"The Orientation of Ring Compounds on Ag(110) by NEXAFS" J.L. Solomon, R.J. Madix, J. Stohr	201
1080Vp	"NEXAFS Studies of Benzene and Benzenethiol on Mo(110)" A.C. Liu, J.T. Roberts, J.R. Swanson, C.M. Friend	203
8000V	"Structural Studies of Schottky Barrier Formation by Means of Partial Photoionization Cross Section and the Asymmetry Parameter: Ag/Si(111)" M. Ardehali, I. Lindau	204
8000V	"Photoemission Study of the Electronic Structure and Magnetic Interaction of High T_c" Z.-X. Shen	205
8104V	"The Effect of Strain on the Band Structure of $In_xGa_{1-x}As$" J. Hwang, P. Pianetta, G.D. Kubiak, R.H. Stulen, C.K. Shih, Y.-C. Pao, Z.X. Shen, P. Lindberg, B. Chow	206
8104V	"First Images from Photoelectron Microscope" P. Pianetta, I. Lindau, P. King, M. Keenlyside, G. Knapp, R. Browning	208
8104V	"A Kinetic Model of Crosslinking in Chemically Amplified Resists" D. Seligson, P. Pianetta, P. King, L. Pan	210
8104V	"X-Ray Absorption Studies Performed at the Silicon K-Edge" J.C. Woicik, B.B. Pate, P. Pianetta	211
9900V	"(1x1)Co/Cu(001) Surface Geometry Determined from Co 1s Photoelectron Diffraction" Z.Q. Huang, L.J. Terminello, L.Q. Wang, Z. Hussain, X.S. Zhang, S. Kim, L. Huckabee, D.A. Shirley, J. Woicik, P. Pianetta	213
9901V	"Sub-KeV Near-Threshold Resonances in Photoabsorption" N.K. Del Grande, K.G. Tirsell	214
9901V	"Optically Detected Absorption in the Soft X-Ray Region" M.J. Weber, M.B. Schneider, K.G. Tirsell	215
9901V	"Resonant Photoemission Study of the NiGa Intermetallic Compound" L. Hsu, R.S. Williams, D. Outka	216
1L05V	"Synchrotron Based Studies of X-Ray Induced Photoconductivity" D.R. Kania, L. Pan, P. Bell, P. Pianetta, J. Trebes, H. Kornblum	217
1L09V	"Radiation Damage in X-Ray Lithography Masks" P.L. King, L. Pan, P. Pianetta, A. Shimkunas, P. Mauger, D. Seligson	218

Materials Proposals

X-RAY ABSORPTION STUDIES OF DISORDERED SYSTEMS

E.D. Crozier, N. Alberding, K.R. Bauchspiess, D. Jiang, A.J Seary
Physics Department, Simon Fraser University
Burnaby, B.C., Canada V5A 1S6

R. Ingalls, J. Freund and B. Houser
Physics Department, University of Washington
Seattle, Wash., 98195, U.S.A.

HIGH T_c SUPERCONDUCTORS

During this reporting period, we initiated an x-ray absorption study of $YBa_2Cu_3O_{7-\delta}$ to examine the valence of Cu and changes in the local structure with temperature and pressure. Two papers were published on the work[1,2] and a third submitted.[3]

Three important results have emerged from the studies: 1) Cu Valence Early speculations suggested that a dynamic fluctuation between Cu^{2+} and Cu^{3+} valence states would enhance the Cu-O breathing modes, increase the electron-phonon interaction and therby contribute to the high T_c. Others suggested that a static partitioning of Cu^{2+} and Cu^{3+} ions between the two different Cu sites in the crystal would produce the same effect. Of particular interest in x-ray absorption spectroscopy is the peak at ~9002 eV in the Cu K-edge XANES, which some have attributed to the presence of Cu^{3+}. In measurements at pressures up to 70 kbar at temperatures below and above T_c we find that the features at ~9002 and ~9010 eV shift to higher energies with increasing pressure in a manner consistent with compression of bonds (Fig.1). We conclude[1,3] that the XANES does not provide evidence for the existence of Cu^{3+} in $YBa_2Cu_3O_{7-\delta}$.

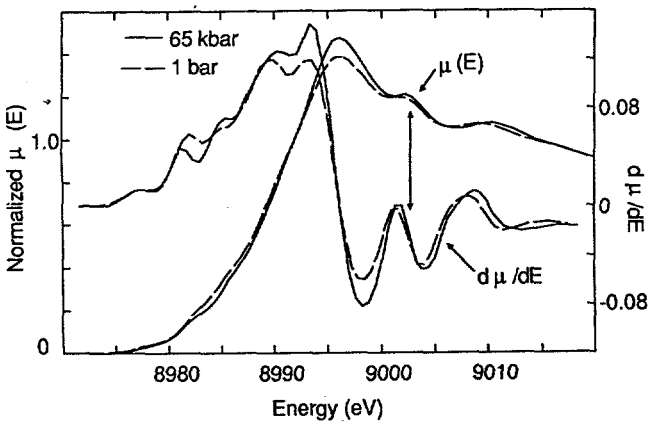

2) Structural changes at low temperatures The most striking feature of the temperature study at 1 bar is the anomalous dependence of the EXAFS mean square relative displacements $\Delta\sigma^2$ shown in Fig. 2. It occurs in all the interatomic pairs that we analyzed: Cu-Ba (long dash), Cu-Y (solid), Cu-O-Cu multiple scattering (dash-dot), and Cu-O (short dash), Y-Y (solid), Y-O (short dash), Y-Ba(long dash), and Y-Cu(dash dot); yet there are no detectable changes in the interatomic distances within ± 0.02 Å. The normal behaviour of $\Delta\sigma^2$ is shown by the dotted lines which represent an Einstein model fit to Cu-Y and Y-O using the 80- and 297-K points. The most obvious interpretation of the anomalous behaviour is that some softening of the bond strengths occurs near 170 K which may involve a subtle structural change.[1,2] This is consistent with recent Raman studies which reveal a softening of a Cu-O mode at the same temperature.

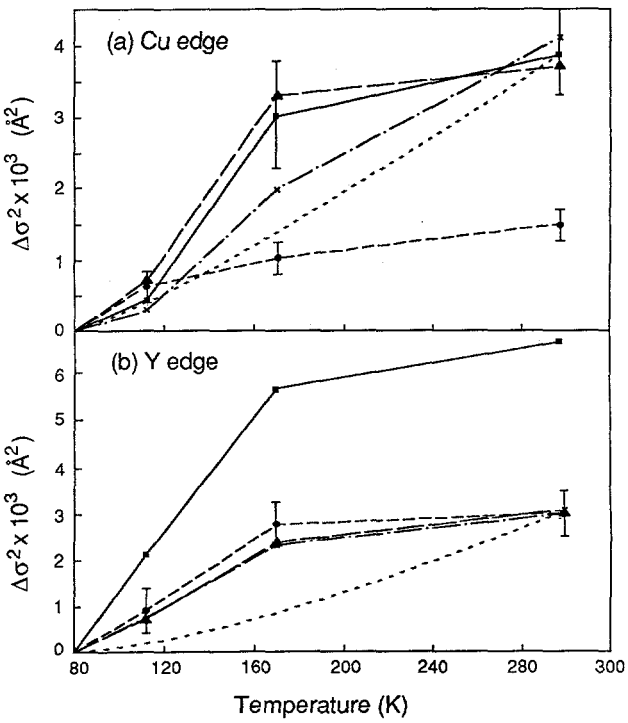

3) Structural changes at high pressures The Fourier transforms of the EXAFS interference function for the Cu K-edge are shown in Fig. 3. for 1 bar and 65.5 kbar.

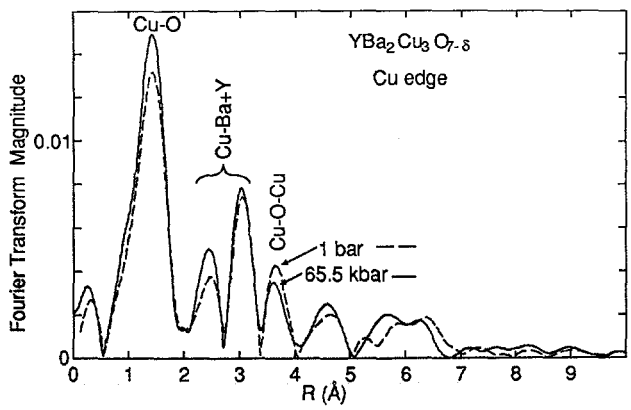

The amplitudes of the Cu-O, Cu-Ba and Cu-Y peaks behave with pressure in the normal way, increasing as the mean square relative displacements, σ^2, decrease with compressibility. The decrease of the height of the Cu-O-Cu peak with pressure is anomalous. At 1 bar the peak is complicated by multiple-scattering contributionsfrom the intervening O atoms in the linear Cu-O-Cu chains and the Cu-O-Cu bonds along the c-axis. The decrease in peak height indicates either an unexpectedly large compression of the c-axis or a bending of the chains. In the latter case, detailed analysis of the multiple scattering indicates that the chains begin to buckle near 20 kbar. This is important to understanding the role that the "one dimensional" chains play in the mechanism for superconductivity. There is general agreement from other studies that T_c increases with pressure in orthorhombic samples of $YBa_2Cu_3O_{7-\delta}$. It thus appears that the buckling of the linear chains does not affect T_c in a serious way.[3]

SURFACES

Obtaining quantitative details of the structure of interfacial regions is a difficult experimental problem, yet of fundamantal interest. It is of particular importance in device physics applications where frequently the interface of interest is buried beneath a passivating layer. In artificially structured materials, prepared by Molecular Beam Epitaxy, x-ray scattering at glancing incidence can be used to examine the surface of thick layers, but for thin layers interpretation is complicated by contributions from the different crystalline layers on either side of the interface. More standard surface techniques, such as LEED and RHEED, probe the surface, but cannot specify completely the three-dimensional structure and cannot provide the structure of buried interfaces. However, with the glancing-angle EXAFS technique the depth or interface can be selected by simply choosing the correct angle of incidence.

We report further results for Ni epitaxially grown on the (100) face of Fe single crystals. The work is being done in conjunction with B. Heinrich, SFU, who has conducted extensive studies of the growth, structure and magnetic properties of the system.[4] It is of interest because the Ni overlayer is ferromagnetic. It is part of a larger study of the possibility of producing superpermanent magnetic materials based upon the large surface magnetic anisotropy of epitaxially grown films.[5] The basic question is how does the crystal structure affect the magnetic anisotropy. It is known that the first 6 layers of Ni grown on Fe(100) have the bcc symmetry of the substrate. When additional layers are grown, their structure is neither bcc nor the normal fcc structure of Ni, but they do exhibit large cubic magnetic anisotropy. Neither LEED nor RHEED have been able to determine the structure. Our initial glancing incidence EXAFS studies were conducted with 50 Å of epitaxially grown Ni and with the sample maintained in nitrogen gas. Definitive results were prevented by nickel oxide contamination. To prevent oxidation, 60 Å of Al were deposited at 150 K in the MBE machine on two samples grown epitaxially with 6 monolayers and 37 monolayers of Ni. From ferromagnetic resonance measurements the sandwiches have similar ferromagnetic behaviour to Ni on Fe. Our Ni K-edge XANES results, at glancing incidence, are shown in Fig. 4 for the $\underline{E}$ vector of the incident x-ray beam parallel to the surface. Both the 6 and 37 monolayer films are significantly different from bulk Ni metal. The differences apparent between the 6 and 37 monolayers are also evident in the EXAFS. Further analysis is in progress.

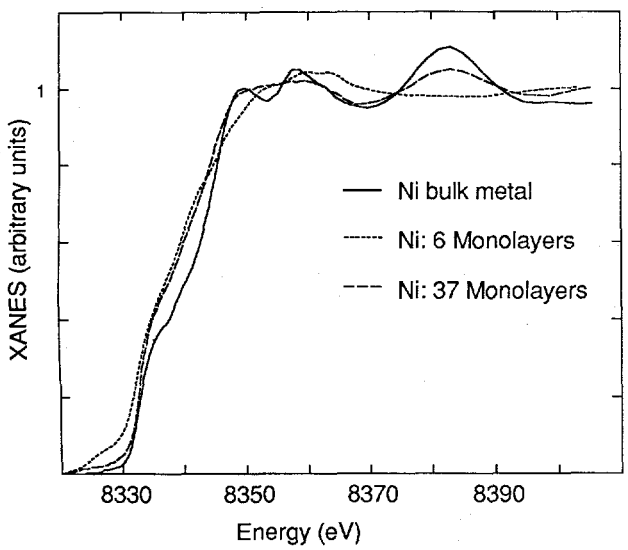

We have also obtained preliminary results for the Hg L_{III}-edge at the $Si/Hg_xCd_{1-x}Te$ interface. This work is being done in conjunction with J. Dubowski, National Research Council, Canada, who pulse-laser evaporated the Si onto the HgCdTe single crystals in an MBE machine. More data will be acquired during the next run. The details of our glancing-incidence EXAFS apparatus have been published.[6]

1. E.D. Crozier, N. Alberding, K.R. Bauchspiess, A.J. Seary and S. Gygax, Phys. Rev. B 36 (1987) 8288.
2. S.Gygax, E.D. Crozier, N. Alberding, K.R. Bauchspiess and A.J. Seary, Proceedings of the Eighteenth International Conference on Low Temperature Physics, Jpn. J. Appl. Phys. 26 (1987) 1051.
3. E.D. Crozier, N. Alberding, K.R. Bauchspiess, S. Gygax, A.J Seary, R. Ingalls and B. Houser (submitted).
4. B. Heinrich, A.S. Arrott, J.F. Cochran, S.T.Purcell, K.B. Urquhart, N.Alberding, and C. Liu, in Thin Film Growth Techniques for Low-Dimensional Structures, eds. R.F.C. Farrow, S.S.P. Parkin, P.J.
5. B. Heinrich, K.B. Urquhart, A.S. Arrott, J.F. Cochran, K. Myrtle, and S.T Purcell, Phys. Rev. Lett. 59 (1987) 1756.
6. D.Jiang, N. Alberding, A.J.Seary, and E.D. Crozier, Rev. Sci Instrum. (Feb. 1988).

TEMPERATURE DEPENDENCE STUDY OF MONOLAYERS AND MULTILAYERS OF THE LANGMUIR-BLODGETT TYPE

W. B. Yun, J. M. Bloch, X. Yang and J. Viccaro

Argonne National Laboratory

9700 S. Cass Avenue, Argoone, IL 60439

INTRODUCTION :

We have extended our previous x-ray studies of Cd-Stearate and Mn-Stearate monolayers and multilayers to investigate the effect of temperature variation on the in-plane structure of the layers and the stacking correlation between the layers. In this work, we have re-examined a previously reported trigonal structure for a monolayer, which did not provide a consistent picture for the in-plane orthorhombic structure observed for 2, 3 and more layers.

RESULTS AND DISCUSSIONS :

A) A Cd-Stearate Monolayer Sample

At room temperature, two diffraction peaks A and B (see Fig.1) were observed. The A peak has been observed priviously by one of us and collabrators on a similar sample (NSLS report 1986, Thin Film Gordon conference - Santa Barbara 1986). The B peak indicates that the structure is not trigonal, as was previously reported from electron diffraction experiments. However the ratio betwen the diffraction intensities of the two diffraction peaks also precludes the interpretation of a simple orthorhombic structure. In the temperature dependence study, it was found that the A peak, which corresponds with the multilayer [11] orthorhombic peak, was practically temperature independent, in both peak position q and linewidth. In contrast the B peak, which corresponds with the multilayer [02] orthorhombic peak, moved away from the [11] peak when the temperature was lowered down to -40 degree C. At temperatures elevated slightly above room temperature the [02] peak position first moved toward the [11] peak and its intensity decreased. At about 35 degrees C the peak disappeared completely. It reappeared when the temperature was lowered again. In the temperature range investigated, the ratio of the B peak intensity to that of the A peak was consistantly lower than what one would expect from a regular orthorhombic structure even at the lowest temperature of the experiment. In order to explain the results, a model of random orthorohmbic structure is proposed.

B) A 15 Layer Cd-Stearate Sample

At room temperature, results similar to those reported by us earlier (NSLS report 1986) were obtained and interpreted as an in-plane orthorhombic structure. Upon cooling, the [020] in-plane peak position, originating with the orthorhombic unit cell, moved towards larger q values, while the [110] in-plane peak position remained unchanged. The shift of the [020] peak position toward larger q values indicates an increase in the orthorhombic distortion away from the trigonal structure at lower temperatures. The effect of temperature variation on the stacking correlation between layers was investigated with scans made along $[11Q_z]$ and $[02Q_z]$ directions with different history of thermal conditions. The results show that the stacking correlation remained unchanged when the sample was cooled down to -40 degree C and the sample exhibited a 3D structure. When the sample was warmed back to room temperature, the stacking correlation in the $[02Q_z]$ was lost. In further temperature cyclings between room temperature and -90 degree C, no further change in the stacking correlation was observed. This indicates that the sample had changed to a new struture after the first temperature cycling and the new structure is thermodynamcally more stable than that originally acquired by the sample at preparation. The new structure has a repeat distance larger than that of the original sample, indicating that the temperature cycling had made the chains perhaps straighter than that in the original sample. The new structure has good stacking correlation along the [11L] direction but poor stacking correlation along the [02L] direction, and is reminiscent of a "one dimensional" Smectic B material.

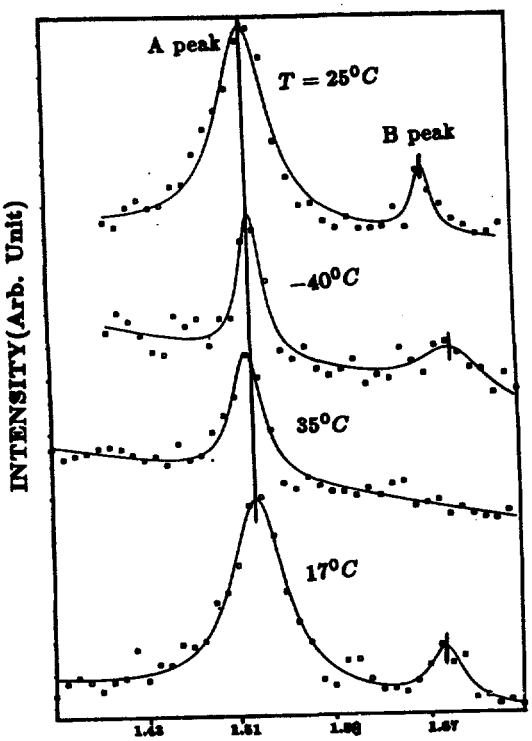

Fig.1 Selected scans from a Cd-stearate monolayer at differnt temperatures. Circles are experimental data and the solid line presents a fit of the corresponding data with two Lorentzians.

ACKNOWLEDGEMENTS:

This work was supported by the U. S. Department of energy, BES-Material Science, under contract W-31-109-ENG-38. Part of this work was performed at SSRL. The support and services provided by SSRL staff are greatly appreciated.

EXAFS STUDIES OF HIGH T_c SUPERCONDUCTORS

J. B. Boyce
Xerox Palo Alto Research Center, Palo Alto, CA 94304, U.S.A

F. Bridges
Physics Department, University of California, Santa Cruz, Santa Cruz, CA 95059, U.S.A

T. Claeson
Physics Department, Chalmers University of Technology, 41296 Gothenburg, Sweden

T. H. Geballe
Department of Applied Physics, Stanford University, Stanford, CA 94305, U.S.A

C. W. Chu
Department Physics, University of Houston, Houston, TX 77009, U.S.A.

J. M. Tarascon
Bell Communications Research, Red Bank, NJ 07701, U.S.A.

INTRODUCTION

The spectacular breakthrough in the field of superconductivity has strongly affected the work of this proposal. The original intent was to study the local structure and vibrations of the superconducting record holders as of the time when the investigation started, i.e., the A15 superconductors. A strongly temperature-dependent electron-phonon coupling, coupled to a two-well potential, had been suggested. One of the motivations of the work was to study the temperature-dependent broadening of the pair distribution function as studied by the Extended X-Ray Absorption Fine Structure, and in particular to compare the information obtained from Nb_3Sn and Nb_3Sb, which have high and low superconducting T_c's, respectively.

However, the appearance of the new class of high T_c superconductors based on copper oxides motivated a shift of attention to these truly high T_c superconductors. The EXAFS method is well suited for the determination of the local structure, local distortions, etc. The structures of the new superconductors were determined at the same time as our EXAFS data was analyzed, and our results could be compared with diffraction-based models.

RESULTS: A15 SUPERCONDUCTORS

EXAFS measurements at the Sn and Sb K-edges were made on Nb_3Sn, Nb_3Sb, and $Nb_3Sn_{1-x}Sb_x$ alloys. No temperature-dependent anomalies were noted within a large temperature range, from 4 K up to room temperature for the alloys and up to above 600 K for the endpoint compounds. The temperature dependence of the broadenings of the Sn-Nb and Sb-Nb distances fit an Einstein oscillator model, with Einstein temperatures of 237 and 254 K for Sn-Nb and Sb-Nb, respectively. The results agreed with calculations by Weger. A localized vibration behavior in the ternary alloys was indicated by the fact that the Debye-Waller-type broadenings in the Sn-Nb and Sb-Nb distances for a particular alloy are not equal to one another, but rather nearly equal those of the binary endpoint compounds.

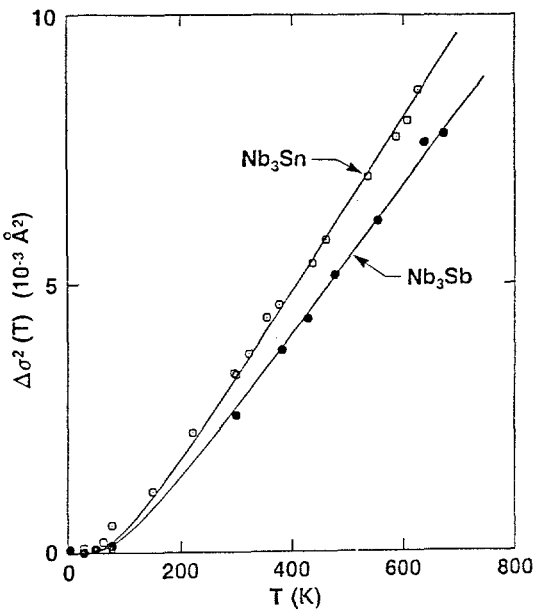

FIG. 1 The Debye-Waller-type broadening $\Delta\sigma^2(T) = \sigma^2(T)-\sigma^2(4.2\ K)$ of the nearest neighbor distances in Nb_3Sn and Nb_3Sb. The solid lines are fits to the data using an Einstein oscillator model with characteristic temperatures of 237 K for Nb_3Sn and 254 K for Nb_3Sb.

RESULTS: DOPED La-Cu-O SUPERCONDUCTORS

No structural transitions that alter the valence or the near-neighbor environment by > 0.01 Å could be detected between 4 and 300 K in $La_{1.8}Sr_{0.2}Cu0_4$ or $La_{1.8}Ba_{0.2}Cu0_4$. Two different Cu-O distances could be distinguished in both compounds. Their values and thermal expansions agree with diffraction results. The doping with Sr and Ba primarily changed the Cu-O distance and width along the c-axis.

The temperature-dependence of the Debye-Waller-like broadening of the two Cu-O distances was used to extract information on the Cu-O vibrational frequencies, the so-called breathing modes of this structure. For the Sr-doped compound, we found an Einstein oscillator temperature of 610±80 K for the Cu-0(1) mode (in the Cu-0 planes), and 500±100 K for the Cu-0 (2) band (perpendicular to the plane, i.e., along the c-axis). Using these vibrational frequencies, it is barely possible to obtain the 40 K superconducting T_c for La-Sr-Cu-O using an electron-phonon coupling mechanism.

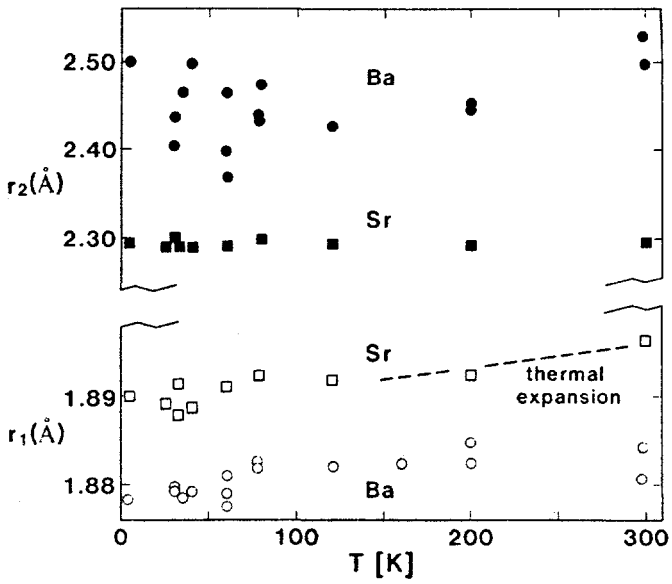

FIG. 2 The Cu-O first neighbor distances as a function of temperature for Ba- and Sr-doped La_2Cu0_4. Two distances to four 0(1) atoms in the basal plane (r_1) and to two 0(2) atoms along the c-axis (r_2) can be distinguished.

ACKNOWLEDGMENTS

The experiments were performed at Stanford Synchrotron Radiation Laboratory, which is supported by the U.S. Department of Energy, Office of Basic Sciences and the National Institutes of Health, Biotechnology Division. Support was also given by the Swedish National Science Research Council and by NSF Grant DMR 85-05549.

INVESTIGATION OF THE α-Fe $\rightleftharpoons$ ϵ-Fe TRANSITION USING SYNCHROTRON RADIATION

M. H. Manghnani, L. C. Ming, Y. H. Kim, and N. Nakagiri
Hawaii Institute of Geophysics, University of Hawaii, Honolulu, HI 96822, USA

INTRODUCTION

Iron is the most important constituent in the Earth's core. Knowledge concerning the phase transitions in iron is essential for understanding the properties of the Earth's core. Fe is stable in the body-centered-cubic (bcc) structure (α-Fe) at ambient conditions and transforms into a hexagonal-closed-packing (hcp) structure (ϵ-Fe) at $\sim$ 13 GPa at room temperature. The $\alpha \rightarrow \epsilon$ transition is displacive and is accomplished through the the distortion in the bcc lattice[1]. This transition is also known to be very sluggish and to exhibit appreciable hysteresis. Thus somewhat inconsistent values for the dP/dT slope of the phase boundary have been reported. The purpose of the present study is to investigate the nature of the $\alpha \rightleftharpoons \epsilon$ transition under simultaneously high pressure and temperature (to 27.5 GPa and 540°C) using a resistively heated diamond-anvil cell and energy-dispersive X-ray diffraction system (EDXRD) interfaced with synchrotron radiation at the Stanford Synchrotron Radiation Laboratory (SSRL).

RESULTS AND DISCUSSION

Figure 1 shows five isothermal runs at 190°C, 270°C, 360°C, 450°C and 540°C and the phase(s) observed at each data point. Because of the hysteresis, four stages are observed in the complete cycle of the forward ($\alpha \rightarrow \epsilon$) and backward ($\epsilon \rightarrow \alpha$) transitions: (1) the start of $\alpha \rightarrow \epsilon$, (2) the completion of $\alpha \rightarrow \epsilon$, (3) the start of $\epsilon \rightarrow \alpha$, and (4) the completion of $\epsilon \rightarrow \alpha$. These stages (i.e., 1 and 2 in the increasing pressure cycle and 3 and 4 in the decreasing pressure cycle) are characterized, respectively, by the appearance of the ϵ phase, disappearance of the α phase, the reappearance of the α phase, and the disappearance of the ϵ phase. The transition pressure for each stage at a certain temperature is evaluated on the basis of the diffraction peak intensity data for both the α and the ϵ phases[2]. The transition pressures thus evaluated for ϵ-in and α-in are, respectively, given by:

$$P(GPa) = 9.57 - 0.0032T(°C) \quad (1)$$

$$P(GPa) = 8.50 - 0.0016T(°C) \quad (2)$$

The equilibrium transition pressure (P_e) in such a transition is considered to be between the stages (1) and (3), and is approximately the average of $P^s_{\alpha\rightarrow\epsilon}$ (i.e., the pressure at which $\alpha \rightarrow \epsilon$ starts) and $P^s_{\epsilon\rightarrow\alpha}$ (the pressure at which $\epsilon \rightarrow \alpha$ starts). Taking the average of eqs. (1) and (2) above, we have:

$$P_e(GPa) = 9.03 - 0.0023T(°C) \quad (3)$$

Various investigations of the $\alpha \rightleftharpoons \epsilon$ transition in Fe have shown that 1) the value of dP/dT slope ranges from +0.002 to -0.006 GPa/deg; 2) the equilibrium phase boundary for this transition is not sensitive to temperature; and 3) except for Akimoto et al.[3], all other experimental data have yielded a negative slope. However, in view of the hysteresis and the sluggish nature of this transition in each study, as well as the limited data (including the three recent synchrotron radiation studies[2-4]), the value of the slope for this transition is tentative. The large discrepancy in the P_0, the transition pressure at room temperature, found amongst the three most recent determinations[2-4], is probably caused by the different samples used (e.g., levels of various impurities, degree of preferred orientation, dislocations and grain size) and to some extent, by the different apparatus employed (e.g., diamond-anvil cell versus cubic anvil press). It is obvious that more detailed experiments are needed for establishing the phase boundary of the $\alpha \rightleftharpoons \epsilon$ transition in Fe.

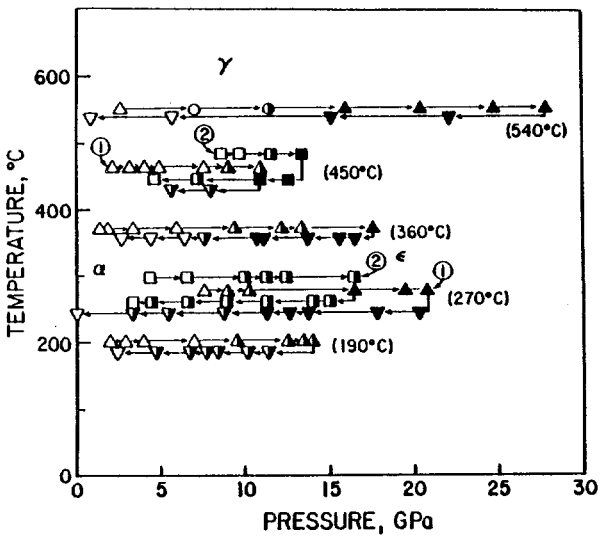

Figure 1. Isothermal runs for the $\alpha \rightleftharpoons \epsilon$ transition in Fe at five temperatures (at 190, 270, 360, 450 and 540°C). The upright and inverted triangles represent the data for increasing and decreasing pressure cycles, respectively, and the arrows indicate the experimental sequence.

ACKNOWLEDGMENT

This research was supported by the National Science Foundation grants EAR84-18125 and EAR87-08482. Thanks are due the staff of the Stanford Synchrotron Radiation Laboratory for facilitating our work.

REFERENCES

1. Mao, H. K., W. A. Bassett and T. Takahashi,, *J. Appl. Phys.*, 38, 272-276, (1967).
2. Manghnani, M. H., L. C. Ming and N. Nakagiri, *in High-Pressure Research in Mineral Physics*, Terrapub/AGU, 155-163, (1987).
3. Akimoto, S., T. Yagi, T. Suzuki and O. Shimomura, *in High-Pressure Research in Mineral Physics*, Terrapub/AGU, 149-154, (1987).
4. Huang, E., W.A. Bassett and P. Tao, *in High-Pressure Research in Mineral Physics*, Terrapub/AGU, 165-172, (1987).

ANOMALOUS X-RAY DIFFRACTION STUDIES OF BIMETALLIC CATALYSTS : Pt-Re on SiO_2

Proposal No. 940M

K. S. Liang, G. J. Hughes and J. H. Sinfelt
Exxon Research and Engineering Co.
Route 22 E, Clinton Township
Annandale, NJ 08801

The formation of bimetallic clusters of immiscible binary alloys has major impacts in industrial catalysis, in particular in the production of aromatic hydrocarbons for automotive fuels. It is generally believed that these clusters are inhomogeneous due to segregation of one constituent to the surface of the small particles. However, to obtain a more precise description of the cluster structure is often a formidable task. In this work, we have employed differential anomalous x-ray diffraction (DAXD) technique to study model Pt-Re bimetallic catalysts. The x-ray measurements were performed on the wiggler station IV-3.

The use of DAXD technique to obtain the diffraction patterns from supported catalytic particles has been demonstrated previously on supported Pt catalysts.[1] The technique provides the capability of atom-type selectivity, as in EXAFS, but emphasizes the low-q part of the interference function. This function contains the essential structural information and can be modeled directly with an assumed structure using the Debye equation.

The catalysts used in this study contain 2.5, 5.0 and 10.0 wt.% of Pt and Re in a one-to-one weight ratio supported on silica as prepared by a usual coimpregnation procedure. Diffraction patterns were collected using x-rays with energies 10 and 100 eV below the absorption maxima (white lines) at the L_{III} edges of Pt (~11564 eV) and Re (~10535eV). The differential diffraction patterns (DDP's)at both edges were obtained after proper normalization of the measured intensities.

Figure 1 compares the Pt-edge DDP's of two catalysts: one with 2.5 wt.% Pt on SiO_2 and the other with 2.5 wt.% Pt and 2.5 wt.% Re on SiO_2. From the widths of the Bragg peaks, one notices that the sizes of Pt particles are substantially reduced (from ~150Å to ~20Å) by the incorporation of Re, indicating the interactions between these two metals. The observed DDP can be modeled very well as small fcc particles (Fig. 1c).

Knowing that in the bulk phase, Pt is fcc and Re is hcp, it is interesting to see that the Re-edge DDP's reveal both fcc and hcp forms (Fig. 2). One plausible explanation is that in the bimetallic particles the fcc Re could be formed due to epitaxy with Pt. To our knowledge, fcc Re has not been reported.

In short, we demonstrate the use of DAXD technique to reveal novel structural features of Pt-Re bimetallic catalysts. The results are succesfully interpreted by direct structural modeling of the measured intensities.

REFERENCE
1. K. S. Liang, S. S. Laderman and J. H. Sinfelt, J. Chem. Phys. 86, 2352 (1987).

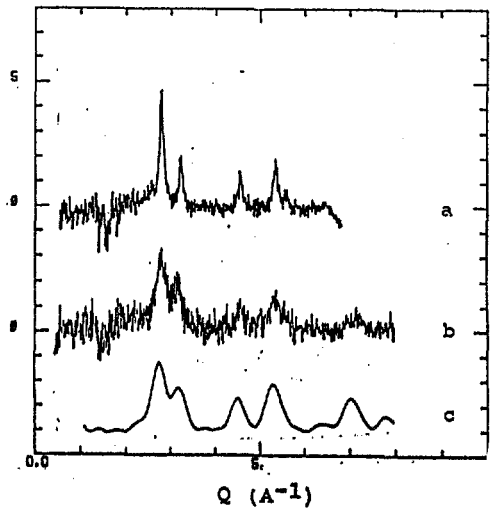

Fig. 1 The differential intensity near Pt L_{III} edge of (a) 2.5 wt.% Pt on SiO_2, (b) 2.5 wt.% Pt-Re on SiO_2, and (c) calculated pattern of 15Å particle of fcc Pt.

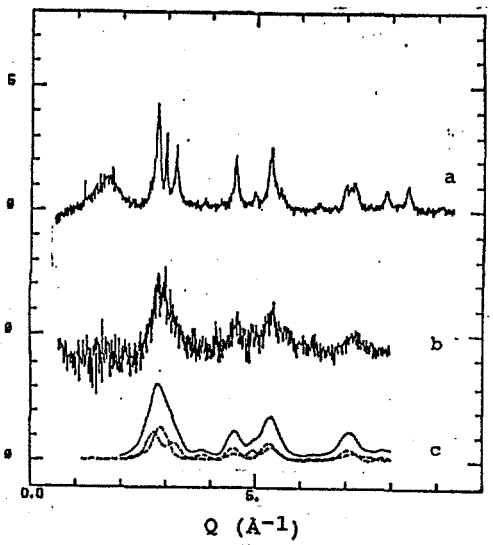

Fig. 2 The differential intensity near Re L_{III} edge of (a) 10 wt.% Pt-Re on SiO_2, (b) 2.5 wt.% Pt-Re on SiO_2, and (c) calculated pattern of mixed fcc and hcp Re particle.

TRANSFORMATION OF Ca AND K CATALYTIC SPECIES IN LIGNITE DURING PYROLYSIS AND GASIFICATION: AN *IN-SITU* EXAFS INVESTIGATION

Frank E. Huggins, Naresh Shah, Gerald P. Huffman,
University of Kentucky, Lexington, KY 40506,

Farrel W. Lytle, Robert B. Greegor,
The Boeing Company, Seattle, WA 98124,
and
Robert G. Jenkins,
The Pennsylvania State University, University Park, PA 16802.

INTRODUCTION

The conversion of coal chars to a gaseous product is known to be considerably easier and faster with lignites than with higher-rank bituminous coals (1). For the most part, this difference is attributed to naturally-occurring, carboxyl-bound alkali and alkaline-earth cations that are highly dispersed throughout the lignite carbonaceous entities (macerals). Such species, which are not present in bituminous coals, catalyze the lignite gasification reactions. Furthermore, it has been found that the activity of these species can be enhanced by a low-severity pyrolysis pretreatment (2).

In this report, we describe how the transformations of calcium and potassium catalytic species in lignites can be investigated using in-situ EXAFS techniques.

EXPERIMENTAL

The hot-cell for in-situ EXAFS experiments (3) consists of a ceramic (boron nitride) disk, which contains a tungsten electrical heating element, inside a stainless steel housing. The coal or char samples are pressed into 1" diameter wafers using, if necessary, a minimum amount of epoxy (<20 wt%) to ensure coherency of the sample wafer. The sample wafer is placed between two stainless gaskets next to the ceramic heating element. Both the gaskets and the heating element contain 3.0x0.6 cm slit windows so that the synchrotron X-ray beam reaching the sample is minimally attenuated. This feature enables relatively low energy X-rays (~2.5-3.0 keV) to be successfully used with the cell. The cell is equipped with an inlet and outlet for gases so that either a reactive or an inert atmosphere can be maintained in the cell. Temperatures are measured with a chromel-alumel thermocouple and temperatures are controlled by varying the power to the electrical heating element with variable voltage transformers. Temperatures as high as 600°C have been recorded in the hot-cell. The hot-cell is placed in a gas-tight aluminum housing, which has both an entrance and exit slit windows covered with thin mylar for the X-ray beam. The hot-cell and its housing are then inserted in a modified Stern-Heald type fluorescent X-ray detector. For EXAFS experiments on Ca and K, helium was used as the detector gas.

Samples in the hot-cell were usually first subjected to pyrolysis under helium up to about 500°C before gasification was initiated by introducing a 90%He/10%O_2 gas mixture to the hot-cell. During pyrolysis or gasification, EXAFS spectra were recorded in fluorescent mode from about 100ev below the Ca or K edge to about 500ev above the edge at typically 15 minute intervals. Spectra were generally recorded at constant temperature (within about ±5°C) during the hot-cell experiments; however, temperatures would typically rise 50°C upon the commencement of gasification due to the exothermic nature of the reaction with oxygen.

RESULTS AND DISCUSSION

Figure 1 shows a sequence of XANES spectra at different temperatures for a Ca-loaded lignite. As seen from this figure, the XANES spectra do not change greatly either during pyrolysis in helium or during gasification in 90%He/10%O_2. There is some broadening of the main XANES peaks and the small pre-edge feature at -2.0eV becomes better defined, but no new peaks occur. Analysis of the EXAFS structure shows the presence in the Fourier transform of one major peak that derives from the shell of nearest neighbor oxygen anions around the Ca cation. With increasing temperature, the Ca-O distance derived from this peak decreases from 2.39Å to 2.32Å. This behavior, which was noted in all samples measured, is inconsistent with expected behavior due to thermal expansion. Furthermore, the changes noted above are partially reversible upon cooling the sample to room temperature. It seems reasonable to conclude, therefore, that a major phase change has not occurred but rather that some relatively subtle change has taken place with the Ca-carboxyl site. Reduction of the average coordination by oxygen around calcium due to devolatilization of H_2O, CO_2, CO, or other molecular species from near the Ca-site would lead to a reduced Ca-O bond distance and would be consistent with all the minor spectral changes.

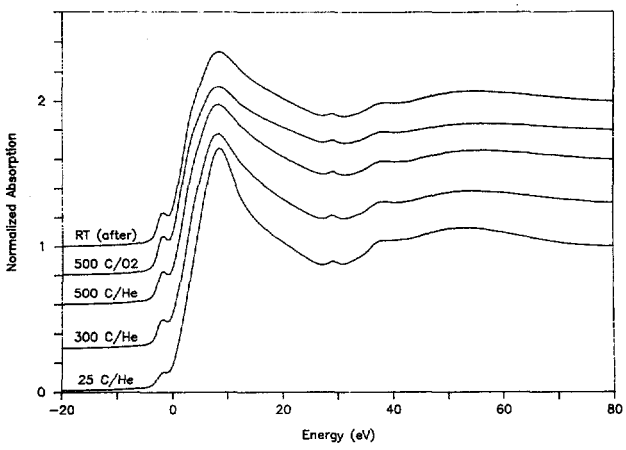

Fig. 1: XANES spectra of Ca-loaded lignite measured under conditions indicated.

For K-loaded lignite samples, the EXAFS regions could not be analyzed due to a major glitch found in all spectra. However, the changes noted in the XANES region were relatively minor until gasification was initiated at about 600°C (Figure 2). At that point, the XANES spectrum undergoes a major change as the main peak splits into two peaks with a separation of about 8eV. This change becomes more apparent upon quenching the sample to room temperature. In this case, it appears that the K-carboxyl sites have transformed and coalesced into a new phase. On the basis of the XANES spectrum alone, the doublet structure and peak positions are similar to that exhibited by K_2CO_3. Further, TGA of potassium benzoate (an analogue compound for the carboxyl-bound potassium in lignite) followed by XRD of the residue confirms that K_2CO_3 can be formed from carboxyl-bound potassium at about 600°C.

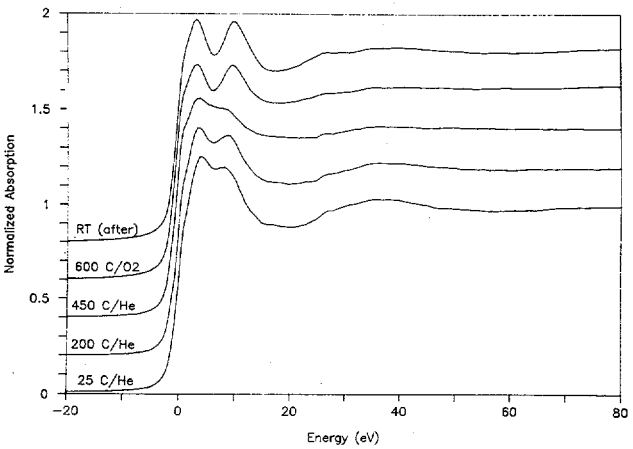

Fig. 2: XANES spectra of K-loaded lignite char measured under conditions indicated.

CONCLUSIONS

This research demonstrates that EXAFS techniques for in-situ investigation of low atomic number elements such as K and Ca can be successfully performed to temperatures of at least 600°C under helium-rich atmospheres. With this technique, we have been able to document the behavior and transformations of noncrystalline, highly dispersed Ca and K catalytic species in chars during pyrolysis and gasification. Based upon the observation of reduced metal-oxygen distances with increasing temperature, it appears that these catalytic species in the chars are activated during pyrolysis by the loss of one or more oxygen atoms from the immediate coordination sphere around the alkali or alkaline-earth ion as a result of devolatilization of small molecules such as H_2O, CO_2, CO, etc. However, whereas the activated Ca species remains little changed upon switching from the inert pyrolysis atmosphere to O_2 gasification, the activated K species rapidly transforms into bulk potassium carbonate upon exposure to O_2 gasification conditions.

Further details of this investigation are being published elsewhere (4,5,6).

ACKNOWLEDGEMENTS

The research described herein is sponsored by the Gas Research Institute, Chicago, Illinois, under Research Contract No. 5084-260-1025.

REFERENCES

1. E.J. Hippo, R.G. Jenkins, and P.L. Walker, Jr. Fuel 58 338-334 (1979).
2. L.R. Radovic, P.L. Walker, Jr., and R.G. Jenkins, Fuel 62 209-212 (1983).
3. Available from The EXAFS Company, Seattle, WA 98168.
4. F.E. Huggins, N. Shah, G.P. Huffman, R.G. Jenkins, F.W. Lytle and R.B. Greegor, 1987 Intern. Conf. Coal Science (Maastricht, The Netherlands), 563-566, (1987).
5. F.E. Huggins, G.P. Huffman, N. Shah, R.G. Jenkins, F.W. Lytle and R.B. Greegor, to be published in Fuel, 67 (1988).
6. F.E. Huggins, N. Shah, G.P. Huffman, F.W. Lytle, R.B. Greegor and R.G. Jenkins, submitted to Fuel.

EXAFS Studies of Organic Sulfur in Coal

Proposal No. 956Mp

G. P. Huffman, N. Shah, and F. E. Huggins
University of Kentucky, 233 Mining and Mineral Resources Bldg.
Lexington, KY 40506-0107
R. B. Greegor and F. W. Lytle
The Boeing Company, Seattle, WA

Introduction

Despite extensive investigation, definitive methods for determining the molecular structure of organic sulfur in coal and coal derivatives have not previously been developed. Moreover, most of the methods that have been used are destructive, requiring pyrolysis, dissolution, or chemical reaction of the sample. Recent measurements[1-3] indicate that EXAFS may be an excellent method of investigating organically bound sulfur.

Experimental

The experiments were carried out during a dedicated run on beam-line VII-3 using a Si(111) monochromator and a fluorescent X-ray ionization detector. An all helium pathway was constructed from the beam entrance into the hutch to the sample and detector in order to minimize absorption of the soft (2472 eV) sulfur K-shell X-rays.

Most of the samples contained little or no inorganic sulfur (pyrite). They included maceral separates prepared by density gradient centrifugation, biologically desulfurized specimens from which all pyrite had been removed, and samples prepared by a supersolvent extraction process.

Results and Discussion

Typical XANES and radial structure functions obtained from maceral separates appear in Figures 1 and 2. The XANES exhibit two sharp peaks at approximately 3 and 5 eV, and an intense, broad peak at 10-12 eV. The sharp peaks occur at the same energies and have qualitatively similar intensities as peaks in the XANES spectrum of dibenzothiophene (dbt). Presumably, they correspond to s ⇒ p transitions characteristic of aromatically bound sulfur. The broad peaks at 10-12 eV may be derived from sulfur bonded to oxygen, since the white lines of several sulfur-oxygen bonded compounds occur at approximately this energy. Alternatively, this feature may be a resonance peak produced by low energy electron scattering from second and third nearest neighbors.[3-6] Contributions to this XANES feature from both of these origins is obviously also a possibility.

Interpretation of the radial structure functions appears straightforward. Assuming the neighbor shells are predominantly carbon, and using an empirical S - C phase shift derived from the EXAFS of dbt, sulfur to carbon distances of 1.75 Å and 2.75 Å are determined for the first two neighbor shells.[2,3] These values seem reasonable for aromatically bound sulfur.

Future work will include obtaining more extensive calibration data, correlating EXAFS results with sample chemistry and other properties, and in situ measurements.

Acknowledgement

This research was supported by the U.S. Department of Energy under DOE Contract No. DE-FC22-86PC90017, which supports the research program of the Consortium for Fossil Fuel Liquefaction Science, and DOE Contract No. DE-FG22-86-PC90520.

References

1. C. Spiro, J. Wong, F. Lytle, R. Greegor, D. Maylotte, and S. Lampson, Science 226, 48 (1984).
2. G. P. Huffman, et al., Processing and Utilization of High Sulfur Coals II, Eds. Y. Chough and R. Caudle, pp. 3-12, Elsevier, 1987.
3. G. P. Huffman, et al., ACS Division of Fuel Chemistry Preprints, Toronto, 1988, in press.
4. F. W. Lytle, R. B. Greegor, and A. J. Panson, "Discussion of XANES: Application to Cu in High T_c Superconductors," submitted to Phys. Rev. B.
5. A. Bianconi, E. Fritsch, G. Calas, and J. Petiaw, Phys. Rev. B 32, 4292-4295 (1985).
6. F. Sette, J. Stohr, and A. P. Hitchcock, Chem. Phys. Letters 110, 517-520 (1984).

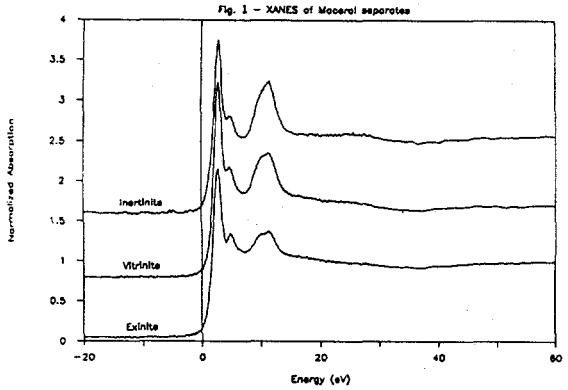

Fig. 2. Radial structure functions of organic sulfur in maceral separates.

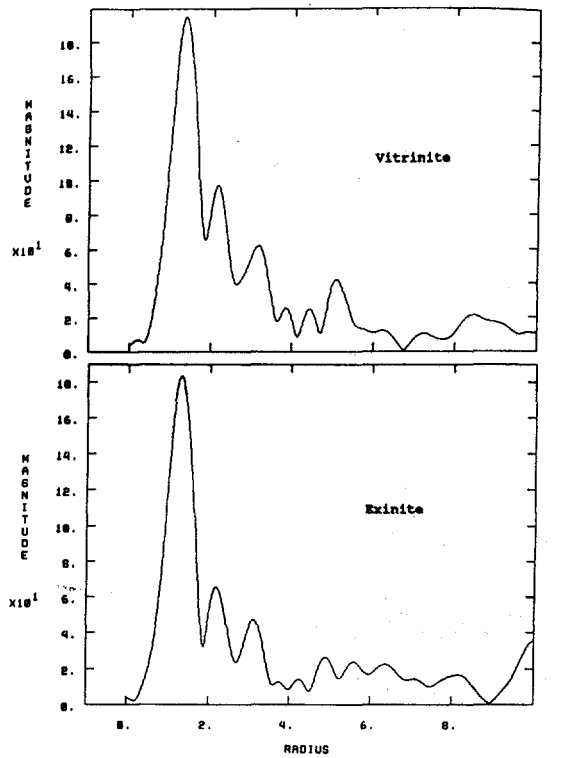

INVESTIGATION OF THE KINETICS OF THE CARBIDE FORMATION IN HSLA STEELS BY EXAFS SPECTROSCOPY

Proposal No. 956Mp

N. Shah, G.P. Huffman, and F.E. Huggins
University of Kentucky
L.J. Cuddy
The Pennsylvania State University, University Park, PA 16802
F.W. Lytle and R.B. Greegor
The Boeing Company, Seattle, WA 98124

Introduction:

Microalloy additions of Nb, V, or Ti to low carbon steels improve the mechanical properties of the HSLA steels by carbide, nitride or carbonitride formations. During hot rolling, precipitates in the austenite phase inhibit recrystallization and permit control rolling to produce fine grain structure with improved strength and toughness. Further precipitation in the ferrite phase during cooling locks dislocations and strengthens the product. To optimize the heat treatment of quenching and tempering, it is necessary to know the kinetics of carbide formation. EXAFS has been successfully used to study the formation of such precipitates, and the partitioning of the microalloying element between solid solution and fine precipitates. (1)

Experimental Conditions:

Three sets of mild steel samples containing 0.1% Nb, 0.2% V, or 0.2% Ti were prepared to study the individual effects of the three most widely used microalloying elements. One square inch sheets of these samples were heated to 1200°C for 30 minutes to dissolve the microalloy addition in the steel and then quenched in water to preserve the disordered solid solution. These samples were then aged at 600°C, 640°C and 680°C for periods from several seconds up to 6000 minutes to promote fine grained carbide or carbonitride formation.

The EXAFS study was carried out during dedicated runs at SSRL. A Si (220) double crystal monochromator was used to scan from -100 to +1000 eV around Nb, V and Ti K-edges in the fluorescence mode at room temperature.

Results:

The radial distribution function for the as-quenched steel sample with disordered solid solution show that the solute atoms are randomly distributed in the bcc Fe matrix. There is no evidence of any carbide formation. When the sample is tempered at 600 to 680°C, there is substantial diffusion of both carbon and the microalloy constituent atoms to form distinct carbide structures.

The ratio of the heights of carbon and microalloy atom peaks of the radial distribution function was the parameter used to monitor the extent of carbide formation.(1) A plot of this amplitude ratio as a function of logarithm of time yields a typical "S" curve. It is obvious that the carbide formation occurs more rapidly at higher temperatures.

Fig. 1 is an Arhennius plot of the inflection points of "S" curves for the vanadium sample. The slope of the plot is related to the activation energy of the carbide formation. The activation energies for the carbide formations are as follows. Vanadium carbide - 84 KCal/mole; Niobium carbide - 127 KCal/mole and Titanium carbide - 44 KCal/mole. These activation energies are in reasonable agreement with those obtained by hardness measurements.

Conclusion:

This method of studying kinetics has several advantages over other methods. The experiment is quick, about 20 minutes per scan and there is no need for elaborate sample preparation as in TEM. Furthermore, it is possible to conduct tempering experiments in situ.(1) Since the K edge is selective for one element, effects of individual elements can be isolated in multi-component systems which is not possible with bulk techniques such as hardness determinations.

In this series of experiments the feasibility of studying the kinetics of the carbide formation by EXAFS spectroscopy has been established. The results are encouraging and further studies of a similar nature are planned, using a wider range of samples and temperatures, with emphasis on in-situ tempering experiments.

(1) G.P. Huffman, F.E. Huggins, L.J. Cuddy, F.W. Lytle, R.B. Greegor, Script. Metall. 18, 719 (1984).

Fig. 1

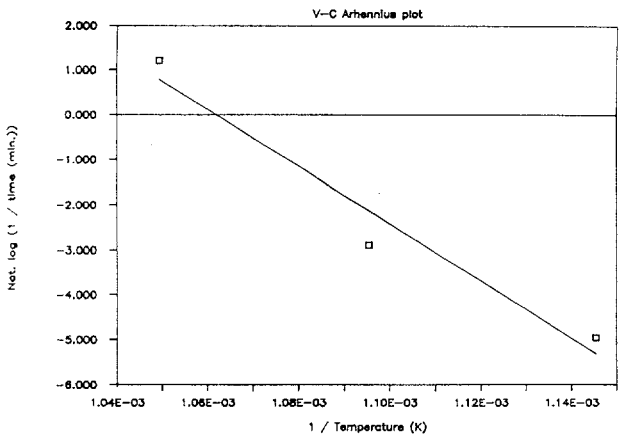

3-D X-RAY MICROTOMOGRAPHY OF CATALYTIC MATERIALS

J. H. Kinney, M.C. Nichols*, Q.C. Johnson, R.A. Saroyan,
U. Bonse†, R. Nusshardt† and R. Pahl†

Lawrence Livermore National Laboratory
Livermore, CA 94550

Introduction:

We have tested our 3-D x-ray microtomography system for characterization of catalysts currently being studied by Sandia National Laboratory. The catalysts are prepared using electroless deposition of Pd on a carbon foam substrate. The carbon foam is manufactured from polystyrene starting material and has pores of roughly 250-μm diameter which are connected by triangular struts having dimensions of 45-μm on edge.

Traditional characterization techniques, most of which are destructive, and can give a distorted representation of the catalysts. Furthermore, these classical characterization techniques have difficulty showing internal surfaces. Using our non-destructive method of 3-D microtomography, we can observe the interiors of the catalysts for information on coating homogeneity and continuity.

Experimental Method:

The experimental apparatus has been discussed in detail elsewhere[1]. Briefly, the x-ray beam from the double crystal monochromator passes through a sample placed on a rotary stage and is converted to visible light in a high-resolution phosphor screen. The phosphor screen is imaged with a CCD array camera which is run in a charge integrating mode. The image data for each view angle through the object is used to reconstruct the three-dimensional structure of the sample. By modulating the energy of the x-ray beam, it is possible to obtain chemical information about the samples as well as structural information in many cases[2].

Tomography was performed on BL I-5 on a 1mm x 1mm x 2mm volume of catalyst. One hundred and eighty view angles were recorded with a reference image taken every four views. This reference period was inadequate to remove all of the circular artifacts in the reconstruction, but was necessitated by time requirements on the low intensity line.

Results:

Figure 1 shows a three-dimensional rendering of a subset of our data. The rendering shows the struts coming together to form a node. Evidence is found that the coating is non-uniform on the node surface, an observation that was supported by subsequent SEM analysis. Figure 2 shows a cross-sectional slice taken through the base of the node which shows that the struts do not completely close. The coating can be seen on both the interior and exterior surfaces of the node.

Acknowledgements:

We wish to thank D. Nissen, C. Bonzo and W.D. Bonivert (SNLL) for preparing and providing the catalyst. Thanks are also due to H. Brand(LLNL) for providing the solid rendering software and A. Knabe (LLNL) for technical support.

Figure 1: Solid rendering of 26 tomography slices of the catalyst. Each slice is approximately 5 - μm, and the strut diameter on edge is nominally 50-μm. Irregularities in the coating thickness can be observed.

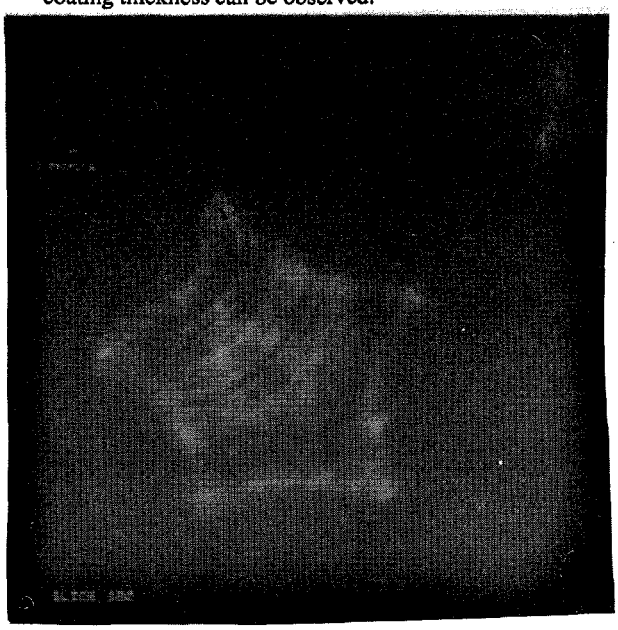

Figure 2: Cross-section of the node near the base (see figure 1). The coating is nominally 5-μm thick, and the internal node surface can be seen to have been coated as well as the external surface.

[1] Kinney, J.H., et al., **Rev. Sci. Instrum., 59,** 196(1988).
[2] Kinney, J.H. et al., **Appl. Opt., 25,** 4583(1986)

*Sandia National Laboratory, Livermore, CA 94550
†Physics Department, University of Dortmund, Dortmund, FRG

Proposal No. 983M

X-RAY ABSORPTION STUDY OF AMORPHOUS GERMANIUM AT HIGH PRESSURE

R. Ingalls and J. Freund

Department of Physics, University of Washington, Seattle, WA 98195

E. D. Crozier

Department of Physics, Simon Fraser University, Burnaby, B.C., V5A 1S6, CANADA

Amorphous materials are of great practical and theoretical interest. Theoretically they pose the problem of calculating their electronic and vibrational properties without resorting to the simplifications due to translational symmetry. In fact, despite the lack of long range order, many properties are similar to their crystalline counterpart. These materials are important from the practical standpoint. For example, ferromagnetic metallic glasses are of interest as memory devices and transformer materials with little hysteresis loss. Amorphous semiconductors are of use for solar cells, thin film transistors, switching and memory devices and image processors.

One of the great strengths of the EXAFS technique is in the study of disordered materials, where diffraction is of limited value. One may obtain average coordination numbers, radial distribution functions and disorder terms quite readily, information crucial to understanding the structure. The latter is of course necessary for a microscopic understanding of the properties.

Amorphous germanium has proven to be an excellent system for study since it can readily be compared with its crystalline counterpart. Our colleagues, E. A. Stern and co-workers,[1] have examined, in considerable detail, the amorphous-to-crystalline transition in this material. Electrical resistance studies[2] indicate that, at about 60 kbar, amorphous germanium undergoes a sharp transition in which the resistivity decreases by a factor of a million. Material taken above this pressure transforms to a metastable tetragonal crystal structure when the pressure is removed.[3]

We are currently analyzing room temperature data on this system taken for pressures over 100 kbar. Our sample was obtained from E. A. Stern et al., who had previously reported the zero pressure results.[1] The sample exhibits no large changes in this pressure range, although higher shells, not apparent at low pressure, become barely discernible. Careful attention is being given the bond compressibility and its mean square disorder as well as the coordination number. This is of interest in comparison with that from crystalline germanium. Moreover, any discontinuities may shed light on the above phase change, if it, in fact, exists in the sample examined.

This work was supported in part by the U.S. D.O.E. Grant DE-FG06-84ER45163 and by the Natural Sciences and Engineering Research Council of Canada.

REFERENCES

1. E. A. Stern, C. E. Bouldin, B. Von Roedern and Y Azoulay, Phys. Rev. B 27, 6557 (1983).
2. K. Tamura, J. Fukushima, H. Endo, S. Minomura, O. Shimomura, and K. Asaumi, J. Phys. Soc. Jpn. 36 558 (1974).
3. S. Minomura in High Pressure Science and Technology B. Vodar and Ph. Marteau, eds. (Permagon Press, NY, 1980), Vol. 1, p. 447.

X-RAY ABSORPTION STUDIES OF HIGH T_c SUPERCONDUCTORS

Proposal No. 984M

J. Whitmore, B. Houser, Y. Ma, M. Qian, R. Ingalls,
E. A. Stern, F. C. Brown, R. Kurosky,* and B. Thiel*

Departments of Physics and Materials Science and Engineering,* University of Washington, Seattle, WA 98195

J. M. Tranquada

Brookhaven National Laboratory, Upton, NY

E. D. Crozier, N. Alberding, and A. J. Seary

Physics Department, Simon Fraser University, Burnaby, B.C. V5A 1S6 CANADA

J. P. Rice, B. G. Pazol, and D. M. Ginsberg

Department of Physics, University of Illinois, Urbana, IL 61801

Several XAFS experiments on the new high T_c superconductors were conducted during this report period on beam time originally allocated for high pressure studies of mixed-valent materials. In the present case, some of the measurements were in fact carried out as a function of pressure. In addition the valence state of the constituents, notably copper, was studied. In all cases the results are still under active analysis.

High pressure studies were performed on high quality samples of both $YBa_2Cu_3O_{7-x}$ ($T_c \simeq 91$ K) as well as $LaBaCuO_4$ ($T_c \simeq 40$ K). In the former case the K-edge spectra of both Cu and Y were obtained. Preliminary results are discussed under Proposal 100. In the latter case only the Cu K-edge was studied. For both studies the L_{111} EXAFS spectra of a gold foil was measured for pressure calibration. Although still under study in both cases the copper appears to remain in the divalent state. There is also possible evidence for a buckling of the Cu-O-Cu bond with pressure.

In another experiment EXAFS data were obtained in transmission at SSRL on a small high quality single crystal of $YBa_2Cu_3O_{7-x}$. The experiments were carried out as a function of angle between the x-ray beam and the normal to the planes of the crystal. As expected, differences appear between the results for the crystal and for polycrystalline samples. Both the near edge and the EXAFS regions of the spectrum show an orientation dependence as the crystal is rotated relative to the x-ray electric field vector.

A study of the doped superconductor $YBa_2(Cu_{1-x}Ni_x)O_{7-x}$ with x=0.02 and 0.05 was investigated. Powder x-ray diffraction and polarized optical microscopy measurements indicate that these materials are more than 95% single phase orthorhombic. Magnetic measurements show sharp superconducting transition with T_c lowered by about 3 K and 8 K, respectively, from the x=0 sample. X-ray absorption fine structure measurements were made on the Cu and Ni K-edges to investigate the Ni site in the two samples. Preliminary results indicate that the Ni atoms do not appear to go in the normal copper sites, Cu(I) or Cu(II) as might have been expected. Analysis is continuing.

This work was supported in part by the U.S. D.O.E. Grants DE FG06-84ER45163, and EE-A505-80ER10742; N.S.F. Grants DMR85-01346, DMR86-12860, and DMR86-16170; and the National Sciences and Engineering Research Council of Canada.

"Actinide and Fission Product Site Speciation in Nuclear Waste Glasses"

Proposal No. 988M

Elizabeth M. Larson and P. Gary Eller
Isotope and Nuclear Chemistry Division, Los Alamos National Laboratory, Los Alamos, NM 87544

R. B. Greegor and F.W. Lytle
Boeing Corporation, Seattle, WA 98124

Michael P. Eastman
Department of Chemistry, University of Texas, El Paso, TX 79968

Introduction

Borosilicate glass is the leading candidate waste form for disposal of high-level nuclear wastes in the United States and in Europe. Despite a considerable amount of phenomenological and engineering-related research, much remains to be learned about the behavior of actinides, fission products, and processing impurities when they are incorporated into the glass. EXAFS has become the method of choice to study site speciation and local order in glassy materials.[1-3] In general, glasses are described as possessing network forming species (e.g. SiO_2 and Al_2O_3) and network modifing ones such as Na_2O and CaO. Lanthanides and actinide dopants as well as transition metals will become network modifiers when introduced into the glass framework. Consequently this becomes an important study when considering the disposal of nuclear waste materials. In this report we describe our results to date with the fission porduct elements Pr, Gd and Lu.

Experimental

Savannah River-Frit 21 was received from ORNL and has been analyzed and described elsewhere [4]. The glass was ground to a fine powder and mixed with oxides of the respective rare earth elements in ratios such that the dopant level was 3 wt %. The samples were heated overnight in air at 1450 °C in Pt boats. Samples were withdrawn from the furnace, quenched, reground and replaced in the oven for an additional firing overnight. Powder diffraction patterns showed no residual oxide lines or crystalline materials present.

EXAFS data were collected on beam line 7-3 at SSRL using a Si(220) monochromator and 1 mm slits. Each sample was ground and enclosed in plastic and suspended in the beam. Both transmission and fluoresence data were collected for all L edges of Pr, Gd, and Lu. Each spectrum was appropriately edge shifted and then background corrected. Rare earth oxides were used as model compounds for experimental phase extraction. A K^2 Fourier transform was performed on the L_{III} edge EXAFS in addition to a least squares fit of the data to obtain first shell distances fom the absorbing element.

Discussion

Values of 2.50, 2.26 and 2.21 Å were obtained from the fitting proceedure of Pr, Gd, and Lu data respectively, for the rare earth-near neighbor oxygen distance in the glass. This compares well with the rare earth-oxygen first shell peaks in the Fourier transforms. A graphic representation of the results of the least squares fitting for each sample is presented as Figure 1.

The near edge and EXAFS data for Gd and Lu are similar to those of the model oxides. In addition, the first neighbor distances for these two elements correspond closely to the sequioxides. The Pr data differs in that the frit exhibits one peak in the near edge, while the oxides PrO_2 and Pr_6O_{11} show double peaks.

The trends in the rare-earth oxide distances are as expected considering the change in ionic radii across the lanthanide series. The difference between the ionic radii for Gd^{+3} and Lu^{+3} in a six-coordinate site is 0.08Å, [5] which corresponds well with the difference in bond lengths derived from the glass EXAFS data. The comparison between Pr^{+3} and Gd^{+3} is not as good. If Pr^{+4} were present, since it is smaller than Pr^{+3}, the discrepancy would be even greater. If Pr^{+3} occupies an eight coordinate site, then the bond length differences (Δ 0.24 Å) match well with the ionic radii (Δ 0.19 Å). We plan to measure the EPR, and uv-visible spectra for these glasses in hopes of gaining more information about the valence state of the dopants.

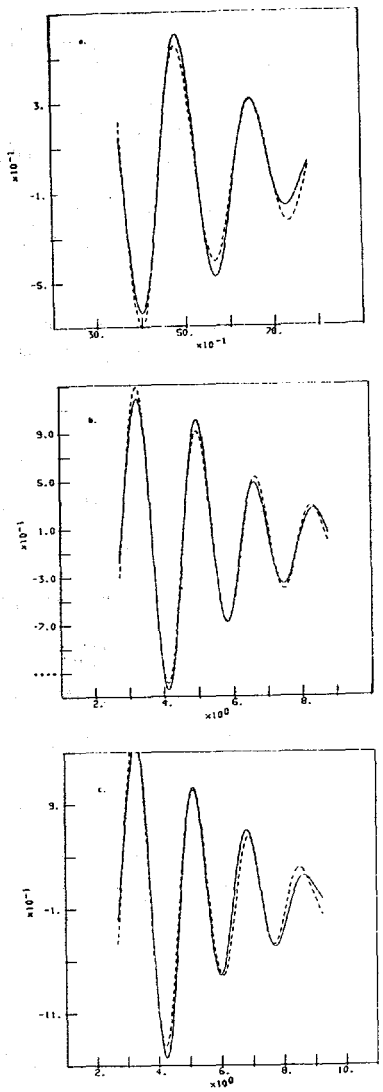

Figure 1.Solid lines represent the data and dotted lines the fit. (a.) Pr; (b.) Gd ; (c.) Lu.

References

1. G.N. Greaves, J. Non-Cryst. Solids , 71, (1985), 203-217.

2. P.H. Gaskell, Nucl. Inst. & Methods, 199, (1982), 45-60.

3. F.W. Lytle & R.B. Greegor, Mat. Res. Soc. Symp. Proc., Vol. 61, (1986), 259-271.

4. P.G. Eller, G.D. Jarvinen, J.D. Purson, R.A. Penneman, R.R. Ryan, F.W. Lytle & R.B. Greegor, Radiochimica Acta, 39, (1985), 17-21.

5. R.D. Shannon, Acta Cryst., A32, (1976), 751-767.

In-situ X-ray Absorption Study of Pb(II) and Co(II) Sorption Complexes at the γ–Al_2O_3/Water Interface

Gordon E. Brown, Jr.,[1], Catherine J. Chisholm[1], Kim F. Hayes[2], A. Lawrence Roe[4], George A. Parks[1], K. O. Hodgson[3], J. O. Leckie[2]

(1) School of Earth Sciences, (2) Department of Civil Engineering, (3) Department of Chemistry, Stanford University, Stanford, CA 94305
(4) W. R. Grace Company, 7379 Rte. 32, Columbia, MD 21044

Introduction

Sorption processes at solid/water interfaces are important in a variety of contexts including contaminant transport in groundwater systems, nuclear waste disposal, formation of ore deposits, electrochemical processes, corrosion control, solar energy conversion and enhanced oil recovery. Few structural probes are available to characterize the types of sorption complexes formed or to constrain the mechanism of sorption reactions at solid/water interfaces. However, synchrotron-based x-ray absorption spectroscopy (XAS) is well suited for this type of investigation because it is elemental specific, it provides quantitative, short-range structural information and it permits *in situ* characterization. By preparing samples in which the element of interest is localized at the solid/water interface, we have been able to use bulk XAS methods to obtain structural data for sorption complexes at less than monolayer coverages on several mineral surfaces in contact with water.

During the first two years of our investigation, we focused on two oxide/aqueous sorption systems: (1) Se oxyanions sorbed to α–FeOOH (goethite) at a sorption density (Γ) of 1.3-3.2 μmole/m^2 and (2) Pb(II) sorbed to α–FeOOH (Γ = 1.3–19 μmole/m^2). In first system, XAS indicated that selenite (SeO_3^{2-}) forms a strongly bound inner sphere sorption complex at pH<5.0 whereas selenate (SeO_4^{2-}) forms a weakly bound outer sphere complex in the same pH range[1]. Our XAS study of the aqueous Pb(II)/goethite system showed that Pb(II) forms inner sphere complexes that cluster at the goethite/water interface with increasing surface coverage [2,3,4]. Evidence for this clustering comes from observation of Pb-Pb scattering in the x-ray absorption near edge structure (XANES) spectra.

In the past year we have extended our work to two additional systems: aqueous Pb(II)/γ–Al_2O_3 (Γ = 0.4–1.2 μmole/m^2) and aqueous Co(II)/γ–Al_2O_3 (Γ = 0.14–1.3 μmole/m^2). These ions were sorbed at much lower surface coverages than in previous studies in order to more closely model the behavior of metal ions in natural systems.

Experimental

XAS data were collected during dedicated runs in May and December 1987 on beam line 1V-1 at a wiggler field strength of 18kG. The sorption samples were centrifuged pastes in contact with water during data collection; samples were loaded into teflon cells with mylar windows to retain their moisture. Data for aqueous samples were collected in fluorescence mode using a Lytle detector with the sample oriented at 45 degrees to the incoming X-ray beam. XAS data for all solid model compounds were collected in transmission mode.

Samples were prepared by adding a known amount of metal nitrate solution to a suspension of 100-120g γ–Al_2O_3/1000g aqueous solution. The pH of the suspension was adjusted so that >95% of the metal cation was removed from solution by the solid; initial solution concentrations for our samples were 5 and 15 mM Pb(II), and 4 and 18mM Co(II). In all cases, the amount of metal ion in the supernatent after the samples were loaded was negligible. Since alumina and water do not absorb x-rays significantly at the energies of the Pb(L_{III}) and Co(K) edges, the sorbed sample spectra have good signal-to-noise ratios. A typical EXAFS spectrum for 15mM Pb on γ–Al_2O_3 is shown in Fig. 1.

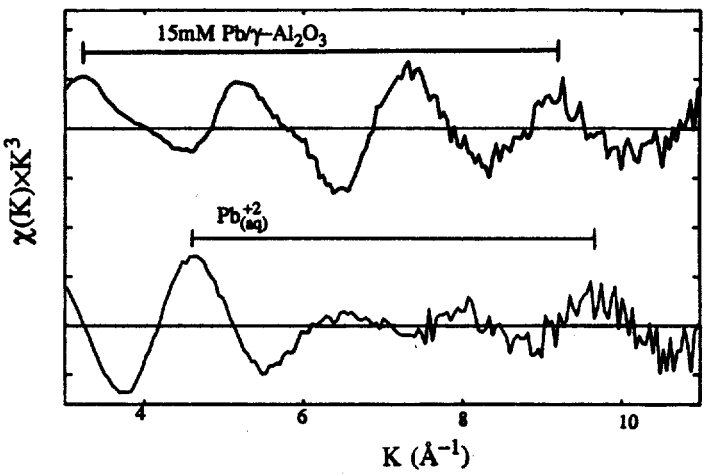

Fig. 1: EXAFS spectra for 15mM Pb(II) sorbed to γ–Al_2O_3 and for aqueous Pb(II). Lines above spectra denote four oscillations.

Pb/γ–Al_2O_3

The study of lead sorbed to γ–Al_2O_3 was undertaken as an extension of the previous work on lead sorbed to goethite[2,3,4]. In their study of the solution chemistry of Pb(II) sorbed to γ–Al_2O_3, Hohl and Stumm[5] concluded that Pb(II) bonds directly to the oxide surface predominantly as a monodentate complex. This conclusion was based on the strong affinity of alumina for lead even at low pH where the surface is positively charged and on the calculated ligand number. Their study, however, provided no structural information about the sorption complex. We reproduced their experiments as closely as possible during our sample preparation with the exception of 5-15 times greater initial lead solution concentrations.

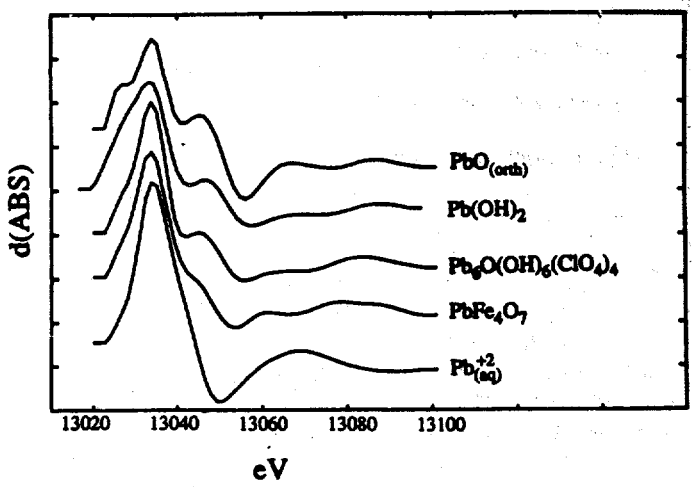

Fig. 2: First derivative of the normalized XANES spectra for five oxygen ligated lead model compounds.

First derivative XANES spectra for a variety of oxygen-ligated lead model compounds are shown in Fig. 2. There is a peak at ≈13045eV in the spectra for all crystalline model compounds but not in the aqueous lead spectrum. Therefore, this peak is interpreted as a result of Pb-Pb interactions. The region of the spectrum from 13060-13100 also contains a signature for Pb-Pb interactions. In the crystalline model compounds, there are two distinct peaks indicative of two different backscatterers (Pb and O) whereas the aqueous lead spectrum only has one peak (due to oxygen backscattering) (Fig. 2). The spectra for lead sorbed to γ–Al_2O_3 are different from both aqueous lead and crystalline lead model compounds (Fig. 3). The 15mM Pb/γ–Al_2O_3 spectrum contains a small feature at about 13045 eV and two peaks in the region of 13060-13100 eV, which suggest that there may be lead in the second coordination sphere of sorbed lead. The amplitude of the feature at 13045eV is much less than that for $Pb_6O(OH)_6(ClO_4)_4$ which implies that a lead precipitate did not form on the alumina surface. The same is true for the 5mM Pb/γ–Al_2O_3 spectrum; the features are subtle but distinct from the aqueous lead spectrum. These observations suggest that the sorbed lead is not a fully hydrated monomeric species.

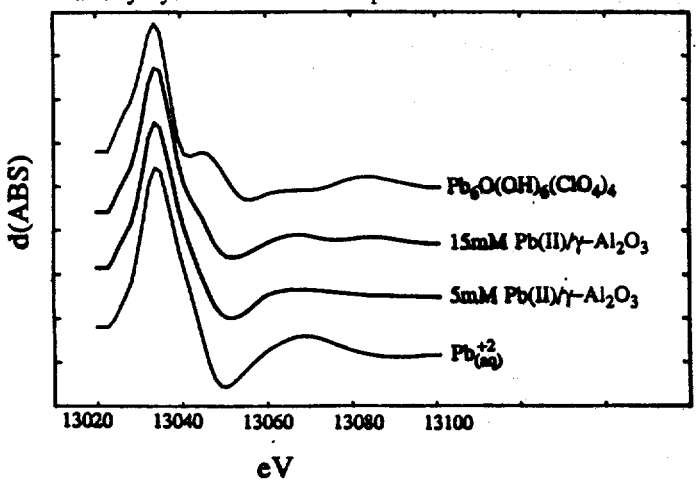

Fig. 3: Comparison of the first derivative of the normalized XANES spectra for 5mM and 15mM Pb(II) sorbed to γ–Al_2O_3 with the spectra for $Pb_6O(OH)_6(ClO_4)_4$ and aqueous Pb(II).

The differences between the XANES spectra of sorbed lead and aqueous lead are further demonstrated by their EXAFS (Fig. 1). The aqueous lead EXAFS spectrum is too noisy for structural analysis, but qualitatively we conclude that the lead-oxygen distance in aqueous lead is greater than that for the sorbed samples based on a comparison of the frequency of the four EXAFS oscillations shown in Fig. 1. The aqueous lead spectrum has a higher frequency and thus a longer average lead-oxygen bond distance. Furthermore, a beat pattern, indicating the presence of a second backscatter, is clearly visible in the EXAFS for 15mM Pb/γ–Al_2O_3 (Fig. 1). Fourier transformation of the EXAFS generates a radial distribution function that contains a small peak at approximately 3.4 Angstroms. Using theoretical phase and amplitude parameters, the backtransform of the radial distribution function can be fit over the range of this peak. The best theoretical fit is achieved by using a combination of Al and Pb backscatterers (Fig. 4a) as opposed to only Pb (Fig. 4b). Therefore, both the XANES and EXAFS data indicate that lead forms complexes which directly bond to the alumina surface and that these complexes contain an average of 2-4 lead atoms.

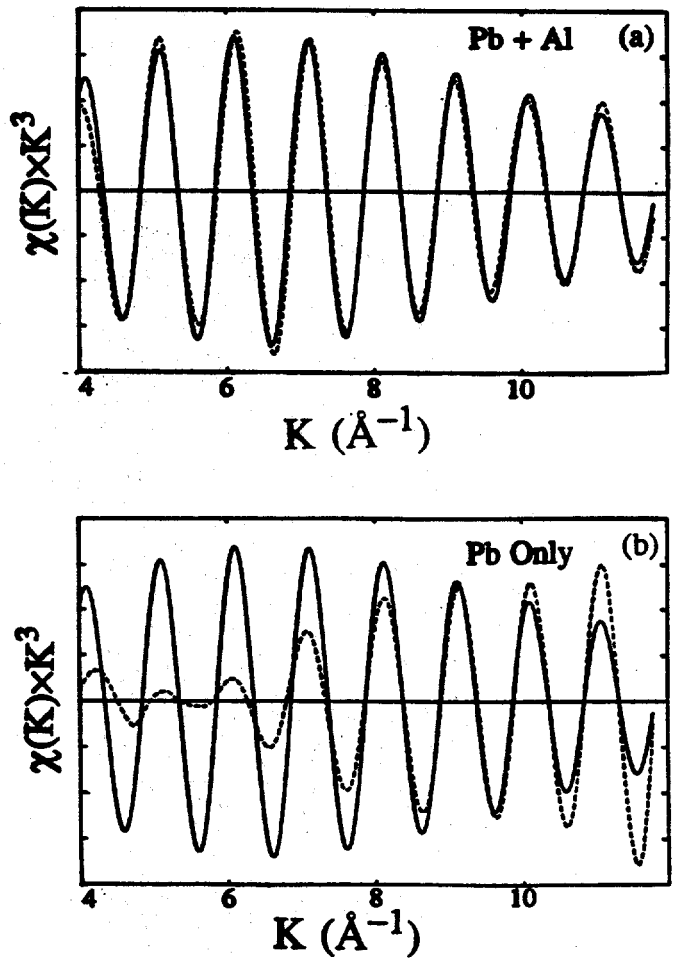

Fig. 4: Comparison of the Fourier filtered second shell EXAFS for 15mM Pb/γ–Al_2O_3 (solid) with theoretical fits (dashed). (a) theoretical fit assuming Pb and Al are backscatters; (b) theoretical fit assuming Pb is the only backscattering atom for this shell.

$Co/\gamma-Al_2O_3$

Previous investigations of Co(II) sorption to $\gamma-Al_2O_3$ have reached different conclusions as to the type of sorption complex formed at this oxide/water interface[6,8]. Uptake of positively charged $Co(II)_{aq}$ from solution by $\gamma-Al_2O_3$ predominantly occurs in the pH range of 6-8 during titration experiments[6]; over this pH range, the solid is positively charged. This behavior implies that Co is not simply electrostatically bound to alumina; it does not indictate whether or not the Co ion retains its inner hydration sheath upon sorption[7]. However, an x-ray photoelectron spectroscopy study of Co sorbed to $\gamma-Al_2O_3$ suggested that the sorption complex was a surface precipitate even under conditions where bulk precipitation of $Co(OH)_2$ would not occur[8].

The radial distribution function of the EXAFS for 18mM Co(II) sorbed to $\gamma-Al_2O_3$ differs from that for $Co(OH)_2$ (Fig. 5). Preliminary analysis of these data indicates that there are fewer second and fourth shell Co atoms in the sorption complex compared with $Co(OH)_2$ and that the neighboring Co atoms are closer together. Atoms arranged colinearly cause an increase in the backscattered amplitude of the EXAFS peaks which results in resolvable peaks for atoms at a greater radial distance from the scatterer. This enhancemment of amplitudes due to the colinear arrangement of atoms may allow detection of outer atoms in complexes at the solid/water interface where high thermal motion will tend to decrease the amplitudes of EXAFS oscillations. Therefore, the presence of a peak at >5 Angstroms for the sorbed sample suggests that, as in $Co(OH)_2$, the second and fourth shell Co atoms are colinear with the central absorber ion. Thus, the EXAFS indicates that Co sorbs to the alumina/water interface as clusters of Co and O in a complex that structurally resembles $Co(OH)_2$. Our EXAFS study does not support Tewari and Lee's[8] suggestion that sorption of Co(II) at the $\gamma-Al_2O_3$ surface results in precipitation of $Co(OH)_2$.

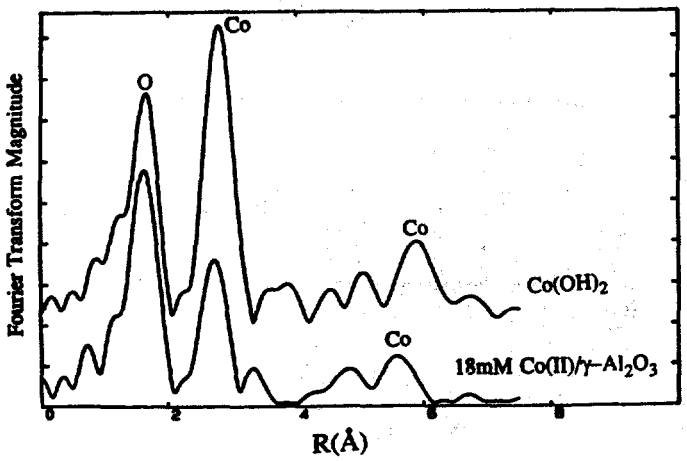

Fig. 5: Radial distribution functions for $Co(OH)_2$ and 18mM $Co/\gamma-Al_2O_3$.

Acknowledgements

This research was supported, in part, by NSF grants EAR-85-13488 and CHE-85-12129. We gratefully acknowledge the experimental assistance of Dr. Britt Hedman.

References

1. Hayes, K. F., A. L. Roe, G. E. Brown, Jr., K. O. Hodgson, J. O. Leckie and G. A. Parks, *Science* **238**, 783 (1987).
3. Roe, A. L., K. F. Hayes, C. J. Chisholm, G. E. Brown, Jr., K. O Hodson, G. A. Parks and J. O. Leckie, *SSRL Report* **87/01**, 142 (1987).
3. Roe, A. L., K. F. Hayes, C. J. Chisholm, G. E. Brown, Jr., G. A. Parks, K. O. Hodgson and J. O. Leckie, *GSA Abstracts with Programs* **19**(7), 823 (1987).
4. Roe, A. L., K. F. Hayes, C. J. Chisholm, G. E. Brown, Jr., G. A. Parks, J. O. Leckie and K. O. Hodgson, (1988) in prep.
4. Hohl, H. and W. Stumm, *J. Colloid Int. Sci.* **55**, 281 (1976).
6. See, for example: Hachiya, K., M. Sasaki, Y. Suruta, N. Mikami and T. Tasunaga, *J. Phys. Chem.* **88**, *23 (1984).*
7. Parks, G. A., in *Adsorption in the Marine Environment, 2nd ed.*, J. P Riberg and G. Skirrow, eds., Academic Press, 241 (1976).
8. Tewari, P.H and W. Lee, *J. Colloid Int. Sci.* **52**, 77 (1975).

Interface Structure of $NiSi_2/Si(111)$

I. K. Robinson and R. T. Tung AT&T Bell Laboratories, Murray Hill, NJ 07974

R. Feidenhans'l Riso National Lab, DK 4000 Roskilde, Denmark

Nickel silicide is very close to being lattice matched to silicon, and forms smooth pseudomorphic films by chemical reaction when Ni is annealed on a Si(111) surface. Because of the ease of preparation and high quality of such films, many structural studies of the interface have been performed using a variety of techniques including transmission electron microscopy[1] (TEM), ion scattering[2] (RBS) and X-ray standing wave fluorescent yield.[3,4] The general conclusions are in agreement with the model of Fig. 1, with an *inward* relaxation of the layer spacing by 0.06 ±0.08Å (ref. 2), 0.11 ±0.03Å (ref. 3) or 0.06 ±0.03Å (ref. 4).

On beam line VII-2, we measured the diffraction near the (111) Bragg peak of one of these interfaces. The sample was a B-type $NiSi_2$ film, 33Å thick, grown on float zone Si(111) ±1/2°, then covered at room temperature by 50Å a-Si to prevent oxidation in the ambient. X-ray measurements were made in air with a wavelength of 1.54Å using 2 mm (horiz) × 10 mm (vert) slits in front of the detector. Very close to the Bragg peak 1 mm × 1 mm slits and an attenuator were used and the results were scaled accordingly. The diffraction pattern was found to consist of a diffuse streak extending from the origin of reciprocal space radially out through the Bragg peak and beyond. Thermal diffuse scattering was also present but could be removed completely by use of ω-scans through the streak. Each data point in Fig. 2 is the integrated intensity of the streak after background subtraction in such a scan. The range of data shown is (0.75, 0.75, 0.75) to (1.3, 1.3, 1.3).

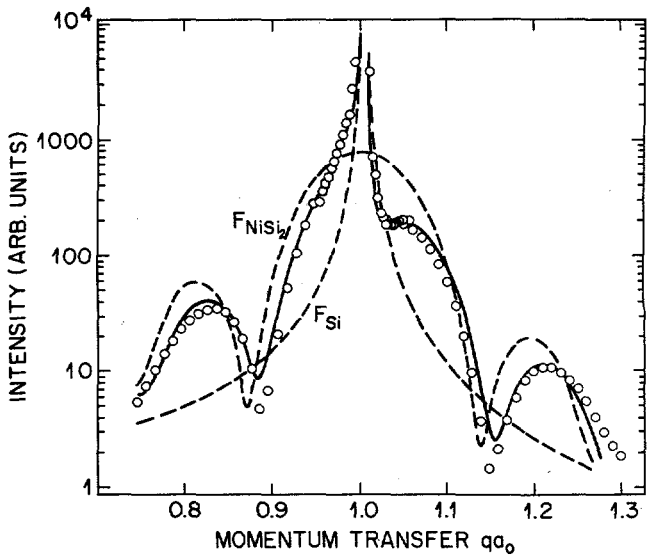

Figure 2. Integrated intensity of the diffracted intensity near the (111) Bragg peak of a $NiSi_2/Si(111)$ interface. The units of momentum transfer q are in inverse Si(111) spacings. The fit is to eqn. 3 and the individual components F_{Si} (eqn. 2) and F_{NiSi2} (eqn. 1) are superimposed as dashed lines.

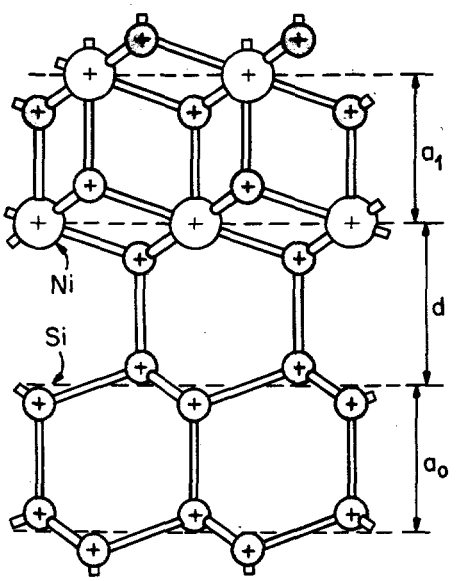

Figure 1. Ball and stick model of a $NiSi_2/Si(111)$ interface. Shown here is a type B interface (ref. 1) which was the type used in the experiments and other work discussed; type A has the overlayer rotated 180° with respect to the substrate.

Both the Si(111) substrate and the $NiSi_2$ film contribute to the streak. The substrate has a crystal truncation rod[5] (CTR) arising from the Fourier transform of its abruptly terminated face. This has an intensity falling off symmetrically as $1/q^2$ on either side of the Bragg peak; this is the same as the Darwin tails predicted by the dynamical theory.[6] The $NiSi_2$ film, being only eight layers thick, has broad diffraction features and subsidiary maxima on either side of the Bragg peak; it is also a symmetric function. What is seen, however, in the data is a dramatic asymmetry of the intensity around (111). This is because the two components *interfere* with each other. Since the relative phase is given by the interface separation, we have a sensitive method to determine that quantity.

The problem reduces to one dimension because all the layers are well ordered parallel to the interface. We can calculate the intensity as the square modulus of the sum of layerwise contributions. Adding up the Si layers and $NiSi_2$ layers separately we obtain (see Fig. 1):

$$F_{Si} = \sum_{n=0}^{\infty} 2f_{Si}\cos\left(\frac{qa_0}{8}\right) e^{-inqa_0}$$
$$= f_{Si}\cos\frac{qa_0}{8}\,\frac{1}{1-e^{-iqa_0}} \qquad (1)$$

$$F_{NiSi2} = \sum_{n=0}^{N-1} (f_{Ni} + 2f_{Si}\cos\frac{qa_1}{4})\, e^{inqa_1}$$

$$= (f_{Ni} + 2f_{Si}\cos\frac{qa_1}{4})\,\frac{1 - e^{iNqa_1}}{1 - e^{iqa_1}} \qquad (2)$$

q is the momentum transfer and a_0 and a_1 are the layer spacings of the substrate and film respectively. Finally, we introduce the interfacial distance d:

$$F_{total} = F_{Si} + e^{iqd}\, F_{NiSi2} \qquad (3)$$

The fit in Fig. 2 is the modulus of F_{tot}, for a value of $d/a_0 = 1.10 \pm 0.02$. Neither F_{Si} nor F_{NiSi2} alone shows any asymmetry; only when they are added together with the appropriate phase in eqn. 3, can we fit the data.

This simple technique allows accurate determination of interface separations by using the interference of the two diffraction contributions. The resulting value of d/a_0 is less than the ideal value of 9/8 seen directly in Fig. 1 assuming no relaxation. The magnitude of the inward relaxation measured is 0.08 ± 0.06Å in good agreement with other determinations.

References

1. R. T. Tung, J. M. Gibson, J. M. Poate, Phys. Rev. Lett. *50*, 429 (1983).
2. E. J. van Loenen, J. W. M. Frenken, J. F. van der Veen, S. Valeri, Phys. Rev. Lett. *54*, 827 (1985).
3. E. Vlieg, A. E. M. J. Fischer, J. F. van der Veen, B. N. Dev, G. Materlik, Surf. Sci. *178*, 36 (1986).
4. J. Zegenhagen, to be published.
5. I. K. Robinson, Phys. Rev. *B33*, 3830 (1986).
6. Z. G. Pinsker, "Dynamical Scattering of X-rays in Crystals", Springer (1978).

EXAFS Study of Rare Earth Element Environments in Quenched Silicate Melts of Geochemical Interest

C.W. Ponader, G.E. Brown, Jr., and W.E. Jackson
Department of Geology, Stanford University
Stanford, California 94305

The local geometry of the site occupied by trace amounts (0.2 wt%) of La, Gd, and Yb, with and without 1-2 wt% F or Cl, has been examined as a function of melt composition using Extended X-ray Absorption Fine Structure (EXAFS) spectroscopy. Spectra were collected in fluorescence mode on BL VII-3 and BL IV-1 during dedicated runs in April, 1986 and January, 1987. The three glass compositions examined are albite, sodium trisilicate, and a peralkaline composition approximately halfway between the two. The results in the halogen-free glasses show that Yb is approximately 6 coordinated (<Yb-O>= 2.21 Å). Gd coordination ranges from 6 in albite glass (<Gd-O>= 2.30 Å) through a mixture of 6 and 7 in peralkaline glass (<Gd-O>= 2.36 Å) to 7 in sodium trisilicate glass (<Gd-O>= 2.43 Å). La is 7-coordinated in the peralkaline and sodium trisilicate glasses (<La-O>= 2.43 Å), but has a coordination of 8-9 in albite glass(<La-O>= 2.59 Å). The irregularity of the rare earth site (*i.e.*, the range of distances to oxygen) appears to increase as tetrahedral polymerization increases. This is caused, in part, by the decreasing number of non-bridging oxygens in the coordination sphere of the rare earth element. The exception to this trend is La in albite glass. The La site in albite glass is more regular than it is in the other glasses because the size of the La ion requires it to occupy a more central position in the "cage" formed by the interconnected rings of Si and Al tetrahedra. This leads to a more regular distribution of La–O bond lengths. The irregularity of the rare earth site also appears to decrease as the size of the rare earth decreases. This is due to the greater ability of the smaller, higher field-strength rare earths to compete for non-bridging oxygens. As the tetrahedral polymerization decreases, the local environment of the rare earth is more strongly influenced by the bonding requirements of the rare earth and is less influenced by the tetrahedral network topology. Increasing the polymerization of the melt or increasing the Si/(Si+Al) ratio of the tetrahedral network should act to increase the crystal/liquid partition coefficients of the rare earths.

EXAFS studies of glasses containing fluorine demonstrate that La, Gd, and Yb form complexes with fluorine in aluminosilicate melts. Gd and Yb are coordinated by eight fluorines with no apparent oxygen neighbors (<Gd-F>= 2.30 Å; <Yb-F>= 2.23 Å). La appears to form mixed O-F complexes consisting of eight ligands approximately evenly divided between fluorine and oxygen (<La-O>= 2.45 Å; <La-F>= 2.46 Å). We found no evidence of Cl complexing of REE in the chlorine-containing compositions studied. The rare earth site in chlorine-containing melts is, however, more regular than the rare earth site in volatile-free melts. This suggests that Cl acts to depolymerize the tetrahedral network. Fluorine, because of complex formation, and chlorine, because of its effect on melt structure, should both act to decrease the crystal/liquid partition coefficients of rare earths in silicate melts.

CHARACTERIZATION OF Co-CONTAINING OXIDES ON STAINLESS STEEL BY e-YIELD XANES SPECTROSCOPY

Farrel Lytle[1], Robert Greegor[1], Zofia Rek[2] and Howard Ocken[3]

1. The Boeing Co., Seattle, WA 98124

2. SSRL, Stanford, CA 94305

3. EPRI, Palo Alto, CA 94303

The passivating oxide layers that form on the inner surface of stainless steel water coolant pipes in nuclear power plants can incorporate the energetic γ-emitter ^{60}Co. Measurements at commercial plants show that this isotope is responsible for ~80% of the occupational radiation exposure incurred by plant maintenance personnel although Co is present in the oxide layer at only ~0.2 wt. %. A number of surface treatments have been shown in laboratory experiments and in limited in-plant demonstrations to inhibit the incorporation of ^{60}Co into the oxide layer. X-ray diffraction and SIMS have been used to characterize the major components of these passive films; however the actual environment of the Co atoms is unknown. To optimize corrective measures a better characterization of the Co environment is necessary.

In this feasibility experiment x-ray absorption spectroscopy was used to investigate the environment of the Co atoms. The samples consisted of sections of Type 304 stainless steel pipe upon which the oxide layer (~4000 Å thick) was present. Samples were prepared by circulating neutral H_2O containing 100 ppt and 20 ppt ^{59}Co at 280 °C for 500 hours. It was estimated that the resulting surface oxides contained ~0.5-1.0 and ~0.1-0.2 wt. % ^{59}Co, respectively. Sections cut from the tubing were examined by simultaneous x-ray fluorescence and total electron yield detection. Since the major constituent, Fe, has a lower excitation energy than Co, the Fe fluoresced intensely throughout the Co spectrum. This made the fluorescent measurement very noisy as shown below. The XANES spectra are shown in Fig. 1 along with reference spectra from Co_3O_4 and CoO. The CoA spectra are from the higher concentration sample. The low concentration sample gave a visible edge but extensive averaging would be necessary for useful data. It is clear that the fluorescent channel CoA, f is too noisy to be useful; however, the e-yield channel CoA, e is not bad and quite similar to Co_3O_4. (Disregard the higher intensity in the near edge peaks of CoA,e compared to Co_3O_4. This is caused by the thickness effect due to self absorption in the Co_3O_4 data.) X-ray diffraction indicated that the primary components of the oxide layer were $Fe_2O_3 > Fe_3O_4$, Fe_2NiO_4, all of which have the spinel structure. Co_3O_4 is also a spinel, thus the tentative identification is to be expected since mixed spinels are common.

Fig. 1 Co K-edge XANES spectra from the surface oxide layer on Type 304 stainless steel. CoA, e and CoA, f are the total e-yield and fluorescent data channels, respectively. Co_3O_4 and CoO are normal absorption mode data from the pure compounds for comparison. A monochromator glitch near the onset of absorption distorts the CoA spectra in the region from 0-10 eV.

The total e-yield technique probes approximately the top 500 Å of the surface. In sample CoA that amounted to ~10^{15} Co atoms which gives a rough estimate of the sensitivity of the technique. Each spectrum in Fig. 1 is the result of one scan through the Co K-edge. In future work we plan to obtain better data by repetitive scanning sufficient to analyze the EXAFS as well as the XANES and thus determine the distrubution of Co-O distances in order to more accurately describe its lattice sites. Samples cut from actual power plant pipes containing ^{60}Co will also be examined. The lack of sensitivity of the e-yield technique to high energy γ-radiation will be an advantage. Also, a monochromator crystal with a different glitch pattern will allow us to inspect the near edge to determine the ratio of Co^{2+}/Co^{3+}. We believe that this more detailed characterization of the Co chemistry and crystal environment will allow a more intelligent choice of procedures to prevent the effect.

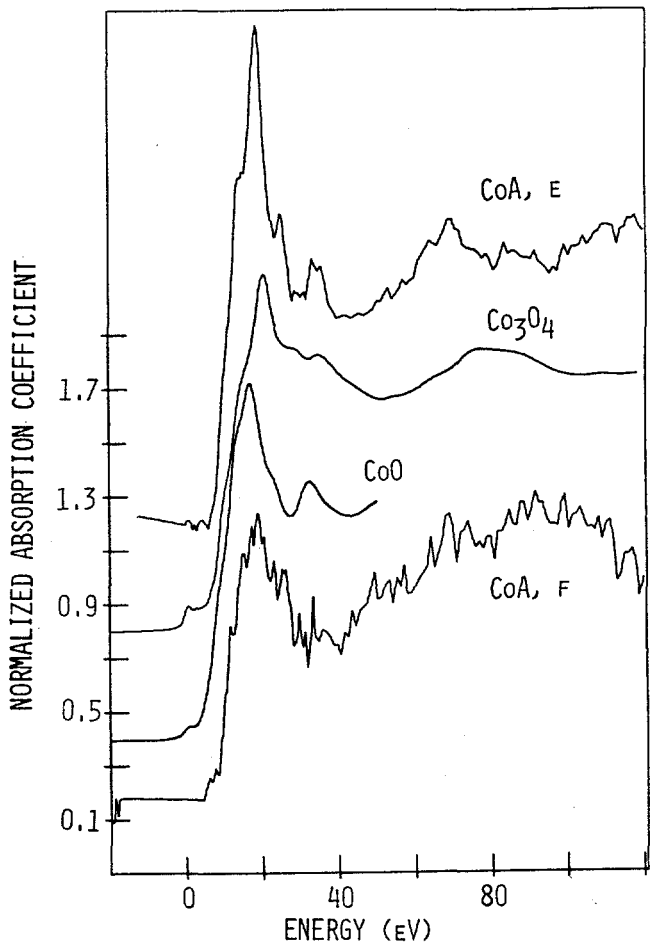

INVESTIGATION OF Pb IMPLANTED TiO_2 and $SrTiO_3$ USING TOTAL ELECTRON YIELD

R.B. Greegor(1), F.W. Lytle(1), B.C. Chakoumakos(2), R.C. Ewing(2), and G.W. Arnold(3)

(1)The Boeing Company, Seattle, WA 98124
(2)Geology Dept., Univ. of New Mexico, Albuquerque, NM 87131
(3)Sandia National Laboratories, Albuquerque, NM 87185

In this investigation Pb ions were implanted in single crystals which were then analyzed using Rutherford backscattering (RBS) and total electron yield EXAFS/XANES measurement techniques. Both 50 and 200 KeV ions were implanted at room temperature to fluences of 2-3 X 10^{14} Pb/cm^2 with a maximum range of approximately 800-900 A for the 200 KeV ions. The RBS channeling measurements were performed only on the 200 KeV Pb-implanted samples. For the TiO_2 sample, the RBS measurements indicated little discernible lattice damage. Planar oscillatory channeling was observed indicating that the near surface region was not appreciably distorted by the implant. The measurements on $SrTiO_3$ indicated that the sample had become completely RBS amorphous.

The surface sensitive electron yield EXAFS/XANES measurements were made simultaneously with conventional fluorescence and transmission techniques which are sensitive to bulk sample characteristics. The results obtained were consistent with the RBS measurements showing little damage for the 200 KeV Pb implanted TiO_2 sample and considerable alteration for the 200 Kev Pb implanted $SrTiO_3$. The transition to the RBS amorphous state in $SrTiO_3$ showed bending of the Ti-O-Ti inter-octahedral angle (as indicated by the relative reduction in the magnitude of the second major peak in the Fourier transform shown in Figure 1 for the surface measurement of the 200 KeV Pb implanted $SrTiO_3$) which is initially 180 for cubic perovskite. The XANES in Figure 2 shows alteration of the doublet in the pre-edge region into a single major pre-edge peak of increased intensity for the surface measurement of the 200 KeV Pb implanted sample. The surface sensitivity in these measurements using electron yield are estimated to be the top approximate 200 A corresponding to the electron escape depth. The 50 KeV Pb implanted $SrTiO_3$ sample did not show significant damage in the top 200 A as measured by the electron yield technique.

This work was supported in part by DOE grant DE-FG06-84ER45121.

Figure 2.
Ti K-EDGE XANES OF Pb IMPLANTED $SrTiO_3$

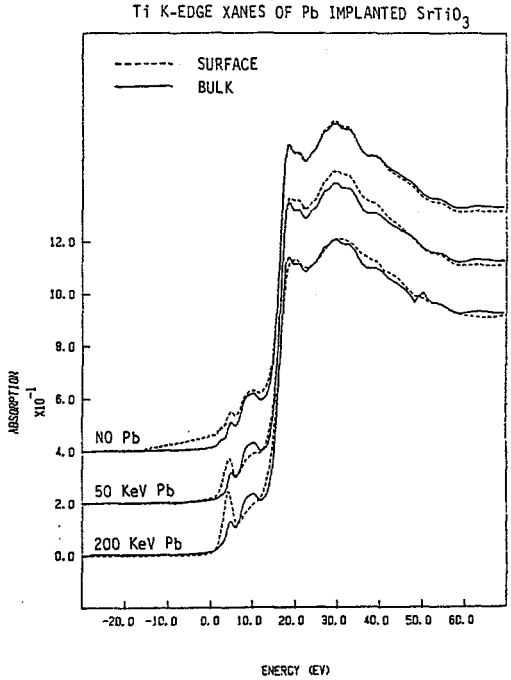

Figure 1.
FOURIER TRANSFORMS OF Ti K-EDGE EXAFS OF Pb IMPLANTED $SrTiO_3$

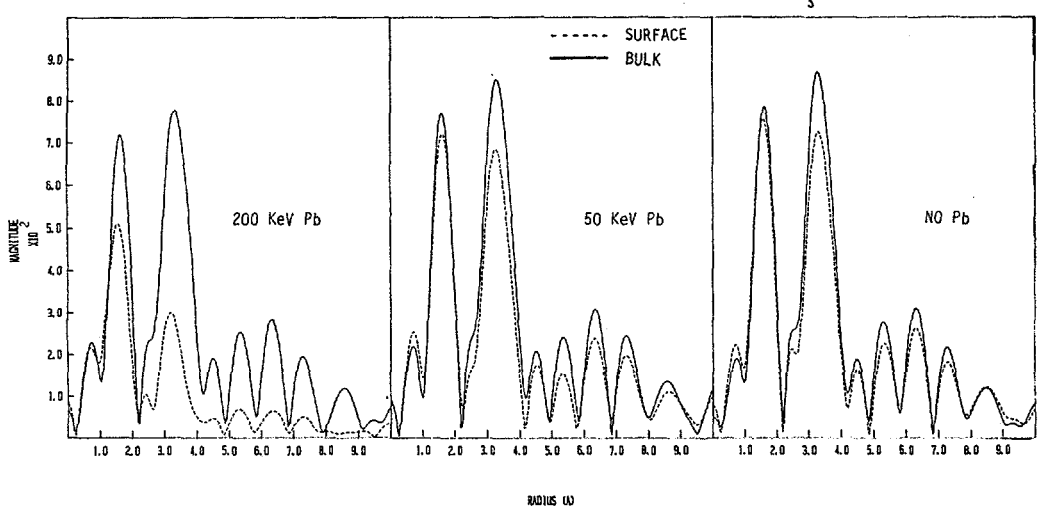

Proposal No. 1000Mp

SITE SELECTIVITY IN Mn GLASS USING OPTICAL XANES

R.B. Greegor, F.W. Lytle and D.R. Sandstrom
The Boeing Company, Seattle, WA 98124

M. Weber and J. Wong
Lawrence Livermore National Laboratory, Livermore, CA 94550

EXAFS and XANES provide information about coordination and bonding of specific atomic species in many types of materials. The information obtained is an average of all the sites present in the material for the given specific atom. In EXAFS or XANES the core hole created by the probing incident x-ray is filled by an electron resulting in radiative emissions including fluorescence at x-ray and optical wavelengths. The fluorescent emissions have been shown to be correlated to the x-ray absorption coefficient. Atoms in different local environments fluoresce at different optical wavelengths. Site selectivity can be obtained in principle by spectral measurements of the x-ray induced optical emissions. Therefore Optical EXAFS can be both atom specific via the x-ray absorption wavelength and site specific via the optical emission wavelength.

Optical EXAFS measurements were made using a holographic grating monochromator (apx. 250 to 800 nm) coupled to a Tracor Northern multi-channel analyzer the output of which was integrated into the data collecting system of SSRL beam line VII-3 using a serial RS232 interface. The samples examined at the Mn K-edge (6539 eV) contained 1% to 5% MnO in sodium glasses having divalent Mn in tetrahedral and octahedral sites. The centers of gravity of the x-ray induced 4T1 > 6A1 optical emission bands for the two sites are shifted because of the different local fields at the respective sites (1). Spectral data was collected at these two bands (apx. 450-550nm T, 600-700nm O as shown in Figure 1) along with the x-ray fluorescence.

Examination of the 1s > 3d transition, which is sensitive to T/O site symmetry, demonstrated the feasibility of simultaneous atom and site selectivity. The Mn K-edge XANES data collected in x-ray fluorescence mode is shown in Figure 2. The characteristic pre-edge feature for Mn in a tetrahedral site is shown in the spectra for the 1% MnO glass. Note that this feature is absent in the spectra 5% MnO glass so that the difference of the fluorescence spectra for the 1 and 5% MnO glass shows the contribution due to Mn in tetrahedral sites. The Mn K-edge optical XANES is shown Figure 3. In this figure all the data was collected on the 1% MnO sample which contained Mn in both octahedral and tetrahedral sites. These sites were separated by setting the appropriate optical regions on the multi channel analyzer as discussed above. The difference spectra in Figure 3 shows the contribution due to Mn in tetrahedral sites and this difference is similar in appearance to the difference shown in Figure 2 which resulted from data taken from two samples (1% and 5%). Thus the principle of simultaneous atom and site selectivity is demonstrated in the 1% MnO glass. With further refinements in signal to noise this method could become a valuable addition to EXAFS/XANES techniques.

This work was supported in part by DOE grant DE-FG06-84ER45121.

1. K. Bingham and S. Parke, Phys. and Chem. of Glasses, 6(6), 224 (1965).

Figure 1.

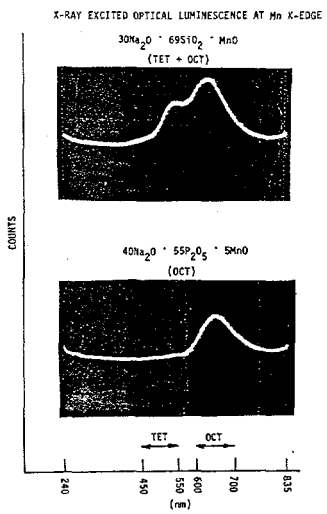

Figure 2.

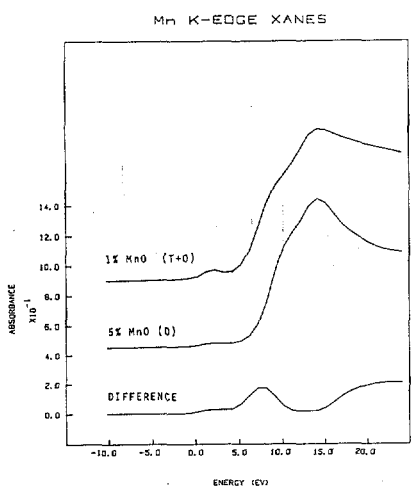

Figure 3.

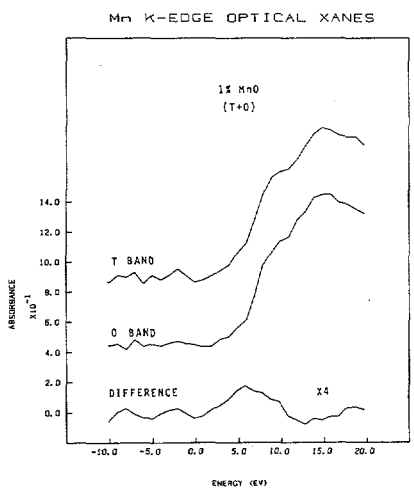

UNIVERSAL INTERACTIONS IN UNDULATING MEMBRANES: A SERIES OF SYNCHROTRON X-RAY STUDIES OF DILUTE 1-DIMENSIONAL FLUID MULTILAYERS

C. R. Safinya, D. Roux*, G. S. Smith and E. B. Sirota
Exxon Research and Engineering Company
Clinton Township, Route 22 East
Annandale, NJ 08801 USA

* Permanent address: Centre de Recherche Paul Pascal
Centre National de la Recherche Scientifique
33405 Talence, Bordeaux, France

The basic stabilizing forces between multilayer systems consisting of stacks of alternating membrane sheets and water is known to originate in usual cases from a balance between van der Waals (electrodynamic), electrostatic and hydration forces(1,2). In these usual surfactant systems the bending modulus of the interface is typically around 40 k_BT so that thermal fluctuation effects can be ignored. Thus, for these flat multimembrane systems the attractive van der Waals forces prevent the layers from separating more than about 30 Å. However, in some recently discovered quaternary and ternary surfactant systems very large dilutions with intermembrane distances of up to a few thousand angstroms has been observed.

In our synchrotron work[3,4] we have studied the precise nature of competing forces in both neutral and charged layered microemulsion and lipidic systems in these novel dilute phases. Aside from the classical regime dominated by detailed intermolecular interactions (e.g. van der Waals, electrostatics), we have discovered a novel universal regime where the forces originate from the entropic undulations of layers and depend only on geometric and elastic parameters such as the layer spacing and the layer rigidity. Our work has also shown that this new regime is distinct from the classical regime in which largely separated layered colloids are stabilized because of their mutual electrostatic repulsion. Our work is consistent with the theoretical work of Helfrich[5] which had suggested that violent out-of-plane fluctuations of membranes, if succiently strong, should give rise to an overwhelmingly large long range repulsive interaction leading to the stability of very dilute (50 Å < d < 5000 Å; d = interlayer spacing) one-dimensional layered colloids.

In each system, we have found that the L_α phase corresponds to a Landau-Peierls system with characteristic power-law behavior for the first and second harmonic of the structure factor with power law exponent η_m scaling as m^2. For this Landau-Peierls system, which consists of condensed matter systems at their lower marginal dimension, δ-function Bragg peaks at $(0,0,q_m = mq_0 = m2\pi/d)$, (m = harmonic order = 1,2,...) are replaced by singularities with asymptotic power law behavior $S(0,0,q_z) \approx |q_z - q_m|^{-2+\eta_m}$ and $S(q_\perp,0,q_m) \approx q_\perp^{-4+2\eta_m}$. Here $\eta_m = m^2 q_0^2 k_B T/(8\pi\sqrt{BK})$ and q_z and $q_\perp$ are components of the wavevector normal and parallel to the layers and B and K are the bulk moduli for layer compression and layer curvature. This lineshape was originally derived by Caillé.

Because B(d) is just the layer compressibility modulus it is directly related to the interlayer interactions; that is, $B = d^2 \frac{\partial^2 F(d)}{\partial d^2}$ where F is the interlayer free energy density. Thus, since $\eta \propto B^{-1/2}$, the scattering allows us to directly access the thermodynamic behavior of the system.

We report on synchrotron X-ray scattering studies in the fluid L_α phase of three systems as a function of the interlayer distance d. In the first system the neutral membrane consists of water layers coated with a mixture of surfactant (SDS) and cosurfactant (pentanol) molecules. The layers are separated by dodecane (i.e. an oil dilution study). In the second system, the negatively charged membranes consisted of a mixture of SDS and pentanol and the layers were separated by water giving rise to long range electrostatic forces. The third system corresponded to a neutral biological membrane consisting of DMPC and pentanol separated by water.

Fig. 1 shows the schematic of our set-up. The monochromator and analyzer consisted of a double bounce Si(111) and a triple bounce Si(111) channel cut crystal set at 8 KeV in the non-dispersive configuration yielding a very sharp in-plane Gaussian resolution function with very weak tail scattering with half-width at half-maximum (HWHM) 8 x 10^{-5} $Å^{-1}$. A sharp Gaussian out-of-plane resolution function (HWHM = 10^{-3} Å) was achieved by use of extremely narrow slits.

In the oil dilution series, we carried out detailed studies for 10 distinct mixtures: x = 0, 0.07, 0.13, 0.18, 0.29, 0.35, 0.47, 0.54, and 0.62. Here x is the percent dodecane by weight of the mixtures. We show in Fig. 2A typical scattering profiles for longitudinal scans through the first harmonic for x between 0 and 0.54 in the L_α phase where the total layer spacing $d = 2\pi/q_0$ increases from 3.82 nm to 11.5 nm. A striking feature of the profiles in Fig. 2A is the tail scattering which becomes dramatically more pronounced as d increases. Fig. 2B shows profiles of the first harmonic of four mixtures along the water dilution path. The % by weight of water is indicated above each profile. The contrast between the two systems is qualitatively clear: In the charged system the ratio of the tail to peak scattering is, to first order, not affected along the dilution. The behavior of S(Q) for the biological membrane system is analogous to that observed in the neutral oil dilution series.

The solid lines in Fig. 2 are fits by the Caillé(3) lineshape giving us $\eta(d)$. Fig. 3 summarizes and plots the variation of the exponent η as a function of the repeat distance d for the three dilution systems. The open squares correspond to the SDS oil dilution system while the filled circles to the biological membrane system. The open triangles correspond to the SDS water dilution case. The solid line is the prediction of pure undulatory intermembrane interactions and the dashed line results from the solution of the Poisson-Boltzman equation associated with long range electrostatic forces(2).

The results clearly show that when diluting a charged membrane with pure water the interaction are dominated by long range electrostatic forces and will be system dependent. In contrast, for neutral flexible membranes where entropically induced undulation forces dominate, $\eta(d) = 1.33\ (1 - \delta/d)^2$ (δ is the membrane thickness) approaches a constant value for dlarge d, as

predicted by Helfrich. We stress that because the undulation forces are entropic in origin, they predict universal behavior as a function of δ/d for any membrane system.

The experiments were carried out both on beam line VI at SSRL and beam line X10A at NSLS. One of us (G.S.S.) was supported in part by an NSF Grant No. DMR-8307157. SSRL and NSLS are supported by the U.S. Department of Energy.

1. G. S. Smith, C. R. Safinya, D. Roux, N. A. Clark, Mol. Cryst. Liq. Crystal 144, 235 (1987).
2. G. S. Smith, E. B. Sirota, C. R. Safinya, N. A. Clark, Phys. Rev. Lett. 60, 813 (1988).
3. C. R. Safinya, D. Roux, G. S. Smith, S. K. Sinha, P. Dimon, N. A. Clark, A. M. Bellocq, Phys. Rev. Lett. 57, 2718 (1986).
4. D. Roux and C. R. Safinya, J. de Physique, in press, February (1988).
5. W. Helfrich, Z. Naturforsch 33a, 305 (1978).

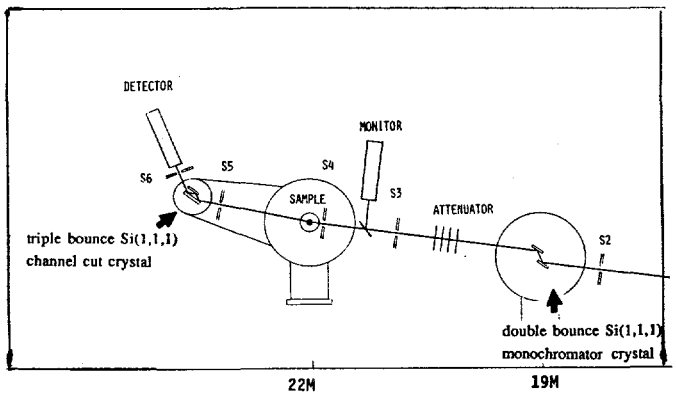

Fig. 1

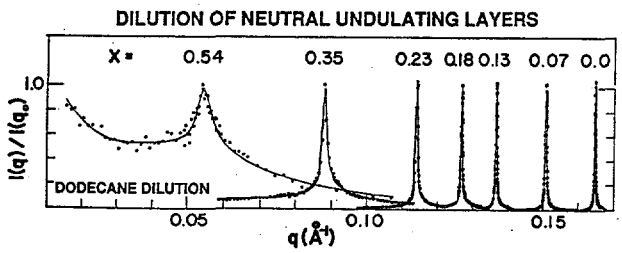

Fig. 2a

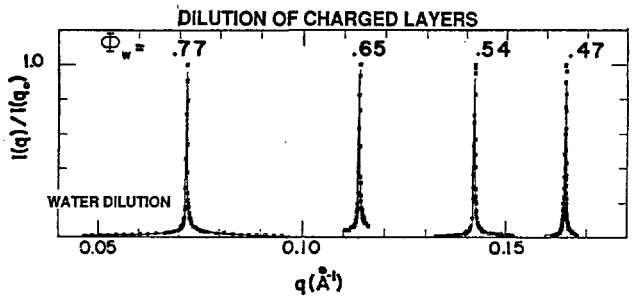

Fig. 2b

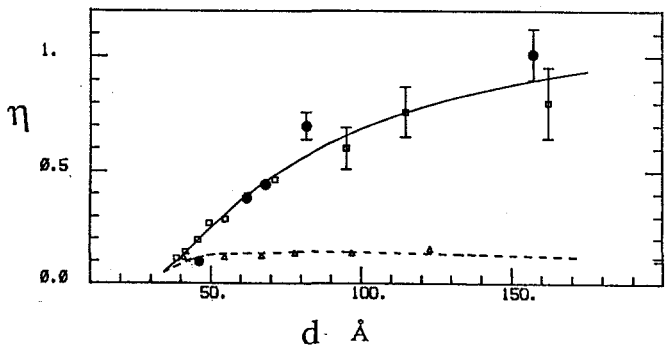

Fig. 3

DYNAMIC "STEADY STATE" MICROSCOPIC STRUCTURE OF COMPLEX FLUIDS STUDIED IN A COUETTE X-RAY SHEAR CELL

Proposal No. 1001Mp

C. R. Safinya, R. Plano, E. B. Sirota and G. S. Smith
Exxon Research and Engineering Co.
Route 22 E, Clinton Township
Annandale, NJ 08801

We present preliminary studies of the microscopic steady state structure of a colloidal suspension of polyballs induced as a consequence of shear. A first prototype of an x-ray Couette cell has just been completed and initial studies are beginning. These types of studies are designed to correlate macroscopic flow properties to microscopic structures. The present shear cell (Fig. 1) has the capability of producing shear rates as large as $\dot{\gamma}$ maximum = 40000Hz. For a given shear rate $\dot{\gamma}$ those dynamical process of the system which have a relaxation time τ greater than a critical time $\tau_c \equiv 1/\dot{\gamma}$ will be affected. For example, in a binary mixture close to the critical point, this relatation time is the time required for a fluctuation to thermally dissipate. For $\tau\dot{\gamma}>1$ then, one expects to spatially distort the density-density correlation function measured in an x-ray experiment. Systems of interest include microemulsions, colloidal suspensions, polymeric fluids and liquid crystals. We show in Fig. 2 at rest, ($\dot{\gamma}$ = 0) the scattering intensity versus $2\theta = \mathrm{Sin}^{-1}(q/2k)$ ($k \simeq 4.0\text{Å}^{-1}$) for a liquid system consisting of polyballs (10% by volume) of diameter 910Å suspended in a solvent (solvent = 50%-50% water-methanol). The first peak of the liquid structure factor is clearly visible.

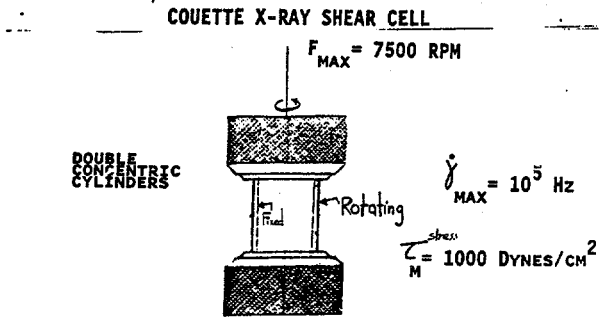

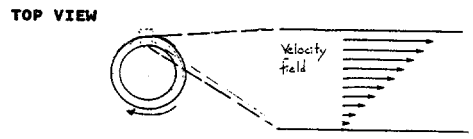

Fig. 1

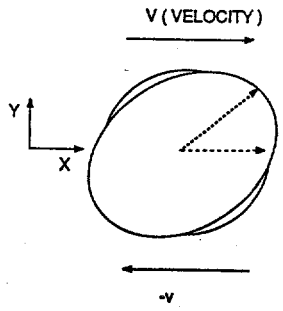

Fig. 3

Fig. 3 shows the geometry for the experiment. The shear plane concides with the x-y plane: the flow direction is along x and ∇v is along y. The circle represents the first peak in S(Q) of a liquid at rest (V=0). The elipse describes the onset of distortion.

Fig. 4 shows radial scans in the shear plane along the $\pi/4$ direction (shown as a dashed line in the x-y plane) through the first peak of S(Q) for $\dot{\gamma}$ = 0 (dashed line), $\dot{\gamma}$ = 100S^1 (solid line) and $\dot{\gamma}$ = 200 S^{-1} (open squares). The onset of distortion is clearly visible with S(Q) moving towards larger Q.

To summarize, our initial limited run time has allowed us to test the newly designed Couette cell and see evidence for the onset of distortion. Future work will concentrate on elucidating the nature of S(Q) at higher shear rates where simulations have predicted novel "steady state" shear induced ordered phases.

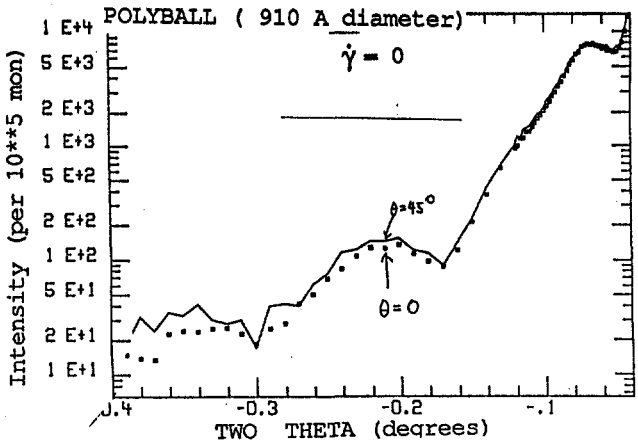

Fig. 2

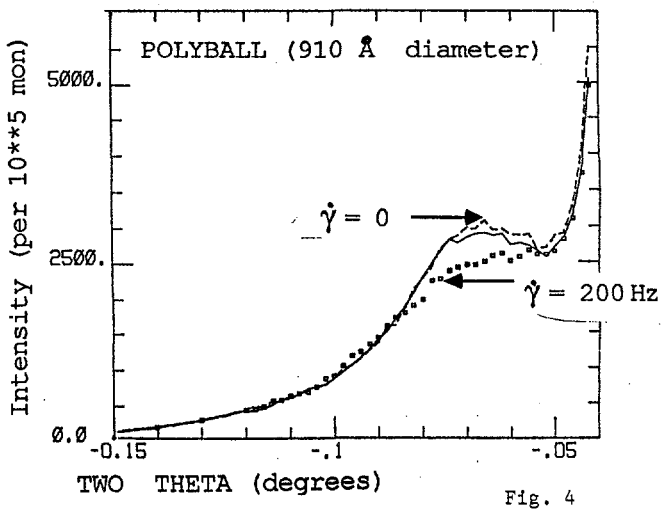

Fig. 4

SAXS STUDY OF COLLOIDAL CRYSTALS

Proposal No. 1001Mp

E. B. Sirota, S. K. Sinha,
H. D. Ou-Yang, P. M. Chaiken, (U. Penna\Exxon)
J. D. Axe (BNL) and Y. Fujii (U. Osaka)
Exxon Research and Engineering
Route 22E Clinton Township
Annandale, NJ 08801

We have performed a small angle x-ray scattering study of the structure of colloidal systems of polystyrene spheres with a 420Å radius. Methanol was used as a solvent instead of water, in order to provide sufficient contrast in electron density between the colloids and solvent. Si(111) monochromator and analyzer were used and the out-of-plane resolution was determined by slits. We were thus able to see peaks occurring as low as $0.005Å^{-1}$. The measurements were performed at the Exxon Beamline X10A using a Si double-bounce monochrometer and a Si analyzer, with tight slits to cut out the tails and background scattering. In the crystalline phases we found it necessary to rotate the sample (which was contained in a 2mm diameter capillary) in order to obtain a powder average.

We have mapped out the phase diagram (Fig. 1) as a function of colloid concentration and the ion concentration (provided by adding HCl) which screened the electrostatic field. We have identified four phases: A liquid, a FCC crystal, BCC crystal and a locally FCC glass phase. There was also a region of coexisting FCC and BCC phases. Since the scattering is weak and the Born approximation can be employed, one can use the intensities of the crystalline peaks to determine the Debye-Waller factor. The minima in the scattering correspond to the minima in the form factor of the spheres.

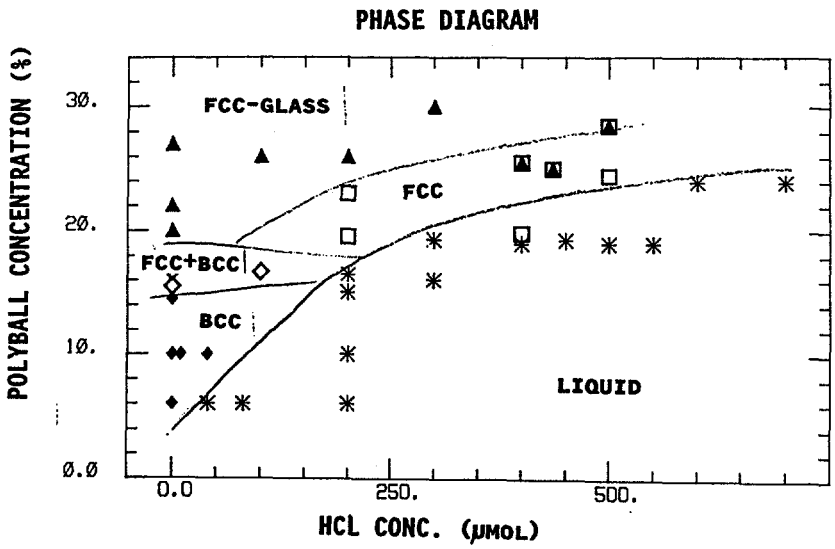

Extended X-ray Absorption Fine Structure (EXAFS) Studies of Platinum-Tin Catalysts

G. Meitzner, G.H. Via, F.W. Lytle (a),
S.C. Fung, and J.H. Sinfelt

Corporate Research Laboratories
Exxon Research and Engineering Company
Annandale, New Jersey 08801

(a) The Boeing Company, Seattle, Washington 98124

Reforming catalysts are used by the petroleum industry in the production of aromatic hydrocarbons for gasoline [1]. One important type consists of platinum and tin dispersed on a refractory alumina [2,3]. We felt that our understanding of this catalyst would benefit from the physical and chemical information on platinum and tin that x-ray absorption spectroscopy could provide.

We made extended x-ray absorption fine structure (EXAFS) and x-ray absorption edge studies of a 1 wt.% Pt - 1 wt.% Sn/Al_2O_3 catalyst which had previously been exposed to hydrogen at high temperature (775-795K) and then cooled to 140K. For comparison, similar studies were conducted on a 1 wt.% Pt - 0.6 wt.% Sn/SiO_2 sample. Beam line VI was essential for measurements of x-ray absorption in the vicinity of the tin K edge since these required high x-ray flux at energies above 29 keV.

For the $Pt-Sn/Al_2O_3$ catalyst the extent of coordination of tin by platinum atoms or by other atoms of tin was small, but the extent of coordination by oxygen was substantial. An analysis of the energy shift of the K absorption edge of the tin indicated that the tin was not present as Sn^{+4} (figure 1). The EXAFS data, coupled with the absorption edge data, suggested that the tin was largely present as Sn^{+2}. There appeared to be a significant interaction between the platinum and the tin, since the platinum was more highly dispersed on alumina when tin was present, and since an unusually short platinum-tin distance contributed to the platinum and to the tin EXAFS. It seems reasonable to regard the catalyst essentially as platinum clusters dispersed on an alumina which had Sn^{+2} present at the surface. The EXAFS data on the $Pt-Sn/SiO_2$ sample lead to very different conclusions. In that case, most of the tin had an oxidation state of zero, and the material consisted predominantly of bimetallic entities of platinum and tin on silica. The work reported here has been accepted for publication [4].

1. Sinfelt, J.H., "Bimetallic Catalysts: Discoveries, Concepts, and Applications"; Wiley: New York, 1983, pp 130-157.

2. Thorn, J.P., Guyer, W.R.F., and Arundale, I., U.S. Patent 2,861,959, 1958.

3. Rausch, R.E., U.S. Patent 3,745,112, 1973.

4. Meitzner, G., Via, G.H., Lytle, F.W., Fung, S.C., and Sinfelt, J.H., J. Phys. Chem., 0000(1987).

TIN K EDGE ENERGY SHIFTS FOR PtSn CATALYSTS AND REFERENCE MATERIALS

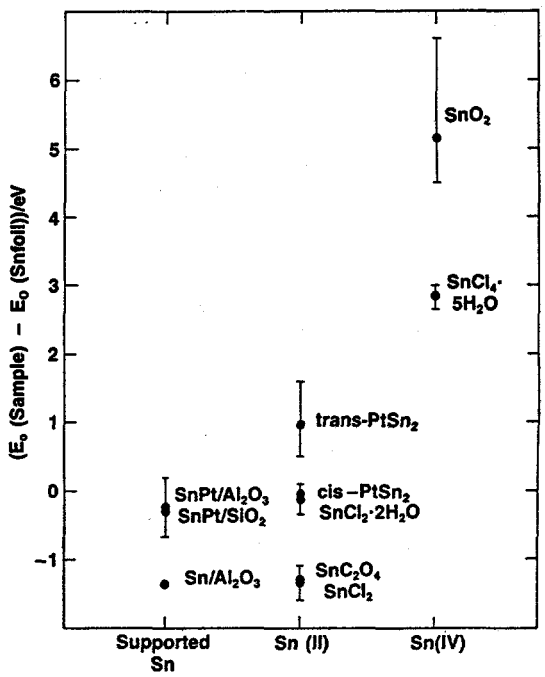

Figure 1. Energy shifts of the K-absorption edges of tin for $Pt-Sn/SiO_2$ and $Pt-Sn/Al_2O_3$, for Sn/Al_2O_3 (0.6 wt.% Sn), and for various Sn(II) and Sn(IV) reference materials. The shifts were determined by using the edge energy of a tin foil as a reference. In each experiment, the absorption edge of the tin foil was determined with the x-rays transmitted through the sample of interest.

Proposal No. 1001Mp

SULFUR K EDGE X-RAY ABSORPTION SPECTROSCOPY OF ASPHALTENES AND MODEL COMPOUNDS

G. N. George and M. L. Gorbaty

EXXON Research and Engineering Co.
Annandale, NJ 08801

INTRODUCTION

A major gap in our current knowledge of the chemistry of heavy hydrocarbons concerns the chemical forms and quantities of organically bound sulfur in these materials. Current knowledge is based almost entirely on the characterization of volatile products, and none of the methods currently in common use (cf. 1) is adequate for determining the forms of organically bound sulfur in native coals or in native petroleum samples. Sulfur K edge X-ray absorption spectroscopy has shown some potential to solve these problems (2).

We have investigated the utility of sulfur K edge X-Ray absorption spectroscopy for the purpose of investigating the forms of organic sulfur in solids and nonvolatile liquids.

Figure 1.

Sulfur K edge spectra of Asphaltenes and selected model compounds.

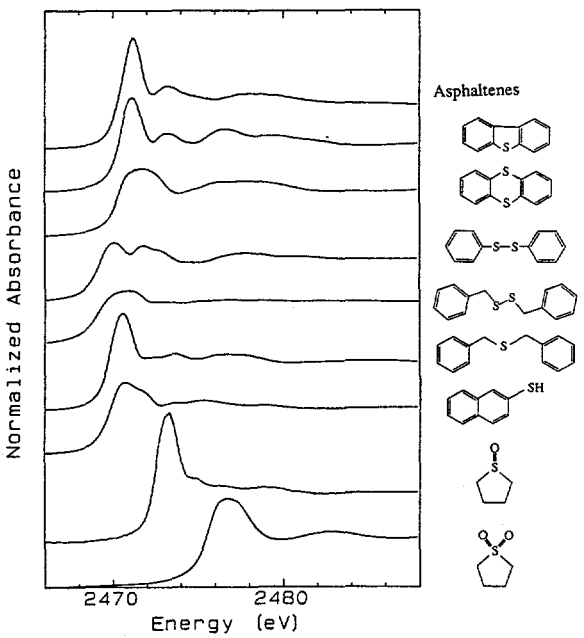

RESULTS AND DISCUSSION

Figure 1 compares the sulfur K edge XANES spectra of a number of model compounds and of an asphaltene sample. The XANES can be seen to vary widely from compound to compound. As might be anticipated, the edge positions of compounds with more oxidized sulfur are notably higher in energy than for those with reduced sulfur. It is apparent that the sulfur XANES can readily be used to distinguish between these types of sulfur and that the asphaltenes do not contain appreciable quantities of oxidized sulfur. Casual inspection of figure 1 might suggest that the spectra from sulfur in different environments can be similar, notably, dibenzyl sulfide and dibenzothiophene. Closer inspection reveals that the edge of dibenzothiophene is displaced from that of dibenzyl sulfide, the first inflection point being some 0.6eV higher for the former compound. A general conclusion is that the sulfur K edge XANES can be used as a fingerprint for the chemical nature of the sulfur under investigation. Thus dibenzothiophene and benzothiophene resemble one another, however dibenzothiophene and, for example, thianthrene are markedly different. The compound whose XANES bears the most resemblance to the asphaltene sample is dibenzothiophene; there are, however, some significant differences, most of which lie in the higher energy region of the spectrum.

We conclude that Sulfur K-edge X-ray absorption spectroscopy can be useful as a tool for determining the environment of sulfur in amorphous materials such as oil products, and that the sulfur in the asphaltene sample examined is mainly present in aromatic ring systems resembling dibenzothiophene, but presumably within far more extensive polynuclear aromatic ring systems.

REFERENCES

1. Van Krevelen, D.W. (1961) Coal, Elsevier Amsterdam p 171
2. Spiro, C.L., Wong, J., Lytle, F.W., Greegor, R.B., Mayolette, D.H. and Lamson, S.H. (1984), Science, **226**, 48

SCATTERING STUDIES OF La_2CuO_4 SINGLE CRYSTALS: CHARGE DENSITY MODULATIONS

D. E. Moncton and K. L. D'Amico
Exxon Research and Engineering Co., Annandale, NJ 08801

J. Bohr and J. Als-Nielsen
Risø National Laboratory, Denmark

R. M. Fleming and J. P. Remeika
AT&T Bell Laboratories, Murray Hill, NJ

D. Vaknin
University of Pennsylvania, Philadelphia, PA

We have studied the structure of single crystals of the high-temperature superconductor parent compound La_2CuO_4 using high resolution X-ray scattering studies on the 54-pole wiggler Beamline VI-2. The samples were grown at Bell Labs and treated in several different ways. Original studies were carried out in April '87 at SSRL. A second run was done at HASYLAB in Hamburg, West Germany in July '87, followed by a third run in November '87 also done at SSRL at Beamline VI-2.

In the initial run in April a charge density wave was observed in the flat-plate single crystal sample along the orthorhombic [001] direction. Previous neutron diffraction studies of powdered samples of the material had identified and characterized an antiferromagnetic phase of the material with a wave vector along [100].[1] This structure was present for the Oxygen deficient stoichiometry for $La_2CuO_{4-\delta}$ with δ approximately equal to 0.015. [2] The powdered sample was observed to have a Néel temperature of ~220K. These studies prompted the search for a weak satellite feature in the single crystal sample of the material which had been heat-treated to reduce the Oxygen content below the stoichiometric value.

Figs. 1 and 2 show the result of the April study. Panel (a) of Fig. 1 shows the allowed bulk (200) and (002) reflections for the Oxygen deficient material at T=9K. Both peaks occur along (h00) because of the twinning in the crystal. Panel (b) is the the scan near (100) showing the presence of the (001) peak and the absence of the (100). Fig. 2 shows the scan near (100) for a non-heat-treated sample from the same boule. Clearly the peak is at least a factor of 10 weaker for the crystal which was not heat-treated to intentionally reduce the Oxygen content.

A subsequent experiment sought to determine the atomic distortions responsible for the CDW in the material. A sample was heat-treated in the same manner and ground to the shape of a sphere for the purpose of doing crystallography. A 200 micron sphere size was chosen for this experiment, which was carried out at the D4 beamline at HASYLAB. This experiment was frustrated by the presence of $\lambda/2$ contamination in the bending magnet beamline's spectrum, however the presence of the CDW peaks in the original rectangular sample was confirmed with the observation of the (1,11,0) reflection. Results from this measurement were used to guide the choice of experimental conditions for the November run at SSRL.

For this experiment, the heat-treated sphere of 200 microns was employed. The CDW peak was again identified for this sample, as seen by the presence of the (hk0) type peaks with measurable intensity. The original (001) peak was too weak to be seen for this sample. In all, 33 CDW peaks were measured, 14 of which had measurable intensity. In addition, 32 other bulk allowed Bragg peaks were measured.

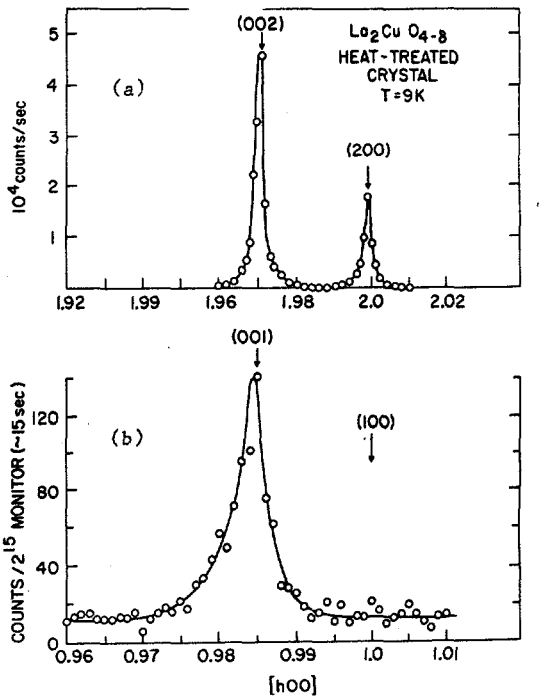

Fig. 1: Bulk reflections (a) and CDW reflection (b) for the Oxygen deficient crystal at T=9K, showing the presence of the peak along [00L] and the absence of the peak along [H00].

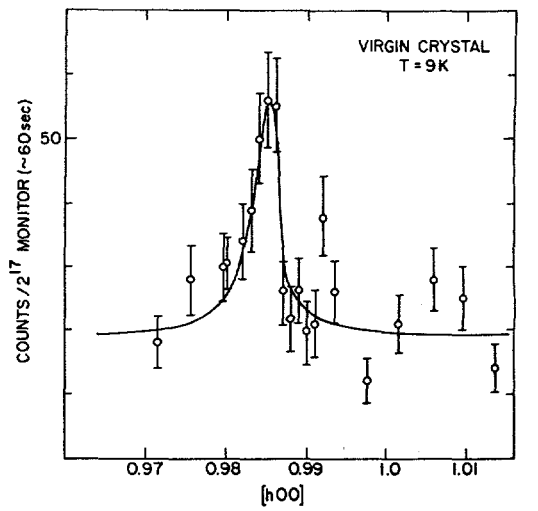

Fig. 2: CDW peak for the non-heat-treated crystal at T=9K. The feature is approximately a factor of 10 weaker than in the heat-treated crystal.

Fig. 3 shows a comparison of the measured and calculated structure factors for the allowed (0k0) peaks for the orthorhombic structure for La_2CuO_4 with k=4,6,8,10,12,14,16 and 18. A correction for both absorption and the Lorentz factor has been applied to the measured data. The data have been arbitrarily normalized to the (004) reflection. Clearly the agreement between the intensity values is quite good. With this as a starting point it is possible to use the measured CDW peak data to determine the distortions responsible for the CDW. The data analysis to determine these distortions is currently in progress.

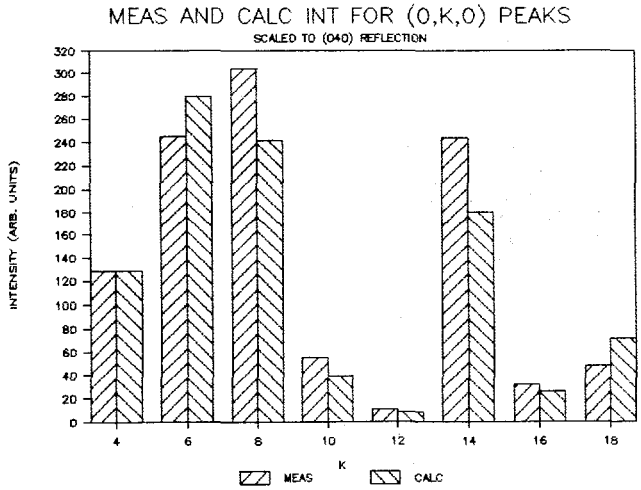

Fig. 3: Comparison of the measured and calculated peak intensities for the heat-treated crystal at T=9K. Peak intensities have been scaled to the (040) peak.

REFERENCES

1. D. Vaknin, S.K. Sinha, D.E. Moncton, D.C. Johnston, J.M. Newsam, C.R. Safinya, and H.E. King, Jr., Phys. Rev. Lett. 58, 5802(1987).

HIGH RESOLUTION POWDER X-RAY DIFFRACTION

J. M. Newsam, K. S. Liang and G. Hughes
Exxon Research and Engineering Company
Clinton Township, Route 22 East
Annandale, NJ 08801 USA

Most technologically important inorganic materials are polycrystalline. Characterization of the structural chemistries of such materials, therefore, generally relies on conventional powder diffraction techniques. This is a major problem because conventional powder diffraction data is generally unsuitable for "ab initio" structure solution. The brightness of the synchrotron source enables microcrystal diffraction experiments, although as a technique this is still under development. Additionally, the brightness and the excellent intrinsic resolution of the source can be exploited in performing high resolution powder diffraction experiments.

In April 1986, during a total of some two and a half days of usable beam time, we conducted a series of powder experiments on BL-VI. The bulk of this time was spent on scans on a vanadyl organophosphonate. The compromises associated with definition of the instrumental resolution by diffracted beam slits or by a LiF analyzer crystal were compared. The diffraction profile $0< 2\theta <45°$ (λ = 1.55 angstroms) was then accumulated at a typical peak width of 0.04°, some 5x better than that accessible on our in-house Siemens system. Solution of the structure of this material using this data is in progress. Additionally, we scanned portions of the diffraction profiles of a standard (Al_2O_3) and two other novel phases, a zeolitic material and the intermetallic KSnAs. Although the diffraction pattern of the former had been indexed on the basis of a large orthorhombic cell, the high-resolution data immediately revealed it to comprise a combination of broad and very sharp peaks (Figure 1). Even this limited data has been helpful in unravelling the complex phase diagram of this system. The intermetallic phase was found to be highly crystalline, but with a lorentzian line-shape component that is index-independent. The component, therefore, arises from inhomogeneity, rather than from the presence of planar defects that had been predicted previously.

These preliminary experiments on BL-VI thus illustrate well the three areas in which high resolution powder diffraction measurements using synchrotron radiation will have a major impact. A report discussing the present experiments in more detail is in preparation.

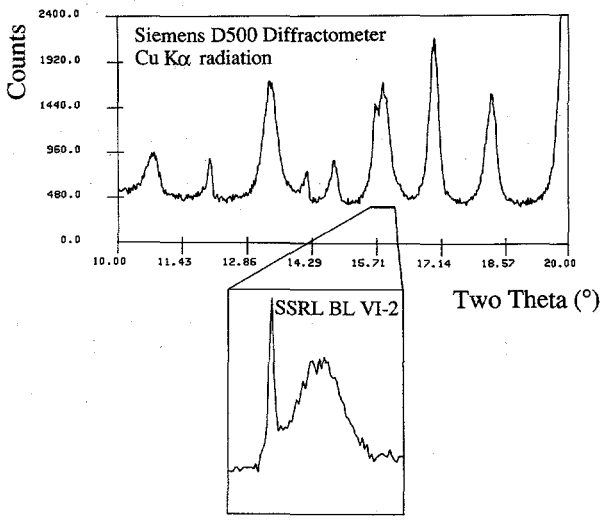

Figure 1. Scans of the powder X-ray diffraction (PXD) profile of a microporous cesium stannosilicate sample. In-house data (fine-focus X-ray tube source) are compared with a portion of the PXD profile accumulated on beam line VI-2.

Bond Orientational Ordering in Tilted Hexatic Liquid Crystal Films

J.D. Brock, R.J. Birgeneau, J. D. Litster, B. McClain, D.Y. Noh
Department of Physics, Massachusetts Institute of Technology, Cambridge, Massachusetts 02139

P.M. Horn
I.B.M. Thomas J. Watson Research Center, Yorktown Heights, New York 10598

Condensed matter systems may be described by independent positional and bond orientational (BO) order parameters. In general, there is no symmetry reason why the positional and BO order must vanish at the same temperature. Thus it is possible to have a phase of matter in which the positional order is short range but the BO order is long range. Indeed, it has been suggested that such an unusual phase could occur in certain smectic liquid crystal materials. This phase has been labeled *stacked hexatic* for hexagonal symmetry systems.

Very interesting theoretical[1] predictions have been made for the so called *tilted hexatics* in which the molecules are tilted with respect to the smectic layer normal. Coupling to the tilt field should induce long-range hexatic order even in the fluid S_C phase. X-Ray scattering studies on *bulk* samples both confirmed the predicted behavior and uncovered a new and unanticipated scaling of the Fourier coefficients describing the hexatic ordering.[2]

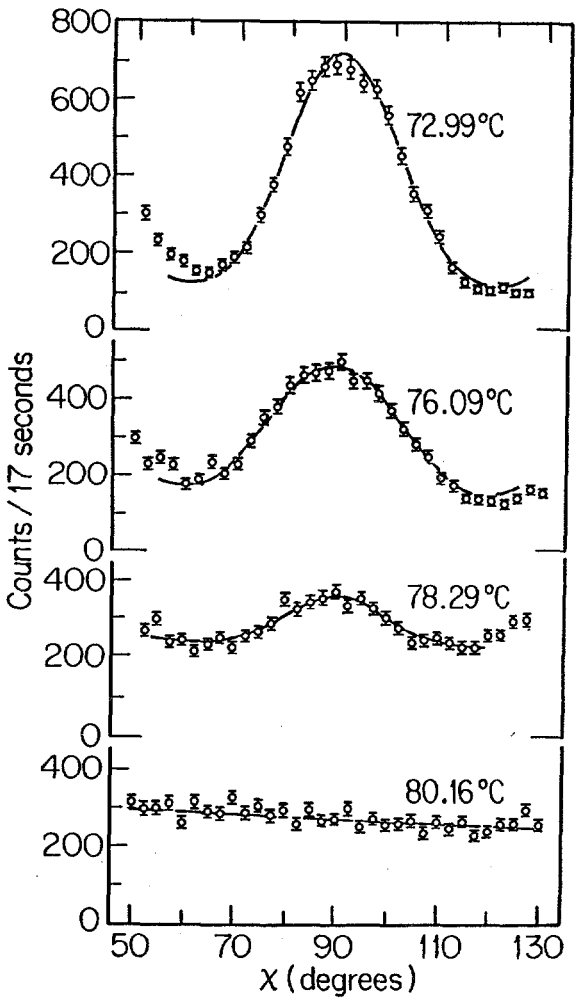

Figure 1: Scans probing development of BO order near the $S_C \rightarrow S_I$ phase boundary.

We report the results of an X-Ray scattering study of the *fluid/hexatic/solid* phase transition in very thin, freely suspended films of 4-(2-methylbutyl)phenyl 4'-(octyloxy)-(1,1')-biphenyl-4-carboxylate (8OSI). A modulation of the diffuse ring of scattering associated with fluid systems is the X-Ray scattering signature of a long range ordered hexatic phase. Figure 1 shows several scans taken along the peak of the fluid and molecular structure factors at several temperatures near the fluid (S_C) to hexatic (S_I) phase transition. Such scans probe the BO order of the system. The sample was a freely suspended film of 8OSI, approximately 23 smectic layers thick. To measure quantitatively the value of the various BO order parameters, the data were fit to the Fourier Series

$$S(\chi) = I_0 \left[\frac{1}{2} + \sum_{n=1}^{13} C_{6n} \cos(90-\chi) \right] + I_{BG}(\chi).$$

The results for the first three Fourier coefficients are plotted in Figure 2. Contrary to the thick film case,[2] the higher Fourier coefficients describing the BO order are suppressed in the hexatic phase in very thin films. This suppression is consistent with a two-dimensional BO order parameter, rather than the manifestly three-dimensional BO order parameter found in very thick films.[3]

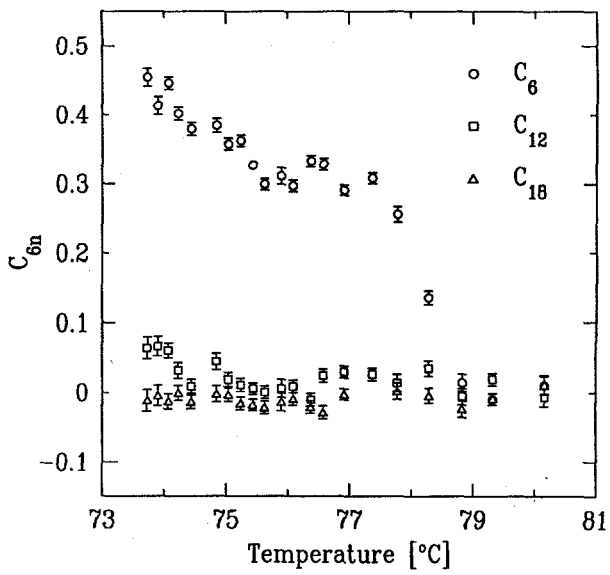

Figure 2: First three Fourier coefficients describing the BO order.

1. D.R. Nelson and B.I. Halperin, Phys. Rev. B **21**, 5312 (1980); R. Bruinsma and D.R. Nelson, Phys. Rev. B **23**, 402 (1981).

2. J.D. Brock, *et al.*, Phys. Rev. Lett. **57**, 98 (1986); Amnon Aharony, *et al.*, Phys. Rev. Lett. **57**, 1012 (1986).

3. J.D. Brock, Ph.D. Thesis, Massachusetts Institute of Technology, 1987 (unpublished).

SYNCHROTRON X-RAY POLYCRYSTALLINE DIFFRACTOMETRY - IV & V

W. Parrish, M. Hart[a], M. Bellotto[b], L Depero and C. Erickson

IBM Research Division, Almaden Research Center, 650 Harry Road
San Jose, California 95120-6099

INTRODUCTION

Improvements of instrumentation continued with a number of developments. The powder diffractometer was mounted on an accurately movable platform which permitted moving the instrument in and out of the beam. This allowed use of a specimen vacuum chamber and made it easier to change specimens. A stepping motor to remotely control the centering of the entrance slit was installed. A He flow path was installed between the pipe to beyond the channel monochromator.

The difference between profile shapes obtained with conventional X-ray tube focusing methods and the synchrotron radiation parallel beam method is shown in Fig. 1 for a pair of quartz reflections. The greater resolution and symmetrical shape make possible higher precision and new diffraction techniques (1).

RESULTS

Data were collected for a number of crystal structure determinations including the high temperature superconductor using four wavelengths for anomalous scattering analysis: CuK-edge, Y-edge, Ba L-III edge and 0.886 Å. Data were also obtained for $CoGaInS_4$ and $MnCrInS_4$. Previous crystal structure studies were published (2,3) together with the determination of f' of Yb at the L-III absorption edge by refinement of the Yb_2O_3 structure using a powder sample (4).

Other studies included profile shape analysis of NBS silicon standards 640 and 640a, NBS and G.E. tungsten and LaB_6. Lattice parameter studies were continued on Si + W samples (5) and two isotopes of tin. Measurement of intensity as a function of wavelength reflected by the channel monochromator were made to determine the effects of window and air absorption on the spectral distribution. Some earlier measurements were repeated on the effect of axial divergence on profile shape and specimen surface displacement which does not shift the peak in the parallel beam geometry.

The development of the grazing incidence method for depth profiling analyses of thin films was continued. Phase identification, lattice spacing changes and profile shapes provide structural characterization of the top 60-200 Å compared to the full film thickness (6). Index of refraction corrections are necessary for lattice spacing changes and are determined experimentally (7).

Run V was not not very productive because of difficulties with instability and low intensity of the source radiation.

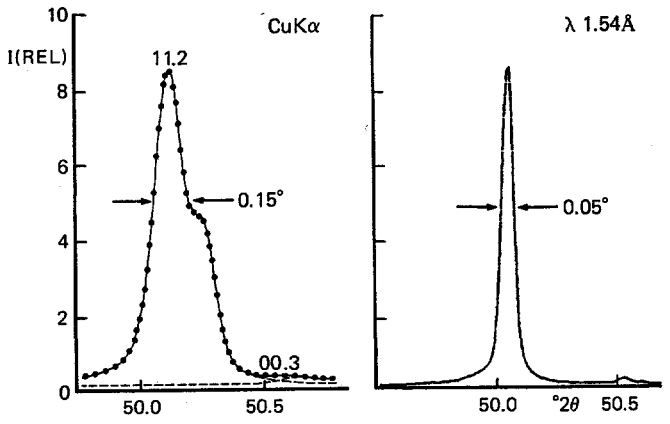

Figure 1. Profiles of quartz (11.2) and (00.3) reflections recorded using (a) the conventional X-ray tube focusing method and (b) the synchrotron radiation parallel-beam method.

REFERENCES

a) Permanent address: Department of Physics, The University, Manchester M13 9PL, United Kingdom.
b) Permanent address: University di Brescia, 25060 Brescia, Italy.

1. W. Parrish, *Australian J. Phys.* **41**, in press (1988).
2. G. Will, N. Masciocchi, W. Parrish and M. Hart, *J. Appl. Cryst.* **20**, 394 (1987).
3. G. Will, M. Bellotto, W. Parrish and M. Hart, *J. Appl. Cryst.* **21**, in press (1988).
4. G. Will, N. Masciocchi, M. Hart and W. Parrish, *Acta Cryst.* **A43**, 677 (1987).
5. W. Parrish, M. Hart, T. C. Huang and M. Bellotto, *Adv. in X-ray Anal.* **30**, 373 (1987).
6. G. Lim, W. Parrish, C. Ortiz, M. Bellotto and M. Hart, *J. Mater. Res.* **2**, 471 (1987).
7. M. Hart, W. Parrish, M. Bellotto and G. S. Lim, *Acta Cryst.* **A44**, in press (1988).

XAS STUDIES OF SYNTHETIC MODELS FOR HYDRODESULFURIZATION CATALYSTS

Geoffrey S. Waldo, Oswaldo Baralt, M. David Curtis, and James E. Penner-Hahn
Department of Chemistry, University of Michigan, Ann Arbor, MI 48109-1055

Recently several M-Mo-S (M = Fe, Co, Ni) clusters have been prepared [1]. When these complexes are supported on metal oxide surfaces (e.g. Al_2O_3, MgO) they form active catalysts for the hydrodesulfurization (HDS) reaction. This is perhaps not surprising, since the current model for commercial HDS catalysts postulates a MoS_2 "raft" with Co atoms bonded at the edges of the raft [2]. In order to follow the structural evolution of M-Mo-S clusters from crystallographically characterized inorganic complexes to active catalysts, we have measured Mössbauer and XAS spectra for the intact clusters, for the clusters adsorbed on oxide supports, for samples heated to 120°C and 400°C, and for samples sulfided under H_2S. We report here our initial results for the cluster $Cp_2Mo_2S_2Fe_2(CO)_8$.

RESULTS

The Fe-XANES spectra are shown in Fig. 1. The pure cluster and the cluster adsorbed on Al_2O_3 at room temperature are very similar (although not identical). The spectra of the two heated samples are identical and are shifted by ca. 5 eV to higher energy relative to the unheated samples. This shift suggests that the iron is oxidized in the heat treated samples. The intensity of the 1s-3d transition in the heat treated samples is consistent with the Fe being in a distorted octahedral environment [3]. Similar conclusions follow from the Mo-XANES (see Fig. 2). The spectra of the pure cluster and the cluster on Al_2O_3 at 25°C are identical, demonstrating that the cluster is adsorbed with no change in the immediate environment of the Mo atoms. The spectra of the heated samples are identical and are shifted ca. 5 eV to higher energies. In addition, a pre-edge feature attributable to Mo=O bonding is present in the heated samples. Sulfiding results in samples having significantly different Fe and Mo XANES (data not shown).

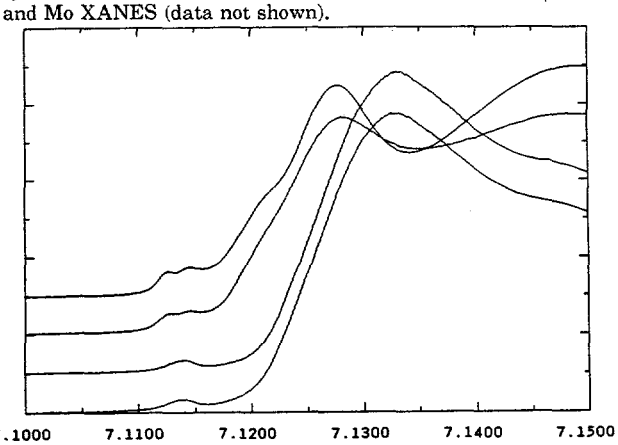

Figure 1. Fe XANES spectra for FeMoS cluster. From top: Neat cluster; adsorbed on Al_2O_3 at room temperature; heated to 120°C; and heated to 400°C

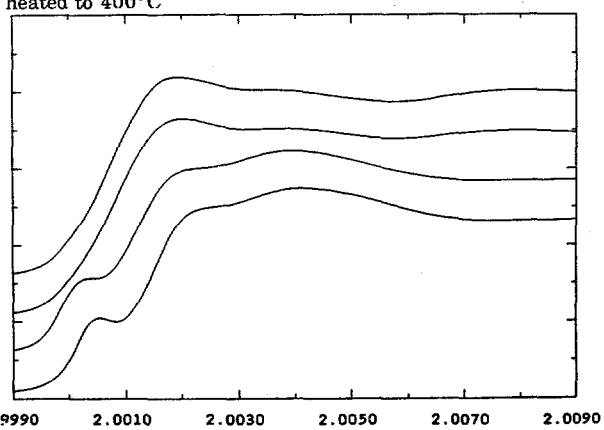

Figure 2. Mo XANES spectra for FeMoS cluster. From top: Neat cluster; adsorbed on Al_2O_3 at room temperature; heated to 120°C; and heated to 400°C

The FT for the Fe-EXAFS is shown in Figure 3. The first peak corresponds to the unresolved Fe-S and Fe-CO contributions and the second peak contains Fe-Fe, Fe-Mo and Fe-CO scattering. Following adsorption on Al_2O_3, the scattering associated with Fe-CO decreases. Curve fitting shows that the adsorbed cluster has lost ca. 1.5-2.0 CO groups per Fe. Upon heating to 120°C under H_2, all of these peaks are lost and a new peak corresponding to Fe-O appears. Curve fitting shows that this peak corresponds to ca. six oxygens at 1.95 Å. Further heating to 400°C causes little additional change in the EXAFS.

Similar results are found for the Mo EXAFS (not shown). Specifically, the Mo environment shows essentially no change prior to heating and the heated samples have a Mo-O environment with no indication of long range order. The lack of long range order in both the Fe and the Mo EXAFS is consistent with diffraction and microscopy studies which show no evidence of sintering.

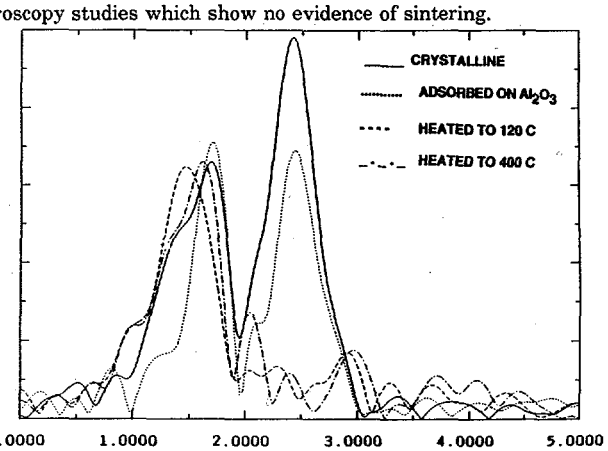

Figure 3. FT of Fe EXAFS for FeMoS cluster under different conditions.

DISCUSSION

Although the samples studied here are not identical to commercial HDS catalysts, they offer a number of advantages for detailed EXAFS studies. Chief among these is the ability to study low metal loadings, since under these conditions the sample is likely to have a single metal environment rather than an ensemble of dispersed and aggregated structures. For the current samples, Mössbauer data suggest that the Fe is present in a single, well defined site. This interpretation is supported by the fact that quantitative curve fitting of the EXAFS gives "normal" coordination numbers (significant site disorder would result in lower apparent coordination numbers). It thus appears likely that the EXAFS data are reflecting the structure of the major form of the Fe and Mo species present and that these samples will be useful for correlating structure with catalytic activity. A more extensive study of related complexes and of samples under catalytic conditions is in progress.

It is also interesting to note that, by an EXAFS criterion, all of the oxidation-decomposition reactions are complete by 120°C. In contrast, temperature programmed decomposition (TPDE) results show continuing evolution of hydrocarbon ligands through 400°C. It thus appears that the TPDE experiment measures the activation energy required to release the hydrocarbon from the surface and is not necessarily a good indicator of cluster decomposition per se. This demonstration is important in view of the extensive use of TPDE for characterizing surface species.

REFERENCES

1. Curtis, M.D. and Williams, P.D., *Inorg. Chem.* **1983**, *22*, 2661.
2. See for example Tops5oe, H.; Clausen, B.S.; Tops5e, N.-Y.; Pedersen, E.; Niemann, W.; Maller, A.; Bmgge, H.; Lengeler, B., *J. Chem. Soc., Faraday Trans I*, **1987**, *83*, 2157-67 and references therein.
3. Roe, A.L.; Scheider, D.J.; Mayer, R.J.; Pyrz, J.W.; Widom, J.; Que, L.Jr. *J. Am. Chem. Soc.*, **1984**, *106*, 1676-1681.

XAS DETERMINATION OF THE CHEMICAL FORMS OF SULFUR IN PETROLEUMS

Geoffrey S. Waldo[1], Robert M. K. Carlson[2] and James E. Penner-Hahn[1]
[1]Department of Chemistry, University of Michigan, Ann Arbor, MI 48109-1055
[2]Chevron Oil Field Research Company, P O. Box 446, La Habra, CA 90631

Next to carbon and hydrogen, sulfur is the most abundant chemical element in petroleum, occuring at concentrations of over ten weight percent in some heavy oils [1,2]. Several factors are generally believed to affect the concentration of sulfur in oil, including depositional source (marine vs. terrestrial), depositional environment (carbonate vs. clastic sequences), thermal maturity, depth of deposition, and extent of biodegradation [1,2]. The lack of suitable analytical techniques has severly limited attempts to characterize the chemical forms of sulfur in heavy oils and source rocks. Such chemical characterization is essential, however, for understanding how sulfur compounds are modified by different geologic processes.

Recent work has shown that sulfur XANES is quite sensitive to both the electronic and structural environment of the absorbing atom [3,4], and thus offers one of the first opportunities for characterizing directly the chemical evolution of sulfur containing compounds in oils and oil source rocks.

Both models and petroleums were studied. Models are necessary since the interpretation of XANES data for unknown samples is based largely on comparison with model spectra. Models studied to date include disulfides, thioethers, thiols, thiophenes, sulfoxides, sulfones, sulfonic acids and sulfate. The 12 eV shift in edge energy from elemental sulfur to sulfate is sufficient, in many cases, to permit unambiguous determination of the oxidation state of the sulfur. Petroleum samples were taken from marine, marine high-sulfur, lacustrine-evaporitic, and lacustrine-deep stratified sources, including samples having different thermal maturities and samples collected at a variety of depths. In addition, asphaltene, maltene polar, and maltene aromatic fractions were examined for several high-sulfur oils.

EXPERIMENTAL. XANES spectra were measured using fluorescence detection. Petroleum samples containing 0.1 to 8.0 wt% sulfur were studied as neat films or as finely ground solids. Model compounds were examined as neat solids, and as dilute (0.3 wt% sulfur) solutions in o-xylene in order to minimize the attenuating and line-broadening effects of self-absorption. All spectra were normalized and placed on a quasi-absolute scale by fitting a single low-order polynomial to both the pre-edge and post-edge regions; the data in these regions were constrained to fit tabulated sulfur x-ray absorption cross-sections (McMaster et al.). This method of normalization is superior to conventional techniques, especially for applications requiring quantitative comparison of XANES [5].

One of the most severe limitation in fluorescence detected sulfur XANES is the occurence of self-absorption. Normalized fluorescence spectra were corrected for self-absorption using a general expression for fluorescence intensity as a function of sample composition, incident x-ray intensity, and sample thickness [6]. Once normalized and corrected for self-absorption, the petroleum spectra can be fitted with linear combinations of model spectra. When applied to chemically defined mixtures, this fitting procedure can be used to determine relative concentrations with an uncertainty of ca. 1%. Quantitative analysis of the petroleum samples is in progress.

RESULTS. In order to evaluate the accuracy of our self-absorption correction algorithm, we measured the XANES spectra for sulfate solutions at concentrations ranging from 10 mM to 1 M. The high concentration samples exhibit pronounced self-absorption, however when normalized and corrected for self-absorption, these spectra agree to within 10%. Since the petroleum samples have lower sulfur concentrations and more importantly, show less variability in concentration, this 10% error is an upper bound for the uncertainty in quantitation.

The spectra for two samples from a low sulfur lacustrine-evaporitic depositional environment are shown in Fig. 1A. The spectra are for an immature petroleum (Gilsonite) from a low sulfur environment (0.65% S) and for a petroleum derived from a similar environment (0.31% S), but of greater thermal maturity. Both samples are primarily thiophenic (~2473 eV feature) with small contributions from thiol/thioether compounds. The thermally mature sample, however, is relatively enriched in a sulfoxide species (~2476 eV feature), and depleted in the thiol/thioether species, suggesting

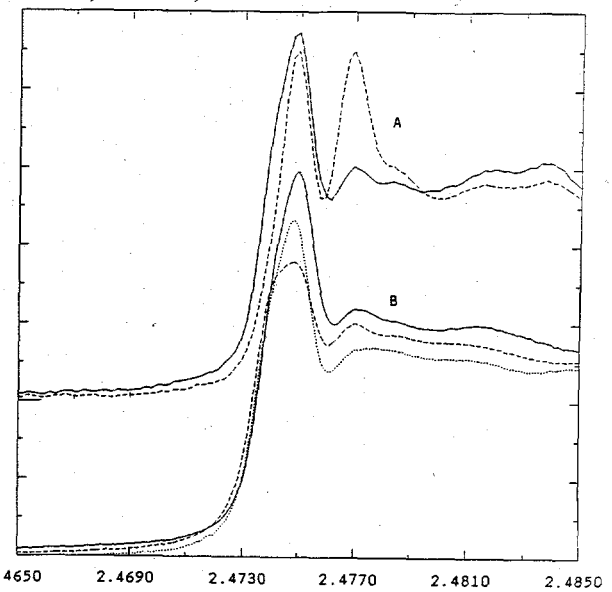

Figure 1. Sulfur XANES spectra. A) Low sulfur lacustrine-evaporitic samples: Gilsonite (solid line) and related petroleum (dashed line). B) Chromatographic fractions for high-sulfur petroleum: asphaltene (solid line), maltene polar (dashed line) and maltene aromatic (dotted line).

that oxidation has occured as a result of geologic processing. The relative enrichment of sulfoxide species as a function of thermal maturity appears to be a general phenomenon and has been observed in the hydrous pyrolysis of source rocks (data not shown).

We have also measured XANES spectra for the different fractions of some of the high sulfur petroleums. Representative spectra are shown in Fig. 1B. The asphaltene fractions are enriched in thiophenic components, while the maltene polar fractions are enriched in thiol/thioether components.

CONCLUSIONS. Sulfur XANES can be used to determine sulfur speciation in geologically interesting samples, at least at the level of sulfur electronic structure. No direct information is available regarding the hydrocarbon side chains in these compounds, however such questions can be addressed by examining the various chromatographic fractions. We have shown qualitatively that there are systematic variations in sulfur speciation as a result of sample history, source, deposition, and thermal maturity. We have developed and tested a procedure to correct sulfur XANES spectra for self-absorption and are in the process of determining the quantitative correlations between sample history and sulfur speciation.

ACKNOWLEDGEMENTS. This work was supported in part by the Donors to the Petroleum Research Fund administered by the American Chemical Society (18073-G3,6).

REFERENCES

1. Hunt, J.M. *Petroleum Geochemistry and Geology*, W.H. Freeman, San Francisco, 1979.
2. Tissot, B.P.; Welte, D.H. *Petroleum Formation and Occurence*, Springer-Verlag, Berlin, 1984.
3. Lytle, F.W.; Greegor, R.B.; Sandstrom, D.R.; Marques, E.C.; Wong, J.; Spiro, C.L.; Huffman, G.P.; Huggins, F.E., *Nucl. Instrum. Methods*, **1984**, *226*, 542. Spiro, C.L.; Wong, J.; Lytle, F.W.; Greegor, R.B.; Maylotte, D.H.; Lamson, S.H. *Science*, **1984**, *226*, 48-50.
4. Frank P.; Hedman B.; Carlson M.K. R.; Tyson, T.A.; Roe, L.; Hodgson, K.O. *Biochemistry*, **1987**, *26*, 4975-4979.
5. Waldo, G.S.; Penner-Hahn, J.E. Manuscript in preparation.
6. Jaklevic, J.; Kirby, J.A..; Klein, M.P. and Robertson, A.S. *Solid State Communications*, **1977**, *23*, 679-682.

COSTER-KRONIG TRANSITION PROBABILITIES IN METALS

S. L. Sorensen,[1] R. Carr,[2] S. J. Schaphorst,[1] S. B. Whitfield,[1] and B. Crasemann[1]

[1]Department of Physics and Chemical Physics Institute, University of Oregon, Eugene, Oregon 97403

[2]Stanford Synchrotron Radiation Laboratory, Stanford, California 94305

INTRODUCTION

Coster-Kronig transitions are Auger transitions in which a vacancy is transferred among subshells within a single inner shell of an atom or molecule. These low-energy radiationless transitions are exceedingly fast, causing large hole-state level widths and taxing the limits of perturbative theoretical approaches. Coster-Kronig rates are very sensitive to transition energy and wave-function overlap, and hence, to details of the atomic model including the effects of relativistic and quantum electrodynamic corrections. Experimental data on Coster-Kronig rates are scarce.

This experiment is designed to measure Coster-Kronig probabilities for the radiationless transfer of vacancies among L subshells of Ni, Cu, Mo, Ag, and Zr by detecting suitable Auger spectra excited by selective photoionization.

EXPERIMENTAL METHOD

Target samples were evaporated <u>in situ</u> onto an aluminum substrate. Radiation from the JUMBO double-crystal monochromator was tuned to ionize selected L subshells of the target elements. The incident photon flux was monitored by measuring photoelectrons ejected from a gold grid placed near the entrance of the target chamber. Auger spectra from the samples were recorded by means of a double cylindrical-mirror electron analyzer.

In order to measure the rate f_{23} of vacancy transfer from the L_2 to the L_3 subshell, the L_3-$M_{4,5}M_{4,5}$ Auger-electron spectrum was recorded when only the L_3 subshell was photoionized, and again, when both L_2 and L_3 subshells were ionized. Comparison of Auger-line intensities in the two cases, normalized to the same incident photon flux and taking into account the respective L-subshell photoionization cross sections,[1] makes it possible to deduce f_{23}. An analogous procedure, based on measurements of L_2-$M_{4,5}M_{4,5}$ Auger spectra, permits determination of f_{12}.

The experiment was completed at the end of the 1987 Fall run at SSRL; the data are currently being analyzed. An example of typical spectra is shown in Fig. 1. Figure 1a shows the raw Mo L_3-$M_{4,5}M_{4,5}$ Auger data. Fig. 1b shows the same data set fitted to a set of peaks described by four continuously varying parameters. The fit is a non-linear least-squares fit, utilizing a linear background function. The low-energy electron scattering background was filtered out. Results are expected to include Coster-Kronig transition probabilities f_{11} that have not previously been measured and that play an important role in characterizing the dynamics of inner-shell electron reorganization following ionization.[2] Data will be compared with state-of-the-art theoretical predictions.[3]

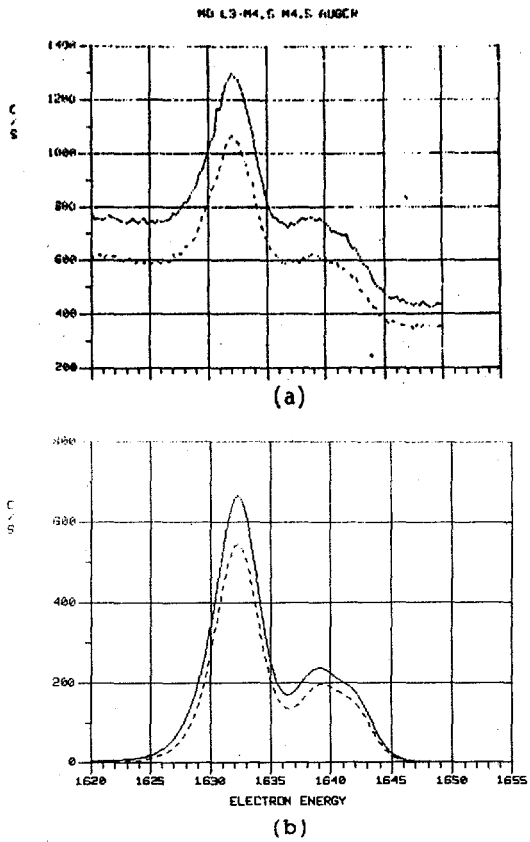

FIG. 1. L_3-$M_{4,5}M_{4,5}$ Auger spectra of Mo, photoexcited by ionization of the L_3 subshell alone (broken curve) and by ionization of both the L_2 and L_3 subshells (solid curve). The spectra have been normalized to the same incident photon flux, corrected for electron energy loss to the lattice and the background has been subtracted.

ACKNOWLEDGMENTS

We gratefully acknowledge the technical assistance and advice of Matt Richter, Michael Rowen, Ann Waldhauer, and Joseph Woicik. We thank W. Jitschin for help and advice in the initial stages of this work. This research is supported in part by National Science Foundation Grant PHY-85 16788 and Air Force Office of Scientific Research Grant AFOSR-87-0026. The experiment was performed at SSRL which is supported by the Department of Energy through the Office of Basic Energy Sciences and the National Institutes of Health through the Biotechnology Resources Program.

REFERENCES

1. J. H. Scofield, Lawrence Livermore National Laboratory Report No. UCRL-51326 (1973) and At. Data Nucl. Data Tables 14, 121 (1974).

2. W. Bambynek, B. Crasemann, R. W. Fink, H.-U. Freund, H. Mark, C. D. Swift, R. E. Price, and P. Venugopala Rao, Rev. Mod. Phys. 44, 716 (1972).

3. M. H. Chen, in Atomic Inner-Shell Physics, edited by B. Crasemann (Plenum, New York, 1985), Chap. 2.

Deep donors in gallium aluminum arsenide semiconductor alloys

T.M. Hayes and D.L. Williamson
Physics Department
Colorado School of Mines, Golden, CO 80401

P. Gibart
Laboratory for Solid State Physics and Solar Energy, CNRS
Sophia Antipolis, 06560 Valbonne, France

Heavily n-doped $Ga_{1-x}Al_xAs$ alloys are of great interest for device applications. For $x < 0.2$, there are several preferred doping elements yielding shallowly bound donor states. For larger x, however, a deep level state appears for each of these dopants, called a DX center.[1] The solution of the resultant serious device problems has been impeded substantially by the absence of direct microscopic structural knowledge of the DX center due to the low concentration of dopants in the materials of interest, typically 10^{17} to 10^{19} cm^{-3}. Addressing this problem, we have undertaken to examine the Sn environment in a variety of Sn-doped $Ga_{1-x}Al_xAs$ alloys using fluorescence detection x-ray absorption spectroscopy (XAS).

We have prepared XAS samples of GaAs and $Ga_{0.7}Al_{0.3}As$ doped with 5×10^{18} cm^{-3} Sn, as well as samples of $ZnSnAs_2$, SnAs, and Al doped with Sn to serve as standards of known structure in the data analysis. The Sn K-edge x-ray absorption spectra of the dilute samples have been measured at 77 K in the fluorescence mode. Separately obtained spectra are added together to reduce statistical noise. The quality of the result is illustrated by the spectrum of the doped $Ga_{0.7}Al_{0.3}As$. The extended fine structure in k space, $k\chi(k)$, extracted from the sum of 12 such spectra is shown in Fig. 1a. All of the extended fine structure shown is of larger amplitude than the apparent noise level. The Fourier transform of this spectrum is shown in Fig. 1b. This result is to be compared with Figs. 1c and 1d, which contain the result of a similar analysis applied to 13 separate spectra from the doped GaAs and to a transmission spectrum of $ZnSnAs_2$. Consider the region of the first neighbor peak, between 1.9 and 2.9 Ang. That region in GaAs (c) is remarkably similar to that in $ZnSnAs_2$ (d), which is due to 4 As atoms at 2.53 Ang. The first peak in $Ga_{0.7}Al_{0.3}As$ (b) is different from these two, and is nearly certain to yield a statistically significant result on further analysis. The differences apparent in the second and third neighbor peaks are possibly within the noise level.

We expect to improve these data through the addition of spectra obtained when beam conditions are less noisy than they were in December 1987. We also have data on the $Ga_{0.7}Al_{0.3}As$ sample under light-soaked conditions chosen to elucidate the persistent photoconductivity found in that material, and on annealed and unannealed Sn-doped Al, both sets of which promise to yield interesting results.

1. D.V. Lang and R.A. Logan, in Physics of Semiconductors 1978 (Inst. Phys. Conf. Ser. No. 43, 1979), p.433

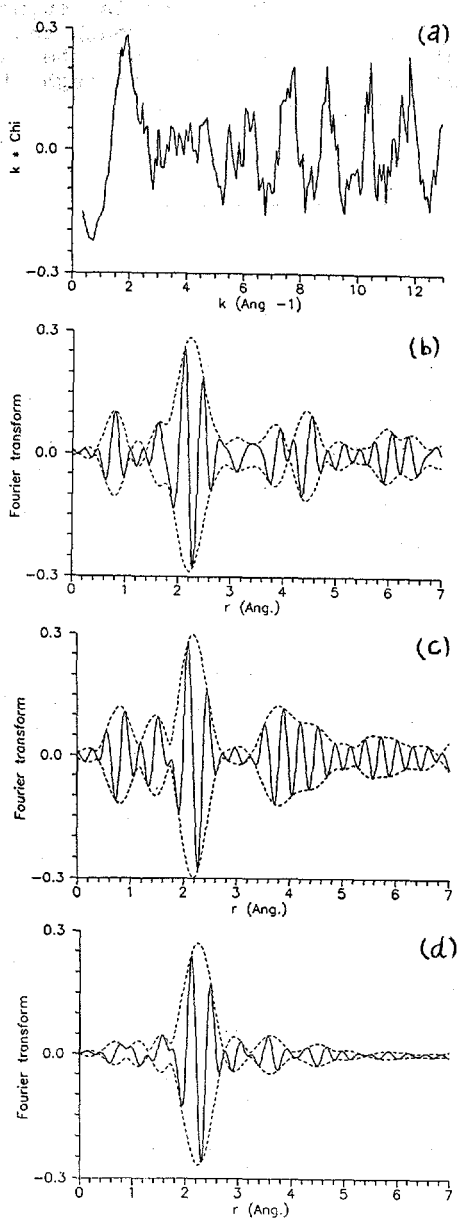

Fig. 1 The extended fine structure in k space, $k\chi$, extracted from the x-ray absorption spectrum associated with the Sn K edge at 77 K in Sn-doped $Ga_{0.7}Al_{0.3}As$ is shown in (a). The remaining three parts are the Fourier transforms of $k\chi$ over k= (2.7,12.8) $Å^{-1}$ for three different Sn K-edge spectra: (b) from (a); (c) from doped GaAs; (d) from the transmission spectrum from $ZnSnAs_2$.

X-Ray Induced Photo-Acoustic Emission

Robert A. Day, Richard W. Ryon, and Steven Benson

Lawrence Livermore National Laboratory
7000 East Avenue, Livermore, CA 94550

Introduction

Materials that have similar linear absorption coefficients, such as aluminum and alumina, are difficult to distinguish by normal x-ray methods. When these materials are mixed with high Z materials such as used in integrated circuits the imaging of small features is even more difficult since the absorption of the higher Z material must also be included.

X-ray induced photo-acoustics holds promise for this type of imaging because the generation of sound is a function of the coefficient of thermal expansion (CTE). For an aluminum wire embedded in an alumina matrix the theoretical sensitivity will be about four times that of x-ray absorption measurement alone. Since we are interested in thick specimens (1-5 mm), absorption edge effects and fluorescence are not useful since absorption is too high to allow penetration.

A second less obvious advantage to acoustic detection is the ability of sound to travel in all directions. This allows detection from any side of the specimen which avoids the need to penetrate high Z materials that may shadow the part of the specimen we wish to image.

Results and Discussion

Prior to doing experiments at Stanford Synchrotron Radiation Laboratory (SSRL) we modelled the photo-acoustic generation in aluminum using a pulsed x-ray source with a 3 nanosecond width (a Febatron). We detected acoustic signals using an acoustic emission tranducer and amplifier. The frequency of this detector was limited to to 100-500 kilohertz region. The low repetition frequency of the Febatron source (0.2 hertz) would require more than a day to form a useful image.

The detection system we designed for use at the synchrotron was based on this Febatron experiment (Fig. 1). A relatively narrow band transducer (PZT-5A) and integral amplifier was designed. The center frequency was 1.1 megahertz with 20% bandwidth to allow detection of the synchrotron ring frequency of 1.28 megahertz. This frequency was chosen because prior work [1] indicated it should work well and because this frequency could allow the use of focused detectors which would allow depth sensitivity to be controlled.

The actual experiments with this system were not successful and it was replaced by a separate transducer bonded to a fused silica flat. The purpose of the flat was to protect the transducer from the intense beam of the synchrotron. The low frequency system was not sensitive enough to detect the higher frequency signals produced by the short x-ray pulses at SSRL.

This system detected photo-acoustic signals (Fig. 2) with an excellent signal-t o-noise ratio (>20dB). Fused silica is not a good generator of photo-acoustic waves because of it's low CTE. The frequency of successful transducers was 25 and 15 megahertz. Lower frequency transducers were insensitive to the sound generated. The very short x-ray pulses (65 picoseconds) generate 15 gigahertz sound which was incapable of exciting the lower frequency detectors, contrary to our experience with the Febatron.

The actual detection was performed at 2 kilohertz using a chopper wheel in the synchrotron beam. During the period the chopper wheel is "open" about 5,000 high frequency x-ray pulses strike the material and the amplifier integrates these into a lower frequency pulse. A signal averager was used to further enhance the signal-to-noise ratio of this signal. Integration times were approximately 10 seconds.

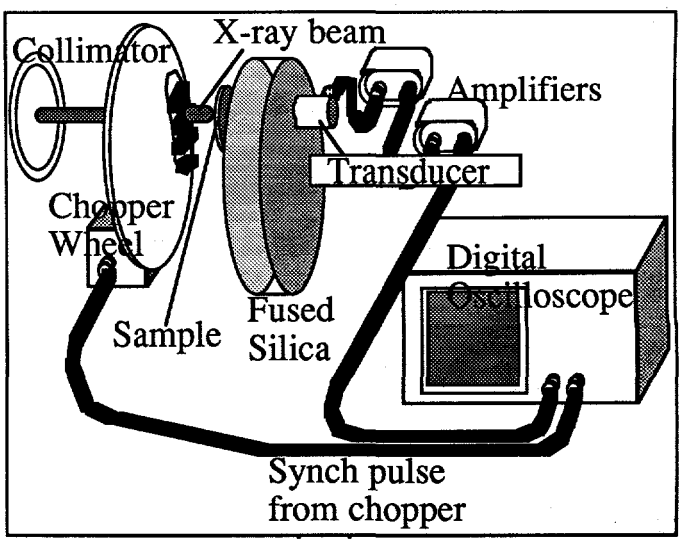

Fig. 1: The experimental system used at SSRL to test x-ray photo-acoustic generation.

The fused silica was 25 mm thick to assure that no x-rays penetrated to the transducer to generate signals through ionization effects or photo-acoustic generation in the transducer itself. Penetration of the silica is 2-4 mm and was verified by radiation darkening.

We assured that no sound was created in the experiment, by the chopper wheel for example, by blocking the x-ray beam at the collimator. No sound was detected by the transducer without the x-ray beam verifying that we were not receiving a noise source from another part of the experiment.

Detection in aluminum, copper, graphite, acrylic plastic and alumina were unsuccessful. The samples of these materials were bonded to the silica with silicon vacuum grease in a thin layer. The

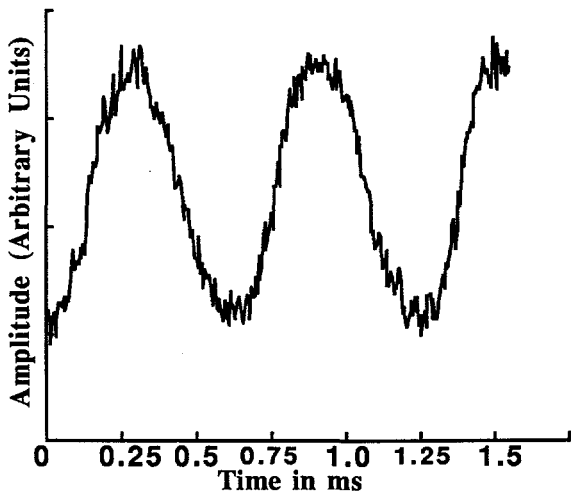

Fig. 2: Signal obtained on fused silica with a 15 megahertz longitudinal wave transducer and 120 dB of amplifier gain. The 25 megahertz transducer gave slightly better signal to noise ratio.

lack of results are in accord with the absorption of the high frequency acoustic pulses by these materials [2]. The very high frequency is absorbed in the first 20 to 30 μ of all of these materials, the minimum thickness was 500 μ. We did not anticipate this high frequency result both because of our Febatron experiment and work by Sachse [3]. The difference between the two x-ray pulses appears minor (65 ps vs 160 ps and different intensity). Different results may be accounted for in the detector and electronics.

The imaging of discontinuities appears promising but much work will be needed to make it practical. Areas we are exploring now include the confirmation of the results of this experiment by use of lasers in transparent and absorbing materials and the use of multi-layer x-ray lens to achieve higher intensity. Optimization of the detector and electronics will be done using the laser model.

Acknowledgements

We would like to acknowledge the help of Jerry Haskins, Walt Kendricks, Mark LaChapell, Jim Brase, Harry Martz, Chuck Valente, Floyd Kirk, Ron Streit and Suzanne Fletcher in helping out in this experiment "beyond the call of duty".

Work performend under the auspices of the U. S. Department of Energy by the Lawrence Livermore National Laboratory under Contract W-7405-Eng-48.

References

1. K. Y. Kim and W. Sachse, *X-ray generated ultrasound*, **Appl. Phys. Lett.**, 43(12), 15 December 1983.

2. H. Wickramsinghe, *Contrast and Imaging Performance in the Scanning Acoustic Microscope*, **J. Appl. Phys.**, 50(2), 1979.

Proposal No. 1056M

Synchrotron White Beam Topography of Striations and Interface Breakdown in Alloyed GaAs

by

S. R. Stock[1], Z. U. Rek[2] and A. G. Elliot[3]

[1]School of Materials Engineering
Georgia Institute of Technology
Atlanta, Georgia 30332-0245

2Stanford Synchrotron Radiation Laboratory

[3]Hewlett-Packard Optoelectronics Divison
San Jose, California 95131

The structure of striations and the morphology of interface breakdown were studied in (001)GaAs with white beam projection topography. Wafers and longitudinal slabs of GaAs alloyed with various atomic species were examined; the majority of samples were low pressure LEC GaAsIn with about 1 at. % indium. Sets of wafers spanning the initiation and development of interface breakdown were studied from three sources, and the structures observed were quite similar despite differences in boule diameters and in some growth parameters.

Well-defined, concentric striations were normally visible before the interface became unstable. Dislocations were present in some specimens but not in others, indicating that the presence of dislocations is not intrinsic to subsequent interface instability. The Burgers vectors of these dislocations could not be identified because they were never out of contrast; decoration with indium may be the cause. Prior to interface breakdown, the normal concentric striations formed a very distorted pattern (Fig. 1). The swirling pattern of striations was reminiscent of turbulence and probably reflected local solidification instability.

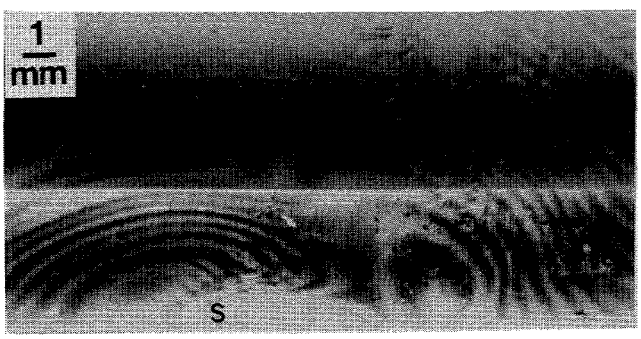

Fig. 1. Transmission topograph of GaAsIn in the earliest stages of interface instability. This topograph was recorded with diffraction vector $\underline{h}$ = [511] and with 0.5 A radiation.

The material solidified approximately 3 mm below that shown in Fig. 1 showed a well-developed breakdown zone and many cells: average diameters were 7 mm and 0.6 mm, respectively. In all of the samples observed the breakdown cells tended to be aligned in rows, but there were numerous faults in the "stacking" and the rows were not close-packed. Some of the cells in this wafer (labeled F in Fig. 2) resemble the faceted pattern observed in reflection topographs and in optical micrographs. The visibility of striations surrounding the breakdown zone varied from boule to boule. A feature common to all of the indium-doped crystals was the presence of alternating light and dark streaks extending from the cells. This structure, labeled S in Fig. 2, was evidently a precursor to cell formation and appeared to be related to the streaks labeled S in Fig. 1.

After further solidification, the range of cell sizes was much greater (Fig. 3). This transmission topograph was from a wafer about 4 mm below that shown in Fig. 2. The larger cells near the center of the breakdown region showed a distinct faceting. These cells evidently have extended along the growth direction from the first cells to nucleate and hence are surrounded by smaller cells which nucleated farther down the boule. Topographs from longitudinal slabs are consistent with this interpretation. The facets are also clear in reflection topographs (Fig. 4) which showed diffraction contrast from the cell walls (not surface relief contrast!). The origin of the contrast may be due to dislocations at the cell walls or to varying indium concentration similar to that producing striation contrast.

Strain mapping with monochromatic topography will be the next step in the study of the cellular interface breakdown morphology.

This work was partially supported by the USAF through contract F49620-85-C-0013/SB5851-0360 P.O. S-760-6MG-103 (SRS).

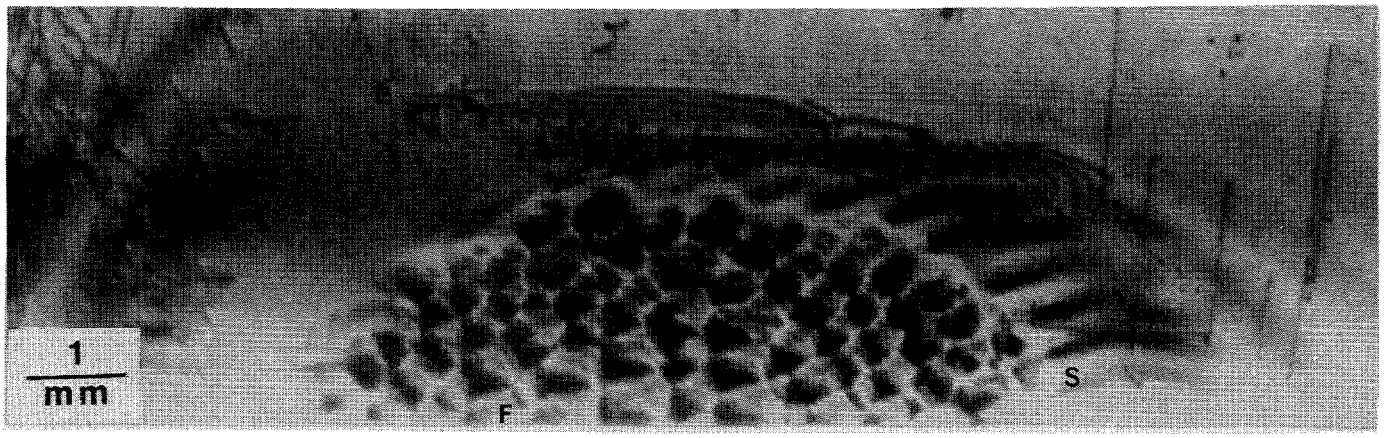

Fig. 2. Cellular structure following interface breakdown recorded with the same parameters as Fig. 1.

Fig. 3. Large, faceted cells surrounded by smaller cells and imaged with the same conditions as Fig. 1 and 2.

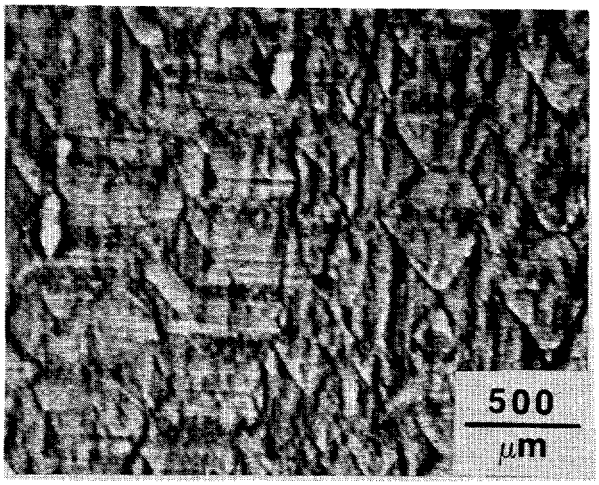

Fig. 4. Reflection topograph of facets after interface breakdown.

Roughening and Deconstruction of the Au (110) Surface

G. A. Held, J. L. Jordan-Sweet, and P. M. Horn
IBM Research Division, T. J. Watson Research Center
P. O. Box 218, Yorktown Heights, NY 10598

and

A. Mak and R. J. Birgeneau
Department of Physics, Massachusetts Institute of Technology
77 Massachusetts Avenue, Cambridge, MA 02139

and

T. Gustafsson
Department of Physics & Astronomy, Rutgers University
P. O. Box 849, Piscataway, NJ 08854

INTRODUCTION

Many noble metal facets are known to favor reconstructed structures at low temperatures. Further, at some temperature T_R a reconstructed surface will typically undergo a reversible "deconstruction" to its unreconstructed state. One such transition which has been studied theoretically[1] as well as with electron diffraction[2,3] is the Au (110) 1x2 to 1x1 deconstruction. While the "missing row" model of the reconstructed 1x2 surface is well established, the nature of the deconstruction transition itself remains controversial[1-3].

We have carried out glancing angle, high resolution synchrotron x-ray scattering experiments as a means of studying the Au (110) 1x3 to 1x1 transition. Observing the temperature dependence of the superlattice and integral order (anti-Bragg) surface peaks[4], we find that at $T_R = 485°C$, the Au (110) 1x3 reconstructed surface becomes incommensurate with the bulk crystalline lattice. During this commensurate-incommensurate transition, the surface both roughens[4] and deconstructs.

EXPERIMENT

This experiment was carried out in an ultrahigh-vacuum chamber equipped with the instrumentation needed to prepare a clean surface, and yet compact enough to fit into a Huber six-circle diffractometer. The Au (110) surface was electropolished and, subsequently, cleaned by cycles of Ar-ion sputtering and annealing until a well ordered surface was obtained.

The scattering measurements were taken at the eight-pole wiggler beam-line VII-2 at SSRL (SLAC). A beam of 8.05 keV photons was focussed onto the sample; the longitudinal (radial) resolution of the spectrometer was set by slits at $0.0075Å^{-1}$ HWHM, less than the radial width of the low temperature Au (001) surface peak. The sample and chamber were oriented such that the in-plane (i.e., grazing incidence) (002) bulk peak, the (001) surface peak, and the superlattice peaks were all observable.

RESULTS AND DISCUSSION

At low temperatures, the equilibrium structure of our Au (110) surface was a 1x3 reconstruction. Typically, ion sputtering at room temperature resulted in a 1x2 reconstruction. Annealing to 300°C resulted in an improved 1x2 surface. However, at temperatures above 300° C, the surface evolved from a 1x2 to a 1x5 to a 1x3 reconstruction. Upon cooling, a highly ordered 1x3 reconstruction would remain (surface domain sizes of at least 1000Å and 3000Å along the (001) and $(1\bar{1}0)$ directions, respectively). At 485°C, the 1x3 reconstruction would undergo a *reversible* deconstruction; it is this transition which we have studied in depth.

It remains unclear precisely why the equilibrium reconstruction of our crystal is 1x3. Morgante, *et. al.*[5] find that 0.3 monolayers of Ag evaporated onto Au (110) induces a 1x3 reconstruction. However, using retarding field Auger spectroscopy, we have determined that there is no substantial Ag coverage on our surface. Calculations by Ercolessi, *et. al.*[6] suggest that the 1x2 and 1x3 reconstructions should have comparable energies. Thus, it is entirely possible that traces of some impurity (undetectable by retarding field Auger) could result in the observed 1x3 reconstruction.

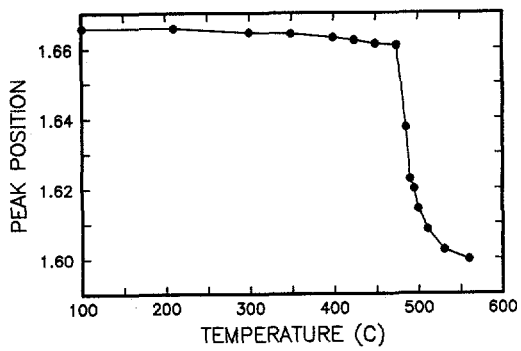

Figure 1. Position of the (0 0 5/3) superlattice peak of Au (110) as a function of temperature. Peak positions have not been corrected for changes in the bulk lattice constant with temperature.

In Fig. 1, we plot the position of the (0 0 5/3) superlattice peak as a function of temperature. It remains essentially constant

until 485°C, at which point the superlattice becomes incommensurate with the bulk. As the (0 0 5/3) peak becomes increasingly incommensurate, it also becomes increasing broad, indicating a decrease in the size of the spatially coherent domains. In addition, we observe that the (001) surface peak broadens and becomes less intense as the surface deconstructs. This suggests that the surface is roughening[4] as well as deconstructing.

Excitations of the 1x2 surface which could result in the 1x2 to 1x1 deconstruction have been discussed theoretically by Villain and Vilfan[1] and are shown in Fig. 2. While the excitations in Fig. 2(a) and (b) could deconstruct the surface without roughening it, the excitations in Fig. 2(c) and (d) would both roughen and deconstruct the surface. We note that these excitations would have the same effect on a reconstructed 1x3 surface. While any of these excitations could account for the observed behavior of the superlattice peaks, only the presence of the excitations in Fig. 2(c) and (d) can result in the observed evolution of the (001) surface peak. These excitations serve as domain walls between commensurate regions of the reconstructed surface. They proliferate above T_R, and the resulting commensurate-incommensurate transition is observed.

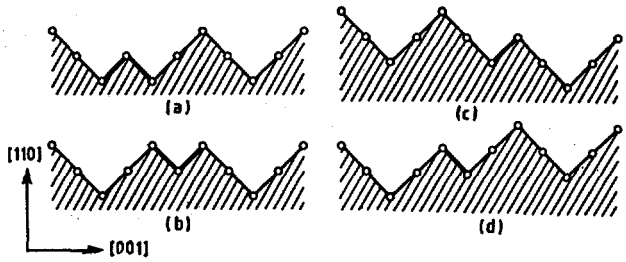

Figure 2. Thermal excitations of the 1x2 Au (110) surface. Excitations (a) and (b) only deconstruct the surface, whereas excitations (c) and (d) both roughen and deconstruct the surface. (Figure from Ref. 1.)

In conclusion, our experiments demonstrate that at 485°C, the Au (110) 1x3 reconstruction undergoes a reversible transition by which it simultaneously roughens and deconstructs.

ACKNOWLEDGEMENTS

We wish to thank W. Haag for technical assistance, I. Robinson for helpful discussions and S. Brennan for advice and assistance at SSRL. Part of this work was performed at SSRL which is supported by the Department of Energy, Office of Basic Energy Sciences. The MIT component of this research was supported by the Army Research Office under Contract No. DAAG29-85-K-0058.

REFERENCES

1. J. Villain and I. Vilfan, preprint.
2. W. Moritz and D. Wolf, Surf. Sci. **163**, L655 (1985); D. Wolf, H. Jagodzinski, and W. Moritz, Surf. Sci. **77** 283 (1978).
3. J. C. Campuzano, *et. al.*, Phys. Rev. Lett. **54** 2684 (1985).
4. G. A. Held, *et. al.*, Phys. Rev. Lett. **59**, 2075 (1987).
5. A. Morgante, *et. al.*, Surf. Sci. **189/190**, 620 (1987).
6. F. Ercolessi, *et. al.*, Surf. Sci. **189/190**, 636 (1987).

THERMAL EXPANSIVITY OF γ-Mg_2SiO_4 AND γ-$(Mg,Fe)_2SiO_4$ SPINELS TO 900°C USING SYNCHROTRON RADIATION

L.C. Ming, M. H. Manghnani, Y. H. Kim, Usha Devi and D. H. Xiong
Hawaii Institute of Geophysics, University of Hawaii, Honolulu, HI 96822, USA

E. Ito
Institute for Study of the Earth's Interior, Okayama University, Misasa, Japan

INTRODUCTION

The olivine → spinel transition in $(Mg,Fe)_2SiO_4$ provides a plausible explanation for the seismic discontinuity at 420 km[1]. Thus the γ-$(Mg,Fe)_2SiO_4$ spinel is considered to be the most abundant phase in the Earth's transition zone. In situ high P-T data for such phase transitions and the equation of state (EOS) of the related phases would provide better constraints for modelling the transition zone (i.e., 420-670 km depth) in term of its chemical composition, dynamics and the thermal state. In this light, we were motivated to carry out in situ high P-T studies on four γ-$(Mg,Fe)_2SiO_4$ spinels using energy dispersive x-ray diffraction (EDXRD) in conjunction with synchrotron radiation at Stanford Synchrotron Radiation Laboratory (SSRL). In this report, we present preliminary results on the thermal expansivity and the nature of the back transition (i.e., γ-spinel → α-olivine).

EXPERIMENTAL RESULTS

The EDXRD measurements on four spinels were carried out at 1 bar to ~ 600°C in air and to ~ 1000°C in vacuum (10^{-4}-10^{-5} torr) using the improved high P-T cell[2]. With the storage ring operating at 3 GeV and 80-40 mA, a high quality spectrum could be obtained in 5 minutes. Figures 1 and 2 show the spectra of the γ-$(Mg_{0.4},Fe_{0.6})_2SiO_4$ at several increasing temperatures, up to 570°C in air and to 740°C in vacuum, respectively. These data demonstrate back-transition from the γ-spinel structure to the α -olivine structure at high temperatures. This is to be expected in the $(Mg,Fe)_2SiO_4$ system, as the α phase is stable at pressures below 6 GPa and at all temperatures to the melting point, whereas the γ phase is stable only at high pressures above 6 GPa[3] . Our preliminary results show that: (1) for iron-rich spinels (i.e., $(Mg_{0.4},Fe_{0.6})_2SiO_4$), the initial transition temperature for the back transition spinel → olivine in air is almost 200°C lower than that in vacuum; (2) the transition temperature increases with increasing Mg content; and (3) the kinetics for the back transition become increasingly rapid with over-temperature and with increasing Fe content. An analysis of the kinetics data for various γ-$(Mg,Fe)_2SiO_4$ spinels is in progress.

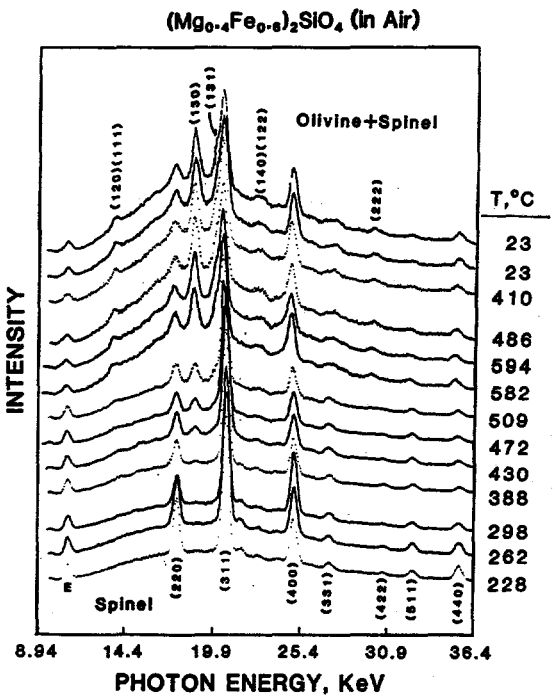

Figure 1. Energy dispersive x-ray diffraction patterns of γ-$(Mg_{0.4},Fe_{0.6})_2SiO_4$ in air at 1 bar and at various temperatures up to 570°C. The data show that the back transition $\gamma \rightarrow \alpha$ starts between 388 and 430°C .

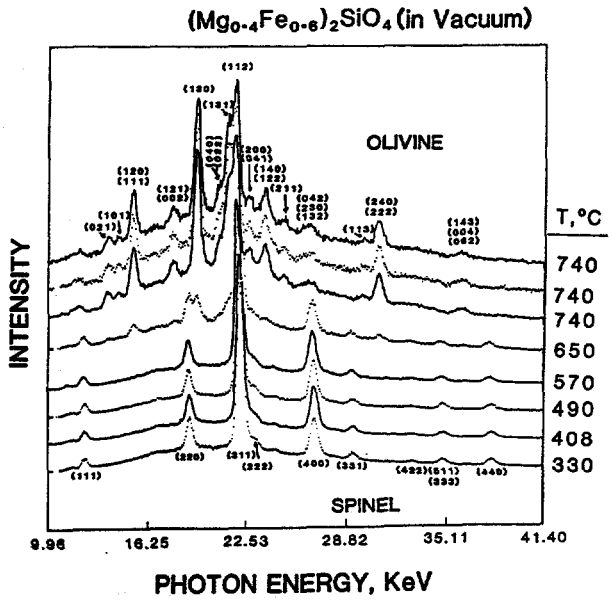

Figure 2. Energy dispersive x-ray diffraction patterns of γ-$(Mg_{0.4},Fe_{0.6})_2SiO_4$ in vacuum at 1 bar and at various temperatures up to 740°C. The data show that the back transition $\gamma \rightarrow \alpha$ starts between 575 and 650°C and the conversion is completed in about five 5 minutes at 740°C.

Figures 1 and 2 also show that there are six to nine diffraction peaks for the spinel phase at all temperatures before the back transition starts. Thus the lattice parameter and the molar volume of the spinel phase (cubic phase) are well constrained.

Plots of $[(V/V_o)-1]$ versus temperature for the γ-$(Mg,Fe)_2SiO_4$ spinels in air and in vacuum are shown in Figures 3 and 4, respectively. The main findings are: (1) in air, the thermal expansivity of iron-rich spinels is anomalous in that it first increases with temperature up to $\sim$ 300°C, then decreases with temperature to $\sim$ 400°C, and then increases very rapidly with

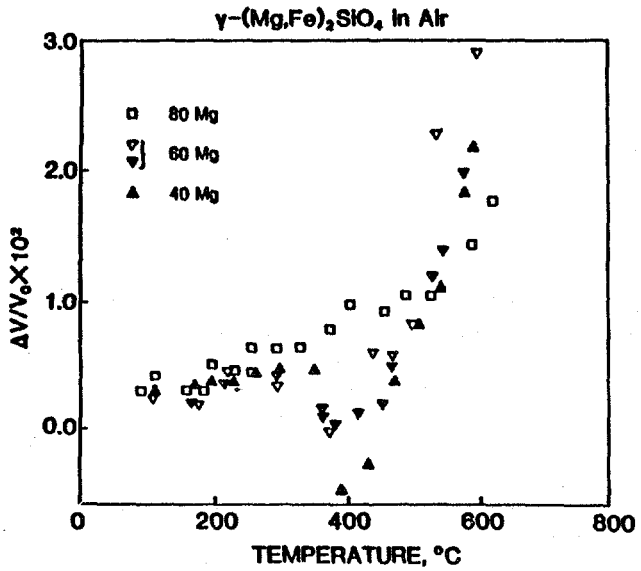

Figure 3. Thermal expansitivity for three γ-$(Mg,Fe)_2SiO_4$ spinels heated in air. It is to be be noted that anomalous behavior is clearly seen in those iron-rich spinels.

temperature to 600°C; (2) the anomalous behavior is suppressed with increasing Mg content and is not observed in the Mg-rich spinels; (3) in vacuum, there is no anomalous behavior; and (4) there appears to be no systematic relationship between composition and the thermal expansivity for the γ-$(Mg,Fe)_2SiO_4$ spinels.

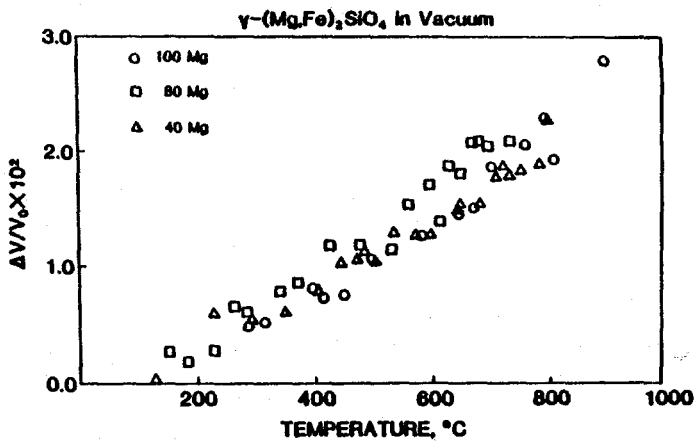

Figure 4. Thermal expansivity for three γ-$(Mg,Fe)_2SiO_4$ spinels heated in vacuum. In contrast to Figure 3, there is no anomalous behavior in the thermal expansivity.

The anomalous behavior observed in the case of iron-rich spinels in air appears to be caused by the oxidation of the spinels that, in turn, facilitates the back transition at much lower temperatures.

ACKNOWLEDGMENT

This research was supported by the National Science Foundation grants EAR84-18125 and EAR87-08482. Thanks are due to the staff of the Stanford Synchrotron Radiation Laboratory for facilitating our work.

REFERENCES

1. Ringwood, A. E., McGraw-Hill Book Co., 618, (1975).
2. Ming, L. C., M. H. Manghnani and J. Balogh, *High Pressure Research in Mineral Physics*, Terrapub/AGU, p. 69-74, (1987).
3. Ringwood, A. E., and A. Major, *Phys. Earth Planet. Interiors*, 3, 89-108, (1970).

IN SITU SURFACE EXAFS OF MONOLAYERS ON SILVER ELECTRODES

Owen R. Melroy, Michael F. Toney, Mahesh G. Samant, and Joseph G. Gordon II

IBM Research Division
Almaden Research Center, K33/802
650 Harry Road, San Jose, CA 95120-6099

Lesser Blum

Physics Department
University of Puerto Rico
PO Box AT, Rio Piedras, Puerto Rico 00931

The solid:solution interface is of fundamental importance in electrochemistry and other interfacial disciplines, but its structure has by-and-large eluded direct experimental study because of the lack of structure sensitive probes that work in condensed phases. Considerable effort has gone into applying UHV based surface science techniques to metal/electrolyte interfaces and these studies have provided valuable insight into structure of atoms and molecules adsorbed from aqueous solutions onto well defined surfaces.[1] However, all of these measurements are *ex situ*. They require transfer of the electrode from the electrochemical environment to vacuum. Because this operation is necessarily accompanied by the removal of solvent and loss of potential control it is uncertain whether the structures observed are those that existed in solution. *In situ* structural measurements are essential and that is the aim of this work which is producing the first reliable look at the atomic structure of the unperturbed metal:liquid interface.

Last year we demonstrated that it is possible, using a combination of grazing incidence excitation and fluorescence detection, to obtain an x-ray absorption spectrum from a monolayer of lead on a silver(111) surface immersed in solution.[2,3] The lead monolayer was deposited electrochemically and maintained under potential control during the experiment. EXAFS above the Pb L_{III} edge revealed that acetate ions were adsorbed at specific sites on the Pb monolayer and that the lead acetate (Pb-O) distance varied with the electrode potential. The SEXAFS provided no information on the internal structure of the lead monolayer, except to suggest that it was incommensurate with the Ag(111) lattice.

This past year, we were able to observe x-ray scattering from the immersed lead monolayer.[4,5] We believe that this is the first example of grazing incidence x-ray scattering (GIXS) from a surface under water. The scattering showed that the lead monolayer is ordered, close packed hexagonal, and epitaxial, with the lead lattice rotated by 4.4° with respect to the Ag lattice and compressed 1.2% compared to bulk lead. Furthermore, between monolayer formation and bulk deposition, the near neighbor distance decreases linearly with the applied potential.

To study the silver surface itself in more detail, we measured SEXAFS spectra from a monolayer of silver on a gold(111) electrode immersed in $NaClO_4$ electrolyte. Because the silver coverage, determined from other measurements, is one silver atom per surface gold atom[6] and because silver and gold are isostructural we expected that silver would form a commensurate (1 x 1) adlayer which should be little perturbed, either structurally or electronically, from bulk silver. Hence, it should be a good model of a silver surface. Indeed, the SEXAFS data reveal that the Ag-Ag and Ag-Au distances are identical and are the same as the distance, 2.89Å in bulk Ag or Au crystals. (Spectra were obtained with the x-ray beam polarized both parallel and perpendicular to the electrode surface so that both in-plane and out-of-plane distances are independently observable.) As was the case with the lead monolayer, backscattering from a low Z element ($Z < 10$), presumably oxygen, was also observed. This is surprising because perchlorate adsorbs very weakly on silver.[7] Further experiments are needed to determine whether the backscattering is from oxygen in water or perchlorate. In contrast to lead, the Ag-O distance is independent of potential between 0.7 and -0.1 V (*vs* Ag/AgCl, 3 M KCl).

We also collected SEXAFS spectra from a simple anionic adsorbate, Br^-, on Ag(111). The radial structure functions derived from this data, are unexpectedly complex and are still being analyzed.

REFERENCES

1. A. Hubbard, *Acc. Chem Res.*, **13,** 177 (1980); E. Yeager, *J. Electroanal. Chem.*, **128,** 1600 (1981); P. N. Ross, *Surf. Sci.*, **102,** 463 (1981).
2. M. G. Samant, G. L. Borges, J. G. Gordon II, L. Blum and O. R. Melroy, *J. Am. Chem. Soc.*, **109,** 5970 (1987)
3. M. G. Samant, G. L. Borges, J. G. Gordon II, O. R. Melroy, and L. Blum, *SSRL Report 87/01*, K. Cantwell, ed., p 79
4. M. G. Samant, M. F. Toney, G. L. Borges, L. Blum, and O. R. Melroy, *Surface Science,* **193,** L29-L36 (1988)
5. M. G. Samant, M. F. Toney, G. L. Borges, L. Blum, and O. R. Melroy, *J. Phys. Chem.*, **92,** 220-225 (1988)
6. W. J. Lorenz, H. D. Hermann, N. Wurthrich and F. Hilbert, *J. Electrochem. Soc.*, **121,** 1167-1177 (1974)
7. G. Valette, *J. Electroanal. Chem.* **122,** 285-297 (1982) and **138,** 37-54 (1982)

Static high pressure equation-of-state (EOS) Studies on thorium to 100 GPa: A preliminary report.

Jagannadham Akella, Quintin Johnson,
Gordon S. Smith and L. C. Ming*

LAWRENCE LIVERMORE NATIONAL LABORATORY
University of California, Livermore, CA 94550

*Institute of Geophysics, University of Hawaii
Honolulu, Hawaii

INTRODUCTION

In recent years there has been renewed interest in the study of the high pressure properties of lanthanide and actinide metals, since such studies can shed light on the systematics in their behavior. Diamond-anvil cell (DAC) apparatus, in conjunction with a synchrotron x-ray source, are the tools used to generate ultra-high static pressures, and to obtain accurate structural and volume data on microgram size samples.

In this report we present volume data for thorium at room temperature to approximately 100 GPa. Thorium the second element in the actinide series (with no 5f-electrons), plays a significant role as a source of internal heat in the earth. Bridgman (1948) studied thorium to 10 GPa. Subsequently Bellussi et. al., (1981) and Benjamin et. al., (1981) extended the static data to 30 GPa and 67 GPa respectively. Shock wave data are available for thorium upto 141 GPa (see Van Thiel 1976).

We used a Mao and Bell (1978) type DAC apparatus and collected data for Th upto 100 GPa. The sample is an electro refined high purity material. Gold was used as an internal pressure calibrant in these experiments.

RESULTS

A thorium sample was loaded into a 100 μm gasket hole along with very fine gold powder (for a complete description of experimental procedure, see Akella et. al., 1987). X-ray diffraction data for the pressurized sample was collected by energy-dispersive method and an intrinsic germanium detector was used in this set up.

In Fig. 1, our thorium data are compared with the data from Bellussi et. al. and Benjamin et. al. These authors fit their experimental data to Birch-Murnghan equation. We have used their EOS parameters in calculating the curves.

There is reasonably good agreement between the present data and those measured by Bellussi et. al. and Benjamin et. al. However, the extension of their data beyond reported experimental range (by using Birch-Murnaghan fit parameters) does not conform to our higher pressure data.

We notice that thorium which is very compressible at low pressures, becomes stiffer beyond ~35 GPa. This is evident from the sharp change in the slope (Fig. 1). We do not see any structural change in thorium around this pressure. We suggest this change of slope may arise out of a possible electronic phase transformation (as for example in cerium). More detailed experiments are planned to explore this possibility.

ACKNOWLEDGEMENTS

We appreciate the help given by the Hawaii Institute of Geophysics Group, especially Dr. Manghnani and Mr. Kim. This work was performed under the auspices of the U.S. Department of Energy under Contract number W-7405-ENG-48.

REFERENCES

1. P. W. Bridgman, Proc. Am. Acad. Arts. Sci., 76 (1948) 55.

2. G. Bellussi, U. Benedict and W. B. Holzapfel, Jou. Less. Com. Metals, 78 (1981) 147.

3. T. M. Benjamin, G. Zou, H. K. Mao and P. M. Bell, Carnegie Geophysical Laboratory Yr. Book, 80 (1981) 280.

4. M. Van Thiel, Compendium of shock wave data, University of California Lawrence Livermore Laboratory, UCRL-50108 (1976).

5. H. K. Mao and P. M. Bell, Carnegie Geophysical Laboratory Yr. Book, 77 (1978) 847.

6. J. Akella, G. S. Smith and A. P. Jephcoat, Jou. Phys. Chem. of Solids (In press), UCRL-96683 (1987).

7. F. Birch, J. Geophys. Res., 57 (1952) 227.

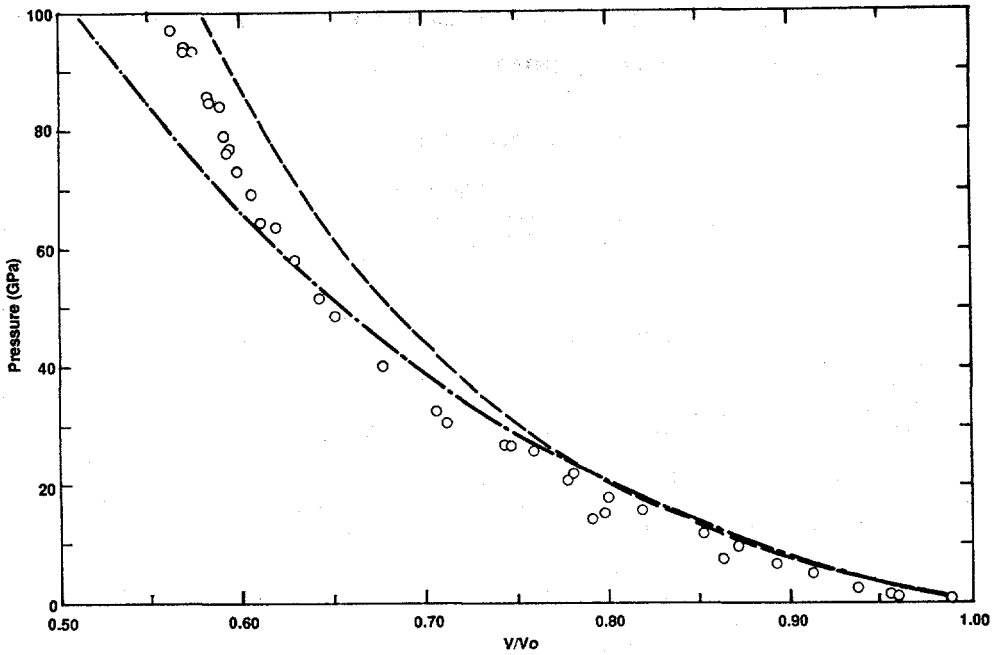

Figure 1. Relative volume of thorium to 100 GPa. Present data (open circles) are compared with Bellussi et. al. (---) and Benjamin et. al. (----) data. Note the extension of their data beyond experimental range does not fit our higher pressure data.

THE USE OF EXAFS SPECTROELECTROCHEMISTRY FOR THE IN SITU STUDY OF THE OXIDATION OF A COPPER(I) COMPLEX IN A POLYMER MODIFIED ELECTRODE

R.C. Elder and William R. Heineman

Department of Chemistry
University of Cincinnati
Cincinnati, OH 45221-0172

The use of EXAFS spectroelectrochemistry has allowed us to study the structural changes occurring in various transition-metal complexes upon electrochemical oxidation or reduction in solution. The advantage of this technique is that it allows the study of materials that can not be obtained in crystalline form and materials that are in oxidation states which are inaccessible by standard synthetic routes. We have recently extended the use of EXAFS spectroelectrochemistry to probe the interaction of transition-metal complexes with ion-exchange polymer membranes on electrode surfaces. In this experiment, an electrical potential is applied to the polymer modified electrode which generates and maintains a given metal-complex, incorporated in a polymer film, in a particular oxidation state while the X-ray absorption spectra is recorded. Information concerning the type and number of atoms surrounding the central absorbing atom and the distance between the corresponding atoms can be extracted from the EXAFS data. XANES spectra are also recorded which give information about the oxidation state of the absorbing atom and the local site symmetry of the ligands surrounding it.

In this report, the construction and evaluation of a new electrochemical cell incorporating a novel thin layer graphite electrode will be discussed. In addition, results pertaining to the structural changes upon oxidation of a Cu(I) complex in a polymer membrane, anchored on the electrode surface, are described (1).

EXPERIMENTAL

The thin layer graphite working electrode was made by spraying three layers of colloidal graphite (Acheson Aerodag G) onto a strip of Mylar. Electrical contact to the film was accomplished using silver paint. An alcohol solution of poly-perfluorosulfonate (Nafion) was applied to the electrode surface and allowed to dry. The copper(I) complex, bis(2,9-dimethyl-1,10-phenanthroline)copper(I) tetrafluoroborate, was incorporated into the Nafion layer by soaking the electrode overnight in a 1 mM solution.

The spectroelectrochemical cell used in this study is shown in figure 1. The cell was machined from 7/16" plexiglass. The solution compartment thickness is 1 mm and the "back" of the working electrode was placed against the Kapton tape window. This configuration is important for the fluorescence EXAFS measurement in that it reduces absorptive losses. The incoming X-ray and outgoing fluorescence photons need only penetrate the polymer and carbon layers, avoiding absorption due to the aqueous solution. To avoid shorting of the working electrode and the counter electrode, kapton tape was interleaved between the two. The holes on the top of the cell were used for filling and insertion of a Ag/AgCl reference electrode. All the electrochemistry was performed on a BAS CV-27 voltamograph. Ammonium acetate was used as the supporting electrolyte and the cell was flushed with fresh electrolyte immediately prior to the X-ray measurement to ensure that the only copoper

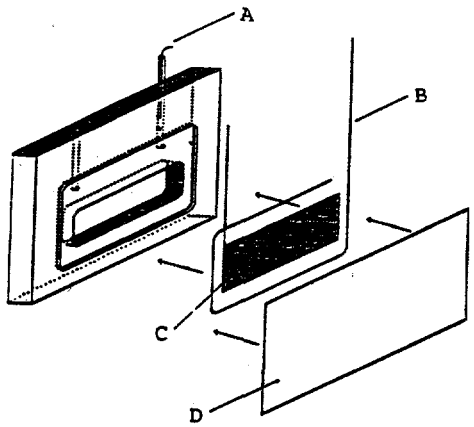

Figure 1: EXAFS spectroelectrochemical cell; (A) Ag/AgCl reference electrode (B) Pt wire counter electrode (C) thin layer graphite working electrode (D) 0.005 in. polyimide Kapton tape window.

present was incorporated in the Nafion film. After the XANES and EXAFS spectra were measured, the electrode potential was set to 1.2 V vs Ag/AgCl for 3 hr. to generate the Cu(II) species followed by a second measurement of the XANES and EXAFS spectra.

RESULTS AND DISCUSSION

The edge spectra shown in figure 2 demonstrate that both oxidtion state and structural changes are taking place upon the application of the 1.2 V potential. The edge spectra of solid $Cu(I)(DMP)_2NO_3$ and the $Cu(DMP)_2^+$ in the

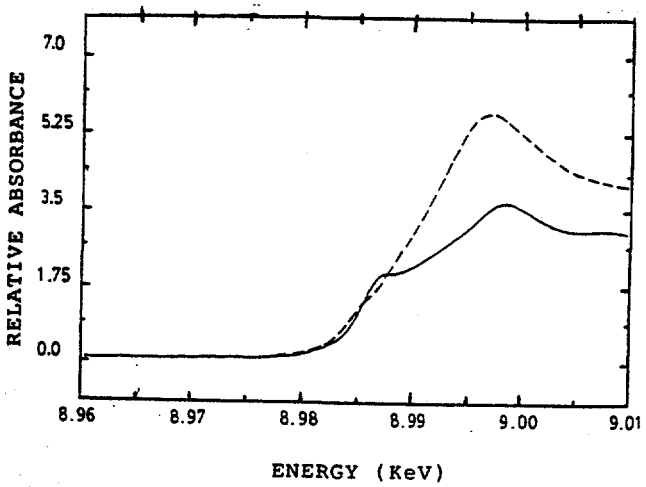

Figure 2: Comparison of the XANES spectra of $Cu(DMP)_2BF_4$ in the Cu(I) state (——) and after electrolysis at 1.2 V vs. Ag/AgCl (- - -).

Nafion membrane were found to nearly superimpose, indicating that the copper species present in the Nafion prior to electrolysis has the same pseudotetrahedral structure found in the solid state. Several significant differences are observed in the comparison of the XANES spectra of the Cu(I) and Cu(II) species (Fig. 2): the pronounced shoulder at 8986 eV is nearly missing in the oxidized species; the maximum has shifted from 8997.5 to 8996.5 eV; and the X-ray absorption has increased by a factor of 1.4. The XANES spectra provide evidence of the exhaustive in situ oxidation of the starting Cu(I) complex.

Curve fitting of the filtered EXAFS data in both oxidation states using the empirical parameters derived from the solid $Cu(I)(CMP)_2NO_3$ complex indicated a Cu-N bond length change of 0.04 A (from 2.06 A for the Cu(I) complex to 2.02 A in the Cu(II) state) and an increase in coordination number from four to five. The increase in coordination number is not unexpected. Cu(II) complexes frequently expand their coordination shell by one or two by adding a water molecule or an oxygen atom from a complex counter ion. The "extra" fifth ligand in the Cu(I) species would most likely be an oxygen atom from one of the sulfonate groups in the Nafion polymer or from water present in the polymer film. The inability of the refinement procedure to distinguish adjacent elements in the periodic table leads to the successful modelling of the four nitrogens and one oxygen system by using five nitrogens. It has been observed that a decrease in the site symmetry about the absorbing atom causes an increase in the spectral transitions obsrved in the XANES spectrum. The increase in the coordination number which causes the reduction in the local site symmetry about the copper center, is also supported by the increase in the XANES spectrum intensity for the Cu(II) species as compared to the Cu(I).

The use of EXAFS spectroelectrochemistry has allowed us to gain insight into this Nafion polymer modified electrode. First, the copper(I) complex is taken up intact and presumably bound by an ionic interaction with the sulfonate groups of the Nafion polymer. Second, upon oxidation the copper(II) coordination sphere is expanded to include a fifth ligand possibly from the sulfonate neighbor. Finally, it appears the techniques utilized here should be of general applicability in characterizing polymer modified electrodes.

Individuals working on this project include Drs. C.E. Lunte, A.F.M.M. Rahman, J.R. Kirchhoff, H.D. Dewald, L.R. Sharpe, and Mr. C. Galiatsatos. Support for this work was provided by NFS Grant CHE 8401525.

REFERENCES

1. Elder, R.C., C.E. Lunte, A.F.M.M. Rahman, J.R. Kirchhoff, H.D. Dewald, and W.R. Heineman, J. Electroanal. Chem., in press.

GLANCING ANGLE EXAFS STUDIES ON Cu-Al INTERFACES

Proposal No. 1072M

S. M. Heald, and H. Chen

Division of Materials Science, Department of Applied Science, Brookhaven National Laboratory
Upton, NY 11973

INTRODUCTION

Cu-Al thin film interfaces have been studied by many techniques. $CuAl_2$ is observed as the first compound to form at the interface by x-ray diffraction and RBS, although the resolution was not much better than 100 A.[1] Photoemission measurements observed intermixing at monolayer coverages, but could not determine compositions.[2] Therefore, the detection of initial interface reactions requires a depth sensitive tool which can resolve local atomic structures. Such a detection is made possible without the need of an UHV environment, via the availability of synchrotron x-rays. Fluorescence EXAFS from an interface region alone can be obtained by using glancing angle incident x-rays.[3] To demonstrate the power of the glancing angle EXAFS technique, Cu-Al thin films prepared under various conditions were studied and compared.

RESULTS AND DISCUSSIONS

Thin films of Al(~600 A)/Cu(~1000 A) were evaporated on glass substrates at near room temperatures (RT) and low temperatures (LT). During the beam time received in December 87 in SSRL, the LT samples were measured and were compared to the RT samples previously measured at CHESS. EXAFS data show that the extent of the initial reaction is about equal for LT and RT. The temperature of the substrate might affect the grain size of films, and hence the reactivity of the interface. Electron microscopy studies are planned to determine the grain sizes. The conclusion one can draw is that the microscopic structures at the initial reacted region for the films prepared at different temperatures are the same to the sensitivity of this technique.

Further studies including oxygen exposures and annealing were performed at CHESS later. More data analysis is required to clarify the results.

ACKNOWLEDGEMENTS

This research was performed under the auspices of the U.S. Department of Energy, Division of Materials Sciences, Office of Basic Energy Sciences, under Contract No. DE-AC02-76CH00016

REFERENCES

1. R. A. Hamm and J. M. Vandenberg, J. Appl. Phys. 56, No. 2, 293 (1984).
2. V. Di. Castro and G. Polzonetti, Surf. Sci. 186, 383 (1987).
3. S. M. Heald, et al., to be published.

X-RAY ABSORPTION STUDY OF OXIDE BASED SUPERCONDUCTORS Proposal No. 1073M

S. M. Heald, C. Y. Yang, and J. M. Tranquada

Brookhaven National Laboratory
Upton, NY 11973

INTRODUCTION

Recently several experimental and theoretical studies have suggested[1] that the Cu-O bond-stretching vibrational modes are responsible for observed high-T_c superconductivity in oxide superconductors. We have demonstrated[2] that EXAFS can be used as a vibrational probe to measure phonon modes. Thus the validity of the phonon mechanisms in $YBa_2Cu_3O_7$ can be put to a critical test by this work.

EXPERIMENTAL

The EXAFS measurements of $YBa_2Cu_3O_7$ were performed at the SSRL on the beam line I-V. The powdered samples were oriented in a magnetic field and potted in epoxy. Measurements were made with the sample oriented in two different configurations: the c-axis perpendicular ($e \perp c$) and parallel ($e \parallel c$) to the x-ray polarization. Measurements were made at 10, 80, 150, 180, 220, 240, and 300 K.

RESULTS AND DISCUSSIONS

For the Cu edge, the Fourier transforms of oriented $YBa_2Cu_3O_7$ (Figs. 1 and 2) show a clear orientation dependence. When $e \perp c$, first shell is due to the contributions from the Cu(I) site (i.e. linear chain site) with two nearest O neighbors at 1.941 A along the b axis and from the Cu(II) site (i.e. square planar site) with four O neighbors at an average distance of 1.944 A in the a-b planes. In Fig. 2, for $e \parallel c$ the first peak is due to the contributions of the two shortest Cu-O bonds at 1.851 A from the Cu(I) site and its shoulder is due to a more distant Cu-O bond at 2.285 A from the Cu(II) site.

The values of mean square relative displacement, σ^2, were extracted using standard techniques.[2] The variation of σ^2 with temperature for the three different Cu-O distances is shown in Fig. 3 along the fits using the Einstein model. Our results strongly indicate that there is no anomalous temperature dependence of σ^2 for Cu-O pairs in $YBa_2Cu_3O_7$. Furthermore, as expected, the long Cu-O bond at 2.285 A (Fig. 3(a)) is weaker than the Cu-O bonds at 1.94 A (Fig. 3(b)) and 1.85 A (Fig. 3(c)). As for a previous study of $La_{2-x}SrCuO_{4-y}$ system,[3] this study has cast doubt on the importance of soft mode phonons for superconductivity in $YBa_2Cu_3O_7$.

ACKNOWLEDGEMENTS

This research was performed under the auspices of the U.S. Department of Energy, Division of Materials Sciences and Division of Chemical Sciences, Office of Basic Energy Sciences, under Contract No. DE-AC02-76CH00016 and one of the authors (C. Y. Yang) was supported by the National Science Foundation under Grant DMR-8407265 and by the U.S. Department of Energy under Contract No. DE-AC05-80-ER10742.

REFERENCES

1. Novel Superconductivity, S. A. Wolf and V. Z. Kresin, Editors, Plenum, New York, 1987 and references therein.
2. C. Y. Yang, M. A. Paesler, and D. E. Sayers, Phys. Rev. B 36, 980 (1987).
3. J. M. Tranquada, S. M. Heald, and A. R. Moodenbaugh, Phys. Rev. B, in press.

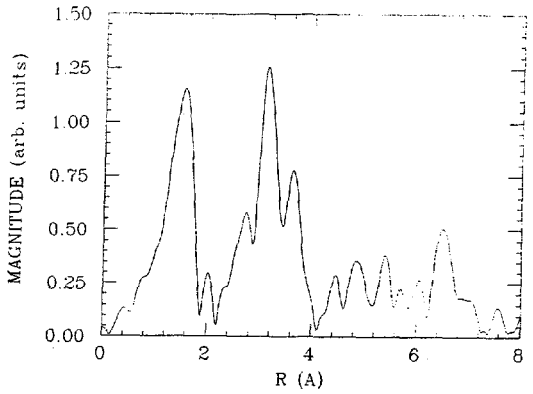

Fig. 1. Magnitude of Fourier transform of $K^2\chi(K)$ for $YBa_2Cu_3O_7$ ($e \perp c$).

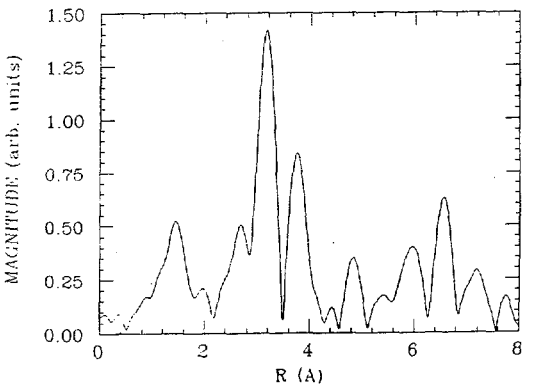

Fig. 2. Magnitude of Fourier transform of $K^2\chi(K)$ for $YBa_2Cu_3O_7$ ($e \parallel c$).

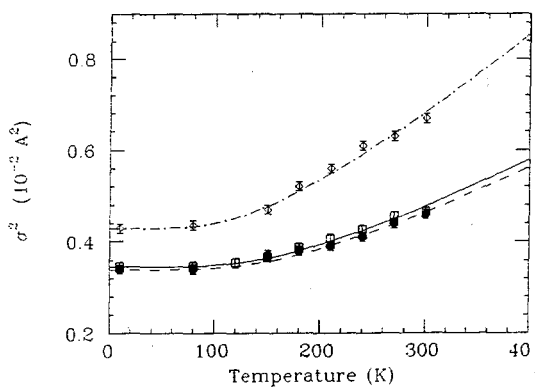

Fig. 3. Changes with temperature of σ^2 for (a) Cu-O pairs along the c-axis at 2.285 A, (b) Cu-O pairs in the a-b planes at 1.942 A, and (c) Cu-O pairs along the c-axis at 1.853 A.

EXAFS Studies on Powders of GaAs Treated with Co Complexes

I. L. Abrahams, C. E. Caley, S. R. Lunt, G. M. Miskelly, M. J. Sailor, P. G. Santangelo, M. H. Schmidt, B. J. Tufts and N. S. Lewis

Department of Chemistry
Stanford University
Stanford, CA 94305-5080

We have been investigating the chemical nature of electrical trap sites at important semiconductor interfaces. Previous work in our laboratory has shown that adsorption of transition metal ions onto GaAs surfaces decreases the surface recombination losses of semiconductor/liquid junctions.[1,2] In order to investigate the structure of these surface species, we have performed detailed Co K absorption edge and EXAFS studies on powders of GaAs that have been exposed to aqueous cobalt(III) ammine complexes. These results represent the first direct structural information for any chemisoprtion reaction at a semiconductor electrode surface. In our last year's work at SSRL, we have collected X-ray data for the chemisorbed metal ion in contact with vacuum at 10K, 77K, and 298K, in contact with H_2O at room temperature, and for a series of model Co(II) and Co(III) complexes. These studies are described below.

The initial studies have been performed with metal complexes of the type $Co^{III}(NH_3)_5X$ (X-NH_3, N_3^-, SCN^-, H_2O, Br^-, NO_2). The EXAFS and Co K absorption edge data were obtained on high surface area GaAs powders (<400 mesh) which were treated with solutions of $Co^{III}(NH_3)_5H_2O$ at pH=10, $Co^{III}(NH_3)_5N_3$ at pH=11, and $Co^{II}(H_2O)_6$ at pH=10. For these studies, samples of GaAs powder (ca. 100 mg) were suspended for 5 minutes in a 10 mM solution of the Co metal complex of interest. Then the solution was filtered, the powder was washed with H_2O, then CH_3OH, and dried in N_2. This procedure resulted in a 1-2% (by weight) loading of Co. EXAFS of GaAs powder exposed to $Co^{III}(NH_3)_5H_2O$, taken at 10K and 10^{-6} torr, yielded a spectrum which was extremely similar to EXAFS data for bulk $Co(OH)_2$, suggesting that the cobalt species on the GaAs surface is similiar to $Co(OH)_2$. The edge absorption position and structure was also quite similar for $Co(OH)_2$ and for the Co/GaAs system, lending further support to the Co(II) oxidation state assignment.

A conventional EXAFS analysis program utilizing model complexes to determine scattering amplitudes and phase factors yielded a best fit for the Co/GaAs sample of 5 oxygen atoms at 2.11 Å. A second peak at 3.13 Å, which was fit to 6 cobalt atoms, was also observed in the EXAFS data. We cannot determine whether any of the second shell atoms are Ga or As, because of the very similiar scattering properties expected for Co, Ga, and As. However, the high coverage of Co (approx. 10 monolayers by radioisotope measurements and by XPS analysis) suggests that most of the Co is in the $Co(OH)_2$ environment.

Comparison of the above data with EXAFS data obtained for a sample measured at room temperature indicated no significant difference in the EXAFS data or Co K absorption edge spectra, implying that cooling and exposure to vacuum did not induce significant changes in the sample. Exposure of GaAs powder to the complex $Co^{III}(NH_3)_5N_3$ in pH=11 solution also yielded an X-ray absorption spectrum that was extremely similar to $Co(OH)_2$. EXAFS data obtained at a temperature of 77K and a pressure of 10^{-6} torr showed the Co atom to be in an environment of 7 oxygen atoms at a distance of 2.08 Å. A second peak at 3.12 Å was also observed in the EXAFS data, and is probably due to 6 Co atoms. The above data is consistent with a mechanism whereby the cobalt(III) complex loses its ligands, is reduced by the GaAs substrate, and forms $Co(OH)_2$ which is insoluble at high pH. At lower pH, the $Co(OH)_2$ dissolves off the surface and no beneficial effect on the I-V behavior of the semiconductor/liquid junction is observed.

If the above mechanism were true, then the chemisorption of cobalt(II) ion onto GaAs should also exhibit similar electrical and structural properties. Electrochemical studies using $Co^{II}(H_2O)_6$ as the starting complex did yield improved I-V properties in the KOH-$Se^{-/2-}$ test electrolyte, though the improvement was not as great as that from treatment by Co^{III} complexes. EXAFS analysis of the data for Co(II)/GaAs samples, obtained at a temperature of 77K and a pressure of 10^{-6} torr, revealed a surface phase similiar in structure to $Co(OH)_2$. The best fit yielded 6 O atoms at 2.08 Å and a second shell scatterer, most likely 8 Co atoms, at 3.13 Å.

The above data gives a good indication of the structure of the surface phase after initial treatment. However, the n-GaAs electrochemical studies are typically performed in KOH-$Se^{-/2-}$ electrolyte, in order to suppress photocorrosion processes.[3] In order to more fully characterize the surface phase in this medium, additional X-ray absorption studies were performed after the Co/GaAs powders were exposed to KOH-$Se^{-/2-}$ solutions. A set of complexes, $Co^{III}(NH_3)_5H_2O$ [pH=10, EXAFS measured both at 298 K and 10K, 10^{-6} torr], and $Co^{III}(NH_3)_6$ [pH=11, 77K, 10^{-6} torr] were reacted with GaAs powder as described above and subsequently exposed to a 1.0 M KOH-1.0 M K_2Se-0.1 M K_2Se_2 solution for 5 minutes, washed with H_2O, and dried. Our EXAFS results demonstrate that for the three compounds and varying conditions, the Co exists in an environment of 3 Se at 2.33 A. This is consistent with XPS experiments which have indicated that both crystalline (100) and powdered GaAs surfaces, when exposed to the various Co ammine complexes under the stated conditions and subsequently exposed to K_2Se solution, yielded identical X-ray photoemission spectra.

In order to be able to make general statements about the mechanisms of metal ion absorption on GaAs surfaces, other systems which also exhibit improvements in photoanode behavior must be studied. Our most recent study is on the behavior of ruthenium ions on GaAs. Based on the initial success of Heller *et. al.*[4,5], Ru^{3+} treatment of the GaAs surface improved the I-V behavior at the n-GaAs/KOH-$Se^{-/2-}$ interface. XPS of single crystal (100 oriented) n-GaAs and

of GaAs powders exposed to $RuCl_3$ has been used to identify the coverage of Ru at approximately 0.5 monolayers. In order to obtain the oxidation state and the chemical environment of the Ru on the surface of GaAs powders, we performed EXAFS on GaAs powders exposed to a 0.1 M HCl-0.1 M $RuCl_3$ solution for 15 minutes. At present, we are in the proccess of analyzing the EXAFS data. The chemical environment of the ruthenium ion is probably quite different from cobalt, since it is at such a low coverage. EXAFS data should yield the oxidation state and nature of the first shell scatterer. At the conclusion of these studies, we expect to have a general picture of the trends in chemical binding to GaAs surfaces, and the resultant structure of the surface species that are responsible for improved electrical behavior of these interfaces.

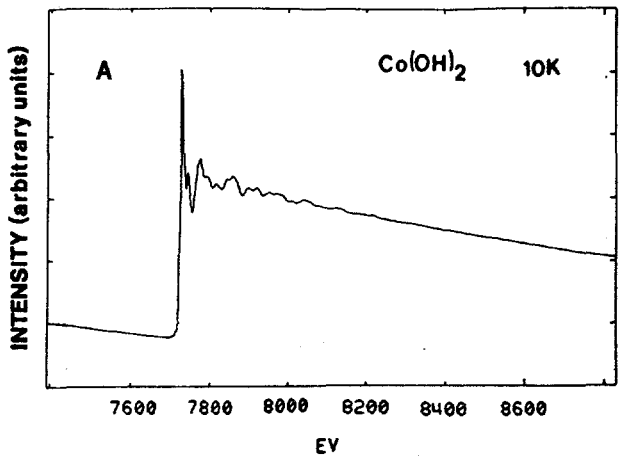

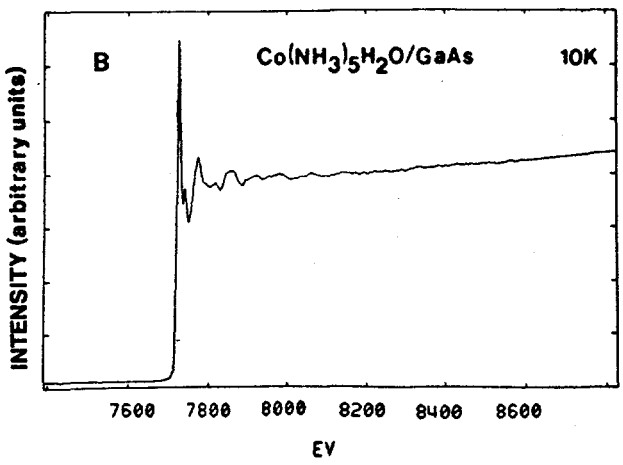

Figure 1. a) X-ray absorption data at 10 K for $Co(OH)_2$ dispersed in BN. The data were collected in transmission mode. b) X-ray absorption data at 10 K for GaAs powder that had been exposed to 10.0 mM $Co(NH_3)_5H_2O^{3+}$ at pH=10. The spectrum is the average of several scans, and was collected in the fluorescence mode.

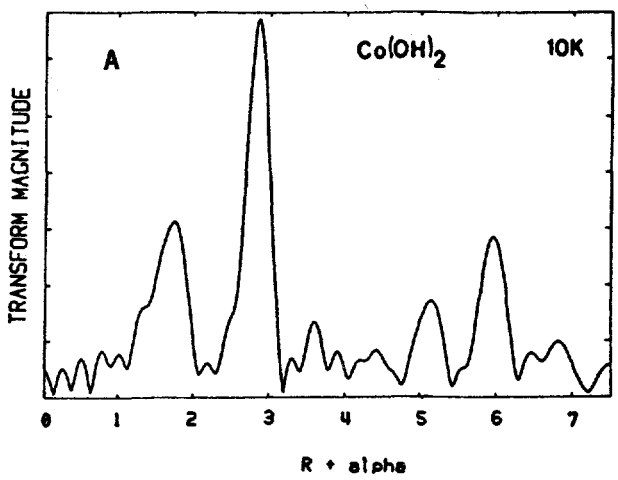

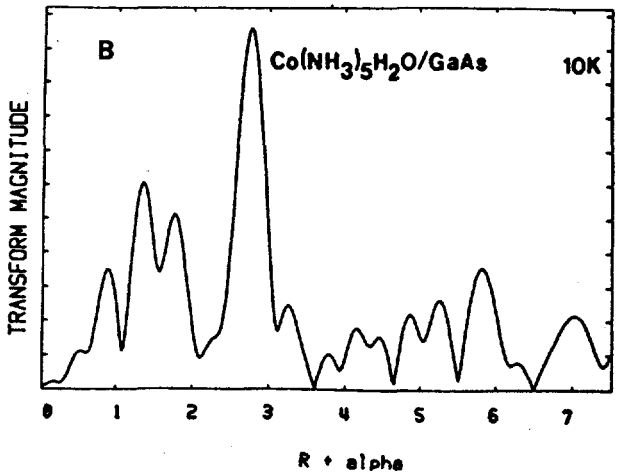

Figure 2. a) Fourier transform of EXAFS data at 10 K for $Co(OH)_2$ dispersed in BN. b) Fourier transform of EXAFS data at 10 K for GaAs powder that had been exposed to 10.0 mM $Co(NH_3)_5H_2O^{3+}$ at pH=10.

ACKNOWLEDGMENT

We acknowledge helpful discussions with Dr. A. Roe, Dr. B. Hedman, and Prof. K. Hodgson of Stanford University and SSRL; and Dr. O. Melroy and Dr. J. Gordon of IBM. We also acknowledge M. Heben, A. Kumar, C. Newcomb, Dr. R. Penner, and G. Ryba of Stanford University.

References:

1. B. Tufts, I. Abrahams, P. Santangelo, G. Ryba, L. Casagrande, N. Lewis, Nature, 326, 861 (1987).

2. I. Abrahams, B. Tufts, N. Lewis, J. Am. Chem. Soc., 109, 3472 (1987).

3. a) K. Chang, A. Heller, B. Schwartz, S. Menezes, B. Miller, Science, 1986, 1097 (1977). b) C. Gronet, N. Lewis, J. Phys. Chem., 88, 1310 (1984).

4. a) W. Johnston, H. Leamy, B. Parkinson, A. Heller, B. Miller, J. Electrochem. Soc., 127, 90 (1980). b) A. Heller, B. Miller, S. Chu, Y. Lee, Proc. IEEE Photovolt. Spec. Conf., 14, 1366 (1980).

5. a) B. Parkinson, A. Heller, B. Miller, Appl. Phys. Lett., 33, 521 (1978). b) B. Parkinson, A. Heller, B. Miller, J. Electrochem. Soc., **126**, 954 (1979). c) R. Nelson, J. Williams, H. Leamy, B. Miller, B. Parkinson, A. Heller, Appl. Phys. Lett., **36**, 76 (1980).

EXAFS OF $YBa_2Cu_3O_{7-\delta}$ AND $GdBa_2Cu_3O_{7-\delta}$ SUPERCONDUCTORS

J. B. Boyce
Xerox Palo Alto Research Center, Palo Alto, CA 94304, U.S.A

F. C. Bridges
Physics Department, University of California, Santa Cruz, Santa Cruz, CA 95059, U.S.A

T. Claeson
Physics Department, Chalmers University of Technology, 41296 Gothenburg, Sweden

T. H. Geballe and R. S. Howland
Department of Applied Physics, Stanford University, Stanford, CA 94305, U.S.A

The local structure and the near-neighbor pair vibrations in two new ceramic superconductors of the 1:2:3 type have been studied. X-ray absorption measurements showed essentially no change in the near-edge and extended fine structure (EXAFS) over a temperature range of 4.2 to 688 K for $YBa_2Cu_3O_{7-\delta}$ and $GdBa_2Cu_3O_{7-\delta}$. The results indicate that the two compounds are very similar to each other in local bonding and electronic structure, and they remain unchanged over the large temperature range, from far below to well above T_c. The EXAFS structural results agree well with the accepted structure modeled from neutron diffraction data. Alternate structures which have been proposed recently are not consistent with the data.

The absorption edge of Cu in a superconductor is broad, covering an energy range between the edges of Cu in CuO (with a formal valence of II) and $KCuO_2$ (with a formal valence of III). An extra peak appears in the near-edge spectrum as oxygen is pumped out from the superconductor. It coincides with a peak in the spectrum for Cu_2O and is associated with the breaking up of 1-d Cu-O chains in the 1:2:3 compound.

From the temperature dependence of the Debye-Waller-like broadening of near-neighbor distances, it is possible to extract information on bond vibrations. The characteristic vibration frequencies of the near-neighbor atoms show that the 2-d Cu-O planes and the 1-d Cu-O chains form the most rigid parts of the structure. These oscillator frequencies are consistent with those for some modes seen by inelastic neutron diffraction as well as by infrared and Raman spectroscopy. The characteristic Einstein temperatures for the Cu-O modes fall in the range of 500-600 K, a value which is lower than the desired value of the breathing modes to describe the superconductivity with a classical electron-phonon coupling.

No evidence of phonon softening is apparent in any of the phonon modes studied over a large temperature interval.

TABLE 1. Number and distances of near neighbors in Y-Ba-Cu-O as determined from fits to EXAFS data for three samples. [The number was kept fixed for Cu-O, as indicated by (f).] The characteristic Einstein temperatures are obtained from the temperature broadening of the distances.

	N	r(Å)	Θ_E(K)
Cu-O	2/3 (f)	1.88±0.02	
	10/3 (f)	1.95±0.01	540±50
	2/3 (f)	2.32±0.05	
Y-O	8±1	2.39±0.01	380±50
Cu-Cu,Y			260±50
Ba-O			310±50

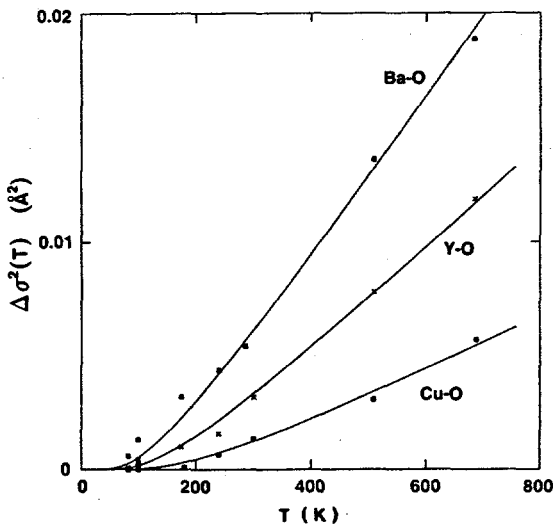

Fig. 1. The change in the square of the width of the pair distribution functions for Cu-O, Y-O, and Ba-O in superconducting Y-Ba-Cu-O as a function of temperature. The solid lines are fits of an Einstein oscillator model to the data. No phonon softening is observed.

MICRORADIOGRAPHY OF CREEP DAMAGE IN COPPER

J.E. Benci and D.P. Pope

Department of Materials Science and Engineering
University of Pennsylvania
3231 Walnut St., LRSM, Philadelphia, PA 19104

INTRODUCTION

There has been a great deal of work done in the last several years using constitutive equations and continuum mechanics to model the development of damage and fracture of materials under slow strain rate, high temperature service conditions[1-6]. Unfortunately,there has been no good experimental check on the accuracy of these models. Most investigators did not even compare their computer predictions with experimental results while a few compared their models to micrographs from polished surfaces of creep damaged samples. Examining a polished surface has the limitation that the surface may not be representative of the bulk sample. Additionally, artifacts may be introduced while other features are concealed during the polishing process. A technique which can reveal information on the size and spatial distribution of creep damage in a bulk sample would be an excellent test for the damage models. Microradiography is such a technique.

RESULTS AND DISCUSSION

A high purity copper alloy which had been heavily doped with oxygen was chosen as the material for this study. This material exhibited a ductility minimum at about 500°C, with a resultant reduction of area of about 3.1%. The fracture at 500°C was totally intergranular due to cavity coalescence. Axisymmetric notched tensile samples were machined from this material. Nearly identical specimens were tested at 500°C at a constant displacement rate of 2.11×10^{-5} mm/sec. Different specimens were interrupted at various fractions of the samples lifetime. Longitudinal cuts were made in the samples using EDM to remove the center sections of each specimen. These 1.5 mm thick slices were then mounted and prepared for microradiographic analysis by polishing both faces.

The development of creep damage as a function of time was observed as well as the spatial distribution of the damage for this material. Fig. 1 is a radiograph from a sample which was interrupted relatively early in its creep life. The small white features, about 150 μm long, emanating from the left notch are microcracks, failed grain boundary facets. Fig. 2 is a radiograph from a nearly identical sample interrupted much later in its creep life. A macroscopic creep crack extends most of the way across the sample. It can be seen from both figs. 1 and 2 that all of the creep damage is located in a fairly narrow band around the minimum cross-section in these samples. This is in marked contrast to previous results from high purity iron samples[7]. The damage in iron developed at fairly sharp angles to the notch or crack plane. This would imply that the damage process in iron is controlled by the effective stress while the formation of damage in this copper alloy is controlled by the maximum principal or hydrostatic stress. The finite element modelling to confirm this hypothesis is currently being performed.

ACKNOWLEDGEMENTS

Part of this work was performed at SSRL which is supported by the Department of Energy, Office of Basic Energy Sciences. This work was funded through the Synchrotron Topography Project of the National Synchrotron Light Source, Brookhaven National Laboratory, which is supported by the Department of Energy under grant DE-FG02-84ER45098.

REFERENCES

1. D.R. Hayhurst, P.R. Dimmer and C.J. Morrison, *Phil. Trans. R. Soc. Lond. A*, A311, 103 (1984).
2. V. Tvergaard, *Int. J. Fracture*, 31, 183 (1986).
3. J.W. Hutchinson, *Acta Met.*, 31, 1097 (1983).
4. H. Reidel, in *Fundamentals of Deformation and Fracture*, eds. Bilby, Miller and Willis, 293 (1985).
5. B.F. Dyson, in *Proc. of the Conference on Mechanisms and Mechanics of Plasticity*, Aussois, France (1987), in press.
6. J.L. Bassani and D.E. Hawk, in *Proc. of the International Seminar on High Temperature Fracture Mechanisms and Mechanics*, Dourdan, France (1987), in press.
7. J.E. Benci and D.P. Pope, *Met. Trans. A*, in press.

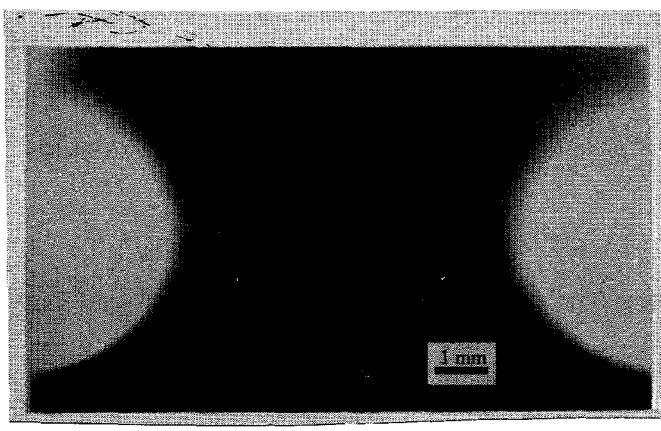

Figure 1. Radiograph of an axisymmetric notched copper sample tested at 500°C and interrupted at 0.75 x (max. stress) while the stress was still increasing.

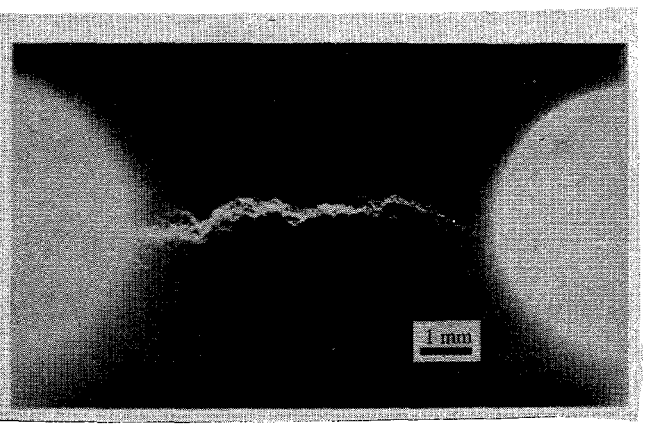

Figure 2. Radiograph of a nearly identical sample as the one from fig. 1 tested at 500°C and interrupted at 0.4 x (max. stress) after the sample had already passed the max. stress.

ANTISITE DISORDER IN $YBa_2Cu_3O_7$

F. W. Lytle, E. C. Marques, R. B. Greegor and H. G. Ahlstrom, The Boeing Co., Seattle, WA 98124
E. M. Larson and D. E. Peterson, Los Alamos National Laboratory, Los Alamos, NM 87545
A. J. Panson, Westinghouse Research and Development Center, Pittsburgh, PA 15235

We have measured and analyzed the 77K EXAFS of Y and Cu in Y $Ba_2Cu_3O_7$ (YBC) and confirm the results reported earlier of antisite disorder between the Y and Cu sites in YBC (1,2,3). Two separate, well characterized samples from Westinghouse and Los Alamos were examined. The data were obtained on beam line VII-3 with Si (220) crystals and 1 mm entrance slits and are shown in Fig.1. Also shown are the Cu-O and Y-O phase corrected transforms. In addition to the expected distances it is evident that Cu and Y share common distances in the structure, i. e. some fraction of the atoms occupy the site of the other. (A long Cu-O bond of 2.31 Å is expected but the peak observed at ~2.4 Å is much too large.) Because of the well known interference between termination ripples and bond distances in R-space, we used fitting in K-space to accurately evaluate the number of bonds and distances. The inverse transform of the region surrounding the first FT peak(s) was fitted using experimentally determined amplitude and phase shift parameters. The fits and components of the fit are shown in Fig. 2 and listed in Table 1. Table 1 lists all the relevant structure data. The values determined by diffraction are an average from the literature with an uncertainty in R of ±.01 Å.

The rationale for the fitting procedure was as follows: We used initial parameters as determined by diffraction from Table 1 and varied N, R, and $\Delta\sigma^2$ for each bond to determine the best possible fit. The resulting parameters were slightly different than the starting ones. Then one extra bond distance was added to the fit and again all N, R, and $\Delta\sigma^2$ were varied. It was found that significantly improved fits could be obtained with an additional Y-O bond of 2.1 Å and a Cu-O bond of 2.5 Å as shown in Table 1 and Fig. 2. The relative number of bond distances as determined from the fitting were used to estimate the mole fraction, x, of Cu and Y involved in the antisite disorder. Note that there are two Cu_2 sites for each Cu_1. It was found that x= 0.16±.05 for either element, Cu on the Y sites or Y on the Cu_2 sites. The data is incompatible with any Y on the Cu_1 sites. It is significant that the 2.5 Å Cu-O distance has a much larger disorder than any of the other bonds. This is to be expected when a small atom occupies a larger site and may be significant in the superconductivity of this compound.

A complete description of this work is found in Ref. 3 along with simulated x-ray diffraction patterns which show that either x-ray or neutron diffraction is insensitive to this degree of disorder.

1. F. Lytle, R. Greegor and A. Panson, Phys.Rev.B37, Feb. 1, 1988.
2. F. Lytle, R. Greegor and A. Panson, in Novel Mechanisms of Superconductivity, p. 1049, Plenum, 1987.
3. F. Lytle, et. al, "Crystal Lattice Measurements in Superconducting Materials", to be published in Superconducting Materials and Instrumentation, SPIE Proceedings, Vol. 879, 1988.

Table 1. Summary of $YBa_2Cu_3O_7$ Structure Data.

	Determined From Diffraction				Determined From EXAFS		
Bond Type	Number, N	Distance, R (Å)	*Average N	*Average R (Å)	N	R (Å)	$\Delta\sigma^2$(Å^2)**
Cu_1-O_4	2	1.84	0.67	1.84	0.9±.3	1.81±.05	-0.0001
Cu_1-O_1	2	1.94					
Cu_2-O_2	2	1.93	3.33	1.94	2.7±.5	1.94±.02	-0.0011
Cu_2-O_3	2	1.96					
Cu_2-O_4	1	2.31	0.67	2.31	0.5±.2	2.25±.05	-0.0006
Cu in Y site					0.9±.3	2.5±.1	0.012
Y-O_2	4	2.38	8.0	2.40	6.8±1	2.38±.02	-.0028
Y-O_3	4	2.41					
Y in Cu site					0.7±.3	2.1±.1	-.0034

*The average represents the resolution expected from EXAFS.

**$\Delta\sigma^2$ is relative to the oxygen envelope extracted from 77 K data for NiO and SrO for Cu-O and Y-O bonds, respectively.

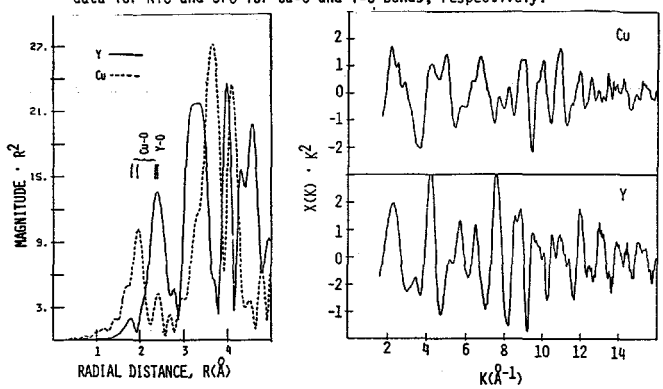

Fig. 1 Right, the measured X(K)·K² EXAFS functions for the K-edges of Y and Cu in YBC. Left, oxygen phase-corrected transforms, note the common distances for Cu and Y.

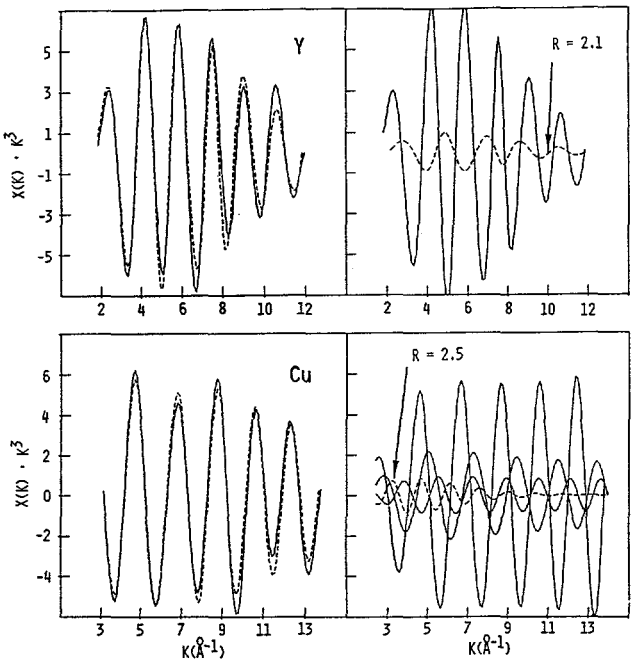

Fig. 2 Left, the data ——, the fit --- and right, the components of the fit.

RARE EARTH L-EDGE SPECTRA IN $Y_{1-x}M_xBa_2Cu_3O_7$

F. Lytle[1], R. Greegor[1], E. Marques[1], E. Larson[2], J. Wong[3] and C. Violet[3]

1. The Boeing Co., Seattle, WA 98124
2. LANL, Los Alamos, NM 87545
3. LLNL, Livermore, CA 94550

It has been observed that substitution of trivalent rare earth elements for Y in $YBa_2Cu_3O_7$ has little effect whereas Ce, Pr and Tb, which have an accessible tetravalent state lower Tc or destroy the superconductivity. Is the effect due to valence? Here we present x-ray absorption L-edge spectra for the following compounds in an attempt to determine valence (1): $Pr_xY_{1-x}Ba_2Cu_3O_7$ where x= 0.2, 0.4 and 0.6; $Gd_xY_{1-x}Ba_2Cu_3O_7$ where x= 0.5 and 1; $CeBa_2Cu_3O_7$ and $HoBa_2Cu_3O_7$. The Gd and Ho compounds were ~90 K superconductors, the Ce compound did not superconduct and the Tc of the Pr compounds was ~80 K, ~40 K and non-superconducting as x= 0.2, 0.4 and 0.6, respectively. The spectra of the superconducting compounds in Fig. 1 were obtained using e-yield detection with a Si(220) monochromator, i. e. resolution better than 1 ev. The spectra of some of the reference compounds were measured in the normal absorption mode and thereby suffer from a thickness effect reduction of the intensity of the L-edge resonances; hence, the relative intensities are not accurate. However, the relative energy positions for each element are accurate to 0.1 eV. The Pr L_2-edges are shown because of a near overlap of the Ba L_1 and Pr L_3. The other edges are all L_3.

The spectra of CeO_2 and PrO_2 have double peaks split by ~ 8eV which had been attributed to mixed valence; however, there is now a consensus(2) that the effect is due to a splitting of the hybridized 4f band. In effect the band splits into low and high energy parts while the total density of states remains approximately constant. The relative intensity and energy position of the doublet is a measure of 4f hybridization rather than a direct indication of valence. The valence information is present in the ~3 eV shift of the first resonance as the valence changes from 3^+ to 4^+. The splitting effect for Ce and Pr is very sensitive to chemical pressure in that the two elements in approximately the same environment show a different degree of the effect. For example, the ratio of the 2nd peak to the 1st in $CeO_2 > Ce_2O_3 > Ce$ in silicate glass, $CePO_4$* and $PrO_2 > Pr_6O_{11}$, Pr_2O_3*, $PrPO_4$*, Pr in silicate glass.* * indicates compounds with no splitting. In Fig. 1 it is evident that in the Pr superconductors the valence is 3+, but there is evidence of a little splitting as marked by the arrow. Compare with the Gd (or Ho) data where there is a dip instead of a bump. This is the only obvious difference in the Pr data (data for all the compounds were identical). The L_3 edge in the Ce compound is shifted relative to the Ce 3+ model compounds indicating a 4+ valence and is broadened and split but different from CeO_2 or other model compounds which were examined. The L spectra of the Gd compounds was identical and very similar to Ho (not shown) and obviously present as 3+. Correlation of these spectra with superconducting properties is not obvious. Ce^{4+} would presumably quench Cu^{3+}; however, Pr is present primarily as Pr^{3+}. The common spectral feature for the two elements is a high energy component of the edge resonance which has been attributed to an unfilled part of the 4f band, albeit $Pr^{3+} << Ce^{4+}$.

1. We thank Brian Maple's group, UCSD, for the Pr and Ce superconductors, Ted Collings, Battelle, for the $Gd_{0.5}$ and Dean Peterson, Los Alamos, for the Gd superconductors. The Ho compound was from Chuck Violet, Livermore.

2. G. Krill, J. de Physique, Colloque C8 47, 907 (1986)

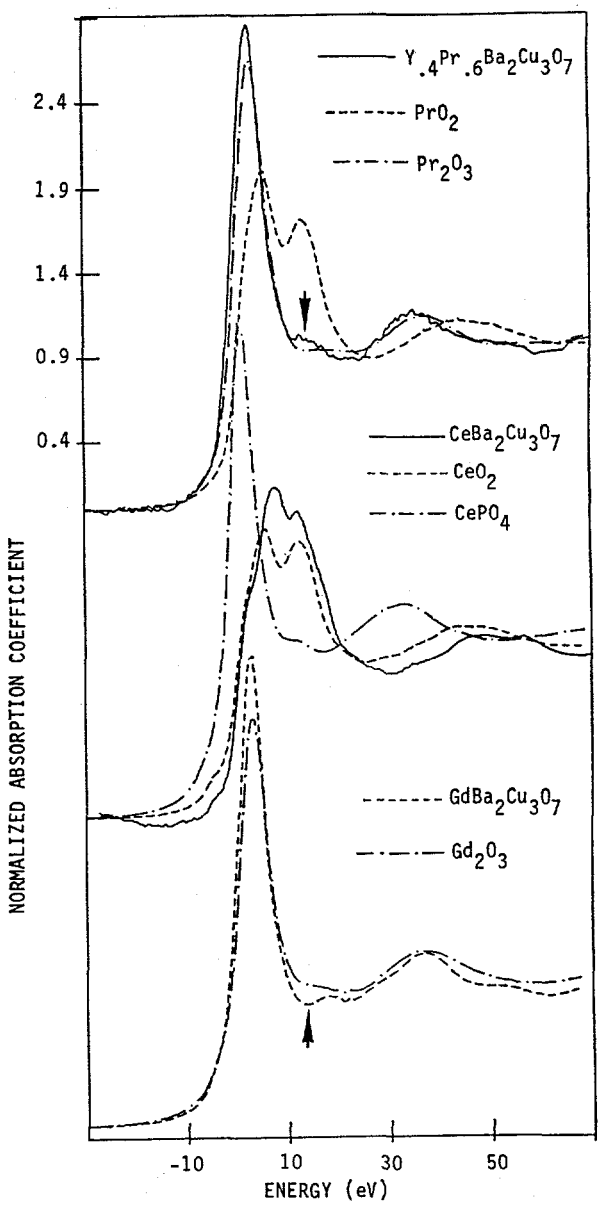

Fig. 1 The Pr L_2, Ce L_3, and Gd L_3 absorption edges vs energy. Relative energy positions for each element are accurate to 0.1 eV. Relative intensities are not accurate, the ordinate for the Gd data has been compressed 17%.

CHARACTERIZATION OF THE ATOMIC AND ELECTRONIC STRUCTURES OF HIGH T_c SUPERCONDUCTING MATERIALS BY XAS

S. D. Conradson, G. H. Kwei, and I. D. Raistrick

INC-4, MS C345
Los Alamos National Laboratory
Los Alamos, NM 87545

INTRODUCTION

The recent observation by Bednorz and Müller[1] of superconductivity at 30 K in a multiphase mixture of La-Ba-Cu-O metal oxides, and the later discoveries of a T_c of 93K in $YBa_2Cu_3O_{7-\delta}$[2] and now of *ca.* 115K in Ca-Sr-Bi-Cu-O systems have prompted intense efforts to understand the origin of the superconductivity in these materials. Although Rietveld refinements of neutron and x-ray powder diffration data have preempted EXAFS as a means of determining their atomic structures, XAS experiments have nevertheless provided contributions towards understanding of their unusual physical properties[3–6]. We also have observed several intriguing spectrum:property relationships in the Cu K XAS of these compounds, paying particular attention to the characteristics of the different samples and the problems of data analysis.

RESULTS AND DISCUSSION

Cu–O amplitudes and phases. It has been noted[4–6] that the use of Cu_2O and CuO as standards for $La_{2-x}M_xCuO_{4-\frac{x}{2}}$ (M = Ba, Sr) and $YBa_2Cu_3O_{7-\delta}$ results in *ca.* 50% overestimates of the total number of O atoms. We found that these errors could be reduced to $\leq$ 10–15% by using La_2CuO_4 as a standard for the Cu–O EXAFS waves. This problem was examined more thoroughly by comparing the Cu–O EXAFS waves from several compounds. The amplitudes of these waves demonstrate a surprisingly large variation in size and shape. The errors in the calculated numbers of O atoms can now be understood as the direct result of the larger per-atom amplitude found in the EXAFS of La_2CuO_4 and related materials. In addition to this difference in size, a shift in the peak of their k^3 weighted amplitude envelopes to higher to near $k = 8$ Å^{-1}. These anomalous amplitudes are related to the potential for superconductivity rather than superconductivity proper, insofar as they have only been found for compounds which are superconducting either as studied or become so when properly doped. We believe that they reflect an unusually anisotropic distribution of the O electrons.

Contributions of more distant shells. We have made a substantial effort to account for the contributions of the La, Y, Ba, and Cu atoms, resulting in consistent metrical values as well as a good correspondence between the data and the fit. This is only true, however, for interplane O and Cu shells; high quality fits were obtained without including the O shell at 2.30 Å or the Cu shells at 3.39 and 4.15 Å . Attempts to include these indicated that their contributions were restricted to the low k region of the spectrum and were rapidly damped. We conclude that, consistent with the thermal parameters found from the combined x-ray/neutron diffraction analysis[7], the interactions between the various Cu–O planes are much weaker than those between atoms within the same plane. We also have observed indications of anomalous vibrational behavior involving the bridging Y and Ba atoms, especially for $YBa_2Cu_3O_6$, but no evidence supporting the claim of Cu–Y substitutional disorder.

Sample dependence of $YBa_2Cu_3O_{7-\delta}$. Our first sample of $YBa_2Cu_3O_{7-\delta}$, which was annealed at only 900°C, exhibited only 50% of the Meissner effect of a second sample prepared by what is now recognized as the optimum procedure. Although single phase, the powder diffraction pattern of this first sample possesses a smaller orthorhombic splitting and the almost complete absence of [00*l*] reflections. Analysis of the EXAFS of these samples demonstrates 10%, 30%, and 5% lower contributions from the Y, Ba, and Cu nearest neighbors, respectively, in the first sample. These observations are most easily explained by invoking a higher degree of substitutional disorder in the first sample, consistent with its lower annealing temperature. The extent of this disorder is apparently not the same for each element, but is greater for the Y and Ba than for the Cu. The effect of this disorder is to decrease the superconducting portion of the sample, but not T_c. In this regard, it is of interest that the XANES of the two samples, reflecting the electronic structure at the Cu atoms, are identical, especially in light of our studies of Zn-doped, depressed T_c samples in which the XANES was affected in a highly specific manner.

REFERENCES

1. J. G. Bednorz and K. A. Müller, Z. Phys. B **64**, 189 (1986).
2. M. K. Wu, J. R. Ashburn, C. J. Torng, P. H. Hor, R. L. Meng, L. Gao, Z. J. Huang, Y. O. Wang, and C. W. Chu, Phys. Rev. Lett. **58**, 908 (1987).
3. a. J. M. Tranquada, S. M. Heald, A. R. Moodenbaugh, and M. Suenaga, Phys. Rev. B **35**, 7187 (1987). b. J. M. Tranquada, S. M. Heald, and A. R. Moddenbaugh, Phys. Rev. B **36**, 5263 (1987).
4. a. J. B. Boyce, F. Bridges, T. Claeson, T. H. Geballe, C. W. Chu, and J. M. Tarascon, Phys. Rev. B **35**, 7203 (1987). b. a. J. B. Boyce, F. Bridges, T. Claeson, R. S. Howland, and T. H. Geballe, Phys. Rev. B **36**, 5251 (1987).
5. a. H. Oyanagi, H. Ihara, T. Matsushita, M. Tokumoto, M. Hirabayashi, N. Terada, K. Senzaki, Y. Kimura, and T. Yao, Jpn. J. Appl. Phys. **26**, L488 (1987). b. H. Oyanagi, H. Ihara, T. Matsushita, M. Tokumoto, M. Hirabayashi, N. Terada, K. Senzaki, Y. Kimura, and T. Yao, Jpn. J. Appl. Phys. **26**, L638 (1987).
6. H. Oyanagi, H. Ihara, T. Matsubara, T. Matsushita, M. Hirabayashi, M. Tokumoto, K. Murata, N. Terada, K. Senzaki, T. Yao, H. Iwasaki, and Y. Kimura, Jpn. J. Appl. Phys **26**, L1233 (1987).

XAS STUDIES OF QUASI-ONE-DIMENSIONAL HALIDE-BRIDGED MIXED VALENCE PLATINUM COMPOUNDS

Proposal No. 2024Mp

S. D. Conradson, B. I. Swanson, and A. P. Sattelberger

INC-4, MS C345
Los Alamos National Laboratory
Los Alamos, NM 87545

INTRODUCTION

A convenient model for the quasi-one-dimensional halogen-bridged mixed-valence metal complexes (HMMC's) is of the form:

$$-[M^{n+\delta} - X^- \cdots M^{n-\delta} \cdots X^-] - .$$

The formation of the charge-density-wave of renormalized metal site, M, d orbitals of amplitude δ is stabilized by strong electron-phonon coupling, i.e., the Peierls displacement of the halide, X^-, off of the central position. We have been engaged in the spectroscopic characterization of anionic and neutral chain Br^--bridged mononuclear Pt-center (n=3)[1] and Br^-- and Cl^--bridged binuclear Pt-center (n=2.5) compounds of this class[2]. Even this limited set of compounds has exhibited a very wide range of behavior in terms of the stabilities of certain types of local (defect) states and metastable ground states. These observations thus raise the following questions in regards to the relationships of the electronic, molecular, and long range structures: 1) what is the magnitude of δ (= 0 for complete charge delocalization); 2) does $\delta^+ = \delta^-$; 3) what factors control the M–M distance; 4) how is the behavior influenced by the halide; 5) how is the behavior influenced by the equatorial ligands and interchain interactions? We (and others[3,4]) have recently been using XAS as an experimental probe for obtaining information concerned with these issues.

RESULTS AND DISCUSSION

The XANES spectra of a number of model compounds corroborate previous observations[5] that, consistent with the higher number of d holes, the height of the Pt L_3 white line is significantly greater for compounds containing Pt(IV) than Pt(II). Changes in the types or, more surprisingly, the arrangement of the Pt first nearest neighbor atoms can, however, cause the transition moment to change by amounts comparable to the Pt(IV)–Pt(II) difference. XANES features at higher energies demonstrate the sensitivity of the Pt L_3 XANES to subtle changes in the Pt environment; these features are conserved when the parent complexes are incorporated into the HMMC. As expected, the white line heights for the HMMC's, with their average Pt oxidation state of +3, fall between those of the Pt(II) and Pt(IV) compounds. Although the differences in the heights between the spectra of these three HMMC's are not large, they follow the order expected from the nephelauxetic β's of these ligands. The ligands therefore do affect the electron densities on the central metal ions of the HMMC's, and apparently do so in ways which are already understood. Significant differences between the Br K XANES of these same three HMMC's, despite the virtual identity of the Pt–Br_{axial} and Pt–$Br_{equatorial}$ distances, demonstrate that bridging halide also has an effect on the electronic structure and, more importantly, that this differs for the axial and equatorial positions.

Tanino *et al.*[3], in a similar series of experiments in which the bridging halide was varied, found that the ratio of the Pt L_3 white line strength of $Pten_2Cl_4$, $[Pt(en)_2][Pt(en)_2Br_2](ClO_4)_4$, and $Pten_2Cl_2$ is 4:3:2 and that the white line height was dependent on the bridging halide in the order $Cl^- > Br^- > I^-$. They interpreted these data as demonstrating that δ can be < 1 but that the average Pt charge is always +3, so that $\delta^+ = \delta^-$. However, considering that core-hole relaxation effects result in a constant offset for the transition intensity[5], the 4:3:2 ratio then means that the Pt charge in $Pten_2Cl_4$ must be less than twice and that of $[Pt(en)_2][Pt(en)_2Br_2](ClO_4)_4$ less than $1\frac{1}{2}$ times that in $Pten_2Cl_2$. As suggested by XPS studies, the calculations of Horsley[5], and our findings, charge is apparently being transferred from the ligands to the Pt ions, the bonds have some covalent character, and $\delta^+ \neq \delta^-$.

These differences in the Pt L_3 and Br K XANES of this set of compounds, especially of the three HMMC's which possess such similar structures, demonstrates the existence of additional, more subtle effects on the Pt d hole density. A better model for these HMMC's may therefore be:

$$-[Pt^{4-\delta_{e4}-\delta_{Br}} - Br^{-1+\delta_{Br}} \cdot Pt^{2-\delta_{e2}} \cdot Br^{-1+\delta_{Br}}] - ,$$

where $\delta_{e4/2}$ are the charges donated by the equatorial ligands to, respectively, the Pt(IV) and Pt(II) ions and δ_{Br} is the charge donated by the axial Br^- to the Pt(IV) ion. A significant difference between this model and the simpler one is the composition and occupancy of the d_{z^2} conduction band. It now has appreciable Br p_z character and is less than half filled.

REFERENCES

1. S. D. Conradson, R. F. Dallinger, B. I. Swanson, R. J. H. Clark, and V. B. Croud. Chem. Phys. Lett. **135**, 463 (1987).
2. a. S. D. Conradson, M. A. Stroud, M. H. Zietlow, B. I. Swanson, D. Baeriswyl, and A. R. Bishop. Solid State Comm. (in press). b. B. I. Swanson, M. A. Stroud, S. D. Conradson, and M. H. Zietlow. Solid State Comm. (in press).
3. H. Tanino, H. Oyanagi, M. Yamashita, and K. Kobayashi, Solid State Comm. **53**, 953 (1985).
4. I. Ikemoto, K. Kikuchi, K. Iwai, M. Yamashita, M. Nomura, K. Asakura, N. Kosugi, K. Yakushi, and H. Kuroda. Bull. Chem. Soc. Jpn. **59**, 3271 (1986).
5. J. A. Horsley, J. Chem. Phys. **76**, 1451 (1982).

Reflectivity of Thin Carbon Films

S. Brennan
Stanford Synchrotron Radiation Laboratory, Stanford, Ca. 94305.
M.F. Toney
IBM Almaden Research Center, San Jose, Ca. 95120.

Carbon films are being considered as protective coatings for thin magnetic films used in recording applications. The films can be produced in a variety of ways which result on a macroscopic scale in differences in density and surface roughness. In this study we have used x-ray reflectivity to study the bulk properties of the films. The reflectivity is very sensitive to the film thickness, density and surface roughness.

We have studied sputtered films approximately 280Å thick. To measure the reflectivity at very low angles it was necessary to slit down the incident beam to roughly 50 microns. The incident photon energy was 9500 eV. The detector slits were set to accept >0.5° of reflected beam and were centered on the incident beam. Figure 1 is a plot of the log of the reflected intensity vs. incident angle for one of the films. The oscillations in the reflectivity are due to the interference between the x-rays reflected from the carbon-air interface and those reflected from the silicon-carbon interface.

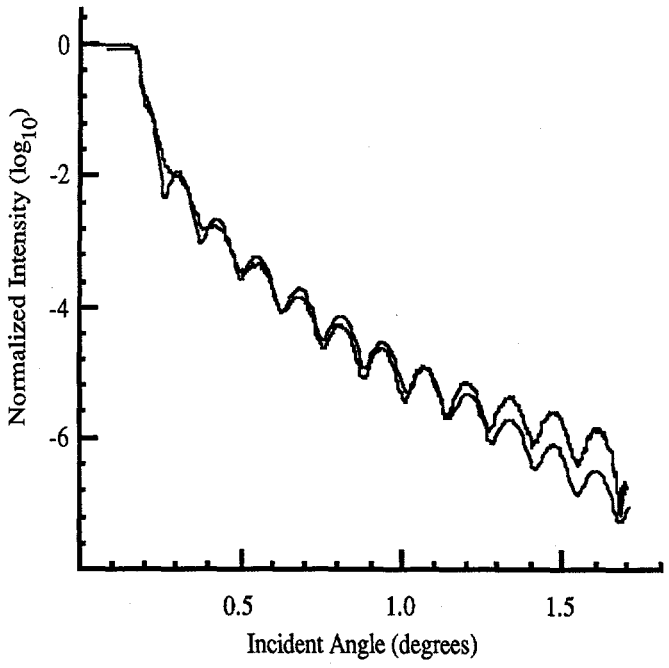

Fig. 1 Normalized Log of the Reflectivity vs. Incident Angle for a ~275Å carbon film sputter deposited on a Si substrate. The dashed line is the fit to the Fresnel theory.

These data were fit using a standard Fresnel theory modified by including an exponential damping term for the surface roughness. The dashed line in Figure 1 shows a fit to the data using that theory. The modulation in the intensity was calculated to be due to a 280 Å thick film. The density of the film was 1.8 gms/cc, well below the value for bulk graphite, which is 2.1 gms/cc. The surface roughness which best fit the data was 7 Å. The theoretical curve had a constant background added to it. As can be seen in the figure the fit is not complete. We are attempting to understand what additional terms are involved.

Figure 2 is a plot of the fluorescence from a 10 Å thick copper layer which had been deposited on the surface of the carbon film. This spectrum was obtained using the same type of scan as was used in Figure 1, scanning the incidence angle on the sample. The fluorescence from the copper layer is a measure of the electric field at the carbon-air interface. The data in Figure 2 were normalized for the change in the number of copper atoms the beam hits with angle. This was done by multiplying each point by the sine of the incidence angle for that point.

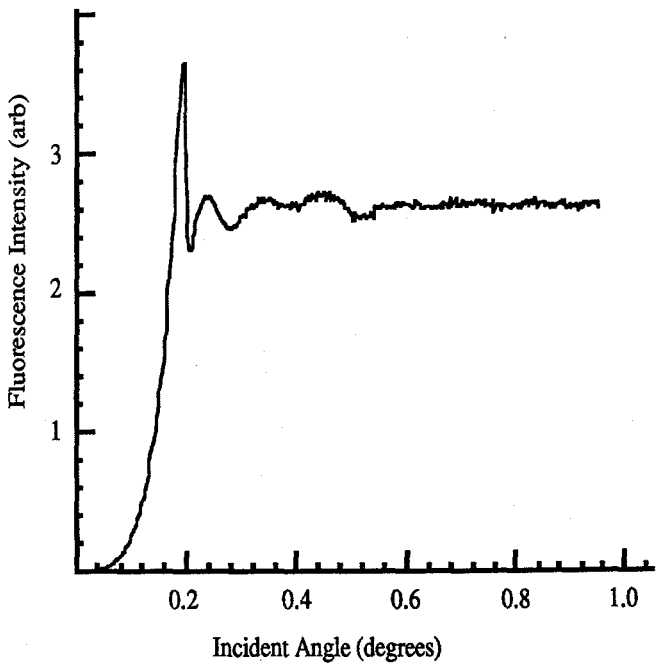

Figure 2. Fluorescence Intensity from 10Å copper layer on surface of carbon film deposited on silicon substrate.

Fluorescence EXAFS Study of Silicon in Neodymium Iron Boron Rare-Earth Magnets

S. Brennan and A. Bienenstock
Stanford Synchrotron Radiation Laboratory, Stanford Ca. 94305
J.E. Keem
Ovonic Synthetic Materials Co., Troy, Mi. 48084

Recently, a material has been described which consists predominantly of a phase similar in structure to $Nd_2Fe_{14}B$ but with the addition of approximately 1 at.% Si. Rapidly solidified ribbon samples of this new material have been fabricated using a melt-spinning process. The resulting ribbons are polycrystalline, as determined by powder diffractometry. To determine the environment of the Si atoms in this structure we have performed fluorescence Extended X-ray Absorption Fine Structure (EXAFS) measurements on the flakes.[1] The advantages of fluorescence EXAFS in this case are its significantly greater sampling depth which avoids the surface sensitivity of electron yield techniques and its better signal-to-background ratio. Previous fluorescence EXAFS studies of low-Z elements have used a proportional counter. For this experiment a Si(Li) solid state detector was used because of its improved energy resolution. The greater energy resolution (~150 eV FWHM) means that the fluorescent signal can be discriminated from the elastically scattered signal, resulting in an improved signal-to-background ratio compared to a proportional counter. This is especially important for polycrystalline samples where elastically scattered diffracted beams can enter the detector.

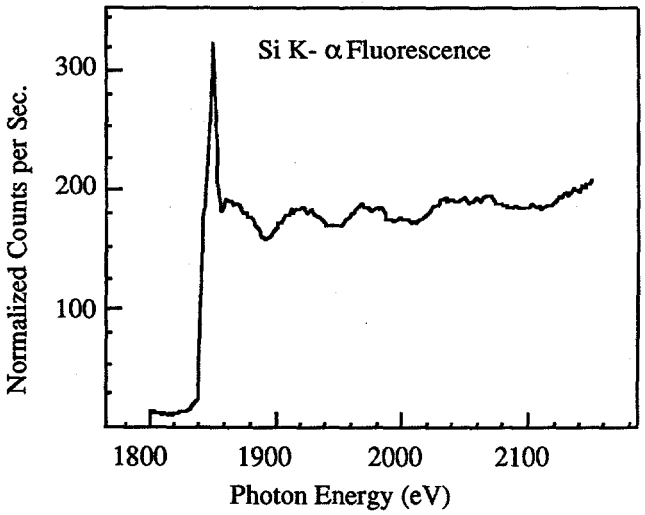

Figure 1 shows the sum of 8 scans obtained with a total of 32 seconds per point, with 2 eV between points. Note that the count rate in the region below the absorption edge is less than 5% of the signal above the edge, indicating the near-total removal of the elastic signal. Figure 2 shows the results of both a k^0 and a k^2 transform. Because the k^0 transform results in better separation of the two dominant features, it was used for the analysis of the distances in the sample.

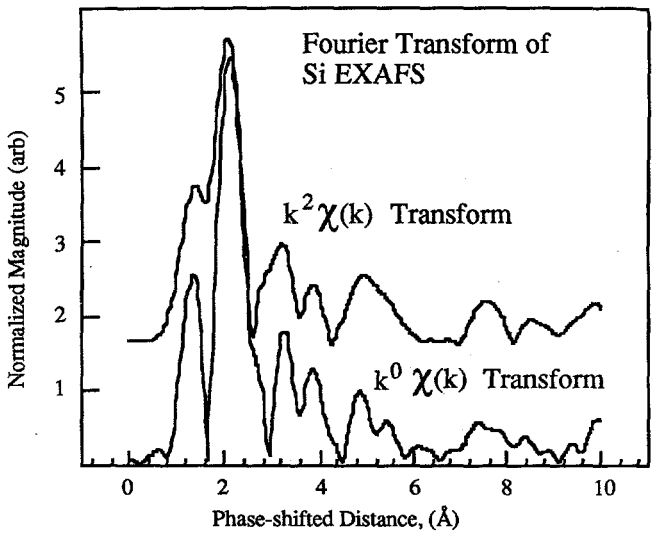

The peak centered at 2.1Å was isolated and back-transformed. This back-transformation isolates the near-neighbor contribution to the EXAFS. Using phase shifts and backscattering amplitudes tabulated by Teo and Lee[1] the result was fit to Si-Fe, Si-Si, Si-Nd and Si-O near-neighbors. The only acceptable fit to the data is for a Si-Fe near neighbor, with a distance of 2.45 Å ±0.05Å. Fitting this shell using calculated back-scattering amplitudes gave the number of near-neighbors as 3.3. After compensating for the contribution of the oxidized silicons to the total signal, the number of near-neighbors was determined to be 4.1. The peak at 1.2Å in Fig 2 was fit using an amplitude and phaseshift derived from a sample of SiO_2. The derived distance is 1.65±0.1 Å with 1.1 near neighbors. The angular dependence of the near edge structure suggest that the Si-O bonds are due to a surface oxide and are not a significant feature of the bulk structure. The EXAFS results indicate that the environment of the Si atom is well characterized by a single shell of Fe atoms. By comparing the environment of the Si atom with possible interstitial and substitutional sites in the $Nd_2Fe_{14}B$ structure it is clear that there are no interstitial sites with enough room. The only substitutional site which has the right set of distances and number of near neighbors is the "C" site in the standard structural model.[2]

References

1. S. Brennan, A. Bienenstock and J.E. Keem, submitted to J. Appl. Phys.
2. J.F. Herbst, J.J. Croat and W.B. Yelon, J. Appl. Phys. **57** 4086 (1985).

Strain Distribution in Thin Aluminum Films using X-ray Depth Profiling

M. F. Doerner
IBM General Products Division San Jose, Ca 95193 and
Dept. of Materials Science and Eng., Stanford University, Stanford, CA 94305
S. Brennan
Stanford Synchrotron Radiation Laboratory, Stanford Ca. 94305

Biaxial stresses are often present in thin films on substrates due to non-equilibrium growth of the film or differential thermal expansion of the film and substrate. The strain distribution can be measure directly in the Grazing Incidence X-ray Scattering (GIXS) geometry in combination with a high brightness x-ray source. At small incident angles, the x-rays do not penetrate the entire thickness of the film so that the strain in the surface region can be determined. With increasing angle, greater depths of the film are sampled. The results of GIXS measurements of Al thin films on Si substrates are described.[1]

Aluminum films were deposited by magnetron sputtering onto (100) oriented silicon wafers at room temperature. The grain size was measured to be roughly the film thickness. The films grow with a strong (111) fiber texture. A thermal oxide 1000Å thick was grown on the wafers prior to thin film deposition, to prevent diffusion of the silicon into the aluminum on heating. An aluminum film of 2600Å was annealed in air for 30 minutes at

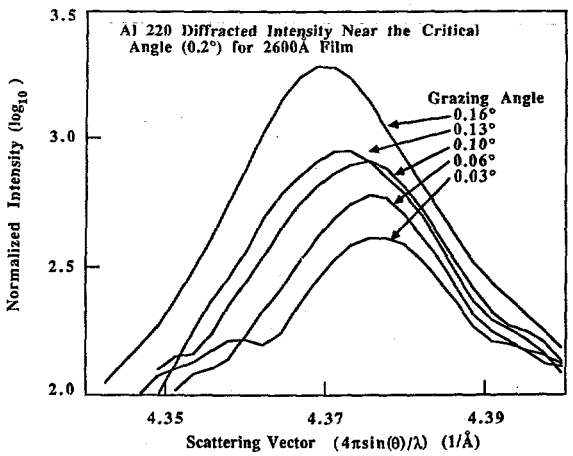

Fig. 1 The measured intensities and positions of the 220 diffracted beam for various incident angles on a strained 2600Å film.

450°C and then cooled to room temperature, in order to produce biaxial tensile stresses in the film. The measured intensities of the 220 diffracted beam in the plane of the film from an annealed 2600Å aluminum film are plotted vs scattering vector for various incident angles in Fig. 1. A shift in the peak to higher values (smaller interplanar spacings) is observed as the incident angle is decreased. Since the penetration depth decreases as the incident angle is decreased, this indicates a decrease in the lattice parameter at the surface. Figure 2 shows a similar set of measurements for a 2600Å film in the as-deposited condition which was found to have very low average strain using the laser-curvature technique. The strain in the film does not change with grazing angle, indicating that the variation seen in the annealed film is not an artifact of the measurement but is due to the strain gradient present in the film.

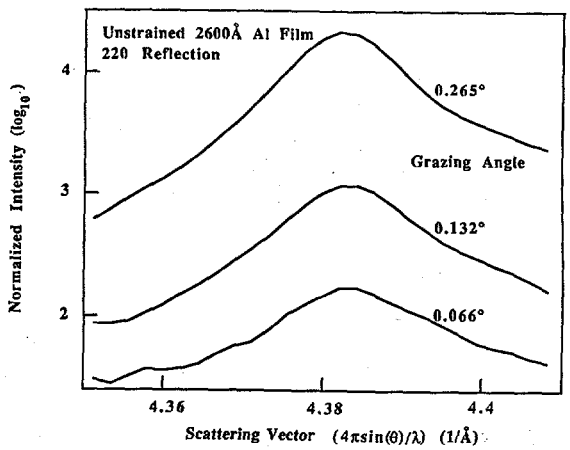

Fig. 2 The 220 diffracted beam intensities and positions for various incident angles on an unstrained 2600Å film.

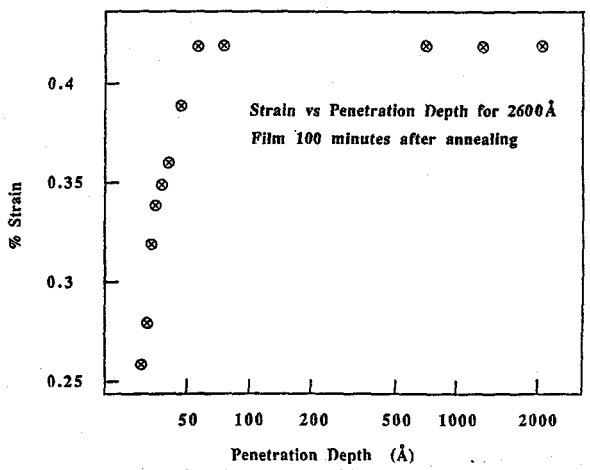

Fig. 3 The strain in the 2600Å Al film plotted vs. penetration depth.

The strain in the film, calculated from the peak center positions at half maximum intensity, is plotted vs. penetration depth in Fig. 3. The strain distribution is constant throughout much of the thickness. The Al diffracted peak position differs from the average value only for penetration depths below 100Å. As the grazing angle is varied through the critical angle the penetration depth scans the entire thickness of the film, yet there is essentially no change in observed peak position in that region.

1. M.F. Doerner and S. Brennan, J. Appl. Phys.63, 126, (1988).

Time-Domain Effects in Resonant Nuclear Scattering of Synchrotron X-Rays

S.L. Ruby, J. Arthur, and D. Brown
Stanford Synchrotron Radiation Laboratory, Stanford, CA 94305
and
G. Shenoy and E. Alp
Argonne National Laboratory, Argonne, IL 60439

The coherent diffraction of X-radiation from a lattice of resonant scatterers, such as Mössbauer nuclei, exhibits time domain effects not found in non-resonant, electronic scattering. Because of its intense, pulsed nature, a high-power synchrotron beam line is an excellent tool for studying these effects. We have observed the time distribution of resonantly scattered X-rays from ^{57}Fe nuclei in a perfect crystal of yttrium iron garnet (YIG), using the new high-power wiggler beam line 10 at SSRL. An average intensity of about 3.5 counts/sec was observed; with minor changes in our scattering geometry we would expect to increase this rate by at least a factor of ten. We observed beats in the time distribution due to the hyperfine splitting of the nuclear levels, and were able to modify the beat pattern by inserting calibrated Mössbauer absorbers into the scattered radiation. We also observed an effective radiative lifetime for the excited nuclear state that was shorter than the normal incoherent ^{57}Fe radiative lifetime by a factor of 38.

Our experiment is similar in design to experiments by Gerdau, et al.[1] A timing detector senses 14.4 keV X-rays diffracted from the YIG (002) planes. Because of hyperfine fields in the magnetic YIG crystal, there are 12 very closely spaced nuclear resonance energies, yielding a time beat pattern with 6 short periodicities (8-35 nsec) and one longer, 390 nsec periodicity. In addition, the nuclear lifetime is expressed in the scattering time distribution. Due to interference between the nuclear scatterers, the effective radiative lifetime for scattering is much shorter than the single-atom radiative lifetime.

Figure 1 shows the time distribution of scattered radiation in our experiment. The solid curve is a fit to our data using a simple kinematic scattering model that includes the expected beat pattern due to the hyperfine splitting. The chief fit parameter measures the radiative speedup factor, which we find to be 38 relative to the single-atom radiative lifetime.

Figure 2 gives a Fourier analysis of the data of Fig. 1, along with the expected hyperfine beat frequencies.

Figure 3 is similar to Fig. 1, except that tuned Mössbauer absorbers have been inserted in the scattered beam to attenuate two of the hyperfine components. In spite of poor statistics for this data, the best fit coefficients give the proper attenuation factor. The speedup factor of 38 also applies to this data.

References

1 E. Gerdau, R. Rüffer, H. Winkler, W. Tolksdorf, C.P. Klages, and J.P. Hannon, Phys. Rev. Lett. **54**, 835 (1985); E. Gerdau, R. Rüffer, R. Hollatz, and J.P. Hannon, Phys. Rev. Lett. **57**, 1141 (1986) and Phys. Rev. Lett. **58**, 2359 (1987).

YIG Data Time Distribution

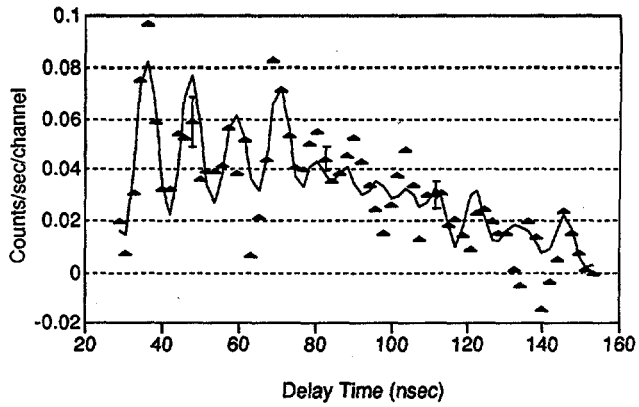

Figure 1

Fourier Analysis of YIG Data

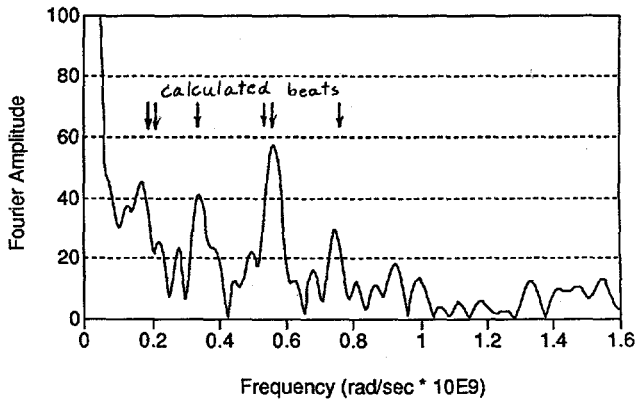

Figure 2

Time Distribution with Absorbers

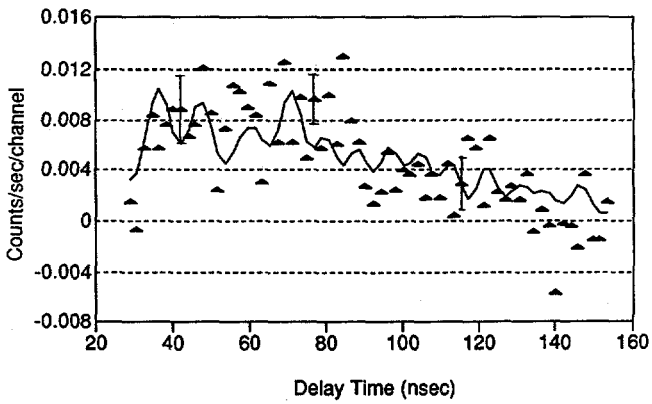

Figure 3

Interferometric Study of Spherical Wave Diffraction

J. Arthur and H. Tompkins
Stanford Synchrotron Radiation Laboratory, Stanford, CA 94305

We have used a monolithic two ear silicon interferometer to observe some effects of the angular coherence present in X-ray waves that have passed through a 5 micrometer wide slit. Diffraction of this radiation in the ears of the interferometer leads to a spatial distribution in the beam leaving the second ear, which is much wider than the 5 micron incident beam. The distribution can be changed by the insertion of phase shifting elements between the interferometer ears. Careful measurements of these distribution patterns provide a test of the fine points of dynamical diffraction theory.

The interferometer used in this experiment consists of two identical thin parallel plates, or ears, which have been cut from but remain attached at the base to a single perfect crystal of silicon. The connecting base keeps the ears parallel to within atomic dimensions. The ear thicknesses are identical to within a few microns; each approximately 300 microns. The ears are separated by 40 mm, and oriented for symmetric Laue diffraction from the crystal (220) or (440) planes.

The dynamical theory of the diffraction of waves produced by a very small source (such as a 5 micron slit) within a crystal slab has been extensively studied[1] and has been applied to the two crystal case.[2] An important result of these studies is the significance of the Pendellösung (or extinction) length, which describes the flow of diffracting energy within the crystal. This length, rather than the X-ray wavelength, is the relevant length for many coherence effects in the interferometer. The Pendellösung length is typically 50 - 100 microns; relative to such lengths a 5 micron source can be considered a point source. The radiation emanating from such a source is for diffraction purposes spherical -- it carries no angular information. (An equivalent viewpoint is that the angular acceptance range for diffraction in a perfect crystal is so small that the single slit diffraction of angstrom-wavelength radiation from a 5 micron slit is enough to completely fill it.)

With such a slit source, the distribution of intensity in the diffracted beam behind the first interferometer ear is a Pendellösung pattern (essentially a Bessel function), spread out over dimensions comparable to the ear thickness. Because of the spherical nature of the source radiation, there is coherence across this widened beam. Diffraction of this beam in the second ear leads to further beam widening and interference, giving a distribution of intensity in the beam leaving the second ear that is a convolution of Pendellösung patterns. This distribution was observed in our experiment.

The experiment was performed at a bending magnet beam line at SSRL. A bent silicon premonochromator was used to focus 26 keV X-rays on the 5 micron entrance slit. This slit consisted of two precision steel roller bearings separated by pieces of 5 micron nickel foil. The interferometer was mounted on a single axis diffractometer, and the exit beam intensity distribution was measured by scanning another 5 micron slit across it, with a NaI detector behind. Changes in the exit beam intensity distribution were induced by placing various acrylic plastic wedges in the beam between the two interferometer ears. Such a wedge introduces a linear phase shift across the beam, changing the interference pattern produced in the second ear. Figure 1 shows two of the intensity patterns that were observed. Although detailed analysis has not been completed, it appears that these patterns are consistent with the predictions of dynamical diffraction theory.

We thank the Quantum Metrology Group of the U. S. National Bureau of Standards, and Dr. Albert Hennins in particular, for hospitality and help in constructing the two ear interferometer.

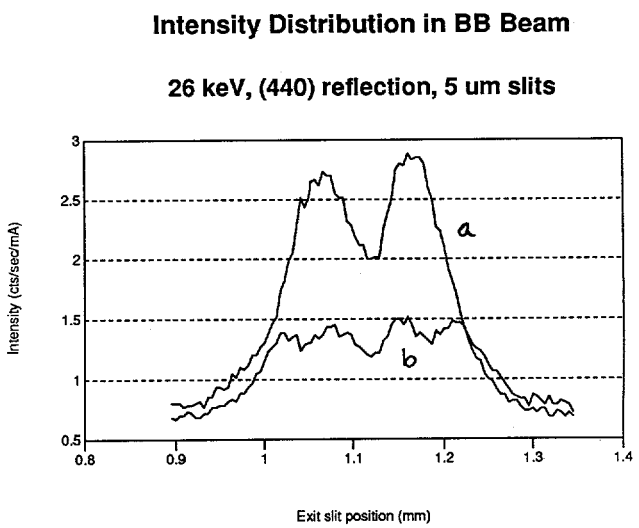

Figure 1
Exit beam intensity distributions with *a)* a narrow wedge inserted and *b)* a wide wedge inserted in the interferometer. There is a broad, flat peak due to incoherent, thermal diffuse scattering underneath the interference pattern in each case.

References

1 See, for example: N. Kato, J. Appl. Phys. **39**, 2225 (1968); L. Azaroff, ed., *X-Ray Diffraction* (McGraw-Hill, N.Y., 1979).
2 V.L. Indenbom, I.Sh. Slobodetskii, and G.I. Truni, Zh. Eksp. Teor. Fiz. **66**, 1110 (1974) [Sov. Phys. JETP **39**, 542 (1974)]; U. Bonse and R. Teworte, Z. Naturforsch. **37a**, 427 (1982); J. Arthur, C.G. Shull, and A. Zeilinger, Phys. Rev. **B32**, 5753 (1985).

Structural Investigations of W-Ge Multilayers and Amorphous W-Ge Alloys

Marybeth Rice
Department of Electrical Engineering
Stanford University

Arthur Bienenstock
Stanford Synchrotron Radiation Laboratory

Anomalous X-ray Scattering and EXAFS experiments were performed on W-Ge multilayers with the aim of understanding the atomic arrangements that occur in these structures as a function of layer thickness and composition. This work is part of a broader effort to understand the structure of multilayers and is a continuation of work started by Wilson and Bienenstock[1] on Mo-Ge multilayers.

The structure of Wilson and Bienenstock's Mo-Ge films, prepared by magnetron sputter deposition, was strongly influenced by the large degree of intermixing of the component materials. This intermixing may be due to the chemical affinity Mo and Ge have for each other as evidenced by the presence of four intermetallic compounds in the equilibrium phase diagram, or it may be a result of the deposition technique. The motivation for undertaking the current research on W-Ge multilayers was to investigate the types of structures that occur in a multilayer system whose components are less chemically interactive. Until very recently the W-Ge system was thought to contain no intermetallic compounds. In the last few years three W-Ge intermetallics have been found that form only at extremes of temperature and pressure orders of magnitude greater than the relatively low temperature and standard pressure intermetallics of the Mo-Ge system. The particular choice of the W-Ge system was predicated on the desire to separate the effects of chemical interaction on the structure from other effects (such as sample preparation techniques).

The W-Ge samples, like the Mo-Ge samples, were prepared by magnetron sputter deposition. Clean Si (100) substrates were affixed to a table that rotated under continuously sputtering targets of W and Ge. This configuration was suitable for fabricating both alloys and multilayers. (So far, the emphasis of this work has been on the fabrication and characterization of W-Ge multilayers. However, an investigation of the structure of a-W-Ge alloys is under way and will be an invaluable aid in characterizing the amorphous components of the multilayers.) The compositions of the films were controlled by varying the sputtering rates of the individual targets while the thicknesses of the deposits, per table revolution, were controlled by varying the rotation speed of the table. The Si substrates were then etched away by immersion for four hours in a 100° C KOH bath. This produced free standing films of W-Ge that were suitable for transmission EXAFS and transmission scattering, as well as reflection scattering. Anomalous scattering was performed at the Ge edge in W rich samples and at the W edge in Ge rich samples.

These investigations were performed on six multilayer samples with nominal layer spacings of: 30 Å W/30 Å Ge, 20 Å W/ 20 Å Ge, 10 Å W/10 Å Ge, 30 Å W/10 Å Ge, 20 Å W/10 Å Ge, and 10 Å W/30 Å Ge. Two Ge rich alloys were also studied with nominal compositions of a-W_8Ge_{92} and a-$W_{20}Ge_{80}$. The nominal atomic compositions of the samples and the nominal thicknesses of the layers were based on the sputtering rates of the individual materials. These vary significantly from the actual compositions as determined by the edge jumps of the EXAFS data. These discrepancies arise from several factors. The sputtering rates were determined by rate tests on the pure elements. These tests are often unreliable because the variation in sputtering rate with current (or power) through the target is non-linear. It is therefore important to perform careful tests near the actual powers at which the targets will be run during sample preparation. However, even under the best of circumstances rate test can give misleading results. For instance, polycrystalline targets with large grains (such as Ge) can have the sputtering rate change with the faces of the crystals that are exposed. Targets also tend to sputter faster as they get thinner. This implies that in W rich W-Ge samples the sputtering rate of the W target increases more rapidly than the sputtering rate of Ge. The W rich samples prepared for this study were generally more W rich than planned while the Ge rich samples were typically more Ge rich than planned.

Even when the sputtering rates are known to a high degree of accuracy, the thicknesses of the layers in the multilayers vary greatly from the nominal thicknesses. Since the nominal rates are based on the bulk pure element rates, no account is taken of the actual non-equilibrium structures- most glaringly, the interfacial structures- that occur in the multilayers. Therefore the nominal layer spacings are necessarily inaccurate. The combination of all the above mentioned errors has produced samples that are different in composition and layer spacing than planned.

The nominal compositions and layer thicknesses of the samples are summarized below along with the actual compositions as determined from the absorption edge jumps of the EXAFS data and the bilayer spacings as determined by the low angle Bragg reflections. Also indicated is the presence of amorphous and/or crystalline structures in the samples.

nominal atomic composition	actual atomic composition	nominal layer spacing	actual bilayer spacing	types of structures present
$W_{59}Ge_{41}$	$W_{68}Ge_{32}$	30 Å W/ 30 Å Ge	35 Å	purely amorphous
$W_{59}Ge_{41}$	$W_{77}Ge_{23}$	20 Å W/ 20 Å Ge	23 Å	amorphous/ crystalline
$W_{59}Ge_{41}$	$W_{77}Ge_{23}$	10 Å W/ 10 Å Ge	15 Å	amorphous/ crystalline
$W_{81}Ge_{19}$	$W_{79}Ge_{21}$	30 Å W/ 10 Å Ge	37 Å	amorphous/ crystalline
$W_{74}Ge_{26}$	$W_{92}Ge_{8}$	20 Å W/ 10 Å Ge	*	purely crystalline
$W_{32}Ge_{68}$	$W_{21}Ge_{79}$	10 Å W/ 30 Å Ge	33 Å	purely amorphous
W_8Ge_{92}	W_8Ge_{92}	cosputtered alloy	cosputtered alloy	purely amorphous
$W_{20}Ge_{80}$	$W_{15}Ge_{85}$	cosputtered alloy	cosputtered alloy	purely amorphous

*insufficient low angle data

A preliminary analysis of the data indicates that trends with composition and thickness are sometimes consistent with the trends observed by Wilson and Bienenstock. However, there are very significant exceptions. These data will be presented elsewhere when the analysis is more complete.

[1] Wilson, L. C., and Bienenstock, A. I., MRS Proceedings, Session on Multilayers, Fall 1987

ANALYSIS OF Co DOPED IRON OXIDE THIN FILMS BY X-RAY DEPTH PROFILING

Michael F. Toney* and Ting C. Huang,
IBM Research Division, Almaden Research Center
650 Harry Road, San Jose, CA 95120

Sean Brennan and Zophia Rek
Stanford Synchrotron Radiation Laboratory
Stanford, California 94305

Thin films used for magnetic storage and electronic devices are sometimes inhomogeneous and consist of several layers of different materials, which can be as thin as 100 Å. Since the properties of these devices depend on the structure of the layers, it is important to be able to determine these structures. Cross section transmission electron microscopy (TEM) is often used to do this. However, the sample preparation is necessarily destructive and can cause structural changes. Difficulties are also encountered with conventional Bragg x-ray diffraction, because the diffraction from thin layers is inherently weak and can be overwhelmed by scattering from thicker layers or the substrate. An alternative, nondestructive structural probe is x-ray diffraction using a grazing incidence geometry. We have used this method to structurally depth profile iron oxide thin films and identified the phase and thickness of a non-magnetic surface layer on a γ-Fe_2O_3 film.

Sputtered γ-Fe_2O_3 thin films have recently been developed for high density magnetic recording media because of their excellent magnetic, chemical, and mechanical properties.[1] These films can be prepared by reactive sputtering of Fe in Ar-O_2 to form Fe_3O_4 and subsequent annealing at high temperature.[2] Since Fe_2O_3 is polymorphic and can exist in a thermodynamically stable anti-ferromagnetic form, α-Fe_2O_3, and a metastable ferrimagnetic form, γ-Fe_2O_3,[3] the properties of the sputtered films are critically dependent on film preparation conditions.[4]

Spin polarized neutron reflection measurements[5] on Co-doped iron oxide thin films revealed a 120-150Å thick non-ferromagnetic layer at the surface of a γ-Fe_2O_3, while the as-deposited Fe_3O_4 film was magnetically uniform throughout its depth. Recently, Auger[6] and secondary ion mass spectrometry (SIMS)[7] depth profiles showed the Co dopant was absent from the top 100Å of the γ-Fe_2O_3, but was present in the Fe_3O_4 film. TEM on these samples has been inconclusive about the possibility of a structurally different top layer in the γ-Fe_2O_3 film.[5]

Our experiments use a grazing incidence asymmetric Bragg geometry.[8,9] The grazing incidence angle is used to vary the penetration depth of the x-rays into the sample. Since the diffracted beams originate from this region of variable depth, multilayered materials produce diffraction patterns that depend on the incidence angle. The exact dependence of the diffracted intensity from each layer is dependent on the depth and extent of each layer.[9] The scattering plane is vertical and the iron oxide sample horizontal. The diffracting planes are thus inclined to the sample surface and the small vertical divergence of the synchrotron is in the plane of the grazing angle. The experiments were performed under dedicated conditions at the 8-pole focused Wiggler station VII-2. A Si(111) double-crystal monochromator was used to select an incident x-ray wavelength of 1.823Å (6800 eV). The incident beam was defined with 1mm vertical and horizontal slits and the scattered beam was collimated with 1 mrad Soller slits and collected with a scintillation counter. Synchrotron radiation is necessary to obtain a high intensity, well-collimated incident beam and to allow easy wavelength selection.

The Fe_3O_4 and γ-Fe_2O_3 samples measured in the neutron study[5] were structurally depth profiled. The diffraction pattern from the Fe_3O_4 film did not depend on incidence angle, showing the film is structurally homogenous throughout its depth. However, the diffraction pattern from the γ-Fe_2O_3 sample did depend on angle. Figure 1 shows the polycrystalline diffraction patterns taken at grazing incidence

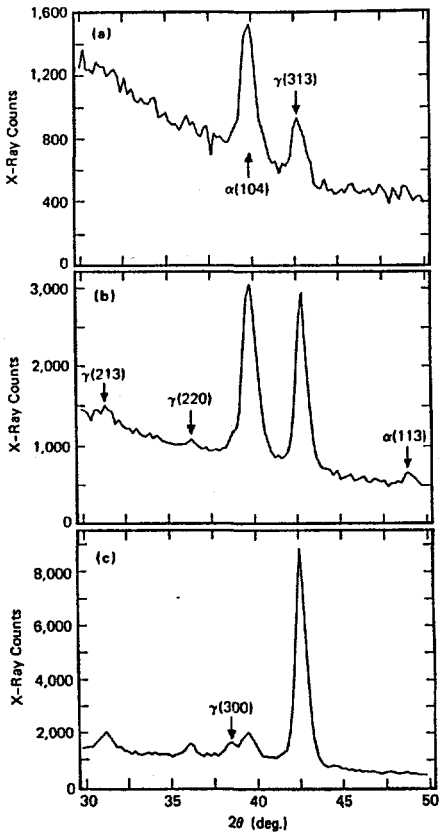

Figure 1. Polycrystalline diffraction patterns of the γ-Fe_2O_3 thin film at three different incidence angles. (a) $\phi = 0.33°$. (b) $\phi = 0.38°$. (c) $\phi = 0.52°$.

angles of 0.33°, 0.38°, and 0.52°. At small angles a pattern characteristic of α-Fe_2O_3 was observed, while at larger angles the pattern was predominately from γ-Fe_2O_3. This shows that the surface of the film is α-Fe_2O_3, but the bulk of the film is γ-Fe_2O_3, confirming earlier work with a conventional source.[10]

To quantify the thickness of the surface α-Fe_2O_3 phase, diffraction patterns were measured at incidence angles from 0.22 to 0.62°. The intensities from the α-Fe_2O_3(104) reflection and from an overlap the α-Fe_2O_3(110) and γ-Fe_2O_3(313) reflections are shown in Figure 2. The average thickness of the surface α-Fe_2O_3 phase was determined by a least squares fit of these data to a two layer (α/γ) model of the film.[9] An excellent fit to the data is obtained with an average thickness $d_\alpha = 90$Å, as shown in Figure 1. Arbitrarily changing the assumed density by up to 10% does not affect the fit or change d_α. The error is estimated as 15Å, since changes by this amount produce significantly poorer fits to the data.

Although the neutron data[5] indicate that the interface between the magnetic and non-magnetic regions is approximately 100Å, our data are best fit with a zero width interface. The fit, however, is insensitive to small variations in this width. Because of the overlap of the α-Fe_2O_3(110) with the γ-Fe_2O_3(313), the data shown in Figure 2(b) contain a small contribution from α-Fe_2O_3 (110), as well as γ-Fe_2O_3(313). This α-Fe_2O_3 contribution causes the insensitivity to the interfacial width. We have determined the interfacial width is less than 120Å.

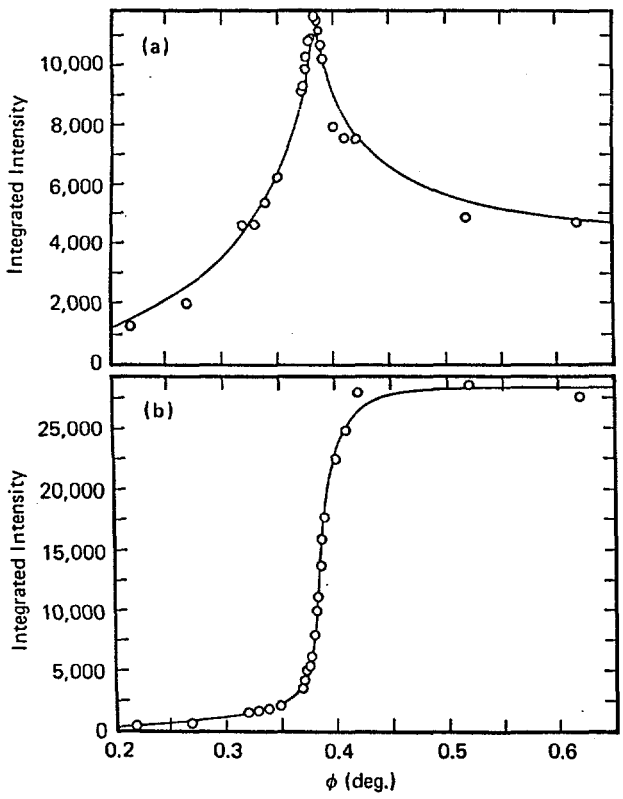

Figure 2. Integrated intensity vs incidence angle. (a) Intensity from α-Fe_2O_3(104). (b) Intensity of the peak resulting from α-Fe_2O_3 (110) and γ-Fe_2O_3(313). The data are shown by the c line shows the calculated intensities with a 90Å thickness for the surface α-Fe_2O_3phase.

The average thickness of the α-Fe_2O_3 surface layer is the same, within experimental error, as the thickness of the non-magnetic layer[5]. This shows that the formation of an antiferromagnetic α-Fe_2O_3 layer at the surface of the thin film caused the non-magnetic layer. The good agreement between the magnetic,[5] chemical,[6,7] and structural data suggest that during oxidation of thin film Fe_3O_4 to γ-Fe_2O_3, the Fe ions diffuse out to the surface to form the new layer of oxide.[6] This changes the as deposited Fe_3O_4 film into γ-Fe_2O_3. The oxide forms as α-Fe_2O_3, the stable, antiferromagnetic Fe_2O_3 phase, not ferrimagnetic γ-Fe_2O_3. However, the formation of the α-Fe_2O_3 phase may be dependent on preparation conditions.

In summary, a γ-Fe_2O_3 thin film was shown to have a surface layer of α-Fe_2O_3, while the bulk of the film was γ-Fe_2O_3, explaining the non-magnetic layer observed earlier.[5] The average thickness of this layer was found to be 90 ± 15Å and the width of the α/γ interfacial region less than 120Å. The as-deposited Fe_3O_4 film was structurally uniform. We have demonstrated the feasibility of structural depth profiling using grazing incidence asymmetric Bragg diffraction (GIAB). This method will be useful for future nondestructive structural measurement of multilayer thin films.

REFERENCES

* IBM Magnetic Recording Institute

1. S. Yoshii, O. Ishii, S. Hattori, T. Nakagawa, and G. Ishida, J. Appl. Phys. **53**, 2556 (1982).
2. Y. Ishii, A. Terada, I. Ishii, S. Ohta, S. Hattori, and K. Makino, IEEE. Trans. Mag. **MAG-16**, 1114 (1980).
3. M. Hansen, *Constitution of Binary Alloys*, (McGraw-Hill, New York, 1958) p. 687.
4. M.M. Chen, C. Ortiz, G. Lim, R. Sigsbee, and G. Castilo, IEEE. Trans. Mag., in press.
5. S. S. P. Parkin, R. Sigsbee, R. Felici, and G. P. Felcher, Appl. Phys. Lett. **48**, 604 (1986).
6. B. Hermsmeier, C.R. Brundle, and J.J. Baglin, J. Vac. Sci. Technol. A **5**, 2864 (1987).
7. C.R. Brundle and V.D. Deline, private communication.
8. T.C. Huang, M.F. Toney, S. Brennan, and Z. Rek, Thin Solid Films **154**, 439 (1987).
9. M.F. Toney, T.C. Huang, S. Brennan, and Z. Rek, J. Mater. Res., in press.
10. T.C. Huang and B.R. York, Appl. Phys. Lett. **50**, 389 (1987).

QUANTIFICATION OF THE SPATIAL VARIATION OF STRAIN FIELDS SURROUNDING LASER-DRILLED HOLES IN SILICON USING WHITE BEAM SECTION TOPOGRAPHY

Proposal No 8103M

Y. H. Chung[1], Z. U. Rek[2], and S. R. Stock[1]

[1]School of Materials Engineering, Georgia Institute of Technology, Atlanta, Georgia 30332-0245

[2]Stanford Synchrotron Radiation Laboratory

Introduction

Synchrotron white radiation allows one to produce transmission Laue patterns, with each spot being a topograph produced by a distinct diffraction vector [hkl] and wavelength. The high flux, the beam's parallelism and large cross-sectional area and the ability to simultaneously record many spots are great advantages. Most topographic studies have focused on discrete defects such as dislocations, stacking faults and microprecipitates. Characterization of continuously varying, long-range strain fields has received less attention. The elastic strains accompanying laser-drilling are prime example of such a field, and results from section topographic strain mapping are presented below.

Section topography uses a narrow, ribbon-like beam to sample a triangular prism of the sample. If the sample is perfect enough and the slits are narrow enough, the interference of the x-ray Bloch waves within the triangular prism results in a pattern of oscillating intensity termed Pendellosung fringes. The presence of elastic strain gradients profoundly alters the Pendellosung fringe pattern, and the spatial variation of strain can be examined by recording section topographs at different positions and by comparing these patterns with those obtained from an undeformed section of the sample.

For small deformations the Eikonal formulation of dynamical diffraction theory [2-4] is an adequate approximation, and one can convert the observed number of Pendellosung fringes to the effective strain gradient β through:

$$\frac{n}{n_0} = \frac{1}{\beta t}\sinh^{-1}\left(\frac{\beta t}{2}\right) + \frac{1}{2}\sqrt{1+\left(\frac{\beta t}{2}\right)^2}, \quad (1)$$

where n_0 is the number of the PF corresponding to the thickness t of a perfect crystal and n is the observed number of fringes. The relationship of β and the displacement u_x along the direction of the diffraction vector is given by

$$|\beta| = \frac{\sin 2\theta}{C|\chi_h|}\left(\frac{\partial^2 u_x}{\partial z^2} - \tan^2\theta\,\frac{\partial^2 u_x}{\partial x^2}\right), \quad (2)$$

where C is the polarization factor, χ_h is the dielectric susceptibility and equals $\left(\frac{e^2}{mc^2}\right)\frac{\lambda^2}{\pi V}F_h$, θ is the Bragg angle, λ is the x-ray wavelength, V is the volume of the unit cell, e^2/mc^2 is the classical electron radius, F_h is the structure factor, $\partial^2 u_x/\partial z$ is the gradient of curvature and $\partial^2 u_x/\partial x^2$ is the gradient in dilation strain. Once the value n is determined from the number of extra fringes on the section topograph, the value of $|\beta|$ can be calculated iteratively.

For the analysis presented here, we have assumed that there is no change in displacement u_x in the z-direction. Noting that $\partial^2 u_x/\partial x^2 = \partial\varepsilon_{xx}/\partial x$, the value of ε_{xx} is obtained by integrating $|\beta(x)|$ as a function of x. The total strain ε_{xx} at point (x_i, y_i) is, therefore, the area under the $|\beta(x, y = \text{constant})|$ curve between x_i and x_∞, where x_∞ is the position where $|\beta|$ is first non-zero. One can then formally write

$$\varepsilon_{xx}(x_i, y_i) = -\frac{C|\chi_h|}{\sin 2\theta \tan^2\theta}\int_{x_\infty}^{x_t}\beta(x, y_i)\,dx. \quad (3)$$

Experimental Methods

Laser-drilled silicon specimens were examined by White Beam topography using Beam Line II-4 at the Stanford Synchrotron Research Laboratory (SSRL). The apparatus consisted of a Huber two-circle goniometer and goniometer head and an adjustable tantalum slit from a Lang camera. Slit widths for white beam section topographs were 10 μm or less, and the film to specimen distance was 89 mm. Exposure times for section topographs were about 10 min, for the 40-50 mA current range.

The film (Kodak SR5, single-sided emulsion) was mounted perpendicular to the incident beam, and a 1 mm thick aluminum sheet and a lead beam stop were used to minimize background. Generally, sets of seven or eight section patterns were recorded on a single piece of film by translating the specimen and film in tandem between exposures. The spacing between adjacent section topographs was 1.0 mm, which prevented overlap. Higher resolution in the strain mapping analysis was obtained by interleaving sets of topographs using a 200 μm offset. The volumes of material sampled in each section topograph were precisely located relative to the position of the hole by superimposing a section and projection topograph.

Subsequent to indexing the patterns, the section patterns were reproduced at 20x magnification. The x-y position of the center of each elliptical Pendellosung fringe (half-period) was plotted, and contours of equal strain gradient were determined.

Linear interpolation was used in transforming the strain gradients to equi-strain contours.

Results and Discussion

The specimen was a 0.5 mm thick, (001) silicon crystal. Drilling was with a 0.1 mm diameter beam from a Nd/YAG laser operated at 10 Hz and 250 mJ/pulse for a total time of 50 sec.

Figure 1 shows a set of section topographs recorded with a very sensitive diffraction vector $\underline{h} = [3\bar{3}3]$. The parallel Pendellosung fringes are quite clear away from the hole, extra periods are introduced nearer the hole and the fringe pattern has been completely disrupted in the very high gradient region near the hole.

Contours of equal number of Pendellosung fringes are shown in Figure 2. The value of n_o is 9.5 for our experimental conditions, and the maximum observed value of n is 12.5. The spatial distribution dilational strain ϵ_{xx} is shown in Figure 3.

The strain gradients and dilational strain are normal to $[1\bar{1}1]$, and for detailed investigation of the relationship between deformation and processing conditions the strain should be transformed to the specimens coordinate system. The contours of strain gradient and dilational strain are similar but not identical; this would only be the case if adjacent contours were parallel and had a constant separation. When assessing different machining or processing techniques, use of strains instead of strain gradients, therefore, provides a more complete description of deformation levels.

The calculated strains and strain gradients are averages over the sample thickness and over the volume of material in the Borrmann triangle. This consequence of the Eikonal approximation is not critical in the present instance of laser drilling. The simplification is not valid, however, for the more rapidly varying fields encountered near devices in silicon; numerical simulation of the dynamical diffraction equations is necessary.

Continuing Research

Section topographs have been recorded around holes drilled (001) Si for a range of drilling conditions. Data for examining whether lattice tilts contribute to the strain gradients (unlikely given the geometry) and for comparing the tangential and radial components of strain have also been collected. Analysis of these results is currently underway. Also being examined is the variable sensitivity of different reflections and the influence of harmonic contamination on the observed Pendellosung fringe patterns.

Acknowledgement

This work was partially supported by the USAF through contract F49620-85-C-0013/SB5851-0360 P.O. S-760-6MG-103 (SRS and YHC).

References

1. A. R. Lang: Acta Met. 5, 358 (1957).
2. P. Penning, and D. Polder: Phillips Res. Rpt. 16, 419 (1961).
3. M. Hart: Z. Physik 189, 269-291 (1966).
4. N. Kato: J. Phys. Soc. Japan, 10, 1785-1791 (1963).

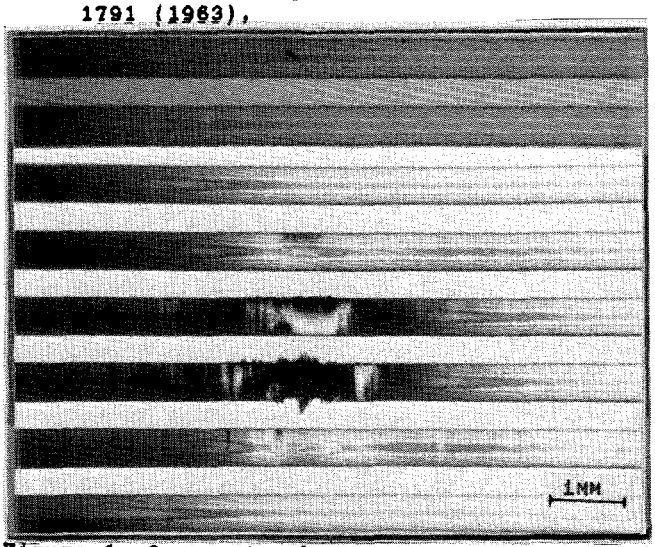

Figure 1. One set of section topographs of the laser-drilled crystal.. The diffraction vector is h = [333] and wavelength is 0.70 Å.

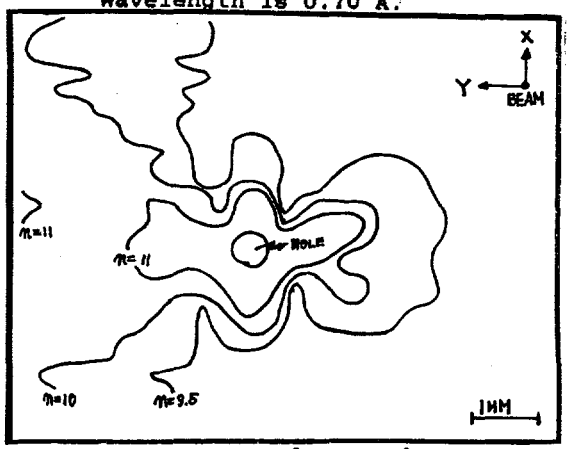

Figure 2. Contours of equal number of Pendellosung fringes from the same crystal as was shown in Fig. 1.

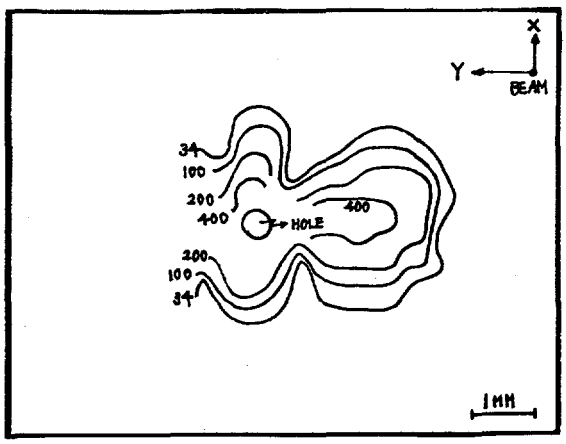

Figure 3. Map of the total dilational strain calculated by integration from Figure 2.

TWO DIMENSIONAL COMPRESSIBILITY

OF ELECTROCHEMICALLY ADSORBED LEAD ON SILVER (111)

P.N. Ross and J.B. Kortright
Lawrence Berkeley Laboratory
University of California
Berkeley, California 94720

O.R. Melroy, M.F. Toney, G.L. Borges, and M.G. Samant
IBM Almaden Research Center
650 Harry Road
San Jose, California 95120

L. Blum
Physics Department
College of Natural Sciences
P.O. Box AT
Rio Piedras, Puerto Rico 99831

We have applied the grazing-incidence scattering geometry to study electrochemical deposition of lead monolayers on silver (111). Measurements were made *in situ* (in contact with solution). For deposition potentials between underpotential monolayer formation and bulk deposition, the near-neighbor distance of the lead monolayer decreases linearly with applied potential, which is proportional to the chemical potential. This variation is shown in the figure. Since the lead monolayer is in equilibrium with lead ions in solution, the isothermal compressibility of the monolayer can be calculated from the potential dependence of the near-neighbor distance and is 0.98 $Å^2$/eV. This potential-dependent strain in the monolayer has implications on the wetting behavior of lead.

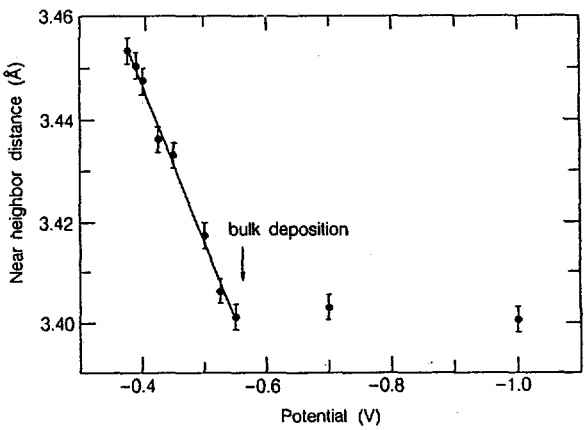

XBL 8712-5761

The research effort at the Lawrence Berkeley Laboratory was supported by the Office of the Director, Program Development Funds, through an agreement with the U.S. Department of Energy under contract DE-AC03-76SF00098. The research at IBM and the University of Puerto Rico was supported by the Office of Naval Research.

VALENCE AND ANTI-SITE DISORDER IN HIGH TEMPERATURE SUPERCONDUCTORS

Joe Wong,(1) F. W. Lytle,(2) R. B. Greegor,(2) C. Violet,(1), G. Xiao,(3)
A. Panson,(4) E. Larson,(5) D. Peterson,(5) T. Collings,(6) and Brian Maple(7)

(1) Lawrence Livermore National Laboratory; (2) The Boeing Company; (3) John Hopkins University;
(4) Westinghouse Research Lab; (5) Los Alamos National Laboratory; (6) Battelle and (7) U.C. at Davis

Introduction

Two variables which appear to be important in the Cu oxide high temperature superconductors are: structure and valence, specifically the detailed distribution of Cu^{2+} and Cu^{3+} among the possible lattice sites. With x-ray absorption spectroscopy there are three detection schemes that can be made site specific: (a) By utilizing single crystal samples and polarized x-rays so that the states probed by the x-ray oscillator are in a given direction. (b) By measurement of the optical emission caused by x-ray absorption (optical EXAFS). It is well known that ions in different lattice sites emit at different optical wavelengths. (c) By utilizing the chemical shift of the absorption edge for different valences in order to resolve scattering resonances from different lattice sites. We have successfully used the optical EXAFS technique to demonstrate site selectivity of Mn in sodium silicate glasses containing both tetrahedral and octahedral sites (1).

Recently it is found that there is extensive anti-site disorder in both $YBA_2Cu_3O_7$(YBC) and $La_{1.8}Sr_{0.2}CuO_4$ (LSC)(2). This was initially realized in the XANES (X-ray Absorption Near-Edge) spectra and confirmed by analysis of the EXAFS. The two superconductors have similar Cu-O bonds with four square planar plus apical oxygens. Fourier transforms of the EXAFS signals for the superconductors show these bonds plus another at about 2.6 A. This distance corresponds to approximately the Y-O or La-O bond distance but can occur for Cu only if Cu substitutes into the Y or La site. Further analysis shows that ca. 20% of Cu in the Y or La site. This should not be an unexpected result since anti-site disorder is found in all perovskite-type structure. In these materials, this disorder may be an important factor in the superconducting mechanism since Cu is a smaller ion than Y or La and would be very loose or "soft" in the Y or La site.

The basic structure of perovskite crystals is composed of a face-centered cubic packing of oxygen atoms where every fourth one is replaced by an A atom. The B atoms are located in 1/3 of the available octahedral interstices and their bonds to oxygen hold the crystal together. There is extensive solubility among various perovskites so that compounds of the form $(A_{1-x}A'_x)\ (B_{1-y}B'_y)O_3$ are common. There is also a region of tolerance to accommodate various sizes of atoms into the basic structure such that for the A site R = 1.2 - 1.6 A and for the B site R = 0.3 - 1.1 A, depending upon the relative sizes of R_A and R_B. Usually there is little exchange between the A and B type atoms but in certain situations when A and B are similar in size and/or there is extensive oxygen disorder A/B site disorder can occur. (3,4)

Experimental

We have performed an extensive series of XANES/EXAFS measurements on copper-oxide-based superconductor materials using the newly commissioned Beamline X-2. (5) A combination of conventional transmission, fluorescence and atomspheric electron yield detection schemes has been employed to measure the room temperature and 77K x-ray absorption spectra of all metal constituents in the following materials:

(a) $YBaCu_{2.7}M_{0.3}O_{7-x}$ where M = Ti, V, Cr, ...Ni, Zn

(b) $REBa_2Cu_3O_{7-x}$ where Re = Ce, Pr, Ho..

(c) La_2CuO_4, (d) $La_2\ Cu_{.95}\ Fe_{.05}\ O_4$

and (e) $La_{1.9}\ Ba_{0-1}\ Cu_{.95}\ Fe_{.05}\ O_4$

Models compounds YN, Y_2O_3, YAG, BaO, Ba ZrO_3, Cu_2O, CuO, SrO, FeO, $FeLaO_3$ and TiO_2 were also studied. The experimental data are being analyzed. The findings of the Y sites substituted with other rare-earths are reported elsewhere in this Activity report (6).

References

1. R. B. Greegor, F. W. Lytle, D. R. Sandstrom, M. Weber and J. Wong, SSRL Users Meeting Abstract, October (1987).
2. F. W. Lytle, R. B. Greegor and A. Panson, Phys. Rev. B (1988), in press.
3. J. Lecomte, J. P. Loup, M. Hervieu and B. Raveau, Phys Stat. Sol. 65, 743 (1981).
4. P. D. Battle, Mat. Res. Bull. 16, 397 (1981).
5. See Beamline X-2 under Beamlines Being Commissioned in this Activity Report.
6. F. W. Lytle et al. current activity report under proposal #1097.

X-RAY TOMOGRAPHY ON BEAMLINE X

J. H. Kinney, Q.C. Johnson, R.Allyn Saroyan, M.C. Nichols*, U.Bonse† and R. Nusshardt†
Lawrence Livermore National Laboratroy, Livermore, CA 94550

Introduction:

We have tested a high resolution solid state CCD array detector for x-ray imaging on the BL-X wiggler. The principal applications of this imaging detector are microradiography and three-dimensional microtomography. Applications to topography can be anticipated.

The intense x-ray flux from the 15 period wiggler makes BL-X an ideal source for CCD imaging methods. In this report, we will describe preliminary results from our use of the CCD array for beam characterization and for three-dimensional microtomography. Future modifications to the existing hardware that will take advantage of the unique properties of BL-X will also be discussed.

Experimental Apparatus:

The experimental apparatus has been discussed in detail elsewhere[1]. Briefly, the x-ray beam from the double crystal monochromator passes through a sample placed on a rotary stage and is converted to visible light in a high-resolution phosphor screen. The phosphor screen is imaged with a CCD array camera which is run in a charge integrating mode. The image data for each view angle through the object is used to reconstruct the three-dimensional structure of the sample. By modulating the energy of the x-ray beam, it is possible to obtain chemical information about the samples as well as structural information in many cases[2].

Applications:

In a preliminary study on the new BL-X wiggler, we used the CCD camera to characterize the x-ray beam and to perform tomography on samples of coal. Figure 1 shows the surface contour plots from a three-second exposure on BL-X operating at 14-kGauss. The x-ray energy is 10-keV. From exposure data, we estimate that the x-ray intensity is roughly 20 times that of the bending magnet line BL-I-5 (accurate flux measurements cannot be made from these measurements, since both lines have not been characterized with the same camera parameters). From these data it is possible to discern a curvature in the intensity profile radiating outward from the center of the beam. We believe that this curvature is due to heat loading of the first crystal[3]. For digital radiography and tomography, this curvature does not pose a problem.

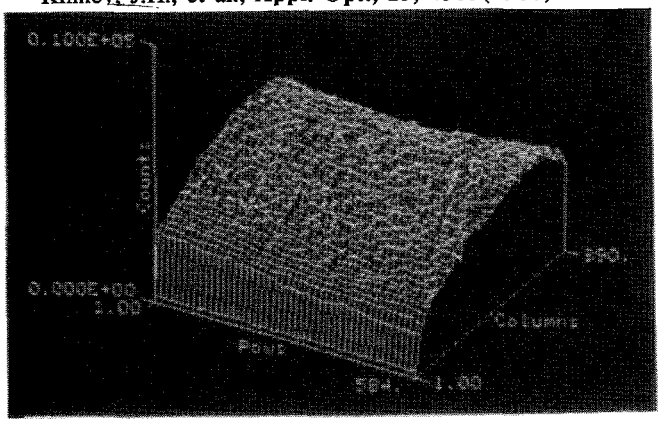

Figure 1: Surface plot of x-ray intensity from BL-X wiggler operating unfocussed at 14-kGauss. Scale is 5-μm.

Figure 2 shows a tomographic reconstruction of a slice through a sample of coal. The beam energy was 7300 eV, which was on the high-absorption side of the k-edge of iron. The bright features in the reconstruction (which are not reproduced well in the black and white screen-print prepared for this publication) are associated with iron rich precipitates that we have subsequently identified as iron sulfide. Pore structures smaller than 10 microns can also be observed. The ring structures are artifacts caused by insufficient detector normalization, and can be corrected by taking a greater number of reference images. The halo surrounding the sample is caused by x-ray scatter, which we believe can be removed by introducing Bragg reflecting optics behind sample.

Future Directions:

Fogging due to x-ray scatter, and grain structure in the phosphor, are the principal limits to the spatial resolution in our CCD imaging system. The high intensity afforded by the wiggler on BL-X allows us to take a new approach to overcome these limitations. We intend to introduce a Bragg reflecting optic between the sample and the phosphor screen. This will eliminate scattered radiation outside of the Bragg angle. By using an asymmetric cut, it is also possible to introduce magnification in one dimension which could increase the spatial resolution in the slice plane.

Acknowledgements:

We would like to thank Al Knabe (LLNL) for his technical support in all stages of this work. Also, we appreciate the support of R. Taylor (LLNL) who supplied us with coal standards.

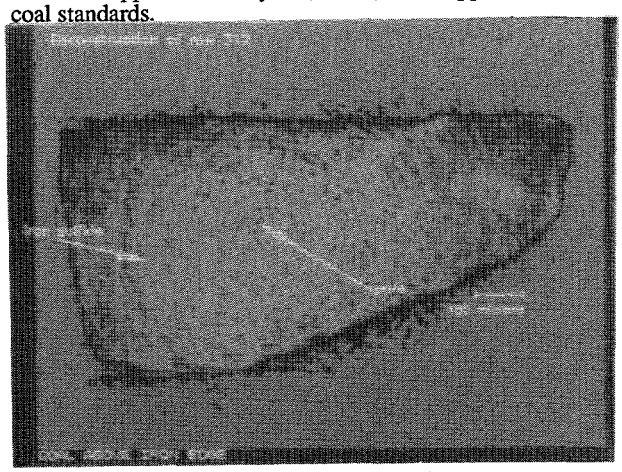

Figure 2: Coal chemistry and structure determined from tomography. Chemical tomography may play an important role in studying low temperature burning of coal.

[1] Kinney, J.H., et al., **Rev. Sci. Instrum., 59,** 196(1988).

[2] Kinney, J.H., et al., **Appl. Opt., 25,** 4583(1986).

[3] Kinney, J.H., Wong, J. and Troxel, T. (accompanying article in this report)

*Sandia National Laboratory, Livermore, CA. 94550.
† Department of Physics, Dortmund University, Dortmund, West Germany.

BEAM LINE X-2 PROFILE MEASUREMENT WITH A CCD IMAGER

J. H. Kinney, J. Wong and T. Troxel*

Lawrence Livermore National Laboratory
Livermore, CA 94550

Introduction:

As part of the characterization and commissioning of Beamline X-2, we have measured a series of initial beam profiles delivered at the sample plane with a high-resolution CCD array camera to map the intensity of the monochromatic beam in two dimensions under various conditions of photon energy, wiggler field strength and focussing. The CCD camera, used principally for high-resolution radiography and tomography, has been described in detail elsewhere[1]. Briefly, the x-rays emerging from the double crystal monochromator are converted to visible light on a high-resolution phosphor screen. The phosphor image is projected onto the CCD array with a bi-convex lens operating in a magnifying geometry. The camera images a 2-mm by 2-mm area of the beam with roughly 5-μm spatial resolution.

Results:

Figure 1 shows the surface plot of the intensity profile of beamline X-2 operating at 14 kGauss. The crystals were tuned to 50% of the peak intensity of the rocking curve at 10keV. We call this the detuned position. The image spans approximately 1-mm on either side of the horizontal center of the beam. The x and y axis units are 5-μm. The intensity units are in CCD pixel units, and are directly proportional to the incident x-ray fluence.

The surface contours indicate a saddle shaped depression in the center of the beam. We believe that this depression is due to crystal heating effects from the high heat load during operation at 14-kGauss. This depression is also present in the tuned beam at the same wiggler field strength.

Figure 2 shows the beam profile for the detuned beam under the same conditions as in figure 1, but in the focussed mode. The tuning compensates for the loss of reflectivity due to thermal loading. Because the exposure times for the two images were different, it is impossible to use this data to accurately determine the increase in intensity from focussing, although an increase is observed.

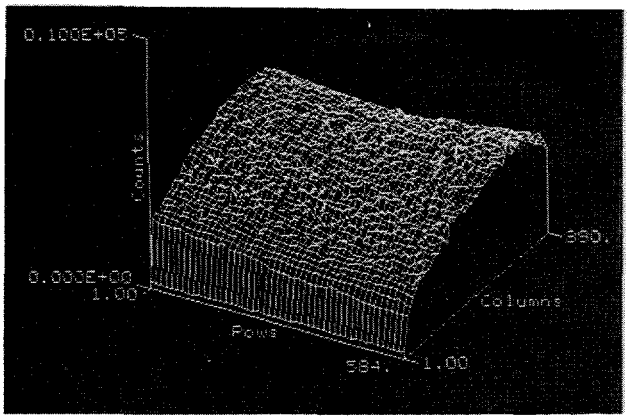

Figure 1: Surface plot of the intensity profile from beamline X-2 operating with a wiggler field strength of 14 kGauss in the detuned mode. The scale is 5 -μm, and the image spans approximately 1mm to either side of the horizontal center. We believe the dip in the intensity profile is indicative of thermal effects on the first crystal.

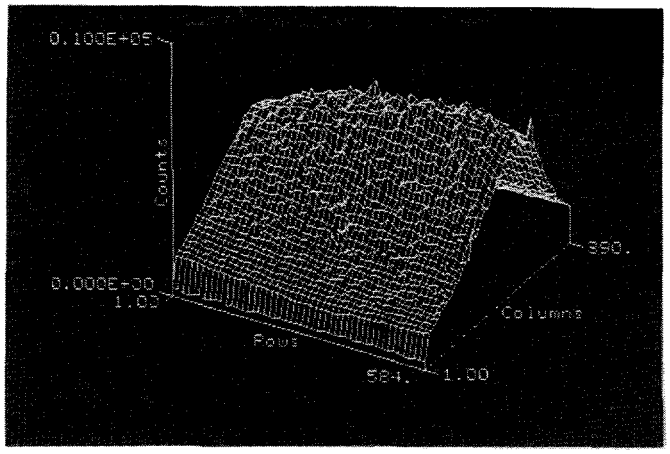

Figure 2: Surface plot of the intensity profile from beamline X-2 operating under identical conditions as in figure 1 with the exception of being focussed with the mirror. Focussing compensates for the dip observed in figure 1.

The depression in the beam was not observed at a wiggler field strength of 8 kGauss, although a direct comparison of the data has yet to be completed. This is a further indication that thermal effects are being seen on the first crystal. Future work will characterize the entire profile of the beam under a variety of wiggler field strengths in order to improve our understanding of the beamline performance.

* Stanford Synchrotron Radiation Laboratory, Stanford, CA

[1] Kinney, J.H., et al., **Rev. Sci. Instrum., 59,** 196(1988).

EXAFS OF NEAR MONOLAYER HAFNIUM FILM

Troy W. Barbee Jr. and Joe Wong

Lawrence Livermore National Laboratory
Livermore, CA 94550

INTRODUCTION

The ability to form perodic synthetic structures with periods of a few monolayers is relevant in both x-ray optic instrumentation development and materials synthesis process science and development. Methods for characterization of such uniquely structured materials are of extreme importance and clearly impact on both scientific and applied areas of investigation. In this activity report we report results of an EXAFS study of a 5 Å thick hafnium film in the vicinity of its L_{III} absorption edge (9561 eV). This film was deposited on a platinum-carbon multilayer having a period of 31.7 Å. This sample had been previously used in a study of evanescent and standing wave fluoresence[1] from the 5 Å hafnium layer and the platinum in the multilayer structure. The results described below indicate that EXAFS studies of films at the 0.01 monlayer level are possible.

The EXAFS spectra were taken on Beamline X-2, a 15-period wiggler source, using a (220) silicon crystal monochromator. The wiggler field was 14 k gauss with a ring electron current of 17 to 25 ma at 3.0 GeV. The sample (20 mm x 70 mm) was mounted on a goniometer and illuminated by a 0.5 X 8 mm beam at grazing angles of 0.3 to 1.0 degrees. A ion chamber Lytle detector was mounted parallel to the sample face at a distance of 20 mm with a 3 μm copper background filter. A standard Keithly picoammeter was used with the sensitivity set at 10^7V/amp.

Figure 1a shows the experimental data, a composite of eight scans of the Hf-L_{III} edge, each scan taking ~8 minutes. Note the strong white line and the large signal to noise. These data were taken at a grazing angle of 0.5 degrees resulting in an effective Hf layer thickness of ~570 Å. The EXAFS function is plotted as χ vs k in Figure 1b. The lack of structure at higher k values indicates that only near neighbors are active in determining the Hf EXAFS spectra as expected for a film of such limited dimensionality. Figures 1c and 1d present the Fourier transform of χ, $\Phi(R)$, and the transform χ^F in the region 0.2-2.4 Å about the central absorbing Hf atom.

The results indicate that the nearest neighbors of the Hf atoms are low Z species due to the gradual decrease of $\Phi(R)$ seen in Figure 1c for $2Å \lesssim R \lesssim 5Å$. This atomic specie is probably carbon as the Hf layer was overcoated with 10 Å of amorphous carbon to stabilize the metal against oxidation. Also, the breadth in R of $\Phi(R)$ for the strong peak at $R \simeq 1.7$ (Å) is consistent with a lack of nearest neighbors and limited dimensionality. I note the phase shift factors for hafnium were not available so that nearest neighbor distances are not reported. This discussion is consistent with the inverse transform, χ^F, shown in Figure 1d.

The primary conclusion of this experiment is that high quality EXAFS spectra may be obtained at monolayer converages on moderately large area samples. The intensity available at Beamline X allows one to project that EXAFS experiments on samples at coverages of 0.01 monolayer or less can be performed with standard experimental techniques. The toal number of atoms in such a sample is no more than 10^{14}.

(1) T. W. Barbee, Jr. and W. K. Warburton, Materials Letters 3, 17 (1984).

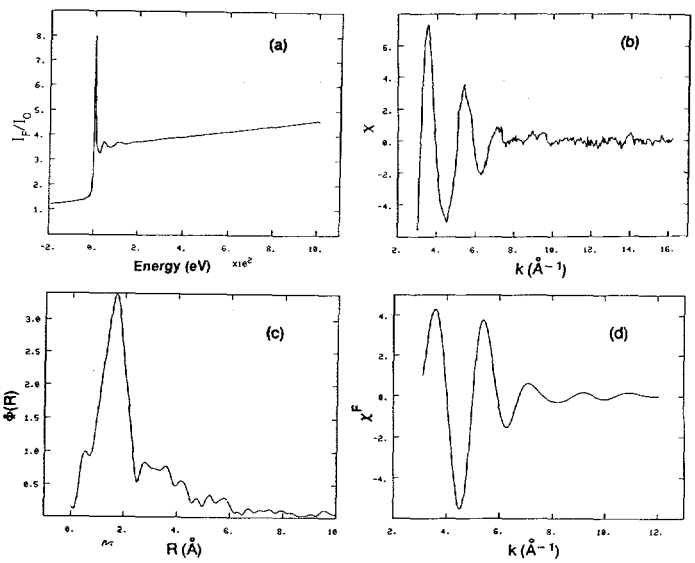

Fig. 1. (a) Experimental scan of Hf L_3-edge EXAFS of 5A of Hf on a C/Pt multilayer, the energy scale is with respect to the Hf L_3-edge first inflection of Hf metal at 9561 eV as zero. (b) Normalized EXAFS plotted as χ vs. k; (c) Fourier transform of χ and (d) Inverse transform χ^F EXAFS in the region 0.2 - 2.4 Å about the central absorbing Hf atom.

BROMINE K-EDGE CELLULAR RADIOSENSITIZATION WITH BROMODEOXYURIDINE

D. Larson[a], W. J. Bodell[b], C. Ling[a], T. L. Phillips[a,c], M. Schell[a], D. Shrieve[a] and T. Troxel[d]

Departments of [a]Radiation Oncology and [b]Neurosurgery and [c]Laboratory of Radiobiology and Environmental Health, University of California, San Francisco, CA 94143, USA
and [d]Stanford Synchrotron Radiation Laboratory, P.O. Box 4349, Stanford, CA 94305, USA

INTRODUCTION

Halogenated thymidine analogs become incorporated into the DNA of proliferating cells during S-phase and may be used clinically to radiosensitize tumors through unknown mechanisms. One possible mechanism involves the production of (highly radiotoxic) Auger electrons following photoelectric absorption of an X-ray by the K-shell of the incorporated halogen. Tisljar-Lentulis et al. [1] has predicted that the contribution by Auger electrons to radiosensitization should be larger for cells containing bromodeoxyuridine (BUdR) than for cells containing iododeoxyuridine (IUdR) in their DNA; Fairchild et al. [2], based on more extensive calculations, has predicted the opposite. In either case one expects increased cell killing for X-ray energies above the K-edge of bromine or iodine compared to below the K-edge, for cells which have incorporated BUdR or IUdR. In this experiment cells with 32% or 0% bromodeoxyuridine (BUdR) incorporated in their nuclear DNA were irradiated with various doses of monoenergetic X-rays, either below (13.450 KeV) or above (13.490 KeV) the K-edge of bromine; measured differences in cell survival reflect Auger contributions to radiosensitization.

METHODS AND MATERIALS

Chinese hamster V79 cells in exponential growth phase were trypsinized and seeded onto one side of plastic tissue culture flasks and grown on this surface with their normal doubling time (9 hr). BUdR was added to the medium of some flasks at the time of innoculation to a final concentration of 3×10^{-6} M. Cultures were incubated (46.5-55.5 hr) until just prior to irradiation, when growth medium was removed and the flasks were completely filled with Ham's F-12 medium without serum. Flasks were translated through an X-ray beam below or above the K-edge of bromine. The dose rate averaged over the cell monolayer area ranged from 7.3 to 18.6 cGy/min. Following irradiation, cultures were trypsinized, washed, counted and plated into 60 mm petri dishes at several cell densities for colony formation; after six days growth in complete medium, cultures were fixed and stained. Colonies containing more than 50 cells were scored and the plating efficiency was calculated by dividing the number of colonies scored by the number of cells plated. Surviving fraction (SF) was calculated by dividing the plating efficiency for treated cells by that for controls. SF data as a function of absorbed radiation dose were fit to linear-quadratic (LQ) and single hit multitarget (SHMT) models. Enhancement ratios (ER) were obtained by dividing the radiation dose necessary to produce a given (0.10, 0.01) SF in controls by that necessary to produce the same SF in cells containing BUdR, for both LQ and SHMT models, and also by dividing the SF slope D_0 for control cells by that for cells containing BUdR. The percent contribution by Auger electrons to radiosensitization was calculated as $(ER_{above}/ER_{below} - 1) \times 100$. The percent replacement of thymidine in DNA was determined by high pressure liquid chromatography.

RESULTS AND DISCUSSION

Model	Energy	ER	Auger(%)
LQ (SF=.10)	above	2.31 ± 0.10	3 ± 6%
	below	2.25 ± 0.10	
LQ (SF=.01)	above	2.09 ± 0.05	12 ± 4%
	below	1.87 ± 0.05	
SHMT (SF=.10)	above	2.27 ± 0.08	7 ± 6%
	below	2.12 ± 0.09	
SHMT (SF=.01)	above	2.05 ± 0.06	6 ± 4%
	below	1.93 ± 0.05	
SHMT (D_0 ratio)	above	1.77 ± 0.10	5 ± 9%
	below	1.68 ± 0.11	

For each model the ER is slightly increased above the K-edge compared to below; the percent radiosensitization due to Auger electrons ranges from 3% to 12%. However, only the LQ model at SF=.01 demonstrates a statistically significant increased ER above the K-edge (12%, $p = 0.003$). No effects related to dose rate or BUdR exposure time were found. We conclude that Auger electrons produced following photoelectric absorption of X-rays by the K-shell of bromine contribute minimally to observed BUdR cellular radiosensitization, and that any clinically important BUdR radiosensitization, utilizing broad-spectrum X-ray sources and lower levels of TdR replacement by BUdR, must be explained mainly by other mechanisms.

ACKNOWLEDGEMENTS

The work reported herein was partially done at SSRL, which is supported by the Department of Energy, Office of Basic Energy Sciences; and the National Institutes of Health, Biotechnology Resource Program, Division of Research Resources. This work was supported in part by the Office of Health and Environmental Research, Department of Energy (DE-AC03-76-SF01012) and by the National Institutes of Health, Department of Health and Human Services (CA-42044 and CA-13525).

REFERENCES

1 Tisljar-Lentulis, G., Feinendegen, L. E. and Bond, V. P. Biologische Strahleneffekte bei Einbau mittelschwerer Kerne ins Gewebe und Verwendung weicher Roentgenstrahlen. Strahlentherapie 145: 656-662, 1973.

2 Fairchild, R. G. and Bond, V. P. Photon activation therapy. Strahlentherapie 160: 758-763, 1984.

Radius of Gyration Measurements of Soluble Chromatin Fibers

S. P. Williams and J. P. Langmore
Biophysics Research Division, University of Michigan

INTRODUCTION

For many years people have been trying to elucidate the structure of chromatin, the molecule containing the genetic code in all plants and animals. Although the subunit of chromatin, the nucleosome, is known at atomic resolution (Richmond, 1984), the arrangement of nucleosomes in the chromatin fiber is not known. There are several models for the structure of chromatin (Finch, 1976; Woodcock, 1984; Worcel, 1981; Williams, 1986). Most models predict that the fiber diameter and mass per unit length are independent of the tissue from which the chromatin was isolated. Earlier sedimentation and scattering results were interpreted assuming a constant diameter and mass per unit length. Only the crossed-linker model (Williams, 1986) specifically predicts that these two parameters will increase in proportion to the amount of DNA in the chromatin subunit. Synchrotron x-ray scattering studies enabled us to compare the structure of the fibers in dilute solution to that in nuclei, and to determine whether the diameter and mass per unit length depend on the chromatin source.

RESULTS AND DISCUSSION

Chromatin fibers were isolated from *Necturus maculosus* (mudpuppy) erythrocytes, *Gallus domesticus* (chicken) erythrocytes, and *Thyone briareus* (sea cucumber) sperm, which have 194 bp, 212 bp, and 233 bp of DNA per nucleosome, respectively.

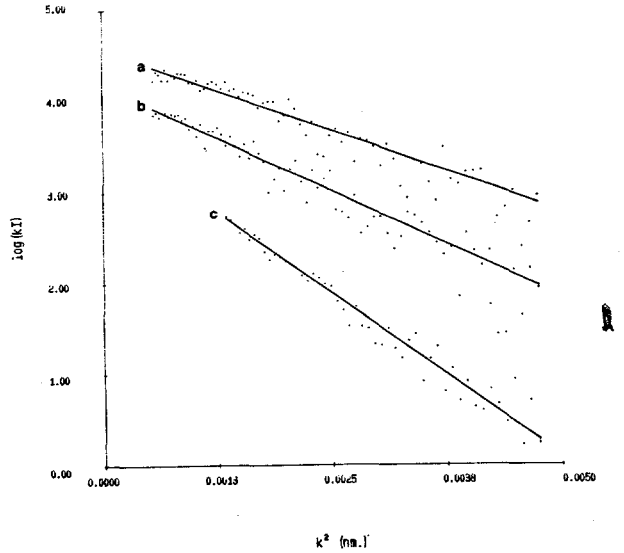

Figure 1
Modified Guinier plot shows different radii of gyration for (a) Mudpuppy, (b) Chicken, and (c) Sea Cucumber.

Chromatin solutions were dialysed against a buffer containing 100 mM monovalent salt and 3 mM EDTA in order to approximate physiological salt concentrations. Solutions of chromatin fibers at 0.05-0.25 mg/ml were diluted for concentration studies. Solution spectra were analyzed by plotting ln(kI) vs. k^2 to get the cross sectional radius of gyration (Luzatti, 1960, Kratky, 1964) where $k = 2\pi\sin\Theta/\lambda$, λ being the incident wavelength. Preliminary values (uncorrected for slit smearing and non-ideality) obtained for the chromatin fibers were 103 ±10 Å for mudpuppy, 120 ±10 Å for chicken, and 142 ± 8 Å for sea cucumber, showing a clear dependence of diameter on DNA content. Our previous low-angle x-ray scattering of nuclei, and electron microscopic measurements of the radius of gyration gave values of 105 Å for mudpuppy, 117 Å for chicken, and 139 Å for sea cucumber, which are in reasonable agreement with the synchrotron results. The results show a trend of fiber diameter with DNA content--in accord with the predictions of the crossed-linker model of chromatin structure.

The structure of fibers in solution at the low concentrations investigated is the same as in cell nuclei. Cross sectional radii of gyration are dependent on the amount of DNA in the nucleosome of the tissue from which the chromatin was isolated. Further studies will investigate concentration dependence, and obtain higher angle data on isolated chromatin fibers for better comparison to spectra of intact nuclei and calculated scattering from the models for chromatin.

ACKNOWLEDGMENTS

We would like to thank T. Russel for his technical expertise, and B. Athey and M. Smith for technical assistance. This work was performed at SSRL which is supported by the Department of Energy, Office of Basic Energy Sciences and supported by NIH grant GM27937

REFERENCES

Finch, J. T., and A. Klug. 1976. *Proc. Nat. Acad. Sci. USA.* 73:1897-1901.
Kratky, O. 1964. *Prog. in Bioph. and Mol. Biol.*13:105-173.
Luzatti, V., and A. Nicollieff. 1959. *J. M. B.*, 1:127-133.
Richmond, T. J., J. T. Finch, B. Rushton, D, Rhodes, and A. Klug. 1984. *Nature* 311:532-537.
Williams, S., B. D. Athey, L. J. Muglia, R. S. Schappe, A. H. Gough, and J. P. Langmore. 1986. *Biophys. J.*49:233-248.
Woodcock, C. L. F., L. Y. Frado, and J. B. Rattner. 1984. *J. Cell Biol.* 99:42-52.
Worcel, A., S. Strogatz, and D. Riley. 1981. *Proc. Nat. Acad. Sci. USA.* 78:1461-1465.

OBSERVATION OF CLUSTER FORMATION IN AN IONOMER

Letter of Intent

A. F. Galambos, W. B. Stockton, J. T. Koberstein, A. Sen, R. A. Weiss

Institute of Materials Science and Department of Chemical Engineering
University of Connecticut, Storrs, Connecticut 06268

T. P. Russell

IBM Research Division, Almaden Research Center
650 Harry Road, San Jose, California 95120-6099

INTRODUCTION

Ionomers exhibit unique mechanical and rheological properties as a consequence of strong associations between the ionic species. Although the spatial arrangement of the ionic groups in ionomers is still an unresolved question, it is now generally agreed that in most ionomers microphase-separated ion-rich aggregates, termed clusters,[1] are the dominant morphological feature. The primary evidence for ionic clusters comes from small-angle x-ray (SAXS) and neutron scattering (SANS) experiments where a maximum corresponding to distance of 2-4.5 nm is observed for most ionomers.[2,3] Here, we report recent results of an experiment in which an ionomer with a microstructure characterized by the absence of a SAXS maximum (herein interpreted as being void of ionic clusters) is heated to elevated temperatures. Using the high flux afforded by a synchrotron radiation source, the formation of the cluster morphology in this material was observed during heating at a controlled rate. To our knowledge, this represents the first time that the development and growth of microphase separation in an ionomer has been reported.

EXPERIMENTAL

SPS containing 7.6 mol% sulfonic acid groups was prepared by the homogeneous sulfonation of polystyrene (Mn = 100,000 and Mw = 260,000) in dichloroethane solution with acetyl sulfate.[4] This was neutralized with the equivalent amount of manganese acetate. A 25 μm film was prepared by casting a 10% solution of the ionomer in a mixed solvent of 90% THF and 10% deionized water onto glass. The solvent was evaporated in air and the film was dried under vacuum for 5 days at 60°C.

The x-ray scattering experiments were performed at Beam Line I-4. The ionomer film was placed in an aluminum sample cell that was fashioned from a conventional DSC pan. The pan contained thin Kapton windows in the top and the bottom so as to maximize the transmission of x-rays. The sample assembly was placed in a Mettler FP82 Hot State that controlled the heating of the sample at a rate of 10°C/min between 40° and 240°C. SAXS curves were collected every 26 seconds, and reflect the scattering integrated over a temperature interval of ca. 4°C.

RESULTS AND DISCUSSION

The corrected SAXS data collected during the heating cycle at controlled heating rate are given in Fig. 1. A scattering maximum is not detectable in the unheated film though substantial zero-angle scattering is evident. This intense zero-angle scattering has been observed in many ionomer samples with no agreement as to its origin. From the changes in the zero-angle scattering observed in these experiments as a function of temperature, it is evident that this scattering must be associated with the presence of ions. As discussed above, the as-cast ionomer film possessed a microphase structure significantly different from that usually observed for similar SPS ionomers.[5-7] We feel that these data are indicative of the absence of microphase-separated ion-rich clusters in the as-cast ionomer.

The fact that the SAXS peak first appeared at about 0.27 nm^{-1} and remained at that position throughout the experiment argues against the explanation that the absence of the peak in the as-cast film could be due to residual water. If the presence of water had shifted the SAXS peak to very low angles, we would have expected the SAXS peak to develop at a lower scattering vectors and shift towards 0.27 nm^{-1} as water diffused from the sample during heating. The growth of the SAXS peak at a constant scattering angle is similar to the behavior we have observed for disorder-order transitions in microphase-separated block copolymers.

Another interesting observation associated with the data in Fig. 1 concerns the zero-angle scattering. As the SAXS peak developed, there was a corresponding decrease in the intensity of the zero-angle scattering. This suggests that the latter phenomenon is also associated with the spatial arrangement of the ions. These two features in the SAXS curves, the peak and the zero-angle scattering, suggest the existence of two distinct environments for the ions (*e.g.*, clusters and multiplets), though at this point, we do not have sufficient information for such assignments.

The SAXS invariant is plotted against temperature in Fig. 2. Due to the limited angular range of the experimental detector configuration, it was not possible to correct the scattering intensity for background contributions arising from thermal density fluctuations.[9] For this reason, the reported invariants are not absolute values, but relative values. A small increase in the invariant for temperatures above Tg (~100°C) is probably associated with the expected increase in thermal density fluctuations with temperature.

A distinct transition in the scattering invariant occurs at ca. 180°C. The invariant increases, coincident with the emergence of a scattering maximum suggesting the development of ion-rich microdomains or clusters. Although the noise level of the invariant data is rather high, the observed transition is nonetheless important, since it is clearly indicative of the development of microphase separation at the transition temperature, rather than a redistribution or reorganization of existing microphases.

REFERENCES

1. Eisenberg, A., *Macromolecules* **1970**, *3*, 147.
2. MacKnight, W. J., Earnest, T. R., *J. Polym. Sci., Macromol. Rev.* **1981**, *16*, 41.
3. Longworth, R. in "Developments in Ionic Polymers-1," Wilson A. D. and Prosser, H. J., eds., Appl. Sci. Publ., London, 1983, chapter 3.
4. Mokowski, H. S., Lundberg, R. D., Singhal, G. H., U.S. Pattent 3,870,841, 1975.
5. Peiffer, D. G., Weiss, R. A., Lundberg, R. D., *J. Polym. Sci., Polym. Phys. Ed.* **1982**, *20*, 1503.
6. Yarusso, D. J., Cooper, S. L., *Macromolecules* **1983**, *16*, 1871.
7. Weiss, R. A., Lefelar, J. A. *Polymer* **1986**, *7*, 3.
8. Owens, J. N., Ph.D. Dissertation, Princeton University, 1986.
9. Koberstein, J. T., Morra, B., Stein, R. S., *J. Appl. Cryst.* **1980**, *13*, 34.

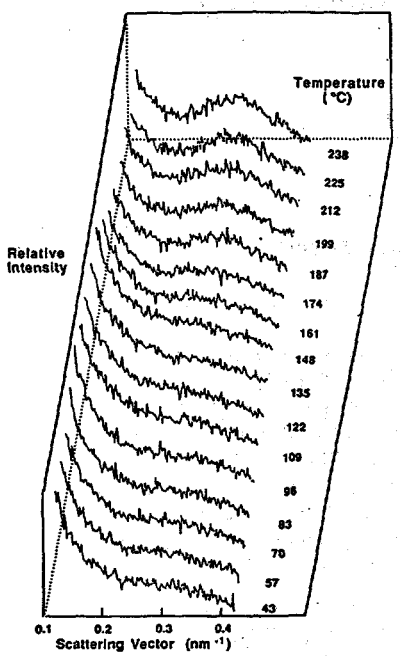

Figure 1. SAXS intensity *versus* scattering vector for 7.6 mol% MnSPS film cast from THF/water as a function of temperature. Heating rate was 10°/min.

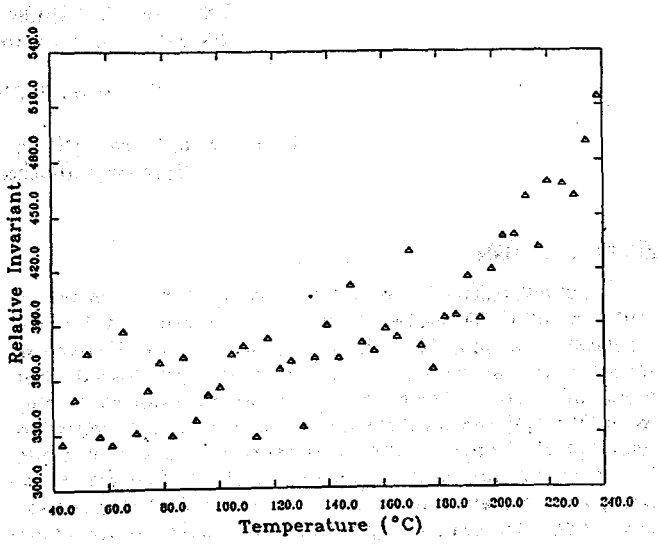

Figure 2. SAXS invariant *versus* temperature for 7.6 mol% MnSPS film cast from THF/water.

THE MICROSTRUCTURE OF BLOCK COPOLYMERS FORMED VIA IONIC INTERACTIONS

T. P. Russell

IBM Research Division, Almaden Research Center
650 Harry Road, San Jose, California 95120-6099

R. Jérôme, P. Charlier, M. Foucart

Laboratory of Macromolecular Chemistry and Organic Catalysis
University of Liége, 4000 Liége, Belgium

INTRODUCTION

The miscibility of two homopolymers is more the exception than the rule. Typically, phase separation exhibited by two polymers occurs on a size scale of several microns which gives rise to opacity and can cause a deterioration of properties due to poor interfacial adhesion. These problems can be circumvented to some extent by copolymerizing the desired monomers. Copolymerization tends to make the two polymers more miscible by covalently linking the otherwise incompatible polymers and it also limits the microphase separation to a size scale comparable to molecular dimensions.[1] An alternate approach to the copolymerization route is to place proton donating end groups on one polymer and proton accepting moieties on the other homopolymer.

EXPERIMENTAL

Polymer blends were prepared by solvent casting techniques. Separate solutions of ion-terminated polymers in toluene were prepared. One solution was then slowly added to the other under vigorous stirring. After the desired volumes were mixed the solutions were allowed to stir for an additional two hours prior to casting. Films were prepared by slow evaporation of the toluene by vacuum drying to constant weight at 50°C. Small angle x-ray scattering studies were performed at SSRL on Beamline I-4.

In Figure 1, the small angle x-ray scattering (SAXS) from a mixture of diamino-terminated poly(isoprene), $M_w = 18{,}000$ ($PIP(NR_2)_2 - 18K$) with disulfonato-terminated poly(α-methylstyrene), $M_w = 14{,}000$ ($P\alpha MST(SO_3H)_2 - 14K$) is shown as a function of temperature at a scanning rate of 10°C/min. A single, well-developed maximum is observed at room temperature. Normalization of the data for plotting purposes only appears to make it look small in the figure. Up to ca. 100°C, only a slight increase in the scattering is observed. Above this, not only does the scattering increase enormously but a pronounced third-order maximum, characteristic of a lamellar morphology with near 50/50 composition, emerges. Symmetry conditions cause the second-order reflection to be absent.

The intensity of the SAXS increases up to 165°C and then begins to decrease. However, rather than vanishing at ca. 200°C, another maximum emerges with a spacing somewhat larger than that observed at lower temperatures. This reflection is much broader and less well defined although it is still intense. This maximum persists up to 260°C, whereupon it shifts to scattering vectors beyond instrumental resolution. These data are quite unusual for multiphase systems and exemplify the power of real time scattering studies using synchrotron light sources. The long period corresponding to the position of the maximum remains relatively constant at an average value of 210Å up to 200°C. Beyond 200°C, the long period increases enormously and suddenly, at 245°C, it decreases sharply up to 265°C. Thus, over the temperature range where a SAXS reflection is clear, the long period passes through a very sharp maximum. Finally, it increases again sharply until the spacing is no longer observable.

The variation in the diffuse phase boundary, E, and the invariant, Q, parallel the changes observed in the long period. Up to ca. 100°C, E remains relatively constant at 60Å, whereupon it increases rapidly by 25% to 75Å; E then remains unchanged to 180°C where it suddenly goes through a sharp drop to ca. 45Å. As the temperature is increased further, E increases rapidly, reaching a maximum value of ca. 75Å near 260°C and then decreases again. Similarly, the invariant shown in Figure 2 gradually increases up to 100°C, then increases sharply up to ca. 180°C, whereupon it goes through a pronounced minimum and is followed by another rapid increase and decrease near 260°C.

The combination of these results at first appears somewhat contradictory in that as Q increases, a decrease in E would be expected. However, clarification of these apparent discrepancies becomes obvious when the magnitudes of Q are examined. For a two-phase system comprised of PαMSt and PIP phases at 25°C, a value of $Q = 7.53 \times 10^{-4}$ (mold $e^-/cm^3)^2$ would be expected. Experimentally, a value of 4×10^{-4} (mole $e^-/cm^3)^2$ is found clearly showing that, as cast, the individual phases are not pure PαMSt or PIP. Due to this, the glass transition temperature of the PαMSt phase is reduced to ca. 100°C. Up to 100°C, thermal expansion can account for the observed changes. At ca. 100°C, there is sufficient mobility in the system to allow the polymers to microphase separate further. The extent to which this will happen will depend upon the temperature of the measurement since this will control the T_g of the PαMSt phase. This will also give rise to the broader phase boundary. At 180°C, the measured value of Q is 1.15×10^{-3} (mol $e^-/cm^3)^2$ which compares well to the value of 1.32×10^{-3} (mol $e^-/cm^3)^2$ calculated assuming pure phases. Consistent with this result is the sharpening of the scattering profiles and the appearance of a third-order reflection. Increasing the temperature further causes Q and E to drop but the long period remains virtually constant and the scattering profiles become more diffuse. As with the $P\alpha MSt(SO_3H)_2 - 8K$ mixtures, these changes can only be described by the approach of the system to an order/disorder transition. Consistent with the $P\alpha MSt(SO_3H)_2 - 8K$ results, the diffuse phase boundary does not broaden, but sharpens which, as stated before, must be attributed to the ionic associations rather than covalent bonding of consecutive blocks. In contrast to the $P\alpha MSt(SO_3H)_2 - 8K$ mixtures, the SAXS of the 14K mixtures shows the effects of this order/disorder transition at lower temperatures. This is also inconsistent with the order/disorder transition observed in covalently bonded block copolymers and results, most likely, from the reduction in the extent of ionic interactions in the system.

At elevated temperatures the $P\alpha MSt(SO_3H)_2 - 8K$ mixtures would be expected to exhibit scattering characteristic of a disordered copolymer. Rather, the SAXS shows the development of a scattering maximum that increases in intensity and shifts to smaller scattering vectors. These data, therefore, show that the system is undergoing a phase separation very much like a spinodal phase separation that is characteristic of a homopolymer mixture below an upper critical solution temperature UCST or above the lower critical solution temperature. Studies on mixtures of polystyrene with polybutadiene,[2,3] which closely resemble a mixture of the constituent telechelic polymers under investigation in this study, would argue in favor of an UCST. Consequently, the ionic

associations of the $-SO_3^-$ and $-NHR_2^+$ are not strong enough at these temperatures to prevent the system from undergoing a coarse phase separation. It should be noted that the behavior of the $P\alpha MSt(SO_3H)_2 - 8K$ mixtures is different in that a coarse phase separation was not observed. Thus, the order/disorder transition must occur at temperatures either above the USCT, *i.e.*, the UCST is reduced by the reduction in the molecular weight or below the temperature at which disruption of the ionic aggregates occurs.

Consequently, a unified description of the phase diagram of the telechelic copolymers arises from these studies. It is apparent that four different features have to be considered to understand the observed SAXS results. These include the mesophase separation temperature of the copolymers formed by ionic associations, the UCST of the constituent homopolymers, the temperature, T_i, at which ionic associations are disrupted and the glass transition temperature T_g. The relative position of these will dictate the morphology. Three such examples are shown in Figures 3 and 4.

REFERENCES

1. Leibler, L. *Macromolecules* **1982**, *19*, 2621.
2. Russell, T. P.; Hadziioannou, Warburton, W. K. *Macromolecules* **1985**, *18*, 78.
3. Russell, T. P.; Ronca, G. *Macromolecules* **1985**, *18*, 665.

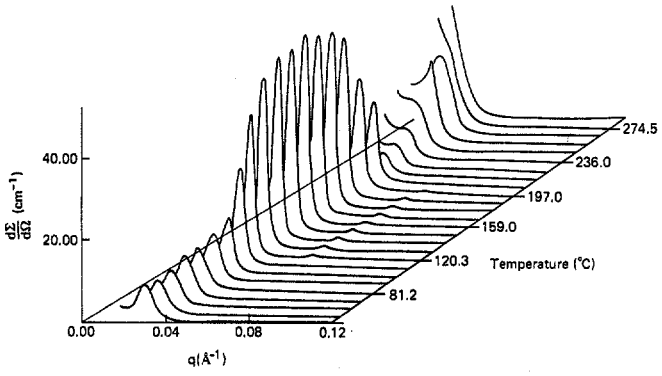

Figure 1. The temperature dependence of the SAXS from a mixture of $PIP(NR_2)_2 - 18K$ with $P\alpha MSt(SO_3H)_2 - 8K$ at a scanning rate of 10°C/min.

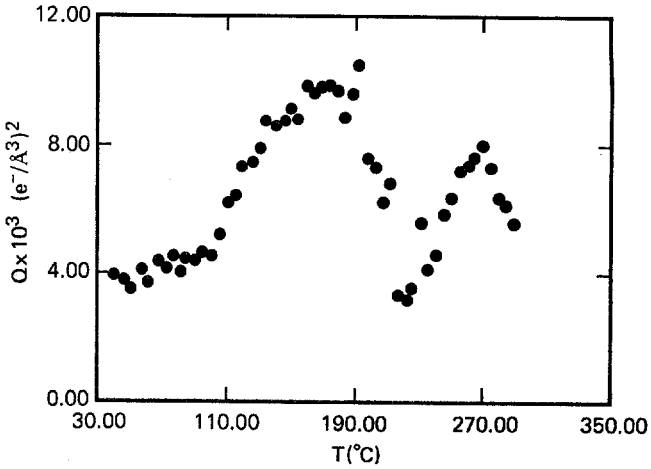

Figure 2. The total integrated scattering as a function of temperature for the scattering profiles shown in Figure 11.

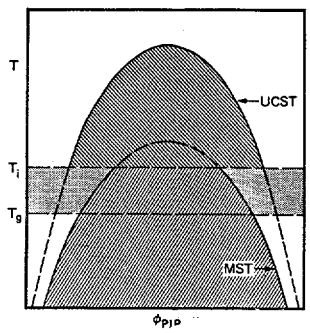

Figure 3. Proposed phase diagram for the $PIP(NR_2)_2 - 18K P\alpha MSt(SO_3H)_2 - 8K$ telechelic mixtures where UCST is the upper critical solution temperature of the constituent telechelic polymers, MST is the microphase separation temperature of the ionic copolymers, T_g is the glass transition and T_i is the temperature at which the ionic associations forming the block copolymers are disrupted. The left to right diagonally hatched area is where the mixtures exhibit a microphase separated morphology similar to that seen in covalently bonded block copolymers. The right to left diagonally hatched area is where the mixtures phase separate in a manner analogous to simple homopolymer mixtures. The stipled area is where the mixtures exist as a disordered copolymer phase and the clear area is where the mixture is a homogeneous mixture of the constituent telechelics. The dashed lines are continuations of the phase diagrams which due to ionic aggregation or disruption of the endgroups are not possible to observe.

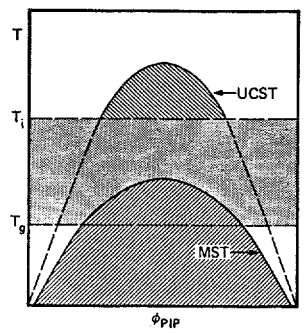

Figure 4. Schematic phase diagram of the $PIP(NR_2)_2 - 18K/P\alpha MSt(SO_3H)_2 - 14K$ telechelic mixtures. The labeling is the same as in Figure 15.

INTERCALIBRATION OF SMALL-ANGLE X-RAY AND NEUTRON SCATTERING DATA

Letter of Intent

T. P. Russell

IBM Research Division, Almaden Research Center
650 Harry Road, San Jose, California 95120-6099

J. S. Lin, S. Spooner, G. D. Wignall

National Center for Small-Angle Scattering Research
Oak Ridge National Laboratory, Oak Ridge, Tennessee 37831

INTRODUCTION

In view of the maturity of small-angle scattering (SAS) techniques, it is surprising that a significant fraction of data are still published in arbitrary units which are functions of the time scale of the experiment, scattering geometry and the sample dimension, *e.g.*, thickness. Data are generally presented in the form of scattered intensity (counts per scattering elements, counts per unit time, *etc.*) *versus* Q, the scattering vector which is given by $(4\pi/\lambda)\sin\theta$ where λ is the wavelength of the incident x-rays or neutrons and 2θ is the scattering angle.

Conversion of the data to an absolute differential scattering cross section $d\Sigma(Q)/d\Omega$, typically in units of cm^{-1}, may be accomplished by multiplying by a calibration constant. Use of absolute scattering is not necessary for the measurement of the interference function. However, placing the data on an absolute scale is necessary for the determination of molecular weights, the number density of particles, the scattering length densities of phases in multiphased systems and to restrict the parameters of a given model to the set which reproduces the observed intensity. It is also a useful means for the detection of artifacts in SAS experiments.

Despite the obvious advantages of placing data on an absolute scale, the use of suitable calibration techniques is by no means universal in the SAS field. This situation is due in part to the fact that many of the primary calibration techniques require special equipment and can be difficult and time consuming (Patel and Schmidt, 1971). In view of the limited time scale of many SAS experiments of steady state reactors, pulsed neutron and synchrotron sources, users are naturally reluctant to devote a significant fraction of beam time to calibration experiments. One solution to this problem is to develop pre-calibrated strongly scattering samples that may be measured rapidly in a given geometry, not detracting significantly from the available beam time.

RESULTS AND INTERCOMPARISON OF STANDARDS

The Debye-Bueche formula is given by[1]

$$\frac{d\Sigma}{d\Omega}(Q)=\frac{d\Sigma}{d\Omega}(O)\frac{1}{(1+Q^2a^2)^2}$$

where a is a correlation length. Thus, a plot of $d\Sigma^{-1/2}(Q)/d\Omega$ *versus* Q^2 should be linear with slope a^2. Figures 1-3 show such plots for small-angle neutron (SANS) and x-ray (SAXS) scattering data of vitreous carbon taken at the Oak Ridge National Laboratory and SSRL. The SSRL SAXS data were calibrated with respect to silica sol standards[2] and the ORNL SAXS data were calibrated with respected to water as described previously.

Because of slight departures from linearity, the data are fitted only for Q values between $0.045 < Q < 0.11 Å^{-1}$ and the correlation lengths from both SAXS and SANS experiments lie in the range $a = 4.75 \pm 0.3 Å$. Based on a neutron cross section $d\Sigma(O)/d\Omega = 5.2 \pm 0.4\ cm^{-1}$, the x-ray cross section can be calculated by multiplying by the ratio $(6 \times 2.82 \times 10^{-13}/0.665 \times 10^{-12})^2$ where $b_c = 0.665 \times 10^{-12}$ cm is the coherent scattering length for carbon and the scattering length of an electron is 2.28×10^{-13} cm. This leads to a predicted SAXS cross section $d\Sigma(O)/d\Omega = 33.3 + 3.2\ cm^{-1}$, in good agreement with the two independent determination of $31.5 \pm 3\ cm^{-1}$ (SSRL) and $38 \pm 4\ cm^{-1}$ (ORNL). Thus, this particular glassy carbon sample yields good quantitative agreement between the techniques.

Measurements on two different polyethylene standards are shown in Fig. 4. The first is the Lupolen (Kratky) standard, whereas the second is a high density polyethylene (Eltex A1050). The first feature to be observed from these data is that despite the fact that both samples are polyethylene, the scattering profiles are profoundly different. This is not surprising since the branching content and the thermal treatment of the samples are different. Clearly, the long period, absolute intensity and the width of the reflection can vary dramatically. Concentrating first on the Lupolen standard, it is seen that a borad weak reflection with a maximum near $0.03 Å^{-1}$ is seen. Separate determinatins of the $[d\Sigma(Q_{max})/d\Omega]$ were found to be $5.3 \pm 0.5\ cm^{-1}$ (ORNL 10-m SAXS) $6.0 \pm 0.5\ cm^{-1}$ (Schelten and Hendricks[4] and $5.0 \pm 0.3\ cm^{-1}$ (SSRL)), thereby yielding an average value of $5.4 \pm 0.5\ cm^{-1}$. The Eltex A1050, on the other hand, shows a pronounced scattering maximum at ca. $0.0275 Å^{-1}$. Vestiges of a third-order reflection are seen near $0.06 Å^{-1}$. The lack of higher-order reflections is due to distribuitons of crystal thickness, diffuse phase boundary between the crystalline and amorphous phases and symmetry since this polyethylene has a degree of crystallinity near 50%. The $[\Sigma(Q_{max})/d\Omega]$ for Eltex A1050 has been measured by Schelten *et al.* as $22.4 \pm 1.5\ cm^{-1}$ and more recently at SSRL as $24.0 \pm 2.0\ cm^{-1}$.

Neither of these samples has a finite coherent cross section for neutrons and comparisons between SAXS and SANS are not possible. For deuterated polyethylene, however, the coherent cross sections should be proportional and Fig. 5 shows SAXS and SANS data for a deuteropolythylene where the SAXS data were calibrated *via* Ludox suspensions. The data can clearly be superimposed to a good approximation by a multiplicative factor after the small incoherent background has been subtracted. Deuteropolyethylene may be regarded as a three-phase system (crystal, amorphous and voids) and level of deuteration is 95%. Because the electron density and scattering length density of the voids are zero, the SAXS and SANS patterns can be scaled as for two-phase systems. The theoretical ratio of SAXS and SANS intensities for a 95% deuterated material is 1.41 compared to the observed ratio over the two scattering patterns (Fig. 5) of 1.31 ± 0.12. Deuteropolyethylene (PED) thus seems to be suitable intercalibration standards for SAXS and SANS data with suitable samle thickness 1.2 mm for each technique.

REFERENCES

1. P. Debye, A. Bueche, *J. Appl. Phys.* **20**, 518 (1949).
2. T. P. Russell, *J. Appl. Cryst.* **16**, 473 (1983).
3. G. D. Wignall, F. S. Buks, *J. Appl. Cryst.* **20**, 28 (1987).
4. J. Schelten, D. G. H. Ballard, G. D. Wignall, G. W. Longman, W. Schmatz, *Polymer* **17**, 751 (1976).

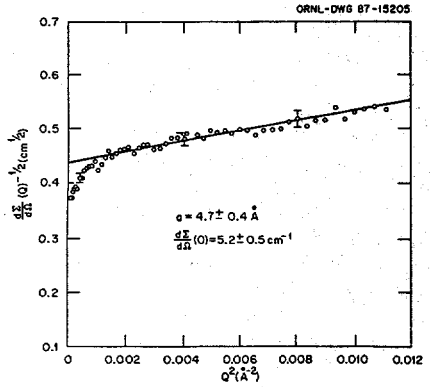

Fig. 1. Debye-Bueche Plot for Vitreous Carbon (ORNL 10M SANS)

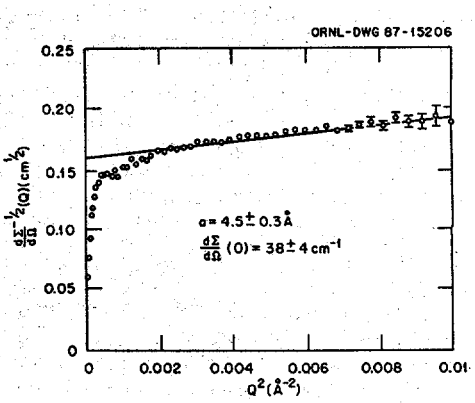

Fig. 2. Debye-Bueche Plot for Vitreous Carbon (ORNL 10M SAXS)

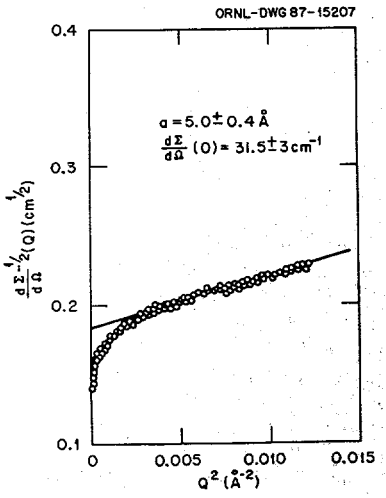

Fig. 3. Debye-Bueche Plot for Vitreous Carbon (SSRL SAXS)

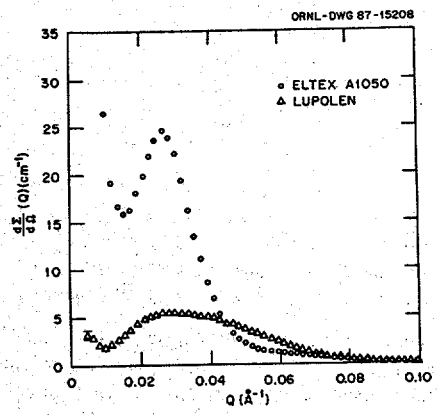

Fig. 4. $\frac{d\Sigma}{d\Omega}(Q)$ vs. Q for ELTEX A1050 and LUPOLEN (Kratky) Standards

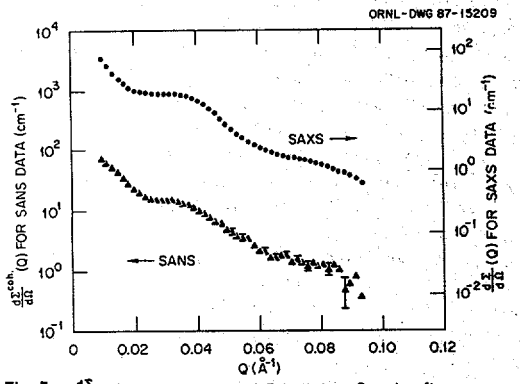

Fig. 5. $\frac{d\Sigma}{d\Omega}(Q)$ vs. Q for Deuterated Polyethylene Sample after Subtraction of Incoherent Background

Solution of phase problem for crystallography at a wavelength of 3.5 Å

Q. Shen & R. Colella

Purdue University, Physics Department, West Lafayette, Indiana 47907, USA

It has been established[1] that one viable method for determining phases in a diffraction experiment is to make use of multiple beam-diffraction, that is, a situation in which two or more reflections are excited simultaneously in a crystal. While the theory had been fully developed and tested in some experiments on a germanium crystal[1], progress was halted by the recognition that such theory could only be applied to perfect crystals such as germanium and silicon, with no mosaic structure. Here we report that considerable progress has been made, to the point of being able now to determine phases of structure factors in the most general situations, with non-centrosymmetric, small mosaic crystals of arbitrary shape. An example will be described here in which the phase of the (202) reflection of an organic molecular crystal (benzil) has been determined.

Important progress was made in 1981[2], when it was shown that certain anomalies observed on the wings of azimuthal plots contain phase information, and extend to wide angular ranges, of the order of degrees. (By azimuthal plot we mean a plot in which each point is an integrated intensity of the (*hkl*) reflection, integrated with respect to θ, angle of incidence on the (*hkl*) lattice planes, as a function of ϕ, the azimuthal angle of the crystal with respect to the scattering vector.) It was found, in ref. 2, that a new mechanism of diffraction is operative in situations in which the main reflection is weak and fully excited, whereas the simultaneous reflection is strong but weakly excited. Such mechanism has been called 'virtual Bragg scattering', (VBS), in analogy with the concept of virtual transitions in atomic and nuclear physics (A. W. Overhauser, personal communication).

It was immediately recognized that, since the VBS situation is one in which the scattering is kinematic (no multiple scattering), it could be used to determine phases in mosaic crystals, by using dynamical theory, the only one that preserves phase information.

As a first step, to test the soundness of our ideas and methods, we confirmed by VBS the sign change[3] of the 'forbidden' (442) reflection in silicon as a function of temperature[4].

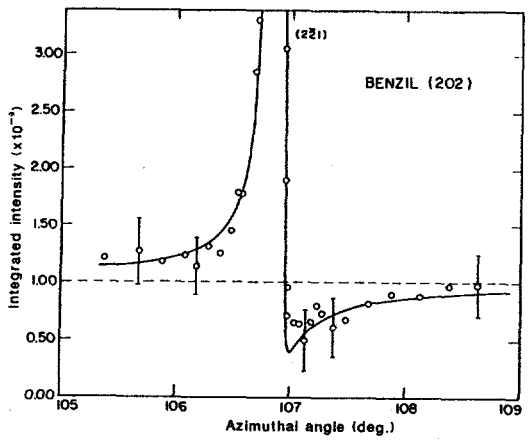

Fig. 1 Azimuthal plot of the (202) reflection, around the excitation point of (2$\bar{2}$1). The dotted line corresponds to the two beam value. The counting rate of the (202) peak value, in the two beam region, was ~1 count s^{-1}. The total number of counts accumulated for each data point was around 1,400 of which 1,000 was background.

The second crucial step, was the phase determinations of some 'forbidden' reflections in V_3Si, a mosaic crystal[5], the first time in which multiple-beam diffraction was used to determine phases *a priori* unknown.

At this point we turned to an organic, molecular, non-centrosymmetrical crystal (benzil: $C_{14}H_{10}O_2$) to check the feasibility of our method on a typical representative of a class of crystals for which phase problems are normally encountered. Preliminary experiments and calculations showed that VBS effects in benzil could only be visible at long x-ray wavelengths (3.5 Angstroms).

A recent experiment, performed on the X-ray 8-pole wiggler line VII-2 at the Stanford Synchrotron Radiation Laboratory, has fully confirmed our expectations. A small quasispherical crystal of benzil (0.3-mm diameter) was set for the (202-2$\bar{2}$1) reflection. The data are shown in Fig. 1, which is essentially identical to Fig. 4 of ref. 6, in which a flat crystal slab was used. Figure 2 shows how the data can be plotted, using the theory of ref. 7, to get the sum of the phases of (2$\bar{2}$1) and (021) with respect to (202), which turns out to be 180°, as expected. The scatter of the data points is due to poor counting statistics, due to the low intensity of the 3.5 keV photons. With the new generation of synchrotron sources and multipole insertion devices and by further reducing the air paths, the counting rates can be easily increased by at least two orders of magnitude. (At 3.5 keV an air path of 30 cm transmits only 1%. In our last experiment at SSRL we had a total of ~21 cm of air paths in the hutch, half of which can certainly be eliminated by constructing special collimators.)

We have therefore confirmed that our method, based on the notion of virtual Bragg scattering, is universally applicable and can be used to solve unknown structures, with no restrictions.

This work was supported by the National Science Foundation and by the Department of Energy.

Received 17 March; accepted 16 June 1987.

1. Colella, R. *Acta crystallogr.* A30, 413-423 (1974).
2. Chapman, L. D., Yoder, D. R. & Colella, R. *Phys. Rev. Lett.* 46, 1578-1581 (1981).
3. Trucano, P. & Batterman, B. W. *Phys. Rev.* B6, 3659-3666 (1972).
4. Tischler, J. Z., Shen, Q. & Colella, R. *Acta crystallogr.* A41, 451-453 (1985).
5. Schmidt, M. C. & Colella, R. *Phys. Rev. Lett.* 55, 715-717 (1985).
6. Shen, Q. &. Colella, R. *Acta crystallogr.* (submitted).
7. Shen, Q. *Acta crystallogr.* A42, 525-533 (1986).

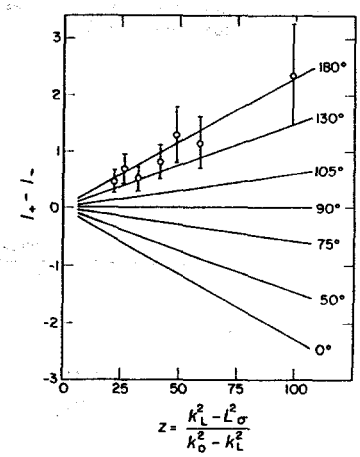

Fig. 2 Plot used to determine $\phi_{2\bar{2}1} + \phi_{021} - \phi_{202}$. The ordinate of each point is the difference in integrated intensity, normalized to the two-beam value, between two experimental points in Fig. 1, symmetrically located with respect to the (2$\bar{2}$1) peak. (The variable *z*, plotted on the horizontal axis, is a geometrical factor which increases as the excitation point of the (2$\bar{2}$1) is approached, and is explained in ref. 6.)

Biology Proposals

X-RAY ABSORPTION SPECTROSCOPY OF MN AND FE IN THE PHOTOSYNTHETIC APPARATUS

R. D. Guiles, Ann E. McDermott, James L. Cole, Vittal K. Yachandra,
Victoria J. DeRose, J.-L. Zimmermann, S. L. Dexheimer,
Kenneth Sauer and Melvin P. Klein

Laboratory of Chemical Biodynamics, Lawrence Berkeley Laboratory
University of California, Berkeley, CA. 94720 USA

Photosystem II (PS II) of cyanobacteria and higher plants consists of a photochemical reaction center quite similar to the reaction center of purple non-sulfur bacteria, together with a donor complex often called the oxygen evolving complex (OEC) that extracts electrons from water. The donor complex couples the four-electron oxidation of water to the one-electron photochemistry of the reaction center by serial accumulation of oxidizing equivalents such that O_2 is released on every fourth charge separation step. The partially oxidized intermediates of the donor complex are called S-states; S_1 is the principal S-state of a long-term dark-adapted preparation, and the OEC advances by one S-state on each charge separation of the reaction center until S_4 is produced, which decays to form S_0 and O_2. In contrast to the solution phase products of serial one-electron oxidation of H_2O to O_2, S_1 is very stable, and S_2 and S_3 are stable on the timescale of a few minutes. PS II exists within the membrane as a complex of several hydrophobic intrinsic proteins and several hydrophilic extrinsic proteins. A Mn complex bound to the PS II proteins is thought to be the catalytic site for water oxidation.

Our X-ray absorption studies of Mn in the OEC provided the first proof that Mn stores oxidizing equivalents during water oxidation [1,2,5]. A more detailed study of the edge position and structure of the 1s to 3d pre-edge features indicates that the advancement from S_1 to S_2 involves an oxidation of Mn(III) to Mn(IV) [3]. EXAFS measurements of samples in the S_1- and S_2-states showed that the Mn is in a cluster with a Mn-Mn distance of ~2.7 Å, with O or N ligand atoms at distances of ~1.8 and ~2.1 Å, which are characteristic of di-μ-oxo bridged Mn complexes [4,6]. XAS studies also indicated that the valence and the bond lengths of the Mn complex in preparations from higher plants and cyanobacteria are remarkably similar [7,8]. More recent experiments address the structure and valence of Mn in the S_3 and S_0 states [9]. We have also examined the structural interactions between the soluble extrinsic proteins of PS II and the Mn complex using XAS [10,11]. Some of the recent results from XAS studies of Mn in PS II are described below.

Pre-edge 1s to 3d Transition in the S_1- and S_2-States

We had shown earlier that the position of the Mn K-edge is a good reporter of the oxidation state of Mn in the S-states. We had also reported the presence of a pre-edge feature which we assigned to a 1s to 3d transition. We have recently collected data of high S/N of the pre-edge region from S_1- and S_2-states and some Mn(III) and Mn(IV) inorganic complexes (Fig 1). The data indicate that the pre-edge region also yields information about the oxidation state of Mn.

Figure 1 shows that the structure of the pre-edge region of the Mn K-edge transitions is systematically different in the Mn(III) and Mn(IV) complexes. Most notably, the pre-edge transitions are resolved from the main edge transition for Mn(IV) complexes, while for Mn(III) complexes they are not. These differences in the edge spectra are presumably related to systematic symmetry differences between Mn(III) and Mn(IV) complexes which give rise to differences in the energies of the d-electron levels and/or differences in the matrix elements for 1s to 3d transitions. The pre-edge region of the K-edge spectra of S_1 samples resembles those of many Mn(III) complexes, while for S_2 samples this region of the spectrum resembles those of Mn(IV) complexes. These results are strongly suggestive that in the S_1 to S_2 transition Mn(III) species are oxidized to Mn(IV).

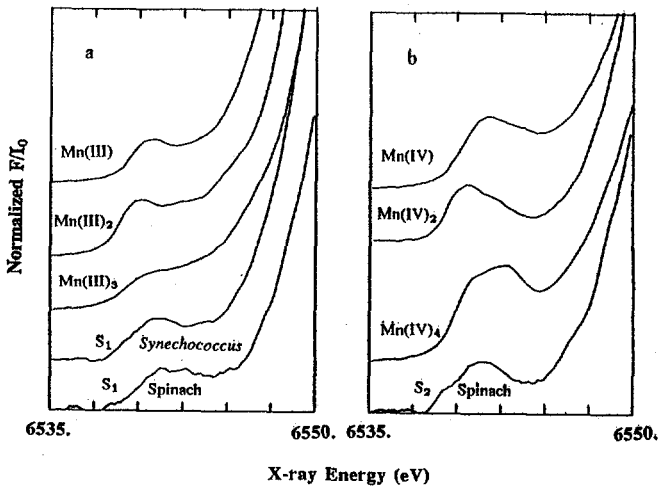

Figure 1. The pre-edge region of the Mn K-edge spectrum of O_2-evolving preparations from spinach and *Synechococcus*, poised in the S_1- and S_2-states. (a) From bottom to top, the pre-edge spectra are: 1. a spinach PS II preparation poised in the S_1-state, 2. a *Synechococcus* preparation poised in the S_1-state, 3. the trinuclear Mn(III) complex, $Mn_3(\mu_3\text{-}O)(OAc)_7.HOAc$, 4. the binuclear Mn(III) complex, $Mn_2(\mu\text{-}O)(OAc)_2(HBpz_3)_2$, and 5. the Mn(III) mononuclear complex, Mn(salen)Cl. (b) The pre-edge spectra of : 1. a spinach PS II preparation in the S_2-state, 2. the tetranuclear Mn(IV) complex, $[Mn_4O_6(tacn)_4](ClO_4)_4$ 3. a binuclear Mn(IV) complex $[Mn_2(\mu\text{-}O)_2(phen)_4](ClO_4)_3.CH_3CN$ and 4. the mononuclear complex, Mn(salicylate)$_2$bipyridine.

The S_3-State

O_2-evolving PS II membranes from spinach have been cryogenically stabilized in the S_3-state of the OEC. The cryogenic trapping of the S_3-state was achieved in a low-temperature, double-turnover illumination of dark-adapted PS II preparations. A double turnover of PS II was accomplished using the high-potential acceptor, Q_{400}, which is associated with the high spin iron of the iron-quinone acceptor complex. EPR spectroscopy was the principal tool establishing the S-state composition and defining the electron transfer events associated with a double turnover of PS II.

The inflection point energy of the Mn X-ray absorption edge of PS II preparations poised in the S_3-state is the same as for those poised in the S_2-state. This is surprising in light of the loss of the multiline EPR signal, which is characteristic of the S_2-state, upon advancing to the S_3-state. This indicates that the oxidative equivalent stored within the OEC during this transition resides on another intermediate donor which must be very close to the Mn complex. Figure 2 shows the Fourier transforms of k^1-weighted EXAFS spectra of samples in the S_1-, S_2- and S_3-states. An analysis of the Mn EXAFS of PSII preparations poised in the S_1-, S_2- and S_3-states indicates that the structure is essentially unchanged in the S_1 to S_2 transition, while a small structural rearrangement occurs during the S_2 to S_3 transition. A detailed comparison of the Mn EXAFS of these two S-states with the EXAFS of multinuclear μ-oxo bridged Mn site models suggests that the subtle differences observed between the S-states are best modelled by an increase in the spread of Mn-Mn distances occurring during the $S_2 \rightarrow S_3$ state transition. This increased disorder in the Mn distances suggests the presence of two inequivalent di-μ-oxo bridged binuclear structures in the S_3-state.

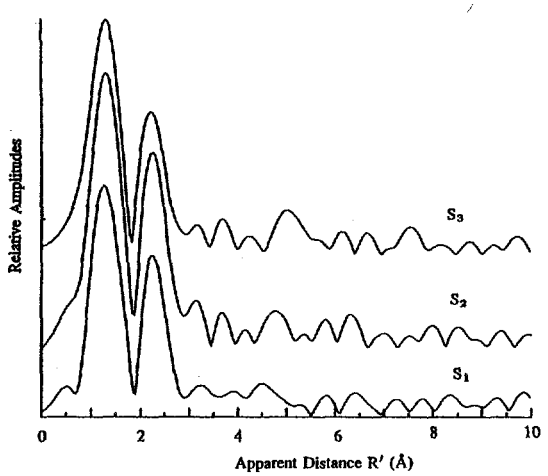

Figure 2. Fourier transforms of the $k^1\chi(k)$ Mn EXAFS data from spinach S_1-, S_2- and S_3-states. The Fourier peak at low R' is due to backscattering from O or N ligand atoms at ~1.8 and 2.1 Å and the peak at higher R' is primarily due to backscattering from Mn at ~2.7 Å. Note the similarity of the Fourier peaks in the S_1- and S_2-states. A small decrease in the amplitude of the Mn peak between the S_2- and S_3-states is also seen.

The S_0-State

Hydroxylamine at low concentrations causes a two-flash delay in the first maximum flash yield of O_2. We used the suppression of the multiline EPR signal to determine the fraction of PS II reaction centers set back to a NH_2OH-induced S_0-like state, S_0^*. The Mn K-edge spectra are virtually identical for dark adapted PS II preparations with and without NH_2OH. This indicates that, despite its high binding affinity to

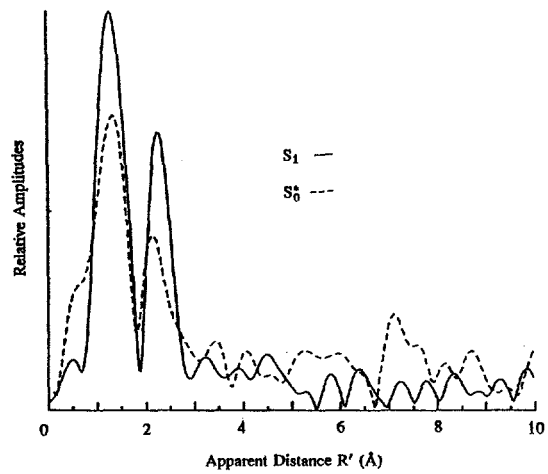

Figure 3. Fourier transforms of the $k^1\chi(k)$ Mn EXAFS data from spinach S_0^*- and S_1-states. The Fourier peak at low R' is again due to backscattering from O or N ligand atoms at ~1.8 and 2.1 Å and the peak at higher R' is primarily due to backscattering from Mn at ~2.7 Å. There is a significant decrease in the amplitudes of the Mn-O or N peaks and the Mn-Mn peak suggesting heterogeneity in the di-μ-oxo bridged Mn structure.

the OEC in the dark, NH_2OH does not reduce the Mn cluster within the OEC in the dark. Furthermore, the similarity of these edges is taken as evidence that NH_2OH does not directly bind to the Mn cluster within the OEC in the dark. After a single turnover of PS II, a shift to lower energy is observed in the inflection of the Mn K-edge of the Mn cluster. We conclude that in the presence of NH_2OH advancement by illumination causes a two electron reduction of the OEC, resulting in a state resembling S_0. This lower Mn K-edge energy of S_0^*, relative to the edge of S_1, implies the storage and stabilization of an oxidative equivalent within the Mn cluster during the $S_0 \rightarrow S_1$ state transition. We have also collected EXAFS spectra of samples in the S_0^*-state, and the Fourier transforms of k^1-weighted EXAFS spectra from S_1- and S_0^*-states are shown in Fig. 3. An analysis of the EXAFS of the S_0^*-state indicates that a significant structural rearrangement is occurring between the S_0- and S_1-states. It is suggested that the differences in the X-ray absorption edge position and the differences in the structure of the Mn cluster in the S_0^*-state are due to a heterogeneous mixture of formal valences of Mn including one Mn(II) which is not present in the S_1-state.

The Role of the 33-kDa Protein in Mn Binding

O_2-evolving PS II membranes containing 4 Mn/PS II were treated with 0.8 M $CaCl_2$ to extract the 33-, 24-, and 16-kDa extrinsic proteins. Mn was not released by this treatment, but subsequent incubation at low Cl^- concentration generated preparations containing 2 Mn/PS II. The Mn K-edge and EXAFS spectrum of the $CaCl_2$-washed preparation containing 4 Mn/PS II is very similar to the spectrum of the native PS II. These results indicate that the structure of the Mn complex is largely unaffected by the removal of the three extrinsic proteins. The K-edge and EXAFS spectrum of the $CaCl_2$-washed sample containing 2 Mn/PS II is dramatically altered indicating that the structure of the Mn complex is disrupted upon depletion of half of the Mn.

Acknowledgements

This work was supported by a grant from the National Science Foundation (PCM 82-16127 and PCM 84-16676) and by the Director, Office of Energy Research, Office of Basic Energy Sciences, Division of Biological Energy Conversion and Conservation of the Department of Energy under contract DE-AC03-76 SF00098. Synchrotron radiation facilities were provided by the Stanford Synchrotron Radiation Laboratory which is supported by the U.S. Department of Energy, Office of Basic Energy Sciences, and by the NIH Biotechnology Program, Division of Research Resources. We gratefully acknowledge Drs. George Christou (Indiana University, Bloomington), Karl Wieghardt (Ruhr-Universität, Bochum) and William H. Armstrong (University of California, Berkeley) for providing the Mn complexes used in this study.

References

1. Goodin, D. B., Yachandra, V. K., Britt, R. D., Sauer, K., & Klein, M.P. (1984) Biochim. Biophys. Acta 767, 209-216.
2. Goodin, D. B., Yachandra, V. K., Guiles, R. D., Britt, R. D., McDermott, A. E., Sauer, K., & Klein, M.P. (1984) in EXAFS and Near Edge Structure III (eds., Hodgson, K. O., Hedman, B. and Penner-Hahn, J. E.), Springer-Verlag, New York, 130-135.
3. Sauer, K., Guiles, R. D., McDermott, A. E., Cole, J. L., Yachandra, V. K., Dexheimer, S. L., Britt, R. D., Zimmermann, J.-L., & Klein, M.P. (1988) Chemica Scripta. In press.
4. Yachandra, V. K., Guiles, R. D., McDermott, A. E., Britt, R. D., Dexheimer, S. L., Sauer, K., & Klein, M.P. (1986) Biochim. Biophys. Acta 850, 324-332.
5. Cole J. L., Yachandra, V. K., Guiles, R.D., McDermott, A. E., Britt, R. D., Dexheimer, S. L., Sauer, K., & Klein, M.P. (1987) Biochim. Biophys. Acta 890, 395-398.
6. Yachandra, V. K., Guiles, R. D., McDermott, A. E., Cole J. L., Britt, R. D., Dexheimer, S. L., Sauer, K., & Klein, M.P. (1987) Biochem. 26, 5974-5981.
7. McDermott, A. E., Yachandra, V. K., Guiles, R. D., Cole, J. L., Dexheimer, S. L., Britt, R. D., Sauer, K., & Klein, M.P. (1988) Biochem. In press.
8. McDermott, A. E. (1987) Ph. D. Dissertation, Univ. of California, Berkeley, CA, USA.
9. Guiles, R. D. (1988) Ph. D. Dissertation, Univ. of California, Berkeley, CA, USA.
10. Cole, J. L. (1987) Ph. D. Dissertation, Univ. of California, Berkeley, CA, USA.
11. Cole J. L., Yachandra, V. K., McDermott, A. E., Guiles, R. D., Britt, R. D., Dexheimer, S. L., Sauer, K., & Klein, M.P. (1987) Biochem. 26, 5967-5973.

ANOMALOUS SCATTERING OF X-RAYS

David H. Templeton and Lieselotte K. Templeton

Department of Chemistry, University of California, Berkeley, CA 94720

INTRODUCTION

In this project we are seeking basic information about anomalous scattering of X-rays to provide a foundation for applications in the study of chemical structure. Synchrotron radiation gives access to the large effects which occur in narrow wavelength intervals near absorption edges. Its strong polarization causes interesting and useful effects which can also be a complication in some experiments. The current emphasis of this work is to explore these polarization effects in X-ray absorption and scattering by crystals.

BIAXIAL TENSORS FOR ANOMALOUS SCATTERING BY SELENIUM

When selenium is bonded to two carbon atoms, as in selenolanthionine (1,2), the X-ray optical constants are free to have independent values for three principal directions of polarization. Last year we reported preliminary measurements of the three absorption spectra and the biaxial tensors which describe the anomalous scattering near the Se K aborption edge. Additional data from December, 1986, have now been analyzed and submitted for publication (3). The tensor components derived from the spectra and from diffraction experiments show the same general features (Fig. 1), but more anisotropy is indicated by the diffraction method. A similar difference was found in earlier work on bromine and platinum (4,5). The anisotropy, nearly 6 for f' and 7 for f'', is the most yet found for a K edge.

OTHER EXPERIMENTS

Experiments with cadmium bromate, designed to measure diffraction effects of the anomalous scattering tensor in a more complicated structure, were done with the area detector in December, 1987, but have not yet been analyzed. A recent publication (6) describes how some structure factor phases are observed in a very direct way in the azimuthal variation of intensity of "forbidden reflections" which are made visible by X-ray birefringence. Some studies of beam polarization are in process of publication (7).

ACKNOWLEDGEMENTS

This research was supported by National Science Foundation Grant CHE-8515298 and was done at SSRL which is supported by the Department of Energy, Office of Basic Energy Sciences; and the National Institutes of Health, Biotechnology Resource Program, Division of Research Resources. It used some facilities of the Lawrence Berkeley Laboratory, supported by DOE Contract DE-AC03-76SF00098.

REFERENCES

1. G. Zdansky, Arkiv Kemi 29, 443-448 (1968).
2. W. A. Hendrickson, Trans. Amer. Cryst. Assoc. 21, 11-21 (1985).
3. L. K. Templeton and D. H. Templeton, Acta Cryst. Sect. A, submitted.
4. D. H. Templeton and L. K. Templeton, Acta Cryst. A41, 133-142 (1985).
5. D. H. Templeton and L. K. Templeton, Acta Cryst. A41, 365-371 (1985).
6. D. H. Templeton and L. K. Templeton, Acta Cryst. A43, 573-574 (1987).
7. D. H. Templeton and L. K. Templeton, J. Appl. Cryst. (in press).

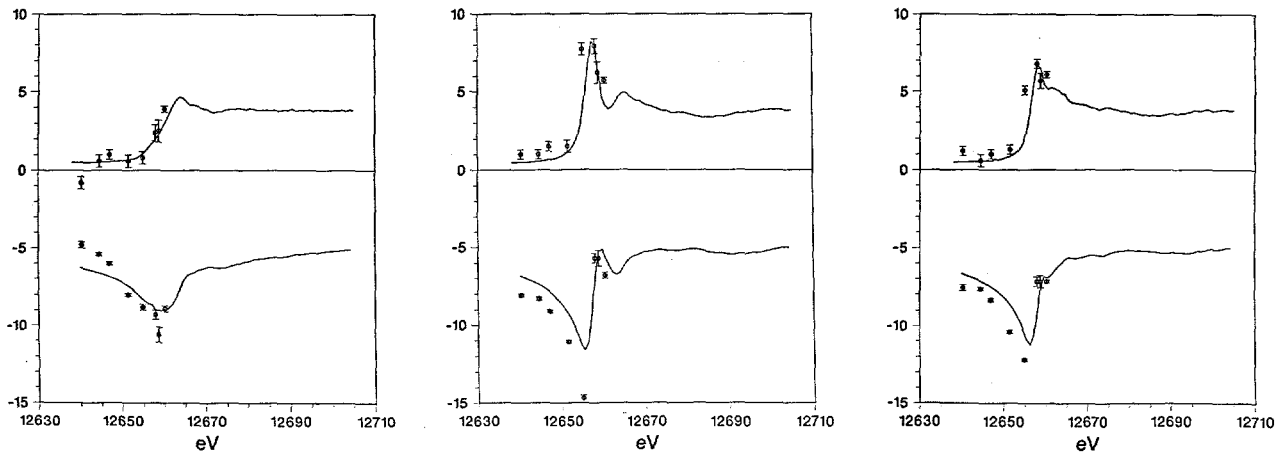

Figure 1. Real and imaginary parts (f', lower; f'' upper) of the principal values of the anomalous scattering tensor of selenium derived from absorption spectra (curves) and from diffraction intensities (points with error bars); left, polarization perpendicular to Se-C bonds; center, polarization in direction of C-C vector; right, polarization along bisector of C-Se-C angle.

STRUCTURE/FUNCTION STUDIES OF OXIDASES, PEROXIDASES AND CATALASES

B. Chance[+*], L. Powers[@], S. Khalid[+], I. Ayene*, R. Waterland*,
T.E. King[+], G. Bunker[+], K. Zhang[+],R. Poyton[#], E. Davidson*

[+]University City Science Center, Institute for Structural & Functional Studies, Philadelphia, PA
*University of Pennsylvania School of Medicine, Department of Biochemistry & Biophysics, Philadelphia, PA
[@]AT&T Bell Laboratories, Murray Hill, NJ
[#]University of Colorado, Department of Molecular, Cellular & Developmental Biology, Boulder, CO

Cytochrome oxidase studies have now been focused largely upon "altered forms of cytochrome oxidase" as obtained by mutation of cytochrome oxidase through the nuclear genes rather than the mitochondrial genes. This affords a variety of altered cytochrome oxidases in which different numbers of subunits are present and in which different activities are observable and, according to our EXAFS study, different structures of the active site will be involved.

The synthesis of altered forms of cytochrome oxidase in genetically altered yeast cells is often inefficient; assembly of cytochrome oxidase may be faulty. Thus, one special goal of the beam time allotments made available has been an increase of the detector sensitivity and reliability to the point that not only do we measure the 100 μM copper of cytochrome oxidase of beef heart membrane-bound preparations as already published (1), but we have, on occasion, obtained edge data at half this concentration. In order to decrease the averaging time and to increase the reliability of the results, a 13-element Germanium detector has been obtained and will be used in a wide-band energy referencing circuit that we believe will decrease the time for accumulation of a satisfactory data set by a factor of two, at least. At the same time, EXAFS studies of these dilute membrane preparations will be undertaken. R.O. Poyton, our collaborator in these studies, together with T.E. King and ourselves will make all efforts to increase the yield of purified cytochrome oxidase from the mutant cells.

Already accomplished are studies of three important aspects of cytochrome structure and function, copper depletion, mercury modification and the structure of the zinc site. Wharton has vastly improved the copper depletion methods for cytochrome oxidase so that an approximation to a single site is achieved in the enzyme. Under these conditions, the algorithms by which we have deconvoluted the separated contributions of the copper atoms in the native enzyme have been checked, and, furthermore, the structure/function of the copper deficient enzyme has been studied in detail (2,3).

The mercuration of cytochrome oxidase was one of the first evidences that an EPR silent copper was involved, and Bickar has recently produced a well-defined derivative on which we have been able to do EXAFS studies (4). The finding is of importance, it is apparent that the mercury ligates the sulfur atom proximal to the a_3-copper binding site. The possibility of ligating a sulfur atom within back scatter distance of the copper further confirms our identification of sulfur as a bridging atom in the resting structure.

Zinc has been identified as a component of the multi-subunit oxidase in the laboratory of Caughey (5). The subunit location and the ligands of the zinc have been identified (6) and found to be consistent with the amino acids sequence and folding properties of subunit VI of cytochrome oxidase; Caughey has shown that several other subunits are not involved and the "three subunit" oxidases is found not to contain zinc. Thus, EXAFS has proved to be most valuable in identifying the nature of the zinc binding site.

Position Noise Study

Our vibrating reed beam position detector has now been used to evaluate Beam Lines II-3, II-2 and VI. A beam tracking circuit has been used on II-2 with a significant decrease (>2x) of noise in EXAFS Recording (7).

Sample Damage Studies

The great sensitivity of dilute cytochrome oxidase to redox perturbations by hydrated electrons has caused the reactivation of research on this topic, particularly at room temperature where eventual kinetics studies are planned. Typically 50% reduction of cytochrome oxidase occurs in 2.5 hours on Beam Line II-2. Use of traps for hydrated electrons is in progress.

Future Plans

The improved detector systems suggests feasibility of EXAFS study of the copper of several yeast mutants of cytochrome oxidase. At the same time, intensified studies on purification and concentration of the preparation to afford a cytochrome oxidase preparation free of other iron components than aa_3 will make possible iron EXAFS studies as well. These data coupled with our detailed analysis of kinetic differences of these oxidases should lead to a better understanding of structure/function relationships in this multinuclear-oxygen reducing enzyme.

REFERENCES

1. Powers, L., Chance, B., Ching, Y.-C., Lee, C.-P. (1987) J. Biol. Chem. 262:3160-3164.
2. Powers, L., Ching, Y., Chance, B., Wharton, D., Bickar, D. (1987) Fed. Proc. 46:2174a.
3. Powers, L., Bickar, D., Wharton, D., Ching, Y., Chance, B. (1988) Ligand environment of the active site copper in cytochrome oxidase, Biochem. (in preparation).
4. Bickar, D., Powers, L., Chance, B. (1987) Biophys. J. 51:298a.
5. Yewey, G.Z., Caughey, W.S. (1987) Biochem. Biophys. Res. Commun. 148:1520-1526.
6. Naqui, A., Powers, L., Lundeen, M., Constantinescu, A., Chance, B. (1988) On the environment of zinc in beef heart cytochrome c oxidase: Am EXAFS Study. J. Biol. Chem. (submitted).
7. Khalid, S., Chance, B., Zhang, M.-Z., Sorge, J., Arthur, J., Hettel, R. (1987) The vibrating reed as a probe to study the monochromatic and white x-ray beam fluctuations coming from the bending magnet, wiggler and undulator at SSRL. Rev. Sci. Instr. (in preparation).

ACKNOWLEDGEMENT

Support: NIH Grants GM-33165,HL-18708,HL-31909, CA-41787,DMB-841452

X-ray Absorption Spectroscopic Studies of Nickel Containing Metalloenzymes.

Andrew K. Shiemke, Marly K. Eidsness and Robert A. Scott

School of Chemical Sciences and Center for Metalloenzyme Studies

University of Georgia

Athens, Georgia 30602

In a recent activity report we demonstrated the use of x-ray absorption near edge spectroscopy in determining coordination geometry and ligand type for various nickel complexes.[1] In particular we found that the edge height is greater for nitrogen or oxygen ligation relative to sulfur ligation in complexes of comparable coordination number. Also, it was found that the forbidden 1s → 3d transition at ~8332 eV is more intense in the non-centrosymmetric tetrahedral complexes than in octahedral or square-planar complexes, and that an intense 1s → 4p transition at ~8336 eV is characteristic of square-planar nickel complexes. We have applied these near edge spectral features to our investigation of the nickel coordination geometry of F_{430}, the nickel-containing tetrapyrrole cofactor of the methylreductase enzyme from methanogenic bacteria.

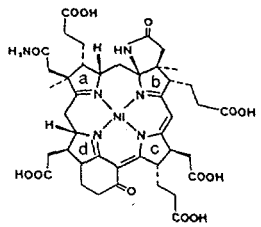

F_{430}

Chromatographically and spectroscopically distinct forms of F_{430} can be isolated, depending on the temperature at which the isolation and purification of the cofactor is done.[2] High temperatures induce an epimerization of the side chains at the 12 and13 positions of pyrrole ring C of the macrocycle.[3] The nickel coordination geometry of the resulting diepimer differs from that of the native cofactor. The intense pre-edge feature at ~8336 eV in the diepimer spectrum (Figure 1a) is characteristic of nickel in a square planar environment, whereas the featureless edge of the F_{430} spectrum is indicative of octahedral coordination.

In addition to the difference in coordination number, these isomeric forms of the cofactor differ in metal-ligand distances as well. Figure 1b shows the Ni K-edge EXAFS for F_{430} and for the diepimer in H_2O. The higher frequency EXAFS for the native cofactor is indicative of increased metal-ligand distances relative to the diepimer. This is dramatically demonstrated in the Fourier transforms of these two species (Figure 1c), which shows that the first shell peak for the native F_{430} occurs ~0.2 Å to longer distance than in the diepimer. Results of curve fitting on the filtered first shell EXAFS of

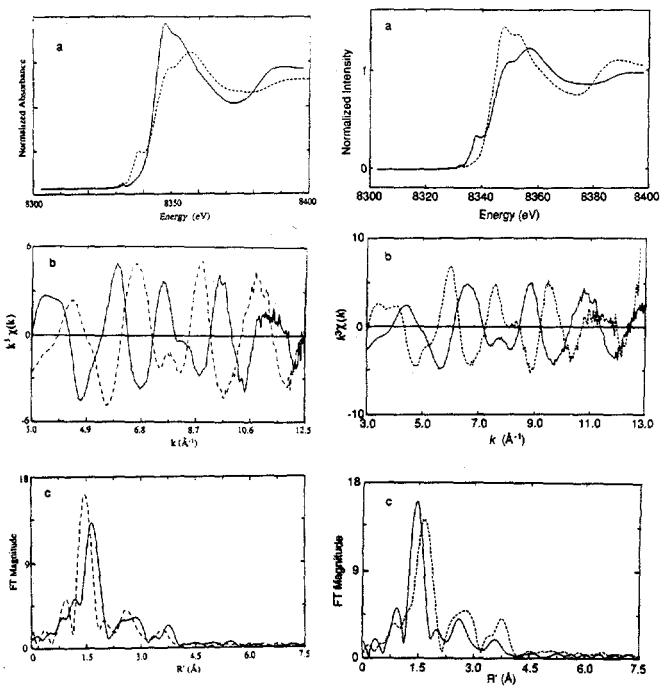

Figure 1 (left). Nickel K-edge spectra (a), EXAFS (b) and Fourier transform (c) for F_{430} (——) and the 12,13 diepimer of F_{430} (- - -). Both samples are in 10 mM phosphate (pH 7.0), and the data was collected at 10K.

Figure 2 (right). Nickel K-edge spectra (a), EXAFS (b) and Fourier transform (c) for the diepimer of F_{430} in 10 mM phosphate, pH 7.0 (——), and in 1-methylimidazole (- - -). Data collected at 10K.

these two samples show that the nickel in F_{430} has 6 nitrogen (or oxygen) ligands at an average distance of 2.1 Å, whereas the diepimer has 4 N (or O) ligands at 1.9 Å. We can therefore conclude that the heat-induced epimerization of the cofactor is accompanied by the loss of axial ligands with a concomitant contraction of the macrocycle core. It is likely that the core contraction of the diepimer macrocycle occurs through an S_4 ruffling of the macrocycle, similar to that observed in the closely related Ni-corphin complexes.[4]

The epimerization at the periphery of the F_{430} macrocycle does not render the central metal incapable of binding axial ligands. In the presence of a large excess of a strongly coordinating species the central nickel will bind axial ligands to become 6-coordinate. Figure 2a shows a comparison of the near edge spectra of the diepimer in water and in 1-methylimidazole. The spectrum of the sample in 1-methylimidazole contains no trace of the $1s \rightarrow 4p$ pre-edge feature seen in H_2O. Comparison of the EXAFS and Fourier transforms of the diepimer in H_2O and in 1-methylimidazole (Figure 2b,c) also indicate axial ligation by 1-methylimidazole. The higher frequency of the EXAFS and the shift of the first shell peak to longer distance in the coordinating solvent are very similar to differences between the native cofactor and diepimer in water (Figure 1). This is confirmed by curve fitting of the filtered first shell EXAFS of the diepimer in 1-methylimidazole which shows that the nickel coordination sphere consists of 6 nitrogen ligands at 2.1 Å. Thus, the axial ligation of the diepimer is accompanied by a core expansion to yield a nickel coordination sphere very similar to the cofactor in its native configuration.

Comparison of the near-edge XAS of isolated F_{430} to that of the protein-bound cofactor also reveals differences in the nickel coordination sphere (Figure 3). Although the central nickel is 6-coordinate in both cases, the edge height of the methylreductase-bound cofactor is reduced relative to that of the isolated F_{430}. In addition the inflection point of the edge is shifted to slightly lower energy in the methylreductase spectrum. These differences may indicate that the axial ligands in the protein-bound cofactor are more polarizable than those of the isolated F_{430} (e.g. sulfur or anionic oxygen ligation in the protein vs. water ligation in isolated F_{430}). Though we cannot yet unequivically identify the axial ligands of either isolated or protein-bound F_{430}, we are continuing to pursue EXAFS studies of both in an attempt to do so.

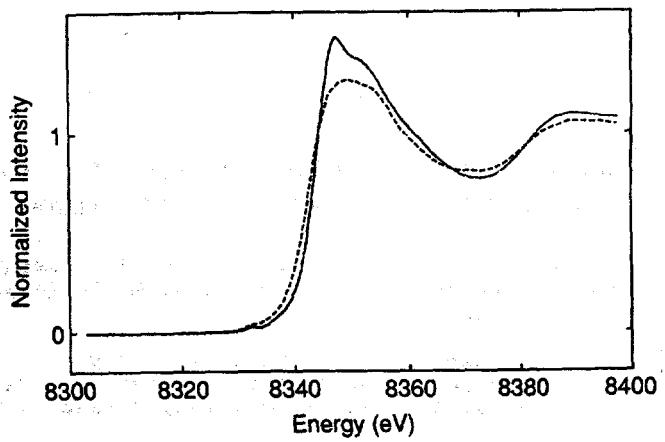

Figure 3. Nickel K-edge absorption spectra of isolated F_{430} (——), and the methylreductase holoenzyme (- - -). Both samples are in 10 mM phosphate (pH 7.0) and the data was collected at 10K.

REFERENCES

1. Scott, R. A. and Eidsness, M. K. *SSRL Activity Report for 1986*, proposal 969, p. 129.
2. Shiemke, A. K.; Hamilton, C. L.; Scott, R. A. *J. Biol. Chem.* **1986**, in press.
3. Pfaltz, A.; Livingston, D. A.; Jaun, B.; Diekert, G.; Thauer, R. K.; Eschenmoser, A. *Helv. Chim. Acta* **1985**, *68*, 1338-1358.
4. Kratky, C.; Fässler, A.; Pfaltz, A.; Kräutler, B.; Jaun, B.; Eschenmoser, A. *J. Chem. Soc. Chem. Comm.* **1984**, 1368-1371.

MATHEMATICAL MODELING OF MULTIPLE WAVE FUNCTIONS FOR IRON PORPHYRIN EXAFS SPECTRA

J. O. Alben, F. G. Fiamingo, A. A. Croteau, C. F. Hemann, K. A. Powell, V. M. Molleran, and S. Park

Biospectroscopy Laboratory, Dept. of Physiological Chemistry, Ohio State University, College of Medicine, Columbus, OH 43210.

INTRODUCTION

The study of heme proteins is critical to the understanding of respiration and electron transfer reactions in living systems. Many of these have been extensively studied by X-ray absorption spectroscopy and have been centrally involved in advances in data collection and analysis. Attempts to extend molecular interpretations to the limits of uncertainty have led to a variety of controversies, especially regarding the presence or absence of axial ligands and their distances from iron. Most of these studies would have benefited by increased signal/noise and resolution (data measured to higher k values). We have therefore begun to reexamine methods of data collection and analysis to more clearly define uncertainties of molecular interpretation.

RESULTS AND DISCUSSION

Iron K-edge and EXAFS data were collected on beam line IV-1 at 4-5 Kelvin in linear k-space increments to 18.4 A^{-1} for several iron-porphyrin derivatives. Extraction of EXAFS and preliminary data analysis were done by standard methods with software kindly made available by Stephen P. Cramer and Graham George. Truncation errors associated with Fourier transforms of finite data sets were avoided by curve-fitting directly to unsmoothed EXAFS data with no Fourier filtering. Metal porphyrins are sufficiently ordered that all ring atoms and at least first shell axial atoms make significant contributions to the EXAFS waveforms. We have therefore implemented a Gauss-Newton algorithm (BMDP3R from UCLA) on an IBM 3081D mainframe with use of parametrized phase and amplitude functions for simultaneous fitting of up to 10 backscatterer wave functions. EXAFS data were fit between k=4 and k=17 A^{-1}. Preliminary fits yield excellent agreement with crystallographic distances for porphyrin ring atoms and some axial atoms. However, refinements may need to be made to the parametrized phase and amplitude functions to make adequate use of the higher resolution data. The residuals (observed minus calculated) are not yet random, but contain one or more waveforms, the physical significance of which is not defined. The fit to the EXAFS spectrum of tetraphenylporphyrin iron(III) chloride and its residual are illustrated in Figure 1.

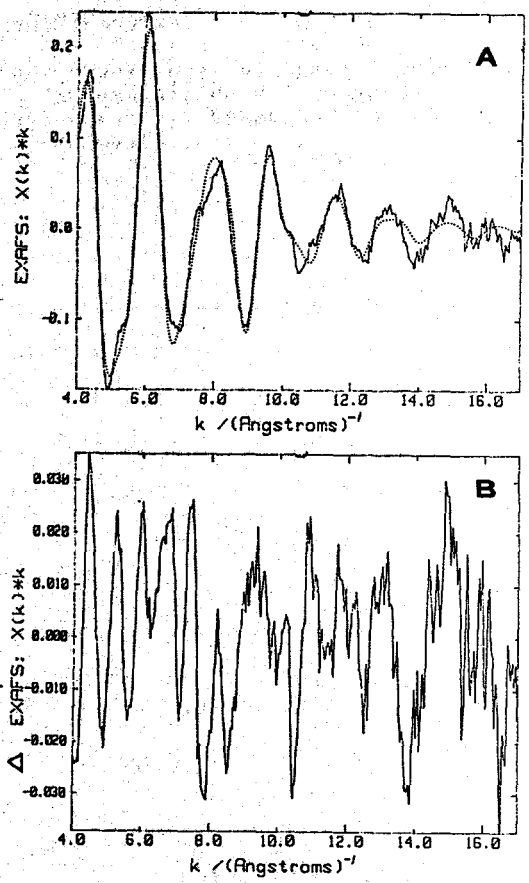

Figure 1. A. Observed (----), and computed (·····) EXAFS of tetraphenylporphyrin iron(III)chloride dissolved in Apiezon N grease at 4 Kelvin.

B. Residual (observed minus computed) EXAFS spectrum.

The computed model was obtained with apparent radial distances for pyrrole N (2.05 A), alpha C (3.12 A), meso C (3.44 A), beta C (4.11 A), and chloride (2.21 A). Phase and amplitude parameters for sulfur were used to estimate the distance for chloride. The residual plot suggests a need for a short period wavefunction at low k-values and some parameter adjustments at high k-values. This will be investigated further.

ACKNOWLEDGEMENTS

We thank Dr. B. Hedman and the SSRL staff for assistance during data collection and Drs. S. P. Cramer and G. George for helpful comments.

TECHNETIUM DIPHOSPHONATE IMAGING AGENTS AND RHENIUM THERAPEUTIC RADIOPHARMACEUTICALS

Richard C. Elder and Edward Deutsch

Department of Chemistry and Radiology and
the Biomedical Chemistry Research Center
University of Cincinnati
Cincinnati, Ohio 45221-0172

Technetium bone imaging agents have been used in clinical practices for many years (1). More recently these have been followed by rhenium therapeutic radiopharmaceuticals. ^{99m}Tc technetium is the imaging isotope of choice because 1) it emits a gamma ray of useful energy 2) it has a 6 hour half-life which is long enough for chemical syntheses but short enought that it quickly decays away and 3) it is available in a "Tc generator" which is readily transported and of low cost. Technetium complexes with a variety of diphosphonate ligands ($O_3PCRR'PO_3^{4-}$) form bone imaging agents. Depending on the nature of the substituents, R and R', and the method of synthesis, the resulting complex mixtures show differing biodistributions. Little is known about the structures of these complexes since they have proven difficult to impossible to crystallize. The crystal structure of one complex, that with the methylenediphosphonate ligand (R=R'=H), has been determined (2). It forms an infinite polymeric chain with a MDP/Tc ratio of 1:1. Although four of the disphosphonate oxygen atoms are bound to technetium, two others are free. It has been proposed that these available oxygen atoms then bind to calcium exposed on growing bone surface and account for the mode of action of these bone imaging agents.

Recently we have developed a method utilizing HPLC to separate single components from a reaction mixture and shown that several of these are stable in solution for a period of months (3). We have isolated the major component of the preparative reaction where TcO_4^- is reduced with $NaBH_4$ in the presence of the methylenediphosphonate ligand and obtained a 8 mM solution for EXAFS studies. Having constructed an adequate cell to guarantee containment of this inherently radioactive solution (99 Tc decays with soft beta emission and a 10^5 year half-life), we have measured EXAFS spectra at the technetium K edge (20.5-22.0 KeV). The Fourier transform of that solution data is given in figure 1.

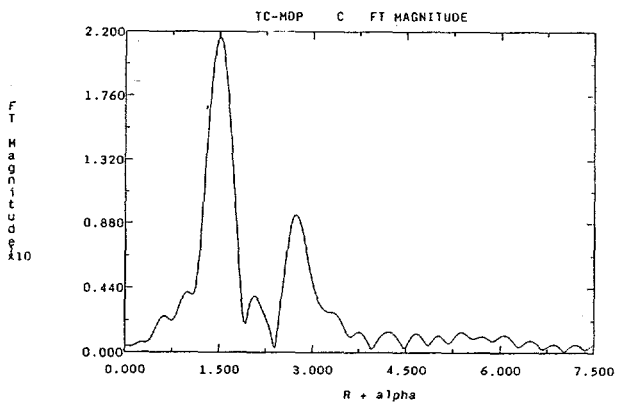

Figure 1

Two distinct peaks are obvious, one centered at 1.5 Å and the other at 2.7 Å. Each of these has been isolated and separately back transformed using a Gaussian window. The filtered EXAFS times k^3 is shown in figure 2A for the 1.5 Å peak and in 2B for that at 2.7 Å. The difference in

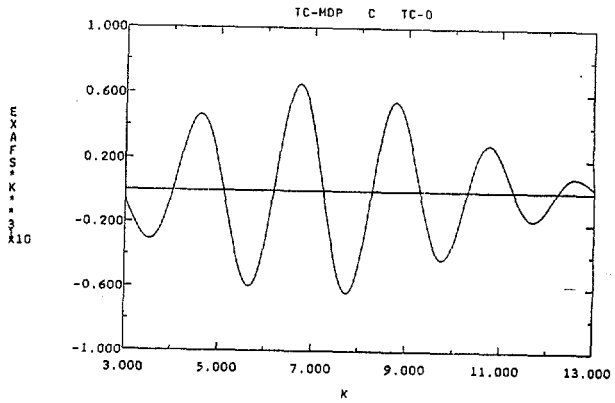

Figure 2A

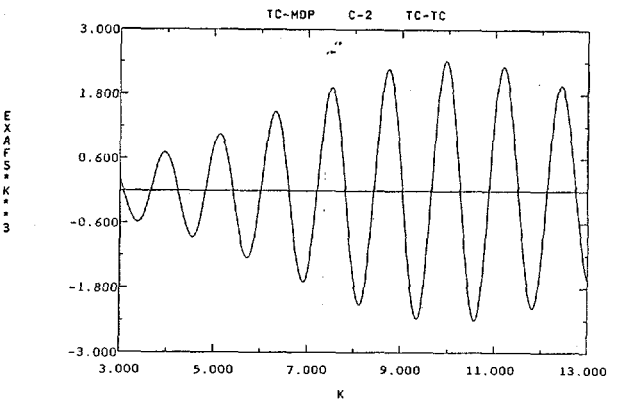

Figure 2B

envelope shapes is readily apparent and suggests that the short distance is from Tc-O whereas the longer value results from a Tc-Tc interaction. Empirical phase and amplitude parameters have been developed from model compounds of known crystal structure kindly supplied by Professor A. Davison of MIT. The results of a preliminary two shell fit to the back transform over the range .88-2.92 Å are as follows: 6.0 O atoms at 1.98 Å and 1.5 Tc atoms at 2.94 Å. Some of our model data is poor and these fitting results are tentative at this time. However, at present these EXAFS studies provide the only clear evidence available for the solution structures of this

important class of imaging agents. The number of 1.5 Tc neighbors suggests a tetrameric chain structure on average with two interior Tc atoms each having two Tc neighbors and the end atoms having a single Tc neighbor. The Tc-O distance of 1.98 and Tc-Tc of 2.94 suggests a nearly square array of two Tc bridged by two O atoms. The O, Tc, O angle would be 85°. Any more detailed interpretation must await the acquisition of higher quality data and further calculations.

Individuals working on this project have included Drs. K. Libson, M. Rahman and D. Pipes as well as Mr. J. Yuan and J. Watkins. Support by NIH grants GM35404 and CA32863 is gratefully acknowledged.

References

1. Deutsch, E., Progr. Inorg. Chem., 1983 30, 120.

2. Libson, K., Deutsch, E., Barrett, B., J. Am. Chem. Soc., 1980 102, 2476.

3. Martin, J., Ph.D. Thesis, University of Cincinnati, 1987.

A Copper XAS Study of Dopamine β-Hydroxylase

Robert A. Scott
Departments of Chemistry and Biochemistry, University of Georgia, Athens, GA 30602

Richard J. Sullivan
School of Chemical Sciences, University of Illinois, Urbana, IL 61801

Walter E. DeWolf, Jr., Roland E. Dolle
Department of Medicinal Chemistry, Smith Kline & French Laboratories, King of Prussia, PA 19406

Larry I. Kruse
Smith Kline & French Research Ltd., Dept. of Medicinal Chemistry, The Frythe, Welwyn, Hertfordshire, England AL6 9AR

Dopamine β-hydroxylase (DBH) is a monooxygenase that catalyzes the benzylic hydroxylation of dopamine to norepinephrine. DBH is a tetramer that is most active with two copper ions per subunit. The oxidized [Cu(II)] form of the enzyme is inactive, but reductive activation occurs in the presence of exogenous electron donors such as ascorbate. In a previous report [1], we showed that the ascorbate-reduced [Cu(I)] DBH active sites exhibit a significantly altered coordination environment. Whereas the Cu(II) sites exhibit mostly (histidine) imidazole ligation, the Cu(I) sites give rise to a split Fourier transform (FT) first-shell peak, reflecting the presence of 2-3 (N,O)-containing ligands at 1.93 Å and 1 S-containing ligand at 2.30 Å [1,2]. In order to determine the effect of organic substrate on the Cu(I) site structure, we have now examined the Cu EXAFS of DBH reduced by ascorbate in the presence of the substrate analog tyramine. We have also examined the Cu(I) site structural changes associated with the binding of the multisubstrate inhibitor 1-(3,5-difluoro-4-hydroxybenzyl)imidazole-2-thione (**1**), which is suspected to bind to Cu through the thione sulfur [3].

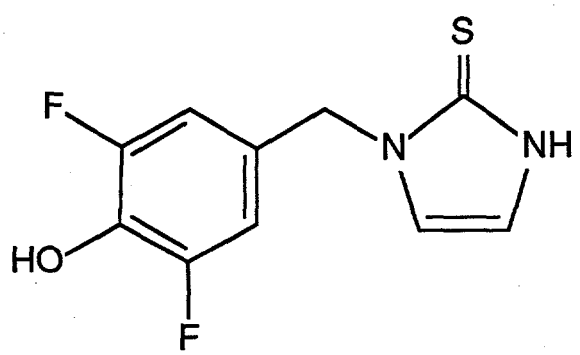

1

Figure 1 shows the raw Cu EXAFS data for two independent samples of ascorbate-reduced DBH and a sample of tyramine-treated DBH after ascorbate reduction. These EXAFS spectra are identical to within the noise in the data, as are the edge spectra for these three samples (not shown). Curve-fitting analysis again gives 2-3 (N,O) @ 1.93 Å and 1 S @ 2.30 Å for the reduced tyramine-treated sample. Thus, the

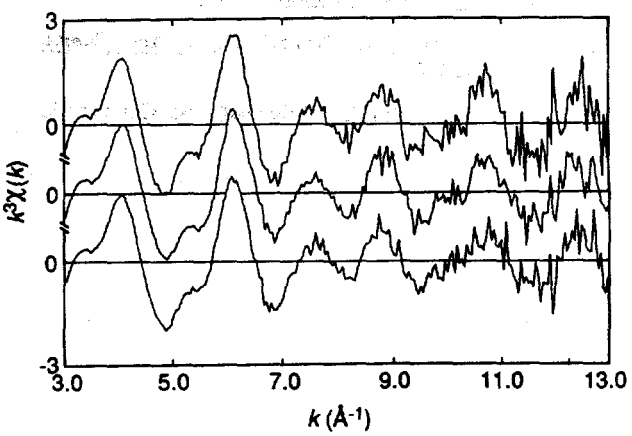

FIGURE 1. Comparison of raw Cu EXAFS data for the Cu(I) (sample A, top; sample B, middle) and the Cu(I)-tyramine bound (bottom) forms of dopamine β-hydroxylase. All three spectra are identical to within the noise of the data.

structural changes associated with reduction of the DBH copper sites are essentially unaffected by the presence of tyramine. We can conclude nothing about the potential binding of tyramine to the copper site, since displacement by tyramine of one of the (N,O)-containing ligands plausibly could result in an insignificant difference in the EXAFS and edge data.

The possibility that a chloride bound to copper could be responsible for the scattering component that we have assigned as Cu-S in the EXAFS of reduced and tyramine-treated reduced DBH prompted us to perform chloride determinations on the XAS samples. The amount of chloride for various samples ranged from 0.23 - 0.64 Cl^-/Cu with an average and standard deviation of 0.39 ± 0.22 Cl^-/Cu. Since our curve-fitting results strongly suggest a (S,Cl) coordination number of one, we prefer to assign this scattering component to a Cu-S interaction.

Figure 2d shows the Cu EXAFS data for an ascorbate-reduced sample of DBH treated with the multisubstrate in-

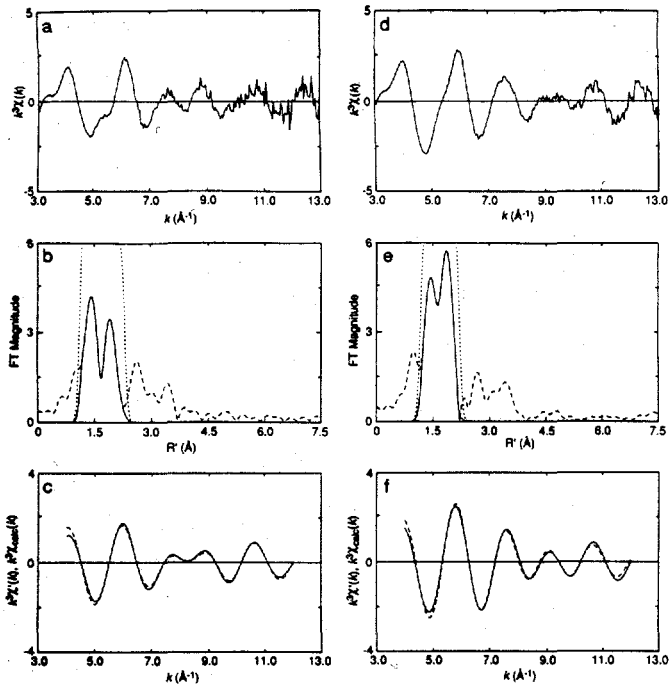

FIGURE 2. Comparison of Cu EXAFS analysis for the Cu(I)-tyramine bound (left) and Cu(I)-inhibitor bound (right) forms of dopamine β-hydroxylase. FTs (k = 3.0 - 13.0 Å^{-1}, k^3 weighting) of the raw Cu EXAFS data [in (a) and (d)] are shown in (b) and (c), respectively. The filter windows (···) in (b) and (e) were used to extract the first-shell contributions that are shown as back-transformed $\chi'(k)$ data (——) in (c) and (f), respectively. The best curve-fitting results are shown as dashed lines in (c) and (f).

hibitor **1**. The copper site structural differences between the inhibited sample and the tyramine-treated sample can be visualized in the FTs (Figures 2b, 2e, respectively) and quantitated by curve-fitting analysis. Figure 2f shows the best curve-fitting simulation of the inhibited Cu(I) site, yielding a coordination environment of 1 (N,O) @ 1.96 Å and 2 S @ 2.30 Å. Thus, the thione S of **1** apparently displaces one of the (N,O)-containing ligands of the Cu(I) site (perhaps blocking substrate binding).

REFERENCES

1. Scott, R. A.; Sullivan, R. J.; Kruse, L. I.; DeWolf, W. E., Jr.; Dolle, R. E. *SSRL Report 87/01* **1987**, 138.

2. Scott, R. A.; Sullivan, R. J.; DeWolf, W. E., Jr.; Dolle, R. E.; Kruse, L. I. *Biochemistry*, submitted for publication.

3. Kruse, L. I.; DeWolf, W. E., Jr.; Chambers, P. A.; Goodhart, P. J. *Biochemistry* **1986**, *25*, 7271-7278.

BIOCHEMISTRY: USE MADE OF BEAMLINE VI-2 IN 1986/1987 Proposal No. 1001B

Graham N. George and Roger C. Prince

EXXON Research and Engineering Co.
Route 22 East, Annandale, NJ 08801

INTRODUCTION

Our X-ray absorption spectroscopy on beamline VI-2 can be divided into soft X-ray (2-3 KeV) and hard X-ray (3-20 KeV) experiments. The 2-3 KeV region has, to date, been relatively little used for biochemical or chemical applications, although it contains the K edges of phosphorus, sulfur, and chlorine as well as the L edges of the second row transition elements and the M edges of tungsten through uranium. Our early work at these energies used line VI-2 as an undulator source to allow the safe removal of the carbon filters normally in place. The x-ray flux was maximized by adjusting the wiggler field so that the undulator third harmonic peaked at the center of the energy region being used. In 1987, developments by SSRL allowed safe removal of the carbon filters at higher wiggler fields, yielding still greater flux.

SULFUR IN FUEL

There still remain some unanswered questions as to the chemical nature of sulfur in oil. This is a problem that X-ray spectroscopy is uniquely suited to address. In collaboration with M. L. Gorbaty, S. P. Cramer, and M. K. Eidsness, we have examined the sulfur K edge spectra of an asphaltene fraction and a number of model compounds. The EXAFS indicated that sulfur is coordinated to two carbons with a mean bond length of 1.74Å, which is typical for an aromatic sulfur involved in a heterocyclic ring system. The edge spectra of the model compounds showed a highly variable structure (Fig. 1). We conclude that the bulk of the sulfur in the asphaltene sample is probably involved in a poly-nuclear aromatic ring system with a local environment similar to that for dibenzothiophene.

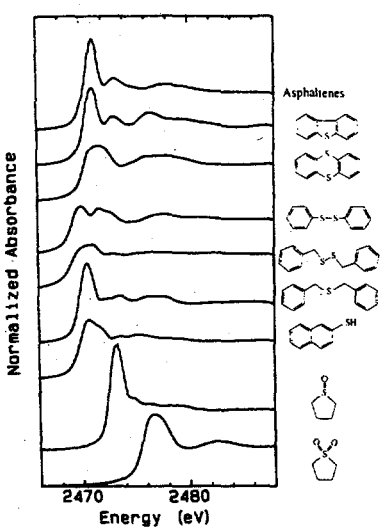

Figure 1. Sulfur K-edge spectra.

MOLYBDENUM L EDGES

The molybdenum L edges of a range of enzyme systems, such as nitrogenase, and numerous model compounds have been investigated, using a combination of proposal and PRT time. This is written up as the reports for proposals 948B and 1030B in the SSRL Activity Report for 1986.

PHOSPHORUS K EDGES

The use of Ge(111) crystal monochromators enabled us, in collaboration with S. P. Cramer, to use line VI-2 to obtain phosphorus K edge spectra for the first time. Preliminary results on a number of systems were obtained, including phosphate minerals, various model compounds (phosphates, etc.) and biological samples (DNA, ATP, etc.). The phosphorus K edge of apatite and sodium phosphate are illustrated in Fig. 2. Although this work is still in its early stages, the utility of phosphorus X-ray Absorption K edge spectroscopy is clearly apparent.

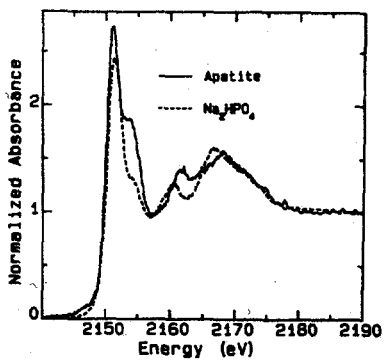

Figure 2. Phosphorus K-edge spectra.

THE ACTIVE SITE OF HYDROGENASE II FROM CLOSTRIDIUM PASTEURIANUM

Hydrogenases are a class of enzymes that catalyze the reversible oxidation of hydrogen. In collaboration with M.W.W. Adams, we have investigated the iron EXAFS of C. pasteurianum hydrogenase II in both oxidized and reduced forms. The data for the oxidized protein indicate an iron environment similar to that found in other iron-sulfur systems; iron being four coordinate to sulfur with an iron-sulfur distance of 2.3Å. Cu-Cu interactions at 2.7Å and 3.9Å have also been tentatively identified. Two genetically engineered copper metallothioneins were also investigated, and found to possess a similar copper environment to the wild type protein.

THE MANGANESE PHOTOSYNTHETIC WATER SPLITTING ENZYME

The photosynthetic water splitting enzyme is perhaps the most important enzyme in the world, being the originator of all the atmospheric oxygen on earth. The enzyme active site is thought to possess 4 manganese atoms but is of unknown structure. In collaboration

with S. P. Cramer, we have performed polarized X-ray absorption spectroscopy on the water splitting enzyme prepared in oriented membranous multilayers, which are ordered in one dimension. The Mn EXAFS Fourier transforms for three different orientations are shown in Fig. 3. The data indicate that the manganese is

Figure 3.

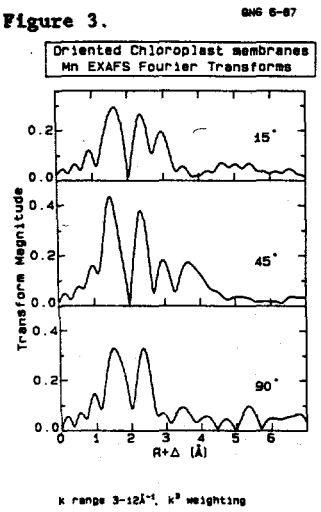

coordinated by oxygen or nitrogen at a mean distance of 1.9Å from the metal. Two different Mn-Mn interactions can be discerned; 2-3 at 2.7Å and 0.5-1 at 3.3Å. The orientation dependence of the latter indicates that the 3.3Å Mn-Mn vector lies approximately along the membrane normal, while for the former a mean angle between the membrane normal and the 2.7Å Mn-Mn vector of about 55° is indicated. The results suggest that the active site contains a tetranuclear manganese cluster. One possible geometry for this is illustrated in Fig. 4.

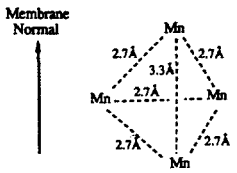

Figure 4. Proposed Mn geometry in the water splitting enzyme.

CRYSTAL STRUCTURE DETERMINATION OF CUCUMBER BASIC PROTEIN USING MULTIPLE ENERGY ANOMALOUS DISPERSION PHASING

Ethan A. Merritt, R. Paul Phizackerley, Keith O. Hodgson, B. Hedman
SSRL, Stanford University, Stanford, California

Hans C. Freeman, J. Mitchell Guss
Dept. of Inorganic Chemistry, University of Sydney, Sydney, Australia

We have determined the crystal structure of Cucumber Basic Protein, a 96 residue blue copper protein, from single crystal x-ray diffraction data collected at four x-ray energies across the Cu K-edge. Crystallographic phases were calculated from the measured difference in Bragg diffraction intensities at the four x-ray energies. The CBP structure has resisted solution using standard crystallographic techniques for some years, and is one of the first macromolecular structures to be solved using Multiple Energy Anomalous Dispersion (MAD) phasing. The successful determination of this M_r 10,000 structure from the anomalous dispersion signal provided by a single copper atom is encouraging for the future importance of the MAD technique.

CBP crystallizes in space group $P2_12_12_1$, with a = 30.88Å, b = 46.41Å, c = 65.57Å, Z = 4 [1]. Though its biological significance remains unknown, CBP has nonetheless attracted interest because its spectroscopic properties and primary structure resemble those of stellacyanin - a much-studied blue copper protein which has never successfully been crystallized. We hope that analysis of the CBP structure will increase our understanding of the copper site in the family of 'blue' copper proteins.

The initial step in the experiment was to characterize the anomalous dispersion terms f' and f" as a function of x-ray energy. These were obtained from fluorescence spectra, measured from the sample crystal prior to crystallographic data collection, using K. Eichhorn's program DISCO (see Figure 1). Four collection energies were chosen so as to maximize the variation in the f' and f" contributions to the total scattering among the selected energies. The SSRL Area Detector system on beamline I-5AD [2] was used to record electronic diffraction images, each corresponding to a small rotation of the sample crystal (0.12° to 0.20°); each rotation and exposure was repeated in succession at the four different x-ray energies. Only two sample crystals were required for this data collection. From these images a total of 85374 integrated Bragg intensitites were extracted. The data set was 95% complete (at the highest x-ray energy) to a resolution of 2.5Å. The data were scaled and averaged over redundant and symmetry equivalent measurements to obtain a consensus value for the intensity of each reflection, resulting in 3550 unique reflections to 2.5Å resolution, where each reflection was represented by up to 8 distinct data points (F^+ and F^- Bijvoet pairs at four energies).

From these values the partial contribution $|F_{Cu}|$ of the copper atom to each reflection was derived using the algorithm of Karle [3] as implemented in W.A. Hendrickson's MADLSQ program. A Patterson synthesis using coefficients $|F_{Cu}|^2$ clearly revealed the crystal coordinates of the copper atom (subject to an ambiguity in the sign of one coordinate). Given the copper coordinates, the f' and f" terms for Cu at each energy, and the observed net diffraction intensities, it was then possible to assign a crystallographic phase to each reflection. The ambiguity in copper coordinates was resolved by inspection of the corresponding electron density maps, only one of which showed a plausible molecular boundary. Crystallographic phases were improved by solvent flattening prior to building an initial atomic model of the structure. The model structure has now been refined to a crystallographic R factor of 0.22 at 2.5Å; further refinement at higher resolution is now in progress.

[1] P.M. Colman, H.C. Freeman, J.M. Guss, M. Murata, V.A. Norris, J.A.M. Ramshaw, M.P. Venkatappa, & L.E. Vickery, J. Mol. Biol. 112, 649-650 (1977).
[2] R.P. Phizackerley, C.W. Cork, & E.A. Merritt, Nucl. Instr. and Meth. A246, 579-595 (1986).
[3] J. Karle, Int. J. Quantum Chem.: Quantum Biology Symp. 7, 357-367 (1980).

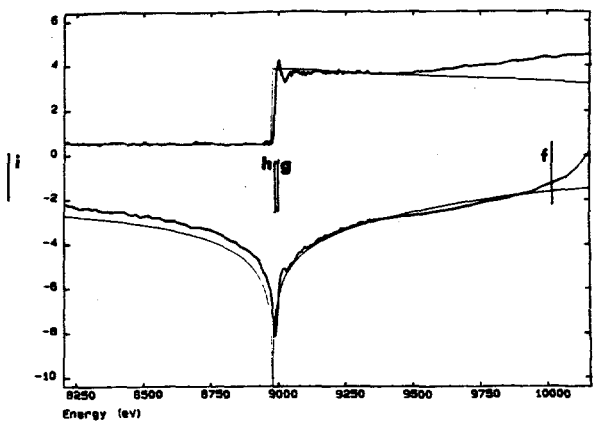

Figure 1: Anomalous dispersion terms f' (bottom) and f" (top), in electrons, as a function of x-ray energy across the Cu K edge. Experimental f" (heavy line) was measured from x-ray fluorescence from a single crystal of CBP, and fit to the ideal Cu K edge (faint line). Values of f' are from numerical integration of the corresponding f" spectra. X-ray energies used for crystallographic data collection are marked f,g,h,i.

LOW TEMPERATURE PHOTOLYSIS/RECOMBINATION OF HEMOPROTEINS UNDER CONDITIONS OF NUCLEAR TUNNELING

B. Chance[+*], G. Bunker*, K. Zhang*, K.S. Reddy[+], H. Oyanagi[#], S. Sligar[@], B. Springer[@]

[+]University City Science Center, Institute for Structural & Functional Studies, Philadelphia, PA
*University of Pennsylvania School of Medicine, Department of Biochemistry & Biophysics, Philadelphia, PA
[#]Electrotechnical Laboratory, Sakuramura, Niiharigun, Ibaraki, Japan
[@]University of Illinois, Department of Biochemistry, Springfield, IL

INTRODUCTION

The goal of our studies is to understand the structural and functional dynamics of myoglobin and hemoglobin using optical, EPR, EXAFS and EXANES techniques. Photolysis and recombination of carboxymyoglobin (MbCO) at low temperature has been studied thoroughly by optical methods. Apart from the static recombination technique, which has been used to determine the rate of various phases of MbCO kinetics, we have used the combination of steady-state photolysis and perturbation of the system by light and heat pulses under steady state conditions. This technique has a great advantage over static kinetic methods, as here one can study the nature of selected populations either by the temperature jump or by the light input method for elucidating the dynamic aspects of the particular selected population. The temperature jump technique indicated that the high temperature photoproduct recombines slower than the low temperature photoproduct. This observation sheds new light on theories of conformational substrates of protein at low temperature (<180 K). The phenomena have important implications on low temperature studies.

Recombination Kinetics of Heme Compounds

We are also studying the MbO_2 and MbNO reaction dynamics using light perturbation techniques. Preliminary studies of MbNO using EPR techniques have been completed.

Effect of Distal Histidine

There are a number of reports where distal histidine (E_7) in myoglobin plays an important role in controlling the reactivity of heme with O_2, CO and NO molecules. In fact, it has been postulated that distal histidine may have a non-bonding interaction with heme iron, and discriminates the O_2 and CO recombination. To test this hypothesis we are collaborating with S. Sligar and B. Springer (University of Illinois), who provided us with a number of mutant myoglobins, where the distal histidine is substituted with a variety of amino acids. The EXAFS study of some mutants Mb were completed; the data are now being analyzed.

EXAFS AND EXANES EXPERIMENTS

EXAFS and EXANES are very important techniques which are capable of providing direct local structural information on proteins in solution state. Our EXAFS studies in 1987 had three implications.

1. Our previous EXAFS studies of MbCO and Mb*CO were in disagreement with other low temperature spectroscopic techniques (1,2). Alben, et al, contradicted our EXAFS results, saying that the MbCO samples of 1 mm and 1 mm thickness cannot be photolyzable. We have repeated these experiments and confirmed that at low temperature (~10 K) we can photolyze MbCO up to 2 mm by using continuous illumination with a tungsten lamp but with a measured sample temperature rise.

2. We have also completed EXAFS experiments with high temperature MbCO photoproduct to determine whether the CO is still near to the Fe atom or further away.

3. A test of the hypothesis of conformational substates by measurements of the Debye-Waller factor for MbCO, MbNO and deoxy Mb at various temperatures below 200 K.

EXAFS DATA ANALYSIS AND RESULTS

We have recently used XANES to analyze our collected data on a continuous basis. The ligand field indicator (LFIR) as defined previously (3) is due to the interference between the first three coordinates around the iron atom in Mb. The LFIR differences found in the photoproducts at different temperatures indicate that the structure depends on temperature. A simulation, in which the LFIR was reconstructed by modeling the first coordination shell, has been performed. It is found that the indicator is indeed sensitive to the iron porphyrin nitrogen distance and also to the Fe-CO distance in MbCO (4). Therefore it can be used to determine the Fe-CO distance in MbCO more accurately or to reduce beam time requirement by taking the LFIR as an indicator for structural changes in hemeproteins.

In addition to the LFIR simulation, we have also done a near edge fit for the data. With a good agreement, both methods give the same structure for deoxyMb and MbCO. The fitting shows that the photoproduct at low temperature (10 K) relaxed towards deoxyMb, and relaxed only a little (40 and 60 K) while at higher temperatures. Further studies are being taken to establish the structures for the photoproducts.

The conformational substate (5) would introduce additional disorder and alter the behavior of the temperature dependence of the Debye-Waller factor. The temperature dependence experiment for various forms of Mb (MbCO, MbNO and deoxyMb) below 200 K were performed. Our preliminary analysis did not find significant changes, other than thermal, of the Debye-Waller factor. The same study on higher temperatures is going to be done when beam time is available.

The preliminary data analysis for the mutant (Methionine replacing distal histidine) deoxyMB and the 10 K photoproduct showed that both spectra of the photoproduct for the mutant and sperm-whale are similar, although the deoxyMb spectra showed some differences. Further investigations are needed to study the effects of distal histadine on photolysis and structure.

Time-resolved studies of the reaction of Hb and CO (1006B) have been carried out and a report is in preparation (G. Zhang, et al.).*

REFERENCES

1. Fiamingo, F.G., Alben, J.L., Biochemistry, 7964:24 (1985).
2. Rousseau, D.L., Argade, P.V., Proc. Natl. Acad. Sci. (USA) 83:1310 (1986).
3. Chance, B., Powers, L., Ching, Y., Poulos, T., Yamazaki, I., Paul, K.G., Arch. Biochem. Biophys., 235, 596 (1984).
4. Zhang, K., Chance, B., Reddy, K.S., Ab. submitted for the APS Meeting, New Orleans, (1988).
5. Austin, R.H., et al., Phys. Rev. Lett., 32, 403 (1974).

ACKNOWLEDGEMENT

Support: NIH Grants HL-18708,GM-31992*, DMB-8414521.

L-EDGE SPECTROSCOPY OF MOLYBDENUM COMPOUNDS AND ENZYMES

G.N. George†, W.E. Cleland, Jr.‡, J.H. Enemark§, B.E. Smith††, C.A. Kipke†, S. Roberts†, and S.P. Cramer¶,*

† Corporate Research Science Laboratories
Exxon Research and Engineering Company
Annandale, New Jersey 08801

‡ Department of Chemistry
University of Mississippi
University, Mississippi 38677

§ Department of Chemistry
University of Arizona
Tucscon, Arizona 85721

†† AFRC Unit of Nitrogen Fixation
University of Sussex
Brighton, UK BN1 9RQ

¶ Electromagnetics Department
Schlumberger-Doll Research
Ridgefield, Connecticut 06877

Molybdenum *L*-edge x-ray absorption spectra for a variety of complexes have been recorded using Beam Line VI-2 and fluorescence detection. The different initial states and relatively sharp 2 eV natural linewidth at the L_2 and L_3 edges allow observation of $4d$ splittings which are unobservable at the *K* edge. To test the relationship between optical and x-ray transitions, *L*-edge spectra of a series of compounds with oxygen and chlorine ligands were collected. In certain cases, 4 distinct $p \rightarrow d$ transitions could be deconvoluted by curve-fitting the second or third derivative spectra. These spectra were compared with the optical data for the same compounds, as well as for Tc analogues. $L_{2,3}$ edge spectra were found to be qualitative probes of the Mo *d*-level splittings, but as shown in Table 1, quantitative interpretation requires significant corrections for the core-hole perturbation and possible electron-electron interactions. Further confirmation of the assignments was obtained by using single crystal spectra for $[N(C_2H_5)_4][MoOCl_4(H_2O)]$.

Table 1 - Mo X-Ray Splittings *vs.* Optical Splittings for Mo Compounds and Tc Analogues

Mo Complex	Tc Analog	Mo,Tc Ground State Configurations	Optical Transition or Splitting	Mo Optical Energy (eV)	Tc Optical Energy (eV)	X-Ray Splitting (eV) L_3	X-Ray Splitting (eV) L_2
MoO_4^{2-}	TcO_4^-	d^0	$E - T_2$	1.68[a]	2.36[a], 2.31[j]	2.48	2.19
MoS_4^{2-}	TcS_4^-	d^0	$E - T_2$	1.25[b], 1.21[a]	-	1.41	1.32
$MoOCl_4^-$	$TcOCl_4^-$	d^1, d^2	$d_{xy} \rightarrow d_{xz,yz}$ $d_{xy} \rightarrow d_{x^2-y^2}$ $d_{xy} \rightarrow d_{z^2}$	1.77[c,d] 2.80[c,d]	1.59[k]	1.21 2.83 4.28	- 2.81 4.12
$MoOCl_3^{2-}$	$TcOCl_3^{2-}$	d^1, d^2	$d_{xy} \rightarrow d_{xy,yz}$ $dxy \rightarrow d_{x^2-y^2}$ $d_{xy} \rightarrow d_{z^2}$	1.71[e,f] 2.78[e,f]	1.32[l] 2.07[l],2.55[l]	1.21 2.85 4.49	0.78 1.99 3.86
$LMoOCl_2$	$LTcOCl_2$	d^1, d^2	$\phi_1 \rightarrow \phi_{2,3}$ $\phi_1 \rightarrow \phi_4$	1.76[g]	1.58	1.26 3.24 4.76	0.9 2.86 4.40
$LMoSCl_2$		d^1	$\phi_1 \rightarrow \phi_{2,3}$	1.13[g]	-		(2.57)

A preliminary spectral analysis of several molybdenum enzymes has been done. L_3-edge splittings of 1.72 and 1.40 eV were observed for nitrogenase and active xanthine oxidase, respectively. Oxidized sulfite oxidase had a more complicated edge structure with L_3-edge splittings of 1.05, 2.14, and 3.05 eV. Since EXAFS indicates similar ligands for sulfite oxidase and desulfo xanthine oxidase (2 Mo=O and at least 2 Mo-SR), some of the differences may arise from geometric effects. In general, the results of this study suggest that *L*-edge spectroscopy is a useful technique for studying the electronic structure of Mo in small molecules, enzymes, and catalysts, especially if such materials are available in oriented forms.

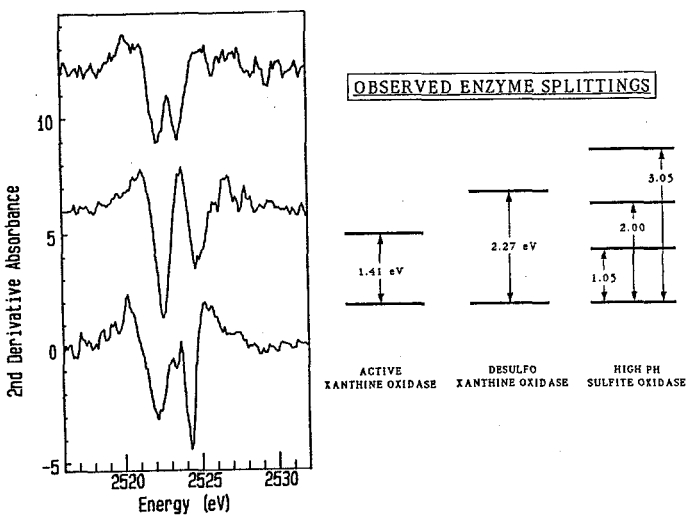

Figure 1. a) L_3-edge 2nd derivative curves for (top to bottom) active xanthine oxidase, desulfo xanthine oxidase, and sulfite oxidase. b) d-orbital splittings for molybdenum enzymes derived from *L*-edge spectra.

XAS INVESTIGATIONS OF RIESKE-LIKE IRON SULFUR CENTERS

Proposal No. 1035B

H.T. Tsang and J.E. Penner-Hahn
Department of Chemistry, University of Michigan, Ann Arbor, MI 48109

C.J. Batie and D.P. Ballou
Department of Biological Chemistry, University of Michigan, Ann Arbor, MI 48109

The phthalate dioxygenase (PDO) from *Pseudomonas cepacia* catalyzes the dioxygenation of phthalate to a dihydrodiol. PDO contains two Fe atoms in a binuclear site and a third, dissociable iron in a mononuclear site. The binuclear site is a [2Fe-2S] Rieske-like cluster. Rieske-like clusters are spectroscopically distinct from other Fe/S clusters, and recent ENDOR measurements have shown that Rieske-like clusters contain at least two nitrogen atoms in place of the more normal thiolate ligands [1]. The mononuclear site is believed to be the site of oxygen activation, however very little is known about the nature of this site.

We have used EXAFS spectroscopy to characterize the Rieske-like and the mononuclear sites in PDO. In order to study selectively the Rieske-like site, we measured data for PDO in which the mononuclear Fe had been removed. In order to study selectively the mononuclear site, we measured Zn and Co EXAFS for PDO samples in which the mononuclear site had been reconstituted with Zn or Co.

EXPERIMENTAL

X-ray absorption data were measured on beam-line 7-3 using Si(220) monochromator crystals. A Stern-Heald detector was used to monitor protein X-ray fluorescence. Protein concentrations were ca. 4 mM. Spectra were measured at 4-10 K. The samples which have been examined include: native (3Fe) protein (fully reduced); 2 Fe (Rieske-like cluster only) protein in both oxidized and reduced forms; and reconstituted protein (2Fe+M, M=Zn,Co). Mixed metal derivatives were studied in forms having oxidized or reduced Rieske-like clusters and in the presence and absence of substrate (phthalate).

RESULTS

RIESKE-LIKE CLUSTER. We previously reported that the EXAFS spectra for the Rieske-like site showed the expected Fe-S and Fe-Fe scattering [2] and that these data indicated a structural rearrangement of the Fe/S cluster on reduction [3]. We have now completed quantitative curve fitting analysis of these data with the results shown in Table I. The structural parameters are consistent with those seen for other Fe/S clusters. The increase in Fe-S bond length on reduction is somewhat greater than that observed for ferredoxin-like clusters, possibly reflecting the less polarizable nature of the ligands in the present case. As previously reported [3], the Rieske-like structure is unaffected by either the metal in the mononuclear site or the binding of substrate.

An interesting observation regarding the Rieske-like site is that it has not proven possible to demonstrate, using EXAFS alone, that the are any nitrogen ligands coordinated to the Fe [4]. The improvement in fit quality for a 2 shell fit (S+N) relative to a 1 shell fit is modest and would not by itself provide convincing evidence for non-sulfur ligation. In spite of this, the position of the nitrogen shell is well defined if this shell is included in the fit. The inability to unambiguously identify ligands which are known to be present in the coordination sphere has important implications for applications of EXAFS to the elucidation of completely unknown structures.

Table I.
Curve Fitting For Rieske-like Cluster[a]

	Fe-S[b]	Fe-N[b]	Fe-Fe[b]
Oxidized	2.20(2)	2.01(5)	2.68(4)
Reduced	2.24(2)	2.08(5)	2.67(4)
ΔR^c	0.031(10)		0
$\Delta\sigma^2$	0.012(5)		0

[a]Isolated shells were fit using 3S+1N (first shell) or 1 Fe (second shell). Amplitude and phase parameters determined empirically.
[b]Tabulated numbers are fitted parameters (estimated uncertainties).
[c]ΔR and $\Delta\sigma^2$ are the change between oxidized and reduced Rieske clusters. These parameters were determined by the phase difference/amplitude ratio method.

MONONUCLEAR SITE. Curve fitting analysis of the Zn EXAFS for the Zn reconstituted protein shows that this site contains predominantly N or O ligation and can be well modeled by 6 nitrogens at 2.01 Å. The EXAFS shows no detectable change in mononuclear-site structure when the Rieske-like site is reduced or when substrate is bound. The Zn-XANES, however, are quite sensitive to these effects, as shown in Fig. 1. In order to explore further these observations, we have recently measured Co XANES for the Co substituted enzyme. These data show the same qualitative effects as were observed for the Zn XANES. Specifically, there is a decrease in the intensity of the principal absorption maximum for oxidized and substrate-bound forms of the enzyme relative to reduced or substrate-free forms. The similarity between the Co and Zn XANES spectra demonstrates that the observed effects are not unique to Zn and suggests that these effects may be relevant to the catalytic functioning of the enzyme.

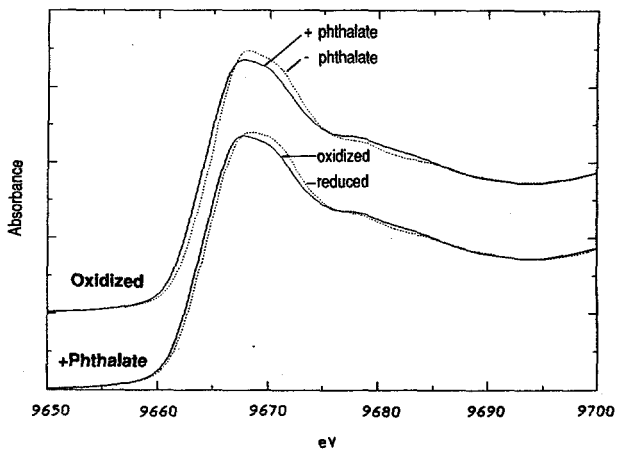

Figure 1. Normalized Zn XANES spectra for 2Fe+Zn derivatives of PDO.

The Co XANES spectra have the additional advantage of containing a 1s-3d transition. It is well known that the intensity of this transition can be correlated with distortions of a site from a centrosymmetric environment [5]. The 1s-3d transition was isolated by fitting the edge with an arctan background and subtracting this background from the observed data. Figure 2 compares the intensity of the 1s-3d transition for the different Co substituted derivatives. The intensity is increased following substrate binding or Rieske-site reduction indicating that the Co site is distorted in these forms of the protein. This may reflect protein rearrangement necessary to bind dioxygen. Quantitative analysis of the Co EXAFS data is in progress.

ACKNOWLEDGEMENTS. This work was supported in part by the NIH (GM-38047). JEPH is the recipient of a Camille and Henry Dreyfus Distinguished Young Faculty Award.

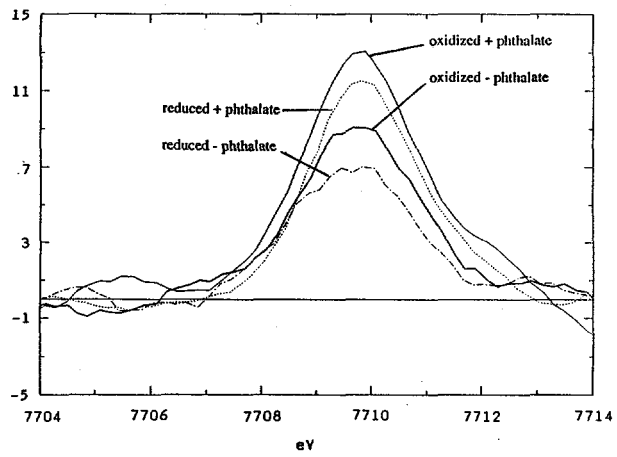

Figure 2. Isolated Co 1s-3d transition for 2Fe+Co derivatives of PDO.

REFERENCES

1. Cline, J.F.; Hoffman, B.M.; Mims, W.B.; LaHaie, E.; Ballou, D.P.; Fee, J.A., **1985**, *J. Biol. Chem.*, **260**, 3251-3254.
2. Penner-Hahn, J.E.; Batie, C.J.; Ballou, D.P., 1986 SSRL Activity Report.
3. Penner-Hahn, J.E.; Tsang, H.-T.; Batie, C.J.; Ballou, D.P. *Recl. Trav. Chim. Pays-Bas*, **1987**, *106* , 228.
4. Penner-Hahn, J.E.; Tsang, H.-T.; Batie, C.J.; Ballou, D.P. Manuscript in preparation.
5. Roe, A.L.; Scheider, D.J.; Mayer, R.J.; Pyrz, J.W.; Widom, J.; Que, L.Jr. *J. Am. Chem. Soc.*, **1984**, *106*, 1676-1681.

EXAFS ANALYSIS OF XANTHINE OXIDASE COMPLEXES WITH ALLOXANTHINE, VIOLAPTERIN AND 6-PTERIDYLALDEHYDE

R. Hille[a], G.N. George[b], M.K. Eidsness[c], and S.P. Cramer[d]

Proposal No 1040B

[a]Department of Physiological Chemistry, Ohio State University, Columbus, OH 43210, [b]Corporate Research Science Laboratories, Exxon Research and Engineering Company, Annandale, NJ 08801, [c]Department of Chemistry, University of Georgia, Athens, GA 30602, and [d]Schlumberger-Doll Research, Ridgefield, CN 06977

Introduction

Xanthine oxidase is a molybdenum-containing enzyme that catalyzes the conversion of xanthine to uric acid[1]. We have undertaken an EXAFS analysis of the enzyme in complex with three aromatic heterocycles: alloxanthine, violapterin and 6-pteridylaldehyde. Alloxanthine forms an extremely tight complex with the reduced molybdenum center of the enzyme that results in the complete loss of enzymatic activity[2]. On the basis of its EPR properties, the alloxanthine complex is presumed to be a stable structural analog to an intermediate in the catalytic cycle (that giving to the so-called Very Rapid EPR signal)[3]. The complexes of reduced enzyme with violapterin[4] and oxidized enzyme with 6-pteridylaldehyde[5] are authentic catalytic intermediates (E_{red}·P and E_{ox}·S, respectively) in the catalytic cycles of enzyme with slow substrates. The present studies have been undertaken in an effort to elucidate the structures of these catalytic intermediates or analogs.

Results and Discussion

The Fourier transforms of the Mo EXAFS data for the various complexes and model compounds studied are shown in Figure 1. In all cases the strongest peak is consistent with a long Mo-S interaction, although it is clear that other interactions are present. The spectra were quantitatively analyzed by curve-fitting the k-space data using previously described empirical phase shift and amplitude functions[6-8]. In all cases, a set of 2-3 sulfur atoms were found at approximately 2.4 A. In addition, all enzyme complexes were found to contain short Mo-O as well. In the oxidized enzyme, unambiguous evidence was found for a Mo=S interaction at 2.2A. Parameters for the final fits are given in Table 1. Surprisingly, in none of the enzyme complexes examined was the data distinguishable from uncomplexed enzyme of the same oxidation state.

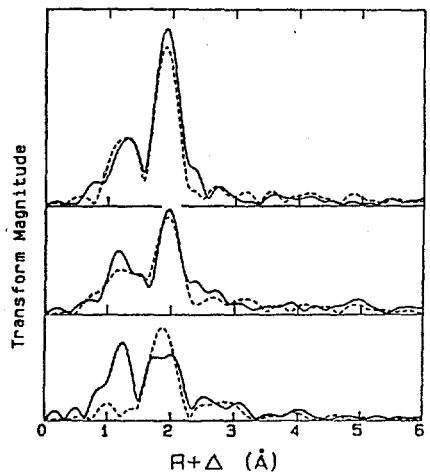

Figure 1. EXAFS Fourier transforms for top: alloxanthine-complexed (---) and free dithionite-reduced xanthine oxidase (---), middle: violapterin-complexed (---) and 6-pteridylaldehyde-complexed (---) xanthine oxidase, and bottom: $LMoO(dtc)_2$ (---) and $LMoS(dtc)_2$ (---), where dtc is the dithiocarbamato ligand.

Table 1. Summary of Curve-Fitting Results

	Mo-SR			Mo=O			Mo=S		
Sample	N*	R*, Å	σ^2*, Å²*	N	R, Å	σ^2, Å²	N	R, Å	σ^2, Å²
dithionite-reduced xanthine oxidase	2	2.38	0.021						
	3	2.38	0.047						
	3	2.38	0.046	1	1.67	0.039			
alloxanthine-inhibited xanthine oxidase	2	2.38	0.0002						
	3	2.38	0.0014						
	3	2.38	0.0032	1	2.70	0.0015			
	3	2.38	0.0023	1	1.68	0.0019			
violapterin-complexed xanthine oxidase	2	2.40	0.0026						
	2	2.40	0.0015	1	1.66	0.0029			
	3	2.40	0.0015	1	1.66	0.0029			
pteridylaldehyde-complexed xanthine oxidase	2	2.47							
	2	2.47		1	1.71				
	2	2.47		1	1.71		1	2.20	

In the case of the alloxanthine complex, the presence of a Mo=O group indicates that previous structures proposed for the complex, wherein the Mo=O bond is either disrupted altogether or elongated due to hydrogen bonding to the alloxanthine molecule[3,8], cannot be correct, and alternate structures must therefore be considered. In the cases of the violaptein and 6-pteridylaldehyde complexes, binding of the heterocycles must result in only minor pertubations of the molybdenum coordination sphere. This is surprising since both complexes exhibit relatively strong charge-transfer bands, indicating substantial interaction between the molybdenum center and the heterocycle in each case. As with the alloxanthine complex, structures in which the Mo=O group, and in the case of the oxidized enzyme complex with 6-pteridylaldehyde the Mo=S as well, is missing may be discounted. The Mo=O group thus appears to be a particularly consistent feature of the molybdenum center of xanthine oxidase throughout the course of catalysis (from E_{ox}·S through the Very Rapid intermediate to E_{red}·). This conclusion is quite surprising given the recent evidence that it is this oxygen atom that is incorporated into substrate in the hydroxylation event[9]. Future work is planned to further examine this apparently paradoxical situation.

Acknowledgements

This work was supported by the National Science Foundation (DMB 85-21645 to R.H.). Part of this work was undertaken at SSRL, which is supported by the Department of Energy, Office of Basic Energy Sciences.

References

1. Hille, R., and Massey, V., in Molybdenum Enzymes (T.G. Spiro, ed.) Wiley-Interscience, New York, p. 443-517 (1985)
2. Massey, V., Komai, H., Palmer, G., and Elion, G.B., J. Biol. Chem. 245, 2837-2844 (1970)
3. Hawkes, T.R., George, G.N., and Bray, R.C., Biochem. J. 218, 961 (1984)
4. Davis, M.D., Olson, J.S., and Palmer, G., J. Biol. Chem. 257, 14730 (1982)
5. Hille, R., and Massey, V., Pharmacol. Ther. 14, 249 (1981)
6. Cramer, S.P., in "EXAFS for Inorganic Systems" (C.D. Garner, and S.S. Hasnain, eds.) Daresbury Laboratory, Daresbury, England (1981)
7. Cramer, L.P., Solomonson, L.P., Adams, M.W.W., and Mortenson, L.E., J. Am. Chem. Soc. 106, 1467 (1984)
8. Bray, R.C., Adv. Enzymol. 51, 107 (1980)
9. Hille, R., and Sprecher, H., J. Biol. Chem. 262, 10914 (1987)

CORONARY ANGIOGRAPHY IN HUMAN SUBJECTS

E. Rubenstein*, G. S. Brown**, J. C. Giacomini*, H. J. Gordon*, R. Hofstadter+, A. C. Thompson ++, H. D. Zeman***

* Department of Medicine, School of Medicine, Stanford University; ** Stanford Synchrotron Radiation Laboratory; + Hansen Laboratories of Physics and Department of Physics, Stanford University, Stanford, CA 94305; ++ Lawrence Berkeley Laboratory, University of California, Berkeley, CA 94720; ***National Synchrotron Light Source, Brookhaven National Laboratory, Long Island, NY 1197

Previous studies have demonstrated the principles of transvenous coronary angiography in humans using synchrotron radiation (1). Investigations have been continued during 1987, in an attempt to define the modifications of the imaging system needed to provide angiograms of clinical usefulness. Three subjects were studied, one of whom had undergone transvenous synchrotron angiography 11 months earlier.

The first patient in the current group of examinations was a 63-year-old man with atypical chest pain and left ventricular hypertrophy. Conventional coronary angiograms had been interpreted as showing normal vessels. Coronary spasm was suspected but not demonstrated. Transvenous coronary angiograms revealed normal appearing vessels. The left anterior descending coronary artery, a diagonal branch, and the obtuse marginal branch of the circumflex artery were visualized (Figure 1). The image was recorded in the right anterior oblique position (-10°). The X-ray exposure for the frame was 0.14 rad.

The second patient was a 64-year-old man with angina pectoris related to narrowing of the middle segment of the left anterior descending coronary artery, which had not responded adequately to three prior transvenous balloon angioplastic procedures. A transvenous synchrotron scan, recorded in the left lateral position, confirmed the persistence of the stenosis. An image recorded with the patient in the left anterior oblique (30°) position at a time when the bolus of contrast agent had largely cleared the right side of the circulation showed a normal-appearing right coronary artery clearly visible through the thinly opacified right ventricle (Figure 2). The X-ray dose for each of these frames was 0.2 rad.

The third patient was a 42-year-old man who had been examined by the synchrotron radiation transvenous angiographic method in May, 1986. During the interval he had undergone revision of an internal mammary artery and a saphenous vein bypass graft, and had suffered a mild myocardial infarction involving the left lateral wall. The second transvenous study revealed improved perfusion of the left anterior descending coronary artery, presumably a consequence of the revision of the internal mammary artery graft, but loss of one of the original vein bypass grafts, believed to have supplied an obtuse marginal branch.

These studies confirm the feasibility of the synchrotron radiation approach, and also confirm that greater X-ray fluence is needed to provide images of clinical quality.

References:
(1) Rubenstein, E., Hofstadter, R., Zeman, H.D., Thompson, A.C., Otis, J.N., Brown, G.S., Giacomini, J.C., Gordon, H.J., Kernoff, R.S., Harrison, D.C., Thomlinson, W. Transvenous coronary angiography in humans using synchrotron radiation. Proceedings of the National Academy of Sciences USA, 83:9724, 1986.

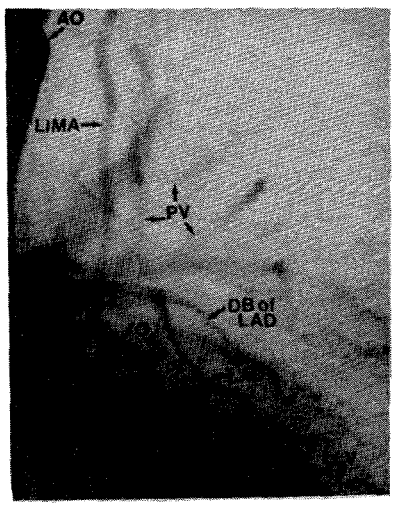

(Fig. 1)

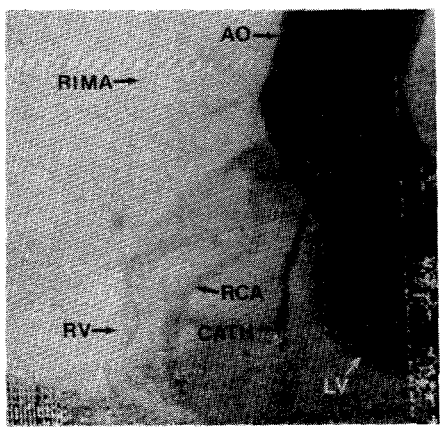

(Fig. 2)

X-RAY ABSORPTION SPECTROSCOPIC CHARACTERIZATION OF THE MN IN BIOLOGICAL SYSTEMS

J. E. Penner-Hahn, V. L. Pecoraro, R. M. Fronko and H.-T. Tsang.
Department of Chemistry, University of Michigan, Ann Arbor, MI 48109-1055.
C. F. Yocum and S. Betts.
Department of Biology, University of Michigan, Ann Arbor, MI 48109-1048.

Manganoenzymes play an important role in mediating the chemistry of O_2 and the various reduced forms of O_2 in the biosphere. In particular, the oxygen evolving complex (OEC) of Photosystem II (PSII) catalyzes the water oxidation reaction while the manganese containing catalase from *L. plantarum* functions in the disproportionation of H_2O_2 to H_2O and O_2. The nuclearity, structure and oxidation state(s) of the manganese cluster associated with the OEC have attracted much interest and effort in recent years. The Mn-catalase, which has only recently been purified, is believed to contain two Mn atoms per subunit but is otherwise essentially uncharacterized.

It is well known that the energy of an x-ray absorption edge is correlated with the oxidation state of the absorbing atom. The current interpretation of x-ray absorption near edge structure (XANES) assumes that the observed edge energy for a mixed valent Mn cluster will be independent of Mn-Mn separation and Mn-Mn geometry, and thus that edge energy may be used to determine the average oxidation state of a multinuclear cluster. In order to evaluate this hypothesis, we have measured the XANES spectra for a series of trinuclear Mn(III/II/III) complexes. The trinuclear complexes have a Mn-Mn separation that varies from 3.50 to 3.27 Å and a Mn-Mn-Mn angle that varies from 138.5 to 180 degrees. In addition, the XANES spectra of a series of mono- and dinuclear Mn(II) and Mn(III) complexes were measured. All of the models are crystallographically characterized and all have oxygen/nitrogen ligation (this is believed to be the ligation for Mn in the OEC [1]).

EXPERIMENTAL. OEC samples were prepared according to Yocum, et al. [2]. A multi-element intrinsic Ge detector (courtesy of S. Cramer) was used to detect the Mn fluorescence for the OEC and Mn-catalase samples. The Mn concentration for the OEC was 1.5 mM and the Mn-catalase was 0.150 mM. All measurements were made at 12 K. Energy calibration was referenced to the $KMnO_4$ pre-edge feature (assigned as 6543.3 eV). The edge energies in Table I are defined as the energy of the first inflection point.

Table I

Complex	Oxid. state, nuclearity	Edge (eV)
$Mn(imidazole)_6^{+2}$	II, mononuclear	6547.2
$Mn(AcO)_2(H_2O)_2$	II, mononuclear	6548.6
Mn_2(SALPS)	II, dinuclear	6547.1
[Mn(DALAPH)]$_c$	II, dinuclear	6549.1
$Mn(urea)_6^{+3}$	III, mononuclear	6551.5
$Mn(acac)_3$	III, mononuclear	6552.9
Mn(SALPN)(AcO)	III, mononuclear	6550.4
{Mn[(2-OH)5-Cl-SALPN]}$_2$	III, dinuclear	6551.2
$(MnSALAHP)_2$	III, dinuclear	6552.2
MVLP	III/II/III, trinuclear	6549.6
MVBM	III/II/III, trinuclear	6549.6
MVLH	III/II/III, trinuclear	6550.7
MVLW	III/II/III, trinuclear	6549.6
Mn-catalase	unknown	6547.9
OEC, dark adapted	unknown, sample 1	6550.1
OEC, dark adapted	unknown, sample 2	6549.7

MVLH = Mn_3[(2-OH)SALPN]$_2$(AcO)$_4$; MVLW = Mn_3(SALADHP)$_2$(AcO)$_4$(H$_2$O)$_2$ 2MeOH; MVLP = Mn_3(SALADHP)$_2$(AcO)$_4$(pyrOH)$_2$H$_2$O; MVBM = Mn_3(SALADHP)$_2$(AcO)$_4$(MeOH)$_2$ (<Mn-Mn-Mn = 138.5°). SALAHP, SALPS, DALAHP, SALPN are Schiff base ligands condensed from salicylic acid and a secondary amine.

RESULTS

BIOLOGICAL STUDIES. The edge energies for several of the complexes are listed in Table I. The increase in edge energy with increasing oxidation state described by Klein, et al. [3], is readily apparent. The XANES for resting state Mn-catalase closely resembles that for Mn(II) complexes, however the low concentration of this sample precludes definitive characterization at this time.

In Figure 1 we compare the XANES spectra for two different OEC samples (solid lines) with those for Mn (II) models (dashed lines) and Mn(III) models (dotted lines). The edge energy of the OEC is consistent with a mixture of Mn(II) and Mn(III) since the OEC edge lies between those of authentic Mn(II) and Mn(III) complexes (see also Table 1). However, the large (ca. 2 eV) spread in edge energies for a given oxidation state suggests that it will be difficult to unambiguously assign oxidation state based solely on the energy of the absorption edge. This concern is particularly important given the breadth of the OEC edge in comparison with the edges for the model compounds (see Fig. 1). This breadth suggests that the Mn in the OEC is present in a number of distinct sites.

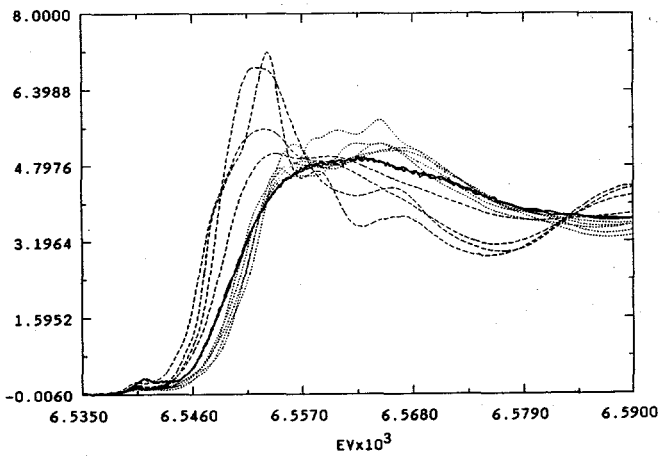

Figure 1. XANES spectra for: the OEC (solid line); Mn(II) model compounds (dashed line); and Mn(III) model compounds (dotted line). All of the model compounds have oxygen/nitrogen ligation.

In addition to XANES data, EXAFS data were also measured for the OEC. The combination of highly concentrated samples and solid state fluorescence detection allowed the measurement of EXAFS data having an excellent signal/noise ratio (see Fig. 2). Analysis of these data is currently in progress.

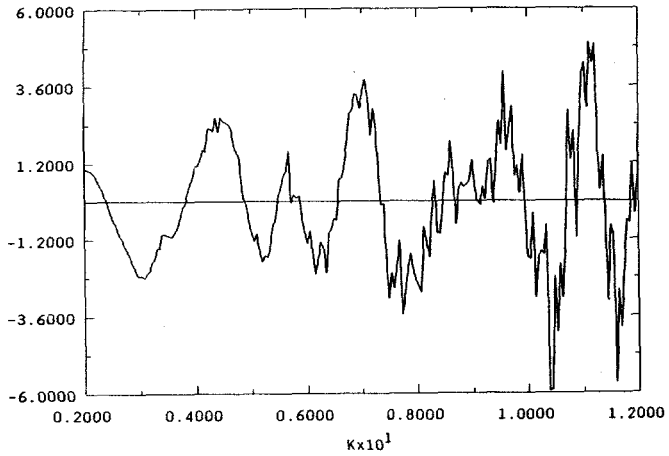

Figure 2. EXAFS data for the OEC. Data are weighted by k^3 and have not been smoothed.

MODEL COMPOUNDS. In order to determine the effect of mixed valence on the XANES, we measured XANES spectra for four crystallographically characterized mixed valence Mn(III/II/III) complexes. These spectra (Fig. 3) demonstrate that small changes in the metal environment can lead to moderately large changes in the XANES spectrum. Thus, the feature at 6564 eV increases in intensity with increasing Mn(II)-O distance, while the feature at 6553 eV seems to be correlated with a long (> 3.4 Å) Mn-Mn distance.

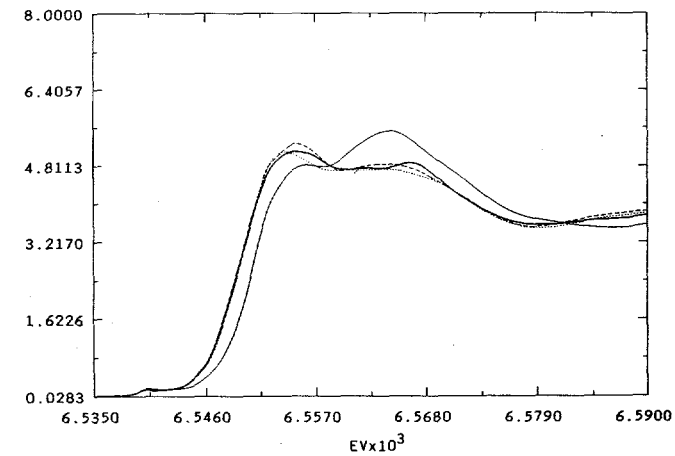

Figure 3. XANES spectra for mixed valence Mn(III/II/III) model compounds. Spectra with lower edge energies are MVLP (solid), MVLW (dash) and MVBM (dotted). The MVLH edge occurs at ca. 1 eV higher energy.

The most striking variation, however, is the ca. 1 eV shift in edge energy amongst the mixed valence complexes. Since the complexes have identical Schiff base ligation and similar coordination environments, we can rule out gross geometrical changes as the origin of this effect. Model studies and polarization dependent measurements are in progress in an attempt to understand this phenomenon. It is unclear what, if any, structural relevance the trinuclear complexes have to the OEC, however it is of interest to note that edge shifts of this magnitude (1 eV) have previously been attributed to oxidation of one of the Mn ions in the OEC [4].

ACKNOWLEDGEMENTS. This work was supported in part by the NIH (GM-38047). JEPH is the recipient of a Camille and Henry Dreyfus Distinguished Young Faculty Award.

REFERENCES

1. Kirby, J.A.; Robertson, A.S.; Smith, J.P.; Thompson, A.C.; Cooper, S.R.; Klein M.P. *J. Am. Chem. Soc.*, **1981**, *103*, 5529.
2. Ghanotakis, D.F.; Demetriou, D.M.; Yocum, C.F. *Biochim. Biophys. Acta* **1987**, *891*, 15.
3. Kirby, J.A.; Goodin, D.B.; Wydrzynski, T.; Robertson, A.S.; Klein, M.P.; Sauer, K. *J. Am. Chem. Soc.*, **1981**, *103*, 5537.
4. a) Goodin, D.B.; Yachandra, V.K.; Britt, R.D.; Sauer, K.; Klein, M.R. *Biochim. Biophys. Acta*, **1984**, *767*, 209. b) Yachandra, V.K.; Guiles, R.D.; McDermott, A.E.; COle, J.L.; Britt, R.D.; Dexheimer, S.L.; Sauer, K.; Klein, M.P. *Biochem.* **1987**, *26*, 5974.

ANOMALOUS DIFFRACTION MEASUREMENTS FROM PROTEIN CRYSTALS

Wayne A. Hendrickson, John R. Horton, Craig M. Ogata, William E. Royer Jr., and Wei Yang

Howard Hughes Medical Institute
Department of Biochemistry and Molecular Biophysics
Columbia University, New York, NY 10032

and

Ethan A. Merritt and R. Paul Phizackerley

Stanford Synchrotron Radiation Laboratory
Stanford, CA 94305

INTRODUCTION

Methods have been developed for the measurement and analysis of diffraction measurements made at a few select wavelengths associated with the absorption edges of appropriate anomalous scatterers in macromolecular crystals. During the past year, we have applied our procedures for analyzing multiwavelength anomalous diffraction (MAD) measurement made earlier at SSRL and at the Photon Factory in Japan. This work has led to a phase evaluation for lamprey hemoglobin and to three-dimensional structure for a bacterial ferredoxin and for streptavidin. New measurements have also been made during 1987 on two other crystalline proteins. The analysis of these data is still in progress.

UROCHIS HEMOGLOBIN

We had previously measured a set of data complete to 5.5A spacing from the hemoglobin of Urechis caupa, an echiuran known as the innkeeper worm. This hemoglobin crystallizes in space group $C222_1$, with a=104.8, b=54.9 and c=110.6A. These crystals were grown and provided by Dr. Marvin L. Hackert and his collaborators at the University of Texas. Unfortunately, these data proved to be too weak and inaccurate to be useful even for the location of iron center. The present work was made possible by the availability of larger crystals.

During January of 1987 we measured data at four wavelengths (1.5000, 1.7382, 1.7400 and 1.8000A) related to the iron K edge. Due to beam conditions, there was inadequate time to complete a full 3A data set. However, with a full quadrant of coverage in rotation about b (100°) and a fill in of 34° about a from one crystal together with additional partial data from rotation about c, a complete 5.5A set was obtained. The MAD data have been processed and are markedly superior to those obtained previously. The phasing analysis has not been pursued, however, as our collaborators meanwhile solved the structure.

THIOREDOXIN

In collaboration with Dr. David LeMaster of Yale University, we have produced E. coli thioredoxin in which the methionine residues have been replaced by selenomethionines. This was done by expression of recombinant DNA in plasmids that had been introduced into an E. coli strain made defective in methionine synthesis. This protein has been crystallized under conditions similar to those used earlier by Holmgren et al. (PNAS 72, 2305, 1975), but ones sufficiently changed that unit cell dimensions differ appreciably. Our crystals are in space group C2 with a=89.2, b=49.6, c=57.8A and $=100.2^\circ$ whereas the earlier crystals had lattice dimensions of a=89.7, b=51.1, c=60.3 and $=113.5^\circ$.

During December 1987 we measured diffraction data at five wavelengths (0.9000, 0.9791, 0.9794, 1.3776 and 1.3787A) associated with absorption edges of the copper and selenium present in these crystals. The crystal had dimensions of 0.3 x 0.3 x 0.6 mm. Data were measured with the detector at 400 mm from the crystal. A full 180° rotation was made about the b-axis, and these data were supplemented by omega-axis fill-ins with 26° of rotation about a* and some additional measurement about c*. Preliminary data reduction results indicate that counting statistics will not be limiting in the analysis.

CRYSTAL STRUCTURE DETERMINATION OF AMICYANIN USING MULTIPLE ENERGY ANOMALOUS DISPERSION PHASING

Ethan A. Merritt, R. Paul Phizackerley
SSRL, Stanford University, Stanford, California

Louis Lim, F. Scott Mathews
Washington University Medical School, St. Louis, Missouri

Amicyanins are small blue copper proteins which mediate the transfer of electrons from methylamine dehydrogenase to c-type cytochromes in several methylotrophic bacteria. The amicyanins share spectroscopic properties with other blue copper proteins, but perform a different biological function than those copper proteins which have been previously studied. We report here our efforts to determine the structure of an amicyanin from the facultative methylotroph P. denitrificans.

P. denitrificans amicyanin is a 129 residue protein which crystallizes in space group $P2_1$ with a = 28.90Å, b = 56.61Å, c = 27.55Å, and β = 96.41° [1]. Crystallographic data were collected from a single crystal of native amicyanin at four x-ray energies (see Table 1) across the copper K absorption edge using the area detector system on beamline I-5AD [2]. After scaling and merging the measured Bragg intensities the data set consisted of 2983 unique **hkl** (15Å to 2.5Å), of which 2729 were represented by four or more of the eight possible observations ($|F+|^2$ and $|F-|^2$ at four energies), and 2311 were represented by all eight. The merging R factor for the intensities to this resolution was 0.052. For each reflection **hkl** an estimate of |Fa|, the anomalous scattering contribution of the copper atom, was derived using the algorithm of Karle [3] as implemented in W. A. Hendrickson's MADLSQ program. A Patterson map was calculated using coefficients $|Fa|^2$ from the 1050 reflections to 3.5Å for which $|Fa|^2 < 1000$. The map (shown in Fig. 1) clearly revealed the Cu-Cu interatomic vectors, and hence the atomic coordinates of the copper atom subject to an ambiguity in the sign of one coordinate. Multiple Energy Anomalous Dispersion (MEAD) phases were assigned based on both possible assignments of copper coordinates. The MEAD phases were used to calculate electron density maps at 2.5Å resolution, which were then sharpened using automated solvent-flattening [4]. A tentative choice of the correct map has been made, and initial interpretation of the map is in progress.

[1] L.W. Lim, F.S. Mathews, M. Husain, V.L. Davidson, J. Mol. Biol. 189, 257-258 (1986)
[2] R.P. Phizackerley, C.W. Cork, & E.A. Merritt, Nucl. Instr. and Meth. A246, 579-595 (1986)
[3] J. Karle, Int. J. Quantum Chem.: Quantum Biology Symp. 7, 357-367 (1980)
[4] B.C. Wang in H. Wyckoff, C.H.W. Hirs, S.N. Timasheff (eds) Methods in Enzymology 115, 90-112.

energy:	10.030	9.002	8.990	8.500
f″:	3.27	4.09	3.12	0.54
f′:	-1.61	-6.03	-7.51	-2.61

Table 1. Amicyanin data collection energies (in keV) are shown, as well as the corresponding anomalous dispersion terms f″ and f′ (in electrons) measured by x-ray fluorescence from a single crystal of amicyanin. Derivation of f″ and f′ from fluorescence spectra was done using K. Eichhorn's program DISCO.

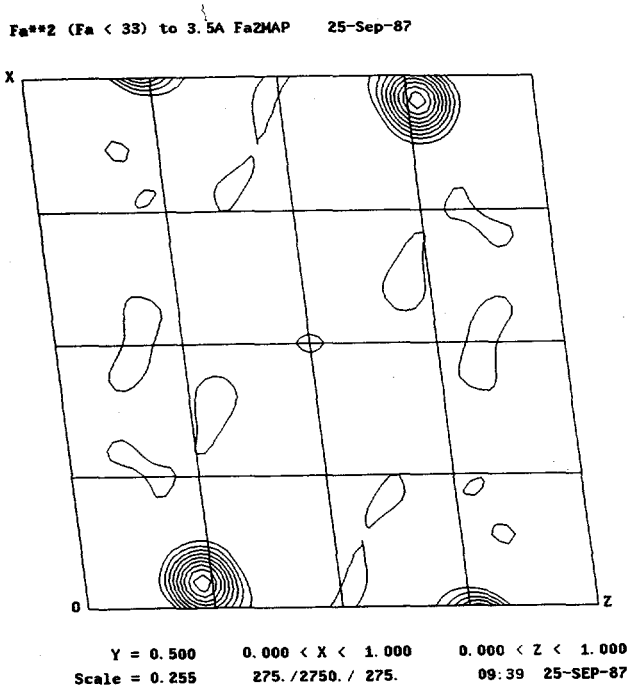

Figure 1. Harker Section at Y=0.5 of a Patterson map which clearly shows the Cu-Cu interatomic vectors.

SMALL ANGLE X-RAY SCATTERING STUDIES ON CATION BINDING SITES AND LINKING REGIONS OF BACTERIORHODOPSIN

Proposal No. 8110B

[1]S. Wakatsuki, [1]K.O. Hodgson, [3]R.M. Stroud, [2]S. Doniach & [1]U. Spann

[3]Departments of [1]Chemistry and [2]Applied Physics, Stanford University
[3]Dep. of Biochemistry and Biophysics, Univ. of California, San Francisco

INTRODUCTION

The retinal group of bacterioRhodopsin (bR) absorbs light energy and pumps protons through the purple membrane. Each bR molecule consists of 7 α-helices that align normal to the membrane plane, and form a 2D crystal with P3 symmetry. The binding of Mg^{2+} and Ca^{2+} cations to bR molecules is believed to have an important function in the photocycle. Anomalous diffraction data from Tb^{3+} ions bound to bR allow location of the cation binding sites in the 3D electron density map of the bR molecules. In electron microscopic studies the diffraction data are restricted to an area in reciprocal space outside of a conical region, called the missing cone. Small angle X-ray diffraction studies in principle can give intensity profiles in the missing cone and allow reconstruction of a complete 3D density map of the bR molecules. The phases can be calculated on the basis of electron microscopic data. Knowledge of the density distribution in the linking regions of the 7 α-helices should help both to define their linking order and to map the primary amino acid sequence onto the helices.

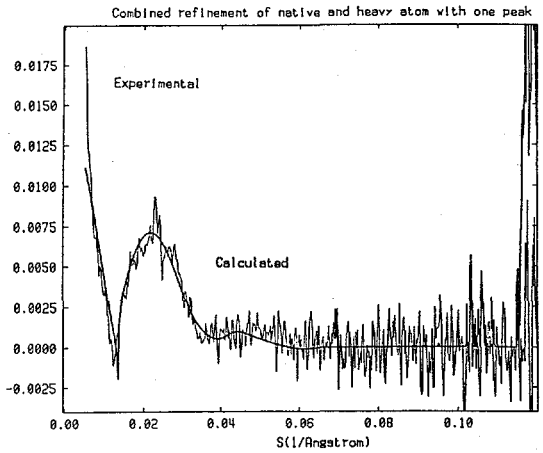

Fig. 1 Difference of amplitudes between data taken below and at the L_{III} absorption edge of Tb^{3+} in the meridional direction. Experimental curve: amplitude difference of the (0,0) rod, calculated curve: result of a non-linear least squares refinement with 2 peaks.

CATION BINDING SITE STUDY

Anomalous diffraction studies were done on pelleted bR samples. Ultracentrifugation of bR suspensions at 50000 rpm for 10 hours resulted in partially oriented bR samples. The membrane layers were randomly rotated about the axis perpendicular to the membrane plane. For data collection the beam lines II-2 and IV-2 at SSRL were used. X-ray energies for anomalous diffraction were chosen around the L(III) edge of Tb^{3+} which is at 7515 eV. By measuring the meridional intensity profile the electron density distribution along the direction normal to the membrane plane was obtained. A finite number of combinations of native phases were determined using Shannon's sampling theorem [1]. The effect of anomalous diffraction is shown best by the difference between data sets collected at energies around the absorption edge of Tb^{3+} (Fig. 1). The anomalous signals follow precisely $\Delta f'(E)$. The locations of the cation binding sites were calculated by non-linear least squares refinement using the anomalous signals and the native phases (Fig. 2). The R factors of the 2 peak solutions ($R \approx 0.05$) were substantially smaller than those of the 1 peak solution ($R \approx 0.35$). The addition of a third binding site did not improve the R factor and the resulting positions were further out of the membrane. The results of the refinement calculations showed that the bR molecules have 2 cation binding sites. They are located close to the lipid head groups, one on each side of the membrane. These results are consistent with FTIR-studies done by Gewert et al. [2]. Due to the smearing effect caused by the misorientation of the membranes it is still difficult to obtain the distribution of cation binding sites in the membrane plane.

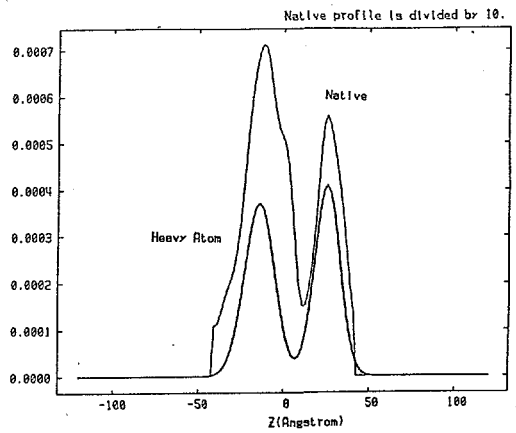

Fig. 2 Electron density profiles along the direction perpendicular to the bR membranes (z). Upper curve: electron density of the native bR sample, lower curve: distribution of Tb atoms after non-linear least squares refinement.

LINKING REGION STUDY

To obtain data in the missing cone, diffraction experiments were performed at angles of grazing incidence on thin, dried bR samples. The membrane layers had a maximum thickness of several μm. Preliminary measurements were done by recording the diffracted intensity with X-ray films. Figures 3 and 4 show the first experimental results. The intensity distribution of several rods in reciprocal space could be measured. To decrease the influence of the misorientation of the membranes, experiments will be continued with thinner samples composed of a few layers or monolayer samples. To assign the cation binding sites in a 3D electron density map of the bR molecules it is necessary to measure the anomalous diffraction along the rods. With an improved camera and by swinging the linear position sensitive detector to appropriate scattering angles it should be possible to measure the anomalous diffraction along the rods.

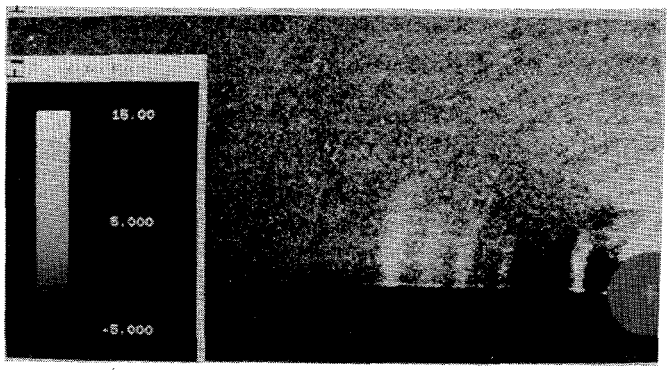

Fig. 3 Scanned and background corrected data from an X-ray film. A thin and dried bR-sample was illuminated at angles of grazing incidence at a photon energy of 7515eV. The intensity distribution from several rods in reciprocal space is shown.

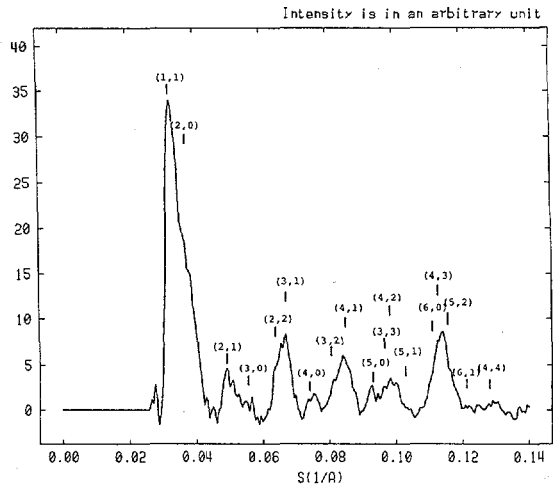

Fig. 4 Same experiment as in Fig. 3. The intensities are integrated on arcs within a 10° cone in the equatorial direction. A least squares spline was calculated through the intensity decay at small angles and regions between the intensity maxima. The splined curve was subtracted from the diffraction data.

REFERENCES

1. A.E. Blaurock & G.I. King (1977), Science, **196**, 1101-1104.

2. K. Gewert, U.M. Ganter, F. Siebert & B. Hess (1987), FEBS letters, 213, 39-44.

A Study of the Electronic Structure of $S_2O_6^{2-}$ by Polarized K-edge X-ray Absorption Spectroscopy

Trevor A. Tyson[1], A. Lawrence Roe[1], Britt Hedman[1,2], Patrick Frank[1] and Keith O. Hodgson[1]

[1] Department of Chemistry, Stanford University, Stanford, Ca. 94305
[2] SSRL, SLAC, Bin 69, P. O. Box 4349, Stanford, Ca. 94305

I. Introduction

Since X-ray photoabsorption by a molecule involves the promotion of a core electrons to a bound or continuum state, the absorption process reveals information about the bonding between the absorbing atom and its ligands. Moreover by performing polarized X-ray absorption (PXA) measurements information about the symmetry of empty molecular orbitals (bound states) and available continuum states can be directly obtained (1).

Here we present the results of a PXA study of the sulfur K-edge excitation spectra of the sulfur oxyanion $S_2O_6^{2-}$ (dithionate). PXA measurements were performed and features in the spectra were labeled.

In concert with these experimental results, MS-Xα calculations using the extended continuum (EC-MS-Xα) scheme (2) were carried out. These calculations served as a cross-check on the ordering of final states determined by our direct experimental measurements and to elucidate properties not made evident by our experimental procedure.

II. Qualitative Physics

Within the single particle approximation, the probability per unit time that an electron in an initial state, $|\phi_i\rangle$, makes a transition to a final state, $|\phi_f\rangle$, due to a perturbation, V, is given by

$$W_{fi} = 2\pi/\hbar \, |\langle \phi_i | V | \phi_f \rangle|^2 \delta(E_i - E_f) \qquad 1$$

where E_i is the total energy of the initial configuration and E_f is the total energy of the final configuration.

For transitions due to the absorption of electromagnetic radiation the above expression, in the dipole approximation, leads to an expression for the photoabsorption cross section :

$$\sigma(\hbar\omega) = 4\pi^2\alpha\hbar\omega \, \Sigma_f |\langle \phi_i | \mathbf{e}\cdot\mathbf{r} | \phi_f \rangle|^2 \, \delta(E_i + \hbar\omega - E_f) \qquad 2$$

where α is the finestructure constant, $\hbar\omega$ is the energy of the absorbed photon, and $\mathbf{e}\cdot\mathbf{r}$ is the scalar product of the electric field polarization vector ($\mathbf{e}$) with the electron position operator ($\mathbf{r}$) (3).

III. Measurements

The polarized absorption measurements were performed on the 54-pole wiggler beam line VI-2 which was operated in undulator mode under dedicated conditions (3 GeV, 40-80 mA, focussed, Si(111) double-crystal monochromator). Only with this setup is there adequate flux to produce high quality data from crystals the size used (0.5 x 0.5 x0.5 mm³). At the energies of interest (2400 - 3000 eV) care had to be taken to insure that the entire beam path was in helium and a goniometer was designed for this purpose.

IV. Results and Interpretations

$K_2S_2O_6$ forms crystals which have three molecules in each unit cell. The unit cell is hexagonal and the space group is P321 (4). The arrangement of the $S_2O_6^{2-}$ (dithionate) anions is ideal for polarized absorption measurements (with the symmetry axes, defined by the sulfur-sulfur bond, of all anions parallel to the unit cell three-fold axis (see fig. 1a)). We were therefore able to obtain sulfur K-edge absorption data for two orientations. In the first orientation (fig 1b thin line) the the symmetry axis (C_3) of the anion was aligned parallel to the electric field vector, $\mathbf{e}$. In the second configuration (fig 1b thick line) the crystal was oriented so that the electric field was perpendicular to the symmetry axes.

The vacant orbital structure and available continuum states of dithionate are complex because of the presence of two sulfur atoms in the molecule. Fortunately, both sulfur atoms are completely indistinguishable when the molecule is in its ground state. However on the absorption of a photon the redistribution of charge on the absorbing sulfur atom (which has a core hole) reduces the molecular symmetry from D_{3d} to C_{3v}. Hence equation 2 reduces to

$$\sigma(\hbar\omega) = 4\pi^2\alpha\hbar\omega \, \{ \Sigma_f |\langle \phi_{1s} | \mathbf{e}_p\cdot\mathbf{X}_p | \phi_e \rangle + \langle \phi_{1s} | \mathbf{e}_z z | \phi_{a1} \rangle|^2 \} \, N(E_i + \hbar\omega - E_f) \qquad 3$$

where (in configuration space) $\mathbf{e}_p$ and $\mathbf{X}_p$ are the vector components of $\mathbf{e}$ and $\mathbf{X}$, respectively, perpendicular to the C_3 axis of the molecule, ϕ_{1s} is the initial state wave function ϕ_{a1} and ϕ_e are the possible final state wave functions and the function N is the density of final states. Only transitions to final states of a1 (e) symmetry are possible in the first (second) orientation.

Even more can be learned by combining observations with the results of the complete calculation of the photoabsorption cross section of the dithionate anion obtained by the EC-MS-Xα method. Features which appear below the computed zero of energy can be attributed to transitions to bound final states while those above can be attributed to transitions to continuum final states.

In figure 1c we show the computed spectra. Based on the positions of the features A, A', B we argue that these features correspond to transitions to molecular orbitals of a1, e and a1 symmetry, respectively. Features B', C', D', E and E' are seen to be transition to continuum states of e, e, e, e and a1 symmetry, respectively. The feature labeled D in the measured spectrum is believed to be residual from the e symmetry feature D'. The origin of the feature C is at this point not clear.

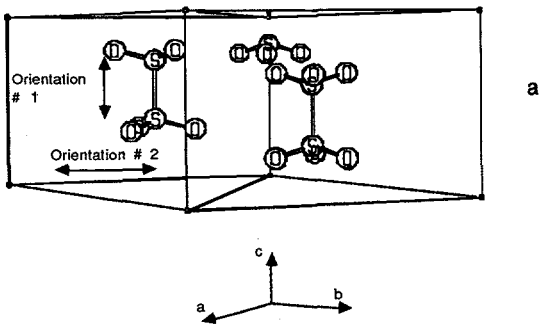

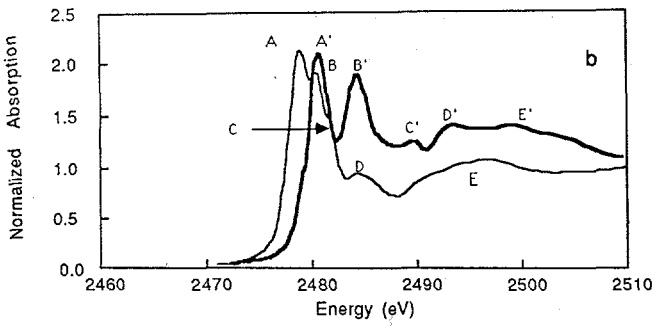

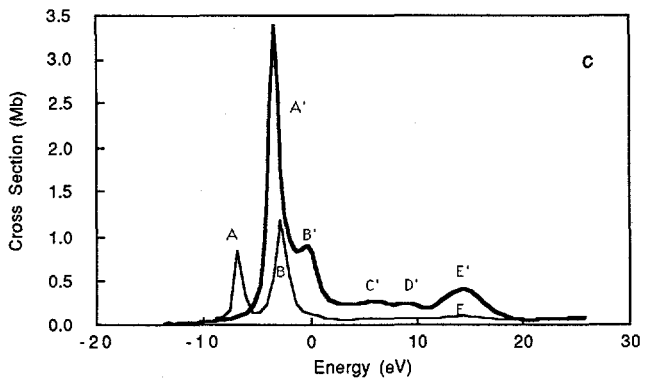

Figure 1. $K_2S_2O_6$: (a) Crystal structure of $K_2S_2O_6$ with unit cell outlined. In orientation #1 the **S-S** vector (C_3) of the anion is held parallel to **e** while for orientation #2 it is rotated so that the C_3 axis is normal to **e**. (b) The experimental data for orientation #1 (thin line) and orientation #2 (thick line). (c) The calculated spectra in which the lines have the same meaning as in (b).

References

[1] J. E. Hahn and K O. Hodgson, "ACS Symposium Series No.211, Inorganic Chemistry:Toward the 21st Century", Malcom H. Chisholm, ed, 1983 ,p. 431

[2] S. Doniach, M. Berding, T. Smith and K. O. Hodgson, "EXAFS and Near Edge Structure III" , K. Hodgson, B. Hedman and J. E. Penner-Hahn eds., Springer Verlag 1984, p. 33

[3] C. R. Natoli and M. Benfatto, Journal de Physique, C8 11 (1985)

[4] E. Stanley, Acta Cryst. 9, 897 (1956)

Acknowledegments

We are indebted to Prof. C R. Natoli (Laboratori Nazionali Di Frascati, Frascati, Italy) for allowing us use of their VAX-8600 for the EC-MS-Xα computations.

This research was supported by NSF grant CHE 85-12129 and was done at SSRL which is supported by the DOE's Office of Basic Energy Science and the NIH's Division of Research Resources, Biotechnology Resource Program.

A Multiple Scattering Analysis of the EXAFS Spectrum of SF_6

Trevor A. Tyson[1], Britt Hedman[1,2] and Keith O. Hodgson[1]

[1] Department of Chemistry, Stanford University, Stanford Ca. 94305
[2] SSRL, SLAC, Bin 69, P.O. Box 4349, Stanford Ca, 94305

Introduction

It is well known that the absorption spectrum of molecules and extended solids can be separated into three distinct regions. The pre-edge region which occurs before the onset of absorption, the XANES or near edge region characterized by white lines and resonances and the EXAFS region of the spectrum which is dominated by single scattering processes (1). Unfortunately, without the assistance of a specific mathematical model the limits of the energy intervals covered by these regions are not well defined.

As an extension of our polarized near edge studies (at the sulfur and chlorine K-edges), we have elected to look at the same problem from the perspective of multiple scattering theory. We have embarked on this new approach by first looking at the dominant multiple scattering paths involved in the near edge region of the gas SF_6.

Theoretical Comments

A unifying scheme for the computation and interpretations of X-ray absorption spectra based on multiple scattering theory has been put forth by Natoli and Benfatto (4). This method follows directly from the well known Xα-MS approach used to study valence and core excitations between bound levels in discrete molecules and clusters (5) and extended to continuum final states by Dill and Dehmer (6). In this model (4) an approximate inversion of the multiple scattering series results in its decomposition (in the EXAFS region) into scattering involving closed scattering paths beginning and ending at the absorber's site. Applied to K-edge absorption, this series can be written as

$$\sigma_{tot}(E) = \sigma_{atom}(E) + \Sigma_n \sigma_n(E)$$

where σ_{atom} corresponds to pure atomic absorption and σ_n corresponds to all closed scattering paths involving the absorber and n-1 neighbors (n greater than 1). This multiple scattering series converges only when the eigenvalues of the matrix $\mathbf{T}_a * \mathbf{G}$ are all less than unity. The model is of a rigorous curved-wave nature and can be shown to reduce to the plane-wave approximation under certain conditions.

Experimental Procedure

The sulfur K-edge absorption spectrum of SF_6 was measured on beam line VI-2 operating in undulator mode with characteristics as already described (2). The fluorescence excitation spectrum was measured using a detector of Heald-Stern design (3) with a gas flow cell adapted to fit into its sample chamber. A constant flow rate of a gas mixture with a two-to-one ratio of He to SF_6 was maintained during the scans. Measurement of the EXAFS region extended up to 3185 eV (k ~ 13.5 Å^{-1}) where oscillations were still noticeable.

Discussion

In figure 1 the edge spectrum of SF_6 is presented. The spectrum is dominated by an intense dipole-allowed a_{1g} (sulfur 1s) to t_{1u} bound-to-bound-state transition (7) straddled on the low energy side by a a_{1g} (sulfur 1s) to a_{1g} feature and on the high energy side by a a_{1g} (sulfur 1s) to t_{2g} transition both of which have final states which are mixtures of s and d symmetry (8). These transitions are dipole-forbidden and hence are much weaker than the main peak.

To facilitate the comparison of the EXAFS data with the computed spectra the onset of the continuum region had to be found. This was done by noting that ΔE, the difference in total energy of 1s to t_{1u} *configuration and 1s to ∞ configuration, gives the energy above* the 1s to t_{1u} feature at which the true continuum starts. From our experimental measurement we found that the 1s to t_{1u} peak was at 2488.5 eV and our MS-Xα computations yielded ΔE = 7.7 eV. Hence we define E_0 to be 2496.2 eV (see ref 10 for a similar procedure).

In figure 2a we have plotted the experimental EXAFS spectrum, where one can note that for k above ~ 6 Å^{-1} the EXAFS spectrum displays the characteristic single damped sinusoidal behavior typical of single scattering processes. For lower values of k, however, this is not the case. Specifically there is an asymmetric peak at ~ 4 Å^{-1} which clearly can not be due to single scattering processes only.

To understand this feature we present the computed single scattering cross section and the partial sums $\sigma_2 + \sigma_4$ and $\sigma_3 + \sigma_5$ in figures 2b and 2c, respectively. The multiple scattering series converges for k > 3.6 Å^{-1} and above this value of k a discussion of scattering paths is appropriate. It can be seen that for the range 3.6 to 13.5 Å^{-1} only σ_2 and σ_4 are necessary to qualitatively reproduce the observed EXAFS spectrum. Moreover we can in particular attribute the sharp asymmetric feature near 4 Å^{-1} to be due preliminary to a sum of single scattering and triple paths.

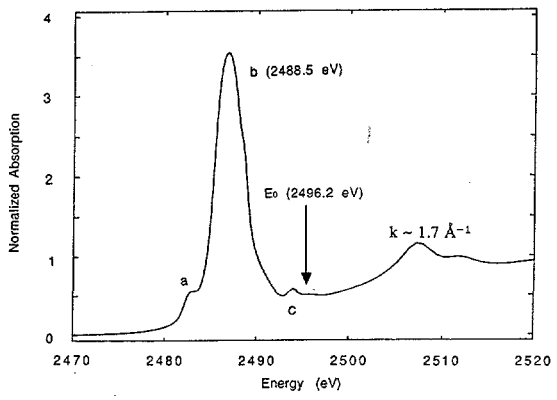

Figure 1. The near edge spectrum of SF_6. The transitions to final states of a_{1g}, t_{1u} and t_{2g} symmetry are labeled a, b and c and the location of E_0 is pointed out. In addition, the first maximum in the EXAFS region (~ 1.7 Å^{-1}) is labeled in order to to facilitate comparison with the EXAFS data shown in figure 2.

It should be noted that since this is just a semiqualitative and preliminary analysis of the data, no attempt was made to place the amplitude of the experimental data on the same scale as that of the computed spectra. In addition, we have used a static Xα exchange for our computations. The main effect of this is to slightly change the energy scale (10). A more complete analysis of the data now being done will address these problems.

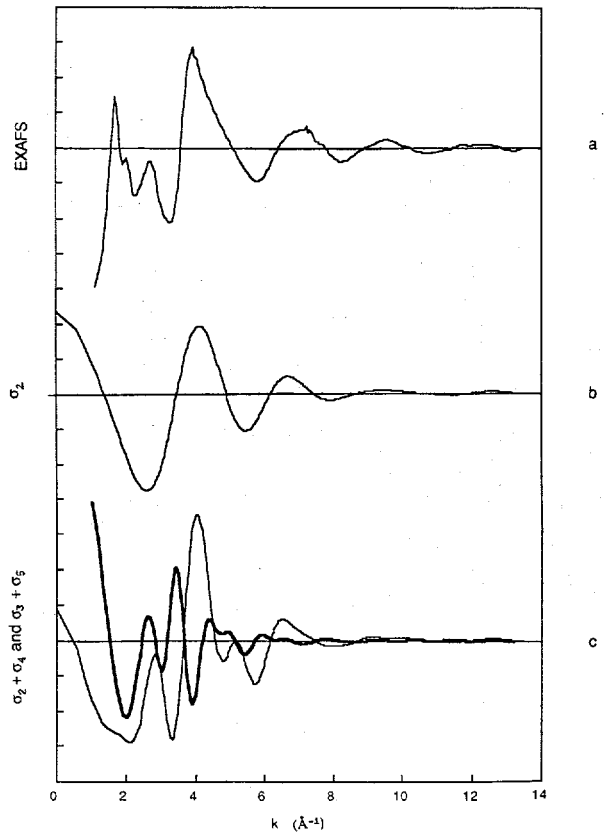

Figure 2. Measured EXAFS and computed cross sections: (curve a) The measured EXAFS spectrum of SF_6, (curve b) the computed single scattering contribution, σ_2, and (curves labeled c) the partial sums $\sigma_2 + \sigma_4$ (thin line) and $\sigma_3 + \sigma_6$ (thick line).

References

[1] A. Bianconi et al, Journal de Physique, C9, 101 (1985)
[2] B. Hedman et al, Nucl. Instr. Meth. A246 797 (1986)
[3] E. A. Stern and S. M. Heald, Rev. Sci Instr. 50, 1579 (1979)
[4] C. R. Natoli and M. Benfatto, Journal de Physique, C8, 11 (1985)
[5] K. H. Johnson, Adv. Quan. Chem. 7, 143 (1973)
[6] D. Dill and J. L. Dehmer, J. Chem. Phys. 61, 692 (1974)
[7] This was determined by the explicit computation of the dipole allowed cross section within the extended continuum scheme. (See S. Doniach et al in "EXAFS and Near Edge Structure III", K. O. Hodgson, B. Hedman and J.E. Penner-Hahn eds. Springer Verlag, 33 (1984) for a discussion of the extended continuum method)
[8] F. A. Gianturco, G. Guidotti and U. Lemanna, J. Chem. Phys., 57, 840 (1971)
[9] S. H. Chou et al, Phys. Rev. B. 35, 2604 (1986)
[10] M. Benfatto et al, Phys. Rev. B. 34, 5774 (1986)

This research was supported by NSF grant CHE 85-12129 and was done at SSRL which is supported by the DOE's Office of Basic Energy Sciences and the NIH's Division of Research Resources, Biotechnology Resource Program.

XANES SPECTROSCOPIC STUDIES OF SULFUR WITHIN BLOOD CELLS FROM THE TUNICATE ASCIDIA CERATODES

Proposal No. 8116B

Patrick Frank[1], Britt Hedman[1,2], Robert M. Carlson[3] and Keith O. Hodgson[1,2]

1. Department of Chemistry, Stanford University, Stanford, CA 94305.
2. Stanford Synchrotron Radiation Laboratory, SLAC, Bin 69, P.O. Box 4349, Stanford, CA 94306.
3. Chevron Oil Field Research Co., P.O. Box 446, La Habra, CA 90631.

Introduction. The study of the status of sulfur within the blood cells of the tunicate Ascidia ceratodes has been extended using sulfur K-edge XANES spectroscopy [1]. Spectra of whole cells from three independent blood samples, derived from specimens collected over a period of about 18 months, have been obtained. These are here compared with K-edge XANES spectra of biologically relevant sulfur-containing model solutions.

Experimental. The experiments were performed on beam-line VI-2 (in undulator mode) or IV-2 during dedicated conditions (3 GeV, 35-80 mA, focused, Si(111) double-crystal monochromater). Details of the experimental conditions have been described previously [2]. Aqueous acidic solutions of V(III) sulfate and V(III) methanesulfonate were prepared as described [3].

Results. In a previous report [1] we noted that sulfur K-edge XANES spectra of sulfate were significantly broadened in solutions of V(III) sulfate. We do not observe this effect in solutions of sodium, ammonium or manganese(II) sulfate of equivalent sulfur concentration. The blood cells of A. ceratodes and other tunicates are known to be rich in vanadium and sulfate [2-6] and the sulfur K-edge sulfate XANES spectrum of blood cells from the former organism also appears to be broadened [1,6]. Investigation of this phenomenon was therefore carried out since it seemed possible thereby to determine whether these two ions (i.e., V(III) and SO_4^{2-}) are colocated within the blood cells of A. ceratodes.

In Figure 1 is shown a sulfur K-edge XANES spectral titration of sulfate with a serially increasing mole-fraction percent of V(III). Two effects of increasing [V(III)] on the sulfate edge spectrum are noted: a. There is a clear increase in linewidth with [V(III)]; b. There is at the same time a small shift in peak maximum to higher energy. At $[V(III)]/[SO_4^{2-}] = .67$, (i.e., in a solution of $V_2(SO_4)_3$), the half-height width of this peak was 2.8 eV, up from an initial value of 2.3 eV.

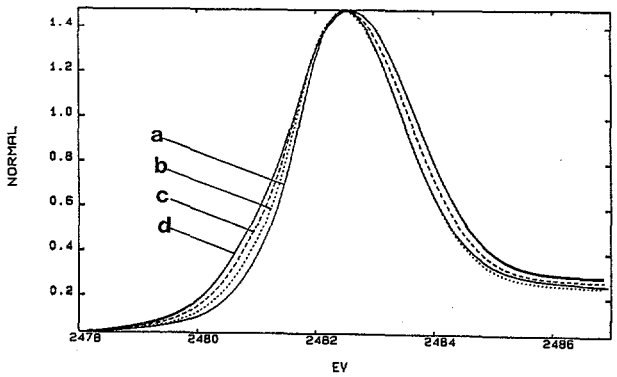

FIGURE 1. Sulfur K-edge XANES spectrum of 1M sulfate pH 1.5 with: a. 0.0 mol-%; b. 18 mol-%; c. 40 mol-%; and d. 67 mol-% V(III) added.

A similar effect on width and position was observed in sulfate XANES spectra on titration of this anion with acid, over the pH range 0.0-5.0. This pH range is equivalent to the transformation of a solution containing purely HSO_4^- (bisulfate ion) to one of pure SO_4^{2-} (sulfate ion).

From the data of Kimura et al. [7] the mole-fraction of sulfate represented by the VSO_4^+ complex ion, in a solution of $V_2(SO_4)_3$, can be estimated to be 0.61. Therefore the vanadium sulfate spectrum in Figure 1 reflects a mixture of free and complexed sulfate ion. The total anticipated increase in half-height peak width for a solution of pure VSO_4^+ is estimated to be 0.8 eV over that for pure sulfate (compare 0.5 eV for the transformation to bisulfate).

These results imply that the underlying phenomenon is the same in each case. That is, the complexation of sulfate, as shown in equation 1.

$$SO_4^{2-} + M^{n+} \Leftrightarrow MSO_4^{(n-2)+} \qquad 1.$$

where M^{n+} is V^{3+} or H^+. (Since complexation occurs on oxygen, the symmetry of sulfate decreases from T_d to C_{3v} in this reaction. Whether this fact accounts for the new XANES spectral features awaits calculation.)

In the case of both the bisulfate ion and the VSO_4^+ compex ion, calculation of the second derivative spectra indicated the appearance of new features near 2480 eV and 2483 eV, accounting for the observed changes in peak width and position. The shape of the second derivative sulfate feature at high acid was comparable to that for sulfate in the presence of a high [V(III)].

Figure 2 shows the sulfur XANES spectrum of a sample of whole blood cells from A. ceratodes, washed free of surface sulfate. The dashed and dotted spectra indicate the presence of both sulfate and an aliphatic sulfonic acid moiety, respectively, within these cells. The close correspondence in peak position and line-shape of the the vanadium sulfate solution spectrum with the sulfate portion of the whole cell spectrum strongly implies the intracellular presence of a vanadium(III)sulfate complex.

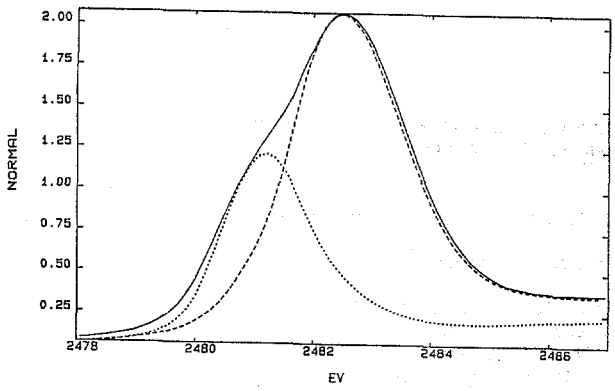

FIGURE 2. Sulfur K-edge XANES spectrum of a washed whole blood-cell preparation from A. ceratodes (solid line); of 0.5M $V_2(SO_4)_3$ in pH 1.5 sulfuric acid (dashed line); and of 100mM methane sulfonic acid (dotted line). The latter spectra have been inserted for illustrative purposes and are not fits to the cellular data. Note the close correspondence between the slopes and positions of the high energy sides of the respective sulfate features.

Figure 3 (top) displays second derivative solution spectra of a mixture of 2:1 sulfate: methane sulfonate. In the solution also containing V(III) the sulfate portion of the spectrum is broadened to higher energy. In addition, the larger sulfate peak-width due to the presence of V(III) has broadened the maximum of the sulfonate portion of the spectrum near 2481 eV. In Figure 3 (bottom), the second derivative spectra of three independent samples of whole blood cells from A. ceratodes is shown. The organisms were collected over a period of about one year. Inspection of the three spectra clearly indicates the presence of considerable V(III) in one sample, a lesser amount of this ion in the second sample, and essentially no V(III) in the third.

Since in each case the blood cell samples contained cells from about 30 animals, the spectra survey an average disposition of cellular constituents. Thus it appears possible that there is some seasonal variation in the colocation of V(III) and sulfate ion. However both ions are certainly always present intracellularly. The question remains, therefore as to where these materials are stored when they are not stored together, i.e., in separate compartments of the same cell, or in separate cells altogether. In addition, when sulfate is not present, what constitutes the counterion for intracellular V(III)? Since a sulfonate ion of unknown structure is also present intracellularly in high concentration in all the blood cell preparations examined thus far, this anion may serve the role of alternative counterion to V(III).

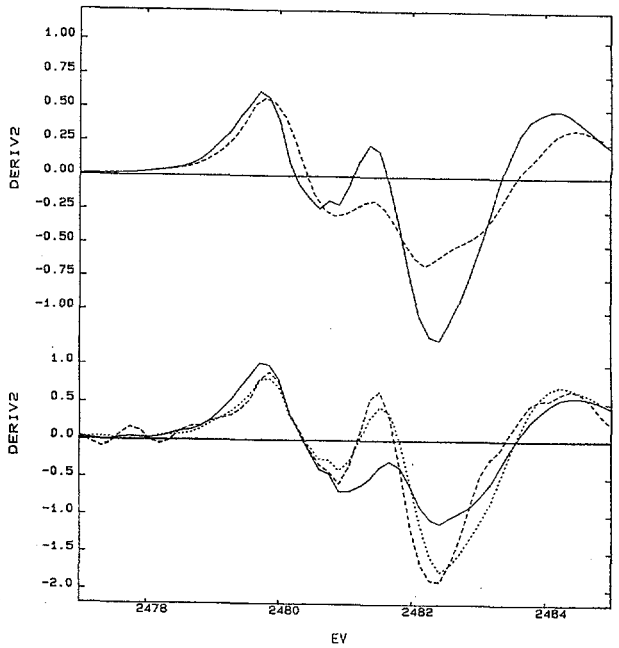

FIGURE 3. Second derivative sulfur K-edge XANES spectra of: (top) 1M sodium sulfate with 0.5M cysteic acid (solid line); and a 2:1 SO_4^{2-}:$MeSO_3^-$ numerical addition spectrum of the XANES solution spectra of 0.5M $V_2(SO_4)_3$ pH 1.5 and 1M aqueous methane sulfonic acid (dashed line). The true sulfate maxima appear at the same energy position in the two spectra despite the broadening induced by V(III) in the vanadium sulfate solution. This suggests the appearance of a new band in the latter solution, rather than a vanadium(III)-induced energy shift of the original sulfate band; (bottom) Washed whole blood-cell preparations from A. ceratodes collected on: 5, June 1985 (solid line); 31, May 1986 (dotted line); and 12, January 1987 (dashed line). Note that the first and second samples, collected approximately 1 year apart, show the greatest relative variance in vanadium-induced broadening.

References.

[1] P. Frank, B. Hedman, R. M. K. Carlson, T. Tyson, A. L. Roe and K. O. Hodgson (1986) SSRL Activity Report, 193-194.

[2] B. Hedman, P. Frank, J. E. Penner-Hahn, A. L. Roe, K. O. Hodgson, R. M. K. Carlson, G. Brown, J. Cerino, R. Hettel, T. Troxel, H. Winick and J. Yang (1986) Nucl. Instr. Meth. Phys. Res. A246, 797-800.

[3] P. Frank, R. M. K. Carlson and K. O. Hodgson (1987) Inorg. Chem. 25, 470-478.

[4] C. J. Hawkins, G. A. James, D. L. Parry, J. H. Swinehart and A. L. Wood (1983) Comp. Biochem. Physiol., B: Comp. Biochem. 76B, 559-565

[5] B. J. S. Pirie and M. V. Bell (1984) J. Exp. Mar. Biol. Ecol. 74, 187-194

[6] P. Frank, B. Hedman, R. M. K. Carlson, T. A. Tyson, A. L. Roe and K. O. Hodgson (1987) Biochemistry 26, 4975-4979.

[7] T. Kimura, M. Morinaga and J. Nakano (1972) Nippon Kagaku Zaishi, 664-667.

This research was supported by NIH Grant RR 01209 and NSF Grant CHE 85-12129

SULFUR K AND MOLYBDENUM L EDGE XANES OF THE IRON-MOLYBDENUM COFACTOR FROM AZOTOBACTER VINELANDII NITROGENASE

Britt Hedman[1], Patrick Frank[2], Stephen F. Gheller[3], A. Lawrence Roe[2], William E. Newton[3] and Keith O. Hodgson[2]

[1]SSRL, SLAC, Bin 69, P.O. Box 4349, Stanford, CA 94309, USA
[2]Department of Chemistry, Stanford University, Stanford, CA 94305, USA
[3]Western Regional Research Center, USDA-ARS, Albany, CA 94710; and Department of Biochemistry and Biophysics, University of California, Davis, CA 95616, USA

The electronic and structural nature of sulfur and molybdenum in the iron-molybdenum cofactor (FeMoco) isolated from the MoFe protein of Azotobacter vinelandii nitrogenase has been studied by x-ray absorption edge and near-edge spectroscopy at the sulfur K and molybdenum L_3 and L_2 edges. In contrast to the relatively poor resolution found for x-ray absorption edges at higher energies, resolution in the 2.4-3.0 keV region is significantly improved, resulting in higher sensitivity to changes in electronic and structural environment at the absorbing atom.

Experimental. The experiments were performed using beam line VI-2 in undulator mode (~1.5 kG; with 250, 125 and 25 μm Be windows and no graphite filters in the beam line) during dedicated conditions (3.0 GeV, 40-80 mA, focused, Si(111) double-crystal monochromator). Details of the experimental conditions have been described previously [1]. A cryostat compatible with the requirements of minimum radiation absorption and anaerobicity for the sample was constructed and used.

Results. Spectra were recorded for FeMoco in its oxidized (ox) and semi-reduced (s-r) forms. For comparison, spectra of a number of inorganic complexes containing molybdenum and/or sulfur were also obtained. In the cofactor isolation process, dithionite is normally added to maintain FeMoco in its semi-reduced state. The sulfur edge spectrum of dithionite (and its oxidation/decomposition products) superimposes upon that of the FeMoco (in Fig. 1, compare spectra for FeMoco samples A and B with that of an aged aqueous dithionite solution). To remove this interference (and other small, unbound molecules in the FeMoco solution), an anaerobic column chromatographic method of purification was developed. Spectra could thus also be obtained for dithionite-free FeMoco(ox) (spectrum C in Fig.1).

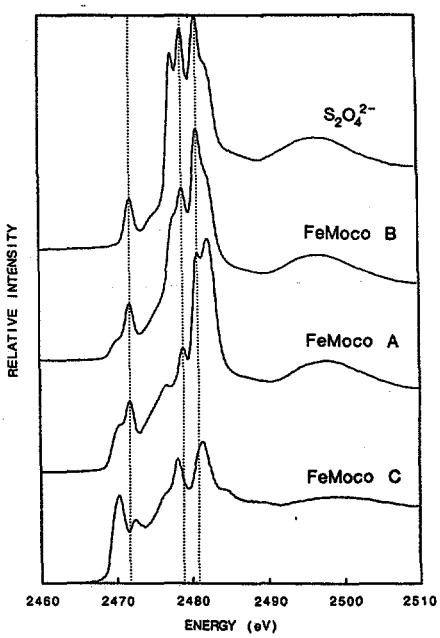

Fig. 1. Sulfur K edges of (in order from the top): aged aerobic aqueous dithionite ($S_2O_4^{2-}$); FeMoco B; FeMoco A (each containing dithionite and/or decomposition products); and FeMoco C (dithionite-free).

The spectrum of dithionite-free FeMoco sample C shows no overlapping features with the dithionite-related spectra. It reveals both expected and new features, and is dominated by four transitions, two near 2470 eV and two around 2480 eV. The main transition at 2470.4 eV is consistent with the presence of both transition metal-bridging sulfide, as seen from the comparison with S edge spectra of, for example, $[Fe_4S_4(SR)_4]^{2-}$ clusters, and of thiolate sulfur liganded to iron. The two features at 2478.2 and 2481.5 eV can only result from sulfur in a high oxidation state with oxygen as a part of its coordination sphere. These two transitions show very close correspondence to those that would be expected from a thiosulfate ($-S-SO_3$) moiety bound to FeMoco through its terminal sulfur. This S K edge study has thus shown the presence of an unprecedented form of sulfur as an integral part of FeMoco. In addition, the identity of some of the terminal ligands of this metal cluster are revealed for the first time.

The MoL_3 and MoL_2 edge spectra of FeMoco, are characterized by a split white-line, where the two features are close in energy and the peaks not resolved (Fig.2). The first transition has lower intensity, and the intensity ratio of the first and second transition is, as also seen in model complexes, lower at the L_3 than at the L_2 edge. When compared to structurally relevant model compounds, the position and shape of the near-edge features indicate a mixed S/O coordination (which is consistent with Mo K EXAFS results [2]) with a formal oxidation state of around +4 (Fig. 2). Comparison of the Mo L edge spectra of FeMoco in its oxidized and semi-reduced forms, shows that there is no observable change in coordination around molybdenum or in its oxidation state (at least within a small fraction of an electron) with the redox change of FeMoco.

Preliminary results of measurements performed in the December 1987 run confirm the results reported here.

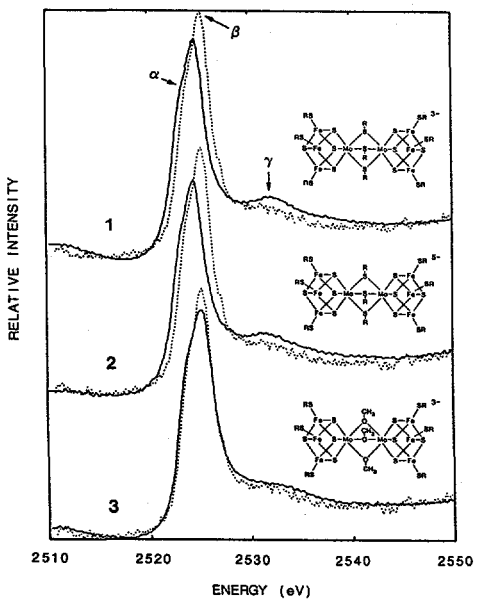

Fig. 2. Molybdenum L_3 edge spectra of the cubane-clusters $[Mo_2Fe_6S_8(SC_6H_5)_9]^{3-}$ (1), $[Mo_2Fe_6S_8(SC_6H_5)_9]^{5-}$ (2) and $[Mo_2Fe_6S_8(OCH_3)_3(SC_6H_5)_6]^{3-}$ (3), solid lines. For comparison with each spectrum, dithionite-free FeMoco C, dotted line, is shown. The best match is with the methoxy-bridged cluster (3).

References.

[1] B. Hedman, P. Frank, J.E. Penner-Hahn, A.L. Roe, K.O. Hodgson, R.M.K. Carlson, G. Brown, J. Cerino, R. Hettel, T. Troxel, H. Winick, J. Yang, Nucl. Instr. Meth. **A246** (1986) 797.

[2] S.D. Conradson, B.K. Burgess, W.E. Newton, L.E. Mortenson, K.O. Hodgson, J. Am. Chem. Soc. **109** (1987) 7507.

Acknowledgements. This research was supported by NSF grant CHE 85-12129 and was done at SSRL which is supported by the DOE's Office of Basic Energy Science, and the NIH's Division of Research Resources, Biotechnology Resource Program.

CRYSTALLOGRAPHY OF RIBOSOMAL PARTICLES

A. Yonath[1],[2], F. Frolow[1], K. vonBoehlen[2], I. Makowski[3],
H. Hope[4], C. Kratky[2],[5], ,K. Bartels[2], and H.G. Wittmann[4]

(1) Weizmann Inst. of Science, Rehovot, Israel.
(2) Max Planck Research Unit for Structural Molecular Biology, Hamburg.
(4) Max Planck Institute for Molecular Genetics, Berlin (West).
(4) U. of Ca. at Davis, Ca. USA.
(5) Univ. of Graz, Graz, Austria.

In order to understand the molecular mechanism of protein biosynthesis, it is necessary to know the molecular structures of the various components involved in this process. To this end we have been engaged in crystallographic studies of ribosomes, the cell organelles which provide the site at which the genetic information is translated into polypeptide chains.

Ribosomes are complex assemblies of several strands of RNA and of a large number of different proteins with no internal symmetry. They consist of two independent subunits of unequal size, which associate upon initiation of protein biosynthesis. The molecular weights of bacterial ribosomes and their two subunits are 2.300.000; 1.600.000 and 700.000 daltons, respectively. A typical bacterial ribosome contains 53 different proteins (32 in the large subunit; 21 in the small one) and 3 RNA chains (2 and 1 respectively).

Despite the tendency of ribosomes to disintegrate, their inherent flexibility, complexity and enormous size, we have been able to grow fifteen crystal forms of intact ribosomal particles and their complexes with components of protein biosynthesis (Table I). So far all crystals were obtained from functionally active particles, and the crystalline material retained its integrity and biological activity for long periods. All crystals which we found useful for crystallographic studies were grown under conditions close to the physiological ones. In spite of their fragility these crystals can be manipulated, mounted in different ways and soaked in heavy-atom solutions.

A common property of the diffraction patterns of all crystals of ribosomal particles is that they show a sharp drop in the intensities at about 20Å. Thus initially we were misled to believe that this was the actual resolution limit. Only later, when crystals grew larger and measuring facilities were improved, we observed that the crystals are ordered internally to a much higher level, and diffracted best to 5.5Å (Fig. 1 and Makowski et al., 1987).

Crystallographic data have been collected from crystals of the following systems : (1) the small (30S) ribosomal subunits from *Thermus thermophilus* (2) the large (50S) subunits from *Halobacterium marismortui* (3) the large subunits from wild and mutated *Bacillus stearothermophilus* and (4) functional complexes of large subunits of both *B. stearothermophilus* and *H. marismortui* with tRNA + a short polypeptide chain. The crystals of types (2)-(4) were grown and studied under conditions close to physiological ones (crystallographic characteristics are given in Table I).

Until 1987 data were collected at temperatures close to 0°C. At these temperatures, in all cases the reflections with resolution better than about 20Å decayed after a few minutes of irradiation. Thus substantial difficulties have been encountered in data collection and processing. Crystals were aligned only visually and over 260 crystals had to be irradiated in order to obtain a (supposedly) complete set of film data.

To overcome these problems we have initiated crystallographic studies at cryo temperature. We have observed, for each crystal form, that at this temperature there was hardly any radiation damage even after hours in the synchrotron X-ray beam, so that a complete data set could be collected from a single crystal. The idea that crystals of biological macromolecules can be coated by an inert viscous material, "flash frozen" at around 100 K (in a stream of nitrogen or in liquid propane) to prevent the internal solution from crystallization, and then mounted exposed to the atmosphere, has been introduced only recently (Hope, 1988).

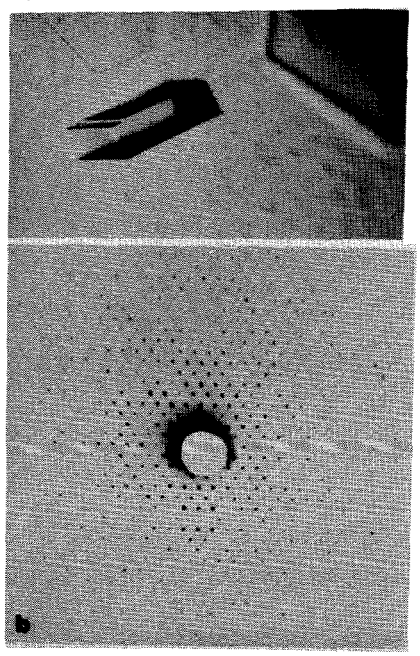

Fig 1. (a) Crystals of the 50S ribosomal subunits from *H. marismortui* grown as in Makowski et al., 1987.
(b) An X-ray diffraction pattern from a crystal similar to that shown in (a), obtained at -180°C at station VII-I at SSRL with 0.3mm collimated X-ray beam (=1.48Å), on a Nonius precession camera. Exposure time=3 min, crystal to film distance=140mm.

Due to the shape of the crystals, which grow as flat plates (Fig. 1) or long needles, attempts to use glass rods for mounting, resulted in bending of the crystals around the rods. This, in turn, caused a significant loss of resolution in the diffraction patterns. We therefore developed a special device for mounting the crystals. Tiny spatulas were constructed from a very thin glass film glued to a thin glass rod, previously soldered to a brass pin which could be mounted on the goniometer head. Several types of spatulas were constructed, differing in the angle between the glass film and the rod, in order to permit mounting of the crystals in any desired orientation. The crystals were extracted from the solution and attached to these "spatulas" by surface tension. A more sophisticated version: the "sandwich" type , was developed later. These spatulas are made of double layers of extremely thin glass films glued to the glass rod. The crystals were placed between the two layers which provide extra protection from evaporation.

Because in all crystal forms the shortest crystal edge coincides with the largest unit cell dimension, the geometry of the spatulas dictates the permissible rotation angle. The natural tendency of the crystals was to lie flat on the glass layer. Because most crystals exhibit a high mosaic spread (up to 3°) there was a severe problem with overlap, in particular when the long (i.e 594 Å) axis was in the direction of the X-ray beam. Therefore, when using "flat" spatulas, there were no fully recorded reflections. In contrast, crystals mounted on perpendicular spatulas could be positioned so that their long axis coincided with the spindle axis, permitting a relatively large rotations (3°-5°) at medium resolution. These data can be used as a "scaling set" for data collected at different orientations at higher resolution.

As viscous materials we used either a hydrophobic hydrocarbon or materials such as methyl pentane diol (MPD), which was used for the growth of the crystals of the 30S subunits, or polyethylene glycol (PEG), which was used for the growth of crystals of large (50S) ribosomal subunits from *Bacillus stearothermophilus*. The latter ribosomal particles are very interesting because they are well characterized chemically and since we are able to split from the ribosomes several proteins in a controlled way, using biochemical and genetic methods (Yonath et al., 1986b; Gewitz et al., 1987). Initially crystals from this source were grown at 4°, using low molecular weight alcohols as precipitants (Yonath et al., 1984; 1986). Since these crystals could not be handled or soaked we have developed procedures for growing crystals using non-volatile materials. Currently we can obtain well shaped crystals from very low concentrations of polyethylene glycol in the presence of low concentrations of salts, conditions which resemble the natural environment of these particles.

We used our beam-time periods for establishing the procedures for cryo temperature crystallography, for examining the newly grown crystal forms and for collecting data from some of them (marked D in Table I). Data have been collected also from several derivatives (using crystals soaked in heavy-atom clusters (marked H in Table I), and from complexes of 50S subunits from *H. marismortui* and *B. stearothermophilus* with tRNA and a short (18-20) segment of the nascent polypeptide chain.

TWO- AND THREE-DIMENSIONAL CRYSTALS OF RIBOSOMAL PARTICLES

Source	Crystal Form	Cell Dimensions, (Å) determined by electron microscopy		X-ray crystallography	Reso-lution	Comments
70S E.coli	A*	340x340x590;	120°; $P6_3$			
70S B.st.	2D[x], AS*	190x420;	91°; $P2_1$		40Å	
30S T.t.	M*			405x405x171; $P42_12$	9.9Å	D,H
50S H.m.	1, P*	310x350;	105°			
	2, P	148x186;	95°	147x181; 97°	13Å	
	3+,P	170x180;	75°	214x306x594; $C222_1$	5.5Å	D,H
50S B.st.	1, A	130x254;	95°			
	2, A	156x288;	97°			
	3, A	260x288;	105°			
	4, A	405x405x256;	120°			
	5, A	213x235x315;	120°			
	6+#, A	330x670x850;	90°	360x680x920; $P2_12_12$	13-18Å	D
	7+#, P			285x380x526; C222	11Å	D,H
	2D, A	145x311;	89°; P2		35Å	
	2D,AS*	148x360;	109°; P1		25Å	

[x] All forms are of three-dimensional crystals, unless marked by 2D.

D = crystallographic data have been collected from native and derivated (H) crystals.

* Crystals were grown by vapor diffusion from low molecular weight alcohols (A), MPD (M), polyethylene glycol (P), or ammonium sulphate (AS).

Same form and parameters for crystals of large ribosomal subunits of a mutant (-L11 protein) of the same source.

+ Same form and parameters for crystals of a complex of 50S subunits+ tRNA+a segment (18-20 mers) of a nacsent polypeptide chain.

B.st = Bacillus stearothermophilus, T.t.= Thermus thermophilus
H.m. = Halobacterium marismortoui

References

H.S. Gewitz, J. Piefke, A. Yonath and H.G. Wittmann, Biochimie, in press (1987)

H. Hope, Amer. Cryst. Assoc. Abstract series 2,13 (1985).

I. Makowski, F. Frolow, M.A. Saper, H.G. Wittmann and A. Yonath, J. Mol. Biol.,193, 819, (1987)

A. Yonath H.D. Bartunik, K.S. Bartels, and H.G. Wittmann, J. Mol. Biol. 177, 201, (1984)

A. Yonath, M.A. Saper, I. Makowski, J. Müssig, J. Piefke, H.D. Bartunik, K.S. Bartels, and H.G. Wittmann J. Mol. Biol., 187, 633, (1986)

X-ray Crystallography of Succinyl-CoA Synthetase from *Escherichia coli* Proposal No. 1A39B

W.T. Wolodko, P.M.D. Fitzgerald*, M.N.G. James and W.A. Bridger

Department of Biochemistry, University of Alberta, Edmonton, Alberta, Canada T6G 2H7

Introduction

Succinyl-CoA synthetase is an enzyme of the tricarboxylic acid cycle, catalyzing the 'substrate-level' phosphorylation step: it performs a vital function in aerobic metabolism. The enzyme, purified from *Escherichia coli,* is a tetramer with a molecular weight of 1.4×10^5. It consists of two types of subunits and is thought to be assembled as a dimer of $\alpha\beta$-dimers (1). Several lines of evidence suggest that although the complete catalytic site is formed by regions in contact from both subunits in the $\alpha\beta$-dimer, these $\alpha\beta$-dimers do not function independently within the active, tetrameric enzyme (2,3). One way to reconcile the catalytic properties of this enzyme with its quaternary structure is to have a clear representation of the conformation of the tetrameric enzyme in three dimensions. Such a determination is in progress. Crystals of succinyl-CoA synthetase suitable for X-ray diffraction study undergo severe radiation damage when subjected to a beam of X-rays. Their lifetime and utility for data collection to high resolution with conventional X-ray sources is limited (4). Fortunately, this problem is solvable using synchrotron radiation.

Experimental

Succinyl-CoA synthetase was purified from *Escherichia coli* and crystallized as described in a preliminary paper (4). Tetragonal crystals were grown by micro-diffusion up to a size of 0.5 x 0.5 x 1.0 mm. The space group is $P4_122$ with unit cell dimensions of 99 x 99 x 399 Å and one tetramer per asymmetric unit. Potential heavy-atom derivatives were prepared by soaking native crystals appropriately with solutions of platinum ammonium cyanide, uranyl acetate, and auric chloride. Diffraction data were collected at SSRL (Beam Line VII-1) using a wavelength of 1.54 Å. Crystals were mounted with c* aligned parallel the spindle axis (except for the blind-cone data). Oscillation ranges of 1.7-2.0° (45° total range) and exposures, in dose mode, of 1.5×10^7 counts/degree oscillation were taken. To minimize the effects of radiation damage, diffraction was carried out at 4°C, only a single setting-still (exposure 1 s) was taken with Polaroid film for preliminary crystal alignment, and only two film packs were exposed per crystal with translation along the crystal between the film packs. Furthermore, the spindle angle was adjusted for an overlap of 0.5° between sequential crystals. The diffraction patterns were recorded on Kodak DEF-5 film, in 3-film packs with aluminum foil attenuation between films, developed by standard procedures using fresh solutions. Films were scanned and digitized at 50 micron raster on a P-1000 Optronics drum scanner linked to a Kennedy 3110 tape drive. Initial processing, merging, scaling and post-refinement of the data have been carried out on an Amdahl 5870 main-frame computer using programs provided by P.M.D.F.

*Present address: Merck Sharp and Dohme Research Laboratory, Rahway, New Jersey 07065, USA

Results and Discussion

Four full data sets (approximately 100 films each) were collected, a native set and three potential heavy-atom derivatives (Pt, U and Au), to a measurable resolution of 2.9 Å (the limit of resolution with standard flat cassettes at a crystal-to-film distance of 100 mm). Preliminary processing of the data sets has been completed and difference Patterson maps are presently being calculated to assess the quality of the derivatives. The merged and scaled intensity data are of good quality producing R(I) factors in the order of 8-10% with a mean multipicity slightly better than 3 reflections.

From the initial processing of these films, two observations are important with respect to the data collection. Firstly, in approximately 5% of the two film packs from a single crystal, refinement of crystal orientation indicated that the correction of the spindle value between film packs had shifted slightly (usually less than a degree) while corrections along the other two axes were unchanged. Either the crystals had slipped unidirectionally (thus, notice to take extra care in drying mounted crystals in future data collection) or the action of translating the X-ray beam to a fresh part of the crystal, which involved the unlocking and retightening of the restraining ring around the dial, resulted in the shift of the spindle value (again, caution for future collection). Secondly, approximately 10% of the data were salvaged following incorporation (by P.M.D.F.) of film tilt and pivot point calculations in the processing programs. It seems that a film cassette and/or a position on the carousel of the rotation camera did not lock orthogonally to the X-ray beam resulting in a forward tilt of approximately one degree.

In summary, good data have been collected from weakly diffracting crystals by taking advantage of synchrotron radiation. The data are in the middle stages of processing. Heavy-atom derivatives are being used to solve the phase problem and, thus, the initial structure of succinyl-CoA synthetase.

Acknowledgements

This work was supported by a grant to the Medical Research Council Group in Protein Structure and Function and by Grant MT-2805, both from the Medical Research Council of Canada. Provision of beam time and assistance by personnel at SSRL has been greatly appreciated.

References

1. Wolodko, W.T., Kay, C.M. and Bridger, W.A. (1986) *Biochemistry* **25**, 5420-5425.
2. Nishimura, J.S. (1986) *Adv. Enzymol.* **58**, 141-172.
3. Bridger, W.A., Wolodko, W.T. and Williams, S.P. (1987) *Enzyme Dynamics and Regulation*, (Chock, P.B. and Huang, C., eds.), Springer-Verlag Publishers, Chapter 2, pp. 6-16.
4. Wolodko, W.T., James, M.N.G. and Bridger, W.A. (1984) *J. Biol. Chem.* **259**, 5316-5320.

Three-Dimensional Structure of an Oncogene Protein: Catalytic Domain of Human c-H-*ras* p21

Abraham M. de Vos*, Liang Tong*, Michael V. Milburn*, Pedro M. Matias*, Jarmila Jancarik*, Kazunobu Miura•, Eiko Ohtsuka•, Shigeru Noguchi§, Susumu Nishimura§, and Sung-Hou Kim*

Introduction

The most commonly found oncogenes isolated from human tumors or transformed human cell lines belong to the *ras* gene family (1). In the human genome there are three distinct cellular *ras* genes: c-H-*ras*, c-K-*ras*, and N-*ras*, the former two having sequence similarity (2-5) to the transforming principles of the Harvey and Kirsten strains of rat sarcoma viruses (6,7), respectively. All proteins encoded by these genes are called p21, have a molecular weight of 21,000 with 188 or 189 amino acid residues, and have practically identical amino acid sequences, with the exception of the COOH-terminal 25 residues (8). The difference between the normal *ras* proto-oncogenes and the activated (transforming) *ras* oncogenes is usually a single base change at one of a few critical positions, resulting in a single amino acid substitution in p21 (9-11).

Knowledge of the three-dimensional structure of this *ras* protein family should be most useful to provide a basis for understanding the known biochemical functions of both normal and activated proteins.

Results.

We have recently crystallized the catalytic domains of normal as well as activated human ras p21 proteins. The space group of the "catalytic domain" crystals is $P6_522$ with cell parameters $a = b = 83.2$ Å and $c = 105.1$ Å. There is one p21 "catalytic domain" per asymmetric unit and 46 percent of the unit cell volume is protein.We collected diffraction data for the native as well as five heavy-atom derivatives on x-ray films using an Enraf-Nonius rotation camera installed on the eight-pole wiggler branch line (Stanford Synchrotron Radiation Laboratory, Palo Alto, California). The x-ray wavelength for the data collection was either 1.5418 or 1.08 Å, and the crystal-to-film distance was 60 or 85 mm. All the data were collected at 4° C. The films were digitized with the use of a drum scanner by Optronix Corp., and the data were processed with the use of computer programs originally written by Rossmann (12). Reflection data from different films were merged together with the use of the PROTEIN program package (13). The native data set contained about 46,000 observations of 10,400 unique reflections, with an $R_{merge}(I)$ of 8% and a maximum resolution of 2.25 Å. About 300 reflections, missing from this data set because of intensity overload and positional overlap on the films, were later measured using a Nicolet P3/F four-circle diffractometer and added to the native data set.

Five heavy-atom derivatives were used for phasing for phasing. An overall view of the three-dimensional backbone structure of p21 is shown below. The crystal structure at 2.7 Å resolution of the normal human c-H-*ras* oncogene protein lacking a flexible carboxyl-terminal 18 residues reveals that the protein consists of a six-stranded β-sheet, four α-helices and nine connecting loops. Four loops are involved in interactions with bound guanosine diphosphate (GDP): one with the phosphates, another with the ribose and two with the guanine base. The majority of transforming *in vivo* and *in vitro* mutants have single amino acid substitutions at one of a few key positions in three of these four loops plus one additional loop. The biological functions of the remaining five loops and other exposed regions are at present unknown. However, one loop corresponds to the binding site for a neutralizing monoclonal antibody and another to a putative "effector region", mutations in which do not alter guanine nucleotide binding or guanosine triphosphatase activity but reduce the transforming activity of activated proteins. The data provides a structural basis for understanding the known biochemical properties of normal as well as activated *ras* oncogene proteins and reveals additional regions in the molecule that may possibly participate in other cellular functions.

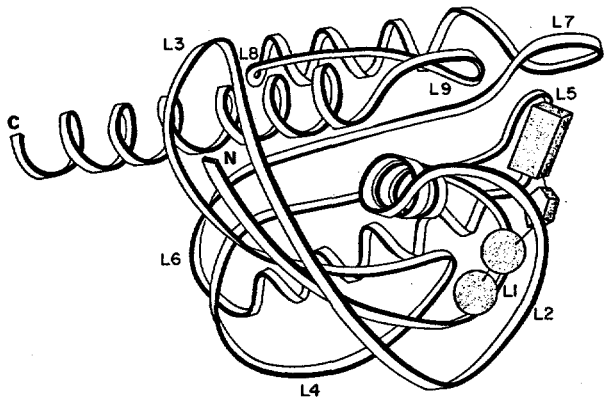

Acknowledgements

We thank Dr. P. Phizackerley, Stanford Synchrotron Radiation Laboratory, Palo Alto, CA for his help in data collection. Supported in part by grants from NIH (GM 29287, CA 45593), and DOE to S.H.K., a gift from Merck, Sharp, and Dohm to the University of California, Berkeley, Grants-in-aid from the Japanese Ministry of Health and Welfare for a Comprehensive 10-Year Strategy for Cancer Control to Su.N., a Research Res ident Fellowship from the Foundation for Promotion of Cancer Research (Tokyo) (Su.N.) and a Damon Runyon-Walter Winchell Cancer Fellowship (P.M.M).

References

*Department of Chemistry and Lawrence Berkeley Laboratory, University of California, Berkeley, CA 94720 USA;
•Faculty of Pharmaceutical Sciences, Hokkaido University, Kita-ku, Sapporo, Japan;
§Biology Division, National Cancer Center Research Institute,Chuo-ku, Tokyo, Japan.

1. S. Nishimura and T. Sekiya, *Biochem.J.* **243**, 313 (1987).
2. C. Shih, L. C. Padhy, M. Murray, and R. A. Weinberg, *Nature (London)* **290**, 261 (1981).
3. T. G. Krontiris and G. M. Cooper, *Proc.Natl.Acad.Sci. U.S.A.* **78**, 1181 (1981).
4. M. Perucho, *et al. Cell* **27**, 467 (1981).
5. S. Pulciani, *et al. Proc.Natl.Acad.Sci.U.S.A.* **79**, 2845 (1982).
6. J. J. Harvey, *Nature (London)* **204**, 1104 (1964).
7. W. H. Kirsten and L. A. Mayer, *J.Natl.Cancer Inst.* **39**, 311 (1967).
8. M. Barbacid, *Ann. Rev. Biochem.* **56**, 779 (1987).
9. C. J. Tabin, *et al. Nature (London)* **300**, 143 (1982).
10. E.P. Reddy, R. K. Reynolds, E. Santos, and M. Barbacid, *ibid.*, p. 149 (1982).
11. E. Taparowsky, *et al.*, *ibid.*, p. 762 (1982).
12. M. G. Rossmann, *J.Appl.Cryst.* **12**, 225 (1979).
13. W. Steigemann, *PROTEIN : A package of crystallographic programs for analysis of proteins.* Max Planck Institute for Biochemistry, Martinsried, West Germany (1982).

STRUCTURAL STUDIES OF ANTIBODIES, ANTIGENS AND ANTIBODY-ANTIGEN COMPLEXES Proposal No. 1A663

I.A. Wilson, E.A. Stura, J.H. Arevalo, G. Lambert and J.M. Rini

Department of Molecular Biology
Research Institute of Scripps Clinic
10666 North Torrey Pines Road
La Jolla, California 92037

INTRODUCTION

In order to understand how the immune system interacts and neutralizes foreign microorganisms such as viruses via surface glycoproteins, it is neccessary to understand the detailed chemistry of antibody-antigen union. In the last decade four antibody Fab' fragments derived from multiple myelomas have been determined to high resolution (1,2). With the advent of the hybridoma technology, specific monoclonal antibodies can now be made against antigens of interest. These advances have aided in the recent successes in the crystal structures of antibody-protein complexes with lysozyme (3,4) and neuraminidase (5) used as immunogens. These studies have provided valuable insights into the detailed interactions of antibodies with proteins and has revealed no major changes in the antigen structure on antibody binding. However, we would like to know the structures of the free antibody, free antigen and antibody-antigen complex for the same system to evaluate changes not only in the antigen but also in the antibody. In addition, different immunogens may produce antibodies which vary in their conformational flexibility such as may be observed when antipeptide antibodies combine with an intact protein. In our laboratory, we have decided to study several antibody systems to advance our knowledge of the detailed interactions in antibody-antigen union. In all of the systems we have not only complex crystals but native Fab crystals as well.

RESULTS AND DISCUSSION

Anti-progesterone Fab' and Fab'-steroid complexes

Crystals have been grown of an anti-progesterone antibody which causes infertility in mice up to 36h after mating (6,7). We have collected several data sets by oscillation photography at SSRL (beam line VII.2) on the anti-progesterone Fab' and steroid-Fab' complexes with progesterone 11-α-OH-progesterone, 11-β-OH-progesterone and aetiocholanolone. In addition, three heavy atoms have been collected, phenyl mercury acetate, ammonium osmium chloride and an iodinated steroid, 11-iodo-benzoyl-progesterone for use in multiple isomorphous replacement methods. Data have been previously collected to 2.8 Å at 1.54 Å wavelength and recently to 2.4 Å at 1.08 Å wavelength. Six data sets have been processed with merging R-factors of 10% on intensities. Difference Patterson maps have been calculated and possible heavy atom positions identified for the three derivatives. The structure determination by multiple isomorphous replacement is well underway. Data from the synchrotron source has been found to be of higher resolution and quality than can be collected in our laboratory on a rotating anode for these hexagonal crystals. Results for this study should enable us to understand the fine specificity of the antibody interactions as well as how even single proton changes in the steroid can completely abolish binding.

Anti-peptide Fab and Fab-peptide complexes

Great interest has been developed recently in the use of synthetic peptides as vaccines. In order to understand how an antibody generated against a short peptide can cross-react with its cognate sequence in the parent protein we have made antibodies against residues 75-100 of the 1975 influenza virus haemagglutinin. We have shown the determinant to be residues 98-106 of the peptide (8). Crystals have been grown of both the free antibody and the antibody-peptide complex (9). Survey of the crystals at SSRL has shown the native crystals to diffract to better than 1.9 Å and the cocrystals to 2.1 Å. The native data can conveniently be collected in our laboratory. However, the synchrotron is necessary to achieve high resolution data on the complex crystals as these are long, thin, plate-like rods.

Catalytic antibody Fab and inhibitor-complex crystals

Crystals of a esterolytic antibody Fab raised against a transition state ester (10) have been crystallized. Surveys at the SSRL have shown the small crystals diffract to at least 3.5 Å resolution but are slightly disordered. Work is in progress to obtain better quality crystals.

Influenza virus HA, PR/8/M5/34

Crystals of the major surface antigen of the 1934 PR/8 influenza virus, the haemagglutinin (HA), have been grown in collaboration with Dr. Walter Gerhard, Wistar Institute. These crystals were tested at the synchrotron and found to diffract significantly better than in our laboratory. However, at present they diffract only to 3.5 Å maximum into the face and 4.5-5.0 Å into the edge of the plate-like crystals. Comparison of this structure with the previously solved 1968 Hong Kong HA (11) will show the extent to which the virus surface can change and be antigenically distinct but still functional for receptor binding and viral fusion.

REFERENCES

1. Amzel, L.M. and Poljak, R.J. (1979) Ann. Rev. Biochem. 48:961-967.
2. Davies, D.R. and Metzger, H. (1983) Ann. Rev. Immunol. 1:87-117.
3. Amit, A.G, Mariuzza, R.A., Phillips, S.E.V. and Poljak, R.J. (1986) Science 233:747-753.
4. Sheriff, S., Silverton, E.W., Padlan, E.A., Cohen, G.H., Smith-Gill, S.J., Finzel, B.C. and Davies, D.R. (1987) Proc. Natl. Acad. Sci. USA 84:8075-8079.
5. Colman, P.M., Laver, W.G., Varghese, J.N., Baker, A.T., Tulloch, P.A., Air, G.M. and Webster, R.G. (1987) Nature 326:358-363.
6. Stura, E.A., Feinstein, A. and Wilson, I.A. (1987) J. Mol. Biol. 193:229-231.
7. Stura, E.A., Arevalo, J.H., Feinstein, A., Heap, R.B., Taussig, M.J. and Wilson, I.A. (1987) Immunology 62:511-521.
8. Wilson, I.A., Niman, H.L., Houghten, R.A., Cherenson, A.R., Connolly, M.L. and Lerner, R.A. (1984) Cell 37:767-778.
9. Schulze-Gahmen, U., Rini, J.M., Arevalo, J.H., Stura, E.A. and Wilson, I.A. (1988) submitted.
10. Tramontano, A., Janda, K.D. and Lerner, R.A. (1986) Science 234:1566-1570.
11. Wilson, I.A., Skehel, J.J., and Wiley, D.C. (1981) Nature 289:366-373.

The Crystal Structure of the Enzyme Phosphoribosyl Transferase

S.L. Edwards, J. Kraut, T. Halloran and S.E. Mills

Departments of Biology and Chemistry
University of California, San Diego
La Jolla, CA 92093

X- ray diffraction data were collected from crystals of the enzyme phosphoribosyl transferase (PRT). These crystals which are moderately unstable and poorly diffracting using standard equipment diffracted quite well using the wiggler beam at port VII-1. With the beam adjusted to a monochromatic wavelength of 1.54 Angstroms the crystals diffracted to a resolution of 3.0 Angstoms, a significant improvement over previous attempts at data collection. These crystals grow in the high symmetry cubic space group, I432. Consequently all of the unique data are represented in a very small wedge of reciprocal space, 1/64 of a sphere. Although our initial intent was merely to investigate the possible resolution enhancement due to the synchrotron source, the actual measurements we recorded on film probably constitute the majority of the data required for a complete data set. These films have yet to be scanned with a densitometer and processed.

This enzyme is important for many reasons. First, it is one of five enzymes that make up the pathway for tryptophan synthesis. The crystal structures of three of these enzymes have been recently solved. If the PRT structure and the one other remaining enzyme structure, anthranilate synthase, could be solved it would represent a major advance in biochemistry: the first complete biosynthetic pathway of an amino acid to be elucidated with crystal structures. The final enzyme of this pathway, tryptophan synthase, was the target used by Dr. Charles Yanofsky of Stanford to prove colinearity between genetic code triplets and amino acids. Of medical interest, PRT is related to the enzyme hypoxanthine guanine phosphoribosyl transferase which is a key enzyme in the mechanism that leads to gout and a particular genetic defect in this enzyme has been identified as the cause of always fatal Lesh-Nyhan's disease. We hope that our continued work will lead to the solution of the crystal structure of this enzyme, a molecule of great biochemical and medical interest.

Crystallographic Studies of Transmembrane Ion Channels

Thomas Earnest, Michael McCarthy, Michael Shuster, Julie Earnest, Kathy Perry, William Montfort, Seunghyon Choe, Robert Stroud

Department of Biochemistry and Biophysics, University of California-San Francisco

Transmembrane ion channels play an important role in various cellular processes such as the signalling between cells and sensory transduction. Until recently it has not been possible to crystallize membrane proteins and obtain a three dimensional structure. The success of Michel, et al., in crystallizing the photosynthetic reaction center, along with the subsequent solution of its structure, has led to an increase in the efforts of many protein crystallographers to crystallize other membrane proteins. Due to the importance of these proteins, the ability to crystallize and solve the three dimensional structure of these systems would represent a significant advance. We are using the rotation camera facility of beam line VII-1 at SSRL to investigate the structure of two transmembrane ion channels which we have recently been able to crystallize: colicin Ia from Escherichia coli and the nicotinic acetylcholine receptor from Torpedo californica. We are also developing low temperature methods (80-130 K) in order to decrease beam damage.

I. Colicin Ia

Colicin Ia is a 70,000 dalton protein consisting of 629 amino acids which can insert into cell membranes to form a voltage dependent ion channel. We have obtained crystals of the soluble form with unit cell dimensions of a=66.3, b=176.6, c=289.8 in the space group $C222_1$. CD studies suggest that alpha helices are the predominant secondary structural motif. We previously collected data to 3.5 angstrom resolution for the native and four putative derivatives at SSRL. These data sets have been scanned and scaled and one derivative solved. This one was unfortunately located on a symmetry axis necessitating more derivatives for phasing.

II. Nicotinic acetylcholine receptor

The nicotinic acetylcholine receptor is the best understood of all of the neurotransmitter receptors. It can be obtained in high concentrations from the electroplax organ of the electric fish Torpedo californica, and consists of a 250,000 dalton multisubunit polypeptide. We have obtained small crystals of detergent solublized AChR in our laboratory which are suitable for x-ray diffraction studies. In our laboratory we have observed reflections out to 15 angstroms. The crystals appear to have a cubic space group with a unit cell length of 257 angstroms. We are continuing to study parameters important for the growth of larger, well ordered crystals. At SSRL we obtained a rotation photograph with reflections out to 19 angstroms.

III. Low temperature x-ray diffraction

Low temperature methods have been used to decrease beam damage to protein crystals for a number of years. Until recently this usually required exchange into a cryo-protecting agent, limiting the general applicability of the method. Recent success in extending the lifetime of ribosome subunit crystals (Yonath and Hope, personal communication) by quick freezing has been quite dramatic. At SSRL and also in our laboratory we have shown that this method could be used to extend the lifetime of our test crystals, lysozyme and thymidylate synthase, although we were unsuccessful, at that time, infreezing our crystals of colicin and AChR. We are presently continuing to develop low temperature methods in our laboratory for use with our crystals of colicin and AChR.

VUV Proposals

The Bonding of Arsenic and Hydrogen to the Si(111) Surface.

Proposal No. 908Vp

R. D. Bringans

Xerox Palo Alto Research Center, 3333 Coyote Hill Rd., Palo Alto, CA 94304

and

M. A. Olmstead

Department of Physics, University of California, Berkeley, CA 94720

INTRODUCTION

The (100) and (111) surfaces of Si and Ge can be passivated very effectively by a single monolayer of As[1-4]. In GaAs-on-Si heteroepitaxy this leads, in part, to island formation rather than two-dimensional growth. This effect has been quantified for GaAs-on-Si(111) in an earlier paper[5] where it was found that the degree of island formation was dependent on the arrival rate of Ga and As atoms and on which species arrived first at the substrate. The details of how the As monolayer on Si surfaces is bonded are thus very important. The stability of Si(111):As against oxygen and air was found to be very great[4] (a 5 minute air exposure only reduced the surface state intensity in UPS spectra by 25%). Interaction of Si(111):As with atomic hydrogen, however, was found to change the surface state density in a reversible way[4]. In the present work we examine the reverse situation. A Si(111) surface which has been terminated with hydrogen atoms was exposed to the type of As_4 fluxes used in molecular beam epitaxy (MBE) of GaAs on Si. The results cast light on the nature of the bonding between Si and As and are also important for understanding how some substrate preparation methods, which leave a hydrogen terminated surface, will interact at moderate temperatures with As.

RESULTS AND DISCUSSION

Photoemission measurements were carried out both on the valence band and on the Si 2p and As 3d core levels. Hydrogen exposures were made with the substrate held at room temperature or at 300°C. A hot filament was placed within 5cm of the surface in order to create H atoms from the H_2 pressure in the chamber. Arsenic exposures were made at As_4 partial pressures in the 10^{-7} to 10^{-6} torr range with the substrate facing away from an effusion cell containing As.

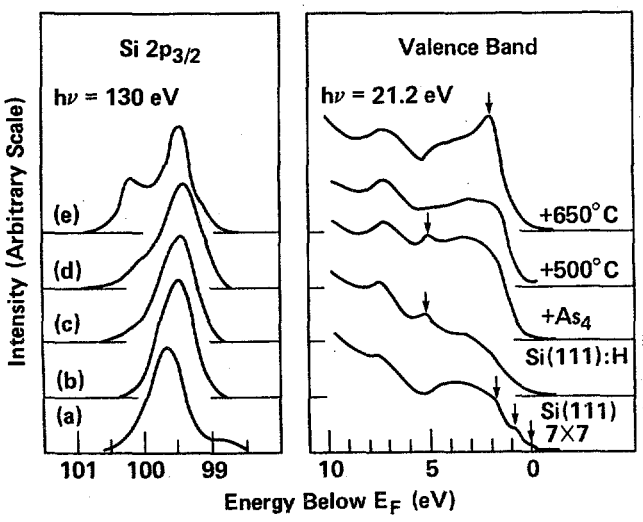

Figure 1. Si $2p_{3/2}$ core level and valence band spectra, taken sequentially on the same surfaces with 130 eV synchrotron radiation and a 21.2 eV He discharge lamp respectively, for (a) the clean Si(111) 7x7 surface and for the same surface (b) after hydrogen exposure plus a 300°C anneal. This hydrogen covered surface was then exposed to As_4 before spectra (c) and subsequently annealed at a number of temperatures with results for 500°C and 650°C being shown in (d) and (e), respectively. Intensities are shown on an arbitrary scale and the plots are aligned in energy at the Fermi energy.

Experiments to study the interaction of arsenic with Si(111):H were carried out under a variety of conditions. The substrate temperature was varied for the H exposure and for the As_4 exposure and annealing studies were made for Si(111):H and for Si(111):H + As. Spectra for one of these surface treatments are shown in detail in Fig. 1. The data correspond to a 1000L hydrogen exposure at room temperature followed by a 6 minute anneal at 300°C to form Si(111):H. This surface was then exposed to As_4 with the substrate held at 300°C for part of the exposure and at room temperature as the As_4 pressure in the MBE chamber was increased and then reduced. The change in the valence band upon hydrogen termination of Si(111) 7x7 can be seen clearly. The three surface states on the Si(111) 7x7 surface (indicated by arrows) disappear and a new peak arises at around 5.0eV below the Fermi energy (shown by the arrow. This latter peak corresponds to the bond between H and Si. There is also a qualitative change in the Si $2p_{3/2}$ spectrum after hydrogen exposure. The surface-related shoulder on the low binding energy side of the main peak disappears and the overall spectrum narrows. Both of these results can be understood as the removal of the complicated Si(111) 7x7 structure, which has many inequivalent Si sites in its unit cell, and its replacement by a 1x1 structure which has only one type of interface Si atom site in addition to the bulk Si site.

Addition of As_4 to the Si(111):H surface increases the photoemission intensity in the region near the top of the valence band, consistent with the increase seen in this region in the earlier angle resolved photoemission experiments[4]. The peak associated with the hydrogen-silicon bond remains visible, suggesting that the As atoms reside on top of the Si(111):H surface. After the 650°C anneal, the valence band and core level spectra are similar to those for Si(111):As. The arrow in (e) shows the peak corresponding to the As lone pair state[4]. The (As 3d / Si 2p) core level intensity ratio decreased by 7% after the 350°C anneal and then remained constant during anneals at successively higher temperatures until the arsenic begins to desorb as the surface was annealed above 750°C.

A measure of the As coverage of the surfaces was determined from the ratio of areas under the As 3d and Si 2p core levels. This ratio was found to be significantly lower for As_4 deposition onto previously hydrogenated surfaces than it was for deposition onto the clean surface. This could be the result of loss of As via AsH_3 desorption or due to the inability of As atoms to find their optimum sites on the Si surfaces when H atoms are present.

The Si 2p core level spectrum for the ideally terminated Si(111):As surface has a bulk contribution and a single, well-defined chemical shift of 0.75eV to higher binding energy[3-5]. This shift identifies the Si atoms at the interface which are each bonded to three As atoms. The Si $2p_{3/2}$ spectrum in Fig 1 for the Si(111):H + As surface after a 650°C anneal has a large shifted component at 0.75eV, but has in addition a small component on the low binding energy side of the bulk peak and significant spectral weight between the bulk and 0.75eV components. This qualitative result can be interpreted to show that the As coverage is not complete after the H atoms have been removed.

It was shown by Uhrberg et al[4] that atomic H interacts in a reversible manner with Si(111):As. The results of the present study show that the inverse reaction is not reversible. We have found that arsenic bonds strongly to the Si(111) surface and displaces hydrogen atoms on the Si(111):H surface. Taken together, these results indicate that if H and As atoms are competing to bond to the Si(111) surface, the As atoms will win. We have also shown that a hydrogen terminated surface is more resistant to bonding to As atoms that is a clean Si(111) 7x7 surface.

ACKNOWLEDGEMENTS

We are grateful for many discussions with J. E. Northrup, and D. K. Biegelsen and for the skillful assistance of J. D. Denlinger, L. E. Swartz, and R. D. Yingling. Part of this work was performed at SSRL which is supported by the DOE Office of Basic Energy Sciences. MAO was partially supported by NSF Grant DMR 8657623.

REFERENCES

1. R. D. Bringans, R. I. G. Uhrberg, R. Z. Bachrach and J. E. Northrup, Phys. Rev. Lett. **55**, 533, (1985).

2. R. I. G. Uhrberg, R. D. Bringans, R. Z. Bachrach, and J. E. Northrup, Phys. Rev. Lett. **56**, 520 (1986).

3. M. A. Olmstead, R. D. Bringans, R. I. G. Uhrberg and R. Z. Bachrach, Phys. Rev. B, **34**, 6401, (1986).

4. R. I. G. Uhrberg, R. D. Bringans, M. A. Olmstead, R. Z. Bachrach and J. E. Northrup, Phys. Rev. B, **35**, 3945, (1987).

5. R. D. Bringans, M. A. Olmstead, R. I. G. Uhrberg and R. Z. Bachrach, Appl. Phys. Lett., **51**, 523, (1987); Phys. Rev. B **36**, 9569, (1987).

Fermi Level Pinning at Sb/GaAs(110) Interface: The Temperature Effects

Renyu Cao, K. Miyano, T. Kendelewicz, I. Lindau, and W. E. Spicer

Stanford Electronics Laboratories

Stanford University, Stanford, CA 94305

Sb/GaAs has been attracting attention for many years due to its unique interface structure. Extensive theoretical and experimental studies have been performed, and nearly perfect interface has been reported even at room temperature. How this interface structure affects the Schottky barrier formation has been a controversial issue. Here we report a systematic study on Sb/GaAs interface with various thermal treatments in order to test several hypotheses. The purpose of this report is to present a summarized view of the band bending issue at this interface. Detailed analysis and discussion has been published else where [1].

The experiment was performed at the Stanford Synchrotron Radiation Laboratory (SSRL) with tunable synchrotron radiation as the source for soft x-ray photoelectron spectroscopy (PES). All the sample preparation and measurements were done in a UHV chamber with base pressure in the mid 10^{-11} torr range. A low coverage evaporator which enables us to do an initial stage band bending study was used. PES core levels (Ga 3d, As 3d, and Sb 4d) and valence band spectra were taken after each step of preparation. A computer deconvolution routine was applied to separate the substrate bulk component from the core level spectra and track them throught the evaporation series to measure band bending.

Figure 1 illustrates the surface Fermi level as a function of Sb coverage on n- and p-type GaAs at room temperature (RT) and low temperature (LT) (-120°C). It shows that at RT band bending is saturated around one monolayer (ML) of Sb coverage and the surface Fermi levels are pinned around 0.75eV and 0.5eV above valence band maximum (VBM), consistent with photoemission measurements in the past [2]. LT band bending measurement has also been done. The dashed line shows that the substrate band bending at LT behaves in a manner similar to that at RT. The similarity in the pinning pattern at RT and LT is in contrast to other systems, where a change in cluster formation at different temperature has been attributed for the drastic change in Fermi level pinning [3].

Figure 2 illustrates the surface Fermi level position of n- and p-type GaAs when Sb/GaAs interfaces were annealed in the range between 300°C and 450°C. Large variation in surface Fermi level position for p-type GaAs has been observed right after annealing, which is qualitatively in agreement with the result reported by Schäffler *et al.* [4] although in our result p-type GaAs does show some dependence of the band bending on the annealing temperatures. In the contrast, change of band bending for n-type GaAs is barely seen in our annealing temperature range.

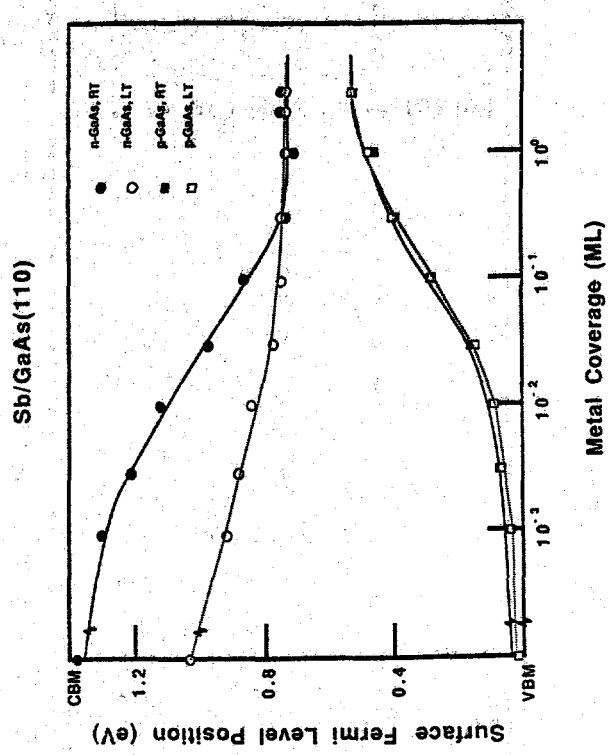

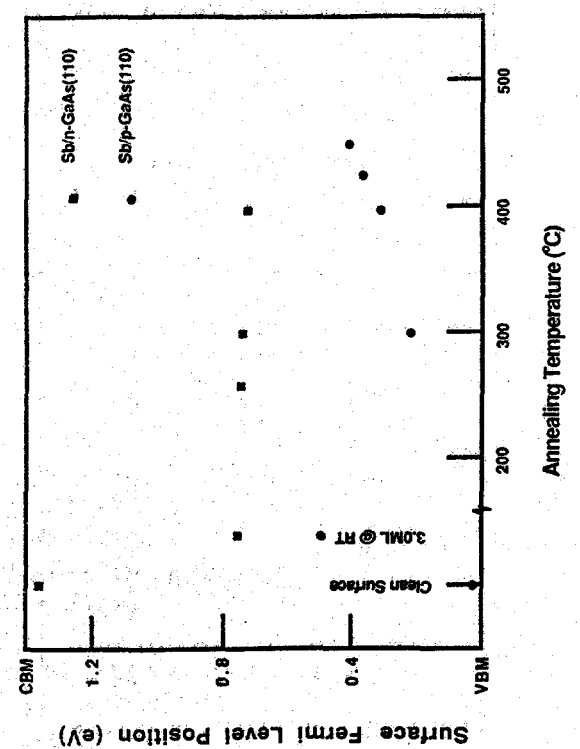

The nature of Schottky barrier formation at the Sb/GaAs interface has been argued for a long time. Theoretical calcutions [5,6] based on a zig-zag chain model suggests that the Sb-derived states lie inside the valence band and conduction band or very close to conduction band minimum, and thus those states can not be responsible for the Fermi level pinning around mid band gap. In another words, any band bending has to be explained by other interface states. The photoemission data show that Sb depostion does induce the band bending for both n- and p-type GaAs. The positions of the surface Fermi levels are 0.75eV for n-type GaAs and 0.5eV for p-type GaAs above the VBM, same as those in other metal or oxide-GaAs systems. The coincidence of the pinning position suggests that even at an interface such that strong chemical bonds are formed, defects [7] may still play a dominant role in the Schottky barrier formation. The Fermi level pinning at LT can also be understood. Detailed analysis has shown that the interface morphological and chemical structure does not change much upon the substrate temperature. Therefore the pinning mechanism is, conceivably, the same at both RT and LT.

Schäffler *et al* [4] argued that room temperature band bending is due to a non perfect Sb/GaAs interface and after annealing the interface, a higher degree of perfection is achieved, resulting in a decrease of band bending. The so-called Sb-derived states have been attributed to the residual 0.28eV band bending. Furthermore same kind of behavior was predicted for Sb/n-GaAs. Clearly it is not the case on the basis of our study. On the other hand, under the framework of defect mode one has to include the change of the relative density of donor states versus acceptor states upon annealing to explain the different pinning behavior of n- and p-type GaAs upon annealing, although it seems plausible to explain the Fermi level pinning at Sb/GaAs interface prepared at RT and LT.

This work was supported by ONR under contract number N00014-85-0736. The experiment was performed at SSRL, which is supported by Department of Energy, Office of Basic Science Research and National Science Fundation, Division of Materials Research.

References

1. R. Cao, K. Miyano, T. Kendelewicz, I. Lindau, and W. E. Spicer, J. Vac. Sci. Technol. **A 6(3)**, in press.
2. P. Skeath, C. Y. Su, I. Lindau, and W. E. Spicer, J. Vac. Sci. Technol, **17**, 874 (1980).
3. R. Cao, K. Miyano, T. Kendelewicz, K. K. Chin, I. Lindau, and W. E. Spicer, J. Vac. Sci. Technol. **B 5(4)**, 998 (1987).
4. F. Schäffler, R. Ludeke, A. Taleb-Ibranimi, G. Hughes, and D. Rieger, J. Vac. Sci. Technol. **B 5(4)**, 1048 (1987); Phy. Rev. **B 36**, 1328 (1987).
5. C. M. Bertoni, C. Calandra, F. Manghi, and E. Molinari, Phy. Rev. **B 27**, 1251 (1983).
6. C. Maihiot, C. B. Duke, and D. J. Chadi, Phy. Rev. Lett. **53**, 2114 (1984); Phy. Rev. **B 31**, 2213 (1985).
7. W. E. Spicer, I. Lindau, P. Skeath, C. Y. Su, and P. Chye, Phy. Rev. Lett. **44**, 420 (1980).

Figure Captions

Figure 1 Band bending diagrams as a function of Sb coverage. The surface Fermi levels are pinnied at 0.75eV and 0.5eV above VBM for n- and p-type GaAs respectively.

Figure 2 Band bending diagram as a function of annealing temperature. Large variation in band bending for p-type GaAs (from 0.5eV to 0.2eV) has been observed but not for n-type GaAs.

Low Temperature Deposition of Ag and Pd on HgCdTe* Proposal No. 935Vp

Glen P. Carey, A. K. Wahi, T. T. Chiang, I. Lindau, and W. E. Spicer

Stanford Electronics Laboratories

Many studies have shown that metal/HgCdTe interfaces formed at room temperature generally exhibit profound intermixing of the semiconductor and overlayer metal, to an extent far greater than for interfaces formed on Si or GaAs. The usual disruption at the interface upon overlayer formation and the concurrent loss of Hg in the near surface cause the interface to be very complex, both morphologically and electrically. Since metal interdiffusion, chemical reactions and Hg loss should be inhibited in interfaces formed at lower temperatures, leading to a simplification of the interface, an experimental approach is followed where Ag and Pd are deposited in ultrahigh-vacuum (UHV) ($p < 10^{-10}$ torr) onto atomically clean (110) $Hg_{0.77}Cd_{0.23}Te$ surfaces cooled to 100 K. These metals have similar telluride heats of formation[1]: $\Delta H_f(Ag_2Te)$ = -8.6 kcal/mole and $\Delta H_f(PdTe)$ = -9.0 kcal/mole, but Pd also has predicted high heats of solution[2] with the cations: $\Delta H_{sol}(Cd;Pd)$ = -32.4 kcal/mole and $\Delta H_{sol}(Cd;Pd)$ = -26.2 kcal/mole. This high of solution for the Pd case results in vastly different interface morphology between these two interfaces formed at room temperature (RT), and the RT interfaces formed between them and HgCdTe have been previously investigated[3,4]. Incremental overlayer coverages ranging from sub-monolayer (ML) at low coverages to several ML at higher coverages were employed in this study. The evolution of both of these low temperature (LT) interfaces are studied using the surface sensitive techniques of photoemission spectroscopy (PES) employing synchrotron radiation and low energy electron spectroscopy (LEED), and compared to the corresponding room temperature (RT) interfaces.[3,4] The HgCdTe crystals used in this study are bulk *p-type*. Preliminary analysis of the data reveals that the LT interfaces are more abrupt than the RT cases, but more in depth analysis of the data is necessary before any concrete conclusions can be drawn from this study.

References

*This work is supported by DARPA contract # N00014-86-K-0854

[1]K. C. Mills, *Thermodynamic Data for Inorganic Sulphides, Selenides, and Tellurides* (Butterworths, London, 1974).

[2]A. R. Miedema, P. F. de Châtel, and F. R. de Boer, Physica B **100**, 1 (1980).

[3]D. J. Friedman, G. P. Carey, C. K. Shih, I. Lindau, W. E. Spicer, and J. A. Wilson, J. Vac. Sci. Technol. A **4**, 1977(1986).

[4]G. P. Carey, D. J. Friedman, and W. E. Spicer, to be published.

Ag/GaAs INTERFACE : REVERSIBILITY OF FERMI LEVEL PINNING

T. T. Chiang, C. J. Spindt, G. P. Carey, A. K. Wahi, I. Lindau, and W. E. Spicer
Stanford Electronics Laboratories
Stanford University, Stanford, CA 94305

The surface fermi level of a well-cleaved, clean GaAs(110) surface lines up with the bulk fermi level, as surface reconstruction has swept all the surface states out of the band gap. As metal is deposited on this clean, "unpinned" surface, midgap electronic states are created, pinning the surface fermi level near midgap. Generally, there is agreement that it is the creation of these midgap electronic states which pin the surface fermi level. However, there is disagreement as to the physical nature of these midgap states. Currently, the two main schools of thought on this issue center around "metal induced gap states" (MIGS) [1] and defects [2].

Attempts to study this problem are complicated by the fact that the metal/semiconductor interface is very complex, with many processes occurring simultaneously. Among these complicating processes are interdiffusion and chemical reaction. To minimize these effects, one would like to choose a metal which reacts weakly with GaAs. Ag is an excellent choice based on this consideration. Evidence of cluster formation even at room temperature is indicative of its low reactivity with GaAs [3], because it reveals the strong preference of the Ag atom to bond to other Ag atoms rather than to a Ga or As atom.

Previous works on the Ag/GaAs interface have concentrated on room temperature [3] and low temperature metal depositions [4]. We complement these studies by annealing to very high temperature after metal deposition [5]. However, this high temperature anneal should not exceed 580°C at which there is significant decomposition of the GaAs crystal [6]. We chose to perform a 500°C anneal and made the interesting observation that the surface fermi level actually moved from the "pinned" position back toward the "unpinned" (bulk) position. This behavior is accompanied with Ag clustering which leaves the vast majority of the surface bare. To gain more perspective on this high temperature annealing process, the experiment was repeated for the Al/GaAs interface. Al was selected because of its strong reactivity with GaAs. Al on GaAs is known to undergo a replacement reaction, in which adsorbed Al goes into a fraction of the surface Ga sites. The result of the Al/GaAs annealing experiment was markedly different from the Ag case. After a 500°C anneal, the surface fermi level remained "pinned" and the Al did not cluster or leave the surface.

By depositing monolayer coverage of Ag on freshly-cleaved, clean GaAs(110) surface, the surface fermi level was found to pin at 0.45±0.05 eV above VBM (valence band maximum) for p-GaAs and 0.65±0.05 eV above VBM for n-GaAs, due to the formation of midgap electronic states. Upon annealing to 500°C, the Ag on the surface clustered into islands and the surface fermi level moved back to within 0.2eV of the bulk position (CBM and VBM for n and p types respectively.) Further deposition of Ag on the annealed surface moved the surface fermi level back to the previously pinned positions. The surface fermi level movement was monitored using Ga3d and As3d photoemission signals (excited by 100eV synchrotron radiation). The Ag clustering was seen both by a dramatic decrease in the Ag4d photoemission signal (excited by 70eV synchrotron radiation) and by scanning Auger microscopy (SAM). Scanning electron microscopy (SEM) also revealed that the Ag clustering formed hemispherical-like islands with a size distribution up to ~500Å in diameter. The average island separation is about a few thousand angstroms (~2000Å). As a comparison with a reactive metal, similar annealing experiments were performed for monolayer coverage of Al on GaAs. For the Al case, the metal remained unclustered after annealing and the surface fermi level remained pinned.

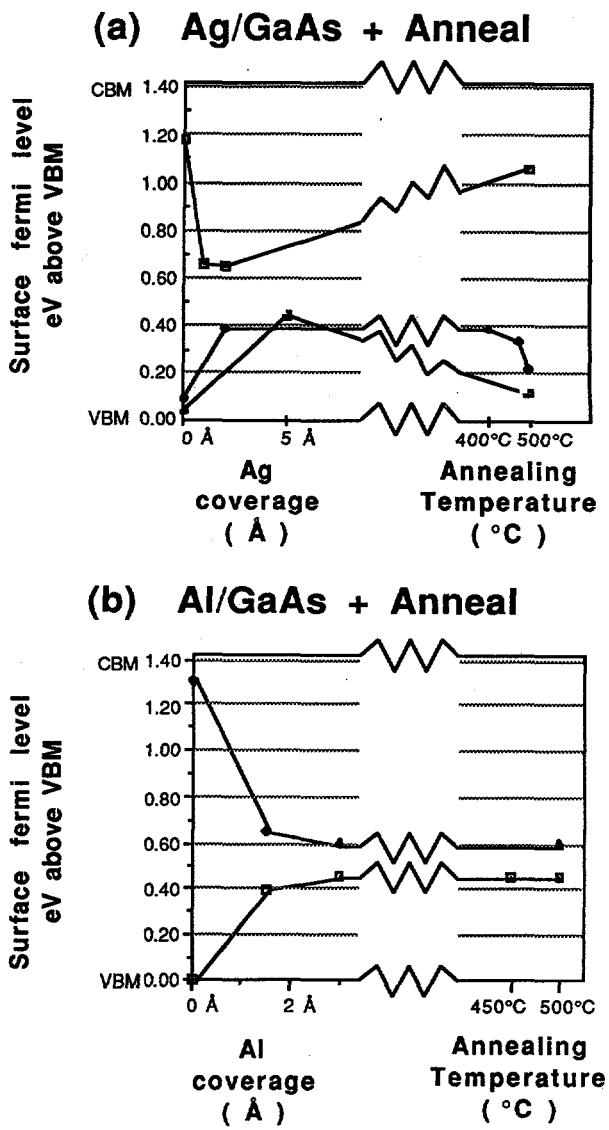

Fig. 1 Movement of surface fermi level as a function of surface treatment. In (a), Ag overlayer is deposited on cleaved, clean GaAs(110) surface, followed by high temperature anneals. In (b), Ag is replaced with Al. p-GaAs samples start from near VBM, while n-GaAs samples start from near CBM.

In summary, our experimental findings indicate that monolayer metal deposition on GaAs pins the surface fermi level near midgap. In the case of Ag, annealing this Ag-covered GaAs surface around 500°C causes the Ag on the surface to cluster and moves the surface fermi level back to within 0.2eV of the bulk position. For the Al case, upon annealing, there is no evidence of clustering and the surface fermi level remains pinned. This result can be adequately explained by both the "metal induced gap state" (MIGS) model and the defect model of Schottky barrier formation [5]. However, even though both models can adequately explain the gross features of these experimental findings, they do have their problems in accounting for particular details. Clearly, more experimental and theoretical work is needed to establish a complete understanding of these results.

This work was supported by the U.S. Defense Advanced Research Projects Agency (DARPA) and the U.S. Office of Naval Research (ONR) under Contract No. N00014-83-K-0073. The SEM (scanning electron microscopy) and SAM (scanning Auger microscopy) experiments were performed at the Center for Integrated Systems (Stanford University) by Dr. R. Browning.

REFERENCES

[1] J. Tersoff, Phys. Rev. Lett. **52**, 465 (1984).
[2] W. E. Spicer, I. Lindau, P.Skeath, C.Y. Su, and P. Chye, Phys. Rev. Lett. **44**, 420 (1980).
[3] R. Ludeke, T.-C. Chiang, and T. Miller, J. Vac. Sci. Technol. **B 1(3)**, 581 (1983).
[4] R. Cao, K. Miyano, T. Kendelewicz, K.K. Chin, I. Lindau, and W. E. Spicer, J. Vac. Sci. Technol. **B 5(4)**, 998 (1987).
[5] For details, see T. T. Chiang, C. J. Spindt, W. E. Spicer, I. Lindau, and R. Browning, submitted for publication in the Proceedings of 15th PCSI conference, to appear in J. Vac. Sci. Technol..
[6] C. T. Foxon, J. A. Harvey, and B. A. Joyce, J. Phys. Chem. Solids **34**, 1693 (1973).

Critical Review of Valence Band Offset Measurements

Proposal No. 935Vp

R. S. List, I. Lindau and W. E. Spicer

Stanford Electronics Laboratories
Stanford University, Stanford, CA 94305

The progress in understanding heterojunction band lineups has increasingly become dependent upon the availability of accurate and reliable measurements. The reported values of the band offset for the Si / GaAs system measured by photoemission range from 0.05 eV to 0.70 eV. Such a large scatter in experimentally determined discontinuities is common for other systems as well and not only makes the evaluation of different theories difficult, but raises the question as to whether such variations are real and representative of technological variations in the offset. Clearly the understanding and control of these variations is essential before any device applications can be realized.

We attempted to study the source of these variations in the Si / GaAs (110) heterojunction. We altered the growth conditions to effect modifications in the overlayer crystalline order, strain and chemical reactivity. The collective consideration of the above factors gives us a coherent overview of the problems involved in discontinuity measurements. To study and characterize the above factors we relied heavily upon photoemission, near edge structure and surface extended x-ray absorption fine structure measurements performed at the Stanford Synchrotron Radiation Laboratory. The Jumbo monochromater beamline at SSRL has unique capabitities of studying absorption across the Si K-edge (1840 eV). In our studies we found the offset to be $0.23 \pm 0.0.5$ eV for both amorphous and crystalline overlayers, either strained or unstrained. We did, however, observe discontinuities as large as 0.7 eV for room temperature growths. We show that such large discontinuities are due to dangling bond type states which extend into the bandgap and change the apparent valence band maximum energy. These states can be removed by annealing the sample without crystallization. Offsets as small as 0.05 eV may be inferred from our data if we fail to account for the contributions of rather subtle chemical effects at the interface. The analysis technique employed in determining the valence band maximum has also been examined and found to yield large absolute variations. Theoretical valence band maxima fitting has been used to remove such errors. Overall we found the discontinuity to be more dependent on the interpretation of the data than on technological variations. If we discern and properly account for extrinsic effects and unambiguously define the discontinuity, photoemission can yield accurate and single valued measurements of the valence band discontinuity.

Direct Measurement of Pinning States in the Band Gap ?

With the recently acquired access to new beamlines at SSRL with greatly enhanced photon flux and resolution, and the anticipation of even brighter sources in the near future, we are attempting to push the sensitivity limits of our photoemission experiments to new limits. A natural system of interest to us is the pinned GaAs surface which is thought to have roughly 0.01 of a monolayer of defect states in the GaAs band gap near midgap. While the importance of the high flux and surface sensitivity of synchrotron radiation is obvious to such an experiment, the high resolution and tunability of synchrotron radiation experiments allow us to resolve these states from the valence band maximum and also sweep the photon energy across the Ga, As and overlayer absorption edges to look for a resonance of the defect states, thereby giving us insight into their nature and origin. A preliminary experiment has been performed during the first run of the new TGM monochromater which demonstrated that there is sufficient flux and resolution for the experiment. We are anticipating the installation of filters in the beamline to greatly reduce the background from second order light and assembling a new high resolution, high throughput hemispherical electron analyzer which combined should allow for the successful completion of this experiment.

Papers published

R. S. List, T. Kendelewicz, M. D. Williams, C. E. Mccants, I. Lindau and W. E. Spicer, "Chemical Reactions at the Si / GaAs (110) and Si / InP (110) interfaces: Efects on Valence Band Discontiuity Measurements," J. Vac Sci. Technol. A, proceedings of the National Symposium of the American Vacuum Society, Anaheim, CA 1987, (in press).

Papers submitted

R. S. List and W. E. Spicer, "Can Photoemission Measure Valence Band Discontinities ?" J. Vac. Sci. Technol. B, Proceedings of the Conference on the Physics and Chemistry of Semiconductor Interfaces, Asilomar, CA 1988.

Proposal No. 935Vp

Data Acquisition Software for the New μ-VAX Beam-line Computers

Peter H. Mahowald

Stanford Electronics Laboratories
Stanford University, Stanford, CA 94305

The data acquisition and data analysis computer programs "Exp" and "Auto",which have been used by Stanford and other groups on the VUV beam lines, now operate on the new μ-Vax beam line computers. Work is in progress to polish the final versions.

These programs take advantage of the features of the new μ-Vax computers. For instance, they use the multiple-window capability of the large μ-Vax operators console, and they use the sophisticated CAMAC control routine called VAXMOTORS.

The main advantages of this software over other existing systems are threefold. One, it is faster to use, both in terms of fast computer response and saving the operator unnecessary interaction with the computer. Second, by its internal design it is less prone to bugs which interrupt data-acquisition. Third, it has a great depth of commands (including commands which can be programmed at the beam line by non-experts). These programs are command oriented (with menus when requested) and the documentation is available from SSRL.

A Substrate Doping Variation Study of the Pinning States at Metal / GaAs(110) Interfaces

Proposal No. 935Vp

K. E. Miyano, R. Cao, T. Kendelewicz, C. J. Spindt, P. H. Mahowald, I. Lindau, and W. E. Spicer

Stanford Electronics Laboratories, Stanford University, Stanford, CA 94305

Schottky barrier formation at metal / n-GaAs(110) interfaces has been studied with photoemission spectroscopy by varying the substrate doping from 4 x 10^{16} to 5 x 10^{18} cm^{-3}. The results challenge certain assumptions that have been made in past barrier formation models. For the clustered systems investigated -- In, Ga, and Ag on n-GaAs -- the issue of lateral inhomogeneity of the interface state density is considered. Assuming that the interface states exist only beneath the clusters, lateral variation of the surface potential is expected. An increase of the substrate doping reduces the lateral depletion and should thereby affect this variation. However the core level lineshapes exhibit no evidence of an inhomogenious surface potential for any doping or coverage, even when the depletion length is in the neighborhood of the average cluster spacing. Consequently scenarios are considered in which pinning states are more uniformly distributed than the overlayer material itself.

In modeling low coverage potential barrier formation, one might suppose that the net interface charge for a given low coverage is independent of the substrate doping. Under this assumption the total band bending for a given coverage is expected to be inversely proportional to the dopant concentration. For the systems examined in this study -- In, Ga, Ag, Sn, and Sb on n-GaAs -- an inverse relationship between band bending and doping is observed, but the dependence is much weaker than a proportionality. The data for Ag, which is representative of all five systems, is displayed below. In the context of a defect model of the interface charge states, this weakened dependence is consistent with a defect state whose nature depends on the local Fermi level position, as has been suggested by Walukiewicz.[1] Metallic screening from the overlayer may also reduce the dependence of band bending on doping, but such an explanation is not valid at the lower coverages of this study.

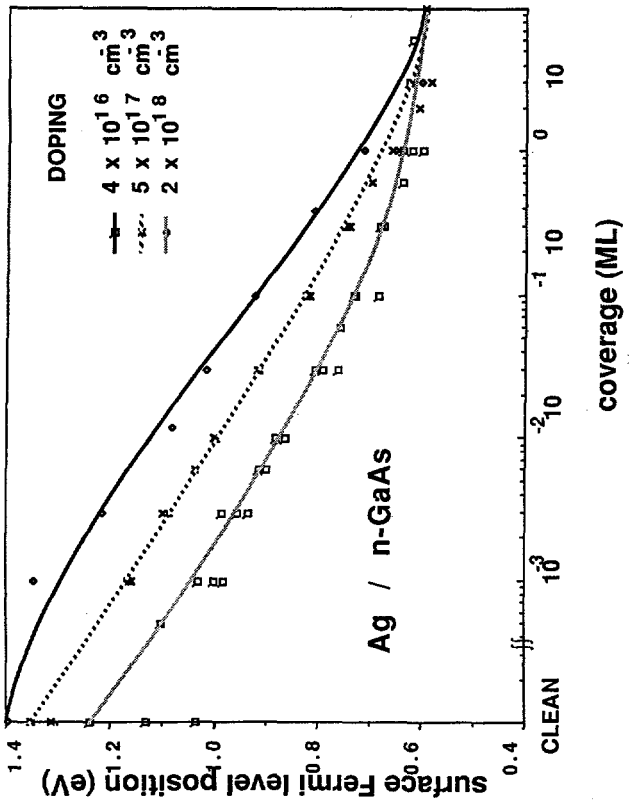

1. W. Walukiewicz, J. Vac. Sci. Technol. B **5**, 1062 (1986); W. Walukiewicz, this Proceedings.

Proposal No. 935Vp

A STUDY OF THE Ag/ZnTe, Al/ZnTe, and Al/CdTe METAL/II-VI (110) INTERFACES

A. K. Wahi, G. P. Carey, T. Chiang
I. Lindau and W. E. Spicer

Stanford Electronics Laboratories
Stanford University, Stanford CA 94305

We have performed a preliminary study of metal/ZnTe interface formation and extend a previous study of metal/CdTe interfaces [1] in order to investigate interfacial chemistry and morphology and also to compare Fermi level pinning behavior in these systems. In comparison to metal/III-V interfaces, interfacial chemistry and morphology in metal/II-VI systems have not been as extensively studied. A photoemission study of metal/CdTe interface formation published recently by Friedman *et al.* [1] determined the final position of the surface Fermi level relative to the valence band *maximum*, E_f-E_{vbm}, for three noble metals on CdTe: Cu, Ag, and Au. Determining whether non-reactive and reactive metal overlayers, which can yield quite different and complex interface morphologies, yield similar Fermi level pinning positions within the semiconductor bandgaps (for CdTe and ZnTe, respectively, 1.5 eV and 2.2 eV) and also comparing the relative pinning positions of the same metals on two different semiconductors can aid in distinguishing metal-dependent effects and those due primarily to the semiconductor substrate. Such information on Fermi level pinning is important as it relates to various models of Schottky barrier formation in metal/semiconductor systems.

Metal interfaces with ZnTe and CdTe are also important in understanding metal/$Hg_{1-x}Cd_xTe$ and metal/$Hg_{1-x}Zn_xTe$ interface formation. Studies of metal/$Hg_{1-x}Cd_xTe$ interfaces [2] point to the role of the weak Hg-Te bond in these alloys and the consequent ease of Hg loss as a major factor contributing to the high degree of interface non-abruptness and semiconductor disruption that occur with metal deposition. Examining the interface morphology of the corresponding binaries CdTe and ZnTe can lead to further understanding of the role of the weak Hg bonding in Hg-containing alloys during deposition of metal overlayers. Determining pinning levels for the two binary extremes of alloy composition can also aid in predicting surface Fermi level positions in the alloys [3].

Ag/ZnTe, Al/ZnTe, and Al/CdTe INTERFACE FORMATION

We have focused on the metals Ag and Al, predicted to be, respectively, non-reactive and highly reactive with Te [2] and thus lead to very different interface morphologies. Differences in heats of solution of Cd or Zn alloying in the metal overlayer also influence resulting interface morphology. Heats of alloying calculated using the Miedema model [4] indicate that Zn alloys in Al more readily than Cd. Initial analysis of Al/ZnTe and Al/CdTe data does show features evolving in the Al2p core level spectra on ZnTe with successive Al metal deposition that indicate a more complex interface is being formed in this case, with possibly more than one other component than reacted Al present. Detailed analysis of core level spectra to determine the presence of dissociated Zn or Cd and reacted Te components at the interface and their evolution with overlayer growth is underway.

Preliminary analysis of band bending results for Al/CdTe and Al/ZnTe indicate the same pinning position, E_f - E_{vbm}, for both semiconductors. In studying Al, a much more reactive metal than the noble metals Ag, Au, or Cu on CdTe, a very different interface morphology is expected; however, a similar Fermi level position is found. This result is at variance with other workers [5] and does not support a model of metal work function-dependent Schottky barrier height. Detailed analysis of data is necessary in order to correlate band bending results with interface evolution.

This work is supported by DARPA/ONR under Contract No. N00014-86-K-0854.

REFERENCES

1. D. J. Friedman, I. Lindau, and W. E. Spicer, submitted for publication.
2. D. J. Friedman, G. P. Carey, C. K. Shih, I. Lindau, W. E. Spicer, and J.A. Wilson, J. Vac. Sci. Technol. A 4,1977(1986).
3. W. E. Spicer, D. J. Friedman, and G. P. Carey, Proceedings of 1987 MCT Workshop, to be published.
4. A. R. Miedema, P. F. de Chatel, and F. R. de Boer, Physica B **100**, 1(1980).
5. R. H. Williams and M. H. Patterson, Appl. Phys. Lett. **40**, 484 (1982).

CORE LEVEL SPECTROSCOPY OF Yb-COMPOUNDS

Proposal No. 941Vp

I.Abbati, L.Braicovich, M.Sancrotti
Istituto di Fisica - Politecnico di Milano
32 Piazza Leonardo da Vinci - 20133 Milano (Italy)

E.Puppin, I.Lindau
Stanford Electronics Laboratories - Stanford University
Stanford - CA 94305 USA

R.Eggenhoffnerr
Dipartimento di Fisica - Universita' di Genova
Via Dodecaneso - 16100 Genova (Italy)

A.Iandelli, G.L.Olcese and A.Palenzona
Istituto di Chimica-Fisica - Universita' di Genova
30 Corso Europa - 16132 Genova (Italy)

INTRODUCTION

In the past years, core level spectroscopies have been widely applied to Rare-Earth (RE) compounds in order to investigate the relationship between their peculiar properties, such as Kondo effect and valence fluctuations, and their electron-states distribution. In the field of light RE-compounds, it is at present well known that valence and core level spectra usually exhibit a rich variety of features which are strictly related to the high-energy nature of the photon excitation and are very indirectly related to the ground-state properties of the samples. Typical examples are shake-up and shake-down satellites and final-state configuration cross-over. On the contrary, core level spectra from heavy RE-compounds, especially Yb-compounds, have been so far interpreted as useful tools capableto give direct informations on the ground-state properties.

Here we report strong final-state effects in the Yb-L_{II} and -L_{III} X-ray absorption spectra of $YbIn_3$ and Yb_2Ag_7. While magnetic susceptibility measurements and shallow core level spectroscopy (XPS,UPS) suggest a divalent configuration for the Yb-ions of these compounds, our XAS spectra reveal strong contributions related to the trivalent configuration.

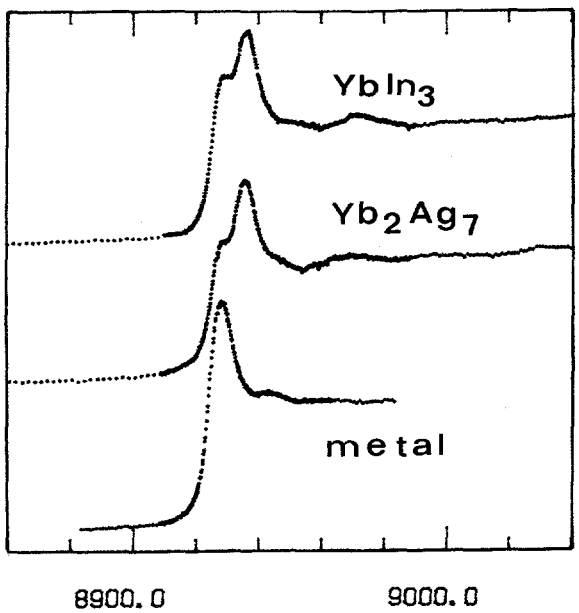

Fig. 1

RESULTS AND DISCUSSION

Clean surfaces were prepared by scraping the samples with a diamond file in a Ultra-High Vacuum chamber. The XAS spectra were collected in the total-yield mode.

Fig 1 shows the XAS spectra, excited at the Yb-L_{III} edge, from $YbIn_3$, Yb_2Ag_7 and Yb-metal (for reference). Strong "white-lines",corresponding to the dipole allowed 2p---5d transitions, are clearly evident in the near edge region of all these spectra. Whereas in the pure metal case only a single white line is observed, which correspond to the divalent configuration, a second peak is present in the other spectra. The two components of this latter double-peak feature can be assigned, respectively, to ions in the $4f^{14}$ (divalent) configuration and ions in the $4f^{13}$ (trivalent) configuration. On the other hand, these Yb-compounds are unambigously recognised as purely divalent samples through an analysis of their magnetic properties and their 4f-photoemission spectra. Thus, the trivalent components in the XAS spectra turn out to be a final-state effect (shake-up), strictly related to the creation of the deep Yb-2p core hole.
Photoemission investigation of accessible core levels in $YbIn_3$ and Yb_2Ag_7 is in progress.

REFERENCES

1) F.U.Hillebrecht and J.C.Fuggle, Phys.Rev. B25, 3550 (1982)
2) E.V.Sampathkumaran, G.Kaindl, W.Krone, B.Perscheid and R.Vijayaraghavan, Phys.Rev.Lett. 54, 1067 (1985)
3) G.K.Wertheim, E.V.Sampathkumaran, C.Laubschat and G.Kaindl, Phys.Rev. B31, 6836 (1985)

Observation of Many New Argon Valence Satellites Near Threshold*

U. Becker,** B. Langer,† H.G. Kerkhoff,† M. Kupsch,† D. Szostak,†
R. Wehlitz,† P.A. Heimann,‖ S.H. Liu, D.W. Lindle,††
T.A. Ferrett,†† and D.A. Shirley

Materials and Chemical Sciences Division
Lawrence Berkeley Laboratory
and
Department of Chemistry
University of California
Berkeley, California 94720

High resolution photoelectron spectra and zero-volt electron scans were measured following synchrotron radiation excitation of argon, to elucidate the photon energy range between threshold and the Cooper minimum region of the Ar 3s photoline. A number of the "correlation satellite" lines show a dramatic increase of fractional intensity toward threshold, yielding a total of about 40 observed photolines at threshold, of which more than half were not previously observed in photoemission (see Figure 1). This effect is interpreted as arising from inelastic scattering of the outgoing photoelectron by the residual ion, yielding high angular momentum ionic states otherwise inaccessible by photoemission.

*This work was supported by the Director, Office of Energy Research, Office of Basic Energy Sciences, Chemical Sciences Division of the U.S. Department of Energy under Contract No. DE-AC03-76SF00098. It was performed at the Stanford Synchrotron Radiation Laboratory, which is supported by the Department of Energy's Office of Basic Energy Sciences.

**Present address: Physikalisches Institut, Universitat Wurzburg, Am Hubland, D-8700 Wurzburg, West Germany.

†Permanent address: Technische Universitat Berlin, Institut fur Strahlungs- und Kernphysik, Sekr PN 3-2, Hardenbergstr. 36, D-1000 Berlin 12, West Germany.

‖Present address: Technische Universitat Munchen, Physik-Department E20, 8046 Garching b, Munchen, W. Germany.

††Present address: National Bureau of Standards, Gaithersburg, MD 20899.

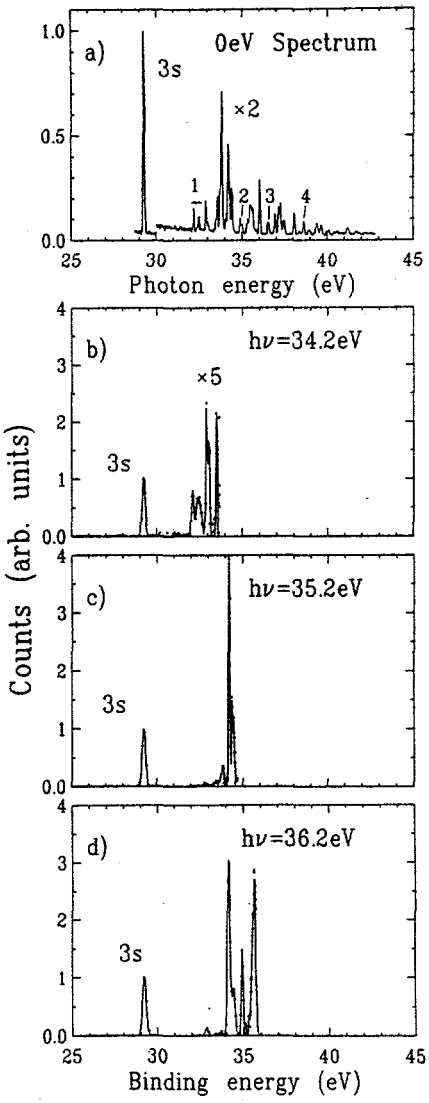

Figure 1. Photoelectron spectra (b-d) taken in the near-threshold region of the satellites with lower binding energy together with a zero-volt electron scan (a) between 29 and 43 eV.

Photoelectron Asymmetry Parameter for the S 2p Level of SO_2*

T.A. Ferrett,† P.A. Heimann,** H.G. Kerkhoff,†† U. Becker,††
D.W. Lindle,† and D.A. Shirley

Materials and Chemical Sciences Division
Lawrence Berkeley Laboratory
and
Department of Chemistry
University of California
Berkeley, California 94720

We present a measurement of the asymmetry parameter (β) for S 2p core-level photoionization of SO_2 in the vicinity of several continuum resonances (see Fig. 1). Results are contrasted with β(2p) for the central atoms of the molecules SF_6 and SiF_4. Atomic calculations for β(S 2p) appear to reproduce qualitatively the molecular curve for SO_2 aside from a shift to lower β-values for the molecular case.

*This work was supported by the Director, Office of Energy Research, Office of Basic Energy Sciences, Chemical Sciences Division of the U.S. Department of Energy under Contract No. DE-AC03-76SF00098. It was performed at the Stanford Synchrotron Radiation Laboratory, which is supported by the Department of Energy's Office of Basic Energy Sciences.

†Present address: National Bureau of Standards, Gaithersburg, MD 20899.

**Present address: Technische Universitat Munchen, Physik-Department E20, 8046 Garching b, Munchen, W. Germany.

††Permanent address: Technische Universitat Berlin, Institut fur Strahlungs- und Kernphysik, Sekr PN 3-2, Hardenbergstr. 36, D-1000 Berlin 12, West Germany.

References

1. T.A. Ferrett, D.W. Lindle, P.A. Heimann, M.N. Piancastelli, P.H. Kobrin, H.G. Kerkhoff, U. Becker, W.D. Brewer, and D.A. Shirley (unpublished results).

2. S.T. Manson (private communication).

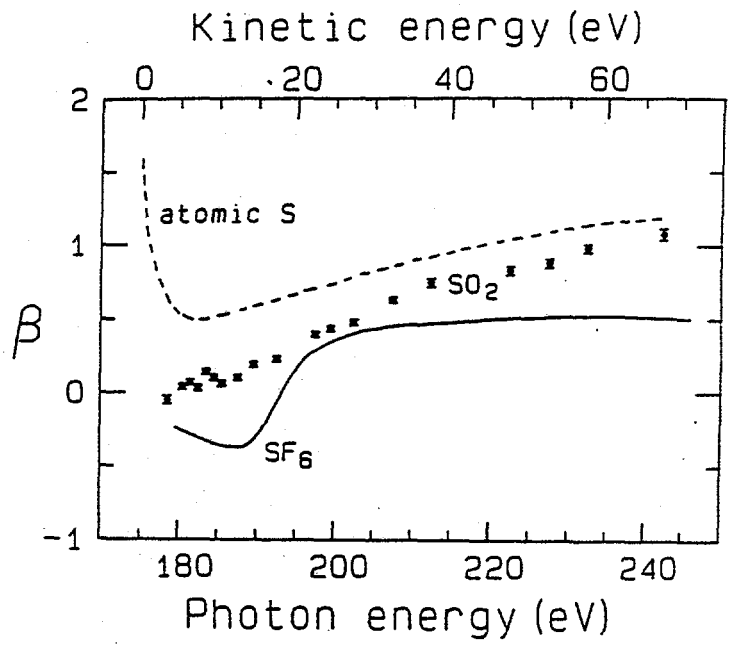

Figure 1. The S 2p symmetry parameter (β) for SO_2 as a function of photon energy (bottom scale) and kinetic energy (top scale). The solid curve represents experimental data for β(S 2p) of SF_6 [1], plotted as a function of kinetic energy. Hartree-Slater theory curve [2] for the atomic β(2p) of sulfur is also shown (dashed), as a function of kinetic energy.

Complete Photoemission Study of the He $1s^2 \rightarrow 3s3p$ Autoionizing Resonance*

D.W. Lindle,† T.A. Ferrett,† P.A. Heimann,** and D.A. Shirley

Materials and Chemical Sciences Division
Lawrence Berkeley Laboratory
and
Department of Chemistry
University of California
Berkeley, California 94720

The total absorption cross section of He (Fig. 1) and the He+(1s) partial cross section have been measured using photoelectron spectroscopy and synchrotron radiation in the photon-energy region of the $1s^2 \rightarrow 3s3p$ resonance. The effects of autoionization are relatively small, causing deviations of 5-10% from the nonresonant cross sections. These new measurements, along with a previous study of the 3s3p resonance behavior of the He+(n=2) satellite cross section, branching ratio, and angular-distribution parameter, allow the complete determination of all the parameters governing the $1s^2 \rightarrow 3s3p$ resonance. From these experimentally determined parameters, we have derived all of the relevant oscillator strengths and individual dipole and Coulomb matrix elements which describe He photoionization in the vicinity of the 3s3p doubly excited state.

*This work was supported by the Director, Office of Energy Research, Office of Basic Energy Sciences, Chemical Sciences Division of the U.S. Department of Energy under Contract No. DE-AC03-76SF00098. It was performed at the Stanford Synchrotron Radiation Laboratory, which is supported by the Department of Energy's Office of Basic Energy Sciences.

---

†Present address: National Bureau of Standards, Gaithersburg, MD 20899.

**Present address: Technische Universitat Munchen, D-8046 Garching b, Munchen, W. Germany.

References

1. G.V. Marr and J.B. West, At. Data Nucl. Data Tables 18, 497 (1976).

2. P. Dhez and D.L. Ederer, J. Phys. B 6, L59 (1973).

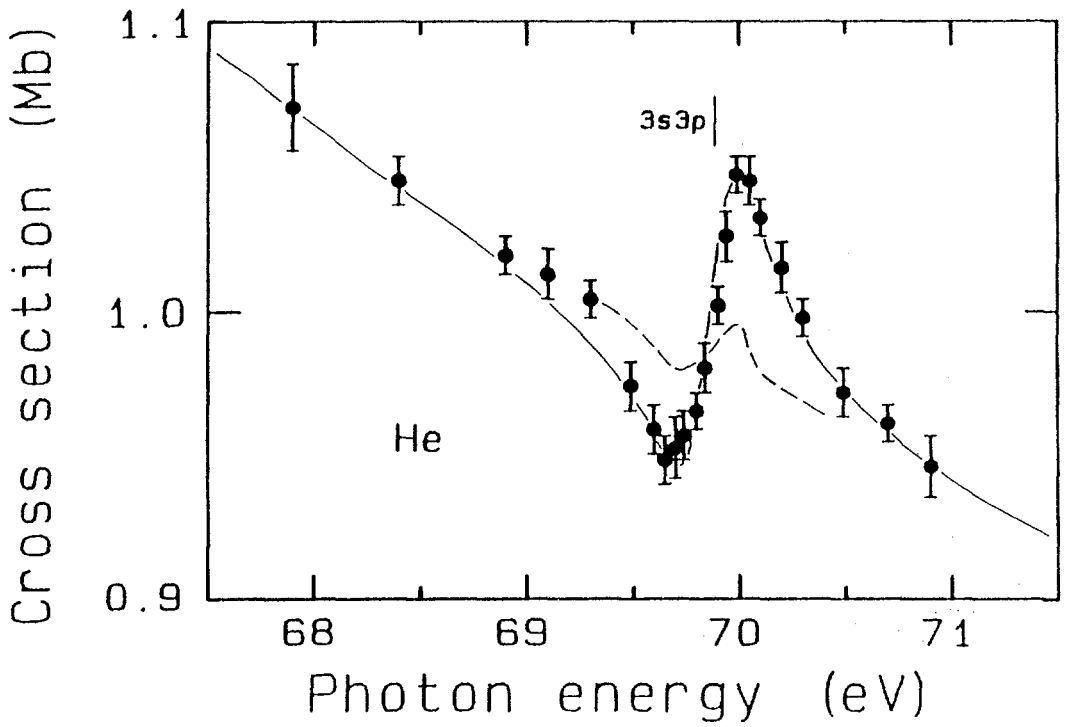

Figure 1. Total cross section of He in the vicinity of the $1s^2 \rightarrow 3s3p$ resonance scaled to Marr and West (Ref. 1) at 68.9 eV. The solid curve is a fit to the data using the Fano formula convoluted with a Gaussian function of 0.19 eV (0.48Å) FWHM to account for monochromator broadening. The dashed curve is an absorption measurement from Ref. 2.

A Photoemission Study of Kr 3d → Np Autoionization Resonances*

D.W. Lindle,† P.A. Heimann,†† T.A. Ferrett,†
M.N. Piancastelli,** and D.A. Shirley

Materials and Chemical Sciences Division
Lawrence Berkeley Laboratory
and
Department of Chemistry
University of California
Berkeley, California 94720

Resonant photoelectron spectra of Kr have been taken in the photon-energy ranges of the $3d_{5/2}$ → 5p,6p and $3d_{3/2}$ → 5p excitations. The spectra shown in the figure, which closely resemble normal Kr^+ $3d^{-1}$ Auger spectra, illustrate the importance of "spectator" Auger-like decay for inner-shell resonances, in which the initially excited electron does not participate in the core-hole deexcitation process, except to respond to the change in the atomic potential. Possible assignments for some of the spectator decay channels are made based on photoemission intensity measurements at the different 3d resonances. These assignments suggest that shake-up (e.g. 5p → 6p) of the "spectator" electron during the decay process is not quite as important as previously suspected. The resonance profiles of some of the more intense satellites have been determined over the 3d → np resonances. Very small resonance effects also were observed in the partial cross section for 4p subshell ionization, which produced asymmetric Fano-type profiles. The 4p angular distribution, in contrast, exhibits a pronounced effect in the resonance energy range. The 4p results demonstrate that non-spectator autoionization also is present.

*This work was supported by the Director, Office of Energy Research, Office of Basic Energy Sciences, Chemical Sciences Division of the U.S. Department of Energy under Contract No. DE-AC03-76SF00098. It was performed at the Stanford Synchrotron Radiation Laboratory, which is supported by the Department of Energy's Office of Basic Energy Sciences.

---

†Present address: National Bureau of Standards, Gaithersburg, MD 20899.

††Present address: Technische Universitat Munchen, D-8046 Garching b, Munchen, W. Germany.

**Permanent address: Department of Chemistry, University of Rome "La Sapienza", 00100 Rome, Italy.

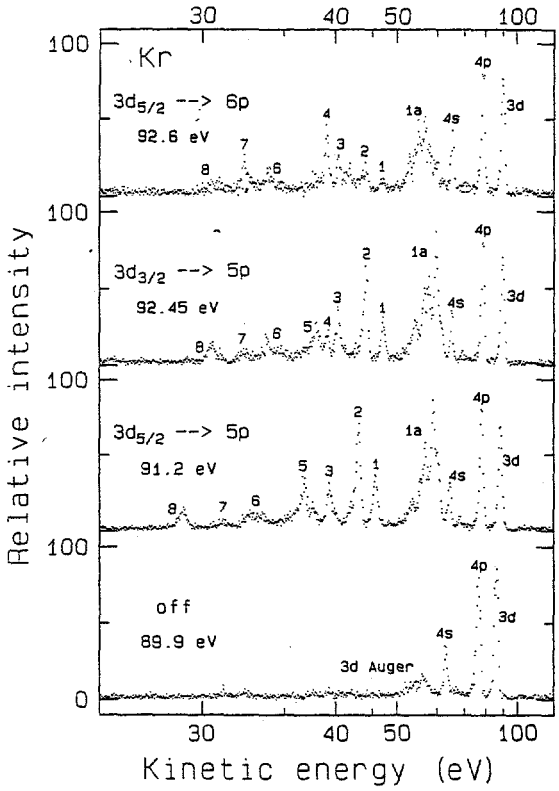

Figure 1. Resonant TOF photoelectron spectra of Kr at 89.9 eV, 91.2 eV, 92.45 eV, and 92.6 eV photon energy, which correspond to off-resonance excitation, and excitation of the $3d_{5/2}$ → 5p, $3d_{3/2}$ → 5p, and $3d_{5/2}$ → 6p resonances, respectively. The spectra are not corrected for analyzer transmission, which varies monotonically from 0.5 to 1 between 30 and 70 eV kinetic energy. The spectra have been scaled so that relative peak intensities in different spectra can be compared. The numbered peaks in the resonant spectra correspond to Kr^+ satellite configurations. The 3d peak is produced by second-order radiation, and the 3d Auger peak in the 89.9 eV spectrum is the $M_4{}_5N_2{}_3N_2{}_3$ Auger from the decay of these "second-order" 3d-hole states. The 3d Auger peak also has a small contribution from valence satellites.

Lithium 1s Main-Line and Satellite Photoemission: Resonant and Nonresonant Behavior*

T.A. Ferrett,† D.W. Lindle,† P.A. Heimann,‖ W.D. Brewer,**
U. Becker,†† H.G. Kerkhoff,†† and D.A. Shirley

Materials and Chemical Sciences Division
Lawrence Berkeley Laboratory
and
Department of Chemistry
University of California
Berkeley, California 94720

We present experimental results on core-level photoemission of atomic lithium (see spectrum in Fig. 1), leading to both main-line and satellite states of the Li^+ ion (1snl where n=2-5). We have compared the measured 1s2s $^{1,3}S$ main-line cross sections with recent relaxed Hartree-Fock calculations and with previous experimental results, finding reasonable agreement in both cases. For the n=3 satellite, our results disagree with earlier photoemission work which was complicated by additional peaks at 52 eV kinetic energy. We discuss possible explanations for these extra peaks. For the doubly excited state 1s(3s3p) at 71.14 eV, we present total cross-section results in good agreement with previous photoabsorption measurements. The qualitative differences among our partial cross-section profiles are discussed, and the phase for the total cross section is rationalized by estimating the signs of pertinent matrix elements.

*This work was supported by the Director, Office of Energy Research, Office of Basic Energy Sciences, Chemical Sciences Division of the U.S. Department of Energy under Contract No. DE-AC03-76SF00098. It was performed at the Stanford Synchrotron Radiation Laboratory, which is supported by the Department of Energy's Office of Basic Energy Sciences.

---

†Present address: National Bureau of Standards, Gaithersburg, MD 20899.

‖Present address: Technische Universitat Munchen, D-8046 Garching b, Munchen, W. Germany.

**Permanent address: Institut fur Atom- und Festkorperphysik, Freie Universitat Berlin, Arnimalee 14, 1000 Berlin 33, West Germany.

††Permanent address: Technische Universitat Berlin, Institut fur Strahlungs- und Kernphysik, Sekr PN 3-2, Hardenbergstr. 36, D-1000 Berlin 12, West Germany.

Reference:

1. C. Moore, Atomic Energy Levels NSRDS-NBS 35 (U.S. GPO, Washington, D.C., 1971) Vol. 1.

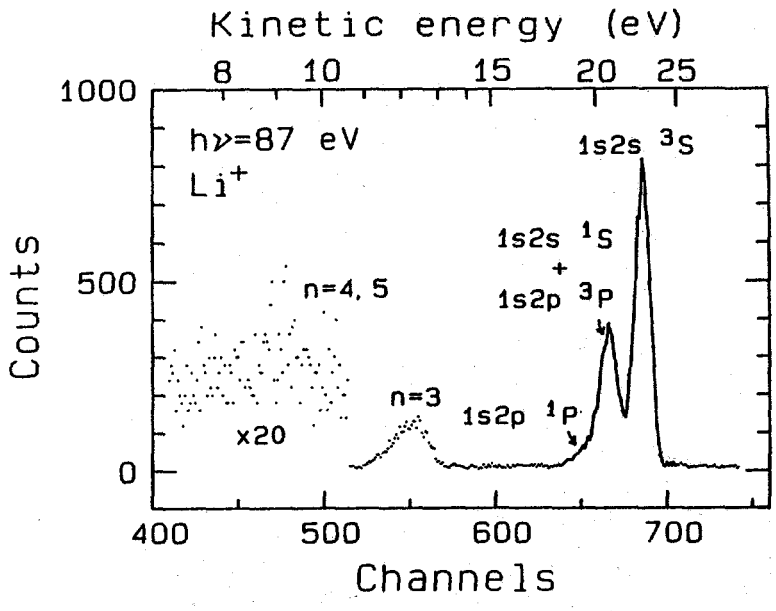

Figure 1. TOF photoelectron spectrum taken at hν=87 eV and θ=54.7°. The 1s2s main-line photoemission is split into ^3S and ^1S components, with the 1s2p $^{1,3}P$ satellites unresolved at slightly higher binding energy. The relatively intense n=3 satellites (1s31) have a binding energy of about 75 eV.[1] The very weak higher n satellites are shown also on an expanded scale (x 20).

C(2x2)S/Cr(001) Surface and Near-Surface Structure Determined Using Angle-Resolved Photoemission Extended Fine Structure*

L.J. Terminello, X.S. Zhang,† Z.Q. Huang, S. Kim,
A.E. Schach von Wittenau, and D.A. Shirley

Materials and Chemical Sciences Division
Lawrence Berkeley Laboratory
and
Department of Chemistry
University of California
Berkeley, California 94720

We report the surface and near-surface structure of c(2x2)S/Cr(001) determined from angle-resolved photoemission extended fine structure (ARPEFS). The sulfur 1s photoemission partial cross section was measured in the [001] and [011] emission directions which yielded fine structure amplitudes up to 50-70%. Qualitative results are obtained from Fourier transforms of the ARPEFS revealing geometrical information beyond 10 Å path-length difference from the photoemitter. Structural parameters are determined with greater precision by comparing the Fourier filtered data to multiple-scattering spherical-wave (MSSW) calculations giving statistically tractable results (as shown in Figure 1). The directional sensitivity of ARPEFS is demonstrated through the analysis of normal [001] and off-normal [011] emission direction data. We show that sulfur adsorbs in the four fold hollow site 1.17 Å above the first chromium layer and that the first to second layer chromium distance contracts to 1.31 Å, 8% less than the 1.44 Å bulk value. Analysis of the near-surface contribution to ARPEFS showed that deeper layers essentially retain the bulk separation.

*This work was supported by the Director, Office of Energy Research, Office of Basic Energy Sciences, Chemical Sciences Division of the U.S. Department of Energy under Contract No. DE-AC03-76SF00098. It was performed at the Stanford Synchrotron Radiation Laboratory, which is supported by the Department of Energy's Office of Basic Energy Sciences.

---

†Permanent address: Department of Physics, Zhejiang University, Hangzhou, Zhejiang, China.

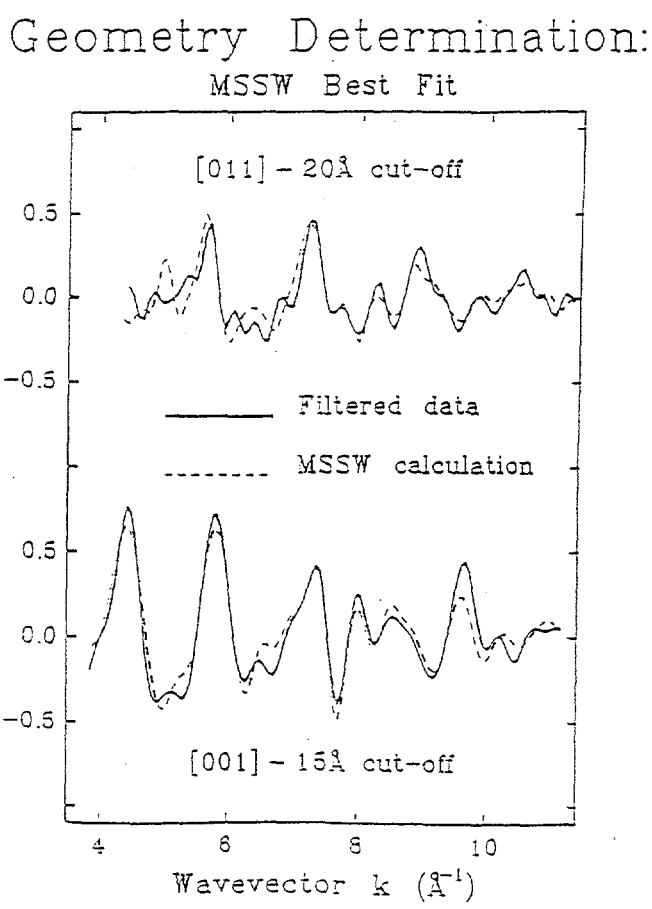

Figure 1. Best-fit MSSW calculations compared to experimental curves. Each experimental curve (solid line) has been Fourier filtered and is compared to the MSSW calculated data (dashed line) that gives an absolute r-factor minimum.

Chemisorption Structure of c(2x2)S/Fe(001) Determined by ARPEFS*

X.S. Zhang,† L.J. Terminello, S. Kim, Z.Q. Huang,

A.E. Schach von Wittenau, and D.A. Shirley

Materials and Chemical Sciences Division
Lawrence Berkeley Laboratory
and
Department of Chemistry
University of California
Berkeley, California 94720

Angle-Resolved Photoemission Extended Fine Structure (ARPEFS) spectroscopy is a very effective method to determine surface structures. In this work, ARPEFS has been studied to measure the chemisorption geometries of c(2x2)S/Fe(001) directions for the two adsorbate systems. We have analyzed the normal and off-normal data of both experiments in two ways. One is direct Fourier transform of the experimental data; another is using multiple-scattering spherical-wave calculations to compare with the experiments, which give the structure in detail. Multiple-scattering calculations (see figure) were done with a cluster size that included path lengths > 15 Å. These long path-length differences were necessary to model the contributions to the ARPEFS signal from near-surface atoms.

The result indicates adsorption in a four fold hollow site for both systems, and 1.10 ± 0.03 Å distance above the Fe surface indicating a S-Fe bond length of 2.30 ± 0.01 Å. The first to second layer iron distance of 1.40 ± 0.02 Å indicates a slight contraction from the bulk value. This result also is in agreement with self-consistent field (SCF) Xα scattered-wave calculations.

*This work was supported by the Director, Office of Energy Research, Office of Basic Energy Sciences, Chemical Sciences Division of the U.S. Department of Energy under Contract No. DE-AC03-76SF00098. It was performed at the Stanford Synchrotron Radiation Laboratory, which is supported by the Department of Energy's Office of Basic Energy Sciences.

---

†Permanent address: Department of Physics, Zhejiang University, Hangzhou, Zhejiang, China.

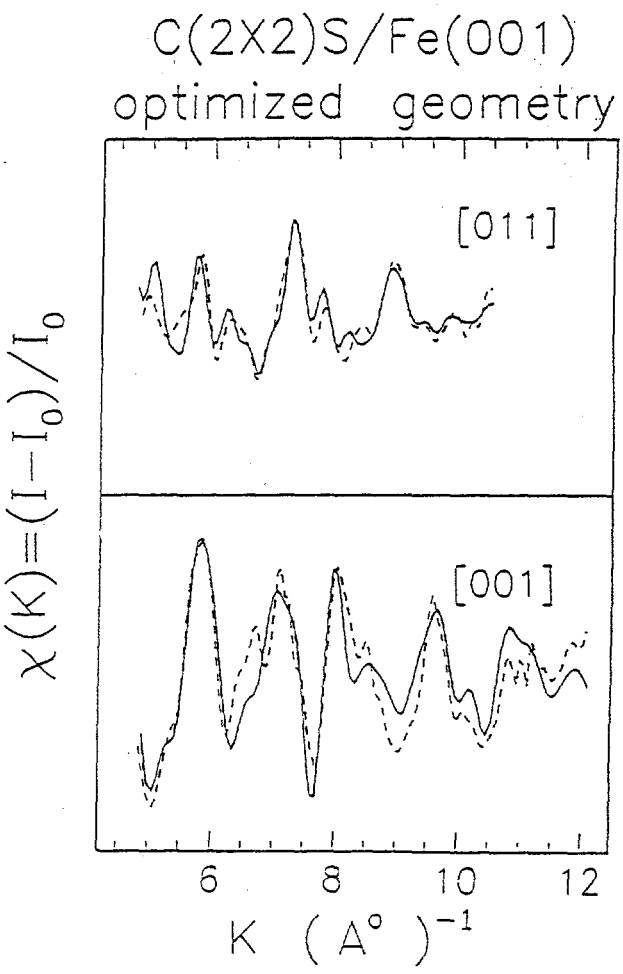

Figure 1. The theoretical calculations for optimized geometry, the solid line, compared to experimental data, the dashed line.

ANISOTROPIC VIBRATIONAL AMPLITUDES OF SURFACE ATOMS STUDIED WITH SEXAFS

P. H. Citrin, F. Sette, T. Hashizume[a]
AT&T Bell Laboratories
Murray Hill, NJ 07974

F. Comin
European Synchrotron Radiation Facility
BP 220, F30043, Grenoble, France

A. A. MacDowell
National Synchrotron Light Source
Brookhaven National Laboratories, Upton, NY 11973

A novel application of SEXAFS was used to investigate the existence of anisotropic surface vibrational amplitudes. This general problem in surface dynamics reflects the shape of the surface potential and is directly related to diffusion, desorption, surface reactions, and epitaxial growth. Previous experimental studies had been unable to probe in-plane and out-of-plane surface modes with comparable sensitivity and without interfering effects of correlated motion. Both problems were solved by analyzing *polarization*- and *temperature*-dependent SEXAFS *amplitudes* from *higher-neighbor* scatterers (up to five shells) located along directions perpendicular and nearly parallel to the surface. Essential to the success of this procedure were very high quality data, which were obtained with fluorescence yield detection.

Figs. 1 and 2 show the raw and Fourier-transformed SEXAFS data from the Cu(100)c(2×2)-Cl system. Peak assignments for the various shells are given in the caption, and the results for the corresponding distances and relative mean square displacements are given in Table I. From straightforward analysis of these latter values it is easy to show that the individual mean square displacements of both Cl and surface-Cu atoms are about twice as large within the surface as along the normal. This anisotropy is very large and disagrees with predictions based on the widely used spring-constant model. The SEXAFS-measured Cl-Cu bond length and the interlayer substrate expansion reveal substantial charge transfer between the Cl and the Cu surface, which we argue to be important in understanding the observed anisotropy. A systematic study of how surface bonding affects surface vibrations is planned to be tested in other related systems. This work provides a clear example of how direct measurements of surface structure modify conventional wisdom and open up new ways of describing surface behavior.

TABLE I. Summary of SEXAFS r_i's and $\Delta\sigma_i^2$'s

i	N_i	r_i(expt) (Å)	r_i(calc)[a] (Å)	$\Delta\sigma_i^2$ (10^{-3}Å^2)
1	4	$2.37\pm0.01_5$	...	5.5 ± 0.5
2	1	3.43 ± 0.02	...	6.5 ± 1
3	4	$3.62\pm0.01_5$	3.62	10 ± 2
4	4	4.25 ± 0.03	4.28	9 ± 2
5	8	4.31 ± 0.02	4.32	12.5 ± 1
6	4	5.05[b]	4.98	...

[a]Calculated with r_1 (expt), r_2(expt), and a_0(Cu).
[b]Multiple scattering from first-neighbor Cu atoms affects this value, evident in the anomalously large E_0 shift from the CuCl model compound.

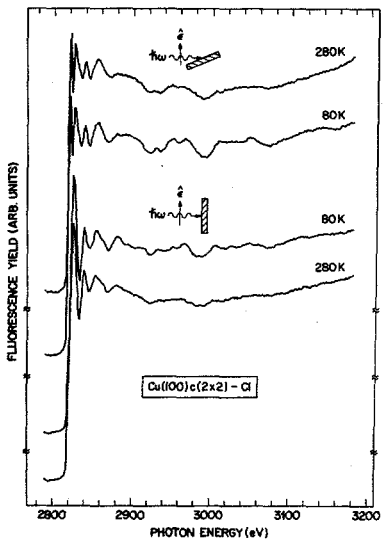

FIG. 1. Raw Cl *K*-edge absorption data from 0.5 monolayer of Cl on Cu(100) taken at 80 and 280 K, with the electric field ϵ_θ parallel ($\theta=90°$) and nearly normal ($\theta=20°$) to the surface.

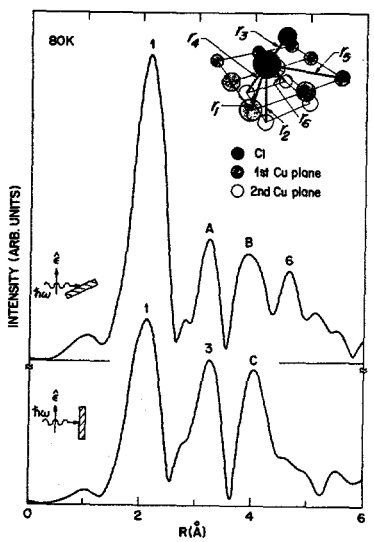

FIG. 2. Fourier transforms of 80-K data shown in Fig. 1. The SEXAFS χ_i from the first six coordination shells at distances r_i around the absorbing Cl atom (see inset) constitute the labeled peaks as follows: 1, χ_1; *A*, $0.88\chi_2+0.12\chi_3$; 3, χ_3; *B*, $0.64\chi_4+0.36\chi_5$; *C*, $0.83\chi_5+0.17\chi_4$; 6, χ_6.

Acknowledgement: We thank C. T. Chen and J. E. Rowe for their contributions to this work.

(a) Institute for Solid State Physics, University of Tokyo, Roppongi,Minato-Ku, Tokyo 106,Japan

Proposal No. 963V

NEXAFS Studies of π-complex Orientation on Ag(110)

A. Muscat and R.J. Madix*
J. Stöhr**

*Department of Chemical Engineering, Stanford University, Stanford, CA. 94305
**IBM Almaden Research Center, 650 Harry Road, San Jose, CA. 95120

The oxidation of organic molecules on silver surfaces has been studied extensively in order to delineate the reaction sequences governing the chemical transformations [1]. The detailed interaction of the reaction intermediates with the metal surface is not understood, however. Near-edge X-ray absorption fine structure (NEXAFS) provides a probe of the structure, orientation, and electronic state of adsorbed molecules [2]. We have used the NEXAFS technique on beam line I-1 at SSRL to investigate two adsorbates on Ag(110): methyl acetylide ($CH_3C{\equiv}C$-), produced from the oxidation of methyl acetylene ($CH_3C{\equiv}CH$), and 2,4-hexadiyne ($CH_3C{\equiv}C$-$C{\equiv}CCH_3$). All NEXAFS spectra were recorded at the carbon edge with the surface at 100K.

The stable surface methyl acetylide was formed by exposing a Ag(110) surface on which oxygen atoms had been preadsorbed to methyl acetylene at 210K. Water was evolved to leave only the methyl acetylide on the surface [3].

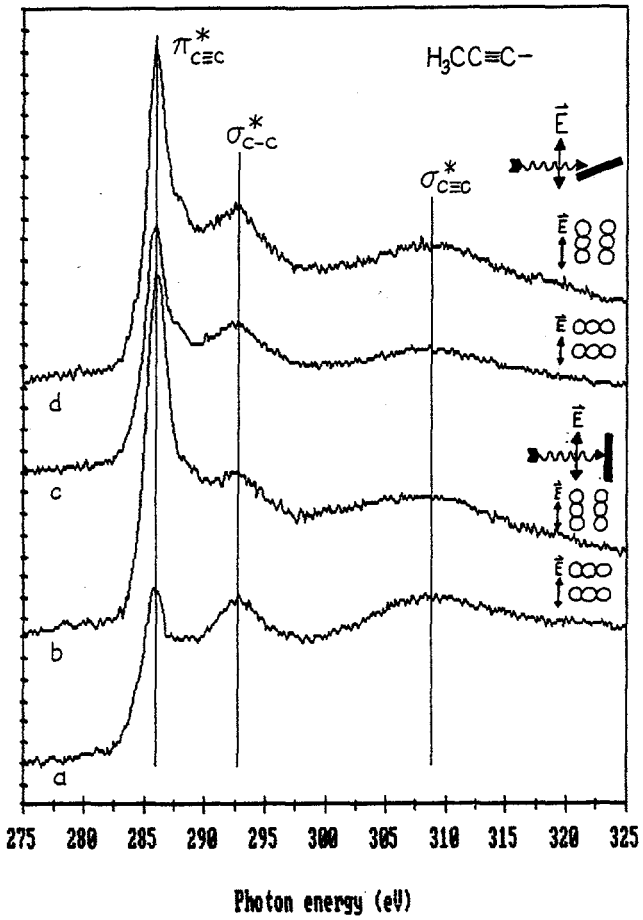

Figure 1. Carbon K edge NEXAFS spectra of methyl acetylide on Ag(110) at 100K.

The attenuation of the π^* feature for the electric field vector, $\vec{E}$, directed along the (100) azimuth (compare figs. 1a and 1b) indicates that the methyl acetylide is azimuthally ordered, lying with the C≡C bond axis preferentially oriented perpendicular to the close-packed direction. The (C≡C) σ^* resonances present near 310 eV (as that for acetylene [4], indicative of retention of the triple bond) in figure 1 indicate that the C≡C bond axis of the intermediate is not parallel to the surface, but canted from the surface plane. A structurally similar intermediate, propargyloxy ($CH{\equiv}CCH_2O$-), has been shown to have the backbone lying perpendicular to the close-packed direction [5].

Previously we have shown that acetylene adsorbs with random orientation in the monolayer state with no perturbation of the C≡C bond length [4]. This run we studied the orientation of the linear, six-carbon diyne, 2,4-hexadiyne. The monolayer state was prepared by exposing the clean Ag(110) surface at 100K to the diyne, then annealing to 220K to desorb the multilayer.

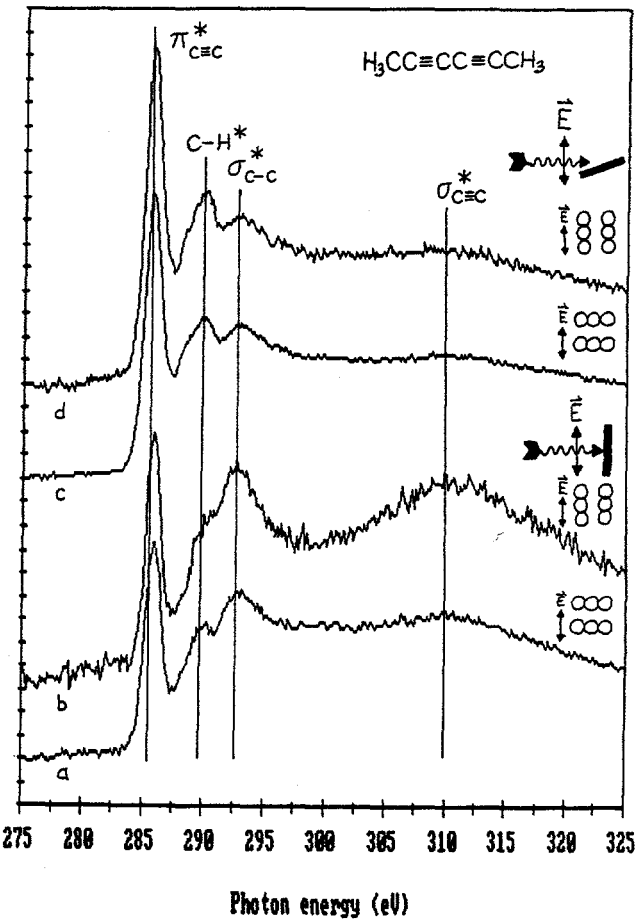

Figure 2. Carbon K edge NEXAFS spectra of 2,4-hexadiyne on Ag(110) at 100K.

The spectra for the 2,4-hexadiyne show evidence for preferential, but not perfect, azimuthal ordering (fig. 2) of the carbon chain along the $(1\bar{1}0)$ azimuth (the close-packed direction). The π^* resonance at 286 eV is attenuated at normal incidence with the electric field vector along the $(1\bar{1}0)$ azimuth (fig. 2b), and the σ^* resonance is most prominant in this orientation, indicating that the carbon backbone is parallel to the close-packed $(1\bar{1}0)$ direction. The σ^* resonance energy of the carbon-carbon triple bond is nearly the same as that for acetylene [4], indicative of retention of the triple bond.

The tilt of the linear $CH_3C{\equiv}C$- species out of the surface plane contrasts sharply to the in-plane orientation of the linear carbon chain in $CH{\equiv}CCH_2O$-. This difference must reflect the relative position of the triple bond with respect to the point of attachment to the surface and the greater rigidity of methyl acetylide. The preferred orientation of the hexadiyne compared to acetylene suggests that intermolecular interactions may assist ordering for larger, more bulky molecules.

[1] M.A. Barteau and R.J. Madix, in The Chemical Physics of Solid Surfaces and Heterogenous Catalysis, D.A. King and D.P. Woodruff, eds., Elsevier: Amsterdam, 1982; Vol. 4, p 95.

[2] F. Sette, J. Stöhr and A.P. Hitchcock, J. Chem. Phys., 81 (1984) 4905.

[3] J.M. Vohs, B.A. Carney and M.A. Barteau, J. Am. Chem. Soc., 107 (1985) 7841.

[4] P.A. Stevens, R.J. Madix and J. Stöhr, in preparation.

[5] J.L. Solomon, R.J. Madix and J. Stöhr, submitted to J. Chem. Phys.

SULFUR DOPED $Al_xGa_{1-x}As$: MICROSCOPIC STRUCTURE OF DX CENTERS AND COMPOSITIONAL ORDERING

F. Sette, J. E. Rowe, J. M. Poate and S. J. Pearton

AT&T Bell Laboratories
600 Mountain Avenue
Murray Hill, NJ 07974

Donors in $Al_xGa_{1-x}As$ induce a class of defects referred to as DX centers [1] which show two characteristic phenomena: persistent photoconductivity and a very large Stoke shift. Both effects have been taken as strong indication for a large lattice relaxation upon electron-hole creation. Macroscopic properties of this class of defects are the proportionality between defects and donor concentrations and the independence of DX properties from the Al content in the alloy composition range $0.2 < x < 0.5$. Conclusive knowledge of the microscopic structure of these defects is not available yet, although various structural models have been suggested [1,2]. A common feature between these efforts, which is substantiated by the observation of DX centers behavior in Si doped pure GaAs at large hydrostatic pressures [3], is the belief that the lattice relaxation associated with the DX centers is induced by localized states in the impurity-defect complex and that these states can be expected as a modification of the random alloy band structure induced by the impurity atom.

We recently studied S impurities in $Al_xGa_{1-x}As$ compounds where the Al concentration was varied from $x = 0.2$ to $x = 0.45$ and the alloys were grown by MBE or by MOCVD. Doping was performed by ion implantation and by annealing following similar proedures to those previously described for S in GaAs [4]. The S concentration was varied between $\bar{n}=10^{19}$ and $\bar{n}=10^{20}$ at/cm^3.

The sulfur K-edge EXAFS data show the surprising result that $90 \pm 10\%$ of the S first-neighbors are Al atoms, independent of the alloy Al concentration x, the S concentration $\bar{n}$, and the alloy growth method. This result is contrary to expectations based on the properties of a random $Al_xGa_{1-x}As$ alloy where the donor first neighbor composition should be a mixture of Al and Ga atoms, proportional to the relative alloy concentration. Furthermore, the S atoms are substitutional as revealed by the S-second-neighbor shell position. This shell is centered at 3.98 ± 0.05 Å from the S atom (4.00 in GaAs) and it is composed exclusively of As, Ga or a mixture of these two atoms without any appreciable amount of Al atoms. The S-Al distance is 2.27 ± 0.02 Å and is strongly relaxed when compared with the alloy effective first-neighbor distance, ~2.45Å.

The unexpected microscopic structure of S impurities in $Al_xGa_{1-x}As$ alloys reveal large differences between the heat of reaction and the diffusion probabilities of S donors with Al or Ga atoms. In particular, the preferred S-Al bonding configuration is responsible for the short S-Al distance and such bond-length contraction in proximity of the impurity site determines a large static displacement of some atoms from the theoretical positions of the host crystal and a non-random variation in the alloy composition. An obvious implication of our study is concerned with the ability of extracting from the structural model derived from the EXAFS data new information on the microscopic structure of DX centers. Indeed, it is reasonable to expect that the static relaxation of the lattice at the impurity site and the non-stochiometric Al enrichment around the S site may induce localized states. These electronic states, by acting as deep electron traps and by being separated from the rest of the lattice by some potential barrier induced by the ordered variation in the alloy composition moving away from the impurity site, are consistent with the general features of DX centers and may explain phenomena like persistent photoconductivity. Furthermore, the independence of the DX properties from the Al concentration x is a natural consequence of the present model, being the impurities concentration always lower than the Al content; the existence of a finite interval of alloy composition where DX behavior is observed can also be understood as a consequence of non-random alloy composition around the impurity site. Although our model provides a consistent picture for the microscopic structure of DX centers in $Al_xGa_{1-x}As$ alloys, which is based on alloy composition ordering in the impurity region, the present model does not seem to offer any immediate hint for the DX behavior observed in pure GaAs under high pressures [3].

ACKNOWLEDGEMENTS

We wish to acknowledge useful discussions with our colleagues G. A. Baraff, F. Capasso, D. V. Lang, R. A. Logan, M. Stavola, C. W. Tu and M. A. Marcus at AT&T Bell Laboratories. We also thank the scientific and support staff of the Stanford Synchrotron Radiation Laboratory (SSRL). SSRL is supported by the D.O.E. and N.I.H. under materials research and biotechnology programs respectively.

REFERENCES

1. D. V. Lang "DX Centers in III-V Alloys" in "Deep Levels in Semiconductors," edited by S. Pantelides, Gordon and Breach, N. Y. (1985).
2. T. N. Morgan, Phys. Rev. B *34*, 2664 (1986).
3. M. Mizuta, M. Tachikawa, H. Kukimoto, and S. Minomura, Jpn. J. Appl. Phys. *24*, L143 (1985); M. Tachikawa, T. Fujisawa, H. Kukimoto, A. Shibata, G. Oomi, and S. Minomura, Jpn. J. Appl. Phys. *24*, L893 (1985).
4. F. Sette, S. J. Pearton, J. M. Poate, J. E. Rowe and J. Stöhr: Phys. Rev. Lett. 2637, 56 (1986).

STRUCTURE OF P IMPURITIES IN GaAs

F. Sette, J. E. Rowe, J. M. Poate and S. J. Pearton

AT&T Bell Laboratories
600 Mountain Avenue
Murray Hill, NJ 07974

We measured the K-edge photoabsorption spectra of impurities in GaAs at $10^{19}-10^{20}$ P at/cm^3 concentrations. Samples were prepared by ion implantation and subsequent annealing at 900°C. Channeling measurements showed no noticeable residual damage. In Fig. 1 we report the Fourier transform magnitude of the EXAFS data for phosphorus. This function is directly related to the radial distribution function and shows the first, second and third neighbor shells of the P atoms. The second and third shells results reveal that the P atoms are substitutional on the As sublattice. The radial distances of these two shells, 4.00±0.02 Å and 4.68±0.03Å respectively, agree extremely well with the analogous values of the GaAs lattice, 4.00Å and 4.68Å. However, the bond-distance between the P atom and its 4 Ga first neighbors is R=2.38±0.01Å, which is 0.07Å shorter than in GaAs, R=2.45Å. This contracted first neighbor distance and the unrelaxed higher shells reveal a large local contraction of the four first-shell Ga atoms toward the P site with distortion of the 2nd shell GaAs bond angles and lengths. This homogenous breathing relaxation of the Ga atoms is due to a trigonal distortion taking place on such Ga sites. The shorter P-Ga bond is consistent with tetrahedrally coordinated first-shell Ga atoms and with the P-Ga bond distance of 2.36Å in bulk GaP; although, it is interesting to observe that the measured distance is still 0.02Å longer than in GaP. This is due to a balance of forces on each first-shell Ga atom provided by the remaining three second-shell As-Ga bonds which are stretched to a value of 2.47Å as required by the first and second shell distances given above.

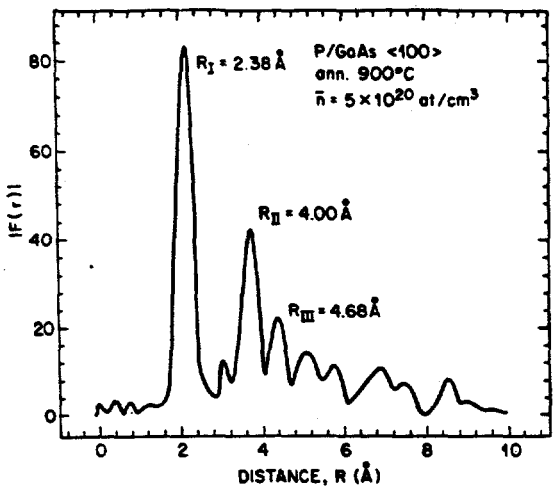

Fig. 1 Fourier transform magnitude |F(r)| of the EXAFS signal obtained from a P doped GaAs sample ($\bar{n}$=5x10^{19} at/cm^3). The sample was doped by ion implantation and annealed at 900°C. The distances of the first three P atomic shells are indicated after phase-shift corrections.

Our results show that local chemical interactions on an isolated isoelectronic impurity in the zincblende lattice are dominant with respect to the crystal structure geometrical constraints. This property arises from weak bond-bending forces which, with small variations of bonding angles, allow large variations in the bond distances of those Ga atoms bound to both As and P atoms. Specifically, the Ga atoms bound to As and P have distances of 2.47Å and 2.38Å, respectively, with only 1% variation in the bond angles.

Summarizing results already pointed out [1,2] for $A_xB_{1-x}C$ III-V alloys, our results show that even in the limit $x\rightarrow 0$, the A-C bond distance is much closer to the bond distance in the A-C compound then to the average bond distance, which in this concentration limit is the B-C bond distance. However, we also experimentally demonstrate that the lattice relaxation is absorbed within the first two shells of the isoelectronic impurity and the average bond distance of the displaced Ga atoms is

$$\bar{d} = (3R_{Ga-As}+R_{Ga-P})/4=2.45\text{Å}, \qquad (1)$$

which is identical to the Ga-As bond in GaAs. The previous relation (1) also confirms the theoretical treatment of local lattice distortion for isoelectronic impurities presented by M. Scheffler [2].

ACKNOWLEDGEMENTS

We wish to acknowledge useful discussions with our colleagues G. A. Baraff, F. Capasso, D. V. Lang, R. A. Logan, M. Stavola, C. W. Tu and M. A. Marcus at AT&T Bell Laboratories. We also thank the scientific and support staff of the Stanford Synchrotron Radiation Laboratory (SSRL). SSRL is supported by the D.O.E. and N.I.H. under materials research and biotechnology programs respectively.

REFERENCES

1. J. C. Mikkelsen and J. C. Boyce, Phys. Rev. Lett., *49*, 1412 (1982).
2. M. Scheffler, Proceedings of the 2nd Int'l. Conf. on Shallow Impurity Centers (Trieste, July 1986, ed. Baldereschi, Elsevier) to be published and private comm.

PHOTOELECTRON SPECTROSCOPIC STUDIES OF METAL ION SITES

Proposal No. 1022Vp

K.D. Butcher, S.V. Didziulis, J. Lin, and E.I. Solomon

Stanford University, Stanford, California 94305

Our work over the past year has focused on PES studies of the electronic structure and bonding in transition metal ion sites related to catalysis. We concentrate here on the $3d^{10}$ metal complexes and the d^5 and d^6 iron chlorides.

We have used variable energy PES to determine the valence band electronic structure and to study the covalent bonding properties of three tetrahedral $3d^{10}$ transition metal complexes with a systematic variation in both ligand and metal ion. The valence band spectra of ZnO were contrasted to those of $ZnCl_4^{2-}$ to evaluate the effect of ligand variation on bonding. Next $ZnCl_4^{2-}$ was compared to CuCl to examine the differences in bonding which occur on changing the d^{10} metal ion in the tetrahedral site. PES data obtained over the energy range of 16.7 - 1486.6 eV (see Fig. 1) show dramatic intensity changes in the valence band feataures which allow detailed assignments to be made using molecular orbital theory and theoretical photoionization cross sections. In general, the ZnO PES spectrum exhibits two sets of peaks, one centered at 10.7 eV binding energy and the second between 4 - 8 eV. The deeper binding energy feature becomes more intense with increasing photon energy, allowing it to be assigned as Zn 3d photoemission. A detailed analysis gives peaks 1 and 2, Zn 3d t_2 and e bonding; peak 3, the Zn 4s-stabilized O 2p bonding; peak 4, the O 2p non-bonding; peak 5, O 2p anti-bonding. Experimental estimates of mixing using the Gelius model give a mixing coefficient of α^2=.21 O 2p averaged over the Zn d orbitals. Similar analyses for $ZnCl_4^{2-}$ and CuCl yielded α^2 values of .08 and .15, respectively.

Spectral differences in the data provide insight into the bonding of these compounds. The larger ZnO_4^{2-} 3d band splitting (see Figure 2) relative to $ZnCl_4^{2-}$ indicates greater ligand field strength (10 Dq) for the oxide ligands which arises from the stronger σ-bonding interaction of the Zn^{2+} 3d with the O^{2-} 2p orbitals. The increased effective nuclear charge on Zn^{2+} shifts the d levels below the ligand levels, making them bonding and reversing the sign of 10 Dq. This greater Z_{eff} on Zn^{2+} also lowers the energy of the empty metal 4s and 4p significantly, resulting in greater covalent stabilization of the ligand bonding levels in $ZnCl_4^{2-}$ relative to CuCl. These results are in agreement with thermodynamic data corrected for charge differences which show that Zn^{2+} complexes with donor ligands are much more stable than their Cu+ counterparts.

Our second research effort is directed toward understanding the active sites in iron-sulfur proteins using tetrahedral iron model complexes. The PES spectra of d^5 $FeCl_4^-$ and d^6 $FeCl_4^{2-}$ were obtained over the range of 25-150 eV and are presented in Figure 3. In $CsFeCl_4$, peak 2 shows the largest drop in intensity through the Cooper minimum and can thus be assigned as the Cl 3p non-bonding peak. In addition, the relative intensity changes show a maximum in the peak 3 bonding levels relative to the peak 1 anti-bonding levels, indicating greater iron character in peak 3. In Cs_3FeCl_5, peak 1 is assigned as anti-bonding levels with dominantly Fe 3d character on the basis of its delayed intensity maximum. Peaks 2 and 3 represent Cl 3p non-bonding and bonding levels, respectively. Peak 4 is assigned as the Fe 4s stabilized $2a_1$ bonding level.

Figure 1.

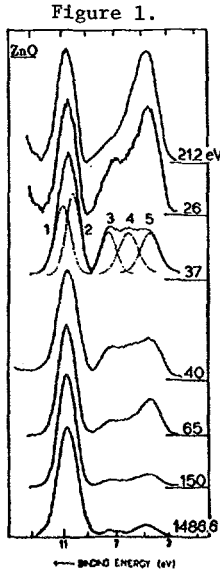

Figure 2.

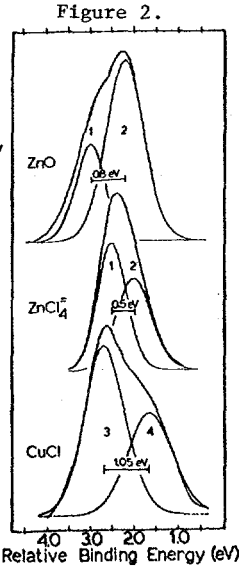

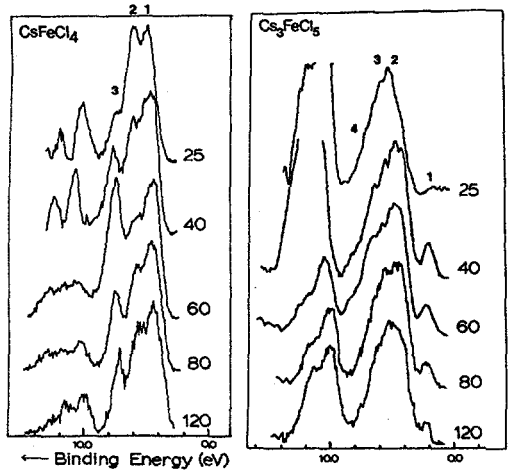

Figure 3.

Spectra taken at the Fe 3p --> 3d absorption edge show resonance enhancement of peak 3 in both salts as well as deep binding energy satellites at 11.0 and 12.5 eV in $CsFeCl_4$. The CIS profiles show a Fano interference pattern for peak 1 in both salts; the maximum resonance in peak 3 corresponds to the peak 1 profile inflection point. The enhancement corresponds to the SCK-auger decay process:

$$3p^6 3d^{5,6} \longrightarrow 3p^5 3d^{6,7} \longrightarrow 3p^6 3d^{4,5}$$

This requires that the dominant peak in resonance have metal character in the final state. Thus peak 3 is associated with the $|3d^4\rangle$ final state in Fe^{3+} and $|3d^5\rangle$ in Fe^{2+}. These results differ from our earlier work on $CuCl_4^{2-}$ in that the greatest enhancement occurs in the main band for iron, but in the

satellite for copper. The deep binding energy Fe satellite shows very little intensity out of resonance, but it does show some enhancement at the absorption edge. The lack of off resonance intensity in the deep binding energy satellite indicates little relaxation upon ionization, again in contrast to our $CuCl_4^{2-}$ results. Spin-restricted and unrestricted SCF-$X\alpha$-SW calculations for both initial and final states have been performed using spheres adjusted to reproduce ligand to metal charge transfer energies. The calculations support these experimental results, indicating that the anti-bonding levels have mostly ligand character, and showing that there is limited relaxation ($\sim$3%) upon ionization for all levels. This has important implications with respect to bonding interactions at iron active sites.

REFERENCES

1. S.V. Didziulis, S.L. Cohen, K.D. Butcher, E.I. Solomon, Inorg. Chem., in press.

2. S.V. Didziulis, S.L. Cohen, A.A. Gewirth, E.I. Solomon, J. Am. Chem. Soc. 110, 250 (1988).

HIGH-PHOTON FLUX PHOTOEMISSION STUDIES IN NARROW BAND MATERIALS

[1]J.W. Allen, [1,2]J.-S. Kang, [3]Z.-X. Shen, [3]J. J. Yeh, [4]W. Ellis, [2]M.B. Maple,
[2]Y.D. Dalichaouch, [2]B.-W. Lee, [5]M.S. Torikachvili, [3]J.-Z. Sun, [3]I. Lindau

[1] Randall Laboratory, University of Michigan, Ann Arbor, MI. 48109-1120

[2]Department of Physics, University of California at San Diego, La Jolla, CA. 92093

[3]Stanford Electronic Laboratory, Stanford University, Stanford, CA. 94305

[4]Los Alamos National Laboratory, Los Alamos, NM. 87545

[5]Physics Dept., San Diego State University, San Diego, CA.

Electronic structure of copper oxide superconductors

An understanding of the origin of the high superconducting transition temperatures T_c of the superconducting copper oxides will require an understanding of their electronic structure. Coulomb interaction effects are usually described by a Hubbard or Anderson model, and it is important to determine at least roughly the magnitude of the model parameters. Therefore we have measured and analyzed valence band resonant photoemission (RESPES) and core level x-ray photoemission spectroscopy (XPS) data using the Anderson Hamiltonian in the impurity cluster approximation.[1]

All the data in Figs. 1–4 were taken at room temperature and the resolution of the data is 0.45 eV , unless otherwise indicated.

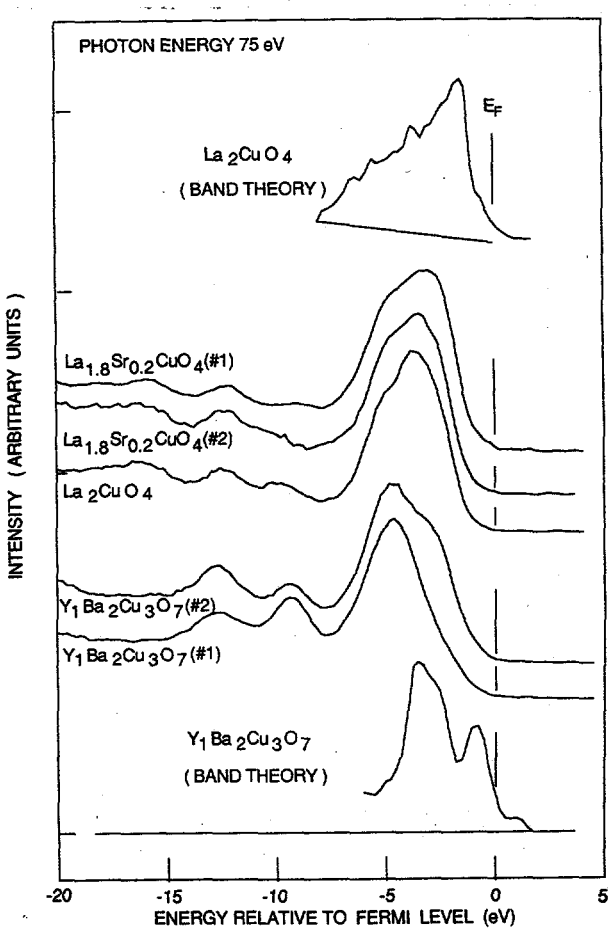

Fig. 1

Fig. 1 compares the experimental valence band spectra to band theoretical spectra[2] with the appropriate photoemission cross-sections taken approximately into account using tabulated atomic cross-sections[3]. The photon energy used maximizes the Cu 3d emission via a cross-section resonance at the Cu 3p edge. Effects due to second order light have been removed from the $YBa_2Cu_3O_{7-\delta}$ spectra.

There are obvious differences between the experimental spectra and the theory. For the large peaks at low binding energy, for all the samples, (a) the experimental centroids are shifted to higher energy than in the theory, (b) the shapes and the widths of the spectra from theory and experiment are quite different, and (c) the experimental density of states at the Fermi energy E_F is much smaller than in the theory. Another difference is the feature at –12.5 eV, discussed next.

Fig. 2 shows the valence band EDC's for photon energies in the Cu 3d resonant photoemission (RESPES) region for $La_{1.8}Sr_{.2}CuO_4$. The inset shows the detail of the Fermi level region at a photon energy of 70 eV. Peaks A,B and D display resonant behavior, implying that they involve Cu 3d states. In our cluster model, peak D gives the Cu d^8 energy, pushed far from the main band by the d-d Coulomb interaction U. Peak C is attributed to oxygen 2p states, consistent with O 2p RESPES data reported by other workers and confirmed recently by us.

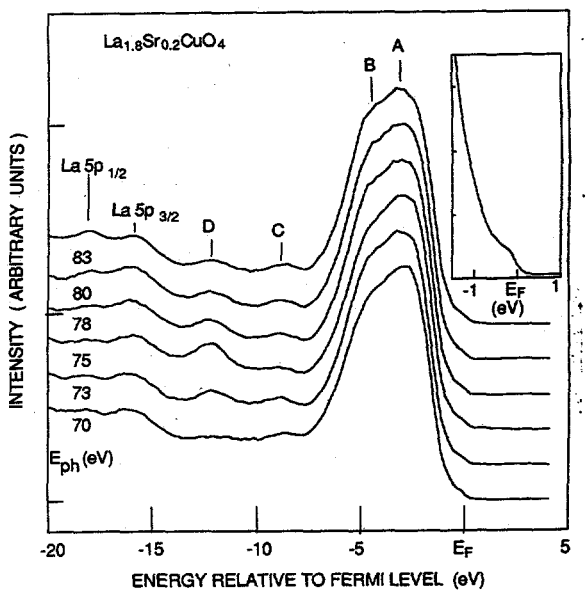

Fig. 2

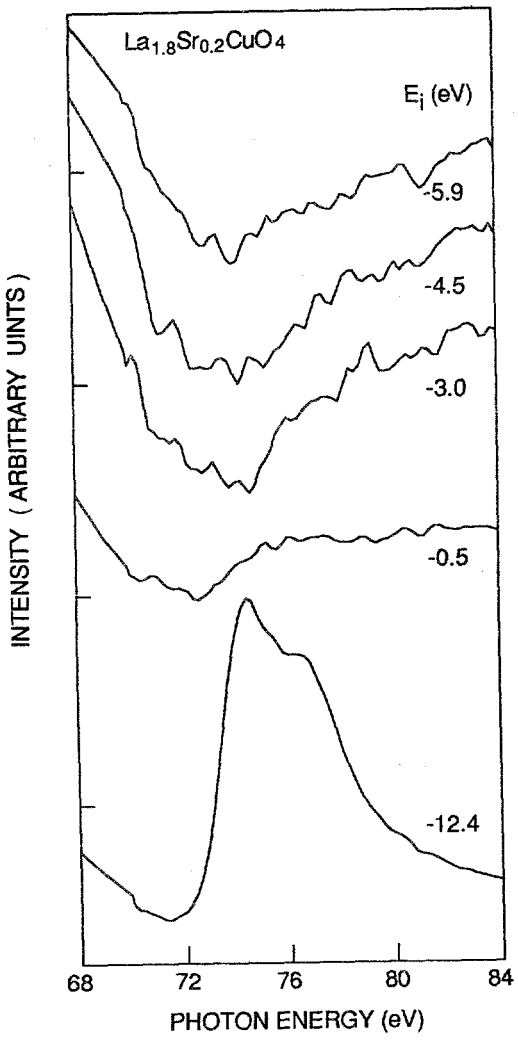

Fig. 3

Fig. 3 shows constant initial state (CIS) spectra in the Cu 3d RESPES region for various binding energies E_i of the valence band spectra of Fig. 2. The spectra are the difference between raw data and a smooth spline fit to the data. The main band emission shows a resonance dip and the satellie emission shows a resonance peak as in CuO and Cu_2O. The vertical scale is aribtrary but the same for all the curves. The CIS taken at E_i=–0.5 eV just above E_F also shows resonance behavior, which means that models for the superconductivity should include the Cu 3d character at E_F. Fig. 4 shows CIS spectra for photon energies at the La 4d edge for various binding energies E_i of the valence band spectra of Fig. 2. For $YBa_2Cu_3O_{7-\delta}$, CIS spectra around the Ba 4d edge for various E_i are similar to those shown in Fig. 4.

We also measured the Cu 2p XPS spectra for our superconducting samples and for Cu and CuO. These show spin-orbit-split $2p_{1/2}$ and $2p_{3/2}$ components, each of which has a main line and a satellite. The separation and intensity ratios for the two $2p_{3/2}$ lines were analyzed using the Anderson model. The separation 8.7 eV is approximately equal to U_{cd}, the Coulomb interaction between the Cu 2p core hole and the 3d electrons. The chemical shift from Cu to CuO agrees with that of a previous measurement and it is significant that the chemical shifts of the superconducting samples are intermediate, indicating that the oxidation of Cu in these samples is less than that of CuO, which provides evidence that Cu^{3+} does not occur. This conclusion is consistent with the large energy of the Cu d^8 state observed in the valence band spectra.

From an analysis of our photoemission data, using the Anderson Hamiltonian, we obtained experimental values of the parameters of the model, the copper-oxygen charge transfer energy Δ~0.4 eV, the d-d Coulomb interaction U~6 eV, and the ligand–3d hybridization T~2.4 eV. Using the parameters, we evaluated the linear Cu-O-Cu superexchange interaction J and found it is dominated by the charge fluctuations. For $\Delta << U$ and $T >> \Delta$ the charge transfer degrees of freedom and the lattice aspects of the Anderson lattice Hamiltonian should not be neglected in constructing models for the high T_c superconductivity.

Recently we have also obtained data on the states above E_F by Bremstrahllung isochromat spectroscopy (BIS), which provides a much more direct measure of the charge transfer energy Δ. From the new data, it is apparent that the Δ–values should be considerably larger (> 2 eV) than those we deduced using photoemission data alone, where Δ is determined mostly by fitting relative line intensities, rather than from line positions. We are now repeating the analysis to take this new data into account.

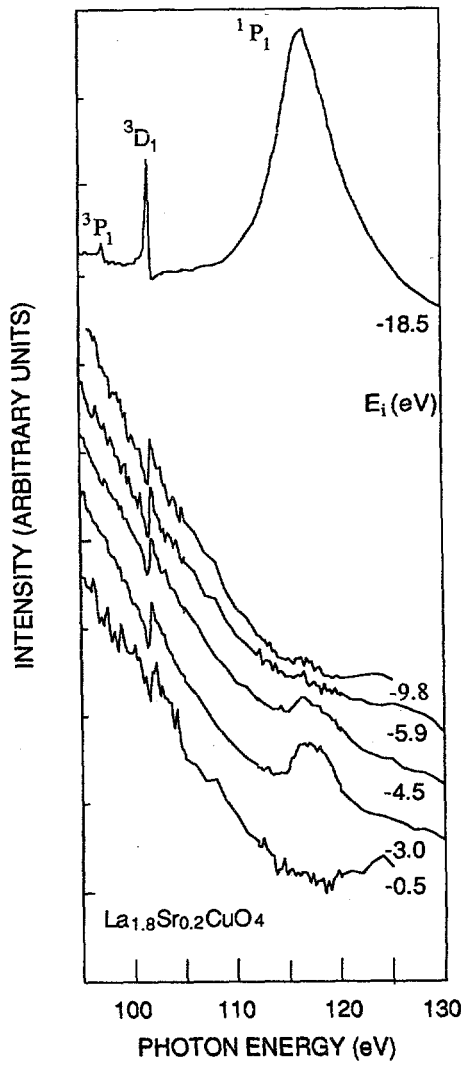

Fig. 4

Electronic structure of $Y_{1-x}Pr_xBa_2Cu_3O_{7-\delta}$

The superconductivity of $Y_{1-x}Pr_xBa_2Cu_3O_{7-\delta}$ is quenched as x is increased[4]. In order to correlate changes in the electronic structure and superconductivity properties of these alloys, we have measured their RESPES, core level XPS and BIS spectra.

Fig. 5 compares the Pr 4f specta obtained by RESPES for several values of x. The spectra are scaled to have the same magnitude of the main peak. Each is obtained by suitably scaling[5] and subtracting the Fano minimum spectrum (photon energy $h\nu$=115 eV) from that of the Fano maximum spectrum ($h\nu$=124 eV), both taken with resolution 0.35 eV. Fig. 6 shows CIS spectra for E_i=–0.8 eV for four values of x.The CIS spectra for other E_i values and x–values are also very similar, suggesting no valence change as a function of x.

From the measured BIS spectra (not shown here) the Pr 4f spectral weight above E_F was extracted by subtracting the spectrum for x=0 from that for each x, using the Ba $4f^0 \rightarrow 4f^1$ peak for normalization. There are 4f peaks at 2eV and 8eV abover E_F. As x increases, the relative intensity of the 2 eV peak decreases. Interpretation of the Cu 2p core level XPS spectra (not shown here) is complicated by overlapping Pr 3d emission just under the Cu 2p main peaks. Analysis is underway to correct for this, and to find a unified interpretation of all the data.

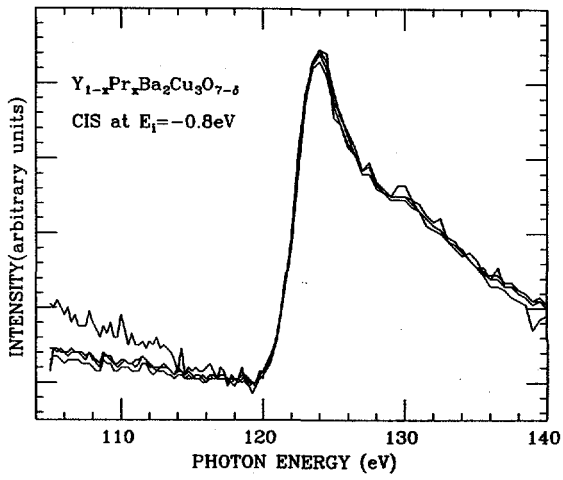

Fig. 6

Spectral Weight of $Y_{1-x}U_xPd_3$.

Cerium and uranium materials have in common that they display a diversity of ground state properties[6]. The f-electrons of these materials are generally regarded as being responsible. For Ce, the major features of the 4f spectra can be understood using the impurity Anderson Hamiltonian, which also provides a description of ground state properties not explicitly related to translational symmetry[7]. The U 5f spectra usually have very much weight around E_F, with a rather bandlike appearance, contrasting sharply to the Ce-4f spectra. There exists no unified picture for the U 5f spectral weight.

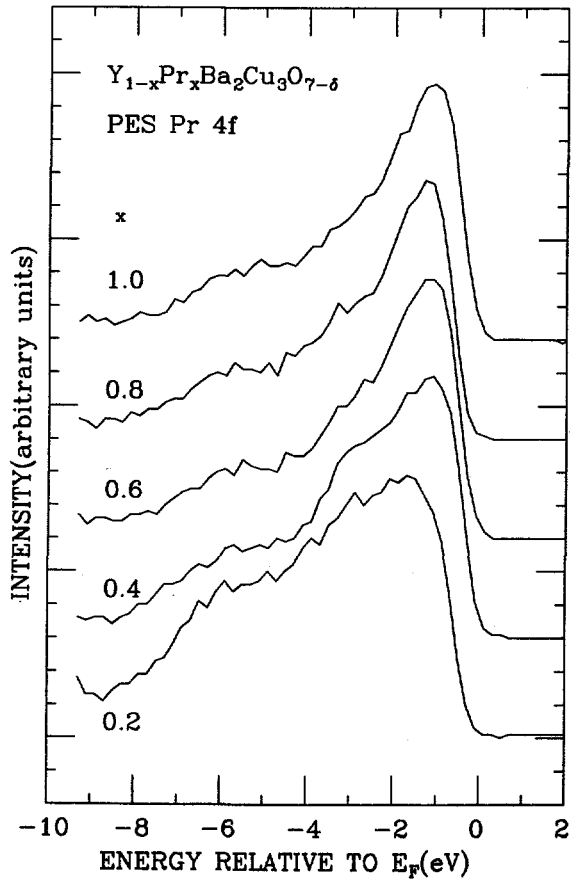

Fig. 5

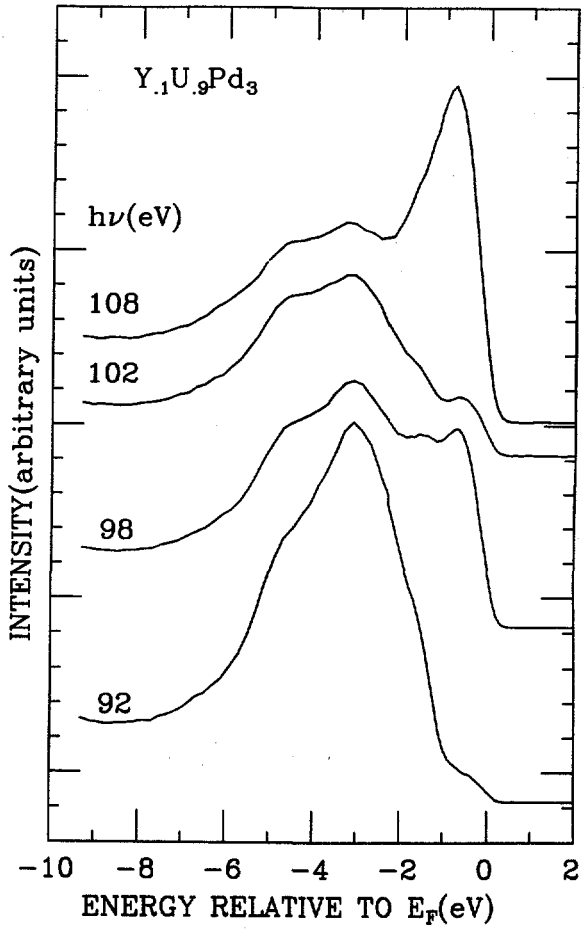

Fig. 7

UPd_3 is very interesting because it is the only intermetallic uranium compound for which the 5f spectrum has little weight at E_F. We have measured RESPES of $Y_{1-x}U_xPd_3$ for x=0, 0.1, 0.5, 0.9, and 1.0 The crystal structure for x=0 is the cubic Cu_3Au structure and that for x=1 is the hexagonal Ni_3Ti structure. There is a crystal structure transition with a rather broad immiscibility gap in the range x=0.5 to x=0.9. In the gap region, samples are 2–phase. The thrust of our study is to determine how the 5f spectrum changes with concentration and crystal structure.

Fig. 7 shows normalized valence band spectra for x=0.1, for several photon energies with 0.35 eV resolution. In the spectrum for $h\nu$=92 eV, the emission occuring at –3 eV is due to Pd 4d states, with a decrease of this emission at higher photon energies approaching the Cooper minimum around $h\nu$=110 eV. The energies $h\nu$=92 eV and 102 eV correspond to Fano minima and the energies 98 eV and 110 eV are Fano maxima of the resonance of the U 5f emission around the U 5d edge. The U 5f spectral weights, extracted from the 102 eV and 108 eV spectra as described in Ref. 5, are shown in Fig. 8.

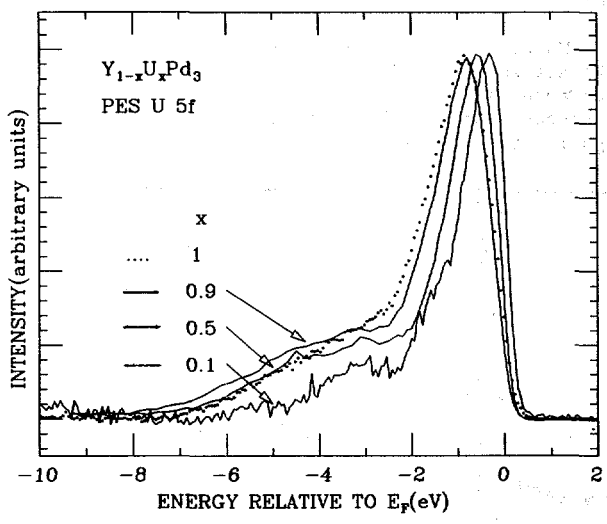

Fig. 8

In Fig. 8 the extracted 5f spectra are scaled to have the same magnitudes. If the Fano minimum spectra are scaled to one another, the resulting 5f spectra have areas which scale roughly with x. As x decreases, the centroid of the 5f peak moves toward E_F and its width becomes narrower. Since there is a change even in the range x=0.1 to 0.5, where the crystal structure is the same, we conclude that the change is due to dilution rather than the crystal structure change. This behavior is different from that[8] observed for $UPd_{3-x}(Pt, Rh)_x$, in which the 5f spectral weight changes abruptly at $x=x_c$, where there is a change in the crystal structure. These results are also different from those[5] for $Y_{1-x}U_xAl_2$, where the major features of the spectra are identical for x=0.02, 0.1 and 1.0.

REFERENCES

1. Z-X. Shen, J.W. Allen, J.J. Yeh, J.-S. Kang, W. Ellis, W. Spicer, I. Lindau, M.B. Maple, Y.D. Dalichaouch, M.S. Torikachvili, J.Z. Sun and T.H. Geballe, Phys. Rev. B **36**, 8414 (1987).
2. L.F. Mattheiss, Phys. Rev. Lett. **58**, 1024 (1987); L.F. Mattheiss and D.R. Hamann, Solid State Commun. **63**, 395 (1987).
3. J.J. Yeh and I. Lindau, At. Data and Nucl. Tables **32**, 1 (1985).
4. Y. Dalichaouch, M.S. Torikachvili, E.A. Early, B.W. Lee, C.L Seaman, K.N. Yang, H. Zhou and M.B. Maple, Solid State Commun. (in press).
5. J.-S. Kang, J.W. Allen, M.B. Maple, M.S. Torikachvili, B. Pate, W. Ellis, and I. Lindau, Phys. Rev. Letters **59**, 493 (1987).
6. G.R. Stewart, Rev. Mod. Phys. **56**, 755 (1984).
7. J.W. Allen, S.-J. Oh, O. Gunnarsson, K. Schönhammer, M.B. Maple, M.S. Torikachvili and I. Lindau, Adv. Phys. **35**, 275 (1986).
8. A.J. Arko, private communication.

J.L. Solomon and R.J. Madix*
J. Stöhr**

*Department of Chemical Engineering, Stanford University, Stanford, CA 94305
**IBM Almaden Research Center, 650 Harry Road, San Jose, CA 95120

Near-edge x-ray absorption fine structure (NEXAFS) is a powerful technique to determine orientation and bonding information of adsorbed molecules [1]. We have used NEXAFS to determine the orientation of benzene (C_6H_6), aniline ($C_6H_5NH_2$), phenol (C_6H_5OH), furan (C_4H_4O), 2,5-dihyrofuran (C_4H_6O), and maleic anhydride ($C_4H_2O_3$) on Ag(110). Multilayers were formed by dosing each compound at 100 K on the clean Ag(110) surface. Monolayer coverages were then obtained by annealing the crystal to desorb the multilayers. Carbon K-edge spectra were taken on beam line I-1 at Stanford Synchrotron Radiation Laboratory with the surface held at 100 K. Final NEXAFS spectra were obtained by dividing the adsorbate covered spectra by spectra taken of the clean surface.

Figure 1 contains spectra for benzene, phenol, and aniline. A clear polar dependance is observed for all three of the molecules as evidenced by dominance of the π^* resonance at glancing incidence (θ = 20°), and the dominance of the σ^* resonances at normal incidence (θ = 90°). Clear similarities in the spectra are also apparent as one would expect from the similar structure of the molecules (i.e. each contains a six member aromatic ring). The π^* resonance at glancing incidence is broadened for aniline and split for phenol, as expected due to the differing C(1s) binding energies for the ring carbons bound to nitrogen and oxygen, respectively.

Monolayer spectra for furan and 2,5-dihydrofuran (DHF) are shown in Figure 2. Again a clear polar dependance is observed. The π^* resonance and the σ^* resonances indicate that both of these five member rings lie parallel to the plane of the surface.

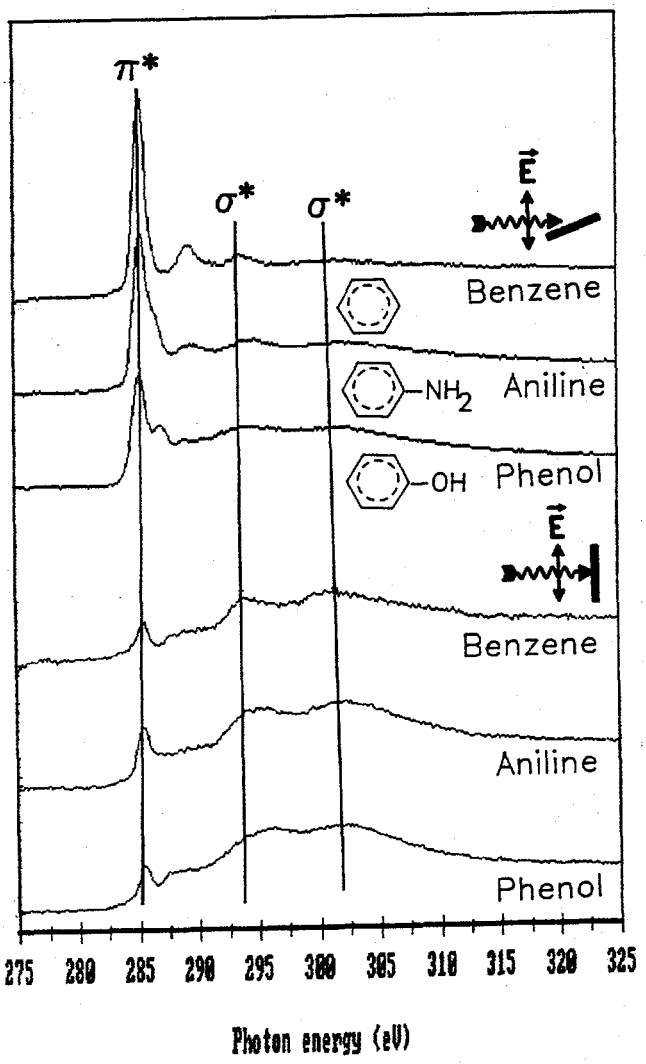

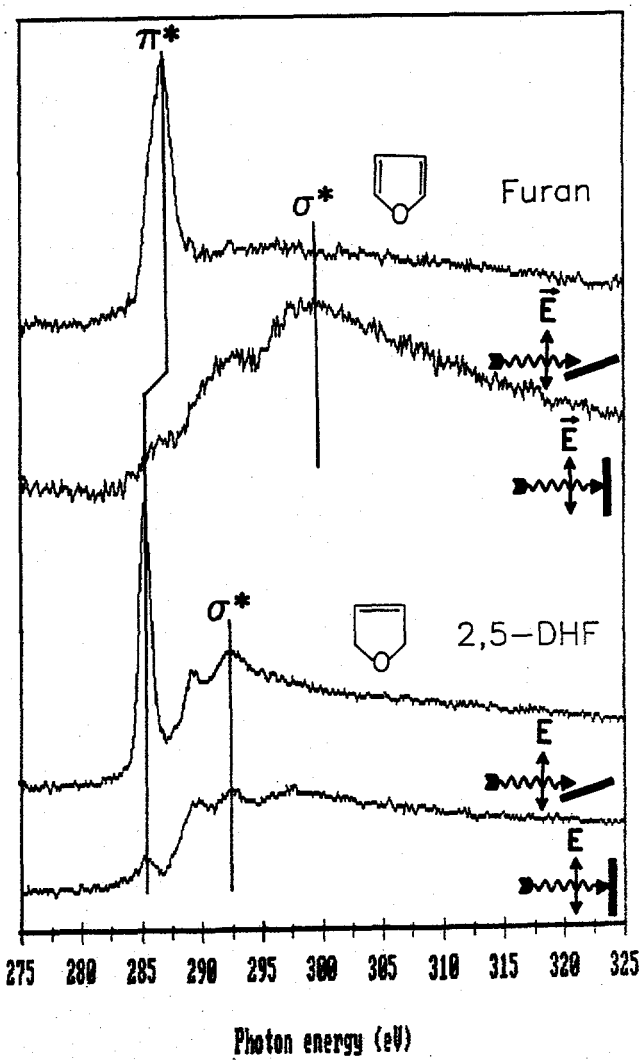

Spectra for maleic anhydride on Ag(110) are shown in Figure 3. In contrast to the previous five molecules, there is little difference between the monolayer spectra taken at glancing incidence and those taken at normal incidence, indicating that surface species is tilted appoximately 54° from the surface normal. The monolayer spectra also exhibit a decrease in the intensity ratio of the $\pi^*_{C=C}$ resonance to $\pi^*_{C=O}$ resonance relative to the ratio observed for the multilayer. The decrease in the intensity ratio means that transitions to the π^* orbitals of the C=C bond are less probable. Reactions at the C=C bond with the metal surface are a very likely explanation of this relative decrease in the transition intensity, and this interesting feature is still under investigation.

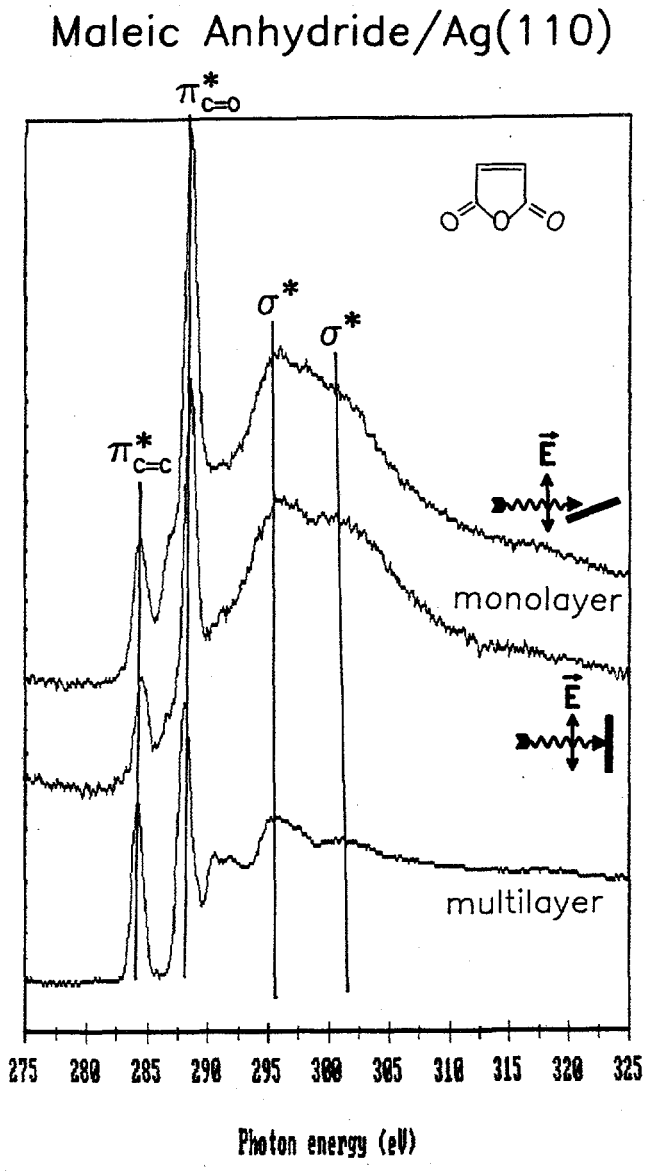

Figure 1. Carbon K edge NEXAFS spectra of monolayer coverages of benzene, aniline, and phenol, respectively, on Ag(110) at 100 K.

Figure 2. Carbon K edge NEXAFS spectra of monolayer coverages of furan and 2,5-dihydrofuran (DHF) of Ag(110) at 100 K.

Figure 3. NEXAFS spectra at the carbon K edge for monolayer and multilayer coverages of maleic anhydride on Ag(110) at 100 K.

[1] J. Stöhr and D.A. Outka, J. Vac. Sci. Technol. A 5 (1987) 919.

NEXAFS STUDIES OF BENZENE AND BENZENETHIOL ON Mo(110)

A. C. Liu, J. T. Roberts, J. R. Swanson and C. M. Friend

Department of Chemistry
Harvard University
Cambridge, Massachusetts 02138

INTRODUCTION

Near-edge X-ray absorption fine structure (NEXAFS) measurements offer a straightforward yet powerful means of investigating the structure of adsorbed species.[1] In particular, NEXAFS studies can yield considerable information on the polar and azimuthal orientation of adsorbed molecules with respect to a surface.[2] Using NEXAFS measurements as a key tool, we have investigated the adsorption and reaction of both benzene (C_6H_6) and benzenethiol (C_6H_5SH) on Mo(110).

RESULTS AND DISCUSSION

On the basis of temperature programmed reaction spectroscopy (TPRS) and X-ray photoelectron spectroscopy (XPS) data, we have found that benzene is molecularly adsorbed on Mo(110) at 120 K.[3] This chemisorbed benzene remains intact until ~350 K, when competing desorption and decomposition reactions begin to occur, resulting in C_6H_6 desorption at 350 K and H_2 evolution at 400 K. A large amount of surface carbon as well as the presence of a hydrocarbon intermediate are detected in XPS data recorded after annealing benzene to 500 K. At ~530 K, this intermediate undergoes complete decomposition, yielding additional H_2 and surface carbon.

Based on TPRS, XPS and high-resolution electron energy loss spectroscopy (HREELS), we have determined that adsorption of benzenethiol on Mo(110) at 120 K results in the immediate formation of phenyl thiolate (C_6H_5S), bound to the surface through the sulfur atom.[4,5] Above 300 K, the thiolate undergoes competing hydrogenolysis of the C-S bond, producing gaseous benzene and atomic sulfur, and, as surface hydrogen is depleted, dehydrogenation at C_2 accompanied by C-S bond scission, leading to surface benzyne (C_6H_4) and additional sulfur. The benzyne intermediate is exceptionally stable, remaining intact until 680 K, when it decomposes to H_2 and carbon.

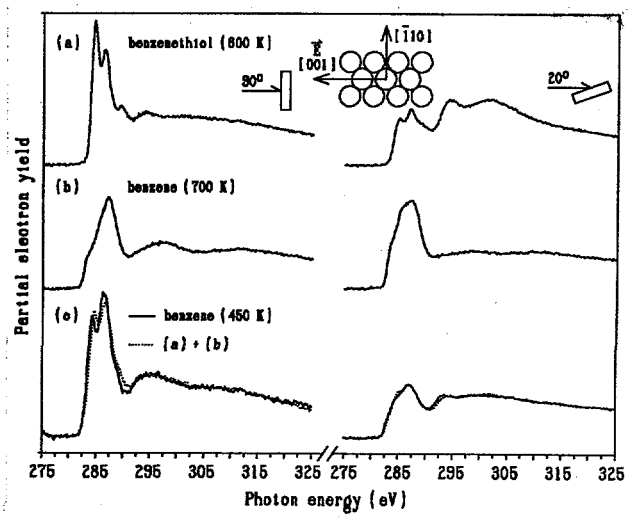

FIG. 1. Carbon K-edge NEXAFS spectra on Mo(110) for (a) benzyne from heating benzenethiol to 600 K, (b) surface carbon from heating benzene to 700 K, (c) surface intermediate(s) from heating benzene to 450 K. The dotted spectra are the best fits of coadded benzyne and surface carbon NEXAFS spectra to the 450 K benzene spectra. The azimuthal orientation of the Mo(110) crystal during these experiments is also shown.

Carbon K-edge NEXAFS spectra of the phenyl thiolate intermediate formed from benzenethiol show that the C-S bond and the phenyl ring are tilted ~20° away from the surface normal.[2,6] This unusual configuration may be due to steric interactions between phenyl hydrogens and surface Mo atoms. The NEXAFS spectra of the benzyne intermediate show two C=C π^* and two C=C σ^* resonances, in addition to a C-H resonance (Fig. 1(a)). Quantitative consideration of the polarization dependencies suggests that the benzyne is bound perpendicularly to the surface and that the ring plane is aligned along the $[\bar{1}10]$ azimuth.

NEXAFS measurements made after annealing benzene to 200 K are similar to those reported previously for monolayers of benzene on Pt(111).[7] The polarization dependencies of the C=C π^* and C=C σ^* resonances clearly indicate that the benzene is bound parallel or nearly parallel to the surface. Spectra for the hydrocarbon intermediate formed after annealing benzene to 450 K are complicated by the presence of absorption structure due to surface carbon atoms; NEXAFS spectra of atomic carbon produced by annealing benzene to 700 K clearly evidence structure due to carbon-metal scattering (Fig. 1(b)). However, least-squares fitting of the coaddition of spectra for benzyne formed from benzenethiol and atomic carbon formed from benzene produces spectra closely resembling the actual spectra recorded after annealing benzene to 450 K (Fig. 1(c)). We therefore propose that thermal reaction of benzene on Mo(110) also results in formation of perpendicularly-bound surface benzyne. The selectivity for benzyne formation from benzene is not as high as it is from benzenethiol; this is likely due to the relative accessibility of C-H bonds in π-bound benzene as compared to phenyl thiolate, thus resulting in substantial amounts of non-selective decomposition.

ACKNOWLEDGMENTS

The authors thank J. Stöhr for his assistance and for the use of his endstation at SSRL. Funding for this research has been provided in part by NSF-ROW, CHE-8710455.

REFERENCES

1. J. Stöhr and R. Jaeger, Phys. Rev. B **26**, 4111 (1982).
2. J. Stöhr and D. A. Outka, Phys. Rev. B **36**, 7891 (1987).
3. A. C. Liu and C. M. Friend, to be published.
4. J. T. Roberts and C. M. Friend, J. Am. Chem. Soc., submitted.
5. J. T. Roberts and C. M. Friend, J. Chem. Phys., in press.
6. A. C. Liu, J. T. Roberts, C. M. Friend, and J. Stöhr, to be published.
7. J. A. Horsley, J. Stöhr, A. P. Hitchcock, D. C. Newbury, A. L. Johnson, and F. Sette, J. Chem. Phys. **83**, 6099 (1985).

Proposal No. 8000V

Structural Studies of Schottky Barrier Formation by Means of Partial Photoionization Cross Section and the Asymmetry Parameter: Ag/Si(111)

Stanford Electronics Laboratories
Stanford University, Stanford, CA 94305

The goal of this work is to assess the possibility of using the energy dependence of the cross section (σ) and the asymmetry parameter[1] (ß) as a surface sensitive tool to probe the degree of hybridization between a transition metal d-states with a semiconductor *sp* valence band during the initial stages of metal deposition onto a clean semiconductor surface. In general, very different interface structures may be formed. In one extreme, the metal atoms may be present as isolated adatoms, with no hybridization with the semiconductor *sp*-states so that the metal wave function at the interface is atomic like. In the other extreme, the metal atoms may nucleate into large clusters and/or form chemical bonding with each other or with the semiconductor *sp*-states so that the metal wave function at the interface is severely distorted with respect to the free atom. It is thus apparent that very complex interface structures may be formed and a structural technique is required to distinguish between the different interface complexes and to yield information about the degree of distortion of the metal wave function at the interface.

We measured the partial photoionization cross section and the asymmetry parameter of Ag atoms deposited at room temperature and at submonolayer coverage onto a vacuum cleaved Si (111) in the energy region near the Cooper minimum (CM).[2] The Ag 4d partial photoionization cross section Fig. 1 in the photon energy range hν = 75-200 eV. It exhibits a dramatic energy dependence and drops by almost 2 orders of magnitude around the CM. Also shown in Fig. 1 are the experimental σ for atomic Ag, the calculated σ for atomic Ag in Herman-Skillman (HS) model, and the calculated σ from the neighboring atom Pd in Relativistic Random Phase Approximation (RRPA). As seen in Fig. 1, the energy dependence of these curves are very similar, all showing a pronounced Cooper effect (since we measured relative cross section, our experimental data are normalized to the theoretical curves at hν=80 eV). Since there is a strong correlation betweem the behavior of σ near the CM and the nature of the initial states,[3] the remarkable agreement between our experimental data and and those for atomic Ag thus suggests that Ag 4d wave function at Ag/Si interface is atomic like.

Measurements of the subshell asymmetry parameter in the condensed phase is experimentally more difficult than in the gas phase (interpretation of the data is also considerably more difficult). In the condensed phase, there are at least three vector quantities associated with any photoemission event, (1) the polarization of the incoming photon ε (for non-polarized light, photon direction), (2) the direction of the outgoing photoelectron p, and (3) the coordinate system characterizing the system which for a disordered system—such as a disordered Ag overlayer prepared by evaporating Ag atoms at room temperature and at submonolayer coverages onto Si (111)—consists of a single vector: the sample normal n. To measure the asymmetry parameter in the condensed phase, it is essential to take photoemission spectra at several ejection angles by varying the angle between the polarization vector and the photoelectron momentum θ, while keeping the angle between the sample normal and the photoelectron momentum (∠n.p) and the angle between the polarization vector and the sample normal (∠n.ε) constant. This can be achieved by rotating the electron analyzer in a cone around the sample normal, thereby achieving θ variability.

The asymmetry parameter of Ag 4d at its interface with Si is plotted in Fig. 2 as a function of photon energy in the energy region around the CM. Also shown in Fig. 2 are the experimental data and the theoretical calculations in Herman-Skillman approximation for the asymmetry parameter of atomic Ag and the theoretical calculations in RRPA for theasymmetry parameter of the neighboring atom Pd. The energy dependence of ß from Ag/Si interface, in the vicinity of the CM, is very close to the atomic results, all showing a pronounced Cooper effect.

The strong oscillation of ß near the CM, and its favorable agreement with the experimental and the theoretical results, indicates that Ag 4d states do not hybridize with Si *sp* valence band since any hybridization would attenuate the oscillation of ß.[4]

References

1. C. N. Yang, Phys. Rev. 74,764 (1948).
2. J. W. Cooper, Phys. Rev. 128, 681 (1962).
3. T. A. Carlson, M. O. Krause, F. A. Grimm, P. Keller, and J. W. Taylor, J. Chem. Phys. 77, 5340 (1982).
4. T. A. Carlson, M. O. Krause, W. A. Svensson, P. Gerard, F. A. Grimm, T. A. Whitely, B. P. Pullen, Z. Phys. D. 2, 309 (1986).

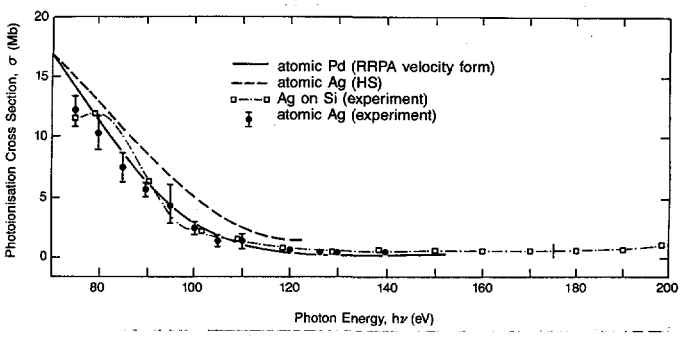

Fig. 1

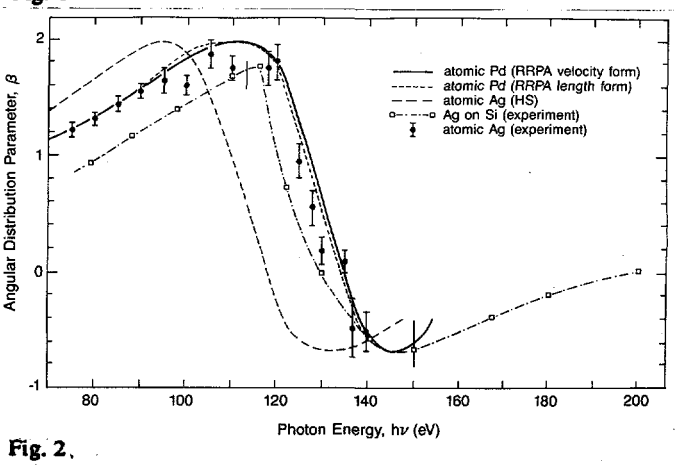

Fig. 2.

Photoemission Study of the Electronic Structure and Magnetic Interaction of High Tc

Z.-X. Shen

Stanford Electronics Laboratories
Stanford University, Stanford, CA 94305

The discovery of the high Tc superconductors have draw many attentions because of their important impacts in understanding of the fundamental physics. The unusually high critical temperature raises the question of whether the traditional theory of superconductivity is sufficient to describe the mechanism of superconductivity. To data, many schools of new theories have been proposed trying to explain the superconductivity at very high temperature, but There are not enough experimental data to distinguish the correct one from others.

In order to understand the properties of the new superconductors, it is necessary to understand their electronic structures. However, the understanding of the electronic structures of the high Tc superconductors remains very controversial. At present, there are three different kind of views upon the electronic structure of the superconductors held by different theories of superconductivity. The First group of theories believe that the electronic structure of the high Tc superconductors can be well described by one electron band theory, and the superconductivity is mediated by more or less conventional way in the form of electron phonon coupling. The second group of theories believe that the one electron band theory breaks down due to the strong coulomb interactions among the 3d electrons of Cu. They describe the electronic structure by a localized Hubbard Model which only take into account the copper 3d states. The third groups of theories believe that the one electron band theory breaks down and a localize picture should be used. However, the Hubbard Model is over simplified. They believe that the charge transfer degree of freedom between oxygen 2p states and Cu 3d states should not be neglected. These theories like to describe the electronic structure of the high Tc superconductors by Anderson Model which reconcile both the strong coulomb interaction U among the localized electrons and the charge transfer between the copper 3d states and oxygen 2p states.

As a very powerful tool of understanding the electronic structure, photoemission has been widely used to study the electronic structure of many materials. Given the controversy among the understanding of the electronic structure of the superconductors, it seems well motivated to perform photoemission study on the electronic structure of the superconductors.

The electronic structure of the high Tc superconductors was studied by resonance photoemission experiment performed at SSRL on Bean line III-4. The result suggested that the Anderson Model gave the most realistic description of the electronic structures of high Tc superconductors.

The EDC's obtained in the experiment were very different from what one electron band theory has predicted [1]. In Comparison with the prediction by band theory, the observed experimental density of states at fermi level was much lower, the centroid of the valence band shifted to higher binding energy, and the valence band EDC lineshape was also very different.

Another important observation which clearly signaled the breakdown of the one electron band theory is A d^8 satellite in the valence band 12.5 ev below the fermi level[1]. The satellite clearly showed a resonance behavior as the photon energy was tuned through the copper 3p to 3d absorption edge around 75 eV. This kind of resonance behavior which was not predicted by one electron band theory but often observed in transition metal compounds. We interpreted its unusually high binding energy position in the valence band as due to the strong coulomb interaction U among two d holes in d^8 configuration. The separation between this satellite and the main valence band gave a measure of U about 6 ev. We then fitted all our experimental data by the Anderson Hamiltonian applied to an configuration interaction cluster model. We obtained the experimental data for coulomb interaction U to be 6 ev, and the charge transfer energy D to be 0.5 ev. We found that the charge transfer degree of freedom dominated the low energy degree of excitation freedom. The lattice aspect of the Anderson Model must be taken into account. We then used the obtained experimental values to estimate the superexchange among O-Cu-O Chain. Again the result showd the importance of the charge transfer between the oxygen and copper. In summary, Our conclusion from the experiment was that the the superconductors are highly correlated, namely there were strong coulomb interactions among the electrons. On the other hand, the charge transfer degree of freedom also had to be considered.

The behavior of the high Tc superconductors below their superconducting transition temperature (93K) was also studied, no significant change in the electronic structure was observed. [2]

References

1. Z.-X. Shen et al, Phys. Rev. B 36, 8414 (1987).

2. Z.-X. Shen et al, to be published in the proceeding of the Fall Meeting of Material Research Society, Boston, December,1987.

The effect of strain on the band structure of $In_xGa_{1-x}As$

Proposal No. 8104V

J. Hwang, and P. Pianetta
Stanford Synchrotron Radiation Laboratory, Stanford, CA 94305
G. D. Kubiak, and R. H. Stulen
Sandia National Laboratories, Livermore, CA 94550
C. K. Shih, Y.-C. Pao, Z. X. Shen, and P. Lindberg
Stanford Electronics Laboratories, Stanford, CA 94305
B. Chow
Varian Operation Laboratory, Santa Clara, CA 94054

The fabrication of pseudomorphic semiconductor heterostructures, which can offer flexibility in tailoring their electronic and optical properties, has been emphasized during the past years. These pseudomorphic heterostructures are grown from lattice mismatched materials. The lattice mismatch between layers is accomodated by internal strain such that the lattice spacing parrallel to the interface of the heterostructure is equal on both sides. It is thought that the epitaxial layers in the pseudomorphic heterostructure exhibit tensile or compressive tetragonal distortion [1-3] which is a functionof the growth sequence of layers dependent on their respective lattice constants.

The availability of molecular beam expitaxy (MBE) provides a method to grow pseudomorphic heterostructures. Combined with band mapping by angle-resolved photoemission spectroscopy (ARPS), we can then directly measure the k-resolved deformation potential of each band, i.e. the strain-induced band shift at a certain k point. In this paper we examined the k-resolved deformation potential in $In_xGa_{1-x}As$ alloys with composition of x=0.0, 0.2, and 0.9. Our primary interest is concentrated in the deformation potential of the first two upper valence bands, i. e. $\Delta 3+\Delta 4$ (P_x+P_y–like) bands and the $\Delta 1$ (P_z–like) band.

Six representive samples with different strain profiles are described and tabulated in Table I. The GaAs(001) strained-layer is under a tensile tetragonal distortion [1-2] which consists of tensile in-plane strain in the (001) surface plane and a compressive uniaxial strain along the surface normal direction . In contrast, the $In_{0.2}Ga_{0.8}As(001)$ and $In_{0.9}Ga_{0.1}As(001)$ layers were designed to have a compressive tetragonal distortion which consists of a compressive in-plane strain in the (001) surface plane and a tensile uniaxial strain along the surface normal direction. These strain profiles are in the opposite direction to that of the strained GaAs(001) layer.

The photoemission spectra in this paper were obtained at Beam line III-2 of the Stanford Synchrotron Radiation Laboratory (SSRL) using a Seya-Namioka monochromator with 1180 line/mm grating. We have examined the MBE grown samples using photon energies between 17 and 30 eV. The polarized light was incident at 45 degrees with respect to the surface normal [001] such that all the valence states can be excited by this mixed s and p polarized radiation. The overall instrument resolution was less than 0.25 eV, however the energy peak positions could be determined to within 0.05 eV.

The arsenic capping technique was used in order to eliminate any oxygen contamination of the MBE grown layers during transfering to the ARPS system. In order to get a good surface, we found that it was important to minimize the time during which the sample was

TABLE I. Description of samples. The value of in-plane strain applies only to strained layer samples.

Sample layer	Unstrained	Strained	In-plane strain
GaAs(001)	1.5 micron thick	50Å GaAs(001) 200Å $In_{0.2}Ga_{0.8}As(001)$ GaAs(001) substrate	+1.3%
$In_{0.2}Ga_{0.8}As(001)$	2000Å thick	50Å $In_{0.2}Ga_{0.8}As(001)$ 1.5 micron GaAs(001) GaAs(001) substrate	−1.3%
$In_{0.9}Ga_{0.1}As(001)$	1000Å thick	40Å $In_{0.9}Ga_{0.1}As(001)$ 3000 Å $In_{0.53}Ga_{0.47}As(001)$ InP(001) substrate	−2.3%

exposed to air. The As cap was then removed by heating the sampleto approximately 500°C as monitored by an infrared pyrometer. Low Energy Electron Diffraction (LEED) was done only after the photoemission study and showed that all these samples have a C(4X4) surface reconstruction.

Normal emission spectra are taken at different photon energies between 17 and 27 eV for unstrained and strained GaAs(001), $In_{0.2}Ga_{0.8}As$(001), and $In_{0.9}Ga_{0.1}As$(001) cases. By using a free electron-like final state model to obtain the band dispersion curves, the detailed analysis described elsewhere [3], we can determine the k-resolved deformation potential. Our results show that the k-resolved deformation potential exhibits a significant k-vector dependence. Thus, we define a strain response function, ΔES, as a indication of the strain-induced effect. The ΔES is the difference of the energy separation between the Δ3+Δ4 bands and the Δ1 band. Fig. 1 shows the strain response functiion of the Δ3+Δ4 (P_x+P_y–like) and the Δ1 (P_z–like) bands for the GaAs(001), $In_{0.2}Ga_{0.8}As$(001) and $In_{0.9}Ga_{0.1}As$(001) cases. Notice that the ES becomes larger as the GaAs layer is put in tension. In contrast, the ES becomes smaller as the $In_{0.2}Ga_{0.8}As$ layer is put in compression. The ΔES value is almost exactly opposite to that in the GaAs case, consistent with the opposite strain condition. This again support our assumption that ΔES is a reliable indication of strain-induced effects. Moreover, the ΔES are quite similar for both the $In_{0.9}Ga_{0.1}As$ and $In_{0.2}Ga_{0.8}As$ layers. This clearly reflects the fact that both the $In_{0.9}Ga_{0.1}As$ and $In_{0.2}Ga_{0.8}As$ layers have compressive tetragonal distortions.

The strain-induced effect on the band structure of $In_xGa_{1-x}As$ shown in Fig. 1 indicates that the opposite trend in the ΔES value is consistent with the the opposite strain condition. This consistent experimental picture suggests that the $In_xGa_{1-x}As$ alloys with composition ranging from x=0 to 1 have the same response function to the strain perturbation. In other words, the cation (Ga or In atom) alloying has a negligible contribution to the k-resolved deformation potential.

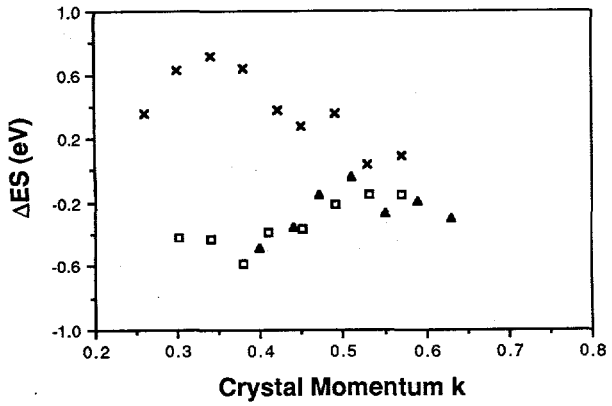

FIG. 1. The ΔES value as a function of crystal momentum along ΓX. The ΔES represents the strain-induced change in the energy separation between the Δ3+Δ4 bands and the Δ1 band. The crystal momentum is in units of $Å^{-1}$. (X: GaAs; : $In_{0.2}Ga_{0.8}As$; Δ: $In_{0.9}Ga_{0.1}As$).

Another interesting aspect in this study is that all these strain-induced effects exhibit k-vector dependence which seems to be periodic in k. The absolute value of ΔES, which is an index of strain–induced effects, has a minimum value at k=0.55 $Å^{-1}$ (about 1/2 ΓX) and reaches a maximum at k=0.34 $Å^{-1}$ for all compositions. |ΔES| becomes smaller as k approaches the Γ point. This evidence suggest that the deformation potential at k=0.34 $Å^{-1}$ is larger than that at the Γ point. However, the possible physics behind this still remains unclear.

ACKNOWLEDGEMENTS

We sincerely acknowledge the help of J. P. Chuang, H. Guyot and A. Waldhauer during the experiment . This work was done at Stanford Synchrotron Radiation Laboratory which is supported by the Department of Energy,Office of Basic Energy Sciences.

REFERENCES

1. S.T. Picraux, L.R. Dawson, G.C. Osbourn, and W.K. Chu, Nucl. Instr. and Meth. 218, 57(1983).

2. S.T. Picraux, L.R. Dawson, G.C. Osbourn, R.M. Biefield, and W.K. Chu App. Phys. Letter 43(11), 1020(1983).

3. J. Hwang, C.K. Shih, P. Pianetta, G. D. Kubiak, R. H. Stulen, L. R. Dawson, Y.-C. Pao, and J. S. Harris, Jr., American Vacuum Society 34th National Symposium, Anaheim, california, Nov. 2-6, 1987.

Proposal No. 8104V

First Images from Photoelectron Microscope

Piero Pianetta , Ingolf Lindau, and Paul King
Stanford Synchrotron Radiation Laboratory
SLAC Bin 69, PO Box 4359, Stanford CA 94031

Michael Keenlyside and Gordon Knapp
Surface Science Instruments Division, Kevex Corporation,
465 National Avenue, Mountain View CA 94043

Ray Browning
Center for Integrated Systems, Stanford University,
Stanford CA 94031

The first results have been obtained using an imaging photoelectron microscope (MicroESCA™) designed and constructed by Surface Science Instruments of Mountain View, CA. This instrument provides for complementary imaging and spectrometry of the photoelectrons excited by monochromatic synchrotron radiation. Lateral resolution is a couple of microns. Examples of images showing aluminum lines and pads on a silicon substrate are given below.

The theory of the photoelectron microscope has been described in detail elsewhere (1,2). In brief, the device relies on the diverging magnetic field from a superconducting magnet to guide drifting photoelectrons from the sample surface to a resistive anode imaging detector. Electrons that escape in a direction other than normal to the sample surface experience a Lorentz force and so follow a helical path to the detector. Radial motion is converted into axial motion by the diverging magnetic field. Electrons arrive at the detector having maintained the spatial and energetic characteristics of the ejected photoelectrons. Magnification is obtained by the electrons spreading out while following the flux lines of the diverging magnetic field. Linear magnification is simply [B(S)/B(D)]^0.5 where B(S) is the field strength at the sample and B(D) is the field strength at the detector.

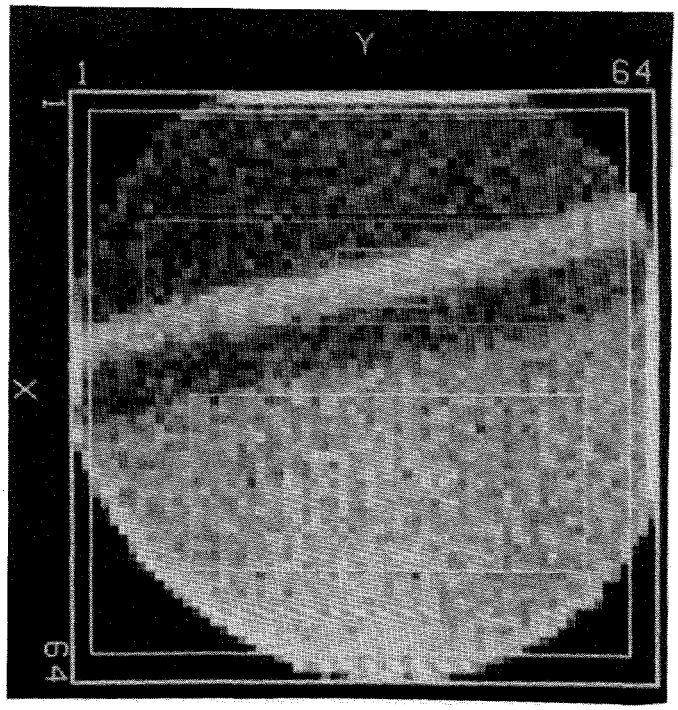

Figure 1. 64 by 64 pixel image is of a 20 um aluminum line and a larger aluminum pad on a silicon substrate. Image contrast is related to the intensity of photoelectrons in a 10 eV window associated with aluminum 2p excitation.

Typical working values are B(S) equal to 7T and B(D) equal to 1.5mT resulting in a linear magnification near 70. Spectrometry is carried out by controlling a retarding voltage at the detector. This allows for the generation of images from electrons in any particular energy window and thus provides a method for elemental and chemical mapping of surfaces.

Figure 1 is an image of the photoelectron intensity of a sample consisting of a 20 um wide aluminum line and a larger aluminum pad on a silicon substrate. Figure 1 represents all photoelectrons with energies associated with the aluminum 2p excitation. Incident photon energy here is 170eV. Figure 2 shows the spectrum of photoelectrons collected from the aluminum line and from the aluminum pad. Surprisingly, the photoelectron peak was found to shift between these two areas. In this instance the possibility of local charging has not yet been excluded. Analysis of this and other image data is still underway.

References

1. G. Beamson, H.Q. Porter, and D.W. Turner, Nature **290**, 556 (1981)
2. I.R. Plummer, H.Q. Porter, D.W. Turner, A.J. Dixon, K. Gehring, and M. Keenlyside, Nature **303**, 599 (1983)

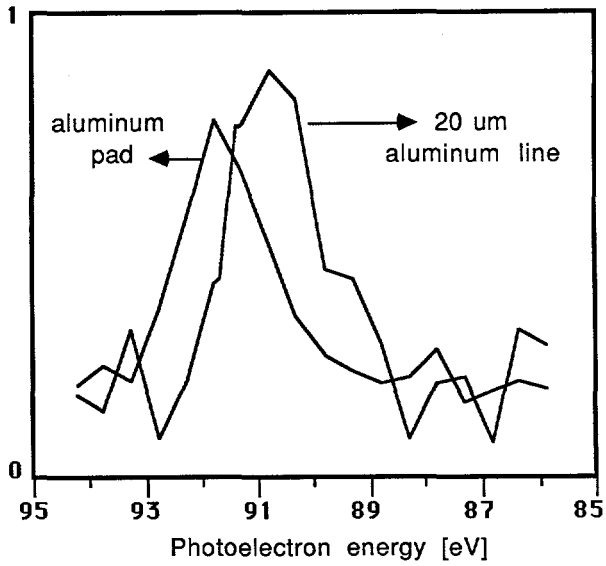

Figure 2. Spectrum of photoelectrons collected from the aluminum line and aluminum pad regions shown in Figure1. An apparent peak shift of the aluminum line to higher binding energies is observed.

A Kinetic Model of Crosslinking in Chemically Amplified Resists

Proposal No.8104V

Daniel Seligson
Intel Corp., 408-765-2381

Piero Pianetta, Paul King, Lawrence Pan
SSRL

We describe work begun in 1986 wherein we examined a series of x-ray resists which differed only in their halogenated sensitizer concentration, n_r. Photoresists are composed mainly of C, N and O. The addition of Br- or Cl-sensitizers increases the x-ray absorption for 1 to 3 keV of interest for lithography. In 1986 we showed that resist sensitivity is inversely proportional to the average mass absorption. (Note: sensitivity is defined as that incident dose, D_{50} which results in 50% of the initial film thickness remaining after development. Greater sensitivity means smaller D_{50}.) The more recent experiments showed that the addition of Cl improved d_{50} more than could be accounted for by the x-ray absorption. We concluded that the Cl participates in the chemistry of the resist exposure process, not just the absorption physics. In 1987 we developed a kinetic model of the exposure process which predicts the dependence of sensitivity on n_r and on the post-exposure processing parameters. From a manufacturing perspective, the most significant result is that we can calculate the effect of process variations on resist performance, basing those calculations on relatively few experimental measurements.

The resists used were provided by Rohm and Haas Research Laboratories. They are novolak polymers containing a photoacid generator (PAG) and crosslinking agent. The photoacid (PA) autocatalytically crosslinks the polymer upon application of heat subsequent to exposure. The resists were prepared with different n_r.

The model employs three critical assumptions. 1) PA is proportional to the absorbed x-ray dose density and to n_r. 2) The rate of crosslinking is equal to the product of PA concentration, a temperature dependent rate constant and the density of uncrosslinked polymer. 3) The rate constant of assumption 2 has an Arrhenius dependence.

We calculate molecular weight and solubility of the polymer, using these to obtain the dependence of D_{50} on n_r, for fixed postexposure bake (PEB) time and temperature (Fig. 1). The model predicts a dependence of n_r^{-1}, but the data seems to fit a $n_r^{-1/2}$

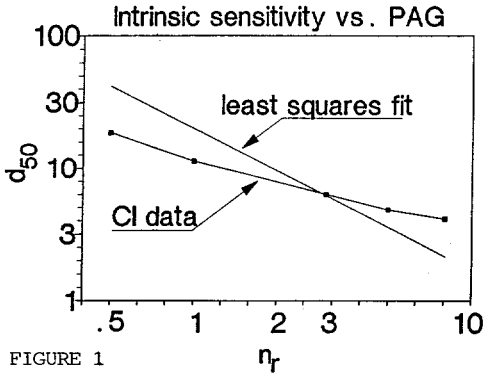

FIGURE 1

dependence. In fact the dependence seems to weaken as n_r increases. This and the square root dependence itself are probably attributable to the fact that the presence of additional sensitizer alters the polymer chemistry adversely, as well as promoting crosslinking as intended.

Examining the dependence of D_{50} on PEB conditions, we fixed n_r and ran an experimental matrix of times (0.5 to 16 minutes) and temperatures (90°C to 130°C). From Arrhenius plots we determined the activation energy, ~9200 Kelvin, and we found that $D_{50} \sim t^{-1/3}$. The rate of crosslinking saturates with time. This is to be expected because as the reaction proceeds, the sensitizer gets locked up in the crosslinked network and cannot migrate outwards to regions of low crosslinking density. This so called 'cage effect' can be included in the model by altering assumption 2.

The model predicts that the data for all doses and PEB conditions can be described by a single contrast curve if we use a suitably defined effective dose, D_{eff}. Data from 9 different processing conditions are plotted using this D_{eff} (Fig. 2). The model does not predict the shape of the curve.

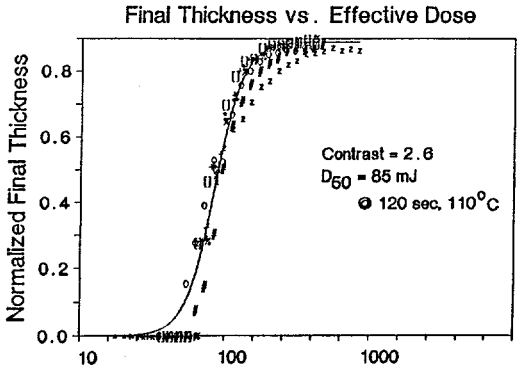

FIGURE 2

From general principles of lithography, we understand the influence of dose variations on the linewidth of printed images. Considering the total variation of D_{eff} we determine analytically the effect of small processing variations on linewidth, or other quantities, as given below.

$$\frac{\text{del } D_{eff}}{D_{eff}} = \frac{\text{del } D}{D} + n\,\frac{\text{del } t}{t} + \frac{E_a}{k_B T}\,\frac{\text{del } T}{T}$$

For the resist in question $E_a/k_BT \sim 25$, so the effect of temperature variations is very pronounced, much more so than variations of either incident dose or PEB time variations. This result therefore has significant implications for the process control that must be exercised in sub-micron lithography.

X-ray Absorption Studies Performed at the Silicon K-edge

J.C. Woicik, B.B. Pate, and P. Pianetta
Stanford Synchrotron Radiation Laboratory
Stanford CA, 94305

Our recent work has focused on the understanding of the lineshape of the Si 1s absorption edge in various silicon based materials and surfaces. Emphasis has been placed on correlating the local geometric structure about the silicon atom with the local electronic structure as derived from the near edge x-ray absorption spectra. The first part of this report briefly describes the conclusions of an earlier study in which we reported the Si 1s absorption near edge spectra of Si and SiGe alloys while the second part of this report briefly describes the conclusions of a later study in which we reported the Si 1s absorption near edge spetra of the clean Si(111) 2x1 and hydrogen terminated Si(111) 1x1-H systems. In both studies, the near edge spectra contributed key information towards the understanding of the electronic structure of the materials.

In order to study the effect of alloying on the electronic structure of SiGe alloys, the evolution of the 'white line' in the Si 1s absorption edge of (1) crystalline Si, (2) a stochiometric crystalline SiGe alloy, and (3) a dilute (<10% Si) crystalline SiGe alloy was studied. It was found that the 1s absorption edge was actually split into two distinct peaks. The splitting (~1 eV for crystalline silicon and ~1.7 eV for the dilute alloy) was found to be a continuous function of alloy composition. In each case, our experimental data closely resembled the calculated density of unoccupied conduction band states for crystalline Si, SiGe (calculated in the virtual crystal approximation), and Ge respectively. Common to each calculated spectrum are two distinct peaks above the conduction band minimum followed by a third, less intense peak. Agreement with the experimental absorption spectrum and the first three peaks of the pertinent calculated density of states was obtained both in regard to energy postition and relative intensity. The apparent splitting of the 'white line' may thus be attributed to the first two large peaks in the density of unoccupied conduction band states. The justification for comparing the dilute alloy with the band structure of Ge is based on the extreme physical and assumed electronic miscibility of the two materials. That is, the band structure of SiGe alloys apparently behaves as an interpolated average of the Si and Ge band structures. Under this assumption, the band structure of dilute SiGe should be identical to that of Ge, and the band structure of SiGe intermediate to both Si and Ge. As seen from our results, this is indeed the case. The slope of the edge was also found to be a continuous function of alloy composition and was sharpest for the dilute alloy. Qualitatively, our results may be accounted for in a one electron picture without invoking many body excitonic effects. The absorption edge of amorphous silicon showed no resolvable double structure which indicates that the splitting of the 'white line' is due to the long range order present in the crystalline lattice. The edge slope of amorphous silicon was identical to that of crystalline silicon. This result showed that it is the short range order, i.e. Si-Si or Si-Ge bonding, which influences the lineshape at threshold.

In order to study the electronic structure of the silicon surface, we measured the Si 1s absorption edges for the Si(111) 2x1 and Si(111) 1x1-H systems in both bulk and surface sensitive modes. Our results showed that in the surface sensitive mode, the Si 1s electron exhibited absorption into the Si(111) 2x1 unoccupied surface states. Subtraction of the bulk from the surface sensitive absorption spectra revealed a surface peak which disappeared upon exposure of the clean surface to atomic hydrogen and which lay ~0.5 eV below the bulk conduction band minimum in agreement with the π bonded chain model for this surface. These surface states are sensitve to the 1s absorption due to the favorable dipole coupling between states of s and p character. Silicon p_z surface states are produced upon cleavage. By selectively tuning the photon energy to this surface peak, we were able to extract the surface contribution to the total Si $L_{2,3}VV$ Auger lineshape. We showed that the surface lineshape differs significantly from that of the bulk. The main differences are that the

bulk plasmon loss at ~70 eV kinetic energy is suppressed at the 2x1 surface, an effect which may be explained by classical arguments, and that the contribution of the surface filled-dangling-bonds shifts the main Auger peak ~1 eV towards higher kinetic energy. The bulk plasmon loss at ~70 eV is greatly intensified at the Si(111) 1x1-H surface due to the passivation of the surface upon hydrogen adsorption and the reordering of the surface from a sp^2 to sp^3 configuration. The high energy $L_{2,3}VV$ Auger satellite peak at ~107 eV kinetic energy was shown to be sensitive to the photon energy within the vicinity of the Si K-edge. This phenomenon was explained by the double ionization of the Si L-shell due to a KLL decay for photon energies above the silicon K-edge. We deduced that ~15 eV is the energy difference between a singly and doubly ionized Si L-shell and is due to the presence of the extra 'spectator' core hole during the LVV decay. Unlike the plasmon loss, this feature was not sensitive to the surface geometry since it is an atomic rather than geometric effect.

(1x1)Co/Cu(001) Surface Geometry Determined From Co 1s Photoelectron Diffraction

Z.Q. Huang, L.J. Terminello, L.Q. Wang, Z. Hussain,† X.S. Zhang,††
S. Kim, L. Huckabee, D.A. Shirley

Materials and Chemical Sciences Division
Lawrence Berkeley Laboratory
and
Department of Chemistry
University of California
Berkeley, California 94720

J. Woicik, P. Pianetta
Stanford Synchrotron Radiation Laboratory
Stanford University, California 94305

Co 1s angle-resolved photoemission was measured over a kinetic energy range of 80-400 eV from a (1x1)Co/Cu(001) adsorbate system. The photoemission measurements were made on Beamline VI and exhibit an intensity modulation arising from photoelectron diffraction. This energy dependent form of photoelectron diffraction, recently termed angle-resolved photoemission extended fine structure (ARPEFS),[1] exhibits large oscillations (see Fig. 1) that permit Fourier analysis and subsequent extraction of structural information. The (1x1)Co/Cu(001) system was prepared by evaporating Co from high purity wire onto a clean (1x1) Cu(001) substrate. Evaporation rates were monitored by a quartz micro-balance and were correlated to effective coverages determined from separate Auger electron intensity analysis. The results of our (1x1)Co/Cu(001) ARPEFS study were compared with the epitaxial structure proposed by LEED[2] and reveal additional physical information. There is evidence that the Generalized Ramsauer-Townsend effect,[3] that arises from particular scattering conditions, is present in our results.

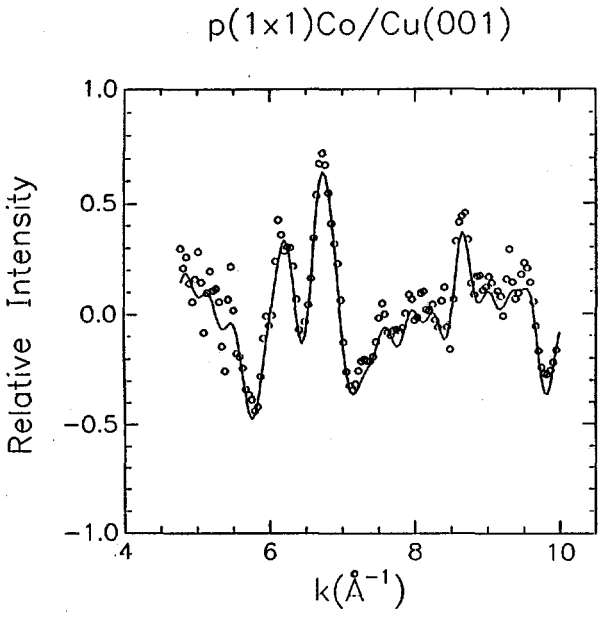

Figure 1. $\chi(k)$ curve for emission direction normal to the Cu(001) surface. The circles represent unfiltered data. The solid line is the same $\chi(k)$ filtered at path-length differences between 1.5Å and 20Å.

Acknowledgement

This work was supported by the Director, Office of Energy Research, Office of Basic Energy Sciences, Chemical Sciences Division of the U.S. Department of Energy under Contract No. DE-AC03-76SF00098. It was performed at the Stanford Synchrotron Radiation Laboratory, which is supported by the Department of Energy's Office of Basic Energy Sciences.

†Permanent address: Department of Physics, University of Petroleum & Minerals, Dhahran, Saudi Arabia

††Permanent address: Department of Physics, Zhejiang University, Hangzhou, Zhejiang, China

References

1. J.J. Barton, C.C. Bahr, Z. Hussain, S.W. Robey, J.G. Tobin, L.E. Klebanoff, and D.A. Shirley, Phys. Rev. Lett. 51, 272 (1983).
2. A. Clarke, G. Jennings, R.F. Willis, P.J. Rous, and J.B. Pendry, Surf. Sci 187, 327 (1987).
3. J.J. Barton, Z. Hussain, and D.A. Shirley, Phys. Rev. B 35, 933 (1987).

SUB-keV NEAR-THRESHOLD RESONANCES IN PHOTOABSORPTION

Proposal No. 9901V

Nancy Kerr Del Grande and K. Glenn Tirsell

Lawrence Livermore National Laboratory, Livermore, CA 94550

Synchrotron radiation was used for absolute photoabsorption experimental cross section (APECS) measurements taken in transmission.[1-3] Among the interesting phenomena observed for a broad range of solid elements (Z=4 through Z=92) at energies from about 50-1500 eV were the resonances/enhancements which seem to accompany virtually every inner shell threshold. Two light elements (e.g., beryllium metal and amorphous carbon) have structural enhancements extending some tens of eV above their respective K-edges which differ significantly from relativistic Hartree Slater (RHS) theory,[4] the Henke compilation[5] and the LLNL data base (CSLOW). The BL-VIII TGM APECS measurement in Figure 1 for solid Be closely parallels the relative atomic photoionization cross section measurement from Auger spectra for the gas.[6] Note the structure for the solid metal is predominantly atomic, although there is significant broadening due to outer conduction band electrons. A broad structural enhancement for amorphous carbon is tentatively explained as a molecular shape resonance, although autoionizing transitions from the 1s state to unoccupied valence bands in the solid are also possible.[1] Recent BL-VIII SGM APECS measurements of the relative intensity and spacing versus Z for the 2p-3d autoionizing resonances of Ti, V, Cr, Fe and Ni reveal features about the interplay between exchange and spin orbit interactions which help explain the coupling scheme of the ions. Other BL-VIII TGM measurements of the 5d giant resonance for uranium are being used to test relativistic time-dependent local density approximation (RTDLDA) calculations for the uranium atom in a spherical "drop" of jellium.[2,7] APECS measurements are providing a valuable tool to test theory and probe the behavior of atoms, ions, molecules and solids.

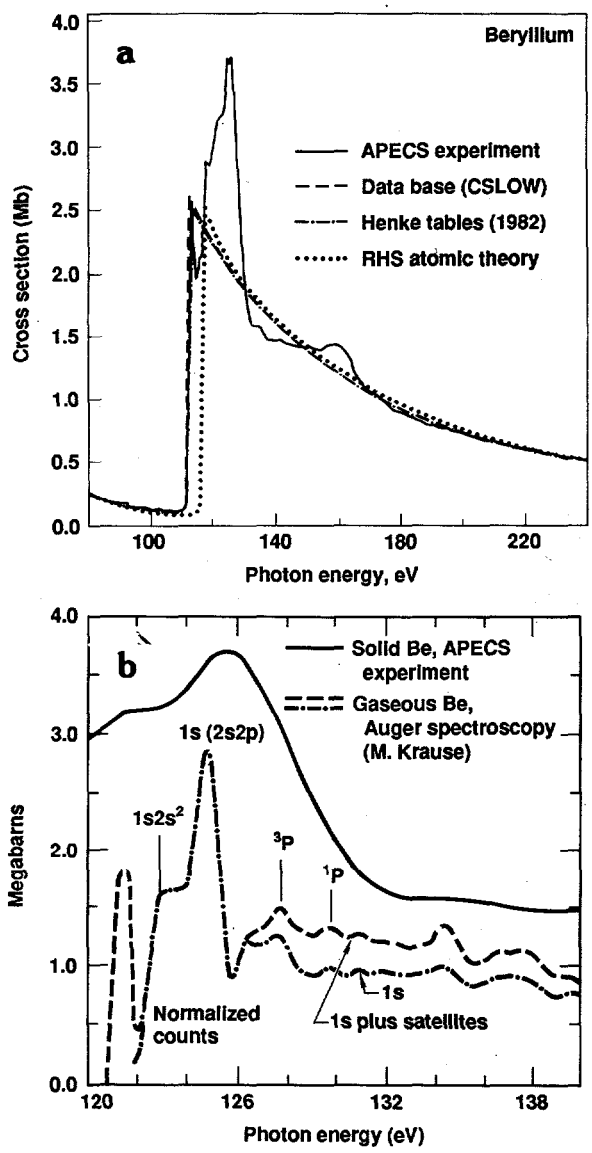

Figure 1. Preliminary APECS measurement of Be metal showing comparison with theory,[4] compilation[5] and data base in 1a and with relative atomic photoiopizaton cross section measurement for Be gas in 1b.[6]

ACKNOWLEDGMENTS

We appreciate the APECS multilayer sample design ideas and measurements of T. Barbee, Jr.; the technical support efforts of J. Batteux, M. Fowler and R. Mazuch; the data acquisition and analysis support of M. Schneider, E. Carr, and P. Mahowald; the collaboration with B. Pate; the UHV work of H. Morales, T. Martinez, T. Neal, and P. Golceff; and the support given by P. Pianetta and his staff. This work was performed under the auspices of the U. S. Department of Energy by the Lawrence Livermore National Laboratory under Contract No. W-7405-ENG-48.

REFERENCES

1. N. K. Del Grande et al., "Resonances in near-threshold x-ray photoabsorption of inner shells," Spec. suppl. to Journ. de Phys. with Proc. of 14th Internat. Conf. on X-Ray and Inner Shell Processes, Paris, France (1988).
2. N. K. Del Grande and K. G. Tirsell, "A program to obtain reliable photoabsorption cross sections," in X-Ray and VUV Interaction Data Bases, Calculations, and Measurements, N. Del Grande et al., Eds., Proc. SPIE 911 (1988).
3. K. G. Tirsell and N. K. Del Grande, "Considerations for the use of synchrotron radiation sources to measure sub-keV x-ray photoabsorption cross sections in transmission," in X-Ray and VUV Interaction Data Bases, Calculations, and Measurements, N. Del Grande et al., Eds., Proc. SPIE 911 (1988).
4. E. B. Saloman, J. H. Hubbell, and J. H. Scofield, "X-ray attenuation cross sections for energies 100 eV to 100 keV and elements Z=1 to Z=92," Atomic Data and Nuclear Data Tables 38, 1-145 (1988).
5. B. L. Henke et al., "Low energy x-ray interaction coefficients: photoabsorption, scattering and reflection, E=100-2000 eV, Z=1-94," Atomic Data and Nuclear Data Tables 27, 1-144 (1982).
6. M. O. Krause and C. D. Caldwell, "Strong correlation and alignment near the Be 1s photoionization threshold," Phys. Rev. Lett. 59, 2736-2739 (1987).
7. A. Zangwill and D. A. Liberman, "Optical response of an embedded atom: Resonant photoemission from uranium," Phys. Rev. B 34, 6705-6707 (1987).

Proposal No. 9901V

OPTICALLY DETECTED ABSORPTION IN THE SOFT X-RAY REGION

M. J. Weber, M. B. Schneider and K. G. Tirsell

Lawrence Livermore National Laboratory
P.O. Box 808, Livermore, California 94550

INTRODUCTION:

Detection of x-ray absorption edges and fine structure by monitoring optical luminescence has been reported for both the hard[1] and soft[2,3] x-ray regions. This technique involves relatively simple sample preparation and experimental apparatus, can be used for spectroscopy of low-Z elements or high-lying core levels having small x-ray fluorescence yields, and in certain cases can provide site and valence specific information. We have demonstrated the further versatility of this method for the soft x-ray region by examining several crystalline and amorphous materials having either intrinsic luminescence or luminescence from transition metals and organic dyes present as dopants. Measurements were made in the 10-200 eV region using beamline VIII-1 (TGM) and in the 100-1200 eV region using beamline VIII-2 (SGM). Fluorescence was observed from the front surface of the sample at 45° to the direction of the x-ray beam with a photomultiplier tube and photon counting electronics. Since the samples were optically thick with respect to x-rays, the edge jumps are negative.[4]

RESULTS:

Rare Earth Materials: Several rare earths fluoresce intensely, even at high concentrations, and therefore are useful activators. The $M_{4,5}$ and $N_{4,5}$ edges corresponding to allowed 3d→4f and 4d→4f transitions of CeF_3, CeF_3-CaF_2 solid solutions, PrF_3, TbF_3, $LiTbF_4$, and KTb_3F_{10} were easily detectable. The complex spectrum observed for CeF_3 was in excellent agreement with that obtained by transmission through thin films.[5] As an example, the luminescence excitation spectrum for a $Tb(PO_3)_3$ glass showing both the Tb $N_{4,5}$ edges and the P $L_{3,2,1}$ edges is given in Fig. 1.

LaF_3:Tb(0.1%): Although the terbium concentration in this sample is small, its luminescence can be used to detect the F K edge and EXAFS and the La $M_{4,5}$ edges as shown in Fig. 2.

BaF_2: The excitation spectrum of the intrinsic luminescence shows Ba and F absorption edges similar to those shown in Fig. 2, but different fine structure.

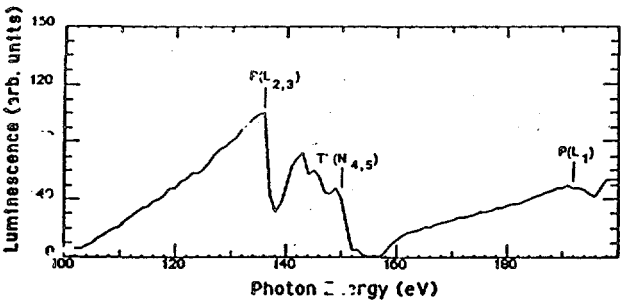

Figure 1. Terbium luminescence excitation spectrum for $Tb(PO_3)_3$ glass at room temperature.

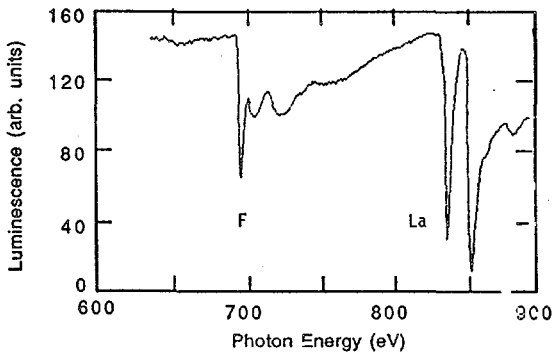

Figure 2. Terbium luminescence excitation spectrum for LaF_3:Tb(0.1%) at room temperature.

$Bi_4Ge_3O_{12}$: The O K edge and EXAFS were observed but there was no clear evidence of other Bi or Ge edges in the 100-1300 eV region (the Bi L edges and Ge K edges have, however, been detected optically).

Europium Aluminoborate Glass: The Eu $N_{4,5}$ edges and the B and O K edges were observed by monitoring the Eu luminescence; the latter absorptions were weak.

Sodium Phosphate Glass (1.0% Mn): By monitoring the Mn^{2+} luminescence, the O and Na K edges and EXAFS and a weak Mn L_3 edge were observed.

Tin-Lead-Fluorophosphate Glass (Rhodamine 6G): The Sn $M_{4,5}$ edge and the O and F K edges were detected by monitoring the dye fluorescence in this low temperature glass.[6]

ACKNOWLEDGEMENTS:

We thank R. Stulen (SNLL) for the loan of the UHV chamber used for the experiments and D. Blackburn (NBS) and P. Tick (Corning) for glass samples. This work was performed under the auspices of the U.S. Department of Energy by the Lawrence Livermore National Laboratory under contract W-7405-ENG-48.

REFERENCES:

1. J. Goulon et al. in EXAFS and Near Edge Structure III, ed. K. Hodgson, B. Hedman, and J.E. Penner-Hahn (Springer-Verlag, Berlin, 1984), 490 and references cited therein.
2. B.X. Yang, J. Kirz and S.Xu, Nucl. Instr. and Meth. A258, 141 (1987).
3. D.B.M. Klaassen, C.M.G. van Leuken and K.M.H. Maessen, J. Lumin. 40/41, 696 (1988).
4. J. Goulon, P. Tola, M. Lemonnier and J. Dexpert-Ghys, Chem. Phys. 78, 347 (1983).
5. C. G. Olson and D. W. Lynch, J. Opt. Soc. Am. 72, 88 (1982)
6. W. R. Tompkin, R. W. Boyd, D. W. Hall and P. Tick, J. Opt. Soc. Am. B 4, 1030 (1987).

Proposal No. 9901V

RESONANT PHOTOEMISSION STUDY OF THE NiGa INTERMETALLIC COMPOUND

Lishing Hsu and R. Stanley Williams
U C L A, Los Angeles, CA 90024-2569

Duane Outka
Sandia National Laboratory, Livermore, CA 94550

The Fe group transition metals form a series of intermetallic compounds with the group-III elements in which the ratio of the transition metal to group-III atom varies from 3:1 to 1:4. Since the transition metals are significantly more electronegative than the group-III metals, these compounds should display a wide range of electron transfer into the transition metal *d*-orbitals. We are using resonant photoemission, i.e., the enhancement in the shake-up satellite of the Ni *d*-bands at the threshold of the Ni *3p* absorption edge,[1] to help characterize this charge transfer.

Figure 1 shows the PES EDCs for NiGa as a function of photon energy from 60 to 80 eV. The resonance enhancement of the weak shake-up feature can be clearly observed at $h\nu$ = 67 eV. By examination of difference spectra, as shown in Fig.2, the contributions from the resonantly enhanced satellite and the MVV Auger peak can be more clearly resolved.

The resonance enhancement observed in NiGa is very similar to that for elemental Ni in terms of the binding energy of the satellite, the resonance photon energy, and the intensity of the enhancement. Thus, the Ni *3d*-band in this intermetallic compound does not appear to have been perturbed much by the Ga. This contrasts with the case of $PtGa_2$, where the Pt *d*-levels are nearly 2 eV below the Fermi level of that compound.[2] No satellites are observed for the Ga *3d* peak, which shows that the resonance enhancement is localized on individual Ni atoms.

1 M.R. Thuler, R.L. Benbow, and Z. Hurych, Phys. Rev. **B 27,** 2082 (1983).

2 S. Kim, L. Hsu, and R.S. Williams, Phys.Rev. **B 36,** 3099 (1987).

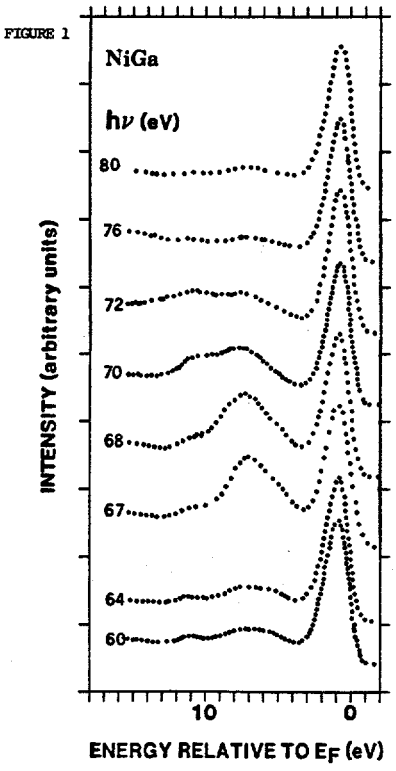

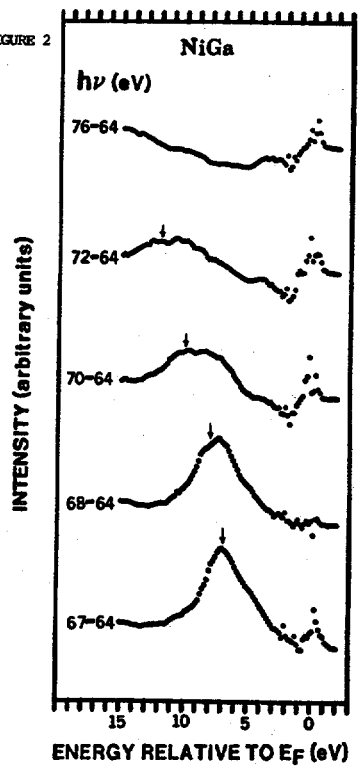

SYNCHROTRON BASED STUDIES OF X-RAY INDUCED PHOTOCONDUCTIVITY*

D. R. Kania, L. Pan,** P. Bell, P. Pianetta,** J. Trebes and H. Kornblum

Lawrence Livermore National Laboratory, University of California
P.O. Box 5508, L-473, Livermore, CA 94550

Introduction

The photoconductive properties of x-ray excited materials permit direct comparison of near and far above band gap excitation when compared to optical (laser) radiation sources. As a part of this effort, the present investigation studied carrier lifetimes in InP, GaAs, and type IIa diamond with kilovolt x-ray excitation. In addition, evidence for carrier velocity as a function of applied electric field was measured for a diamond sample.

Results and Conclusions

Bulk samples of neutron damaged GaAs,[1] iron doped InP, and natural type IIa (insulating) diamond were tested in this study. The samples were 1 x 1 x 3 mm cubes with Ohmic contacts placed on two opposite faces of the cubes. The samples were placed in high speed transmission lines to permit direct, time resolve measurements of the x-ray generated photocurrents. The samples were illuminated on a face parallel to the electric field generated by the contacts. Beam line III-4 (Lithography) was used with thin foil filters as the x-ray source. This configuration gave the necessary large peak x-ray power in the range of 1-3 keV to excite the samples. The data were recorded on a high speed sampling system with a net rise time of less than 50 ps.[2]

The carrier lifetime in the samples was measured. The neutron damaged GaAs and InP:Fe results were consistent with optical laser excitation of these samples. The speed of the GaAs samples was 60 ps, sufficiently fast to resolve the ring x-ray pulses (see Fig. 1). The InP:Fe samples showed slower carrier life-times of 400-600 ps. By varying the filtration, the photoresponse of the GaAs and diamond samples were measured to be independent of photon energy between 1 and 3 keV in agreement with theory for above band gap excitation.[3]

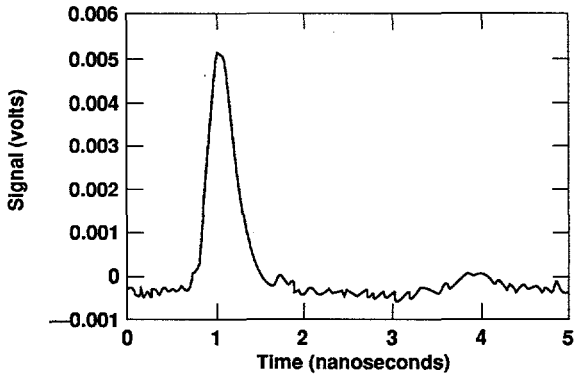

The carrier lifetimes for valence to conduction band transitions of five natural, insulating diamond samples were directly measured. The lifetimes varied from 150 to 650 ps. This is attributed to the sample to sample variations in the natural material. In addition, we were able to measure the effects of carrier velocity saturation with increasing electric-field in diamond. Figure 2 shows the bias polarity independent roll-off of the output voltage with applied electric field. At electric fields greater than 3000 V/cm, significant departures from linearity are observed.

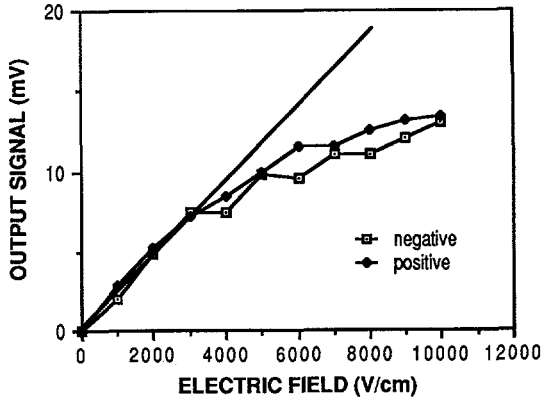

Figure 2. The output signal of a type IIa diamond crystal as a function of applied electric field. The effects of carrier velocity saturation are evident for electric fields greater than 3000 V/cm for both positive and negative bias. A linear fit to the low electric field points is included (——).

Conclusions

We have directly measured carrier lifetimes for several samples of three different materials: 1) InP:Fe, 2) GaAs (neutron damaged) and 3) type IIa, natural diamond. the diamond measurements represent the first direct measurements of carrier lifetimes for conduction to valence band transitions. In addition, the effects of carrier velocity saturation in diamond were directly measured in these experiments.

References

* Work performed under the auspices of the U.S. Department of Energy by the Lawrence Livermore National Laboratory under contract number W-7405-ENG-48.

** SSRL, P.O. Box 4349, Bin 69, Stanford, CA 94305

1) R. S. Wagner, R. M. Bradley, and R. B. Hammond, IEEE Trans. Nucl. Sci 33, 250 (1986).

2) D. R. Kania, r. J. Bartlett, and P. Pianetta, Nucl. Instr. Meth. A246, 534 (1986).

3) D. R. Kania, A. E. Iverson, D. L. Smith, R. S. Wagner, R. B. Hammond and K. A. Stetlar, Jour. Appl. Phys. 60, 2596 (1986).

RADIATION DAMAGE IN X RAY LITHOGRAPHY MASKS

Paul L. King, Lawrence Pan and Piero Pianetta
Stanford Synchrotron Radiation Lab, SLAC Bin 69, PO Box 4349, Stanford CA 94305

Alex Shimkunas and Philip Mauger
Nano Structures Inc., 1245 Pear Ave., Mountain View, CA 94043

Daniel Seligson
Intel Corporation, POB 58126, Santa Clara CA 95052-8126

The thin (2-5 um thick) pellicles used to support the absorbing pattern in an x ray lithography mask must be able to withstand large cumulative doses of soft x rays without degrading. We have studied a number of pellicles made of different materials during exposure to soft x rays in order to judge their long term behavior and acceptability in x ray lithography systems.

Boron nitride. Although hydrogenated boron nitride membranes have performed satisfactorily with conventional electron impact sources, Johnson et al. (1) raised questions about the stability of CVD boron nitride during exposure to x rays in high intensity synchrotron environments. Our boron nitride samples were deposited at 400C on <100> silicon by CVD using ammonia and diborane as source gases. Transmission is typically 50% at 633 nm for a 5 um thick window. Membranes transmit about 75% of the incident x rays. The x ray transmission spectrum has been measured using the beamline's multilayer monochromator and is in good agreement with predicted values assuming the measured density of 1.9 g/cm3 and a stoichiometry of B_4NH_1. We also looked at samples produced by chemical vapor deposition at 600C and at samples produced from the pyrolysis of diborane at 600C.

The transmission through a 400C CVD boron nitride window falls from 50% to 20% after absorbing 250 kJ/cm3 of soft x rays (1-2 KeV). This represents severe degradation as this dose would be absorbed after little more than 500 PMMA exposures. We observed that the CVD films produced at higher temperatures (600C) are much less affected by absorbed radiation; the pyrolytic BN:H seems to be completely immune in these dose ranges. These effects are correlated with the hydrogen content of the films (1, 2).

The change in optical transmission in the 400C samples is accompanied by a decrease in membrane tension . After intense exposure this can result in buckling of the membranes due to a relaxed exposed region surrounded by a taut unexposed region. We have quantified the change in stress by constructing simple cantilever beams of the film on silicon and monitoring the change in curvature at various doses. Film tension, initially around 4E8 dyne/cm2, becomes compressive after absorbing a dose near 300 kJ/cm3 i.e. less than 1000 PMMA exposures (Figure 1). Again this represents severe degradation. It is interesting to note that all damage to the 400C boron nitride samples was annealable at 350C. The growth kinetics of the damage and effect of annealing suggest that ionization induced point defects associated with hydrogen are resposible for the damage rather than hydrogen evolution.

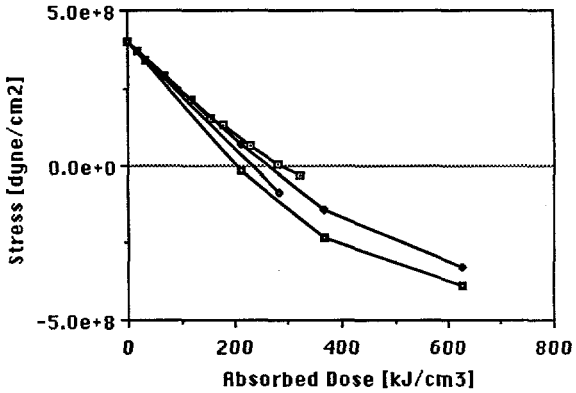

Figure 1. Change in stress in boron nitride thin films during soft x ray irradiation

Silicon nitride, silicon carbide, silicon, and diamond. Pellicles of various other materials were also studied during soft x ray exposure. Silicon nitride and silicon carbide windows produced through plasma enhanced CVD, boron doped silicon windows produced by the differential etching rates between doped and undoped silicon, and diamond windows were exposed. No macroscopic deterioration in these samples was observed.

REFERENCES

1. W.A. Johnson, R.A. Levy, D.J. Resnick, T.E. Saunders, A.W. Yanof, H.Betz, H.Huber and H. Oertel, J. Vac.Sci. Technol. B5(1), 257 (1987)
2. P.L. King, L. Pan, P. Pianetta, A. Shimkunas, P. Mauger, and D. Seligson, J. Vac.Sci. Technol. to be published (Jan/Feb 1988)

VIII ACTIVE PROPOSALS

As of December 31, 1987 there were 158 active SSRL proposals. Proposals remain active for two years after their initial rating by the Proposal Review Panel. Since October 1974 SSRL has received a total of 2048 proposals. The Spokesperson for each proposal is underlined and their institution shown in parentheses. The letter suffix appended to the proposal number indicates the sub-panel of the Proposal Review Panel to which the proposal is assigned: Materials (M), Biology (B) or Vacuum Ultra-Violet (V). The small (p) indicates a program proposal.

No.	Received	Experimenters	Title
100Mp *(PRT)*	9/7/83	DARYL CROZIER ANDREW J SEARY FARREL W LYTLE ROBERT B GREEGOR ROBERT L INGALLS P VIRAN J E WHITMORE NEIL ALBERDING K R BAUCHSPIESS *(SIMON FRASER UNIVERSITY)*	**X-ray Absorption Studies of Disordered Systems**
882Mp	3/1/84	MATI BLOCH PETER M EISENBERGER *(ARGONNE NATIONAL LABORATORY)*	**Structural Studies of Organic Thin Films on the Solid Gas and Liquid Gas Interface**
897Vp	4/3/84	GERALD M ROTHBERG MARTIN L DENBOER INGOLF LINDAU *(STEVENS INSTITUTE OF TECHNOLOGY)*	**Spin Polarized Photoelectron Studies of Magnetism in Solids (SPEXAFS)**
898Mp	5/3/84	L D GIBBS KEVIN L D'AMICO JOHN D AXE JAKOB BOHR DAVID MONCTON *(BROOKHAVEN NATIONAL LABORATORY)*	**Magnetic X-Ray Scattering from Ho**
906Bp	8/29/84	DALE E SAYERS ELIZABETH C THEIL PAULINE HARRISON E A STERN KENNETH RAYMOND *(NORTH CAROLINA STATE UNIVERSITY)*	**X-Ray Absorption Studies of the Protein-Iron Interaction in Ferritin**
908Vp	8/31/84	ROSS D BRINGANS ROBERT Z BACHRACH ROGER I G UHRBERG J E NORTHRUP *(XEROX)*	**Influence of Surface Reconstruction on Electronic Properties of Semiconductor Surfaces**

910Mp	8/31/84	CHARLES E BOULDIN M I BELL R A FORMAN *(NATIONAL BUREAU OF STANDARDS)*	**Structural Studies of Ion Implants in III-V Semiconductors with Reflectance EXAFS**
922Bp	9/6/84	RICHARD C ELDER KATHERINE TEPPERMAN *(UNIVERSITY OF CINCINNATI)*	**Gold-Based Antiarthritis and Anticancer Drugs and Metabolites: XAS, WAXS, DAS**
928Mp	9/11/84	PETER M EISENBERGER KENG S LIANG *(EXXON RESEARCH & ENGINEERING)*	**Grazing-Incidence X-ray Scattering Program**
935Vp	9/20/84	INGOLF LINDAU TOMAS F KENDELEWICZ WILLIAM E SPICER JOEL SILBERMAN M D WILLIAMS JOE WOICIK C BOWMAN J J YEH S J EGLASH K K CHIN K SHIH S LIST C MCCANTS KRISTINE BERTNESS T CHIANG CARLO R CARBONE PETER MAHOWALD DANIEL FRIEDMAN JUN NOGAMI N NEWMAN EZIO PUPPIN *(SSRL)*	**Electronic Structure, Chemistry, and the Fermi Level at Semiconductor Surfaces and Interfaces**
941Vp	9/26/84	LUCIO BRAICOVICH O BISI IVANO ABBATI STEFANO NANNARONE CARLO CALANDRA Z SHEN EZIO PUPPIN MASSIMO SANCROTTI UMBERTO DEL PENNINO WILLIAM E SPICER INGOLF LINDAU *(POLITECNICO DI MILANO)*	**Study of the Formation of Rare Earth/ Elemental Semiconductor (Ge, Si) Interfaces and Compounds**

943Vp	9/6/84	DAVID A SHIRLEY DENNIS W LINDLE TRICIA FERRETT ALLEN L JOHNSON JOHN J BARTON ERNESTO PAPARAZZO BAOHUA NIU TONG LEUNG SEHUN KIM ALEXIS SCHACH V WITTENAU ZHENG-QING HUANG SHIHONG LIU STEVEN W ROBEY PHILIP A HEIMANN LAISHING WANG LOUIS J TERMINELLO MARIA NOVELLA PIANCASTELLI XUN-SHENG ZHANG LAURA MEDHURST CHARLES C BAHR *(LAWRENCE BERKELEY LABORATORY)*	**Electron Spectroscopy of Gases, Solids, and Surfaces**
947V	10/15/84	PAUL H CITRIN FABIO COMIN *(AT&T BELL LABORATORIES)*	**Proposal to Perform SEXAFS from Substrate Surfaces**
956Mp	2/27/85	G P HUFFMAN ROBERT B GREEGOR FARREL W LYTLE F E HUGGINS NARESH SHAH R G JENKINS *(UNIVERSITY OF KENTUCKY)*	**Applications of EXAFS Spectroscopy in the Steel and Coal Industries**
957Bp	2/28/85	DAVID H TEMPLETON L K TEMPLETON *(LAWRENCE BERKELEY LABORATORY)*	**Anomalous Scattering of X-rays**
959Vp	3/1/85	ROBERT Z BACHRACH ROSS D BRINGANS *(XEROX)*	**Core Level and Near Edge Structure Study of Interface Formation**
963Vp	3/6/85	JOACHIM STOHR *(IBM RESEARCH LABORATORY)*	**NEXAFS and SEXAFS Studies by Means of X-ray Fluorescence Detection: Local Structure Around Low-Z Atoms**
969Bp	3/14/85	ROBERT A SCOTT STEPHEN P CRAMER *(UNIVERSITY OF GEORGIA)*	**X-ray Absorption Spectroscopic Studies of Nickel-Containing Metalloenzymes**

973M	4/12/85	CHARLES E BOULDIN M I BELL R A FORMAN G K HUBLER E D DONOVAN *(NATIONAL BUREAU OF STANDARDS)*	**EXAFS Study of Damage and Annealing of Ion Implanted Semiconductors**
981Bp	9/3/85	JAMES O ALBEN STEPHEN P CRAMER ALLAN A CROTEAU CRAIG F HEMANN KIMBERLY A POWELL FRANK G FIAMINGO *(OHIO STATE UNIVERSITY)*	**High Resolution EXAFS Spectroscopy of Iron and Copper Proteins**
991Bp	9/4/85	RICHARD C ELDER EDWARD A DEUTSCH *(UNIVERSITY OF CINCINNATI)*	**Technetium and Rhenium Imaging Agents and Therapeutic Radiopharmaceuticals**
994Mp	9/5/85	GLENN A WAYCHUNAS GORDON E BROWN, JR *(STANFORD UNIVERSITY)*	**High Temperature EXAFS Study of Fe and Ca in Silicate Crystals and Melts**
995Mp	9/6/85	GORDON E BROWN, JR KEITH O HODGSON GEORGE A PARKS GLENN A WAYCHUNAS JAMES O LECKIE KIM F HAYES *(STANFORD UNIVERSITY)*	**XAS Study of Cation Adsorption at Aqueous/Oxide Interface**
997Mp	9/10/85	I K ROBINSON P J ESTRUP M ALTMAN ROBERT J BIRGENEAU *(AT&T BELL LABORATORIES)*	**The Surface Phase Transition of Clean W(100)**
998M	9/10/85	K K CHAN KENG S LIANG G J HUGHES PETER M EISENBERGER *(Brookhaven National Laboratory)*	**Order-Disorder Transition of Adsorbates on Nickel**
999Mp	9/10/85	GORDON E BROWN, JR W A JACKSON C W PONADER GLENN A WAYCHUNAS S ROTHFUS *(STANFORD UNIVERSITY)*	**EXAFS Study of Trace Element Environments in Quenched Silicate Melts of Geochemical Interest**

1001Mp *(PRT)*	1/1/86	PETER M EISENBERGER S K SINHA C R SAFINYA KENG S LIANG GRAYSON H VIA JOHN H SINFELT J M NEWSAM DAVID MONCTON *(EXXON RESEARCH & ENGINEERING)*	**EXXON PRT Proposal - Beam Line VI**
1008Mp	10/4/85	WILLIAM K WARBURTON KARL F LUDWIG ARTHUR BIENENSTOCK *(ARACOR)*	**Binary Liquid Structures Determined by Anomalous X-ray Scattering**
1010M	10/14/85	C R SAFINYA BILL VARADY N A CLARK *(EXXON RESEARCH & ENGINEERING)*	**Synchrotron Studies of Freely Suspended Discotic and Ordered Microemulsion Strands**
1012Bp	11/4/85	ROBERT H FAIRCLOUGH STEVEN R HUBBARD KEITH O HODGSON SEBASTIAN DONIACH D RICHMAN *(UNIVERSITY OF CHICAGO)*	**Membrane X-Ray Diffraction Studies of the Acetylcholine Receptor**
1013Vp	11/18/85	FRANCESCO SETTE J E ROWE JOHN M POATE *(AT&T BELL LABORATORIES)*	**NEXAFS and EXAFS Studies of Shallow Inpurities in Semiconductors by Soft X-ray Fluorescence**
1015Vp	2/28/86	JOHN L GLAND DANIEL A FISCHER FRANCISCO ZAERA *(EXXON RESEARCH & ENGINEERING)*	**The Structure and Reactivity of Adsorbed Intermediates Using NEXAFS and SEXAFS**
1017M	3/3/86	JAMES B BOYCE J C MIKKELSON FRANK G BRIDGES *(XEROX)*	**Local Structure of Icosahedral Materials**
1018Mp	3/3/86	D DE FONTAINE B E C DAVIS JEFF J HOYT B CLARK M KRAITCHMAN *(UNIVERSITY OF CALIFORNIA)*	**Diffusion in Ternary Multilayer Thin Films**

1019B	3/3/86	F SCOTT MATHEWS LOUIS LIM R PAUL PHIZACKERLEY ETHAN A MERRITT *(WASHINGTON UNIVERSITY)*	**Crystallographic Study of Amicyanin by Anomalous Scattering Using Synchrotron Radiation**
1021Mp	3/3/86	WILLIAM PARRISH TING C HUANG GEORGE WILL MAURIZIO BELLOTTO CURT ERICKSON MICHAEL HART *(IBM RESEARCH LABORATORY)*	**Synchrotron X-ray Polycrystalline Diffractometry**
1022Vp	3/3/86	EDWARD I SOLOMON STEVE V DIDZIULIS JIAN-YI LIN KRISTINE BUTCHER *(STANFORD UNIVERSITY)*	**UPS Studies of the Coordination Chemistry of Metal Oxides, Chlorides and Sulfides**
1025M	3/4/86	S C WEAVER ANTHONY D COX M CHEN LEI P ZIA J V ACRIVOS *(CALIFORNIA STATE UNIVERSITY)*	**Structure of Multiple Valence Compounds such as Prussian Blue vs Temperature**
1026M	3/4/86	DONALD R SANDSTROM FARREL W LYTLE (BOEING COMPANY)	**Transition Metal Ion Complexes in the Gas Phase**
1027Bp	3/5/86	STEVE D CONRADSON WILLIAM WOODRUFF BASIL SWANSON *(LOS ALAMOS NATIONAL LABORATORY)*	**Dispersive XAS Development: Time Resolved and Diamond Anvil Applications**
1028Vp	3/5/86	JIM ALLEN INGOLF LINDAU *(UNIVERSITY OF MICHIGAN)*	**High-Photon Flux Photoemission Studies of Narrow Band Materials**
1029B	3/5/86	MICHAEL SEUL SRIRAM SUBRAMANIAM *(AT&T BELL LABORATORIES)*	**X-ray Diffraction by Molecular Films on Solid Substrates in Aqueous Environment**
1030Bp	3/17/86	STEPHEN P CRAMER B E SMITH M WW ADAMS E I STEIFEL V MINAK L S SOLMONSON J ENEMARK W CLELAND GRAHAM N GEORGE *(SCHLUMBERGER DOLL RESEARCH)*	**Soft X-ray Spectrocopy of Molybdenum Enzymes, Cofactors and Model Compounds**

1031M	3/18/86	JAMES E PENNER-HAHN M DAVID CURTIS OSWALDO BARALT LEVI THOMPSON *(UNIVERSITY OF MICHIGAN)*	**XAS of Synthetic Models for Hydrodesulfurization Catalysts**
1032M	3/19/86	CHARLES E BOULDIN P BOOLCHAND *(NATIONAL BUREAU OF STANDARDS)*	**EXAFS Study of Local Chemical Coordination of Cation and Anion Sites in Chalcogenide Glass**
1033M	3/19/86	JAMES E PENNER-HAHN ROBERT MK CARLSON GEOFFREY WALDO *(UNIVERSITY OF MICHIGAN)*	**XAS Determination of the Chemical Forms of Sulfur in Petroleums**
1034Mp	3/4/86	PETER S PERSHAN ERIC SIROTA SUZANNE AMADOR L B SORENSEN *(HARVARD UNIVERSITY)*	**Structure and Phase Transitions of Hexatic Phases in Thin Liquid Crystal Films**
1035B	4/14/86	JAMES E PENNER-HAHN DAVID P BALLOU CHRISTOPHER J BATIE HIM-TAI TSANG JAMES A FEE *(UNIVERSITY OF MICHIGAN)*	**XAS Investigations of Rieske-Like Iron Sulfur Centers**
1036M	4/14/86	BERND CRASEMANN GEORGE S BROWN G BRADLEY ARMEN W JITSCHIN S L SORENSEN U WERNER S B WHITFIELD ROGER CARR *(UNIVERSITY OF OREGON)*	**Coster-Kronig Transition Probabilities**
1037M	5/19/86	TIMOTHY M HAYES D L WILLIAMSON G KRAUSS *(COLORADO SCHOOL OF MINES)*	**Grain Boundary Segregation of Impurities in Iron and Steel**
1038M	5/19/86	TIMOTHY M HAYES D L WILLIAMSON P GIBART *(COLORADO SCHOOL OF MINES)*	**Deep Donors in Gallium Aluminum Arsenide Semiconductor Alloys**

1039B	6/3/86	STEPHEN P CRAMER TERRENCE G FREY ROGER C PRINCE GRAHAM N GEORGE ROBERT A SCOTT *(SCHLUMBERGER DOLL RESEARCH)*	**Polarized XANES and EXAFS of Cytochrome Oxidase in Hydrated, Oriented Mitochondrial Multilayers**
1040B	6/3/86	RUSSELL HILLE STEPHEN P CRAMER *(OHIO STATE UNIVERSITY)*	**X-Ray Absorption Spectroscopy of Xanthine Oxidase**
1041B	9/3/86	ROBERT A SCOTT MARLY EIDSNESS *(UNIVERSITY OF GEORGIA)*	**Measurement of Metal-Metal Distances in Proteins by X-ray Anomalous Scattering**
1042B	9/3/86	BRITTON CHANCE BARTON HOLMQUIST DAVID AULD MARK CHANCE JAMES RIORDAN LINDA S POWERS B VALLEE *(UNIVERSITY CITY SCIENCE CENTER)*	**Studies of Intermediates in the Mechanism of Carboxypeptidase-A**
1043B	9/3/86	BRITTON CHANCE GRANT BUNKER PETER REICHARD S M KHALID BRITT-MARIE SJOBERG ALI NAQUI GUANG ZHANG *(UNIVERSITY CITY SCIENCE CENTER)*	**X-Ray Absorption Spectroscopy of Iron-Iron Interactions: Ribonucleotide Reductase**
1044M	9/3/86	MATTHEW A MARCUS CHING-LONG TSAI J BEVK *(AT&T BELL LABORATORIES)*	**Structural Effects of Ultrahigh Strains and Dislocation Densities**
1045M	9/3/86	MATTHEW A MARCUS CHING-LONG TSAI *(AT&T BELL LABORATORIES)*	**Multiple and Unusual Siting in Dilute Solid Solutions**

1046B	9/3/86	EDWARD RUBENSTEIN W THOMLINSON ALBERT C THOMPSON GEORGE S BROWN ROBERT HOFSTADTER DONALD C HARRISON JOHN OTIS ROBERT KERNOFF HELEN GORDON JOHN GIACOMINI HERBERT D ZEMAN *(STANFORD UNIVERSITY)*	**Iodine Dichromography with Monochromatic X-ray Beams for Angiography**
1047M	9/3/86	ROBERT L INGALLS J FREUD DARYL CROZIER *(UNIVERSITY OF WASHINGTON)*	**High Pressure Transition Mechanisms via EXAFS**
1048Mp	9/11/86	CAROLINE KILBOURNE SEAN BRENNAN ARTHUR BIENENSTOCK *(STANFORD UNIVERSITY)*	**High Resolution Compton Profiles of Iron and Silicon**
1049Mp	9/11/86	ROBERT B GREEGOR R C EWING FARREL W LYTLE B C CHAKOUMAKOS *(BOEING COMPANY)*	**X-ray Spectroscopic Investigation of Radiation Damaged Materials**
1050Mp	9/11/86	GLENN A WAYCHUNAS GREG J EXARHOS JAMES E PENNER-HAHN MICHAEL J APTED *(STANFORD UNIVERSITY)*	**X-ray Anomalous Scattering and EXAFS Study of Heavy Metal Complexes in Aqueous Solutions**
1051M	9/11/86	GLENN A WAYCHUNAS LAWRENCE R BERNSTEIN *(STANFORD UNIVERSITY)*	**Crystal and Aqueous Chemistry of Germanium in Geochemically Important Systems**
1052M	9/11/86	IVAN SELLIN C S O S B ELSTON D A CHURCH J LEVIN H CEDERQUIST *(OAK RIDGE NATIONAL LABORATORY)*	**Measurement of Recoil Energies of Multiply Charged Recoil Ions and Molecular Fragments**

1053B	9/15/86	ROBERT A SCOTT DAVID M DOOLEY *(UNIVERSITY OF GEORGIA)*	**Copper EXAFS Spectroscopy of Non-Blue Copper Proteins. Amine Oxidases**
1054M	9/15/86	RICHARD W RYON HARRY E MARTZ SUZANNE FLETCHER ROBERT A DAY JOHN H KINNEY *(LAWRENCE LIVERMORE NATIONAL LABORATORY)*	**X-Ray Induced Photoacoustic Emission**
1055B	9/15/86	KEITH O HODGSON STEPHEN F GHELLER FRANK A SCHULTZ BRITT HEDMAN A LAWRENCE ROE W E NEWTON *(SSRL)*	**XAS of Iron-Molybdenum Cofactor of Nitrogenase under Electrochemical Control**
1056Mp	9/16/86	S R STOCK B COULMAN Y H CHUNG ZOPHIA U REK *(GEORGIA INSTITUTE OF TECHNOLOGY)*	**Section Topographic Strain Mapping Using Synchrotron White Radiation**
1058M	9/16/86	PAUL M HORN GLENN HELD *(IBM RESEARCH LABORATORY)*	**Roughening Transition of Metal Surfaces**
1059M	9/16/86	MURLI H MANGHNANI L C MING *(UNIVERSITY OF HAWAII)*	**In Situ High P-T Equation-of-State, Phase Transformations and Kinetics Studies on Mantle Mineral Phases using Synchrotron Radiation**
1060Mp	9/16/86	MARYBETH RICE ARTHUR BIENENSTOCK *(STANFORD UNIVERSITY)*	**Structural Investigations of Layered Synthetic Microstructures and Binary Amorphous Alloys**
1061Bp	9/16/86	JAMES O ALBEN ALLAN A CROTEAU CRAIG F HEMANN KIMBERLY A POWELL FRANK G FIAMINGO *(OHIO STATE UNIVERSITY)*	**Iron Porphyrin Models for EXAFS Analysis**
1062Vp	10/1/86	DONALD C LORENTS R L SHARPLESS *(SRI INTERNATIONAL)*	**Spectroscopy and Kinetics of Excited Gases**

1064M	3/1/87	J AKELLA H K MAO L C MING MURLI H MANGHNANI G S SMITH QUINTIN C JOHNSON *(LAWRENCE LIVERMORE NATIONAL LABORATORY)*	**Static High Pressure and High Temperature X-Ray Diffraction Studies of Some Rare-Earth Elements Using Diamond-Anvil Apparatus**
1065Mp	3/1/87	MICHEL BOUDART R J DAVIS *(STANFORD UNIVERSITY)*	**Characterization of Supported Pd/Au Alloys by X-Ray Absorption Spectroscopy**
1066Mp	3/1/87	RICHARD C ELDER WILLIAM R HEINEMAN *(UNIVERSITY OF CINCINNATI)*	**X-Ray Spectroscopy of Electrochemically Generated Species**
1067Bp	3/1/87	ROBERT A SCOTT SUNNEY I CHAN P MARK LI *(UNIVERSITY OF GEORGIA)*	**Active Site Structures of Cytochrome c Oxidase**
1068Bp	3/1/87	R H FELTON E A STERN *(GEORGIA INSTITUTE OF TECHNOLOGY)*	**Structure of Transients in the Catalytic Cycle of Dioxygenases**
1069M	3/1/87	NOLAN MANGELSON MAX W HILL FARREL W LYTLE *(BRIGHAM YOUNG UNIVERSITY)*	**Characterization of Vanadium, Chromium, Nickel and Arsenic in Particulate Matter**
1070M	3/1/87	THOMAS BEIN KARIN MOLLER *(UNIVERSITY OF NEW MEXICO)*	**Anchoring Chemistry of Transition Metal Complexes and Clusters to Intrazeolite Surfaces**
1071M	3/1/87	MICHEL BOUDART G P VALENCA *(STANFORD UNIVERSITY)*	**Characterization of Clusters of Pt/Y-Zeolite and rh/ -A1 0 by X-Ray Absorption Spectroscopy**
1072M	3/1/87	STEVE M HEALD HEATHER CHEN *(BROOKHAVEN NATIONAL LABORATORY)*	**Glancing Angle EXAFS and Reflectivity of Aluminum-Metal Interfaces**
1073M	3/1/87	STEVE M HEALD J M TRANQUADA M SUENAGA *(BROOKHAVEN NATIONAL LABORATORY)*	**X-Ray Absorption Study of La CuO Based Superconductors**

1074M	3/1/87	STEVE M HEALD DALE E SAYERS JIM VICCARO ERIC ZIEGLER *(BROOKHAVEN NATIONAL LABORATORY)*	**X-Ray Absorption and Reflectivity Studies of Interfaces in Multilayer Optics**
1076B	3/1/87	SEBASTIAN DONIACH S WAKATSUKI ROBERT M STROUD KEITH O HODGSON *(STANFORD UNIVERSITY)*	**Study of Conformational Changes in Bacteriorhodopsin using Time-Resolved Small Angle X-Ray Diffraction**
1077M	3/1/87	KRISHNA M CHOUDHARY *(UNIVERSITY OF NOTRE DAME)*	**Photoemission EXAFS Studies of Surfaces and Interfaces in Compound Semiconductors**
1078M	3/1/87	N S LEWIS KEITH O HODGSON BRUCE J TUFTS *(STANFORD UNIVERSITY)*	**X-Ray Absorption Studies of Metal Ion Absorption at Semiconductor Surfaces**
1079M	3/1/87	JAMES B BOYCE T CLAESON THEODORE H GEBALLE FRANK G BRIDGES *(XEROX)*	**Local Atomic Structure of High-T_c Superconductors**
1080Vp	3/1/87	ROBERT J MADIX C M FRIEND J T ROBERTS B FACTOR A C LIU J SOLOMON PAUL STEVENS *(STANFORD UNIVERSITY)*	**Adsorption Structure of Heteroatom-Containing Molecules on Transition Metal Surfaces**
1081M	3/1/87	DAVID P POPE JOHN E BENCI *(UNIVERSITY OF PENNSYLVANIA)*	**A Study of Creep Damage Using Microradiography**
1082B	3/1/87	DAVID A LARSON TERESA TROXEL MICHAEL SCHELL CLIFF LING THEODORE L PHILLIPS DENNIS SHRIEVE *(UNIVERSITY OF CALIFORNIA)*	**Contribution of Auger Electrons to Radiation Sensitization with IUdR**

1083B	3/1/87	M IKEDA-SAITO ROGER C PRINCE GRAHAM N GEORGE *(UNIVERSITY OF PENNSYLVANIA)*	**X-Ray Absorption Spectroscopy of Myeloperoxidase and Lactoperoxidase**
1084Bp	3/1/87	GRAHAM N GEORGE STEPHEN P CRAMER ROGER C PRINCE *(EXXON RESEARCH & ENGINEERING)*	**Polarized X-Ray Spectroscopy of the Oriented Choiroplast Water-Oxidizing Complex**
1085Bp	3/1/87	JAMES E PENNER-HAHN HIM-TAI TSANG V L PECORARO W D FRASCH R FRANKO C F YOCUM M STERN J T GROVES D GHANOTAKIS *(UNIVERSITY OF MICHIGAN)*	**X-Ray Absorption Spectroscopic Characterization of the Manganese in Biological Systems**
1086V	3/1/87	RICHARD D DESLATTES PAUL L COWAN SEAN BRENNAN DENNIS W LINDLE *(NATIONAL BUREAU OF STANDARDS)*	**Polarization in Molecular X-Ray Flourescence**
1087Bp	3/1/87	WAYNE A HENDRICKSON R PAUL PHIZACKERLEY ETHAN A MERRITT STEVEN R HUBBARD JOHN HORTON WEI YANG WILIAM E ROYER ARNO PAHLER MARIANNE CUFF HM KRISHNA MURTHY CRAIG OGATA *(COLUMBIA UNIVERSITY)*	**Anomalous-scattering Studies of Protein Crystal Structures**
1088M	3/1/87	JAMES E PENNER-HAHN GEOFFREY WALDO SHENGKE WANG RICHARD FRONKO GLENN A WAYCHUNAS *(UNIVERSITY OF MICHIGAN)*	**Polarized X-Ray Absorption Near Edge Structure**
1089M	3/1/87	JAMES HOWARD WILLIAM MURPHY JULIA PECK STEPHEN P CRAMER GRAHAM N GEORGE *(SCHLUMBERGER DOLL RESEARCH)*	**X-Ray Absorption of Iridium in K-T Boundary Samples and Meteorites**

1090MP	6/9/87	T E FURTAK TIMOTHY M HAYES *(COLORADO SCHOOL OF MINES)*	**Electrolyte-Metal Interfaces**
1091Mp	6/9/87	D L WILLIAMSON TIMOTHY M HAYES F M KUSTAS *(COLORADO SCHOOL OF MINES)*	**Characterization of Ion-Implanted Aluminum and Titanium**
1092M	6/19/87	JAMES HOWARD N WADA S WHITTINGHAM D. R. HINES STEPHEN P CRAMER *(SCHLUMBERGER DOLL RESEARCH)*	**Structural Investigation of Interlayer Potassium and Sodium in Phyllosilicates**
1093Mp	8/7/87	R S HOWLAND K CHAR J MOLL B OH N MISSERT J Z SUN A D KENT ALICE FISCHER-COLBRIE THEODORE H GEBALLE STEPHEN LADERMAN *(STANFORD UNIVERSITY)*	**Structure of Superconducting Thin Films**
1094M	8/20/87	JAKOB BOHR I K ROBINSON E JOHNSON L SARHOLT-KRIST L F GRAABAEK H H ANDERSEN A JOHANSEN *(BROOKHAVEN NATIONAL LABORATORY)*	**X-Rays Studies of Rare Gas Inclusions in Single Crystal Aluminium**
1095Mp	8/7/87	PAUL H FUOSS LAURA NORTON D W KISKER *(AT&T BELL LABORATORIES)*	**EXAFS and NEXAFS Investigation of OMPVE Growth of II-VI Compounds**
1096Mp	8/20/87	PAUL H FUOSS D W KISKER LAURA NORTON *(AT&T BELL LABORATORIES)*	**In-Situ X-Ray Scattering Studies of OMVPE Growth of II-VI Compounds**
1097Mp	8/20/87	FARREL W LYTLE ROBERT B GREEGOR *(BOEING COMPANY)*	**Anti-Site Disorder in High T_c Superconductors**

1098M	9/1/87	DANIEL A SCHERSON PHILIP N. ROSS *(CASE WESTERN RESERVE UNIVERSITY)*	**In-Situ EXAFS Transition Metal Macrocycles Absorbed on Electrode Surfaces**
1099M	9/15/87	J V ACRIVOS M CHEN LEI S S P PARKIN R ITHNIN D HELMOLDT J SATCHER S ARNOLD C BUSTILLO *(CALIFORNIA STATE UNIVERSITY)*	**Study of Organic Metals**
2000M	9/15/87	J V ACRIVOS MELVIN P KLEIN S S P PARKIN M CHEN LEI R ITHNIN S ARNOLD J SATCHER D HELMOLDT C BUSTILLO *(CALIFORNIA STATE UNIVERSITY)*	**Study of Cation, Anion X-Ray Edges in S Intercalated Perovskites** $[Y_1Ba_2Cu_3(O/S)_{7+\delta}]$ **n**
2001M	9/15/87	JEFFREY R LINCE PAUL D FLEISCHAUER *(THE AEROSPACE CORPORATION)*	**Extended X-Ray Absorption Fine Structure of Transition Metal Dischalcogenide Materials**
2002Mp	9/15/87	J D BROCK J D LITSTER ROBERT J BIRGENEAU *(MIT)*	**Bond Orientational Order in Tilted Hexatic Liquid Crystal Films**
2003M	9/15/87	MIKE TONEY W H SMYRL OWEN MELROY *(IBM RESEARCH LABORATORY)*	**In-Situ X-Ray Scattering Study of the Structure of Passive Oxides on Single Crystal Ti**
2004M	9/15/87	STEPHEN E DERENZO JAN LITTON WILLIAM W MOSES *(LAWRENCE BERKELEY LABORATORY)*	**Search for Ultra-Fast Heavy Atom Scintillators**
2005M	9/15/87	ROBERT L INGALLS DARYL CROZIER B HOUSER E A STERN J M TRANQUADA *(UNIVERSITY OF WASHINGTON)*	**X-Ray Absorption Studies of Perovskites as a Function of Pressure**

2006Mp	9/15/87	D DE FONTAINE JEFF J HOYT M KRAITCHMAN S SPOONER M WIEDENMEIR *(UNIVERSITY OF CALIFORNIA)*	**Kinetics of Phase Separation in Al-Li**
2007B	9/15/87	JAMES PHILLIPS *(BROOKHAVEN NATIONAL LABORATORY)*	**Protein Folding Studied by Synchrotron X-Ray Scattering**
2008B	9/15/87	DOUGLAS S CLARK GREGG A MARG R MARK GUINN *(UNIVERSITY OF CALIFORNIA)*	**EXAFS of Active-Site Metals in Glucose Isomerase and Methane Monooxygenase**
2009Vp	9/17/87	JOACHIM STOHR THOMAS P RUSSELL W JARK *(IBM RESEARCH LABORATORY)*	**Structural Studies of Thin Polymer Films on Surfaces**
2010Bp	9/17/87	MELVIN P KLEIN R GUILES ANN MCDERMOTT SUSAN DEXHEIMER J L ZIMMERMANN VITTAL K YACHANDRA VICKIE DEROSE KENNETH SAUER *(LAWRENCE BERKELEY LABORATORY)*	**X-Ray Spectroscopy of Manganese and Iron in Chloroplasts**
2011V	9/17/87	DON KANIA PIERO PIANETTA J TREBES (LAWRENCE LIVERMORE NATIONAL LABORATORY)	**Synchrotron Based Studies of X-Ray Induced Photoconductivity**
2012M	9/17/87	E E ALP L SODERHOLM GOPAL K SHENOY PEDRO A MONTANO (ARGONNE NATIONAL LABORATORY)	**Electronic Structure of High T_c Oxide Superconductors by X-Ray Absorption Spectroscopy**
2013M	9/17/87	DAVE WARK HAMISH ROBERTSON DAVE KNAPP WALTER J. TRELA RICH MARTIN TOM BOWLES JOHN WILKERSON JOHN HENDERSON BERND CRASEMANN GEORGE S BROWN ROGER J BARTLETT S B WHITFIELD S L SORENSEN *(LOS ALAMOS NATIONAL LABORATORY)*	**Photoelectron Spectrometry of Correlation Satellites in KR**

2014M 9/17/87 ROBERT M SUTER
J D SHINDLER
R F HAINSEY
(CARNEGIE MELLON UNIVERSITY)
Melting of Xe/TiS_2: Structure and Thermodynamics

2015Mp 9/17/87 S R STOCK
G WEBB
S D ANTOLOVICH
ZOPHIA U REK
(GEORGIA INSTITUTE OF TECHNOLOGY)
In-Situ Synchrotron Microradiography of Delamination in Graphite/Epoxy Composites

2016M 9/17/87 GEORGE KWEI
ANDREW C LAWSON
ROBERT B VON DREELE
JOYCE A GOLDSTONE
ART WILLIAMS
(LOS ALAMOS NATIONAL LABORATORY)
Anomalous X-Ray Powder Diffraction Studies of the Structure of Materials

2017Mp 9/17/87 BENJAMIN OCKO
DAVID M ZEHNER
S G J MOCHRIE
L D GIBBS
(BROOKHAVEN NATIONAL LABORATORY)
Structure and Stability of Metal Surfaces: A Proposal for X-Ray Scattering Experiments

2018M 9/21/87 JEFFREY B KORTRIGHT
ROSS D BRINGANS
JONATHAN DENLINGER
MARJORIE OLMSTEAD
(LAWRENCE BERKELEY LABORATORY)
Structural Study of Hetero-Epitaxial CaF_2 on Si(111) Using Standing Wave Fluorescence

2019V 9/21/87 MARJORIE OLMSTEAD
JONATHAN DENLINGER
ROSS D BRINGANS
(UNIVERSITY OF CALIFORNIA)
Heteroepitaxial Interface Formation Between Insulators and Semiconductors

2020Mp 9/21/87 S H LIN
T GROY
J R SCHOONOVER
(ARIZONA STATE UNIVERSITY)
X-Ray Diffraction of Solid State Reactions and Phase Transitions

2021M 9/21/87 NOLAN MANGELSON
MAX W HILL
ROBERT B GREEGOR
FARREL W LYTLE
(BRIGHAM YOUNG UNIVERSITY)
Structures of Silver(I)-Crown Complexes in Liquid and Solid Phases

2022B 9/21/87 BRITTON CHANCE
HIROYUKI OYANAGI
GRANT BUNKER
KE ZHANG
S G SLIGAR
(UNIVERSITY CITY SCIENCE CENTER)
Structural Features of Low Temperature Recombination of Hemoproteins, Carbon Monoxide and Oxygen

2023Mp	9/21/87	STEVE D CONRADSON IAN D RAISTRICK ZACHARY FISK ANTONIO REDONDO *(LOS ALAMOS NATIONAL LABORATORY)*	**High T_c Superconducting Materials: Their Structural and Electronic Characterization by XAS**
2024Mp	9/21/87	STEVE D CONRADSON BASIL SWANSON ALFRED SATTLEBERGER *(LOS ALAMOS NATIONAL LABORATORY)*	**XAS Studies of Quasi-One-Dimensional Halide-Bridged Mixed Valence Platinum Compounds**
2025B	9/21/87	BRITTON CHANCE GRANT BUNKER TSOO E. KING KE ZHANG ROBERT POYTON EDGAR DAVIDSON *(UNIVERSITY CITY SCIENCE CENTER)*	**Altered Structures of Cytochrome Oxidase**
2026Mp	9/21/87	PIERO PIANETTA JENNCHANG HWANG GLENN KUBIAK JEFF NELSON RICHARD H STULEN *(SSRL)*	**The Bonding Behaviour in Strained Semiconductor Heterostructures**
2027M	9/22/87	SEAN BRENNAN ARTHUR I BIENENSTOCK ROLAND TIMSIT B FACTOR *(SSRL)*	**Structural Studies of Co-Sputtered Amorphous AlTa Thin Films**
2028M	9/29/87	HOWARD OCKEN ZOPHIA U REK FARREL W LYTLE *(EPRI)*	**Characterization of Cobalt-Bearing Passive Oxides on Stainless Steel by EXAFS**
2029Bp	9/29/87	KEITH O HODGSON BRITT HEDMAN BARBARA K BURGESS STEVEN A VAUGHN *(SSRL)*	**Mo and Se XAS Studies of Small-Molecule Binding to Nitrogenase**
2030Bp	9/29/87	KEITH O HODGSON STEPHEN J LIPPARD BRITT HEDMAN ROBERT H BEER JAMES G BENTSEN *(SSRL)*	**XAS Structural Characterization of the Binuclear Iron-Center in Methane Monooxygenase**

2031Bp	9/29/87	KEITH O HODGSON LUNG-SHAN KAU BRITT HEDMAN GRACE TAN EDWARD I SOLOMON *(SSRL)*	**X-Ray Absorption Studies of Coupled Binuclear Copper Sites in Proteins**
2032Bp	9/29/87	KEITH O HODGSON BRITT HEDMAN MASANORI SONO JOHN H DAWSON *(SSRL)*	**XAS Studies of Heme-Iron Enzymes: Cytochrome P-450 and Peroxidases**
2033Mp	9/29/87	TERESA A SMITH BRITT HEDMAN KEITH O HODGSON *(EASTMAN KODAK RESEARCH LABORATORY)*	**Sulfur K Edge XAS Studies of Photographic Sensitizing Centers**
2034M	9/29/87	KEITH O HODGSON BRITT HEDMAN MATTHEW B ZISK HITOSHI ASAHINA JAMES P COLLMAN *(SSRL)*	**XAS Studies of Liquid Crystalline Ruthenium Phthalocyanines and Porphyrins**
2035B	9/29/87	SEBASTIAN DONIACH S WAKATSUKI ROBERT M STROUD U W SPANN KEITH O HODGSON *(STANFORD UNIVERSITY)*	**X-Ray Diffraction Studies of Helix Linking Regions of Bacteriorhodopsin**
2036M	9/29/87	R S HOWLAND D B MITZI J MOLL THEODORE H GEBALLE STEPHEN LADERMAN MARTIN P SCOTT ALICE FISCHER-COLBRIE AHARON KAPITULNIK *(STANFORD UNIVERSITY)*	**Structural Study of** $Ln_{3-x}Ba_{3+x}Cu_6O_{14+\sigma}$
2037Vp	9/29/87	PIERO PIANETTA DANIEL SELIGSON PAUL KING LAWRENCE PAN *(SSRL)*	**X-Ray Lithography Process Development**
2038M	10/1/87	P G ELLER E M LARSON FARREL W LYTLE J D PURSON ROBERT B GREEGOR *(LOS ALAMOS NATIONAL LABORATORY)*	**EXAFS Study of Actinide and Fission Product Speciation in Nuclear Waste Storage Media**

2039Vp	10/1/87	JON ERICKSON SANDY LANGSJOEN TSU-WIE NEE CAREY SCHWARTZ WAYNE WIEMER PHILLIP LAROE VICTOR REHN AROLD K GREEN *(NAVAL WEAPONS CENTER)*	**Superconductor-Semiconductor Heterostructure Research**
2040M	10/4/87	FRANK G BRIDGES JAMES B BOYCE *(UNIVERSITY OF CALIFORNIA)*	**EXAFS Study of Off-Center Behavior and Aggregation in Dilute Immissible Systems**
2041B	10/4/87	JOHN P LANGMORE SHAWN WILLIAMS BRIAN D ATHEY MICHAEL F SMITH *(UNIVERSITY OF MICHIGAN)*	**Synchrotron Studies of Ordered Chromatin Fibers for Model Calculations**
2042M	10/12/87	ERIC SIROTA GREG S SMITH N A CLARK C R SAFINYA *(EXXON RESEARCH & ENGINEERING)*	**Synchrotron Scattering Studies of Dilute Membrane Systems**
2043V	10/12/87	PIERO CHIARADIA GIORGIO MARGARITONDO L J BRILLSON *(ISITIUTIO DI STRUTTURA DELL MATERIA)*	**Schottky Barrier Formation in GaP Single Crystals**
2044Mp	11/5/87	PAUL H FUOSS SEAN BRENNAN LAURA NORTON ARTHUR I BIENENSTOCK J KAHN *(AT&T BELL LABORATORIES)*	**Direct Scattering Studies of Surface Premelting**
2045M	11/5/87	MARYBETH RICE PAUL H FUOSS ARTHUR I BIENENSTOCK LANE C WILSON *(STANFORD UNIVERSITY)*	**Grazing Incidence X-Ray Scattering Study of Ge Epitaxy on Mo**
2046M	11/5/87	R COLELLA Q ZHAO *(PURDUE UNIVERSITY)*	**X-Ray Study of Charge Density Waves (CDW's) in Layer Compounds**

2047B	11/16/87	JAMES E PENNER-HAHN HIM-TAI TSANG THOMAS V O'HALLORAN JEFF WRIGHT DIANA RALSTON RICHARD FRONKO *(UNIVERSITY OF MICHIGAN)*	**X-Ray Absorption Spectroscopy of the MER-R Gene Product**
2048B	11/16/87	JAMES E PENNER-HAHN RICHARD FRONKO ROBERT KERTAYASA JAMES D WHITTAKER *(UNIVERSITY OF MICHIGAN)*	**X-Ray Absorption Spectroscopy of Galactose Oxidase**

ROTATION CAMERA PROPOSALS

Access to the rotation camera facility for protein crystallography is through the submittal of a brief application which is reviewed by the Biology Sub-panel of the PRP on a short turnaround basis. The 15 rotation camera proposals active in 1987 are listed below:

1A57	2/1/87	BRIAN W MATTHEWS STEVE RODERICK LARRY WEAVER *(UNIVERSITY OF OREGON)*	**Structural Studies of Luciferase and other Proteins**
1A62	7/1/87	C D STOUT S A COLLETT ARTHUR ROBBINS *(RESEARCH INSTITUTE OF SCRIPPS)*	**High Resolution Data Collection on Ferredoxin**
1A63	7/8/87	JANUSZ M SOWADSKI SUSAN TAYLOR GORDON GILL *(UNIVERSITY OF CALIFORNIA)*	**Catalytic Subunit of Protein Kinase (cAMP Dependent)**
1A66	7/14/87	IAN WILSON JAIRO AREVALO GUY LAMBERT JAMES RINI ENRICO STURA *(RESEARCH INSTITUTE OF SCRIPPS)*	**The Structure of Antibodies, Antigens and Antibody-Antigen Complexe**

1A68	7/5/87	MICHAEL G ROSSMANN S KRISHNASWAMY PHILIPPE DUMAS KLAUS PIONTEK THOMAS J SMITH JOHN BADGER SANGSOO KIM *(PURDUE UNIVERSITY)*	**Virus Structure**
1A71	9/23/87	MARCOS H HATADA BRADFORD GRAVES JULANN MILLER *(HOFFMANN-LA ROCHE INC.)*	**Interleukin 2**
1A72	9/23/87	MARCOS H HATADA BRADFORD GRAVES JULANN MILLER *(HOFFMANN-LA ROCHE INC.)*	**Interleukin 2: Interleukin 2 Receptor**
1A73	9/23/87	MARCOS H HATADA BRADFORD GRAVES JULANN MILLER *(HOFFMANN-LA ROCHE INC.)*	**Interleukin 1 Δ**
1A74	9/23/87	C D STOUT ARTHUR ROBBINS S A COLLETT *(RESEARCH INSTITUTE OF SCRIPPS)*	**High Resolution Data Collection on Aconitase**
1A75	9/23/87	ROBERT M STROUD V RAMALINGAM THOMAS EARNEST MICHAEL SHUSTER CYNTHIA WOLBERGER MICHAEL MCCARTHY KATHY KANTARDJIEFF *(UNIVERSITY OF CALIFORNIA)*	**Crystal Structure of Colicin Ia**
1A76	11/5/87	IVAN RAYMENT *(UNIVERSITY OF ARIZONA)*	**Crystallographic Studies of Myosin Subfragment-1**
1A78	12/17/87	ADA YONATH FELIX FROLOW ILONA MAKOWSKI KLAUS BARTELS KLAUS V BOEHLEN HAKON HOPE *(WEIZMANN INSTITUTE)*	**Crystallographic Studies on Ribosomal Particles**

1A79	12/28/87	SUNG-HOU KIM MIKE MILBURN BART DE VOS LIANG TONG CHULHEE KANG *(UNIVERSITY OF CALIFORNIA)*	**Redesignal Sweet Protein**
1A80	1/1/88	THOMAS EARNEST JULIE EARNEST MICHAEL MCCARTHY MICHAEL SHUSTER CYNTHIA WOLBERGER ROBERT M STROUD *(UNIVERSITY OF CALIFORNIA)*	**Crystal Structure of Transmembrane Ion Channels: Colicin Ia and the Nicotinic Acetylcholine Receptor**
1A81	1/1/88	DOUGLAS C REES *(UNIVERSITY OF CALIFORNIA)*	**Structures of Electron-Transfer Proteins**

IX SSRL EXPERIMENTERS AND PROPOSALS BY INSTITUTIONS

As of December 31, 1987 there were 535 experimenters from 114 institutions officially involved with active proposals at SSRL. In addition, over a 100 others (graduate students, etc.) participated in work at the laboratory in collaboration with these scientists. The 89 United States institutions included 49 Universities, 27 private corporations and 13 government laboratories.

U.S CORPORATIONS: ARACOR, AT&T BELL LABORATORIES, BECTON DICKINSON & COMPANY RESEARCH CENTER, BOEING COMPANY, CHEVRON OIL FIELD RESEARCH COMPANY, CHEVRON RESEARCH COMPANY, EASTMAN KODAK RESEARCH LABORATORY, EPRI, EXXON RESEARCH & ENGINEERING, HEWLETT PACKARD LABORATORIES, HOFFMANN-LA ROCHE INC., IBM RESEARCH LABORATORY, INTEL CORPORATION, KMS FUSION, LOCKHEED RESEARCH LABORATORY, 3M CENTRAL RESEARCH LABORATORY, MACROATOM, INC, MARTIN MARIETTA, MONSANTO COMPANY, PALO ALTO VETERANS HOSPITAL, SCHLUMBERGER-DOLL RESEARCH, SIGNETICS CORPORATION, SRI INTERNATIONAL, THE AEROSPACE CORPORATION, UNIVERSITY CITY SCIENCE CENTER, W.R. GRACE & COMPANY, XEROX

U.S. LABORATORIES: ARGONNE NATIONAL LABORATORY, BROOKHAVEN NATIONAL LABORATORY, LAWRENCE BERKELEY LABORATORY, LAWRENCE LIVERMORE NATIONAL LABORATORY, LOS ALAMOS NATIONAL LABORATORY, NATIONAL BUREAU OF STANDARDS, NAVAL RESEARCH LABORATORY, NAVAL WEAPONS CENTER, OAK RIDGE NATIONAL LABORATORY, PACIFIC NORTHWEST LABORATORY, SANDIA NATIONAL LABORATORY, STANFORD SYNCHROTRON RADIATION LABORATORY, WESTERN REGIONAL RESEARCH CENTER

U.S. UNIVERSITIES: AMHERST COLLEGE, ARIZONA STATE UNIVERSITY, BRIGHAM YOUNG UNIVERSITY, BROWN UNIVERSITY, CALIFORNIA INSTITUTE OF TECHNOLOGY, CALIFORNIA STATE UNIVERSITY, CARNEGIE INSTITUTE, CARNEGIE MELLON UNIVERSITY, CASE WESTERN RESERVE UNIVERSITY, CITY UNIVERSITY OF NEW YORK, COLORADO SCHOOL OF MINES, COLUMBIA UNIVERSITY, FLORIDA-ATLANTIC UNIVERSITY, GEORGIA INSTITUTE OF TECHNOLOGY, HARVARD MEDICAL SCHOOL, HARVARD UNIVERSITY, HUNTER COLLEGE CUNY, MASSACHUSETTS INSTITUTE OF TECHNOLOGY, NORTH CAROLINA STATE UNIVERSITY, NORTHWESTERN UNIVERSITY, OHIO STATE UNIVERSITY, PENNSYLVANIA STATE UNIVERSITY, PRINCETON UNIVERSITY, PURDUE UNIVERSITY, RESEARCH INSTITUTE OF SCRIPPS CLINIC, STANFORD UNIVERSITY, STEVENS INSTITUTE OF TECHNOLOGY, TEXAS A&M UNIVERSITY, UNIVERSITY OF ARIZONA, UNIVERSITY OF CALIFORNIA, UNIVERSITY OF CHICAGO, UNIVERSITY OF CINCINNATI, UNIVERSITY OF COLORADO, UNIVERSITY OF GEORGIA, UNIVERSITY OF HAWAII, UNIVERSITY OF ILLINOIS, UNIVERSITY OF KENTUCKY, UNIVERSITY OF MICHIGAN, UNIVERSITY OF MINNESOTA, UNIVERSITY OF MISSISSIPPI, UNIVERSITY OF NEW MEXICO, UNIVERSITY OF NOTRE DAME, UNIVERSITY OF OREGON, UNIVERSITY OF PENNSYLVANIA, UNIVERSITY OF SOUTH CAROLINA, UNIVERSITY OF SOUTH FLORIDA, UNIVERSITY OF WASHINGTON, UNIVERSITY OF WISCONSIN, WASHINGTON UNIVERSITY

FOREIGN: ALCAN INTERNATIONAL LIMITED, CHALMERS INSTITUTE OF TECHNOLOGY, CNRS, ELECTROTECHNICAL LABORATORY, EUROPEAN SYNCHROTRON RADIATION FACILITY, HC ORSTED INSTITUTE, ISTITUTO DI FISICA DEL POLITECNICO, ISTITUTO DI STRUTTURA DELLA MATERIA, KAROLINSKA INSTITUTE, KING'S COLLEGE, LINKOPING UNIVERSITY, MAX-PLANCK INSTITUTE FUR MED FORSCH, MEDICAL NOBEL INSTITUTE, MPG HAMBURG, POLITECNICO DI MILANO, SIMON FRASER UNIVERSITY, UNIVERSITA DI BRESCIA, UNIVERSITA DI MODENA, UNIVERSITA DI ROMA, UNIVERSITAT BIELEFELD, UNIVERSITAT BONN, UNIVERSITY OF SHEFFIELD, UNIVERSITY OF SUSSEX, WEIZMANN INSTITUTE, ZHEJIANG UNIVERSITY

SSRL EXPERIMENTERS AND PROPOSALS BY INSTITUTION

UNITED STATES INSTITUTIONS

AMHERST COLLEGE

D.M. DOOLEY	1053

ARACOR

W.K. WARBURTON	1008

ARGONNE NATIONAL LABORATORY

E.E. ALP	2012
M. BLOCH	882
G.K. SHENOY	2012
L. SODERHOLM	2012
J. VICCARO	1074

ARIZONA STATE UNIVERSITY

T. GROY	2020
S.H. LIN	2020
J.R. SCHOONOVER	2020

AT&T BELL LABORATORIES

J. BEVK	1044
M. CHANCE	1042
P.H. CITRIN	947
P.H. FUOSS	1095, 1096, 2044, 2045
D.W. KISKER	1095, 1096
M.A. MARCUS	1044, 1045
S.G.J. MOCHRIE	2017
L. NORTON	1095, 1096, 2044
J.M. POATE	1013
L.S. POWERS	1042
I.K. ROBINSON	997, 1094
J.E. ROWE	1013
F. SETTE	1013
M. SEUL	1029
J.J. YEH	935

BECTON DICKINSON & COMPANY RESEARCH CENTER

A. NAQUI	1043

BOEING COMPANY

R.B. GREEGOR	100, 956, 1049, 1097, 2021, 2038
F.W. LYTLE	100, 956, 1026, 1049, 1069, 1097, 2021, 2028, 2038
D.R. SANDSTROM	1026

BRIGHAM YOUNG UNIVERSITY

M.W. HILL	1069, 2021
N. MANGELSON	1069, 2021

BROOKHAVEN NATIONAL LABORATORY

J.D. AXE	898
J. BOHR	898, 1094
H. CHEN	1072
D.A. FISCHER	1015
L.D. GIBBS	898, 2017
S.M. HEALD	1072, 1073, 1074
S.M. KHALID	1043
B. OCKO	2017
J. PHILLIPS	2007
M. SUENAGA	1073
W. THOMLINSON	1046
J.M. TRANQUADA	1073, 2005

BROWN UNIVERSITY

M. ALTMAN	997
P.J. ESTRUP	997

CALIFORNIA INSTITUTE OF TECHNOLOGY

S.I. CHAN	1067
P.M. LI	1067

CALIFORNIA STATE UNIVERSITY

J.V. ACRIVOS	1025, 1099, 2000
S. ARNOLD	1099, 2000
C. BUSTILLO	1099, 2000
D. HELMOLDT	1099, 2000
R. ITHNIN	1099, 2000
M.C. LEI	1025, 1099, 2000
J. SATCHER	1099, 2000
S.C. WEAVER	1025
P. ZIA	1025

CARNEGIE INSTITUTE

H.K. MAO	1064

CARNEGIE MELLON UNIVERSITY

R.F. HAINSEY	2014
J.D. SHINDLER	2014
R.M. SUTER	2014
J.D. WHITTAKER	2048

CASE WESTERN RESERVE UNIVERSITY

D.A. SCHERSON	1098

CHEVRON OIL FIELD RESEARCH COMPANY

R.M.K. CARLSON	1033

CHEVRON RESEARCH COMPANY

G. ZHANG	1043

CITY UNIVERSITY OF NEW YORK

P.A. MONTANO	2012

COLORADO SCHOOL OF MINES

T.E. FURTAK	1090
T.M. HAYES	1037, 1038, 1090, 1091
G. KRAUSS	1037
D.L. WILLIAMSON	1037, 1038, 1091

COLUMBIA UNIVERSITY

M. CUFF	1087
W.A. HENDRICKSON	1087
J. HORTON	1087
S.J. LIPPARD	2030
H.M.K. MURTHY	1087
A. PAHLER	1087
W.E. ROYER	1087
W. YANG	1087

EASTMAN KODAK RESEARCH LABORATORY

T.A. SMITH	2033

EPRI

H. OCKEN	2028

EXXON RESEARCH & ENGINEERING

M.W.W. ADAMS	1030
K.L. D'AMICO	898
P.M. EISENBERGER	882, 928, 1001
G.N. GEORGE	1030, 1039, 1083, 1084, 1089
J.L. GLAND	1015
K.S. LIANG	928, 1001
V. MINAK	1030
D. MONCTON	898, 1001
J.M. NEWSAM	1001
R.C. PRINCE	1039, 1083, 1084
C.R. SAFINYA	1001, 1010, 2042
J.H. SINFELT	1001
S.K. SINHA	1001
E. SIROTA	1034, 2042
G.S. SMITH	2042

EXXON RESEARCH & ENGINEERING - (Continued)

E.I. STEIFEL	1030
B. VARADY	1010
G.H. VIA	1001

FLORIDA-ATLANTIC UNIVERSITY

F.A. SCHULTZ	1055

GEORGIA INSTITUTE OF TECHNOLOGY

S.D. ANTOLOVICH	2015
Y.H. CHUNG	1056
R.H. FELTON	1068
S.R. STOCK	1056, 2015
G. WEBB	2015

HARVARD MEDICAL SCHOOL

D. AULD	1042
B. HOLMQUIST	1042
J. RIORDAN	1042
B. VALLEE	1042

HARVARD UNIVERSITY

S. AMADOR	1034
C.M. FRIEND	1080
A.C. LIU	1080
P.S. PERSHAN	1034
J.T. ROBERTS	1080

HEWLETT PACKARD LABORATORIES

A. FISCHER-COLBRIE	1093, 2036
S. LADERMAN	1093, 2036
J. MOLL	1093, 2036
M.P. SCOTT	2036

HOFFMANN-LA ROCHE INC.

B. GRAVES	1A71, 1A72, 1A73
M.H. HATADA	1A71, 1A72, 1A73
J. MILLER	1A71, 1A72, 1A73

HUNTER COLLEGE CUNY

M.L. DENBOER	897

IBM RESEARCH LABORATORY

C. ERICKSON	1021
G. HELD	1058
P.M. HORN	1058
T.C. HUANG	1021
W. JARK	2009

IBM RESEARCH LABORATORY - (Continued)

K.F. LUDWIG	1008
O. MELROY	2003
S.S.P. PARKIN	1099, 2000
W. PARRISH	1021
T.P. RUSSELL	2009
J. STOHR	963, 2009
M. TONEY	2003

INTEL CORPORATION

D. SELIGSON	2037

KMS FUSION

L. THOMPSON	1031

LAWRENCE BERKELEY LABORATORY

C.C. BAHR	943
J.J. BARTON	943
S.E. DERENZO	2004
V. DEROSE	2010
S. DEXHEIMER	2010
T. FERRETT	943
R. GUILES	2010
P.A. HEIMANN	943
A.L. JOHNSON	943
M.P. KLEIN	2000, 2010
J.B. KORTRIGHT	2018
J. LITTON	2004
A. MCDERMOTT	2010
W.W. MOSES	2004
E. PAPARAZZO	943
M.N. PIANCASTELLI	943
S.W. ROBEY	943
P.N. ROSS	1098
K. SAUER	2010
D.A. SHIRLEY	943
D.H. TEMPLETON	957
L.K. TEMPLETON	957
L.J. TERMINELLO	943
A.C. THOMPSON	1046
A. SCHACH V WITTENAU	943
V.K. YACHANDRA	2010
J.L. ZIMMERMANN	2010

LAWRENCE LIVERMORE NATIONAL LABORATORY

J. AKELLA	1064
R.A. DAY	1054
S. FLETCHER	1054

LAWRENCE LIVERMORE NATIONAL LABORATORY - (Continued)

J. HENDERSON	2013
Q.C. JOHNSON	1064
D. KANIA	2011
J.H. KINNEY	1054
D. KNAPP	2013
H.E. MARTZ	1054
R.W. RYON	1054
G.S. SMITH	1064
G. TIRSELL	9901
J. TREBES	2011
M.J. WEBER	9901
L.C. WILSON	2045

LOS ALAMOS NATIONAL LABORATORY

R.J. BARTLETT	2013
T. BOWLES	2013
S.D. CONRADSON	1027, 2023, 2024
P.G. ELLER	2038
J.A. FEE	1035
Z. FISK	2023
J.A. GOLDSTONE	2016
G. KWEI	2016
E.M. LARSON	2038
A.C. LAWSON	2016
R. MARTIN	2013
J.D. PURSON	2038
I.D. RAISTRICK	2023
A. REDONDO	2023
H. ROBERTSON	2013
A. SATTLEBERGER	2024
B. SWANSON	1027, 2024
W.J. TRELA	2013
R.B. VON DREELE	2016
D. WARK	2013
J. WILKERSON	2013
A. WILLIAMS	2016
W. WOODRUFF	1027

3M CENTRAL RESEARCH LABORATORY

C.-L. TSAI	1044, 1045

MACROATOM, INC

F.E. HUGGINS	956

MARTIN MARIETTA

F.M. KUSTAS	1091

MASSACHUSETTS INSTITUTE OF TECHNOLOGY

R.H. BEER	2030
J.G. BENTSEN	2030
R.J. BIRGENEAU	997, 2002
J.D. BROCK	2002
J.D. LITSTER	2002
S. SUBRAMANIAM	1029

MONSANTO COMPANY

L. LIM	1019

NATIONAL BUREAU OF STANDARDS

M.I. BELL	910, 973
C.E. BOULDIN	910, 973, 1032
P.L. COWAN	1086
R.D. DESLATTES	1086
R.A. FORMAN	910, 973
D.W. LINDLE	943, 1086

NAVAL RESEARCH LABORATORY

E.D. DONOVAN	973
G.K. HUBLER	973

NAVAL WEAPONS CENTER

J. ERICKSON	2039
A.K. GREEN	2039
S. LANGSJOEN	2039
P. LAROE	2039
T.-W. NEE	2039
V. REHN	2039
C. SCHWARTZ	2039
W. WIEMER	2039

NORTH CAROLINA STATE UNIVERSITY

D.E. SAYERS	906, 1074
E.C. THEIL	906

NORTHWESTERN UNIVERSITY

T.V. O'HALLORAN	2047
D. RALSTON	2047
J. WRIGHT	2047

OAK RIDGE NATIONAL LABORATORY

H. CEDERQUIST	1052
B.C. CHAKOUMAKOS	1049
S.B. ELSTON	1052
J. LEVIN	1052
C.S. O	1052
I. SELLIN	1052

OAK RIDGE NATIONAL LABORATORY - (Continued)

S. SPOONER	2006
D.M. ZEHNER	2017

OHIO STATE UNIVERSITY

J.O. ALBEN	981, 1061
A.A. CROTEAU	981, 1061
F.G. FIAMINGO	981, 1061
C.F. HEMANN	981, 1061
R. HILLE	1040
K.A. POWELL	981, 1061

PACIFIC NORTHWEST LABORATORY

M.J. APTED	1050
G.J. EXARHOS	1050

PALO ALTO VETERANS HOSPITAL

J. GIACOMINI	1046
H. GORDON	1046

PENNSYLVANIA STATE UNIVERSITY

R.G. JENKINS	956

PRINCETON UNIVERSITY

J.T. GROVES	1085
M. STERN	1085

PURDUE UNIVERSITY

J. BADGER	1A68
R. COLELLA	2046
P. DUMAS	1A68
S. KIM	1A68
S. KRISHNASWAMY	1A68
K. PIONTEK	1A68
M.G. ROSSMANN	1A68
T.J. SMITH	1A68
Q. ZHAO	2046

RESEARCH INSTITUTE OF SCRIPPS CLINIC

J. AREVALO	1A66
S.A. COLLETT	1A62, 1A74
G. LAMBERT	1A66
J. RINI	1A66
A. ROBBINS	1A62, 1A74
C.D. STOUT	1A62, 1A74
E. STURA	1A66
I. WILSON	1A66

SANDIA NATIONAL LABORATORY

G. KUBIAK	2026
J. NELSON	2026
R.H. STULEN	2026

SCHLUMBERGER-DOLL RESEARCH

S.P. CRAMER	969, 981, 1030, 1039, 1040, 1084, 1089, 1092
D.R. HINES	1092
J. HOWARD	1089, 1092
W. MURPHY	1089
J. PECK	1089
N. WADA	1092
S. WHITTINGHAM	1092

SIGNETICS CORPORATION

B. COULMAN	1056

SRI INTERNATIONAL

D.C. LORENTS	1062
R.L. SHARPLESS	1062

STANFORD UNIVERSITY

H. ASAHINA	2034
L.R. BERNSTEIN	1051
K. BERTNESS	935
M. BOUDART	1065, 1071
C. BOWMAN	935
G.E. BROWN, JR.	994, 995, 999
K. BUTCHER	1022
C.R. CARBONE	935
K. CHAR	1093
T. CHIANG	935
J.P. COLLMAN	2034
R.J. DAVIS	1065
S.V. DIDZIULIS	1022
S. DONIACH	1012, 1076, 2035
S.J. EGLASH	935
B. FACTOR	1080, 2027
D. FRIEDMAN	935
T.H. GEBALLE	1079, 1093, 2036
D.C. HARRISON	1046
K.F. HAYES	995
R. HOFSTADTER	1046
R.S. HOWLAND	1093, 2036
S.R. HUBBARD	1012, 1087
J. HWANG	2026
W.A. JACKSON	999

STANFORD UNIVERSITY - (Continued)

J. KAHN	2044
A. KAPITULNIK	2036
L.-S. KAU	2031
T.F. KENDELEWICZ	935
A.D. KENT	1093
R. KERNOFF	1046
C. KILBOURNE	1048
P. KING	2037
J.O. LECKIE	995
N.S. LEWIS	1078
J.-Y. LIN	1022
S. LIST	935
R.J. MADIX	1080
R. MAHOWALD	935
C. MCCANTS	935
N. MISSERT	1093
D.B. MITZI	2036
N. NEWMAN	935
J. NOGAMI	935
B. OH	1093
J. OTIS	1046
L. PAN	2037
G.A. PARKS	995
C.W. PONADER	999
E. PUPPIN	935, 941
M. RICE	1060, 2045
S. ROTHFUS	999
E. RUBENSTEIN	1046
Z. SHEN	941
K. SHIH	935
J. SILBERMAN	935
E.I. SOLOMON	1022, 2031
J. SOLOMON	1080
W.E. SPICER	935, 941
P. STEVENS	1080
J.Z. SUN	1093
G. TAN	2031
B.J. TUFTS	1078
G.P. VALENCA	1071
S. WAKATSUKI	1076, 2035
G.A. WAYCHUNAS	994, 995, 999, 1050, 1051, 1088
M.D. WILLIAMS	935
J. WOICIK	935
H.D. ZEMAN	1046
M.B. ZISK	2034

STANFORD SYNCHROTRON RADIATION LABORATORY

A. BIENENSTOCK	1008, 1048, 1060, 2027, 2044, 2045
S. BRENNAN	1048, 1086, 2027, 2044
G.S. BROWN	1036, 1046, 2013
R. CARR	1036
A.D. COX	1025
B. HEDMAN	1055, 2029, 2030, 2031, 2032, 2033, 2034
K.O. HODGSON	995, 1012, 1055, 1076, 1078, 2029, 2030, 2031, 2032, 2033, 2034, 2035
I. LINDAU	897, 935, 941, 1028
E.A. MERRITT	1019, 1087
R.P. PHIZACKERLEY	1019, 1087
P. PIANETTA	2011, 2026, 2037
Z.U. REK	1056, 2015, 2028
U.W. SPANN	2035
T. TROXEL	1082

STEVENS INSTITUTE OF TECHNOLOGY

G.M. ROTHBERG	897

TEXAS A&M UNIVERSITY

D.A CHURCH	1052

THE AEROSPACE CORPORATION

P.D. FLEISCHAUER	2001
J.R. LINCE	2001

UNIVERSITY CITY SCIENCE CENTER

G. BUNKER	1043, 2022, 2025
B. CHANCE	1042, 1043, 2022; 2025
T.E. KING	2025
K.E. ZHANG	2022, 2025

UNIVERSITY OF ARIZONA

J. ENEMARK	1030
I. RAYMENT	1A76

UNIVERSITY OF CALIFORNIA

F.G. BRIDGES	1017, 1079, 2040
B.K. BURGESS	2029
B. CLARK	1018
D.S. CLARK	2008
B.E.C. DAVIS	1018
D. DE FONTAINE	1018, 2006

UNIVERSITY OF CALIFORNIA - (Continued)

B. DE VOS	1A79
J. DENLINGER	2018, 2019
J. EARNEST	1A80
T. EARNEST	1A75, 1A80
G. GILL	1A63
R.M. GUINN	2008
H. HOPE	1A78
J.J. HOYT	1018, 2006
Z.-Q HUANG	943
C. KANG	1A79
K. KANTARDJIEFF	1A75
S. KIM	943
S.-H. KIM	1A79
M. KRAITCHMAN	1018, 2006
D.A. LARSON	1082
T. LEUNG	943
C. LING	1082
S. LIU	943
G.A. MARG	2008
M. MCCARTHY	1A75, 1A80
L. MEDHURST	943
M. MILBURN	1A79
B. NIU	943
C. OGATA	1087
M. OLMSTEAD	2018, 2019
T.L. PHILLIPS	1082
V. RAMALINGAM	1A75
K. RAYMOND	906
D.C. RESS	1A81
M. SCHELL	1082
D. SHRIEVE	1082
M. SHUSTER	1A75, 1A80
J.M. SOWADSKI	1A63
R.M. STROUD	1076, 2035, 1A75, 1A80
S. TAYLOR	1A63
L. TONG	1A79
S.A. VAUGHN	2029
L. WANG	943
M. WIEDENMEIR	2006
C. WOLBERGER	1A75, 1A80
F. ZAERA	1015

UNIVERSITY OF CHICAGO

R.H. FAIRCLOUGH	1012
D. RICHMAN	1012

UNIVERSITY OF CINCINNATI

P. BOOLCHAND	1032
E.A. DEUTSCH	991
R.C. ELDER	922, 991, 1066
W.R. HEINEMAN	1066
K. TEPPERMAN	922

UNIVERSITY OF COLORADO

N.A. CLARK	1010, 2042
R. POYTON	2025

UNIVERSITY OF GEORGIA

M. EIDSNESS	1041
R.A. SCOTT	969, 1039, 1041, 1053, 1067

UNIVERSITY OF HAWAII

M.H. MANGHNANI	1059, 1064
L.C. MING	1059, 1064

UNIVERSITY OF ILLINOIS

S.G. SLIGAR	2022

UNIVERSITY OF KENTUCKY

G.P. HUFFMAN	956
N. SHAH	956

UNIVERSITY OF MICHIGAN

J. ALLEN	1028
B.D. ATHEY	2041
D.P. BALLOU	1035
O. BARALT	1031
C.J. BATIE	1035
M.D. CURTIS	1031
W.D. FRASCH	1085
R. FRONKO	1085, 1088, 2047, 2048
D. GHANOTAKIS	1085
R. KERTAYASA	2048
J.P. LANGMORE	2041
V.L. PECORARO	1085
J.E. PENNER-HAHN	1031, 1033, 1035, 1050, 1085, 1088, 2047, 2048
M.F. SMITH	2041
H.-T. TSANG	1035, 1085, 2047
G. WALDO	1033, 1088
S. WANG	1088
S. WILLIAMS	2041
C.F. YOCUM	1085

UNIVERSITY OF MINNESOTA

W.H. SMYRL	2003

UNIVERSITY OF MISSISSIPPI

W. CLELAND	1030

UNIVERSITY OF NEW MEXICO

T. BEIN	1070
R.C. EWING	1049
K. MOLLER	1070

UNIVERSITY OF NOTRE DAME

K.K. CHIN	935
K.M. CHOUDHARY	1077

UNIVERSITY OF OREGON

G.B. ARMEN	1036
B. CRASEMANN	1036, 2013
B.W. MATTHEWS	1A57
S. RODERICK	1A57
S.L. SORENSEN	1036, 2013
L. WEAVER	1A57
S.B. WHITFIELD	1036, 2013

UNIVERSITY OF PENNSYLVANIA

J.E. BENCI	1081
E. DAVIDSON	2025
T.G. FREY	1039
M. IKEDA-SAITO	1083
D.P. POPE	1081

UNIVERSITY OF SOUTH CAROLINA

J.H. DAWSON	2032
M. SONO	2032

UNIVERSITY OF SOUTH FLORIDA

L.S. SOLMONSON	1030

UNIVERSITY OF WASHINGTON

J. FREUND	1047
B. HOUSER	2005
R.L. INGALLS	100, 1047, 2005
L.B. SORENSEN	1034
E.A. STERN	906, 1068, 2005
P. VIRAN	100
J.E. WHITMORE	100

UNIVERSITY OF WISCONSIN

G. MARGARITONDO	2043

WASHINGTON UNIVERSITY

F.S. MATHEWS	1019

W.R. GRACE & COMPANY

A.L. ROE	1055

WESTERN REGIONAL RESEARCH CENTER

S.F. GHELLER	1055
W.E. NEWTON	1055

XEROX

R.Z. BACHRACH	908, 959
J.B. BOYCE	1017, 1079, 2040
L.J. BRILLSON	2043
R.D. BRINGANS	908, 959, 2018, 2019
J.C. MIKKELSON	1017
J.E. NORTHRUP	908

SSRL EXPERIMENTERS AND PROPOSALS BY INSTITUTIONS
FOREIGN INSTITUTIONS

ALCAN INTERNATIONAL LIMITED *(Canada)*
R. TIMSIT 2027

CHALMERS INSTITUTE OF TECHNOLOGY *(Sweden)*
T. CLAESON 1079

CNRS (France)
P. GIBART 1038

ELECTROTECHNICAL LABORATORY *(Japan)*
H. OYANAGI 2022

EUROPEAN SYNCHROTRON RADIATION FACILITY *(France)*
E. ZIEGLER 1074

HC ORSTED INSTITUTE *(Denmark)*
H.H. ANDERSEN 1094
L.F. GRAABAEK 1094
A. JOHANSEN 1094
E. JOHNSON 1094
L. SARHOLT-KRIST 1094

ISTITUTO DI FISICA DEL POLITECNICO *(Italy)*
I. ABBATI 941
M. S. ANCROTTI 941

ISTITUTO DI STRUTTURA DELLA MATERIA *(Italy)*
P. CHIARADIA 2043
F. COMIN 947

KAROLINSKA INSTITUTE *(Sweden)*
B.-M. SJOBERG 1043

KING'S COLLEGE *(England)*
M. HART 1021

LINKOPING UNIVERSITY *(Sweden)*
R.I.G. UHRBERG 908

MAX-PLANCK INSTITUTE FUR MED FORSCH *(Germany)*
K. BARTELS 1A78

MEDICAL NOBEL INSTITUTE *(Sweden)*
P. REICHARD 1043

MPG HAMBURG *(Germany)*
K.V. BOEHLEN 1A78

POLITECNICO DI MILANO *(Italy)*
L. BRAICOVICH 941

SIMON FRASER UNIVERSITY *(Canada)*
N. ALBERDING 100
K.R. BAUCHSPIESS 100
D. CROZIER 100, 1047, 2005
A.J. SEARY 100

UNIVERSITA DI BRESCIA *(Italy)*
M. BELLOTTO 1021

UNIVERSITA DI MODENA *(Italy)*
O. BISI 941
C. CALANDRA 941
U. DEL PENNINO 941

UNIVERSITA DI ROMA *(Italy)*
S. NANNARONE 941

UNIVERSITAT BIELEFELD *(Germany)*
W. JITSCHIN 1036
U. WERNER 1036

UNIVERSITAT BONN *(Germany)*
G. WILL 1021

UNIVERSITY OF SHEFFIELD *(England)*
P. HARRISON 906

UNIVERSITY OF SUSSEX *(England)*
B.E. SMITH 1030

WEIZMANN INSTITUTE *(Israel)*
F. FROLOW 1A78
I. MAKOWSKI 1A78
A. YONATH 1A78

ZHEJIANG UNIVERSITY *(PRC)*
X.-S ZHANG 943

X SSRL PUBLICATIONS

The following is a partial list of papers published or submitted in 1987 based on work at SSRL. The list represents 183 publications. A list of 1987 theses follows.

Abbati, I., Braicovich, L., Carbone, C., Nogami, J., Lindau, I., Iandelli, I., Olcese, G., Palenzona, A., **Photoemission Studies of Mixed Valence in Yb_3Si_5, YbSi, and Yb_5Si_3: Equivalent Versus Inequivalent Yb Sites:** Solid State Comm 62, 35 (1987)

Allen, J.W., Kang, J.-S., Lassailly, Y., Maple, M.B., Torikachvilli, M.S., Ellis, W., Pate, B., Lindau, I., **Electron Spectroscopy Study of the Heavy Fermion Compound URu_2Si_2:** Solid State Comm 61, 183 (1987)

Armen, G.B., Tulkki, J., Aberg, T., Crasemann, B., **Quantum Theory of Post Collision Interaction in Inner-Shell Photoionization: Final-State Interaction Between Two Continuum Electrons:** Phys Rev A 36, 5606 (1987)

Armen, G.B., Sorensen, S.L., Whitfield, S.B., Ice, G.E., Levin, J.C., Crasmann, B., **Vanishing Post-Collision Interaction During Photon-Excited Coster-Kronig Decay:** Phys Rev A 35, 3966 (1987)

Bachrach, R.Z., Bringans, R.D., Olmstead, M.A., Uhrberg, R.I.G., **Synchrotron Radiation Studies of MBE Formed Semiconductor Interfaces: Si-GaAs and GaAs-Si:** Modern Phys Lett B 1, 97 (1987)

Bachrach, R.Z., Bringans, R.D., Olmstead, M.A., Uhrberg, R.I.G., **Surface Structure and Interface Formation of Si on GaAs(100):** J Vac Sci Technol B 5, 1135 (1987)

Bachrach, R.Z., Bringans, R.D., Swartz, L., Lindau, I., Pate, B.B., Carr, R.G., Hower, N., Youngman, B., Morales, H., Pianetta, P., **Multi-Undulator Beam Line V at SSRL: A Progress Report:** accepted Nucl Instrum & Methods

Barbee, T.W., Pianetta, P., Tatchyn, R., Redaelli, R., Barbee, T.W. III, **Molybdenum-Silicon Multilayer Monochromator for the Extreme Ultraviolet:** App Phys Lett 50, 644 (1987)

Barton, J.J., Hussain, Z., Shirley, D.A., **Generalized Ramsauer-Townsend Resonance in Angle-Resolved Photoemission Extended Fine-Structure Oscillations:** Phys Rev B 35, 933 (1987)

Becker, U., Langer, B., Kerkhoff, H.G., Kupsch, M., Szostak, D., Wehlitz, R., Heimann, P.A., Liu, S.H., Lindle, D.W., Ferrett, T.A., Shirley, D.A., **Observation of Many New Argon Valence Satellites Near Threshold:** submitted Phys Rev Lett

Bertness, K.A., McCants, C.E., Chiang, T.T., Mahowald, P.H., Wahi, A.K., Kendelewicz, T., Lindau, I., Spicer, W.E., **Comparison of Low Intensity Laser Enhancement of Oxygen Chemisorption on GaAs Using O_2 and N_2O:** Mat Res Soc Sym Proc 75, 575 (1987)

Bertness, K.A., Chiang, T.T., McCants, C.E., Mahowald, P.H., Wahi, A.K., Kendelewicz, T., Lindau, I., Spicer, W.E., **Comparative Uptake Kinetics on N_2O and O_2 Chemisorption on GaAs(110):** Surf Sci 185, 544 (1987)

Bienenstock, A., **SSRL Development - Recent and Planned:** accepted Nucl Instrum & Methods

Bouldin, C.E., Forman, R.A., Bell, M.I., **Silicon Photo-Diode Detector for Fluorescence EXAFS:** Rev Sci Instrum 58, 1891 (1987)

Bouldin, C.E., Forman, R.A., Bell, M.I., **Conversion Electron EXAFS Measurements of Ion-Damage GaAs:** Phys Rev B35, 1429 (1987)

Bouldin, C.E., Forman, R.A., Bell, M.I., Donovan, E.P., **Structural Relaxation in Ion-Damaged Amorphous Ge:** submitted Phys Rev B

Boyce, J.B., Bridges, F., Claeson, T., Howland, R.S., Geballe, T.H., **X-Ray Absorption Studies of $YBa_2Cu_3O_{7-\sigma}$ and $GdBa_2Cu_3O_{7-\sigma}$ Superconductors:** Phys Rev B 36, 5251 (1987)

Boyce, J.B., Bridges, F., Claeson, T., Geballe, T.H., Chu, C.W., Tarascon, J.M., **X-ray Absorption Studies of the High-Tc Superconductors $La_{1.8}Sr_{0.2}CuO_4$ and $La_{1.8}Ba_{0.2}CuO_4$:** Phys Rev B 35, 7203 (1987)

Bringans, R.D., Olmstead, M.A., Uhrberg, R.I.G., Bachrach, R.Z., **Summary Abstract: Core Level Spectroscopy of the GaAs-on-Si Interface:** J Vac Sci Technol A5, 2141 (1987)

Bringans, R.D., Uhrberg, R.I.G., Olmstead, M.A., Bachrach, R.Z., Northrup, J.E., **Model Semiconductor Surfaces: Arsenic Termination of the Ge(111), Si(111), and Si(100) Surfaces:** Physica Scripta T17, 7 (1987)

Bringans, R.D., Olmstead, M.A., Uhrberg, R.I.G., Bachrach, R.Z., **Formation of the Interface Between GaAs and Si: Implications for GaAs-on-Si Heteroepitaxy:** Appl Phys Lett 51, 523 (1987)

Bringans, R.D., Olmstead, M.A., Uhrberg, R.I.G., Bachrach, R.Z., **GaAs-on-Si Epitaxy: Results for Coverage of ~1 Monolayer:** Mat Res Soc Symp Proc 94, 201 (1987)

Brown, G.S., Cerino, J., Hofmann, A., Liu, R., Troxel, T., Wang, P., Wiedemann, H., Winick, H., Berndt, M., Brown, R., et al., **Operation of PEP in a Low Emittance Mode:** accepted IEEE

Cao, R., Miyano, K., Kendelewicz, T., Chin, K.K., Lindau, I., Spicer, W.E., **Kinetics Study of Initial Stage Band Bending at Metal GaAs (110) Interfaces:** J Vac Sci Technol B5, 998 (1987)

Carey, G.P., Friedman, D.J., Lindau, I., Spicer, W.E., **Photoemission Studies of the Room Temperature Si/$Hg_{1-x}Cd_xTe$, Si/HgTe and Si/CdTe Interfaces:** J Vac Sci Technol A5, 3198 (1987)

Chin, K.K., Cao, R., Kendelewicz, T., Miyano, K., Yeh, J.J., Doniach, S., Lindau, I., Spicer, W.E., **Photoemission Study of the Physical Nature of the InP Near-Surface Defect States, in Interface, Superlattices, and Thin Films:** Mat Res Soc Sym Proc 77, 429 (1987)

Chin, K.K., Cao, R., Kendelewicz, T., Miyano, K., Williams, M.D., Doniach, S., Lindau, I., Spicer, W.E., **Transition from Schottky Limit to Bardeen Limit in the Schottky Barrier Formation of Al on n- and p-GaAs(110) Interfaces:** Mat Res Soc Symp Proc 77, 297 (1987)

Chin, K.K., Miyano, K., Cao, R., Kendelewicz, T., Yeh, J., Lindau, I., Spicer, W.E., **Chemical Reaction at the In on GaAs (110) Interface: A Synchrotron Radiation Photoemission Study:** J Vac Sci Technol B5, 1080 (1987)

Cole, J., Yachandra, V.K., Guiles, R.D., McDermott, A.E., Britt, R.D., Dexheimer, S.L., Sauer, K., Klein, M.P., **Assignment of the g=4.1 EPR Signal to Manganese in the S2 State of the Photosynthetic Oxygen-Evolving Complex: An X-Ray Absorption Edge Spectroscopy Study:** Biophysical Acta 890, 395 (1987)

Cole, J., Yachandra, U.K., McDermott, A.E., Guiles, R.D., Britt, R.D., Dexheimer, S.L., Sauer, K., Klein, M.P., **Structure of the Mn Complex of Photosystem II Upon Removal of the 33 Kilodalton Extrinsic Protein: An X-Ray Absorption Edge Spectroscopy Study:** Biochemistry 26, 5967 (1987)

Comelli, G., Stohr, J., Pate, B., **Extended X-ray Absorption Fine Structure Studies of Diamond and Graphite:** submitted Phys Rev B

Conradson, S.D., Burgess, B.K., Hodgson, K.O., Newton, W.E., Mortenson, L.E., **Structural Studies of the Molybdenum Site in the MoFe Protein and its FeMo-Cofactor by EXAFS:** J Am Chem Soc 109, 7507 (1987)

Cox, L.E., Ellis, W.P., Cowan, R.D., Allen, J.W., Oh, S.-J., Lindau, I., Pate, B.B., Arko, A.J., **Valence-Band Photoemission in UO_2(111) Near the 5d Resonant Photon Energy:** Phys Rev B 35, 5161 (1987)

Cramer, S.P., Eidsness, M.K., Pan, W.-H., Morton, T.A., Ragsdale, S.W., DerVartanian, D.V., Ljungdahl, L.G., Scott, R.A., **X-Ray Absorption Spectroscopic Evidence for a Unique Nickel Site in Clostridium Thermoaceticum Carbon Monoxide Dehydrogenase:** Inorg Chem 26, 2477 (1987)

Crozier, E.D., Alberding, N., Bauchspiess, K.R., Seary, A.J., Gygax, S., **Structure of $YBa_2Cu_3O_{7-\Delta}$ vs Temperature by X-ray Absorption Spectroscopy:** Phys Rev B

Doniach, S., Chin, K.K., Lindau, I., Spicer, W.E., **Microscopic Metal Cluster and Schottky Barrier Formation:** Phys Rev Lett 58, 591 (1987)

Eberhardt, W., Plummer, E.W., Lyo, I.W., Carr, R., Ford, W.K., **Auger Electron Ion Coincidence Studies of Soft X-Ray Induced Fragmentation of N_2:** submitted Phys Rev Lett

Eberhardt, W., **Core Electron Excitation and Decay in Molecules:** submitted Phys Scripta

Elder, R.C., Eidsness, M.K., **Synchrotron X-ray Studies of Metal-Based Drugs and Metabolites:** Chem Rev 87, 1027 (1987)

Ellis, W.P., Albers, R.C., Allen, J.W., Lassailly, Y., Kang, J.-S., Pate, B.B., Lindau, I., **Valence-Band Densities of State in NiAs:** Solid State Comm 62, 591 (1987)

Ericson, A., Hedman, B., Hodgson, K.O., Green, J., Dalton, H., Bentsen, J.G., Beer, R.H., Lippard, S.J., **Structural Characterization by EXAFS Spectroscopy of the Binuclear Iron Center in Component A of Methane Monooxygenase from Methylococcus capsulatus (Bath):** in press J Amer Chem Soc

Feldman, R.D., Austin, R.F., Fuoss, P.H., Dayem, A.H., Westerwick, E.H., Nakahara, S., Boone, T., Menendez, J., Pinczuk, A., Valladares, J.P., Brennan, S., **Phase Separation in $Cd_{1-x}Zn_xTe$ Grown by Molecular-Beam Epitaxy:** J Vac Sci Technol B 5, 690 (1987)

Ferrett, T.A., Heimann, P.A., Kerkhoff, H.G., Becker, U., Lindle, D.W., Shirley, D.A., **Photoelectron Asymmetry Parameter for the S 2p Level of SO_2:** Chem Phys Letts 138, 607 (1987)

Ferrett, T.A., Piancastelli, M.N., Lindle, D.W., Heimann, P.A., Medhurst, L.J., Liu, S.H., Shirley, D.A., **Resonance Effects on the Inner-Valence Levels of SF_6 in the Photon-Energy Range 52-72 eV:** Chem Phys Lett 134, 146 (1987)

Ferrett, T.A., Lindle, D.W., Heimann, P.A., Brewer, W.D., Becker, U., Kerkhoff, H.G., Shirley, D.A., **Lithium 1s Main-Line and Satellite Photoemission: Resonant and Nonresonant Behavior:** Phys Rev A 36, 3172 (1987)

Frank, P., Hedman, B., Carlson, R.M.K., Tyson, T.A., Roe, A.L., Hodgson, K.O., **A Large Reservoir of Sulfate and Sulfonate Resides within Plasma Cells from Ascidia ceratodes, Revealed by X-ray Absorption Near-Edge Structure Spectroscopy:** Biochem 26, 4975 (1987)

Friedman, D.J., Carey, G.P., Lindau, I., Spicer, W.E., Wilson, J.A., **Overlayer-Cation Reaction at the $Pt/Hg_{1-x}Cd_xTe$ Interface:** Phys Rev B 35, 1188 (1987)

Friedman, D.J., Carey, G.P., Lindau, I., Spicer, W.E., **Systematics of Metal Contacts to $Hg_{1-x}Cd_xTe$:** J Vac Sci Technol A5, 3190 (1987)

Friend, C.M., Stevens, P.A., Serafin, J.G., Baldwin, E.K., Madix, R.J., **Bonding and Absorption Structure of CO on W(100)-(5x1)-C:** submitted J Chem Phys

Fuller, A., Tatchyn, R., Csonka, P., Lindau, I., **Studies of Interfacial Structure in WC Multilayers:** SPIE 733, 286 (1987)

Giauque, R.D., Jaklevic, J.M., Thompson, A.C., **Biological Trace-Element Measurements Using Synchrotron Radiation:** Biological Trace Element Reseach 12, 185 (1987)

Guiles, R.D., Yachandra, V.K., McDermott, A.E., Dexheimer, S.L., Sauer, K., Klein, M.P., **EXAFS and XANES Studies of Manganese Complexes: Models for the Photosynthetic Oxygen-Evolving Complex:** submitted

Guiles, R.D., Cole, J., McDermott, A.E., Yachandra, V.K., Britt, R.D., Dexheimer, S.L., Sauer, K., Klein, M.P., **Structure of Manganese in the SO State of Photosynthetic Oxygen-Evolving Complex:** submitted

Guiles, R.D., Yachandra, V.K., Cole, J., McDermott, A.E., Dexheimer, S.L., Sauer, K., Klein, M.P., **Structure of the S3 State of the Photosynthetic Oxygen Evolving Complex:** submitted

Gygax, S., Crozier, E.D., Alberding, N., Bauchspiess, K.R., Seary, A.J., **Temperature-Dependent EXAFS Spectra of $_{Y}Ba_2Cu_3O_{7-\Delta}$:** Jpn J Appl Phys 26, 1051 (1987)

Hahn, S., Arst, M., Rek, Z.U., Stojanoff, V., Bulla, D.A., Castro, W.E., Jr., Tiller, W.A., **Effects of 450 C Thermal Annealing upon Oxygen Precipitation in Heavily B- and Sb-doped Czochralski Si:** Appl Phys Lett 50, 401 (1987)

Hart, M., Parrish, W., Bellotto, M., Lim, G.S., **The Refractive Index Correction in Powder Diffraction:** submitted Acta Crystallogr

Hayes, K.F., Roe, A.L., Brown, G.E., Hodgson, K.O., Leckie, J.O., Parks, G.A., **In-Situ X-Ray Absorption Study of Surface Complexes: Selenium Oxyanions on Alpha-FeOOH:** Science 238, 783 (1987)

Hedman, B., Frank, P., Gheller, S.F., Roe, A.L., Newton, W.E., Hodgson, K.O., **New Structural Insights into the Iron-Molybdenum Cofactor from Azotobacter Vinelandii Nitrogenase through Sulfur K and Molybdenum L X-ray Absorption Edge Studies:** in press J Amer Chem Soc

Heimann, P.A., Lindle, D.W., Ferrett, T.A., Liu, S.H., Medhurst, L.J., Piancatelli, M.N., Shirley, D.A., Becker, U., Kerkhoff, H.G., Langer, B., et al., **Shake-off on Inner-Shell Resonances of Ar, Kr and Xe:** J Phys B: At Mol Phys 20, 5005 (1987)

Hernandez, P., Lamelas, F., Clarke, R., Dimon, P., Sirota, E.B., Sinha, S.K., **Time-Resolved X-Ray Scattering Study of Ordering Kinetics in $SbCl_5$-Intercalated Graphite:** Phys Rev Lett 59, 1220 (1987)

Hitchcock, A.P., Stohr, J., **K-Shell Shape Resonances and Intramolecular Bond Lengths Comments on "The Relationship Between Shape Resonances and Bond Lengths":** J Chem Phys 87, 3253 (1987)

Horsley, J.A., Wachs, I.E., Brown, J.M., Via, G.H., Hardcastle, F.D., **Structure of Surface Tungsten Oxide Species in the WO_3/Al_2O_3 Supported Oxide System from X-ray Absorption Near-Edge Spectroscopy and Raman Spectroscopy:** J Phys Chem 91, 4014 (1987)

Huang, T.C., Toney, M.F., Brennan, S., Rek, Z., **Analysis of Co-doped Iron Oxide Thin Films by Synchrotron Radiation:** Thin Solid Films 154, 439 (1987)

Huggins, F.E., Huffman, G.P., Shah, N., Jenkins, R.G., Lytle, F.W., Greegor, R.B., **Further EXAFS Examination of the State of Calcium in Pyrolyzed Char:** in press Fuel

Huggins, F.E., Shah, N., Huffman, G.P., Lytle, F.W., Greegor, R.B., Jenkins, R.G., **In-Situ EXAFS Investigation of Ca and K Catalytic Species During Pyrolysis and Gasification of Lignite Chars:** in press Fuel

Hwang, J., Shih, C.K., Pianetta, P., Spicer, W.E., Pao, Y.-C., Harris, J.S., **Determination of the Natural Valence Band Offset in the $In_xGa_{1-x}As$ System:** Appl Phys Lett 51, 1632 (1987)

Ingalls, R., Crozier, E.D., Alberding, N., Seary, A.J., Bauchspiess, K.R., Houser, B., Freund, J., **X-ray Absorption Spectroscopy at High Pressure:** Naukuva Dumka

Jaklevic, J.M., Bouret, E., Scott, M.P., Laderman, S.S., **Application of Tunable Monochromatic Synchrotron Radiation to Topographic Studies of Dislocations in GaAs:** in preparation

Joensen, P., Crozier, E.D., Alberding, N., Frindt, R.F., **A Study of Single-Layer and Restacked MoS_2:** J Phys C 20, 4043 (1987)

Kalkowski, G., Kaindl, G., Brewer, W.D., Krone, W., **Near Edge X-ray Absorption Fine Structure in Uranium Compounds:** Phys Rev B 35, 6 (1987)

Kang, J.S., Allen, J.W., Maple, M.B., Torikachvili, M.S., Pate, B., Ellis, W., Lindau, I., **Spectral Evidence for the Importance of Single-Site Effects in Heavy-Fermion Uranium Materials:** Phys Rev Lett 59, 493 (1987)

Kendelewicz, T., Mahowald, P.H., McCants, C.E., Bertness, K.A., Lindau, I., Spicer, W.E., **Chemical Reaction and Schottky Barrier Formation at the Ti/InP (110) and Sn/InP (110) Interfaces: Reactive Versus Nonreactive Case:** J Vac Sci Technol B 5, 1033 (1987)

Kendelewicz, T., Mahowald, P.H., Bertness, K.A., McCants, C.E., Lindau, I., Spicer, W.E., **Surface Shifts in the In 4d and 2p Core Level Spectra of InP(110):** Phys Rev B 36, 6543 (1987)

King, P., Pan, L., Pianetta, P., Shimkunas, A., Mauger, P., Seligson, D., **X-ray Induced Damage in Boron Nitride, Silicon, and Silicon Nitride Lithography Masks:** SPIE 773, 126 (1987)

Kortright, J.B., Fischer-Colbrie, A., **Standing Wave Enhanced Scattering in Multilayer Structures:** J Appl Phys 61, 1130 (1987)

Kortright, J.B., Denlinger, J., **Study of Atomic Arrangements in Tungsten-Carbon Multilayers of X-ray Optical Interest:** in preparation

Kortright, J.B., Bienenstock, A., **X-ray Structural Study of Amorphous Mo-Ge Films:** accepted Phys Rev B

Kortright, J.B., Laderman, S.S., Scott, M.P., Fischer-Colbrie, A., **Study of Defects in GaAs on Si (100) by X-Ray Diffraction Techniques:** submitted

Laderman, S.S., Kortright, J., Scott, M., Fischer-Colbrie, A., **Grazing Incidence X-Ray Scattering Study of Defect Structures in MBE GaAs/Si Using Synchrotron Radiation:** Mat Res Soc Sym Proc 91, 143 (1987)

Lassailly, Y., Allen, J.W., Ellis, W., Cox, L., Pate, B., Fisk, Z., Lindau, I., **Electron Spectroscopy Study of the Heavy Fermion Compound U_2Zn_{17}:** J Magn & Magn Mat 63 & 64, 512 (1987)

Li, P.M., Gelles, J., Chan, S.I., Sullivan, R.J., Scott, R.A., **Extended X-Ray Absorption Fine Structure of Copper in Cu(A)-Depleted pHMB-Modified and Native Cytochrome c Oxidases:** Biochem 26, 2091 (1987)

Liang, K.S., Laderman, S.S., Sinfelt, J.H., **Structure Study of Small Catalytic Particles Using Differential Anomalous X-ray Scattering:** J Chem Phys 86, 2352 (1987)

Liang, K.S., Eisenberger, P., **Grazing Incidence X-ray Scattering Study of Surface Defects:** Mat Res Soc Symp Proc 82, 493 (1987)

Lim, G., Parrish, W., Ortiz, C., Bellotto, M., Hart, M., **Grazing Incidence Synchrotron X-Ray Diffraction Method for Analyzing Thin Films:** J Mater Res 2, 471 (1987)

Lindau, I., **Interfacial Properties of Metal Overlayers on III-V Compounds:** Vacuum 37, 385 (1987)

Lindle, D.W., Heimann, P.A., Ferrett, T.A., Piancastelli, M.N., Shirley, D.A., **Photoemission Study of Kr 3r np Autoionization Resonances:** Phys Rev A 35, 4605 (1987)

Lindle, D.W., Heimann, P.A., Ferrett, T.A., Shirley, D.A., **Helium Photoelectron Satellites: Low Energy Behavior of the n=3-5 Lines:** Phys Rev A 35, 1128 (1987)

Lindle, D.W., Ferrett, T.A., Heimann, P.A., Shirley, D.A., **Complete Photoemission Study of the He $1s_2$ 3s3p Autoionizing Resonance:** Phys Rev A 36, 2112 (1987)

Lindle, D.W., Ferrett, T.A., Heimann, P.A., Shirley, D.A., **Photoemission from Xe in the Vicinity of the 4d Cooper Minimum:** submitted Phys Rev A

List, R.S., Woicik, J., Mahowald, P.H., Lindau, I., Spicer, W.E., **The Si/GaAs (110) Heterojunction Discontinuity: Amorphous Versus Crystalline Overlayers:** J Vac Sci Technol A5, 1459 (1987)

List, R.S., Woicik, J.C., Lindau, I., Spicer, W.E., **The Si/GaAs (110) Heterojunction: Strain, Disorder, and Valence-Band Discontinuity:** J Vac Sci Technol B 5, 1279 (1987)

Ludwig, K.F., Warburton, W.K., Wilson, L., Bienenstock, A.I., **Liquid $GeBr_4$. I.- A Test of the Anomalous X-ray Scattering Method as Applied to Disordered Materials:** J Chem Phys 87, 604 (1987)

Ludwig, K.F., Wilson, L., Warburton, W.K., Bienenstock, A.I., **Liquid $GeBr_4$. II. - Molecular Packing and Liquid Structures:** J Chem Phys 87, 613 (1987)

Lytle, F.W., Greegor, R.B., Panson, A.J., **Discussion of X-Ray Absorption Near Edge Structure: Application to Cu in the High T(c) Superconductors $La_{1.8}Sr_{.2}CuO_4$ and $YBa_2Cu_3O_7$:** submitted Phys Rev B

McCants, C.E., Kendelewicz, T., Bertness, K.A., Mahowald, P.H., Williams, M.D., List, R.S., Lindau, I., Spicer, W.E., **Chemical and Electronic Properties of the Pt/GaAs (110) Interface:** J Vac Sci Technol B 5, 1083 (1987)

Meitzner, G., Via, G.H., Lytle, F.W., Sinfelt, J.H., **Structure of Bimetallic Clusters Extended X-ray Absorption Fine Structure (EXAFS) of Pt-Re and Pd-Re Clusters:** J Chem Phys 87, 6354 (1987)

Meitzner, G., Via, G.H., Sinfelt, J.H., Lytle, F.W., **Extended - X-ray Absorption Fine Structure Spectroscopic (EXAFS) Studies of Model Reforming Catalysts:** Petroleum Chem 32, 733 (1987)

Moon, D.W., Cameron, S., Zaera, F., Eberhardt, W., Carr, R., Bernasek, S.L., Dwyer, D.J., **A Titled Precursor for CO Dissociation on the Fe(100) Surface:** Surf Sci 180, L123 (1987)

Nogami, J., Friedman, D.J., Kendelewicz, T., Lindau, I., Spicer, W.E., **Binding Energy Shifts from Alloying at Metal/II-VI Compound Semiconductor Interfaces:** J Vac Sci Technol A5, 591 (1987)

Olmstead, M.A., Uhrberg, R.I.G., Bringans, R.D., Bachrach, R.Z., **Photoemission Study of Bonding at the CaF_2-on-Si(111):** Phys Rev B 35, 7526 (1987)

Olmstead, M.A., Bringans, R.D., Uhrberg, R.I.G., Bachrach, R.Z., **Bonding at the CaF_2-on-Si(111) Interface:** Mat Res Soc Symp Proc 94, 195 (1987)

Outka, D.A., Stohr, J., Jark, W., Stevens, P., Solomon, J., Madix, R.J., **Orientation and Bond Length of Molecular Oxygen on Ag(110) and Pt(111): A NEXAFS Study:** Phys Rev B 35, 4119 (1987)

Outka, D.A., Stohr, J., Rotermund, H.H., Madix, R.J., Solomon, J., Hermsmeier, B., **NEXAFS Studies of Complex Alcohols and Carboxylic Acids on the Si(111)(7x7)** Surface: Surf Sci 185, 53 (1987)

Outka, D.A., Stohr, J., Rabe, J., Swalen, J.D., Rotermund, H.H., **Orientation of Arachidate Chains in Langmuir-Blodgett Monolayers on Si(111):** Phys Rev Lett 59, 1321 (1987)

Outka, D.A., Stohr, J., Madix, R.J., Rotermund, H.H., Hermsmeier, Solomon, J., **NEXAFS Studies of Unsaturated Carboxylic Acids and Alcohols Adsorbed on the Si(111) Surface:** Mat Res Soc Symp Proc 90, (1987)

Parrrish, W., Hart, M., **Advantages of Synchrotron Radiation for Polycrystalline Diffractometry:** submitted Z Kristallogr

Parrish, W., **Advances in Synchrotron X-Ray Polycrystalline Diffraction:** submitted Aust J Phys

Parrish, W., Hart, M., Huang, T.C., Bellotto, M., **Lattice Parameter Determination Using Synchrotron Powder Data:** accepted Adv X-ray Anal

Parrish, W., Hart, M., **Accurate Measurement of Powder Diffraction Intensities using Synchrotron Radiation:** submitted Aust J Phys

Pearton, S.J., Poate, J.M., Sette, F., Gibson, J.M., Jacobson, D.C., **Ion Implantation in GaAs:** Nucl Instrum & Methods Phys Res 19, 369 (1987)

Penner-Hahn, J.E., Murata, M., Freeman, H.C., Hodgson, K.O., **Low Temperature X-ray Absorption Spectroscopy of Plastocyanin:** submitted J Am Chem Soc

Persson, I., Penner-Hahn, J.E., Hodgson, K.O., **X-ray Absorption Spectroscopy of Mercury(II) Halide Complexes in DMSO and Pyridine:** submitted Inorg Chem

Piestrup, M.A., Moran, M.J., Berman, B.L., Pianetta, P., Seligson, D., **Transition Radiation as an X-ray Source for Lithography:** SPIE 733, 37 (1987)

Puppin, E., Nogami, J., Carbone, C., Shen, Z.X., Lindau, I., Pate, B., Abbati, I., Braicovich, L., **A Photoemission Study of the Si (111)/Gd Interface: A Comparison with Bulk Silicides:** J Vac Sci Technol B 5, 1083 (1987)

Robey, S.W., Barton, J.J., Bahr, C.C., Liu, G., Shirley, D.A., **An Angle-Resolved Photoemission Extended Fine-Structure Spectroscopy Investigation of c(2x2)S/Ni(011):** Phys Rev B 35, 1108 (1987)

Robey, S.W., Bahr, C.C., Hussain, Z., Leung, K.T., Lou, J., Schach von Witenau, A.E., Barton, J.J., **Surface Structure of (2x2)S/Ge(111) Determined by Angle-Resolved Photoemission Fine Structure:** Phys Rev B 35, 5657 (1987)

Robinson, C.J., Samant, M.G., Stohr, J., Speriosu, V.S., Guarnieri, C.R., Cuomo, J.J., **Structural Studies of Hydrogenated Amorphous Carbon Infrared Coatings:** Mat Res Soc Sym Proc, 90 (1987)

Robinson, I.K., **Symmetry of the Si(111)7x7 at an a-Si Interface:** Phys Rev B 35, 3910 (1987)

Rotermund, H.H., Hermsmeier, B., Solomon, J., **NEXAFS Studies of Complex Alcohols and Carboxylic Acids on the Si(111) Surface:** Surf Sci 185, 53 (1987)

Rubenstein, E., **Synchrotron Radiation for Angiography:** Ann Rev Biophy Biophy Chem 16, 161 (1987)

Rubenstein, E., Brown, G.S., Giacomini, J.C., Gordon, H.J., Hofstadter, R., Kernoff, R.S., Otis, J.N., Thomlinson, W., Thompson, A.C., Zeman, H.D, **Angiograhy using Synchrotron Radiation:** in press Phys Scripta

Samant, M.G., Borges, G.L., Gordon, J.G., Melroy, O.R., Blum, M., **In-Situ Surface Extended X-Ray Absorption Fine Structure Spectroscopy of a Lead Monolayer at a Silver(111) Electrode/Electrolyte Interface:** Amer Chem Soc 109, 5970 (1987)

Savborg, O., Schoonover, J.R., Lin, S.H., Eyring, L., **Time-Resolved X-ray Diffraction by Synchrotron Radiation: The Thermal Decomposition of $Cd(OH_2)$ Powders:** J Solid State Chem 68, 214 (1987)

Sette, F., Pearton, S.J., Poate, J.M., Rowe, J.E., **Extended X-Ray Absorption Fine Structure Studies by Soft X-Ray Fluorescence Detection:** Physica Scripta T17, 209 (1987)

Sette, F., Pearton, S.J., Poate, J.M., Rowe, J.E., **Local Structure of S Impurities in Implanted GaAs:** Nucl Instrum & Methods Phys Res 19, 408 (1987)

Shen, Z.-X., Allen, J.W., Yeh, J.J., Kang, J.-S., Ellis, W., Spicer, W.E., Lindau, I., Maple, M.B., Dalichaouch, Y.D., Torikachvili, M.S., et al, **Anderson Hamiltonian Description of the Experimental Electronic Structure and Magnetic Interactions of Copper Oxide Superconductors:** Phys Rev B 36, 8414 (1987)

Shih, C.K., Silberman, J.A., Wahi, A.K., Carey, G.P., Lindau, I., Spicer, W.E., Berding, M.A., Sher, A., **Angle Resolved Photoemission Study of the Alloy Scattering Effect in $Hg_{1-x}Cd_xTe$:** J Vac Sci Technol A5, 3026 (1987)

Short, R.T., O, C.-S, Levin, J.C., Sellin, I.A., Johnson, B.M., Meron, M., Jones, K.W., Church, D.A., **Synchrotron Radiation Inner-Shell Photoionization of Atomic and Molecular Gases:** Nucl Instrum Methods B24/25, 417 (1987)

Siedle, A.R., Markell, C.G., Lyon, P.A., Hodgson, K.O., Roe, A.L., **Bifunctional Rhodium-Oxometalate Catalysts:** Inorg Chem 26, 219 (1987)

Sirota, E.B., Pershan, P.S., Amador, S., Sorensen, L.B., **Synchrotron X-ray Observation of Surface Smectic-I Hexatic Layers on Smectic-C Liquid Crystal Films:** Phys Rev A 35, 5 (1987)

Sirota, E.B., Pershan, P.S., Sorensen, L.B., Collett, J., **X-Ray and Optical Studies of the Thickness Dependence of the Phase Diagram of Liquid-Crystal Films:** Phys Rev A 36, 2890 (1987)

Stohr, J., Outka, D.A., Madix, R.J., **Near Edge X-ray Absorption Fine Structure Studies of Molecules and Molecular Chains Bonded to Surface:** J Vac Sci Technol A5, 919 (1987)

Stohr, J., Outka, D.A., **Determination of Molecular Orientations on Surfaces from the Angular Dependence of NEXAFS Resonances:** Phys Rev B36 7891 (1987)

Stohr, J., Outka, D.A., Baberschke, K., Arvanitis, D., Horsley, J.A., **Identification of C-H Resonances in the K-Shell Excitation Spectra of Gas Phase, Chemisorbed and Polymeric Hydrocarbons:** Phys Rev B 36, 2967 (1987)

Stura, E.A., Feinstein, A., Wilson, I.A., **Crystallization and Preliminary Crystallographic Data for an Antiprogesterone Monoclonal Antibody Fab' and Steroid-Fab' Complexes:** J Mol Biol 193, 229 (1987)

Stura, E.A., Arevalo, J.H., Feinstein, A., Heap, R.B., Taussig, M.J., Wilson, I.A., **Analysis of an Anti-Progesterone Antibody: Variable Crystal Morphology of the Fab' and Steroid-Fab' Complexes:** Immunology 62, 511 (1987)

Tatchyn, R., Lindau, I., **Off-Axis Radial Properties of Undulator Light:** SPIE 733, 115 (1987)

Templeton, D.H., Templeton, L.K., **X-ray Birefringence, Forbidden Reflections, and Direct Observation of Structure-Factor Phases:** Acta Cryst A43, 573 (1987)

Thompson, A.C., Wu, Y., Underwood, J.H., Barbee, T.W., **Focusing of Synchrotron Radiation X-Ray Beams Using Synthetic Multilayer Mirrors:** Nucl Instrum Methods A255, 603 (1987)

Thompson, A.C., Zeman, H.D., Rubenstein, E., Otis, J.N., Hofstadter, R., Brown, G.S., Harrison, D.C., Kernoff, R.S., Giacomini, J.C., Gordon, H.J., Thomlinson, W., **Transvenous Coronary Angiography in Dogs Using Synchrotron Radiation:** J Cardiac Imaging, in press

Thompson, A.C., Hofstadter, R., Otis, J.N., Zeman, H.D., Kernoff, R.S., Rubenstein, E., Giacomini, J.C., Gordon, H.D., Brown, G.S., Thomlinson, W., **Transvenous Coronary Angiography using Synchrotron Radiation:** in press Nucl Instrum & Methods

Tobin, J.G., Robey, S.W., Klebanoff, L.E., Shirley, D.A., **Development of a Three-Dimensional Valence-Band Structure in Ag Overlayers on Cu(001):** Phy Rev B 35, 9056(1987)

Toney, M.F., Huang, T., Brennan, S., Rek, Z., **Summary Abstract: Analysis of Co Doped Iron Oxide Thin Films by Grazing Incidence X-ray Diffraction:** accepted J Vac Sci

Toney, M.F., Huang, T.C., Brennan, S., Rek, Z., **X-ray Depth Profiling of Iron Oxide Films:** submitted J Mat Res

Tulkki, J., Armen, G.B., Aberg, T., Crasemann, B., Chen, M-H, **Quantum Theory of Post-Collision Interaction in Inner-Shell Photoionization:** Z Physik D5, 241 (1987)

Uhrberg, R.I.G., Bringans, R.D., Olmstead, M.A., Bachrach, R.Z., **Electronic Structure, Atomic Structure and the Passivated Nature of the Arsenic Terminated Si(111) Surface:** Phys Rev B 35, 3945 (1987)

Vijay-Kumar, S., Senadhi, S.E., Ealick, S.E., Nagabhushan, T.L., Trotta, P.P., Kosecki, R., Reichert, P., Bugg, C.E., **Crystallization and Preliminary X-Ray Investigation of a Recombinant Form of Human Gamma Interferon:** J Biol Chem 262, 4804 (1987)

Warburton, W.K., Ludwig, K.F., Wilson, L., Bienenstock, A., **Differential Anomalous X-ray Scattering Techniques for Determination of Liquid and Amorphous Structures:** Mat Res Soc Symp 57, 211 (1987)

Watkins, J.W., Greene, B., Darnall, D.W., Elder, R.C., **Determination of Gold Binding in an Algal Biomass using EXAFS and XANES Spectroscopies:** Inorg Chem 26, 1147 (1987)

Wenzel, L., Arvanitis, D., Daum, W., Rotermund, H.H., Stohr, J., Baberschke, K., Ibach, H., **Structural Determination of an Adsorbate Induced Surface Reconstruction: c(2x2)N Versus c(2x2)O on Ni(100):** Phys Rev B 36, 7689 (1987)

Wilson, L., Bienenstock, A., **Atomic Arrangements in Short Period Mo-Ge Multilayers Determined by Anomalous Scattering and EXAFS:** submitted Mat Res Soc Proc

Winick, H., **Wiggler Magnets as X-ray Sources for Angiography Studies:** to be published

Winick, H., **Synchrotron Radiation:** Sci Am 255, 88 (1987)

Winick, H., **Status of Synchrotron Radiation Facilities Outside the USSR:** Nucl Instrum & Methods A261, 9 (1987)

Yachandra, V.K., Guiles, R.D., McDermott, A.E., Cole, J., Britt, R.D., Dexheimer, S.L., Sauer, K., Klein, M.P., **Comparison of the Structure of the Manganese Complex in the S1 and S2 States of the Photosynthetic Oxygen Evolving Complex: An X-Ray Absorption Spectroscopy Study:** Biochemistry 26, 5974 (1987)

Yeh, J.J., Bertness, K.A., Cao, R., Hwang, J., Lindau, I., **Bonding Characteristics of the Ag/Si Interface Identified by the Energy Dependence of the Photoemission Cross Section:** Phys Rev B 35, 3024 (1987)

Book Articles and Conference Proceedings

Bienenstock, A., Brennan, S., Fischer-Colbrie, A., Fuoss, P.H., Ludwig, K.F., Jr., Lorentz, R.D., Warburton, W.K., Wilson, L., **X-ray Synchrotron Radiation Structural Studies of Amorphous Materials** in Proceedings Second Intl Conf on Effects of Modes of Formation on the Structure of Glass (Nashville, Tenn, June 1987)

Bienenstock, A., Brennan, S., Fischer-Colbrie, A., Fuoss, P.H., Ludwig, K.F., Jr., Lorentz, R.D., Warburton, W.K., Wilson, L., **Synchrotron Radiation as a Tool for the Determination of Atomic Arrangements in Amorphous Materials** in A. K. Bhatnagar (editor) Metallic and Semiconductor Glasses I: (Trans Tech Pub, Switzerland, 1987) pp. 59-70

Boyce, J.B., Mikkelsen, J.C., Jr., **Local Structure of Ternary Alloys: EXAFS Studies** in S.K. Deb, A. Zanger (editors) Ternary and Multinary Compounds: (Mat Res Soc, Boston, 1987) pp. 359-364

Bringans, R.D., Uhrberg, R.I.G., Olmstead, M.A., Bachrach, R.Z., **Core Level Study of Bonding at the GaAs - on Si Interface** in Proceedings 18th Intl Conf on the Physics of Semiconductors (1987)

Chin, K.K., Cao, R., Miyano, K., McCants, C.E., Lindau, I., Spicer, W.E., **An Investigation of the Cause of the Initial Band Bending of a Cleaved Clean n-GaAs (110) Surface** in R.J. Nemanich, et al. Thin Films-Interfaces and Phenomena (Materials Research Society, 1987)

Crozier, E.D., Rehr, J.J., Ingalls, R., **Amorphous and Liquid Systems** in Prins, R., Konigsberger, D. (editors) in X-ray Absorption: Principles, Applications, Techniques of EXAFS, SEXAFS and XANES: (John Wiley and Sons, NY, 1987) pp. 373-442.

Eidness, M.K., Sullivan, R.J., Cramer, S.P., Scott, R.A., **Electronic and Molecular Structure of Biological Nickel as Studied by X-ray Absorption Spectroscopy** in J.R. Lancaster (editor) Bioinorganic Chemistry of Nickel: (VCH, Deerfield Beach) accepted for publication

Friedman, D.J., Lindau, I., Spicer, W.E., **Surfaces of and Interfaces with Mercury Cadmium Telluride** in J. Brice, P. Capper (editors) Properties of Mercury Cadmium Telluride, EMIS Datareviews Series No 3, INSPEC: (Inst of Elec Engineers, London, 1987) pp. 157-178

George, G.N., Cramer, S.P., Frey, T.G., Prince, R.C., **X-ray Absorption Studies of Oriented Cytochrome Oxidase** in Kim, C.H., et al. (editors) Advances in Membrane Biochemistry and Biophysics: (Plenum Press, 1987) p. 429-438

Gygax, S., Crozier, E.D., Alberding, N., Bauchspiess, K.R., Seary, A.J., **Temperature-dependent EXAFS Spectra of $YBa_2Cu_3O_{7-\sigma}$** in Proceedings Intl Conf on Low Temperature (Tokyo, 1987)

Huffman, G.P., Huggins, F.E., Shah, N., Bhattacharyya, D., Pugmire, R.J., Davis, B., Lytle, F.W., Greegor, R.B., **Investigation of the Atomic and Physical Structure of Organic and Inorganic Sulfur in Coal** in Y. P. Chugh, R. D. Caudle (editors) Proceedings and Utilization of High Sulfur Coals II: (Elsevier Science Pub Company, 1987) pp. 3-12

Huggins, F.E., Shah, N., Huffman, G.P., Jenkins, R.G., Lytle, F.W., Greegor, R.B., **Structures of Alkali and Alkaline-earth Gasification Catalysts from EXAFS Spectroscopy** in J. A. Moulijn, et al. (editors) 1987 Intl Conf on Coal Science: (Elsevier Science Publishers, 1987) pp. 563-566

Kortright, J.B., Denlinger, J.D., **Tungsten-carbon Multilayer System Studied with X-ray Scattering** in T. W. Barbee, et al. (editors) Multilayers: Synthesis, Properties and Nonelectronic Applications: (Mat Res Soc, Boston, 1987)

McDermott, A., Yachandra, V. K., Guiles, R.D., Britt, R.D., Dexheimer, S.L., Sauer, K., Klein, M.P., **Iron X-ray Absorption Spectra of Acceptors in PS I** in J. Biggins (editor) Progress in Photosynthesis Research: (Martinus Nijhoff Pub, 1987) pp. 249-252

McDermott, A., Yachandra, V.K., Guiles, R.D., Cole, J., Britt, R.D., Dexheimer, S.L., Sauer, K., Klein, M.P., **The State of Iron and Manganese in the Photosynthetic Apparatus Determined by X-ray Spectroscopy** in A. Bianconi (editor) Proceedings Intl Conf on Biophysics and Synchrotron Radiation (Frascati, 1987) (Springer-Verlag, Heidelberg)

Nogami, J., Lindau, I., **Rare Earth Metal/Semiconductor Interface Formation** in O. Engstrom (editor) 18th Intl Conf on the Physics of Semiconductors (World Scientific, Singapore, 1987) pp. 343-346

Olmstead, M.A., Uhrberg, R.I.G., Bringans, R.D., Bachrach, R.Z., **The Interface Between a Covalent Semiconductor and an Ionic Insulator: CaF_2 on Si(111)** in Proceedings 18th Intl Conf on the Physics of Semiconductors (World Scientific, Singapore, 1987)

Parrish, W., Hart, M., Huang, T.C., Bellotto, M., **Lattice Parameter Determination using Synchrotron Powder Data** in C.S. Barrett, et al. (editors) Advances in X-ray Analysis, Vol., 30 (Plenum Press, NY, 1987) pp. 373-382

Penner-Hahn, J.E., Hodgson, K.O., **X-ray Absorption Spectroscopy of Iron Porphyrins** in A.B.P. Lever, H.B. Gray (editors) Physical Bioinorganic Chemistry (in press 1987)

Plummer, E.W., Gustafsson, T., Hamann, D.R., Lindau, I., Mills, D.L., Quate, C.F., Shen, Y.R., **New Ways of Looking at Surfaces** in P.A. Psaras, H.D. Langford (editors) Advancing Materials Research (National Academy Press, 1987) pp. 283-306

Rubenstein, E., Zeman, H.D., Thompson, A.C., Thomlinson, W., Otis, J.N., Kernoff, R.S., Hofstadter, R., Gordon, H.J., Giacomini, J.C., Brown, G.S., **Recent Results in SYRDA at the Stanford Synchrotron Radiation Laboratory** (Societe Italiana di Fisica, in press, 1987)

Rubenstein, E., Brown, G.S., Giacomini, J.C., Gordon, H.J., Hofstadter, R., Kernoff, R.S., Otis, J.N., Thomlinson, W., Thompson, A.C., Zeman, H.D., **Progress Report on Synchrotron Radiation Angiography on Human Subjects** in Proceedings 14th Intl Conf on X-ray and Inner-shell Processes (Les Editions de Physique, 1987)

Uhrberg, R.I.G., Bringans, R.D., Olmstead, M.A., Bachrach, R.Z., **Arsenic Passivation of the Si(111) Surface** in Proceedings 18th Intl Conf on the Physics of Semiconductors (1987)

Warburton, W.K., Ludwig, K.F., Wilson, L., Bienenstock, A., **Differential Anomalous X-ray Scattering Techniques for Determination of Liquid and Amorphous Structures** in G.S. Cargill III, et al. (editors) Phase Transitions in Condensed Systems-Experiment and Theory (Mat Res Soc, Pittsburgh, 1987) p. 211

Yachandra, V.K., Guiles, R.D., McDermott, A., Cole, J., Britt, R.D., Dexheimer, S.L., Sauer, K., Klein, M.P., **The State of Manganese in the Photosynthetic Apparatus: An X-ray Absorption Study** in J. Biggins (editor) Progress in Photosynthesis Research Vol. 1 (Martinus Nijhoff Pub, 1987) pp. 557-560

Zaera, F., Fischer, D., Carr, R., Kollin, E., Gland, J., **Study of Kinetics of Ethylidyne Formation on Pt(111) using NEXAFS** in ACS Symposium on Molecular Phenomena at Electrode Surfaces (New Orleans, 1987) submitted

THESES BASED ON RESEARCH AT SSRL

Thirteen theses based on work at SSRL were completed in 1987 bringing the total number of completed theses to 127 from 20 different Universities. For the complete list consullt earlier Activity Reports.

R.T. Short	University of Tennessee	"Recoil-Energy Measurements of Slow Highly-Charged Ions Produced by Synchrotron Radiation and by Swift-Ion Impact" (Advisor - I.A. Sellin)
S.R. Hubbard	Stanford University	"Small-Angle X-Ray Scattering Studies of Calcium-Binding Proteins in Solutions" (Advisor - K.O. Hodgson)
L.-S. Kau	Stanford University	"Chemical and Spectroscopic Studies on Metal Active Sites in Metalloproteins and Heterogeneous Catalysts" (Advisor - K.O. Hodgson)
J.L. Cole	UC-Berkeley	"Photosynthetic Oxygen Evolution Studied by Electron Paramagnetic Resonance and X-Ray Absorption Spectroscopy" (Advisor - M.P. Klein)
A.E. McDermott	UC-Berkeley	"Structural Studies of Iron and Manganese in Photosynthetic Reaction Centers" (Advisor - M.P. Klein)
R.E. Guiles	UC-Berkeley	"X-Ray Absorption and EPR Studies of the Role of Mn in the Photosynthetic Oxygen Evolving System" (Advisor - M.P. Klein)
J.J. Yeh	Stanford University	"Metal/Silicon Interfaces and Their Oxidation Behavior - A Photoemission Spectroscopy Analysis" (Advisor - I. Lindau)
D. Friedman	Stanford University	"Metal Interfaces with Mercury Cadmium Telluride" (Advisor - I. Lindau)
A. Viescas	Stanford University	"Photoemission Studies of Core Level Energy Shifts in Clean and Adsorbate Covered Tungsten and Platinum Single Crystal Surfaces" (Advisor - I. Lindau)
P. Jupiter	Stanford University	"Correlation Between the Electronic Structure and Surface Chemistry of Tungsten and Tungsten Carbide 4" (Advisor - W.E. Spicer)
K.A. Bertness	Stanford University	"Photoemission Studies of Oxygen Chemisorption on Gallium Arsenide and Indium Phosphide Surfaces" (Advisor - W.E. Spicer)
J.R. Schoonver	Arizona State	"Time Resolved X-ray Diffraction using Synchrotron Radiation" (Advisor -S.H. Lin)
J.N. Otis	Stanford University	"Minimally Invasive Coronary Angiography with Monochromatic X-Rays: Developmental Studies Utilizing Synchrotron Radia tion" (Advisor - R. Hofstadter)

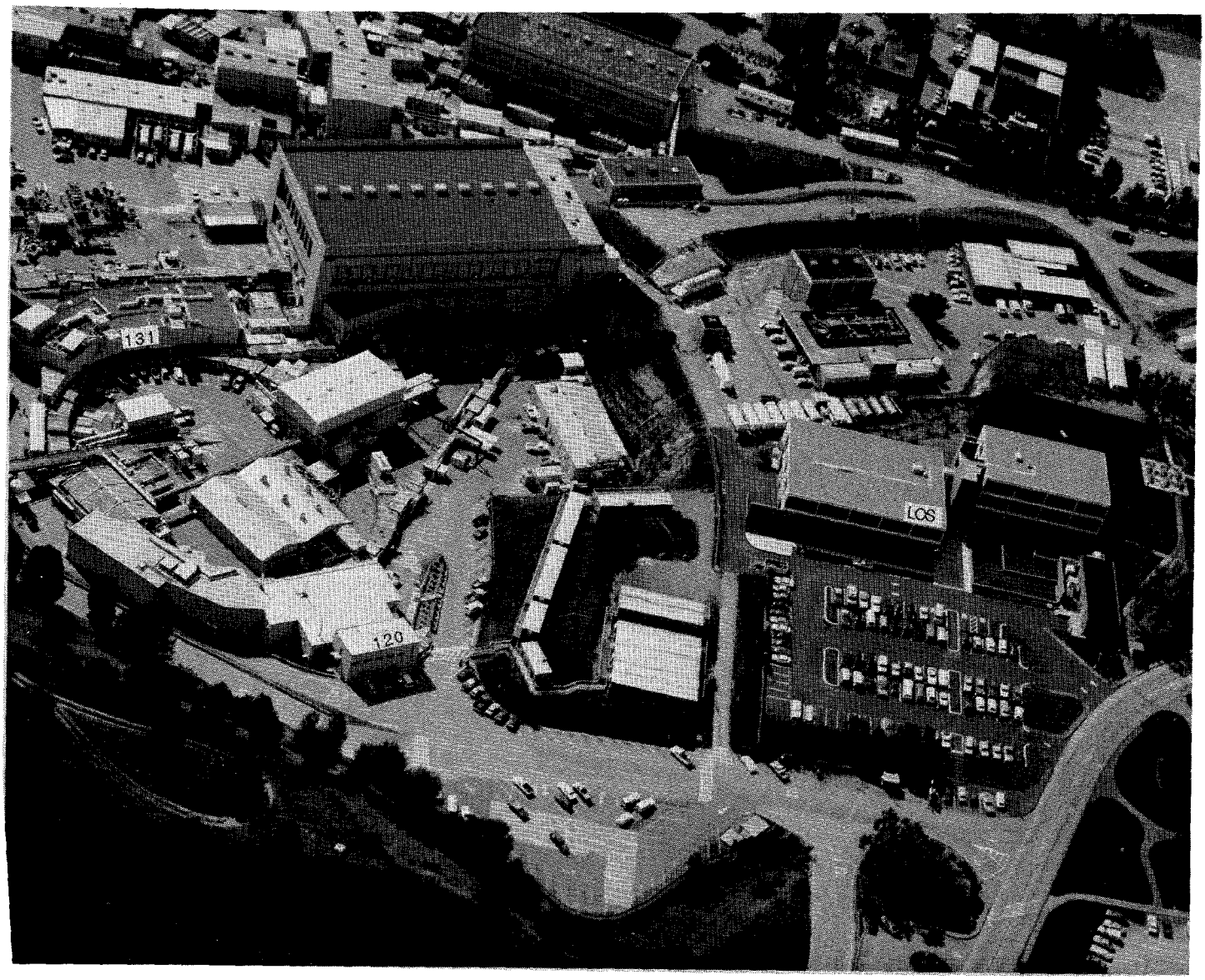

Photo - J. Faust

Overview of SLAC Research yard
SSRL Site

SSRL is located in 3 buildings in and adjacent to the SLAC research yard. The new LOS building houses laboratories and offices. The two buildings (120 and 131) adjacent to the SPEAR ring house the 22 experimental stations, operations staff offices and user facilities. The trailer complex between the LOS and SPEAR houses the Injector Group and user offices.

☆U.S. GOVERNMENT PRINTING OFFICE: 1988- 587- 742/99147